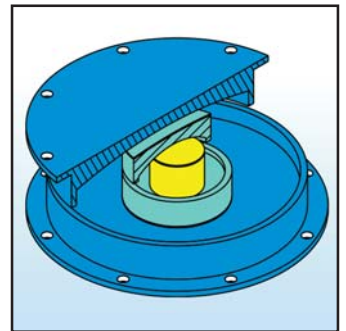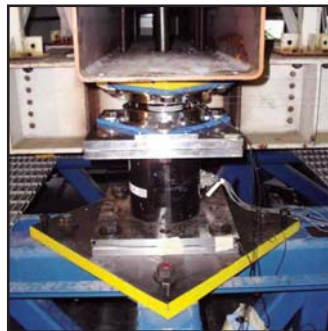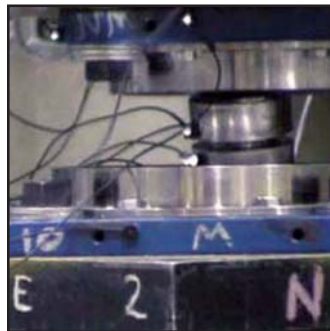# Development, Implementation and Verification of Dynamic Analysis Models for Multi-Spherical Sliding Bearings

by

Daniel M. Fenz and Michael C. Constantinou

NOTICE

This report was prepared by the University at Buffalo, State University of New York as a result of research sponsored by MCEER through a grant from the Earthquake Engineering Research Centers Program of the National Science Foundation under NSF award number EEC-9701471 and other sponsors. Neither MCEER, associates of MCEER, its sponsors, the University at Buffalo, State University of New York, nor any person acting on their behalf:

a. makes any warranty, express or implied, with respect to the use of any information, apparatus, method, or process disclosed in this report or that such use may not infringe upon privately owned rights; or

b. assumes any liabilities of whatsoever kind with respect to the use of, or the damage resulting from the use of, any information, apparatus, method, or process disclosed in this report.

Any opinions, findings, and conclusions or recommendations expressed in this publication are those of the author(s) and do not necessarily reflect the views of MCEER, the National Science Foundation, or other sponsors.

Development, Implementation and Verification of Dynamic Analysis Models for Multi-Spherical Sliding Bearings

by

Daniel M. Fenz[1] and Michael C. Constantinou[2]

1   Ph.D. Candidate, Department of Civil, Structural and Environmental Engineering, University at Buffalo, State University of New York
2   Professor, Department of Civil, Structural and Environmental Engineering, University at Buffalo, State University of New York

MCEER
University at Buffalo, State University of New York
Red Jacket Quadrangle, Buffalo, NY 14261
Phone: (716) 645-3391; Fax (716) 645-3399
E-mail: *mceer@buffalo.edu*; WWW Site: *http://mceer.buffalo.edu*

NTIS DISCLAIMER

Preface

The Multidisciplinary Center for Earthquake Engineering Research (MCEER) is a national center of excellence in advanced technology applications that is dedicated to the reduction of earthquake losses nationwide. Headquartered at the University at Buffalo, State University of New York, the Center was originally established by the National Science Foundation in 1986, as the National Center for Earthquake Engineering Research (NCEER).

Comprising a consortium of researchers from numerous disciplines and institutions throughout the United States, the Center's mission is to reduce earthquake losses through research and the application of advanced technologies that improve engineering, pre-earthquake planning and post-earthquake recovery strategies. Toward this end, the Center coordinates a nationwide program of multidisciplinary team research, education and outreach activities.

MCEER's research is conducted under the sponsorship of two major federal agencies: the National Science Foundation (NSF) and the Federal Highway Administration (FHWA), and the State of New York. Significant support is derived from the Federal Emergency Management Agency (FEMA), other state governments, academic institutions, foreign governments and private industry.

MCEER's NSF-sponsored research objectives are twofold: to increase resilience by developing seismic evaluation and rehabilitation strategies for the post-disaster facilities and systems (hospitals, electrical and water lifelines, and bridges and highways) that society expects to be operational following an earthquake; and to further enhance resilience by developing improved emergency management capabilities to ensure an effective response and recovery following the earthquake (see the figure below).
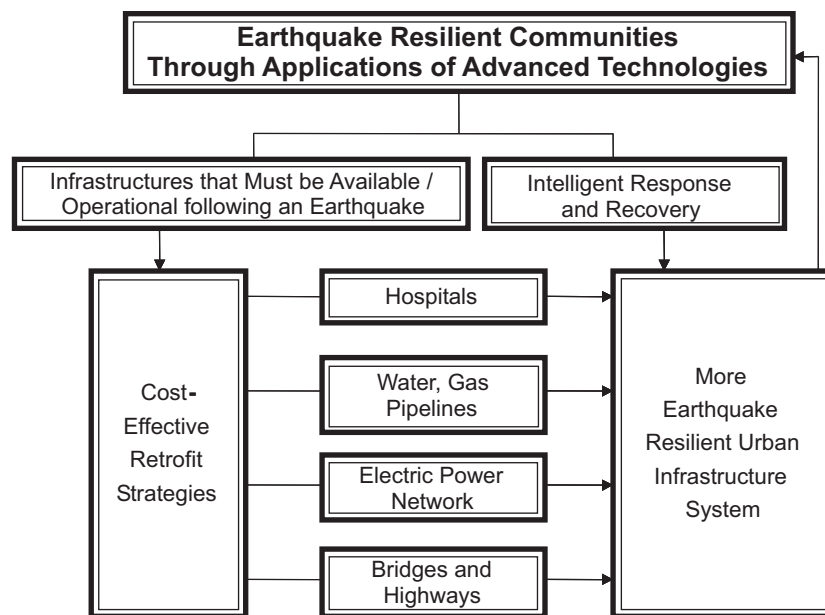
A cross-program activity focuses on the establishment of an effective experimental and analytical network to facilitate the exchange of information between researchers located in various institutions across the country. These are complemented by, and integrated with, other MCEER activities in education, outreach, technology transfer, and industry partnerships.

This report describes the formulation, implementation and validation of multi-spherical sliding bearing models proposed for response history analysis of double and triple Friction Pendulum (FP) bearings. These bearings exhibit hysteretic behavior that is more complex than current seismic isolation devices. Since double FP bearings behave like two single concave FP bearings connected in series, the proposed model considers a series arrangement of single FP elements. Additionally, it is shown that a series arrangement can be used to capture the behavior of triple FP bearings provided that the model parameters are appropriately modified. The proposed models can be implemented in currently available structural analysis programs such as SAP2000 and 3D-BASIS. The FP bearing models presented in this report are verified by comparing the results obtained from shake table testing of a quarter-scale six-story building model to those predicted by response history analysis. Good agreement is observed even in cases of extreme response, which attest to the robustness and validity of the proposed models.

ABSTRACT

This report describes the formulation, implementation and validation of multi-spherical sliding bearing models that can be used for response history analysis. When configured to exhibit adaptive behavior, double and triple Friction Pendulum (FP) bearings exhibit hysteretic behavior that is more complex than that exhibited by current seismic isolation devices. Therefore, in their present form existing models are not applicable to double and triple FP bearings.

Since the true behavior of the double FP bearing is that of two single concave FP bearings connected in series, the approach taken to model its behavior is to use a series arrangement of single FP elements. Additionally, it is shown that a series arrangement can be used to capture the behavior of the triple FP provided that the input parameters are modified appropriately – despite the fact that its true behavior is not that of three single FP bearings connected in series. Elements for modeling the behavior of single FP bearings are available in programs such as SAP2000 and the 3D-BASIS suite. Therefore, the proposed models can be implemented with no need for revision to the current software.

The methodologies described in this report are verified by comparing the results obtained from shake-table testing of a quarter-scale, six-story model to those predicted by response history analysis. There is generally good agreement even in cases of extreme response, which attests to the proposed models' robustness and overall validity.

ACKNOWLEDGEMENTS

TABLE OF CONTENTS

TABLE OF CONTENTS (CONT'D)

LIST OF ILLUSTRATIONS

LIST OF ILLUSTRATIONS (CONT'D)

LIST OF ILLUSTRATIONS (CONT'D)

LIST OF ILLUSTRATIONS (CONT'D)

LIST OF TABLES

LIST OF TABLES (CONT'D)

SECTION 1
INTRODUCTION

Multi-spherical sliding bearings, namely the double and triple Friction Pendulum (FP) bearings, have proven to be one of the more promising recent developments in the field of seismic isolation. The construction of these devices is characterized by multiple concave surfaces upon which sliding can occur. Drawings of the double FP and triple FP bearings are shown in figures 1-1 and 1-2 respectively. Since sliding is shared among multiple concave surfaces, each individual surface needs to accommodate only a portion of the total demand. This allows for the bearings to be manufactured much more compactly in size than traditional spherical sliding bearings, which obviously provides substantial savings in the cost of these devices. In addition to the economic benefits, there are also performance benefits resulting from sharing displacements among multiple surfaces. For example, in double FP bearings, sliding velocities are approximately halved compared to single FP bearings. As a result, frictional heating and associated problems such as wear and variability in friction are reduced.

These benefits are achieved even in the simplest configurations of double and triple FP bearings in which the primary sliding surfaces are of equal friction. In this case, the hysteretic behavior is rigid linear (in the case of the double FP) or approximately bilinear (in the case of the triple FP). In either case the devices can be modeled for dynamic analysis using commonly available hysteretic models in software used for analysis of seismically isolated structures. To date, primarily equal friction configurations of double and triple FP bearings have been used in practical implementation due to the aforementioned economic and performance benefits combined with the relative ease with which these devices can be modeled.

Previous work (Fenz and Constantinou, 2006, 2008a, 2008b, 2008c) has established that multi-stage sliding behavior results when concave surfaces of unequal friction are used. The stiffness and effective friction change as the surfaces upon which sliding is occurring change. The behavior is adaptive, meaning that the stiffness and effective friction change to predictable values at calculable and controllable displacement amplitudes. This results in hysteretic behavior that is more complex than that exhibited by seismic isolation devices currently employed in practice.

The behavior of adaptive double FP bearings has been described in detail in Fenz and Constantinou (2006, 2008a, 2008b, 2008c). When the concave surfaces are of unequal friction, motion initiates upon the surface of least friction when the applied horizontal force, F, exceeds the friction force, $F_{f1} = \mu_1 W$ on this surface (where μ_1 is the velocity-dependent coefficient of friction of surface 1 and W is the vertical load supported by the bearings). Until the friction force is overcome on the surface of higher friction, sliding occurs only on the surface of least friction with stiffness inversely proportional to the effective radius of curvature of this surface ($R_{eff1} = R_1 - h_1$). This is referred to as sliding regime I. When the applied horizontal force exceeds the friction force on the surface of higher friction, $F \geq F_{f2} = \mu_2 W$, motion initiates on this surface and simultaneous sliding

1
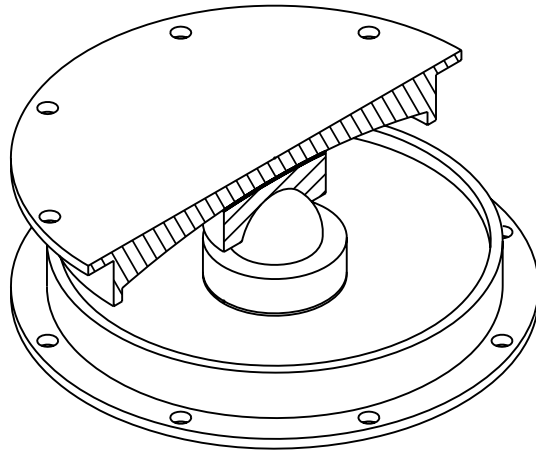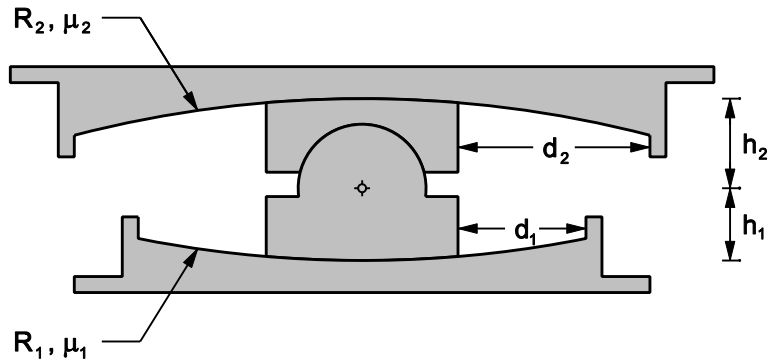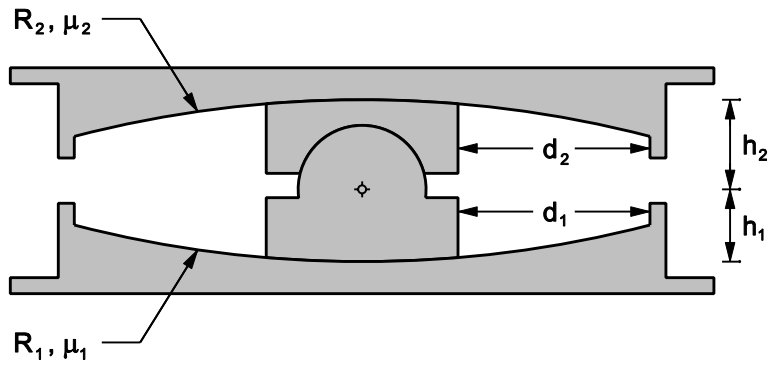
FIGURE 1-1 Cutaway (a) and Cross Section Views (b) of the Double Concave FP Bearing with Surfaces of Both Equal and Different Displacement Capacity

(a)

(b)
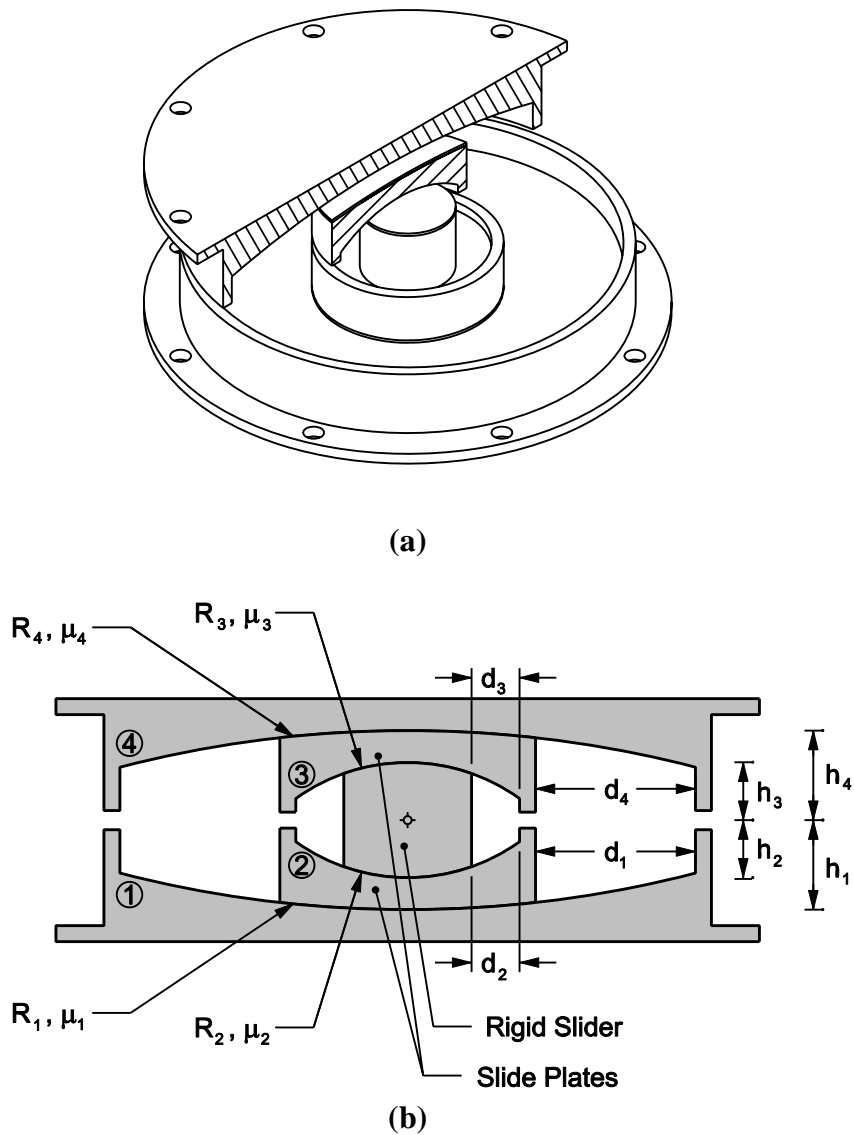
FIGURE 1-2 Cutaway (a) and Cross Section Views (b) of the Triple Concave FP Bearing

occurs. For simultaneous sliding occurring on both surfaces, the stiffness is inversely proportional to the sum of the effective radii of the upper and lower concave surfaces ($R_{eff1} + R_{eff2} = R_1 + R_2 - h_1 - h_2$). This is referred to as sliding regime II. At large displacements, stiffening behavior is achieved when the slider comes into contact with the displacement restrainer. This is referred to as sliding regime III. The surface whose displacement restrainer the slider contacts first is determined by the relative values of the displacement restrainer contact forces on the lower and upper surfaces, F_{dr1} and F_{dr2}, respectively. These forces are defined in table 1-1. This table provides a summary of double FP's behavior in each of the three sliding regimes. The hysteresis loops in sliding regimes I, II and III are provided in figures 1-3, 1-4 and 1-5 respectively.

3

TABLE 1-1 Summary of Double FP Bearing Behavior (Nomenclature Refers to Figure 1-1)

Regime	Description	Force-Displacement Relationship
I	Sliding on surface 1 only	$F = \dfrac{W}{R_{eff1}} u + F_{f1}$ *Valid until:* $\;F = F_{f2}, \quad u = u^* = (\mu_2 - \mu_1) R_{eff1}$
II	Simultaneous sliding on surfaces 1 and 2	$F = \dfrac{W}{R_{eff1} + R_{eff2}} u + \dfrac{F_{f1} R_{eff1} + F_{f2} R_{eff2}}{R_{eff1} + R_{eff2}}$ *Valid until:* $\;F = F_{dr1} = \dfrac{W}{R_{eff1}} d_1 + F_{f1}, \quad u = u_{dr1} = d_1 \left(1 + \dfrac{R_{eff2}}{R_{eff1}} \right) - (\mu_2 - \mu_1) R_{eff2}$
III	Slider bears on restrainer of surface 1; Sliding on surface 2	$F = \dfrac{W}{R_{eff2}} (u - d_1) + F_{f2}$

Assumptions: (1) $\mu_1 < \mu_2$, (2) $d_1 < \dfrac{R_{eff1}}{R_{eff2}} d_2 + (\mu_2 - \mu_1) R_{eff1}$
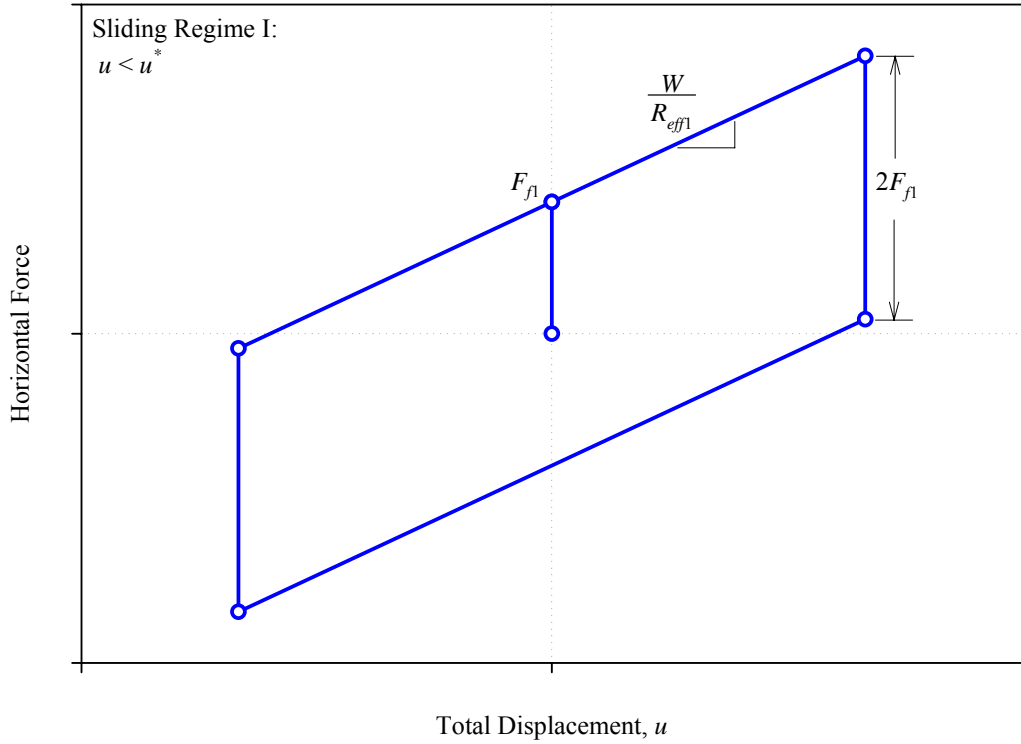
FIGURE 1-3 Force-Displacement Relationship of Double FP for Sliding Regime I

In the figure above (Sliding Regime I):
- Sliding Regime I: $u < u^*$
- Slope labeled $\dfrac{W}{R_{eff1}}$
- F_{f1}
- $2F_{f1}$
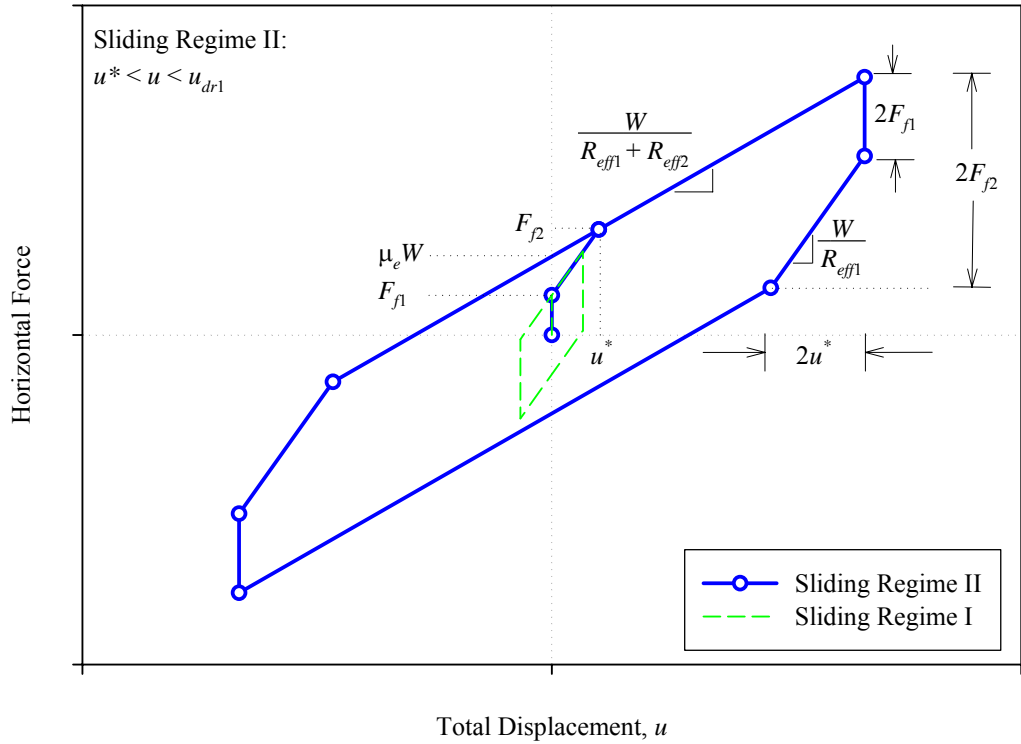
FIGURE 1-4   Force-Displacement Relationship for Sliding Regime II Shown in Comparison to Sliding Regime I

In the figure above (Sliding Regime II):
- Sliding Regime II: $u^* < u < u_{dr1}$
- Slope labeled $\dfrac{W}{R_{eff1} + R_{eff2}}$
- Slope labeled $\dfrac{W}{R_{eff1}}$
- F_{f2}
- $\mu_e W$
- F_{f1}
- u^*
- $2u^*$
- $2F_{f1}$
- $2F_{f2}$
- Legend: Sliding Regime II; Sliding Regime I

Sliding Regime III(a):

$u_{dr1} < u_{max} < u_{dr1} + 2R_{eff2}(\mu_2 - \mu_1)$

$\dfrac{W}{R_{eff2}}$

$2F_{f2}$

F_{dr1}

$F_{dr1} - 2F_{f1}$

$\dfrac{W}{R_{eff1}}$

$\dfrac{W}{R_{eff1} + R_{eff2}}$

u_{dr1}

(a)

Horizontal Force

Total Displacement, u

Sliding Regime III(a)
Sliding Regimes I - II

Sliding Regime III(b):

$u_{max} > u_{dr1} + 2R_{eff2}(\mu_2 - \mu_1)$

$\dfrac{W}{R_{eff2}}$

$2F_{f2}$

F_{dr1}

$F_{dr1} - 2F_{f1}$

$\dfrac{W}{R_{eff2}}$

$\dfrac{W}{R_{eff1} + R_{eff2}}$

u_{dr1}

(b)

Horizontal Force

Total Displacement, u

Sliding Regime III(b)
Sliding Regimes I - III(a)

FIGURE 1-5 Force-Displacement Relationship (a) for Sliding Regime III(a) Shown in Comparison to Sliding Regimes I-II and (b) for Sliding Regime III(b) Shown in Comparison to Sliding Regimes I-III(a)

Since there are more concave surfaces upon which sliding can occur, the behavior of the triple FP is inherently more complex than that of the double FP bearing. In its most fully adaptive configuration, there are five sliding regimes. These are summarized in table 1-2 and are described fully in Fenz and Constantinou (2008a, 2008b, 2008c). To achieve the most fully adaptive behavior, the two innermost sliding surfaces (surfaces 2 and 3 with reference to figure 1-2) must be of the lowest friction, one of the outer surfaces (say surface 1) must be of intermediate friction and the second outer surface must be of the highest friction. Typically, the effective radii of the inner surfaces will be small and equal effective radii and the outer surfaces will be of larger and equal effective radii, that is $R_{eff2} = R_{eff3} \ll R_{eff1} = R_{eff4}$.

When configured in this way, motion initiates on the two innermost surfaces and is characterized by high stiffness and low damping. With increasing horizontal force, motion will initiate on the outer surface of intermediate friction. An important feature of the device's behavior is that the instant motion starts on the outer surface, it stops on the corresponding inner surface. For example, with reference to figure 1-2, the instant sliding starts on surface 1 it stops on surface 2. Therefore, motion during the second regime consists of sliding on surfaces 1 and 3. This transition in sliding behavior is accompanied by a decrease in stiffness and an increase in damping. With increasing horizontal force, motion starts on the surface of highest friction (surface 4) when its friction force is overcome. During this regime, sliding occurs on surfaces 1 and 4 due to the fact that motion stops on surface 3 the instant that it starts on surface 4. Accordingly, transition to this sliding regime is accompanied by further reduction in stiffness and increase in damping.

With further increase in applied horizontal force, the outer slider will come into contact with the displacement restrainer. The exact equations for determining which surface contacts the restrainer first are provided in table 1-2, however for the typical case in which $R_{eff1} = R_{eff4}$ and $d_1 = d_4$ the slider will contact the intermediate friction surface prior to the high friction surface. When contact with restrainer of surface 1 occurs, motion stops on this surface and resumes on the corresponding inner surface (surface 2). Therefore, for this regime sliding occurs on surfaces 2 and 4 which is accompanied by an increase in the stiffness. With further increase in the applied horizontal force, the slider will come into contact with the restrainer of the second outer surface. Transition to this sliding regime is accompanied by further increase in stiffness as sliding occurs on surfaces 2 and 3 to the full displacement capacity of the device. The hysteretic behavior in each sliding regime is summarized in figures 1-6 through 1-10.

Clearly these types of hysteretic behavior are inherently more complex than the seismic isolation devices that exhibited by the devices that are currently implemented in practice. Therefore, in their present form, rigid-linear and bilinear hysteretic models that are used to model single concave FP and elastomeric bearings are not exactly applicable to multi-spherical sliding bearings. This report discusses various methodologies for modeling double and triple FP bearings for response history analysis with emphasis on implementation in SAP2000 structural analysis software. The analytical results predicted using the proposed methodologies are subsequently verified using the results from shake

table testing of a six-story seismically isolated structure. The model structure was tested with various configurations of double and triple FP bearings in order to more fully validate the analytical model across a broader range of behaviors.

Robust and valid methodologies for modeling structures isolated with multi-spherical sliding bearings in adaptive configurations are needed to investigate how best to implement these devices in practice. In order to draw meaningful conclusions from parametric studies, the results must be based on accurate and reliable analytical models. Moreover, the validity of the models must be established prior to using them for analysis and design of actual structures.

TABLE 1-2 Summary of Triple FP Bearing Behavior (Nomenclature Refers to Figure 1-2)

Regime	Description	Force-Displacement Relationship
I	Sliding on surfaces 2 and 3 only	$$F = \frac{W}{R_{eff2}+R_{eff3}}u + \frac{F_{f2}R_{eff2}+F_{f3}R_{eff3}}{R_{eff2}+R_{eff3}}$$ *Valid until:* $\quad F = F_{f1}, \quad u = u^* = (\mu_1-\mu_2)R_{eff2}+(\mu_1-\mu_3)R_{eff3}$
II	Motion stops on surface 2; Sliding on surfaces 1 and 3	$$F = \frac{W}{R_{eff1}+R_{eff3}}u + \frac{F_{f1}(R_{eff1}-R_{eff2})+F_{f2}R_{eff2}+F_{f3}R_{eff3}}{R_{eff1}+R_{eff3}}$$ *Valid until:* $\quad F = F_{f4}, \quad u = u^{**} = u^* + (\mu_4-\mu_1)(R_{eff1}+R_{eff3})$
III	Motion is stopped on surfaces 2 and 3; Sliding on surfaces 1 and 4	$$F = \frac{W}{R_{eff1}+R_{eff4}}u + \frac{F_{f1}(R_{eff1}-R_{eff2})+F_{f2}R_{eff2}+F_{f3}R_{eff3}+F_{f4}(R_{eff4}-R_{eff3})}{R_{eff1}+R_{eff4}}$$ *Valid until:* $\quad F = F_{dr1} = \dfrac{W}{R_{eff1}}d_1 + F_{f1}, \quad u = u_{dr1} = u^{**} + d_1\left(1+\dfrac{R_{eff4}}{R_{eff1}}\right) - (\mu_4-\mu_1)(R_{eff1}+R_{eff4})$
IV	Slider contacts restrainer on surface 1; Motion remains stopped on surface 3; Sliding on surface 2 and 4	$$F = \frac{W}{R_{eff2}+R_{eff4}}(u-u_{dr1}) + \frac{W}{R_{eff1}}d_1 + F_{f1}$$ *Valid until:* $\quad F = F_{dr4} = \dfrac{W}{R_{eff4}}d_4 + F_{f4}, \quad u = u_{dr4} = u_{dr1} + \left[\left(\dfrac{d_4}{R_{eff4}}+\mu_4\right) - \left(\dfrac{d_1}{R_{eff1}}+\mu_1\right)\right](R_{eff2}+R_{eff4})$
V	Slider bears on restrainer of surface 1 and 4; Sliding on surfaces 2 and 3	$$F = \frac{W}{R_{eff2}+R_{eff3}}(u-u_{dr4}) + \frac{W}{R_{eff4}}d_4 + F_{f4}$$

Assumptions: (1) $R_{eff1}=R_{eff4} \gg R_{eff2}=R_{eff3}$, (2) $\mu_2=\mu_3<\mu_1<\mu_4$, (3) $d_1>(\mu_4-\mu_1)R_{eff1}$, (4) $d_2>(\mu_1-\mu_2)R_{eff2}$

(5) $d_3>(\mu_4-\mu_3)R_{eff3}$
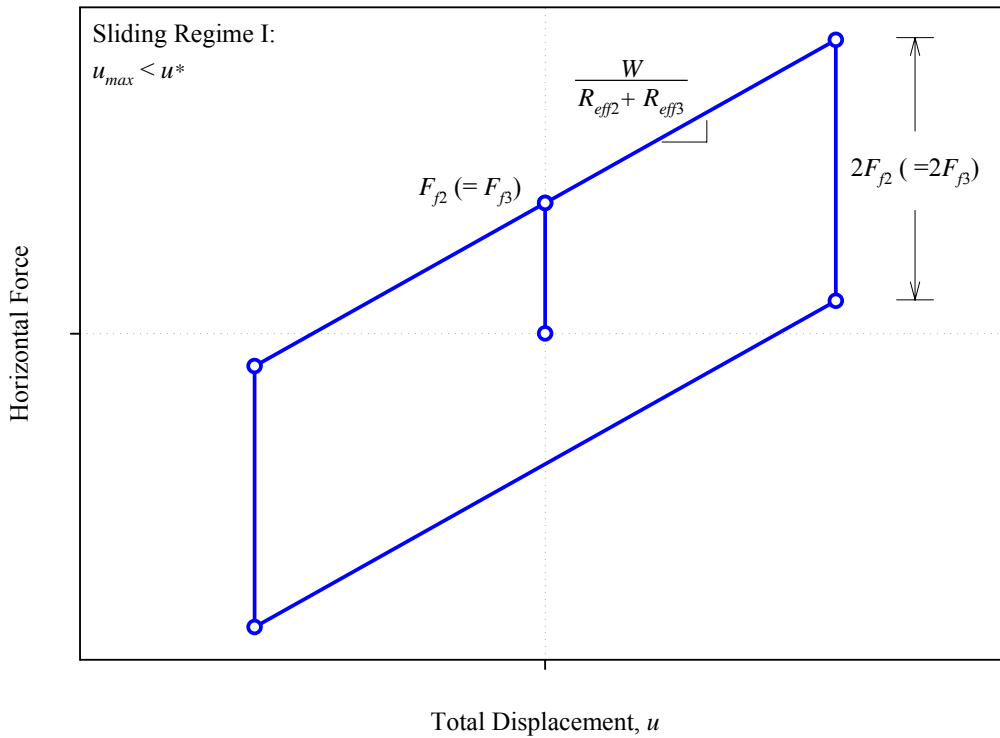
FIGURE 1-6 Force-Displacement Relationship During Sliding Regime I

In the figure:
- Sliding Regime I: $u_{max} < u^*$
- $\dfrac{W}{R_{eff2} + R_{eff3}}$
- $F_{f2} (= F_{f3})$
- $2F_{f2} (=2F_{f3})$
- Horizontal Force
- Total Displacement, u
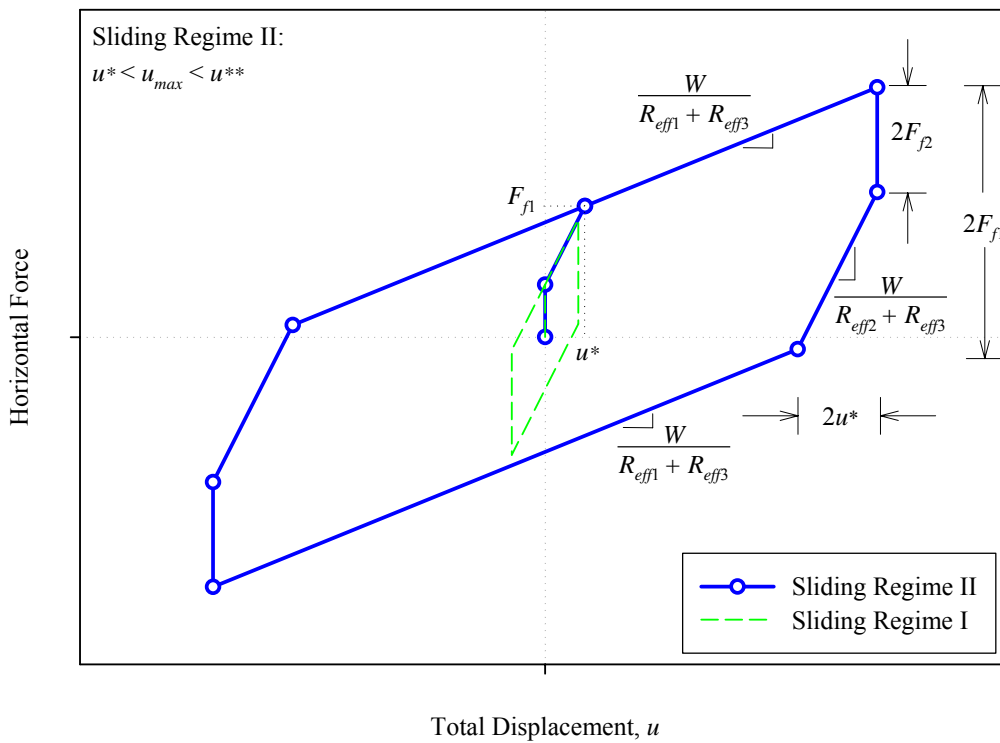
FIGURE 1-7 Force-Displacement Relationship During Sliding Regime II Shown in Relation to Sliding Regime I

In the figure:
- Sliding Regime II: $u^* < u_{max} < u^{**}$
- $\dfrac{W}{R_{eff1} + R_{eff3}}$
- F_{f1}
- $2F_{f2}$
- $2F_{f1}$
- $\dfrac{W}{R_{eff2} + R_{eff3}}$
- u^*
- $\dfrac{W}{R_{eff1} + R_{eff3}}$
- $2u^*$
- Horizontal Force
- Total Displacement, u

Legend:
- Sliding Regime II
- Sliding Regime I

10
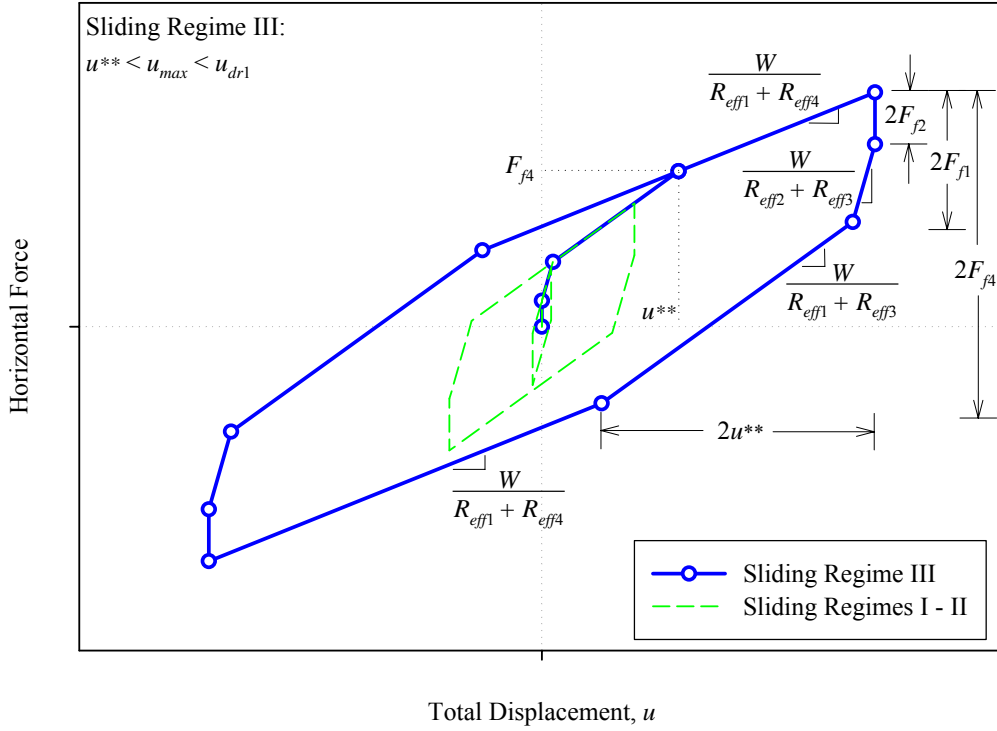
FIGURE 1-8 Force-Displacement Relationship During Sliding Regime III Shown in Relation to Sliding Regimes I-and II
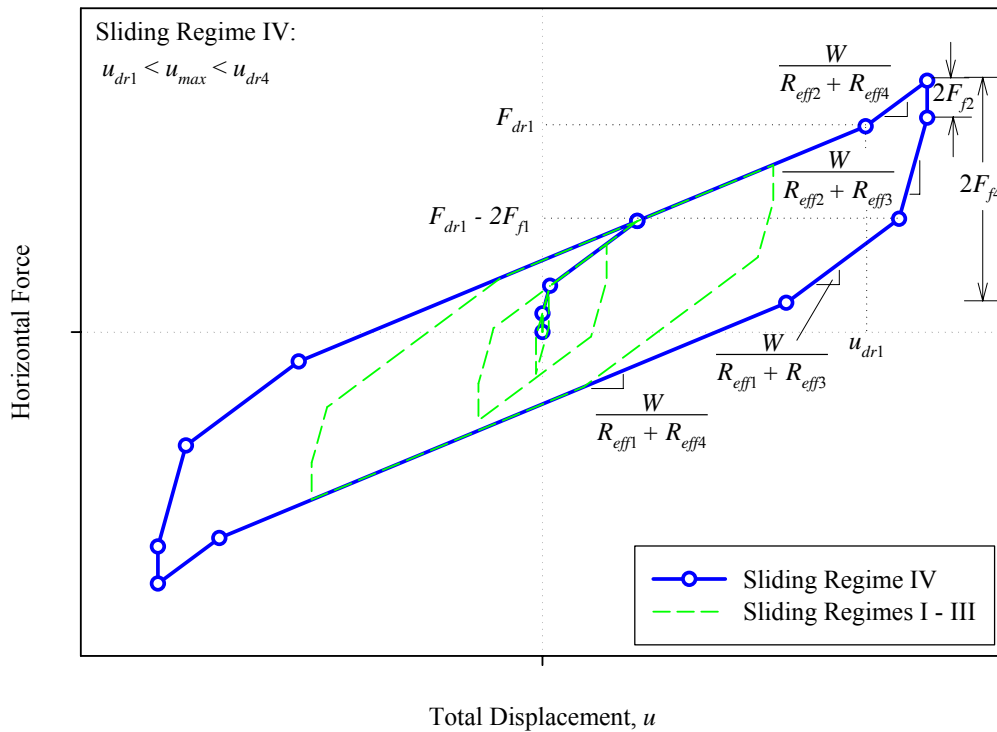
FIGURE 1-9 Force-Displacement Relationship During Sliding Regime IV Shown in Relation to Sliding Regimes I-III

11
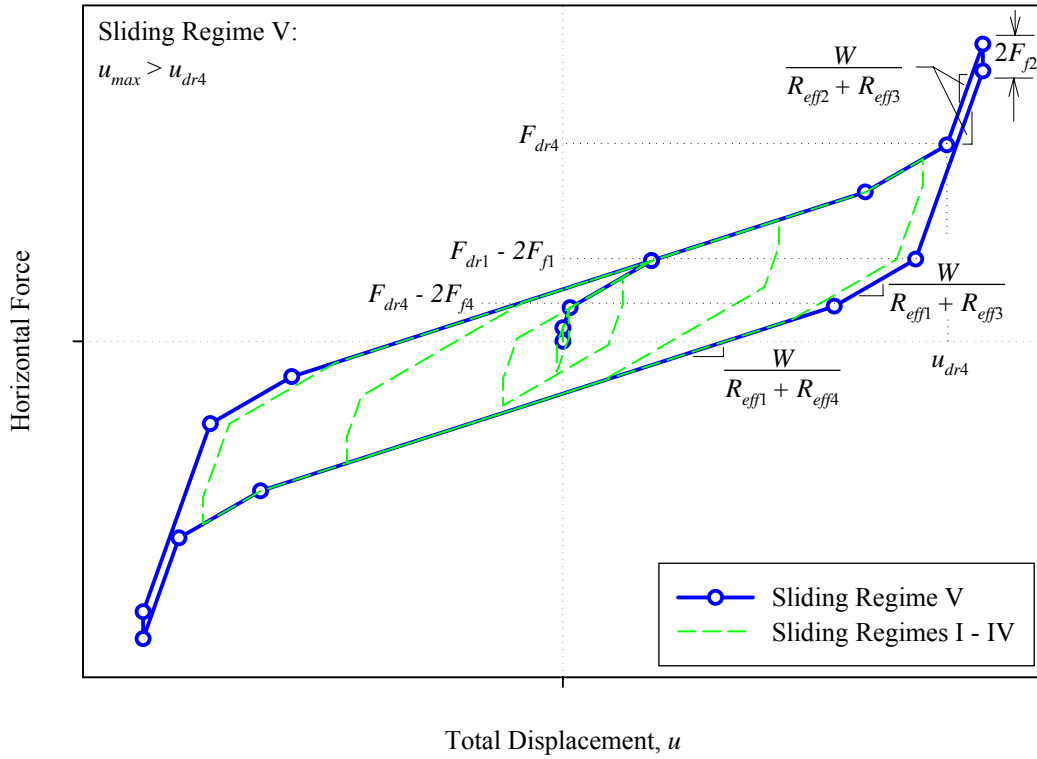
FIGURE 1-10 Force-Displacement Relationship During Sliding Regime V Shown in Relation to Sliding Regimes I-IV

SECTION 2
MODELING DOUBLE FRICTION PENDULUM BEARINGS FOR RESPONSE HISTORY ANALYSIS

2.1 Introduction

Establishing the mechanical behavior of the double and triple FP bearings was an essential prerequisite for the development of analytical models used for response history analysis. The remaining sections of this document discuss the development, implementation and experimental verification of these dynamic models.

One of the key aspects of the behavior of the double FP bearing is that it acts as two single concave FP elements connected in series. This makes the modeling of double FP bearings for response history analysis relatively straightforward. In the simplest case of equal radii and equal friction, the behavior can even be modeled using the same basic approaches as for single concave FP bearings.

This section first describes how to implement models double FP bearings software used for dynamic analysis of seismically isolated structures. Subsequently, a separate approach in which the equations of motion are formulated and numerically integrated using MATLAB is described.

2.2 Modeling for Dynamic Analysis in Structural Analysis Software

Various options exist for modeling double FP bearings in programs used for response history analysis of seismically isolated structures. Currently, SAP2000 is the most widely used program in industry with the 3D-BASIS suite of programs and ABAQUS used for verification and more specialized applications. Both SAP2000 and 3D-BASIS have predefined nonlinear link elements that are used to model the behavior of single concave FP bearings. For the simplest case in which $R_{eff1} = R_{eff2}$ and $\mu_1 \approx \mu_2$, the behavior of the bearing can be modeled as that of a single FP bearing with radius of curvature $R_{eff1} + R_{eff2}$ and coefficient of friction as determined from testing.

The velocity dependence of the coefficient of friction is described by (Constantinou *et al.*, 1990)

$$\mu = f_{max} - (f_{max} - f_{min})\exp(-a|\dot{u}|) \tag{2-1}$$

where $\dot{u}$ is the sliding velocity, f_{max} and f_{min} are the sliding coefficients of friction at large velocity and nearly zero sliding velocity, respectively and a is a rate parameter that controls the transition from f_{min} to f_{max}. Typically, f_{max} is determined in the prototype bearing testing program and the parameters f_{min} and a are selected on the basis of

13

previous experimental results. For more information on the selection of these parameters, the reader is referred to Constantinou *et al.* (2007).

Logically, for double FP bearings the velocity dependence of the coefficient of friction is a function of the sliding velocity on each concave surface and not the total sliding velocity of the top plate relative to the bottom plate. However, the analysis program calculates the velocity of the top node of the FP link with respect to the bottom node, denoted $\dot{u}$. For double FP bearings of equal radii and friction, the actual sliding velocities on each surface are equal and have magnitude of $\dot{u}/2$. This means that the exponential in equation (2-1) must have a value of $\left(-a|\dot{u}|/2\right)$ in order to correctly model the velocity dependence. Therefore, in the analysis, if a value of $a/2$ is specified as the rate parameter then the exponential has the same value and the phenomenon is properly captured. For example, a value of $a = 100$ s/m is often used for the type of material commonly used in single FP bearings. To model double FP bearings with the same type of sliding material, the value $a = 50$ s/m should be specified in the analysis program.

For the general case of a double FP bearing with unequal radii and unequal friction, the behavior can be modeled using two traditional FP link elements acting in series. It was shown earlier that the overall force-displacement can be decomposed into the components on each sliding surface, giving a hysteresis loop for each concave surface identical to that which would be obtained for a traditional FP bearing with the same radius of curvature and coefficient of friction. Therefore, by defining two separate single concave FP elements with the radii of curvature and coefficients of friction of each corresponding surface and then connecting them in series with a small point mass representing the articulated slider, the overall behavior of the double FP bearing is obtained. The velocity dependence of the coefficient of friction is still governed by equation (2-1), though the velocities of each isolator element represent the true sliding velocities on each surface. Therefore, the rate parameter a need not be modified.

2.3 State Space Formulation of the Equations of Motion

The governing equations in dynamic analysis programs such as 3D-BASIS and SAP2000 model FP bearings as a parallel arrangement of a linear elastic spring element with stiffness based on the curvature of the spherical dish and a friction element with plasticity governed by a modified Bouc-Wen model (Nagarajaiah *et al.*, 1989; Tsopelas *et al.*, 2005; Computers and Structures, Inc., 2007). The idea for the parallel arrangement of nonlinear elements used to represent the FP bearing follows from the multiple spring representation of hysteretic behavior described by Sivaselvan and Reinhorn (2000). In addition to these two terms, a gap component can be added in parallel to model the stiffening that occurs when contact is made with the displacement restrainer. Zero force is exerted by the gap element for displacements below a predefined value. Beyond this displacement, the element behaves as a linear spring with large stiffness. Therefore the horizontal force, F_i, exerted by FP element i is given by

$$F_i = \frac{W}{R_{eff\,i}} u_i + \mu_i W Z_i + \underbrace{k_{ri}\left(\left|u_i\right| - d_i\right)\text{sign}\left(u_i\right)\text{H}\left(\left|u_i\right| - d_i\right)}_{F_{ri}} \tag{2-2}$$

where W is the vertical load on the bearing, $R_{eff\,i}$ is the effective radius, u_i is the relative displacement of the slider on the concave surface, μ_i is the velocity dependent coefficient of friction governed by equation (2-1), Z_i is a hysteretic variable ranging between -1 and 1 that is governed by equation (2-3), k_{ri} is the stiffness exhibited by the displacement restrainer, d_i is the displacement capacity of surface i and H is the Heaviside step function. The hysteretic variable Z_i is governed by the differential equation

$$\frac{dZ_i}{dt} = \frac{1}{u_{yi}}\left\{A_i - \left|Z_i\right|^{\eta_i}\left[\gamma_i sign\left(\dot{u}_i Z_i\right) + \beta_i\right]\right\}\dot{u}_i \tag{2-3}$$

where u_{yi} is the yield displacement, $\dot{u}_i$ is the sliding velocity on the given surface and γ_i, β_i, η_i and A_i are dimensionless variables that control the shape of the hysteresis loop. In 3D-BASIS and SAP2000, this model is used with $A_i = 1$ and $\beta_i = \gamma_i = 0.5$. Essentially, the second term of equation (2-2) and equation (2-3) represent the frictional hysteresis with a smooth continuous function that approaches pure frictional behavior as the yield displacement u_{yi} approaches zero.

To formulate the equations of motion, consider the SDOF superstructure mounted on a double FP isolation system as shown in figure 2-1. In the figure, m_3 is the mass of the superstructure, m_2 is the basemat mass and m_1 is a very small mass that must be assigned to represent the articulated slider in order allow for the formulation of the equations of motion for the bottom concave surface. The superstructure stiffness is k_s and the equivalent viscous damping in the superstructure is represented with damping coefficient c_s. The damping coefficient of any dampers included at the isolation level is given by c_b. All parameters associated with the isolators have been defined previously.

As illustrated by the free body diagrams in figure 2-2, the equation of motion of the superstructure mass, m_3, for ground acceleration $\ddot{u}_g(t)$ is

$$m_3\ddot{u}_3 + c_s\left(\dot{u}_3 - \dot{u}_2\right) + k_s\left(u_3 - u_2\right) = -m_3\ddot{u}_g(t) \tag{2-4}$$

The equation of motion of the basemat mass m_2 is

$$m_2\ddot{u}_2 + \frac{W}{R_{eff\,2}}\left(u_2 - u_1\right) + \mu_2 W Z_2 + \underbrace{k_{r2}\left(\left|\left(u_2 - u_1\right)\right| - d_2\right)\text{sign}\left(u_2 - u_1\right)\text{H}\left(\left|\left(u_2 - u_1\right)\right| - d_2\right)}_{F_{r2}} - ...$$
$$c_s\left(\dot{u}_3 - \dot{u}_2\right) - k_s\left(u_3 - u_2\right) = -m_2\ddot{u}_g(t) \tag{2-5}$$

where Z_2 is governed by

15
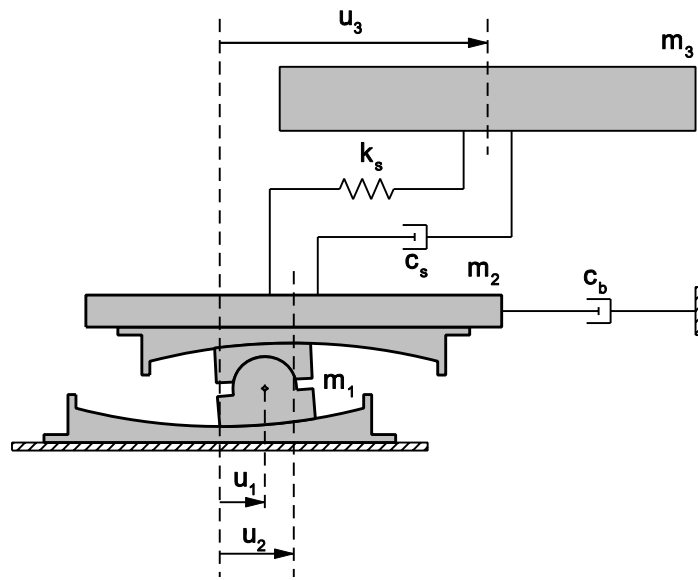
FIGURE 2-1 Definition Sketch of SDOF System Isolated with Double FP Bearings
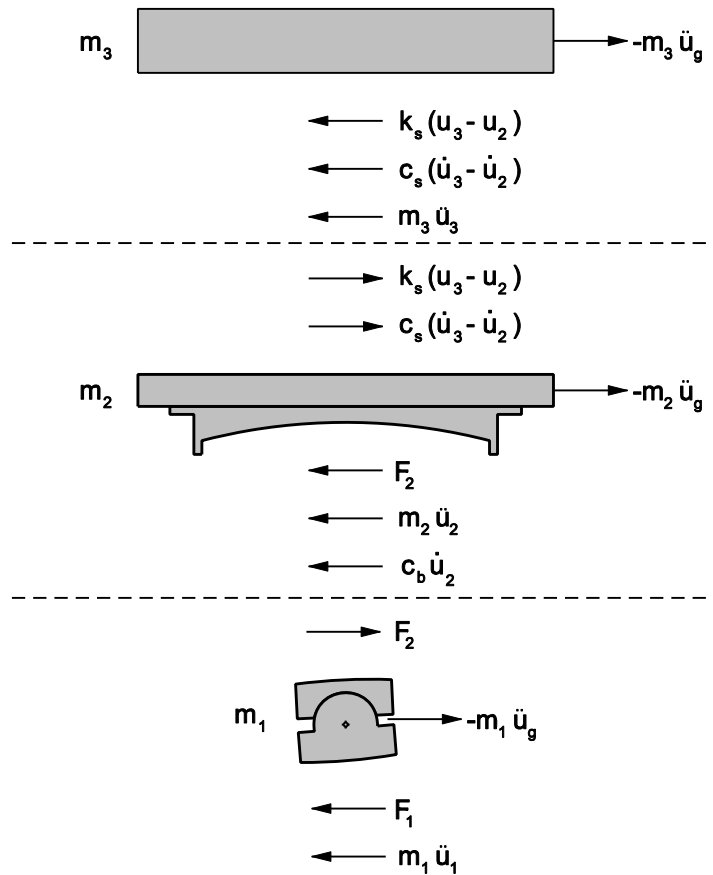
FIGURE 2-2 Free Body Diagrams of Masses m$_1$, m$_2$ and m$_3$ Used to Formulate the Equations of Motion of the SDOF System Isolated with Double FP Bearings

16

$$\frac{dZ_2}{dt} = \frac{1}{u_{y2}}\left\{A_2 - |Z_2|^{n_2}\left[\gamma_2 \text{sign}\left((\dot{u}_2 - \dot{u}_1)Z_2\right) + \beta_2\right]\right\}(\dot{u}_2 - \dot{u}_1) \tag{2-6}$$

Lastly, for the articulated slider mass m_1 the equation of motion is

$$m_1\ddot{u}_1 + \frac{W}{R_{eff1}}u_1 + \mu_1 W Z_1 + \underbrace{k_{r1}\left(|u_1| - d_1\right)\text{sign}\left(u_1\right)\text{H}\left(|u_1| - d_2\right)}_{F_{r1}} - \frac{W}{R_{eff2}}(u_2 - u_1) - \dots$$

$$\mu_2 W Z_2 - \underbrace{k_{r2}\left(|(u_2 - u_1)| - d_2\right)\text{sign}\left(u_2 - u_1\right)\text{H}\left(|(u_2 - u_1)| - d_2\right)}_{F_{r2}} = -m_1\ddot{u}_g(t) \tag{2-7}$$

where Z_1 is governed by

$$\frac{dZ_1}{dt} = \frac{1}{u_{y1}}\left\{A_1 - |Z_1|^{n_1}\left[\gamma_1 \text{sign}\left(\dot{u}_1 Z_1\right) + \beta_1\right]\right\}\dot{u}_1 \tag{2-8}$$

These equations are the same as used in 3D-BASIS and SAP2000, except modified to model two single concave elements with finite displacement capacity in series. Equations (2-4) through (2-8) can be expressed as a system of first order ordinary differential equations of the form

$$\{\dot{\mathbf{x}}\} = [\mathbf{A}]\{\mathbf{x}\} + \{\mathbf{B}\} \tag{2-9}$$

where the state vector $\{\mathbf{x}\}$ is

$$\{\mathbf{x}\} = \{u_1 \quad u_2 \quad u_3 \quad \dot{u}_1 \quad \dot{u}_2 \quad \dot{u}_3 \quad Z_1 \quad Z_2\}^T \tag{2-10}$$

With the state vector is formulated in this way, each term of the derivative $\{\dot{\mathbf{x}}\}$ is:

$$\dot{u}_1 = x(4) \tag{2-11a}$$
$$\dot{u}_2 = x(5) \tag{2-11b}$$
$$\dot{u}_3 = x(6) \tag{2-11c}$$

$$\ddot{u}_1 = -\left[\frac{W}{m_1 R_{eff1}} + \frac{W}{m_2 R_{eff2}}\right]u_1 + \frac{W}{m_1 R_{eff2}}u_2 - \frac{\mu_1 W Z_1}{m_1} + \frac{\mu_2 W Z_2}{m_1} + \frac{F_{r2} - F_{r1}}{m_1} - \ddot{u}_g \tag{2-11d}$$

$$\ddot{u}_2 = \frac{W}{m_2 R_{eff2}}u_1 - \left[\frac{W}{m_2 R_{eff2}} + \frac{k_s}{m_2}\right]u_2 + \frac{k_s}{m_2}u_3 - \dots$$

$$\frac{(c_s + c_b)}{m_2}\dot{u}_2 + \frac{c_s}{m_2}\dot{u}_3 - \frac{\mu_2 W Z_2}{m_2} - \frac{F_{r2}}{m_2} - \ddot{u}_g \tag{2-11e}$$

$$\ddot{u}_3 = \frac{k_s}{m_3} u_2 - \frac{k_s}{m_3} u_3 + \frac{c_s}{m_3} \dot{u}_2 - \frac{c_s}{m_3} \dot{u}_3 - \ddot{u}_g \qquad (2\text{-}11f)$$

$$\dot{Z}_1 = \frac{1}{u_{y1}} \left\{ A_1 - |Z_1|^{\eta_1} \left[\gamma_1 \text{sign}(\dot{u}_1 Z_1) + \beta_1 \right] \right\} \dot{u}_1 \qquad (2\text{-}11g)$$

$$\dot{Z}_2 = \frac{1}{u_{y2}} \left\{ A_2 - |Z_2|^{\eta_2} \left[\gamma_2 \text{sign}(\dot{u}_2 Z_2) + \beta_2 \right] \right\} \dot{u}_1 + \dots$$

$$\frac{1}{u_{y2}} \left\{ A_2 - |Z_2|^{\eta_2} \left[\gamma_2 \text{sign}(\dot{u}_2 Z_2) + \beta_2 \right] \right\} \dot{u}_2 \qquad (2\text{-}11g)$$

Based on the right-hand side of equations (2-11a) through (2-11g), the $[\mathbf{A}]$ matrix and $\{\mathbf{B}\}$ vector are populated accordingly. It should also be noted that in equations (2-11d) and (2-11e) the force from the displacement restrainer, F_{ri} is calculated using the displacement at the previous time step. The coefficient of friction is also calculated based on the appropriate sliding velocity form the previous step. Although this is not perfectly correct, the error introduced in negligible compared to other sources of uncertainty and a more computationally intensive implicit solution algorithm is avoided.

These 8 first order ordinary differential equations can be solved simultaneously using the `ode15s` solver in MATLAB. The `ode15s` solver is a variable order, multi-step algorithm that is efficient in solving systems of stiff differential equations (Shampine and Reichelt, 1997). The system is stiff due to the Z_i variables, which change very slowly when the bearing is sliding (Z_i variables are continuously either +1 or -1) and change very rapidly in the region of where the motion reverses direction or sticking occurs. In addition, since the time step in the solution algorithm differs from the time step of the supplied earthquake acceleration history, the acceleration at each solution time step is calculated by linear interpolation of the ground acceleration values. A MATALB code that performs this analysis is included at the end of this section.

To demonstrate the capabilities of this analysis algorithm, a SDOF structure atop a double FP isolation system is investigated. The data in this example is based on simplified analysis of a four-story hospital in the Bay Area of Northern California. The superstructure mass is $m_3 = 92,555\text{kN/g}$ with stiffness $k_s = 283\text{kN/mm}$ and damping coefficient $c_s = 2.07\text{kN-sec/mm}$. The basemat mass is $m_2 = 24,242\text{kN/g}$, so the total weight supported by the bearings is $W = 116,800\text{kN}$. The isolation system is comprised of double FP bearings of equal radii and unequal friction$- R_{eff1} = R_{eff2} = 2134\text{mm}$, $\mu_1 = 0.03$ at slow speed and 0.06 at high speed and $\mu_2 = 0.04$ to 0.08. For both sliding interfaces the rate parameter is $a_1 = a_2 = 0.024\text{sec/mm}$. Also, the parameters of the plasticity models assigned to both elements are the same: $u_y = 0.10\text{mm}$, $A = 1$, $\eta = 2$ and $\beta = \gamma = 0.5$. The ground excitation used, shown in figure 2-3, is the fault normal component of the 1999 Düzce, Turkey earthquake scaled to the 950 year return period at the hospital site.
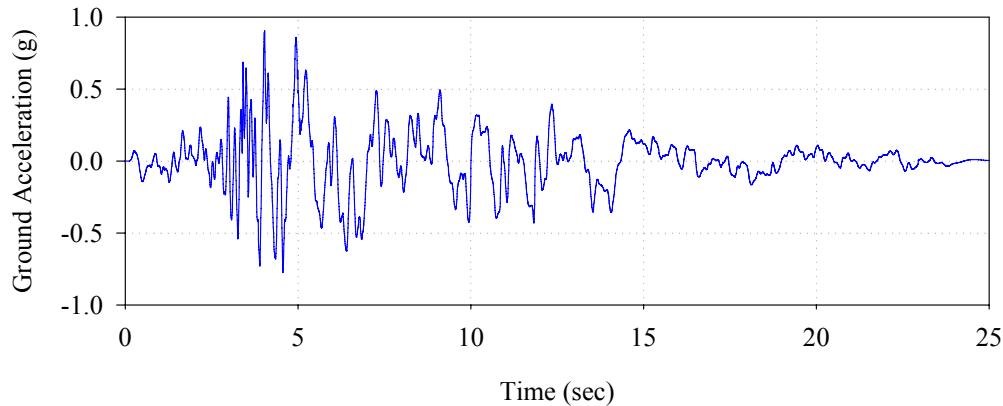
FIGURE 2-3 Duzce Fault Normal Ground Motion Scaled to the Level of the 950 Year Return Period at the Specific Site Used in the Example

Three separate analysis cases are carried out to compare the results obtained using this analysis algorithm solved with MATLAB and the SAP2000 structural analysis program. For the SAP2000 analysis, the double FP bearings are modeled using two FP link elements in series as described earlier. In the first analysis case, no dampers are used at the basemat and large displacement capacities are assigned so that no contact is made with the displacement restrainer. The results of this analysis are shown in figure 2-4 and demonstrate that there is good agreement between the two methods of analysis. This helps to validate both models. The agreement is also very good in cases in which there are dampers at the isolation level (figure 2-5) as well as both dampers at the isolation system level and contact with the displacement restrainer (figure 2-6). In the second analysis case, the isolation system dampers are linear dampers assigned a value $c_b = 15.4 \text{kN-sec/mm}$. For the final analysis case, the concave surface of least friction is assigned a displacement capacity of 305mm and a stiffness of 17,500kN/mm upon contact. In the SAP2000 analysis, this behavior is modeled using the gap element.

19

Matlab Analysis   **SAP2000 Analysis**

Peak Displacement = 1769mm   Peak Displacement = 1755mm
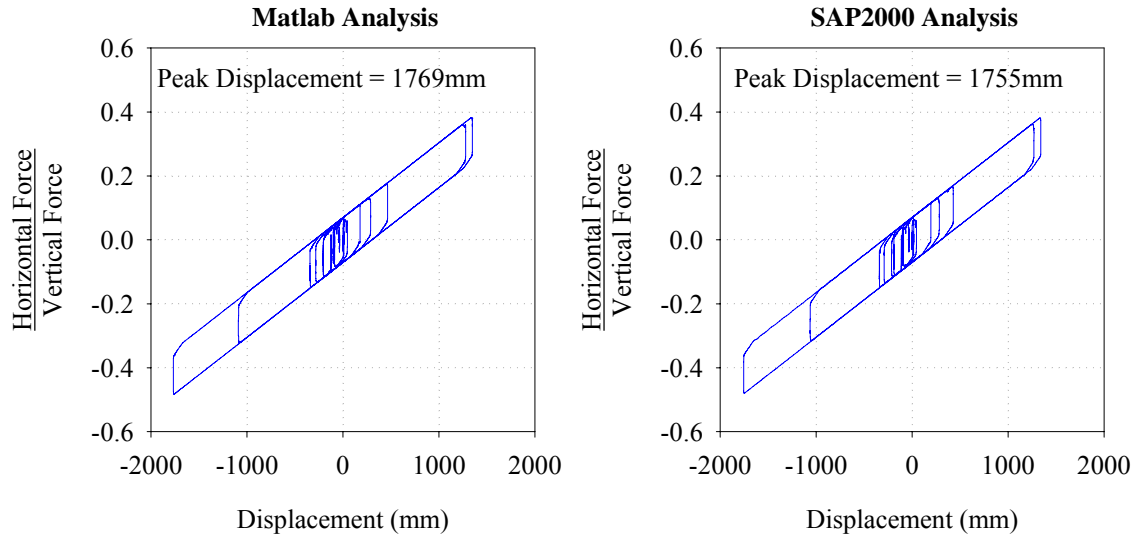
FIGURE 2-4 Comparison of Analysis in MATLAB and SAP2000 for SDOF System Isolated with Double FP Bearings (No Dampers)

Matlab Analysis   **SAP2000 Analysis**

Peak Displacement = 778mm   Peak Displacement = 782mm

Bearings
Bearings+Dampers

Bearings
Bearings+Dampers
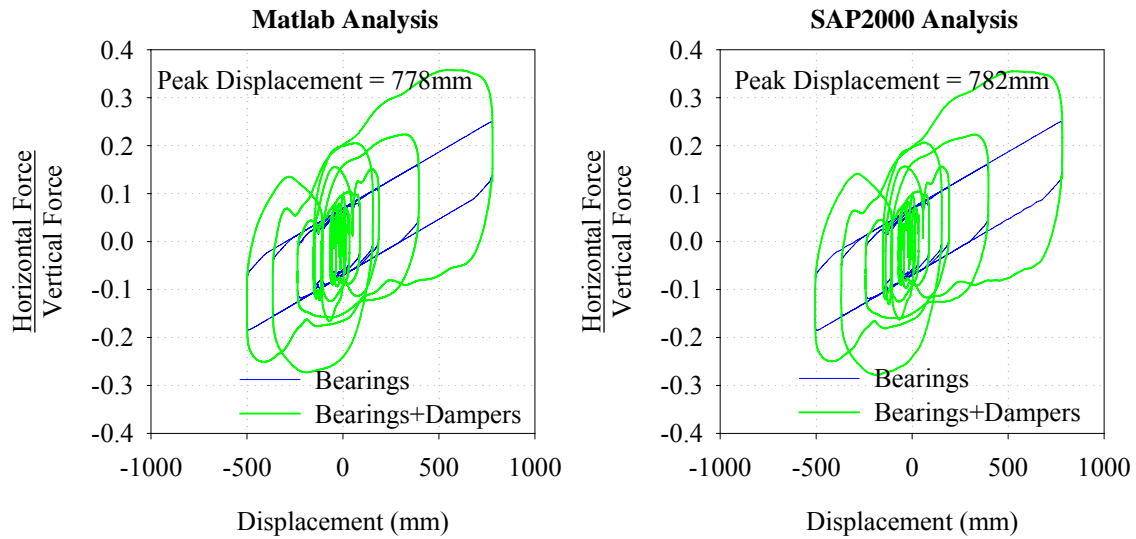
FIGURE 2-5 Comparison of Analysis in MATLAB and SAP2000 for SDOF System Isolated with Double FP Bearings and Viscous Dampers
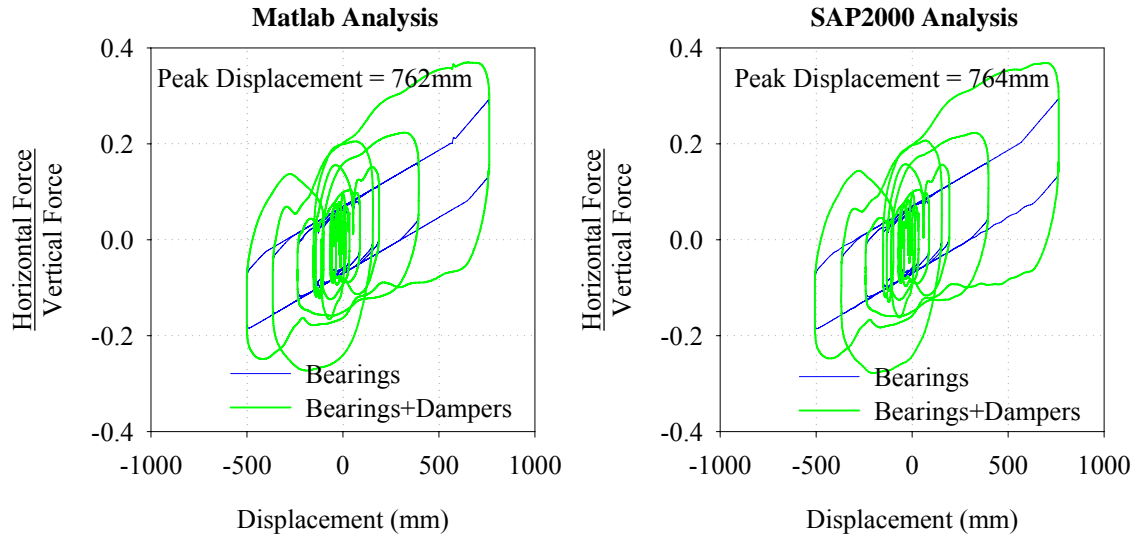
FIGURE 2-6 Comparison of Analysis in MATLAB and SAP2000 for SDOF System Isolated with Double FP Bearings and Viscous Dampers (Contact with Displacement Restrainer of Low Friction Surface)

```matlab
clear;
set(0,'defaultAxesFontName', 'courier new')
global g isp stp hystp tstep accl W;    %declare global variables
g = 386.4;                              % accel due to gravity (in/sec^2)

%%%%%%%%%%%%%%%%%%%%%%%%%%%%%%%%%%%%%%%%%%%%%%%%%%%%%%%%%%%%%%%%%%%%%%%%%
% INPUT OF SYSTEM PROPERTIES AND GROUND ACCELERATION RECORD
%%%%%%%%%%%%%%%%%%%%%%%%%%%%%%%%%%%%%%%%%%%%%%%%%%%%%%%%%%%%%%%%%%%%%%%%%

% Lower concave plate
Reff1 = 84; fmin1 = 0.03; fmax1 = 0.06; alpha1 = 0.6; m1 = 10/g;
d1 = 36; kr1 = 1e5;
% Upper concave plate
Reff2 = 84; fmin2 = 0.04; fmax2 = 0.08; alpha2 = 0.6; m2 = 5450/g;
d2 = 36; kr2 = 1e5;

% HYSTERETIC PROPERTIES
uy1 = 0.005;  A1 = 1; eta1 = 2; gamma1 = 0.9; beta1 = 0.1;
uy2 = 0.005;   A2 = 1; eta2 = 2; gamma2 = 0.9; beta2 = 0.1;

%Load isolator properties into a single vector and save
isp = [Reff1 Reff2; ...
       fmin1 fmin2; ...
       fmax1 fmax2; ...
       alpha1 alpha2; ...
       m1 m2; ...
       d1 d2;...
       kr1 kr2];
hystp = [uy1 uy2; ...
         A1 A2; ...
         eta1 eta2;...
         gamma1 gamma2;...
         beta1 beta2];

%SUPERSTRUCTURE PROPERTIES
Tn = 1.15; zeta = 0.02; m3 = 20808/g; cb = 88;
ks = m3* (2*pi/Tn)^2; cs = zeta*2*m3*sqrt(ks/m3);
stp = [ks; cs; m3; cb];
W = (m2+m3)*g;                          % Total weight on the isolators
                                        %(neglecting ficticious slider mass)
%ACCELERATION TIME HISTORY
tstep = 0.005;                          % time step of accel record
load duz950fn.DAT; accl = duz950fn;  % load ground acceleration data
tspan = [0:tstep:25];                    % time interval and output step size




%%%%%%%%%%%%%%%%%%%%%%%%%%%%%%%%%%%%%%%%%%%%%%%%%%%%%%%%%%%%%%%%%%%%%%%%%
%SOLVE THE DIFFERENTIAL EQUATIONS GOVERNING MOTION
%%%%%%%%%%%%%%%%%%%%%%%%%%%%%%%%%%%%%%%%%%%%%%%%%%%%%%%%%%%%%%%%%%%%%%%%%

x0 = [0 0 0 0 0 0 0 0]';
options = odeset('RelTol',1e-6,'AbsTol',1e-6,'Stats','on');
[t,x] = ode15s('xdot',tspan,x0,options);

%%%%%%%%%%%%%%%%%%%%%%%%%%%%%%%%%%%%%%%%%%%%%%%%%%%%%%%%%%%%%%%%%%%%%%%%%
%POST-PROCESSING OF RESPONSE QUANTITIES
%%%%%%%%%%%%%%%%%%%%%%%%%%%%%%%%%%%%%%%%%%%%%%%%%%%%%%%%%%%%%%%%%%%%%%%%%

%Displacements
u1 = x(:,1); u2 = x(:,2)-x(:,1); u3 = x(:,3)-x(:,2);
%Velocities
v1 = x(:,4); v2 = x(:,5)-x(:,4); v3 = x(:,6)-x(:,5);

%Velocity dependent friction
mu = zeros(length(t),2);
mu(:,1) = isp(3,1) - (isp(3,1)-isp(2,1))*exp(-isp(4,1)*abs(x(:,4)));
mu(:,2) = isp(3,2) - (isp(3,2)-isp(2,2))*exp(-isp(4,2)*abs( x(:,5)-x(:,4) ));
```

```matlab
%Restrainer ring force
gap = zeros(length(t),2); Fr = zeros(length(t),2);
gap(:,1) = abs(u1)-isp(6,1);
gap(:,2) = abs(u2)-isp(6,2);
Fr(:,1) = isp(7,1)*gap(:,1).*sign(u1).*heaviside(gap(:,1));
Fr(:,2) = isp(7,2)*gap(:,2).*sign(u2).*heaviside(gap(:,2));

%Normalized horizontal Force
F = zeros(length(t),4);
F(:,1) = u1/isp(1,1) + mu(:,1).*x(:,7) + Fr(:,1)/W;
F(:,2) = u2/isp(1,2) + mu(:,2).*x(:,8) + Fr(:,2)/W;
F(:,3) = (F(:,1)+F(:,2))/2;
F(:,4) = F(:,3)+stp(4)*x(:,5)/W;   %combined force (isolators+dampers)

%Absolute accelerations
%Ground
accg = zeros(length(t),1);
for n=1:length(t)
    i= fix(t(n)/tstep);
    accg(n) = accl(i+1) + (accl(i+2)-accl(i+1))/tstep.*(t(n)-i*tstep);
end
%Basemat
acc2 = ((W/isp(5,2)/isp(1,2))*(x(:,1)-x(:,2)) + ...
        (stp(1)/isp(5,2))*(x(:,3)-x(:,2)) - ((stp(2)+stp(4))/isp(5,2))*x(:,5) + ...
        stp(2)*x(:,6)/isp(5,2) - mu(:,2).*x(:,8)*(W/isp(5,2)) - ...
        Fr(:,2)/isp(5,2))/g;
%Superstructure
acc3 = ((stp(1)/stp(3))*(x(:,2)-x(:,3)) + (stp(2)/stp(3))*(x(:,5)-x(:,6)))/g;

%Drift and Structure Shear
Vs = u3*stp(1)/(m3*g);
```

```matlab
function y = xdot(t,x)    %XDOT Calculate xdot given x and t

global g isp;

%Find State Transformation Matrix
A = fnamatrix(x);
Fr = fnRestrForce(x);
ag = fnaccl(t)*g;
y = A*x + [0 0 0 (Fr(2)-Fr(1))/isp(5,1)-ag -Fr(2)/isp(5,2)-ag -ag 0 0]';

function A = fnamatrix(x)    %FNAMATRIX Calculates the A matrix
global W hystp isp stp;

mu = fnfriction(x);

z1 = (hystp(2,1)-(abs(x(7))^hystp(3,1))*(hystp(4,1)*sign(x(4)*x(7))+hystp(5,1)))/hystp(1,1);
z2 = (hystp(2,2)-(abs(x(8))^hystp(3,2))*(hystp(4,2)*sign((x(5)-x(4))*x(8))+hystp(5,2)))/hystp(1,2);

A = [0 0 0 1 0 0 0 0;...
     0 0 0 0 1 0 0 0;...
     0 0 0 0 0 1 0 0;...
     -(W/isp(5,1)/isp(1,1)+W/isp(5,1)/isp(1,2))  W/isp(5,1)/isp(1,2)  0 0 0 0  -mu(1)*W/isp(5,1)  mu(2)*W/isp(5,1);...
     W/isp(5,2)/isp(1,2)  -(W/isp(5,2)/isp(1,2)+stp(1)/isp(5,2))  stp(1)/isp(5,2)  0  -(stp(2)+stp(4))/isp(5,2)  stp(2)/isp(5,2)  0  -mu(2)*W/isp(5,2);...
     0 stp(1)/stp(3) -stp(1)/stp(3) 0 stp(2)/stp(3) -stp(2)/stp(3) 0 0;...
     0 0 0 z1 0 0 0 0;...
     0 0 0 -z2 z2 0 0 0];

function mmu = fnfriction(x)  %FNFRICTION Calculates velocity dependent coefficient of friction
global isp;
mmu(1) = isp(3,1) - (isp(3,1)-isp(2,1))*exp(-isp(4,1)*abs(x(4)));
mmu(2) = isp(3,2) - (isp(3,2)-isp(2,2))*exp(-isp(4,2)*abs( x(5)-x(4) ));

function a = fnaccl(t)  %FNACCL Function to interpolate the ground motion acceleration
global accl tstep;
i = fix(t/tstep);
a = accl(i+1) + (accl(i+2)-accl(i+1))/tstep.*(t-i*tstep);

function FFr = fnRestrForce(x)  %FNRESTRFORCE Calculates force imposed by restriner ring (gap element)
global isp
gap(1) = abs(x(1))-isp(6,1);
gap(2) = abs(x(2)-x(1))-isp(6,2);

FFr(1) = isp(7,1)*gap(1)*sign(x(1))*heaviside(gap(1));
FFr(2) = isp(7,2)*gap(2)*sign(x(2)-x(1))*heaviside(gap(2));
```

SECTION 3
MODELING TRIPLE FRICTION PENDULUM BEARINGS FOR RESPONSE HISTORY ANALYSIS

3.1 Introduction

There are currently no applicable hysteresis rules or nonlinear elements available in structural analysis software that can be used to exactly model triple FP bearings for response history analysis. Series models composed of existing nonlinear elements are proposed since they can be immediately implemented in currently available analysis software. However, the behavior of the triple FP bearing is not exactly that of a series arrangement of single concave FP bearings - although it is similar. This section describes how to modify the input parameters of the series model in order to precisely retrace the true force-displacement behavior exhibited by this device. Recommendations are made for modeling in SAP2000 and are illustrated through analysis of a simple seismically isolated structure. The results are confirmed by (a) verifying the force-displacement behavior through comparison with experimental data and (b) verifying the analysis through comparison to the results obtained by numerical integration of the equations of motion. These really only verify the modeling scheme at the component level, however. Subsequent sections of this report describe a program of shake table testing carried out to validate the analytical models when the bearings are part of a complex structural system.

The triple FP bearing exhibits multi-phase sliding that results in a distinct force-displacement relationship more complex than any exhibited by currently used seismic isolation devices. Consequently, in their present form models used to describe the behavior of seismic isolators for nonlinear response history analysis are not applicable as they do not capture the multiple changes in stiffness and damping inherent in the behavior of the triple FP. Two approaches can be taken to model the behavior of this new device: (a) develop and implement a new hysteresis rule to trace the overall behavior or (b) combine existing nonlinear elements in such a way that the overall behavior is captured. This section focuses on the later approach and discusses how to model the triple FP using an assembly of gap elements and single concave FP elements connected in series.

Series models are favored due to their feasibility of implementation in currently available structural analysis programs. Software such as SAP2000 already has nonlinear elements which model the rigid-linear behavior of traditional FP bearings. However, one behavioral phenomenon in particular precludes exact modeling of the triple FP bearing as three single FP bearings connected in series. This is the fact that simultaneous sliding cannot occur at both interfaces of the internal slide plate (surfaces 1 and 2 for example, with reference to figure 1-2). This was observed in experimental testing and is also predicted analytically. Sliding on the inner spherical recess of the slide plate occurs in the initial stage of motion, then stops when sliding begins at the outer sliding interface and subsequently starts again when the slide plate contacts the displacement restrainer. Series models do not exhibit this start-stop-start behavior.

25

Although a series model cannot reproduce the complex sliding behavior of all the internal parts, in this section it is described how to capture the overall behavior of the bearing exactly through appropriate modification of the model's input parameters. That is, the horizontal force-total displacement relationship for the assembly of elements will be correct, though the relative displacement response of the individual FP elements will not correspond exactly to the actual internal sliding behavior. Admittedly, this approach may be less computationally efficient than an explicit hysteresis rule; however the benefit is that it can be immediately implemented using currently available analysis software.

3.2 Behavior of Three FP Elements in Series

A schematic of three single FP elements connected in series is shown in figure 3-1. The individual elements are constrained to have the same force, but the relative displacements of each are independent. Each single FP element consists of a parallel arrangement of (a) a linear elastic spring element representing the restoring force provided by the curvature of the spherical dish, (b) a rigid plastic friction element with velocity dependence and (c) a gap element to account for the finite displacement capacity of each sliding surface. For element i, the stiffness of the spring is given by $1/\overline{R}_{effi}$ where $\overline{R}_{effi}$ is the effective radius of curvature, the velocity dependent coefficient of friction is $\overline{\mu}_i$ and the displacement at which the gap element engages is $\overline{d}_i$. Herein, over-bar notation is used to denote parameters and responses associated with the series model and standard notation is used to denote parameters and responses associated with the true behavior of the triple FP bearing.
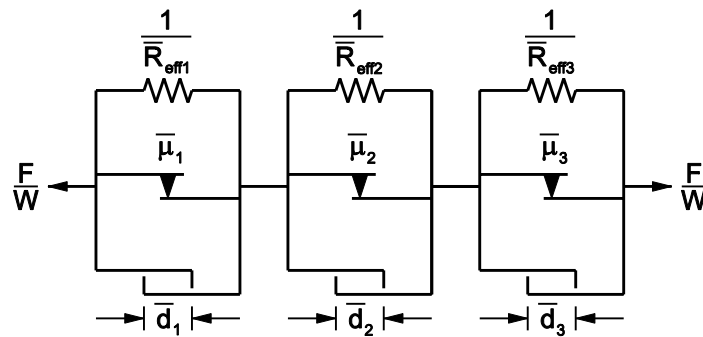
FIGURE 3-1 Three Single FP Elements in Series Used to Model the Behavior of the Triple FP Bearing

Examining the series model, displacement of element i initiates when the applied horizontal force F exceeds the friction force, $\overline{F}_{fi} = \overline{\mu}_i W$, where W is the vertical load supported by the bearing. Motion of element i stops when the relative displacement on the ith surface becomes equal to the displacement capacity $\overline{d}_i$. This occurs at an applied horizontal force of

$$\overline{F}_{dri} = \frac{W}{\overline{R}_{effi}} \overline{d}_i + \overline{F}_{fi} \qquad\qquad (3\text{-}1)$$

The overall stiffness is inversely proportional to the sum of the effective radii of curvature of the surfaces upon which sliding is occurring. Once sliding starts on a given surface it does not stop until motion reverses direction or the displacement capacity of this surface is achieved. The resulting hysteretic behavior obtained by considering three single FP elements in series is shown in figure 3-3. To construct this loop it has been assumed that $\overline{F}_{f1} < \overline{F}_{f2} < \overline{F}_{f3} < \overline{F}_{dr2} < \overline{F}_{dr3}$. The shape of this loop is identical to the actual force-total displacement relationship exhibited by triple FP bearings. Therefore, the approach taken will be to match each branch of the loop of figure 3-2 to the actual behavior through appropriate modification of the input parameters to the series model.
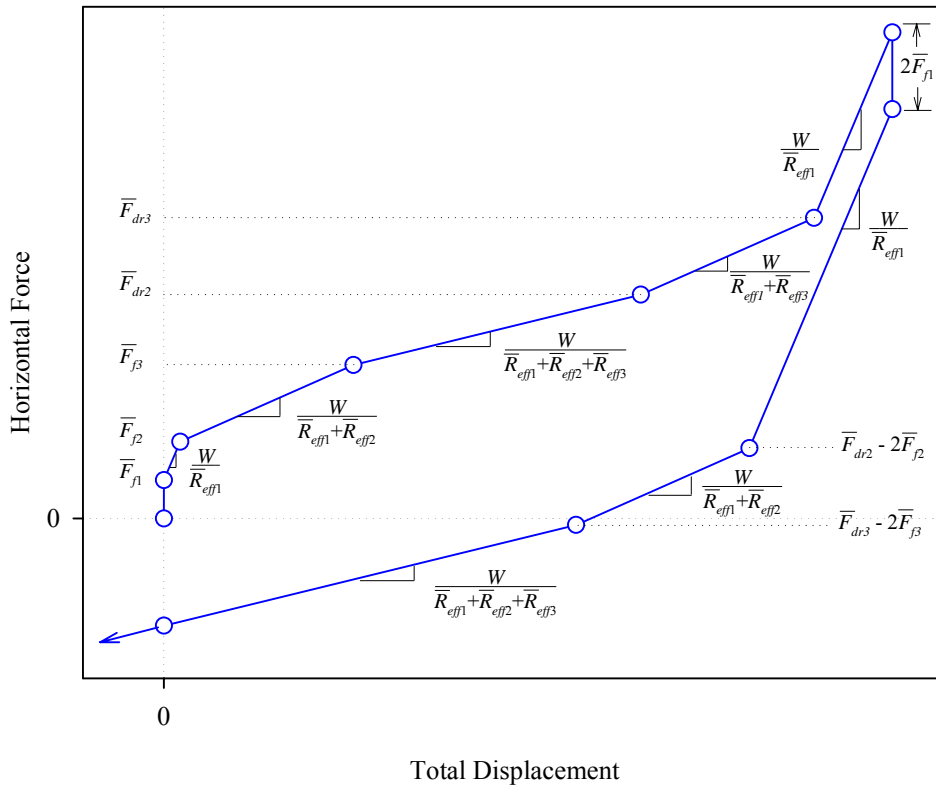
FIGURE 3-2 Force-Displacement Behavior of Three Single FP Elements Connected in Series

3.3 Input Parameters to the Series Model

The modifications made to the input parameters of the series model are calculated assuming that three single FP elements are used to represent a triple FP bearing in the most general or fully adaptive configuration. Referring to figure 1-2, this means that (a)

27

$R_{eff\,2} = R_{eff\,3} \ll R_{eff\,1} = R_{eff\,4}$, (b) $\mu_2 = \mu_3 < \mu_1 < \mu_4$, (c) $d_2 > \left(\mu_1 - \mu_2\right) R_{eff\,2}$ and $d_3 > \left(\mu_4 - \mu_3\right) R_{eff\,3}$ so that $F_{f1} < F_{dr2}$ and $F_{f4} < F_{dr3}$ and (d) $F_{f4} < F_{dr1}$. The behavior of less adaptive configurations, such as the common case in which $\mu_2 = \mu_3 < \mu_1 = \mu_4$, can also be modeled within this framework simply by specifying the appropriate friction coefficients.

In the proposed series modeling scheme, the first FP element represents the combined behavior of inner surfaces 2 and 3, the second element represents the behavior of outer surface 1 and the third represents outer surface 4. Since there is no adjustment made to the vertical load supported by the bearings, to ensure that sliding initiates correctly for each element there are no modifications made to the coefficients of friction. That is

$$\bar{\mu}_1 = \mu_2 = \mu_3 \qquad\qquad (3\text{-}2a)$$

$$\bar{\mu}_2 = \mu_1 \qquad\qquad (3\text{-}2b)$$

$$\bar{\mu}_3 = \mu_4 \qquad\qquad (3\text{-}2c)$$

For $F_{f2} = F_{f3} < F < F_{f1}$ (*i.e.* sliding regime I), the true behavior is sliding occurring only on surfaces 2 and 3. In the series model, there is sliding occurring only for element 1. Therefore, to properly model the stiffness during this sliding regime, it is necessary that

$$\bar{R}_{eff\,1} = R_{eff\,2} + R_{eff\,3} \qquad\qquad (3\text{-}3)$$

For $F_{f1} < F < F_{f4}$ (*i.e.* sliding regime II), sliding occurs on surfaces 1 and 3 only in the actual bearing - motion stops on surface 2 the instant it starts on surface 1. However the series model cannot capture the stoppage of motion for one element once it has begun for another. The effective radius of the second FP element in the series model is obtained by equating the stiffness given by the series model with the actual stiffness exhibited by the bearing:

$$\frac{W}{\bar{R}_{eff\,1} + \bar{R}_{eff\,2}} = \frac{W}{R_{eff\,1} + R_{eff\,3}} \qquad\qquad (3\text{-}4)$$

Combining equations (3-3) and (3-4):

$$\bar{R}_{eff\,2} = R_{eff\,1} - R_{eff\,2} \qquad\qquad (3\text{-}5)$$

For $F_{f4} < F < F_{dr1}$ (*i.e.* sliding regime III), the true behavior is sliding on surfaces 1 and 4 only - motion stops on surface 3 the instant it starts on surface 4. The effective radius of

the third FP element in the series model is obtained by again equating the series model stiffness with the actual stiffness exhibited by the bearing:

$$\frac{W}{\overline{R}_{eff1} + \overline{R}_{eff2} + \overline{R}_{eff3}} = \frac{W}{R_{eff1} + R_{eff4}} \tag{3-6}$$

Combining equations (3-3), (3-5) and (3-6):

$$\overline{R}_{eff3} = R_{eff4} - R_{eff3} \tag{3-7}$$

To ensure that the onset of stiffening behavior marking the start of sliding regime IV is appropriately captured, the force at which the first gap element engages in the series model, $\overline{F}_{dr2}$, is set equal to the force at which the slider contacts the displacement restrainer of surface 1, F_{dr1}:

$$\frac{\overline{d}_2}{\overline{R}_{eff2}} + \overline{\mu}_2 = \frac{d_1}{R_{eff1}} + \mu_1 \tag{3-8}$$

Using equations (3-2b) and (3-5),

$$\overline{d}_2 = \frac{R_{eff1} - R_{eff2}}{R_{eff1}} d_1 \tag{3-9}$$

Similarly, to ensure that $\overline{F}_{dr3} = F_{dr4}$, it is necessary that

$$\overline{d}_3 = \frac{R_{eff4} - R_{eff3}}{R_{eff4}} d_4 \tag{3-10}$$

For $F > F_{dr4}$ (*i.e.* sliding regime V), sliding occurs only on surfaces 2 and 3 to the maximum displacement. The series model gives sliding only for element 1. The stiffness is predicted correctly by the series model during this sliding regime per equation (3-3). If desired to model the total displacement capacity of the bearing, the displacement capacity of the first FP element can be assigned

$$\overline{d}_1 = \left(d_1 + d_2 + d_3 + d_4 \right) - \left(\overline{d}_2 + \overline{d}_3 \right) \tag{3-11}$$

29

or it can be left unspecified (infinite displacement capacity for the entire bearing). When equating the actual behavior of the bearing with the behavior given by the model with three elements in series, the stiffness during each sliding regime as well as the forces at which transitions in stiffness occur were enforced to be equal. It follows that the overall displacements at which the transitions in stiffness occur must also be equal.

Adjustments must also made to properly capture the velocity dependence of the coefficient of friction (equation (2-1)). The velocity dependence on surface 1 of the actual bearing will be properly modeled provided that $\bar{a}_2 \dot{\bar{u}}_2 = a_1 \dot{u}_1$. This is guaranteed by specifying

$$\bar{a}_2 = \frac{R_{eff1}}{R_{eff1} - R_{eff2}} a_1 \tag{3-13}$$

Similarly, for surface 4 of the actual bearing

$$\bar{a}_3 = \frac{R_{eff4}}{R_{eff4} - R_{eff3}} a_4 \tag{3-14}$$

For the first FP element of the series model, the rate parameter can be specified as half of the average of the rate parameters on surfaces 2 and 3 of the actual bearing because the actual sliding velocities on surfaces 2 and 3 are half of the relative velocity $\dot{u}_1$ calculated using the series model. Therefore

$$\bar{a}_1 = \frac{1}{2} \frac{(a_2 + a_3)}{2} \tag{3-15}$$

Equation (3-15) will correctly represent the velocity dependence during stages when sliding is occurring only on surfaces 2 and 3 of the actual bearing. Table 3-1 summarizes the values assigned to the input parameters of the three element series model.

Table 3-1   Parameters of the Series model of the Triple FP Bearing Calculated Assuming the Standard Configuration

Element	Coefficients of Friction	Radii of Curvature	Displacement Capacity (Nominal)	Rate Parameter
1	$\bar{\mu}_1 = \mu_2 = \mu_3$	$\bar{R}_{eff\,1} = R_{eff\,2} + R_{eff\,3}$	$\bar{d}_1 = d_{tot}{}^1 - \left(\bar{d}_2 + \bar{d}_3\right)$	$\bar{a}_1 = \dfrac{1}{2}\dfrac{\left(a_2 + a_3\right)}{2}$
2	$\bar{\mu}_2 = \mu_1$	$\bar{R}_{eff\,2} = R_{eff\,1} - R_{eff\,2}$	$\bar{d}_2 = \dfrac{R_{eff\,1} - R_{eff\,2}}{R_{eff\,1}} d_1$	$\bar{a}_2 = \dfrac{R_{eff\,1}}{R_{eff\,1} - R_{eff\,2}} a_1$
3	$\bar{\mu}_3 = \mu_4$	$\bar{R}_{eff\,3} = R_{eff\,4} - R_{eff\,3}$	$\bar{d}_3 = \dfrac{R_{eff\,4} - R_{eff\,3}}{R_{eff\,4}} d_4$	$\bar{a}_3 = \dfrac{R_{eff\,4}}{R_{eff\,4} - R_{eff\,3}} a_4$

1. d_{tot} is the total displacement capacity of the actual bearing. Alternatively, parameter d_{tot} may be left unspecified (infinite displacement capacity)

3.4 Implementation and Validation

To capture the complete range of behavior exhibited by triple FP bearings, the assembly of two-joint FP link elements, gap elements and rigid beam elements shown in figure 3-3 is proposed. The displacement capacities of gap elements G2 and G3 are $\bar{d}_2$ and $\bar{d}_3$ respectively. In order for gap element G2 to engage at a *relative* deformation of $\bar{d}_2$, the assembly of rigid beam elements is required. The gap elements are pin-ended to approximately model the capability of the slider to rotate freely when against the displacement restrainer. Furthermore, the overall height of the entire assembly should approximately correspond to the height of the actual bearing. Additional guidelines for modeling FP bearings for response history analysis in SAP2000 are provided in Scheller and Constantinou (2002) and Constantinou *et al.* (2007) and are generally applicable.
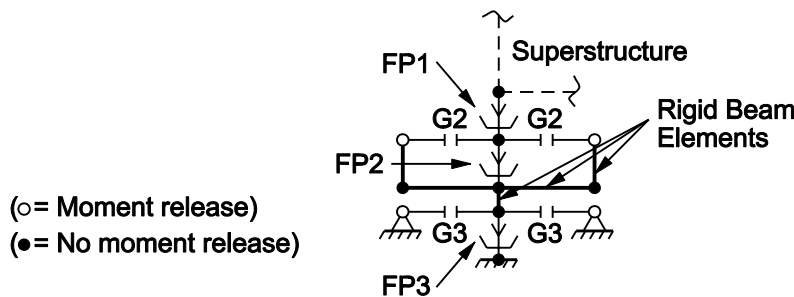
FIGURE 3-3   Assembly of Friction Pendulum Link Elements, Gap Elements and Rigid Beam Elements Used to Model the Behavior of the Triple FP Bearing in Software Used for Response History Analysis

It should be noted that the complete arrangement shown in figure 3-3 is needed only for modeling all sliding regimes of the most general (fully adaptive) configuration of triple FP bearing. In many cases, certain elements can be omitted from the model to make the analysis more efficient. For example, the gap elements can be omitted in lower amplitude excitations or in cases in which the engineer does not wish to utilize the stiffening capability of the device. When this is done however, the actual relative displacements must be checked to verify that the displacement restrainers in the actual bearing are not contacted. Also, in simpler configurations, such as equal friction on the inner two surfaces along with equal friction on the outer two interfaces, the behavior can be properly modeled using only two FP link elements - the first having friction $\mu_2 = \mu_3$ and effective radius $R_{eff\,2} + R_{eff\,3}$ and the second having friction $\mu_1 = \mu_4$ and effective radius $R_{eff\,1} + R_{eff\,4} - R_{eff\,2} - R_{eff\,3}$.

The arrangement described here is exact only for horizontal excitation in one direction (collinear with the gap elements). One may be tempted to include gap elements in both orthogonal horizontal directions and perform a full three dimensional analysis. However, the results would be flawed because the gap element's properties in SAP2000 are uncoupled, that is, they are independent in each deformational degree of freedom (Computers and Structures, Inc., 2007). Physically, this represents a bearing that is square in plan. Obviously the bearing is circular in plan which means that the gap element must engage when the *resultant* relative displacement equals the displacement capacity $\bar{d}_i$. However, a coupled gap element is not currently available in SAP2000. To work around this, additional gap elements can be used radially around the assembly to approximate a circle using straight line segments. Although this assembly becomes somewhat complex, the "replicate radial" command in the software can be used to efficiently build the model. Alternatively, a preliminary analysis can be conducted without gap elements to determine the directions in which they would be engaged. The model can subsequently be modified to include gap elements in these directions.

General purpose finite element software can also be used for the analysis. ABAQUS for example has a cylindrical gap element (GAPCYL) which can be employed in bidirectional analysis. This element is used to model contact between two rigid tubes of different diameter, where the smaller tube is located inside the larger tube (Hibbitt, Karlsson and Sorensen, Inc., 2004). Clarke *et al.* (2005) describes a study in which ABAQUS was used to analyze an offshore oil platform isolated with single concave FP bearings. Also, Tsopelas *et al.* (2005) used ABAQUS in verification studies of 3D-BASIS-ME-MB in the analysis of a seismically isolated structure under uplift conditions.

The force-displacement behavior predicted by the series model was validated by comparison to experimental data generated from characterization testing of the small scale triple FP bearing. The bearings used in the analysis have the properties of the Triple 1 configuration described in Fenz and Constantinou (2008b). The properties of the bearing from characterization testing and the attendant properties of the series model are listed in table 3-2. Based on this, the various sliding isolator and gap link elements used in SAP2000 are defined per table 3-3. Parameters such as the coefficients of friction, radii and gap size are important properties controlling the overall behavior and total response

of the isolators. Other parameters such as the element mass, vertical stiffness, unloading stiffness, rate parameter and gap element stiffness do not substantially influence the response in terms of displacement demands and shear forces, but do affect the efficiency and accuracy of the analysis.

Table 3-2 Actual Properties of Isolator from Testing and those Assigned to the Elements of the Series Model (The Two Coefficients of Friction Listed for Each Surface and for Each Element are the Values at Low Speed and High Speed Respectively)

Actual Properties from Testing (Fenz and Constantinou 2008b)				
Surface 1	$R_{eff1} = 435$ mm	$\mu_1 = 0.02 - 0.04$	$d_1 = 64$ mm	$a_1 = 0.10$ sec/mm
Surface 2	$R_{eff2} = 53$ mm	$\mu_2 = 0.01 - 0.02$	$d_2 = 19$ mm	$a_2 = 0.10$ sec/mm
Surface 3	$R_{eff2} = 53$ mm	$\mu_3 = 0.01 - 0.02$	$d_3 = 19$ mm	$a_3 = 0.10$ sec/mm
Surface 4	$R_{eff4} = 435$ mm	$\mu_4 = 0.06 - 0.13$	$d_4 = 64$ mm	$a_4 = 0.10$ sec/mm
Properties of Series Elements				
Element 1	$\overline{R}_{eff1} = 106$ mm	$\overline{\mu}_1 = 0.01 - 0.02$	$\overline{d}_1 = -$	$\overline{a}_1 = 0.05$ sec/mm
Element 2	$\overline{R}_{eff2} = 382$ mm	$\overline{\mu}_2 = 0.02 - 0.04$	$\overline{d}_2 = 56.2$ mm	$\overline{a}_2 = 0.11$ sec/mm
Element 2	$\overline{R}_{eff3} = 382$ mm	$\overline{\mu}_3 = 0.06 - 0.13$	$\overline{d}_3 = 56.2$ mm	$\overline{a}_3 = 0.11$ sec/mm

Small masses are assigned to the isolator elements to provide modes associated with the isolators required for the modal response history analysis to converge. These are selected iteratively since they must be small enough such that they have negligible dynamic effect, but large enough that the analysis converges within a reasonable time period. The unloading stiffness and yield displacement were calculated per the recommendations in Constantinou *et al.* (2007), but using a much smaller value of yield displacement. A smaller value is specified in this analysis because (a) the total yield displacement of the assembly is three times the yield displacement of a single isolator element and (b) the isolator displacements for the reduced-scale bearing are smaller than those expected in full-scale seismic applications. Lastly, it should be noted that the horizontal effective stiffness of the link elements is actually arbitrary for nonlinear modal response history analysis. However, as explained in Wilson (2001) a good estimate will accelerate the rate of convergence. Therefore, the value assigned to each element is the horizontal effective stiffness at half of the element's displacement capacity, *i.e.* K_{eff} at $D = \overline{d}_i / 2$.

Table 3-3 Properties of Sliding Isolator and Gap Link Elements Used in SAP2000 Analysis

Sliding Isolator Link Elements			
	FP1	FP2	FP3
Mass (kN-sec^2/mm)	5.0×10^{-7}	5.0×10^{-7}	5.0×10^{-7}
Element height (mm)	50	25	50
Vertical stiffness (kN/mm)	4,000	8,000	4,000
Horizontal effective stiffness (kN/mm)	0.524	0.202	0.362
Shear deformation location (mm)	25	12.5	25
Yield displacement (mm)	0.01	0.01	0.01
Unloading stiffness (kN/mm)	50	100	300
Coefficient of friction - slow[†]	0.01	0.02	0.06
Coefficient of friction - fast[†]	0.02	0.04	0.13
Rate parameter (sec/mm)	0.05	0.112	0.112
Radius (mm)	106	382	382
Rotational stiffness (kN-mm/rad)	3.0×10^6	3.0×10^6	3.0×10^6
Gap Link Elements			
		Gap2	Gap3
Mass (kN-sec^2/mm)		1.0×10^{-9}	1.0×10^{-9}
Element length (mm)		150	150
Effective stiffness (kN/mm)		0.5	0.5
Gap size (mm)		56.2	56.2
Stiffness after closing (kN/mm)		250	250

Note: Velocity dependent coefficients of friction are used only for the nonlinear response history analysis. Single valued friction coefficients based on the experimental results are used for the displacement controlled analysis.

In figure 3-4, the results of displacement-controlled analysis with SAP2000 are compared to both the experimental data and the analytical behavior based on the algebraic equations governing the force-displacement behavior. Using the model shown in figure 3-3, the analysis was carried out by fixing the bottom node and imposing a sinusoidal displacement history to the top node. The loops shown have displacement amplitudes corresponding to those from the experiment - 1.2mm, 25mm, 75mm, 115mm and 140mm. Recall that in the experiment the frequency of the excitation was very low to minimize absolute variation of the coefficient of friction due to velocity dependence. Accordingly, single-valued coefficients of friction were specified in the analysis as well. Since the exact values of friction cannot be known beforehand, the friction coefficients specified in the analysis are those measured from each test. As shown in figure 3-4, the

proposed modeling scheme accurately reproduces both the experimental results using the algebraic equations of table 1-2 for all five regimes of sliding behavior.
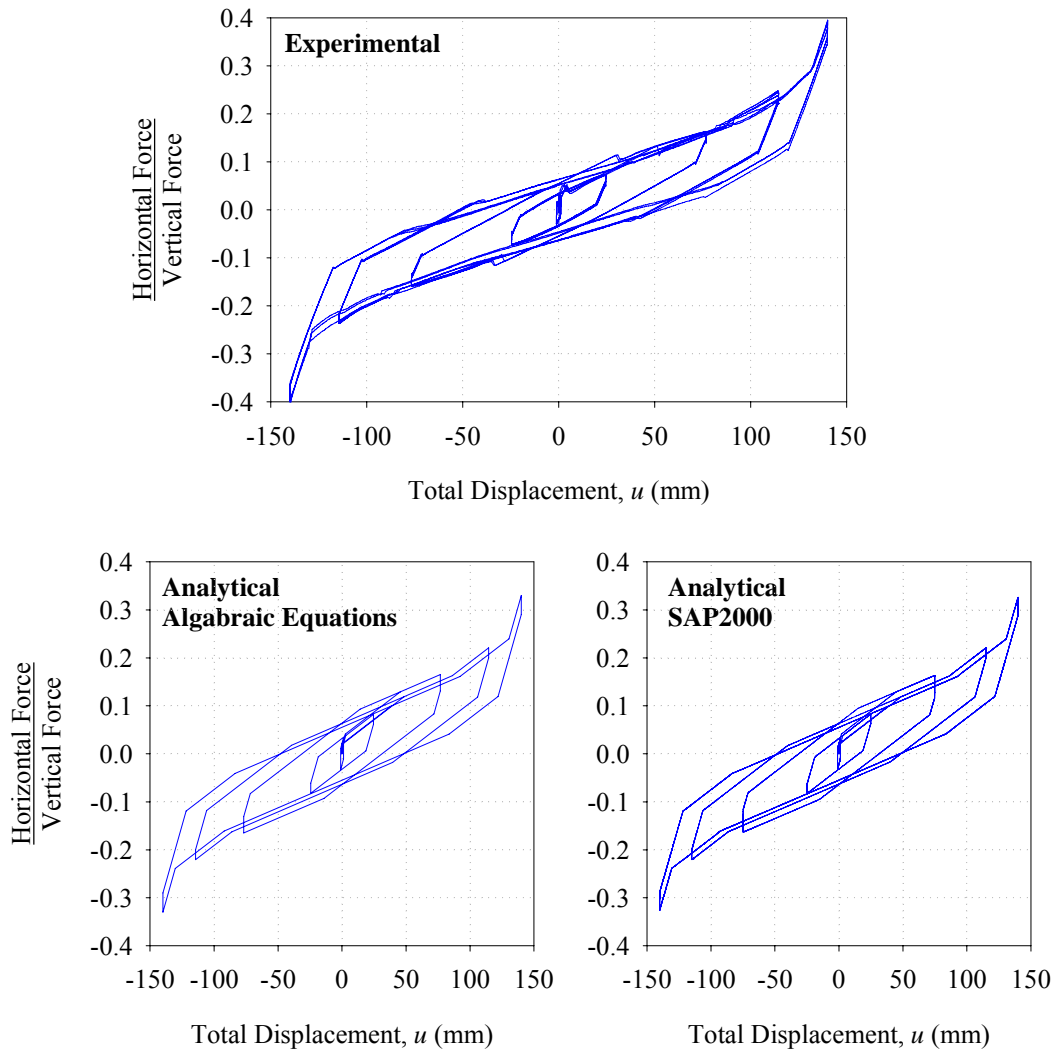
FIGURE 3-4   Comparison of the Experimentally Measured Force-Displacement Relationship of the Triple FP Bearing, the Analytical Prediction Based on the Algebraic Equations and the Behavior Obtained from Displacement-Controlled Nonlinear Analysis in SAP2000

This first analysis case serves to physically validate the force-displacement relationship given by the assembly of nonlinear elements with properly modified input parameters. Next, to verify the basic numerical accuracy of the dynamic response history analysis with the proposed assembly, a simple single story shear building isolated with triple FP bearings is analyzed. The isolators are modeled the same way as the previous analysis except now incorporating the effect of velocity dependence on the coefficients of friction. The analytical model of the superstructure is shown in figure 3-5. The total weight is 200 kN, divided two-thirds to the story mass and one-third to the basemat. All frame elements

are idealized as massless, with the superstructure and basemat masses lumped at the intersections of the beams and columns. Relevant properties assigned to the "Column" and "Rigid" type frame elements are listed in figure 3-5. The moments of inertia of the "Column" elements are selected to give a fixed base superstructure period of 0.20 sec in each principal direction (assuming shear building behavior). "Rigid" elements are assigned large moments of inertia in each direction in order to eliminate bending deformations. For both types of elements, the cross section area, torsion constant and shear area are assigned large values in order to effectively suppress deformations in the associated degrees of freedom.
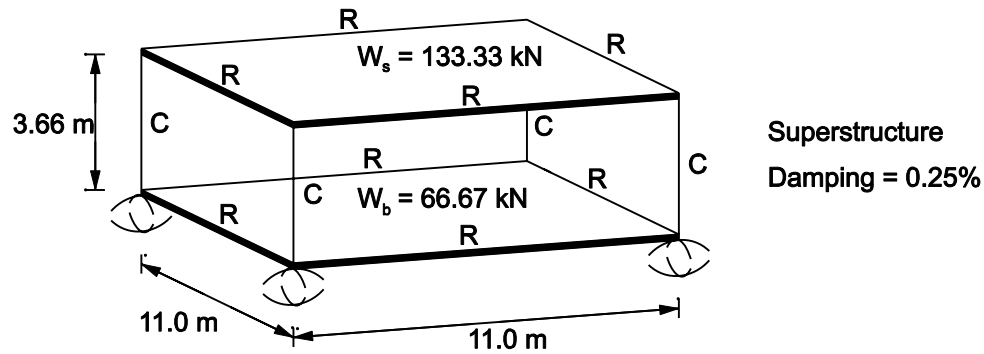
Section Property	Area (mm^2)	Moments of Inertia (mm^4)	Torsion Constant (mm^4)	Shear Area (mm^2)	Mass (kg)	Weight (kN)
"Column" (C)	5.0×10^6	6.851×10^7	1.0×10^8	5.0×10^6	0	0
"Rigid" (R)	5.0×10^6	1.0×10^{11}	1.0×10^8	5.0×10^6	0	0

FIGURE 3-5   Description of Simple Seismically Isolated Structure that was Analyzed in the Validation Study

The story height and bay width are typical values of 3.66m and 11m respectively – chosen to minimize the variation in isolator axial force and the likelihood of uplift for this simple example. Similar to single FP bearings, triple FP bearings are capable of safely accommodating localized uplift over short durations. The upper concave plate temporarily lifts off and there is impact when the bearing returns down, however the effects on the structure are localized and this typically does not result in permanent damage to the bearing. Uplift of individual isolator units is accounted for in the SAP2000 response history analysis since gap behavior is specified in the vertical direction for the FP link elements.

The solution algorithm used in the SAP2000 analysis is the Wilson Fast Nonlinear Analysis algorithm, described in Wilson (2001). This algorithm uses the results of dynamic analysis with Ritz vectors and is particularly efficient for analysis of systems with a limited number of discrete nonlinear elements. Prior to the earthquake analysis

cases, a separate nonlinear modal analysis case must be run to apply the gravity load to the isolators. The load is applied using a ramp function with 10 sec rise time. At the end of the gravity loading case, unidirectional excitation along one axis of the building is applied using the 180 component of the 1940 El Centro record (PGA of 0.31g) available from the PEER NGA database. The motion was amplitude scaled by a factor of 2.15, which was specified simply to induce isolator displacements that were large enough to show all possible sliding regimes.

The results from the SAP2000 analysis were compared to the results obtained from an independent solution method. For the same El Centro 180 excitation used in the SAP2000 analysis, the equations of motion for three FP elements connected in series and attached to a viscously damped SDOF superstructure were formulated using a state-space approach and then integrated numerically using the `ode15s` solver in MATLAB. The formulation and program used were the same as described in Section 2-3, simply extended to incorporate an additional FP element. The SDOF superstructure had the same mass, stiffness, and damping properties (W_s=133.33 kN, $T_s = 0.20$ sec and $\zeta_s = 0.25\%$.) as the superstructure in the SAP2000 model. The very small amount of superstructure damping was chosen to minimize differences in the calculated response caused by the two different ways in which the analysis methods incorporate viscous damping.

Figures 3-6 through 3-8 compare the results obtained using the two analysis methods. There is good agreement in both the response of the isolation system and of the superstructure. Peak values of isolation system displacements agree within 2% and the peak values of absolute superstructure acceleration and drift agree within 5%. The histories of each response quantity also correspond closely to each other. The agreement of the results given by the two independent formulations and solution methods gives added confidence in the validity of this proposed approach. Furthermore, this analysis represents extreme response of the isolators – in practice it is unlikely that engineers will design into the final stiffening regime. It should be emphasized however that these results are verified only for a very simple structure isolated with only four bearings. The validity of the results for more sophisticated analysis cases such as those involving uplift or more realistic buildings that are irregular and have dozens of isolators remain untested.

Lastly, bidirectional analysis was carried out using the El Centro 180 and 270 components (scaled again by a factor of 2.15) applied in each principal direction of the model structure. The assembly of rigid elements and gap elements were arranged radially around the FP elements at 45° increments. Therefore, the bearing which is circular in plan is approximated by a regular octagon. This discretization results in a maximum error of 8% in the displacement capacity of a particular surface based on the difference between the radius of the inscribed circle and the distance from the center to the vertex of the polygon. More elements can be arranged at smaller radial increments just as easily using the "replicate radial" command. The coarse refinement is chosen here to better illustrate the modeling scheme and associated errors.
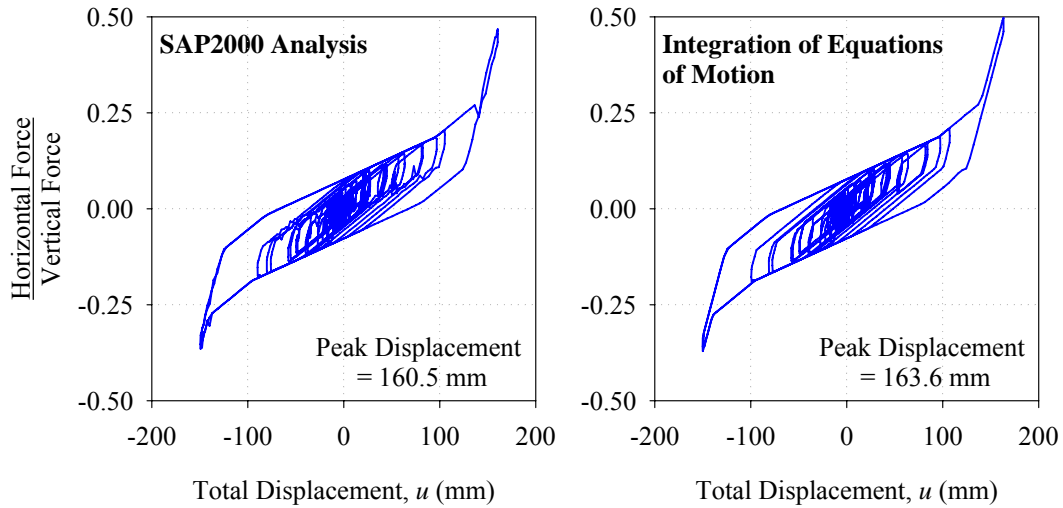
FIGURE 3-6 Comparison of Isolation System Response Predicted by Analysis Using SAP2000 and from Numerical Integration of the Equations of Motion
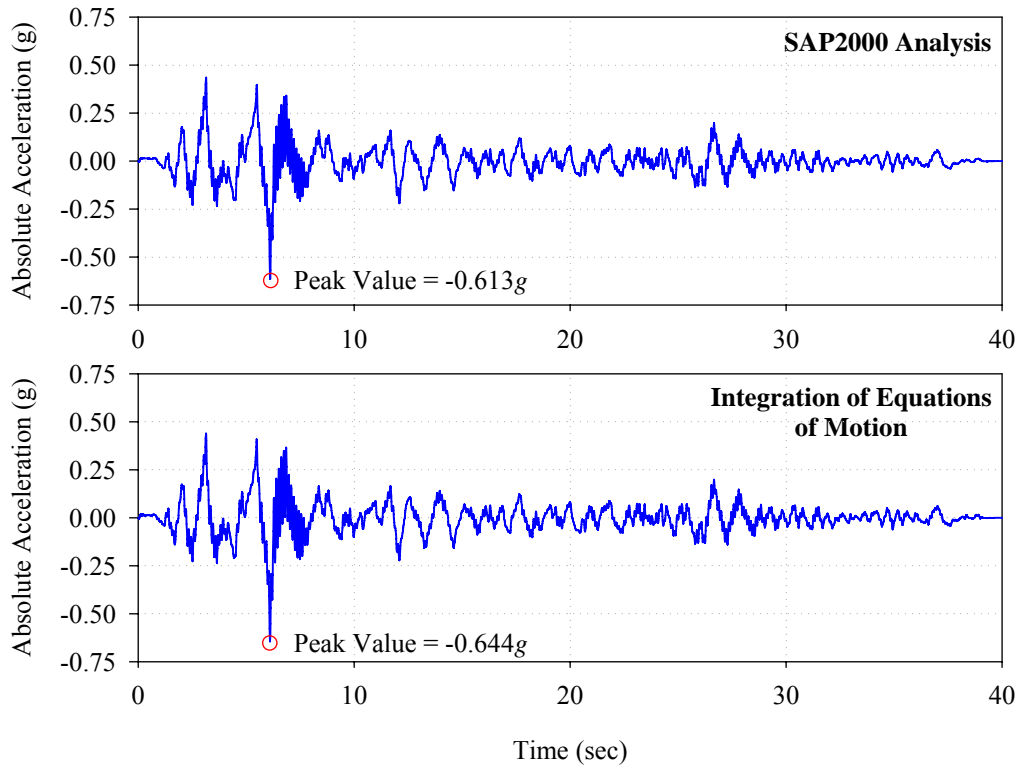
FIGURE 3-7 Comparison of the Histories of Superstructure Absolute Acceleration Response Determined from Analysis using SAP2000 and from Numerical Integration of the Equations of Motion
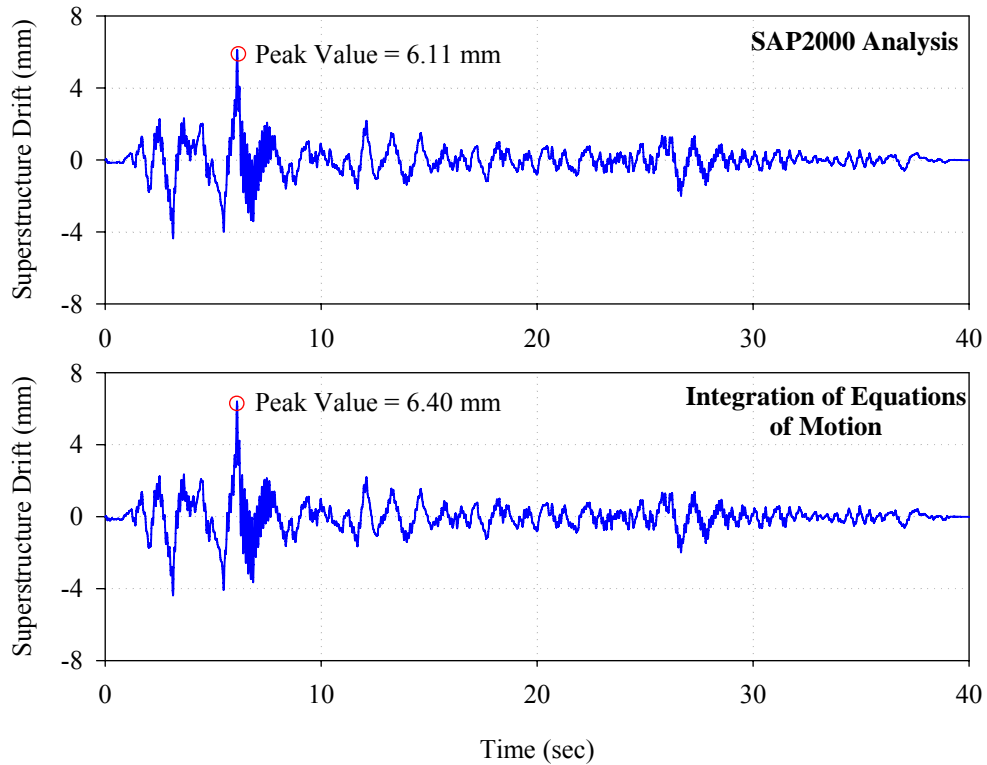
FIGURE 3-8 Comparison of the Histories of Superstructure Drift Determined from Analysis using SAP2000 and from Numerical Integration of the Equations of Motion

The relative displacement trajectories of the slider on surfaces 2 and 3 calculated by modal response history analysis using SAP2000 are provided in figure 3-9. This demonstrates that the radial arrangement of nonlinear elements effectively stops sliding on a surface when the resultant relative displacement on a surface attains the displacement capacity. Given that the FP link elements in SAP2000 have coupled properties in both shear degrees of freedom (Computers and Structures, Inc., 2007), it can be concluded that the proposed arrangement will reasonably approximate the true bidirectional behavior of the triple FP. In Section 10, this is assessed further by comparing the results of multi-component shake table testing to analytical results.
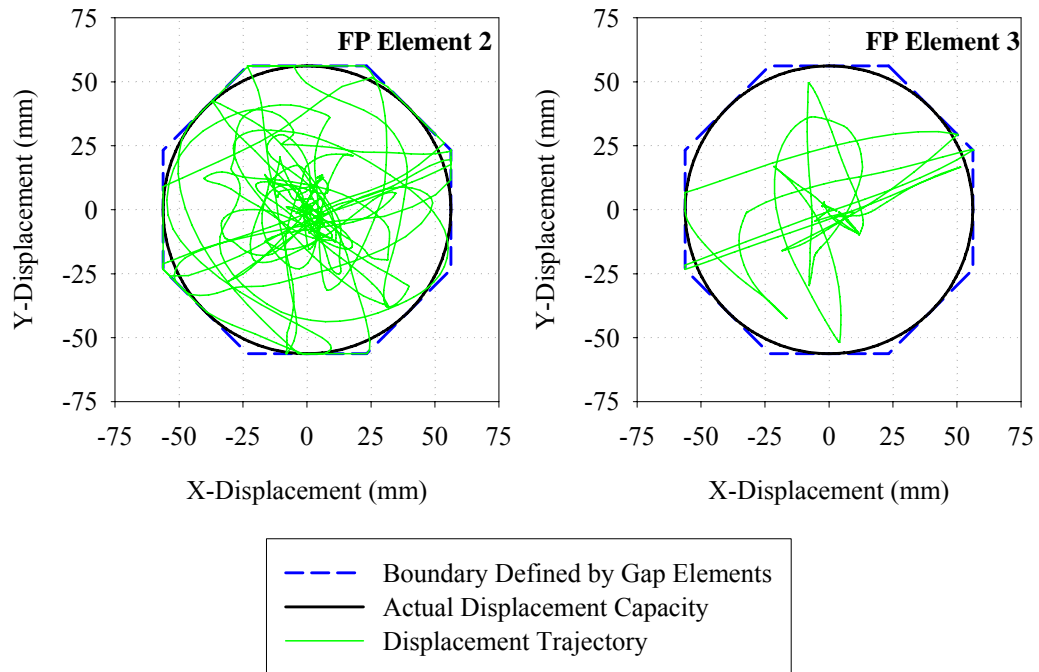
FIGURE 3-9 Displacement Trajectories for FP Elements 2 and 3 Obtained from Response History Analysis of the Model Subjected to the 2.15 El Centro Ground Motion (180 Component in the *x*-Direction and 270 Component in the *y*-Direction

SECTION 4
DESCRIPTION OF SHAKE TABLE TESTING PROGRAM

4.1 Introduction

This section describes an experimental program in which shake table testing of a quarter-scale, six-story seismically isolated steel structure was carried out. Different variations of multi-spherical sliding bearings were tested ranging from double FP bearings with surfaces of equal friction to the most fully adaptive configuration of triple FP bearing. The principal objective was to generate experimental data for bearings exhibiting a wide range of adaptive behaviors when subjected to ground motions of varying magnitudes. This data is subsequently used to validate the existing methods of dynamic analysis and is also archived for validating future software. Therefore, emphasis was placed on collecting highly reliable data from a limited number of exceptional tests (quality over quantity). Provided the analytical models compare favorably to the experimental results in terms of capability to predict (a) isolation system response, (b) primary superstructure response quantities such as story shear and drift and (c) secondary superstructure response quantities of interest for nonstructural components, they can then be used as the basis for analytical studies to investigate how to most efficiently implement these devices in practice.

In addition to validating the basic mechanics of these devices and the dynamic analysis models, investigation of phenomena such as isolator uplift and contact with the displacement restrainer was also of interest. Understanding the behavior under these conditions (and having the ability to predict it analytically) is of importance in practice and can be realistically simulated through shake table testing. Therefore, the experimental setup had to make provisions for examining these localized phenomena as well. If the models can predict extreme types of response such as uplift with suitable accuracy, there is also added confidence in their ability to predict more moderate response.

The shake table testing described herein occurred in two phases. The first stage took place in fall 2004 and examined an isolation system consisting of equal friction double FP bearings. This test program also served to demonstrate the capabilities of the newly constructed NEES equipment site at the Structural Engineering and Earthquake Simulation Laboratory (SEESL) at the University at Buffalo. The second phase occurred in fall 2007 and was a much more extensive study in which several variations of double FP and triple FP bearings were examined. Based on observations from the preliminary tests in 2004, the six-story model was modified slightly prior to the second phase. The details and motivation for these adjustments are discussed in more detail in section 4.2.

4.2 Description of Model Structure

The model shown in figures 4-1 through 4-3 is a six-story structure representing a section in the weak direction of a steel moment resisting frame. It has been extensively used in

FIGURE 4-1 Photograph of Six-Story Isolated Model in the Structural Engineering and Earthquake Simulation Laboratory at UB (Braced Frame Configuration)

FIGURE 4-2 Photograph of Six-Story Isolated Model in the Structural Engineering and Earthquake Simulation Laboratory at UB (Moment Frame Configuration)
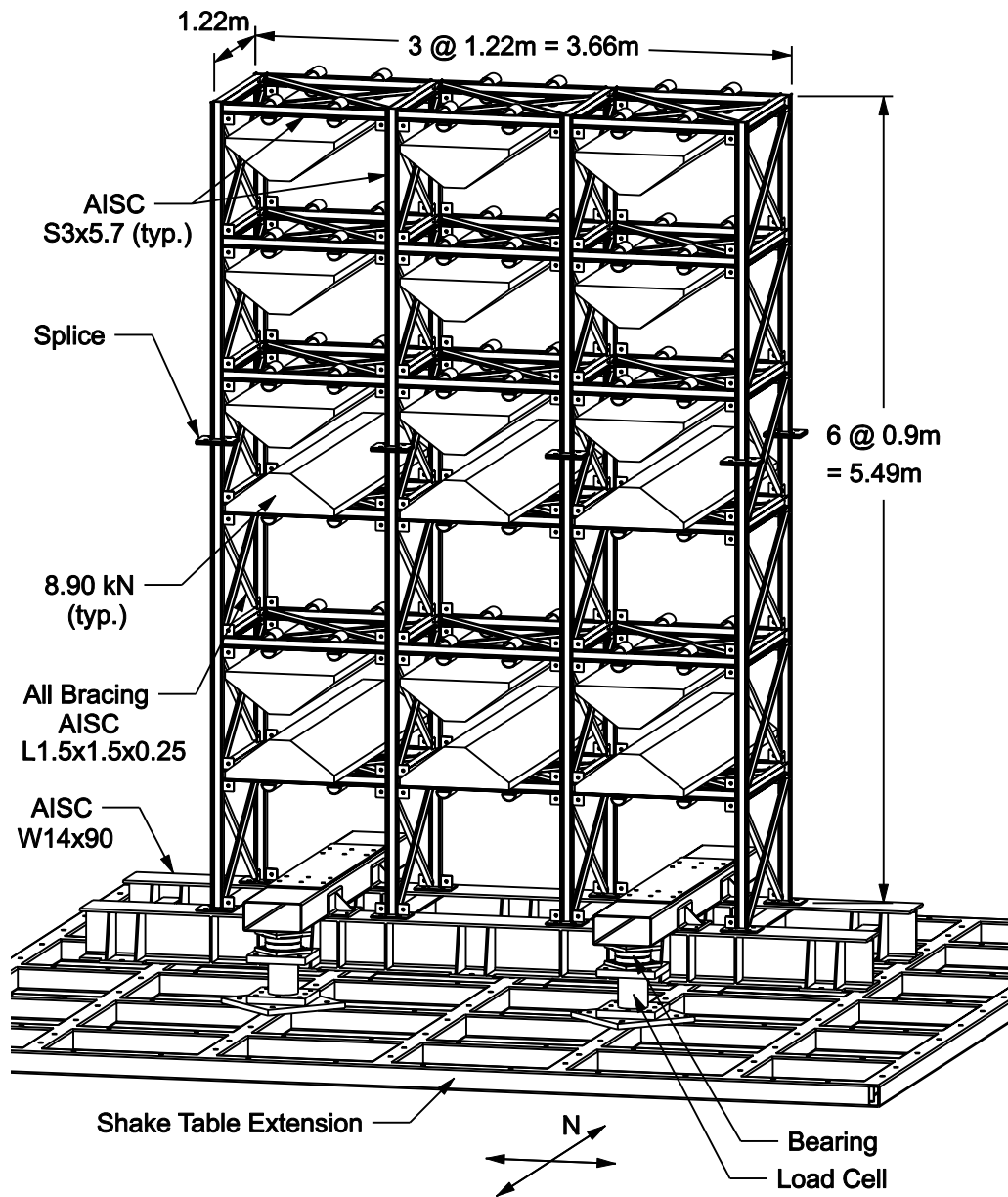
FIGURE 4-3   Six-Story Isolated Model (Moment Frame Configuration with Stiffened Basemat)

testing of seismic isolation and seismic energy dissipation systems at the University of Buffalo. Previous studies using the same superstructure model include Reinhorn *et al.* (1989), Mokha *et al.* (1990), Constantinou *et al.* (1991) and Wolff and Constantinou (2004). The model used in this study is the same except for a basemat modified with a larger footprint in order to reduce the risk of overturning during bidirectional excitation.

All beams and columns are S3×5.7 (SI designation S75×8.5) and all bracing is L1½×1½×¼ (SI designation L38×38×6.4). The beam-column connections are all fully

welded. Each column is spliced at the mid-height of the fourth story so the model can be disassembled and transported by truck. There is permanent diaphragm bracing as well as permanent bracing in the transverse (north-south) direction. Additionally, there are removable braces in the longitudinal (east-west) direction. In this way the superstructure can be tested with longitudinal bracing giving a stiffer braced frame configuration and without the longitudinal bracing giving a more flexible moment frame configuration.

The model structure is three bays wide (bay width = 1.22m) and one bay deep (bay depth = 1.22m). Each story is 0.9m tall giving a scale factor for length of $\lambda_L = 4$. The acceleration scale was chosen to have a value of unity, $\lambda_a = 1$. Since the same material is used for the prototype and model, the scale factor for elastic modulus also has a value of unity, $\lambda_E = 1$. Following the principles of similitude and dimensional analysis described in Bracci *et al.* (1992), all other scale factors are dependent on these three. These are listed in table 4-1.

TABLE 4-1   Comparison of Required and Provided Scale Factors for Six-Story Model Used in Study

Quantity	Scaling Law	Same Material and Acceleration Model		
		Required	Provided (No Added Mass)	Provided (With Added Mass)[1]
Length[2]	λ_L	4	4	4
Elastic Modulus[2]	λ_E	1	1	1
Acceleration[2]	λ_a	1	1	1
Density	$\lambda_\rho = \lambda_E/(\lambda_L\lambda_a)$	0.25	1	0.28
Mass	$\lambda_m = \lambda_\rho\lambda_L^3$	16	64	17.8
Frequency	$\lambda_f = \sqrt{\lambda_E/\lambda_\rho}/\lambda_L$	0.5	0.25	0.47
Gravity Force	$\lambda_{Fg} = \lambda_\rho\lambda_L^3$	16	64	17.8
Time (Period)	$\lambda_T = \sqrt{\lambda_L/\lambda_a}$	2	2	2
Force	$\lambda_F = \lambda_E\lambda_L^2$	16	16	16
Velocity	$\lambda_v = \sqrt{\lambda_L\lambda_a}$	2	2	2

1. Actual scale factors for tested model with 160 kN added mass
2. Independent, predefined scale factors

Based on the three independent predefined scale factors, the required scaling factor for material density is $\lambda_\rho^{req} = 1/\lambda_L = 1/4$. However, the model structure is the same material as the prototype, meaning that the provided material density is the same as the prototype or $\lambda_\rho^{prov} = 1$. Since the required and provided material densities are different, additional mass must be added to the model so that the dependent quantities (mass, gravitational force and frequency) are scaled properly. The floor loads necessary to satisfy similitude requirements were achieved by attaching 26.7kN of concrete blocks to each story so that

45

the total added weight was 160kN. The total weight of the structure from load cell measurements during the experiments was approximately 225kN, meaning that the added weight corresponded to 2.5 times the weight of the bare frame. Based on the similitude requirements, theoretically the added mass should be 3 times the weight of the bare frame. Despite this small discrepancy, the actual scale factors for this amount of provided mass (shown in the last column of table 4-1) compare well with those required to exactly satisfy the similitude laws.

More importantly for this study however, the additional mass was necessary to achieve realistic pressures on the bearings. To do this without the added mass, the sliders would have had to be made so small that there would be the risk of instability at the expected displacements. In other words, the additional mass was more important for ensuring realistic and proper performance of the isolation system rather than for meeting the dynamic similitude requirements for the superstructure. It is emphasized that the goal of the study was not to extrapolate to the behavior of a fictional prototype, but instead to show that the analytical models are capable of predicting behavior for a given structure and set of isolator properties.

Dynamic properties of the superstructure in each principal direction were determined experimentally using white noise structural identification. The base was fixed by bolting locking side plates to the bearings and the structure was subjected to white noise excitation with 0-40Hz frequency content and a peak acceleration of 0.20g. The transfer functions shown in figures 4-4 through 4-7 were obtained as the ratio of the Fourier transform of the horizontal acceleration of each floor to the Fourier transform of the basemat's horizontal acceleration. In each case, the acceleration is the average of the acceleration readings recorded on opposing sides of the model. Transfer functions were calculated with respect to the basemat acceleration rather than the ground acceleration to remove any influence of the foundation's flexibility (the two results were generally the same, however). When the transfer functions are calculated in this way, the local maxima correspond to the modal frequencies. By measuring the amplitude at each lateral degree of freedom, the mode shapes are determined from the ratios of the peak values for the frequency corresponding to one mode of vibration. Phase angles were also determined to obtain the sign of the mode shape. Damping ratios in each mode were determined using the half-power bandwidth method around the transfer function peaks (Bracci *et al.*, 1992).

The dynamic properties from the structural identification tests in the longitudinal and transverse directions are listed in tables 4-2 through 4-5. Results are shown for the braced frame and moment frame configurations and are in good agreement with those previously reported by Wolff and Constantinou (2004). In the directions where the structure is braced, only the first three modes could reliably be identified due to slippage of the braces at high frequencies. In these cases, the peaks of higher modes are closely spaced and not as well defined. A similar phenomenon is apparent in testing of concrete structures where micro-cracking obscures the transfer function peaks of higher modes (Bracci *et al.*, 1992).

46
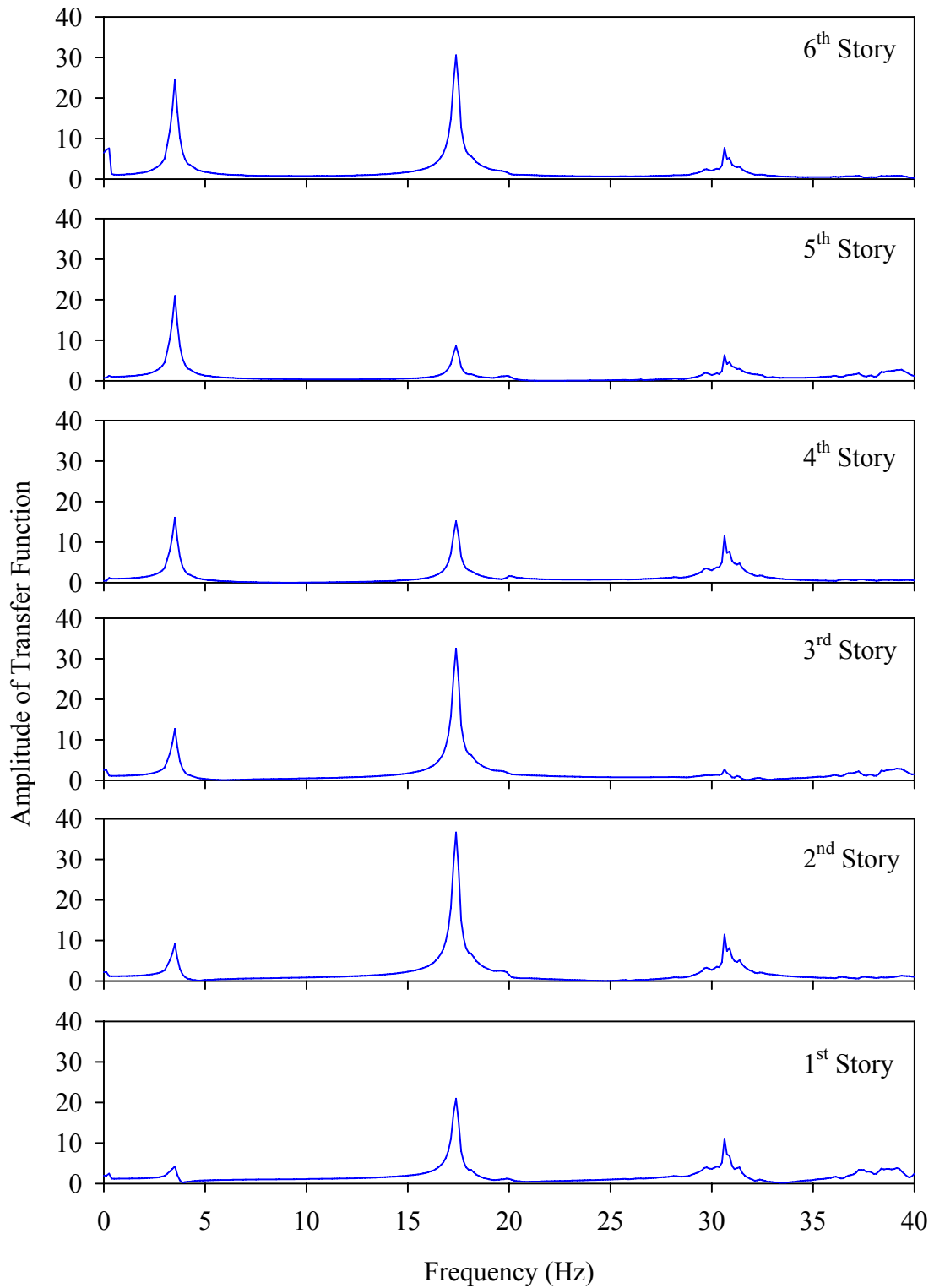
FIGURE 4-4 Transfer Function Amplitudes Obtained from Longitudinal White Noise Excitation of Braced Frame
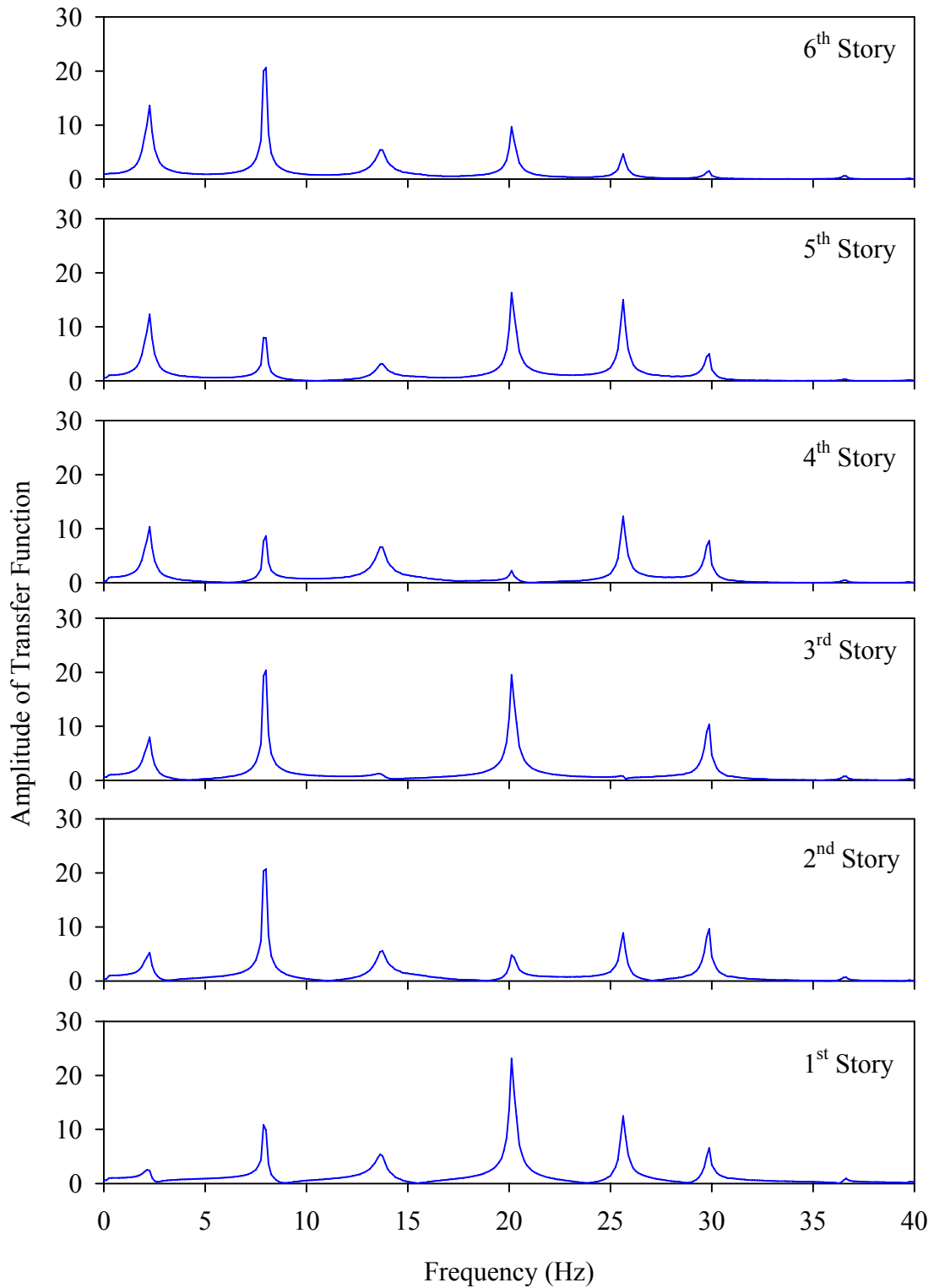
FIGURE 4-5 Transfer Function Amplitudes Obtained from Longitudinal White Noise Excitation of Moment Frame
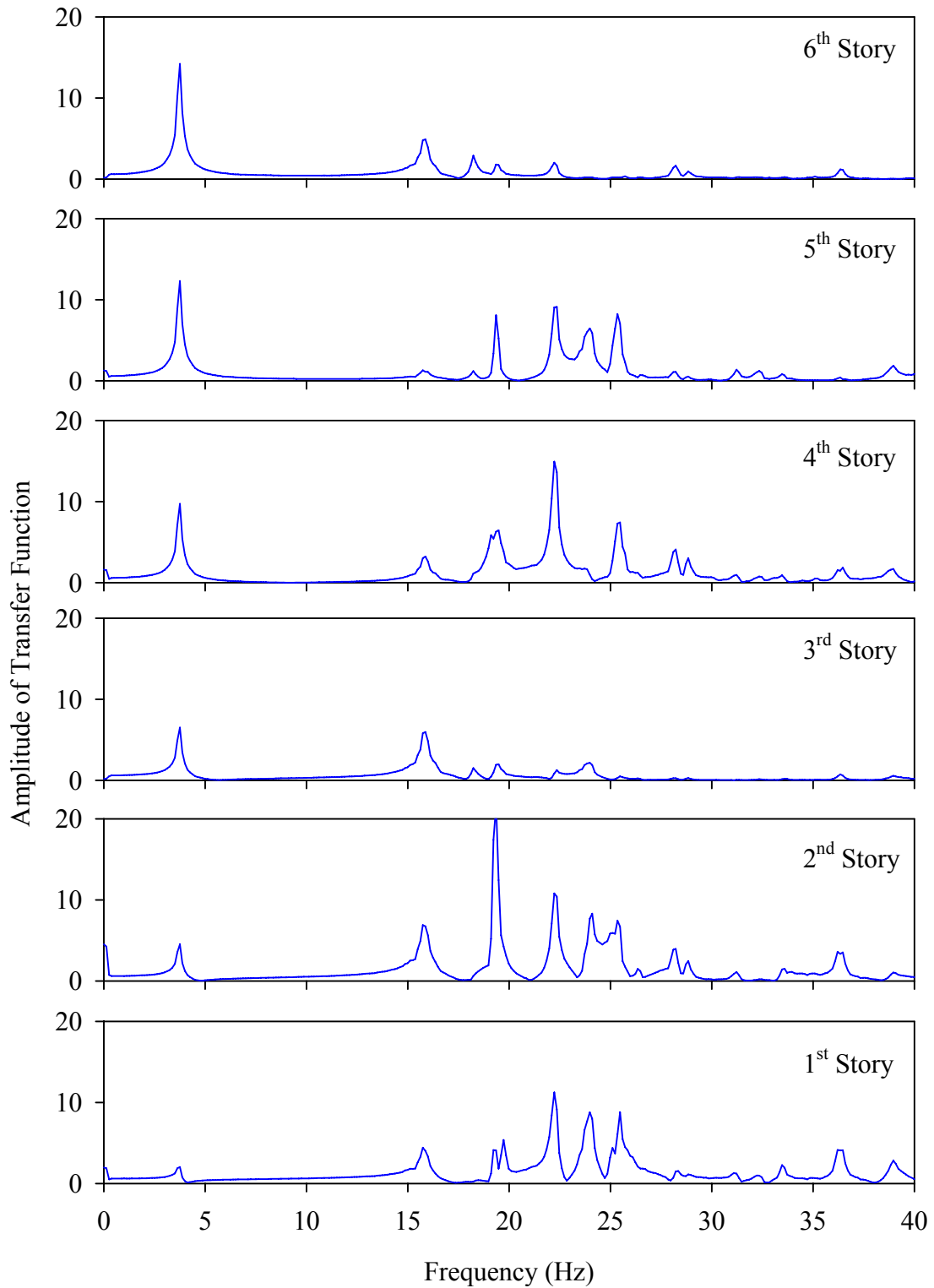
FIGURE 4-6   Transfer Function Amplitudes Obtained from Transverse White Noise Excitation of Braced Frame
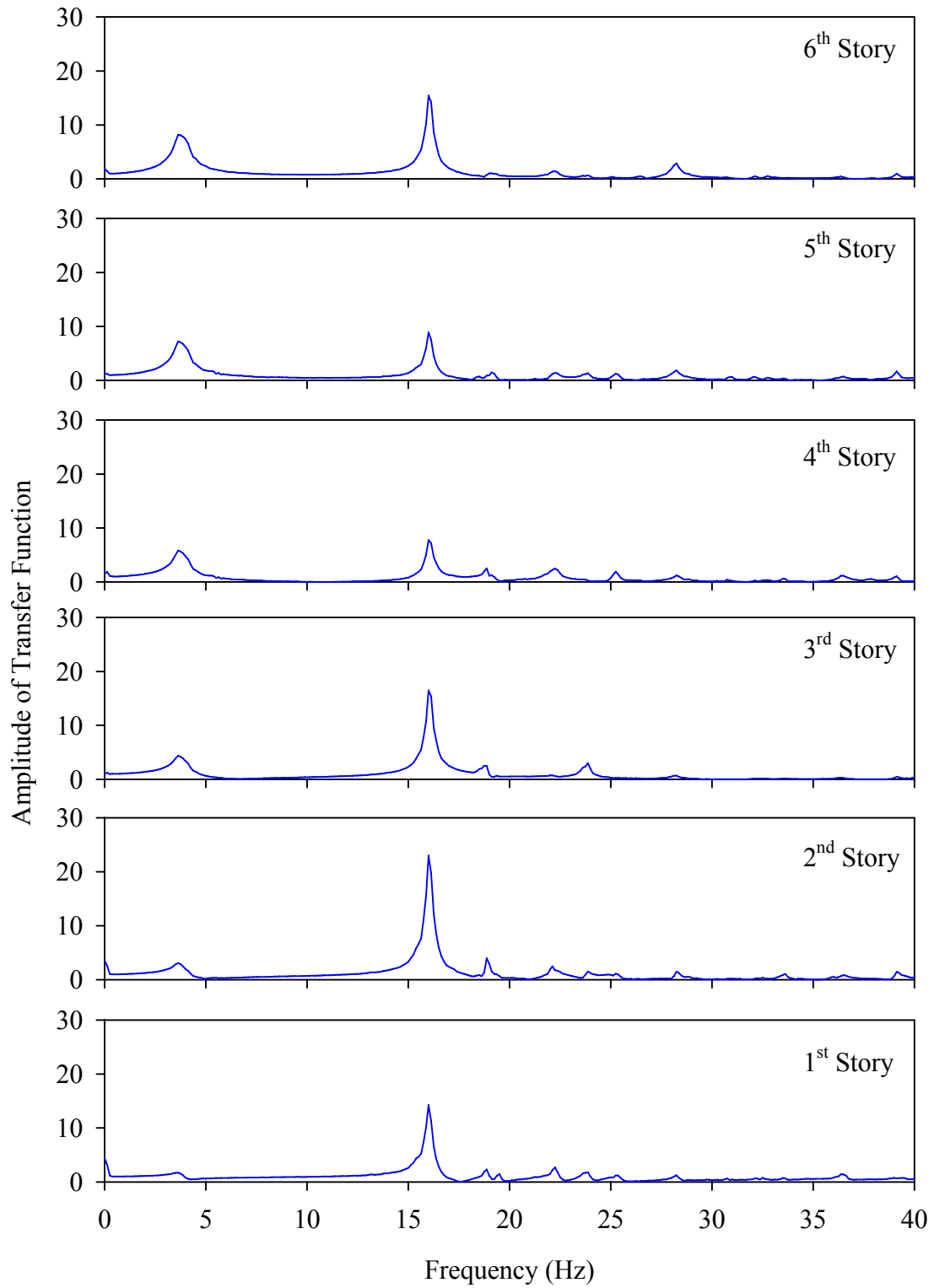
FIGURE 4-7   Transfer Function Amplitudes Obtained from Transverse White Noise Excitation of Moment Frame

TABLE 4-2 Frequencies and Mode Shapes of Braced Frame in Longitudinal Direction

		Mode		
		1	**2**	**3**
Frequency (Hz)		**3.50**	**17.38**	**30.63**
Damping Ratio		**0.033**	**0.017**	**0.003**
Story	6th	1.000	0.834	0.669
	5th	0.850	0.235	-0.551
	4th	0.652	-0.414	-1.000
	3rd	0.513	-0.888	-0.236
	2nd	0.371	-1.000	0.996
	1st	0.173	-0.572	0.958

TABLE 4-3 Frequencies and Mode Shapes of Moment Frame in Longitudinal Direction

		Mode					
		1	**2**	**3**	**4**	**5**	**6**
Frequency (Hz)		**2.25**	**8.00**	**13.63**	**20.13**	**25.63**	**29.88**
Damping Ratio		**0.056**	**0.015**	**0.019**	**0.006**	**0.004**	**0.004**
Story	6th	1.000	0.998	0.819	0.419	0.311	0.145
	5th	0.904	0.383	-0.464	-0.705	-1.000	-0.480
	4th	0.760	-0.418	-1.000	-0.097	0.821	0.748
	3rd	0.585	-0.986	-0.185	0.845	0.051	-1.000
	2nd	0.384	-1.000	0.816	-0.207	-0.593	0.930
	1st	0.177	-0.479	0.817	-1.000	0.834	-0.631

TABLE 4-4 Frequencies and Mode Shapes of Braced Frame in Transverse Direction

		Mode		
		1	**2**	**3**
Frequency (Hz)		**3.75**	**15.86**	**19.36**
Damping Ratio		**0.029**	**0.012**	**0.006**
Story	6th	1.000	0.728	0.084
	5th	0.867	0.166	-0.377
	4th	0.686	-0.481	-0.292
	3rd	0.457	-0.881	-0.089
	2nd	0.318	-1.000	1.000
	1st	0.144	-0.597	0.190

TABLE 4-5   Frequencies and Mode Shapes of Moment Frame in Transverse Direction

		Mode		
		1	**2**	**3**
Frequency (Hz)		**3.63**	**16.00**	**18.88**
Damping Ratio		**0.110**	**0.010**	**0.005**
Story	6th	1.000	0.671	0.184
	5th	0.879	0.387	-0.222
	4th	0.710	-0.338	-0.638
	3rd	0.532	-0.717	-0.615
	2nd	0.377	-1.000	1.000
	1st	0.210	-0.620	0.587

The superstructure is bolted to a basemat consisting of a grid of two W14×90 sections (SI designation W360×164) and two HSS16×8×$^5/_{16}$ sections (SI designation HSS406.4×203.2×7.9). It is shown in figure 4-8 and has a weight of approximately 22.7kN. For this study, the basemat was modified from its original configuration to accommodate bidirectional excitation by adding the tubes, which gave the bearings a more stable 2.44m square footprint. For previous tests in which there was only longitudinal excitation, the four bearings were in a 2.44m×1.22m pattern (longitudinal by transverse), which would easily induce isolator uplift for excitation in the transverse direction.
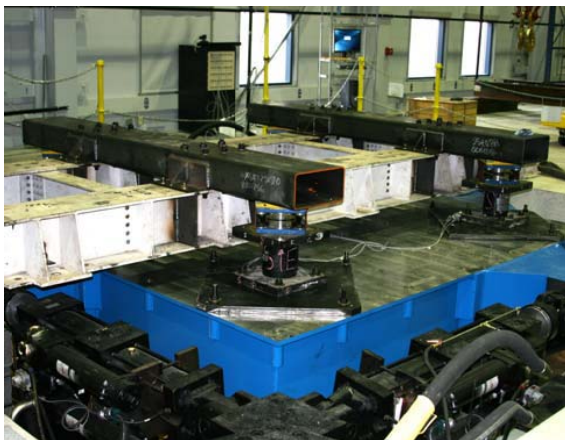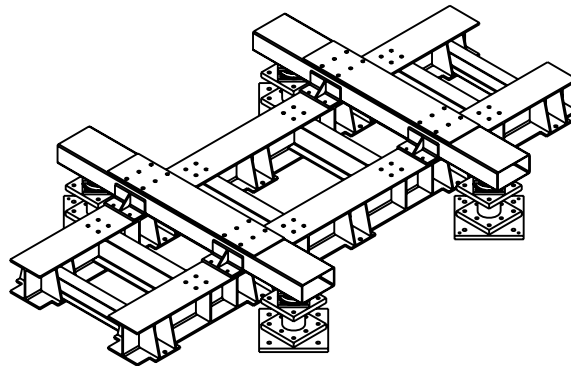
(a)   (b)

FIGURE 4-8 HSS Sections Installed to Give Bearings a 2.44m×2.44m Footprint

4.2.1 Modifications to Model After 2004 Tests

In the preliminary tests of 2004 the model was tested in the braced frame configuration. This was favored for safety and redundancy since the beam to column connections are fully welded. The stiffer superstructure also induced greater isolation system response.

However, this configuration proved somewhat inconsistent and problematic. Over the course of previous studies, the bolt holes in the brace gussets had become elongated slightly, which led to slippage of the braces during testing. This is not an issue in terms of structural strength and does not affect the performance of the isolation system, but it does lead to increased error in the analytical predictions of superstructure response. The braces are engaged during the phases of sticking and bearing, but become disengaged during the sliding phase. This is virtually impossible to model analytically due to the fact that each brace slips independently at a force that is determined by the tightness of the bolt and the roughness of the bearing surfaces. Furthermore, the amount of slippage is determined by how much the bolt hole has opened up over time, which is likely different for each connection. Consequently, to achieve more accurate predictions of superstructure response the longitudinal bracing was removed and the more flexible moment frame configuration was used for the 2007 testing.

An additional problem noticed during the 2004 testing was that the basemat tubes were vertically flexible. This resulted in noticeable rocking response of the superstructure, which was amplified due to interaction with the vertical actuators of the shake table. To reduce this problem for the 2007 tests, the tubes were stiffened by stitch-welding ½ in (12.7mm) thick cover plates over each flange. Other options considered included filling the tubes with high modulus concrete, but based on simple calculations of the moment of inertia, flange stiffening with cover plates proved the most effective and expedient solution.

A comparison of the transfer functions of the basemat vertical acceleration response with respect to the shake table platform's vertical acceleration is presented in figure 4-9. The vertical acceleration of the basemat was taken as the average vertical acceleration of the four accelerometers mounted at each corner of the W14×90 grid and the input vertical acceleration was calculated as the average of the four accelerometers at each corner of the shake table platform. Using the same modal identification techniques as described previously, the fundamental vertical mode changes from f=12.99Hz to f=15.25Hz due to the addition of the cover plates. In both cases the equivalent viscous damping ratio for this vertical mode is $\zeta=0.007$. The stiffening effect was somewhat less than expected since perimeter stitch welding likely did not engage the cover plates across their full cross section.

4.3 Design and Installation of the Isolation System

As previously mentioned, the intent of the shake table testing was primarily to generate data of high quality to demonstrate that response can accurately be predicted analytically for a known set of isolator and superstructure properties. Different variations of bearing had to be tested in order to verify the analytical models for the various types of hysteretic behavior that could be exhibited. The design objective differed from what is commonly done in practice. Due to the somewhat unique circumstances experienced during shake table testing, the effort during the design phase was directed towards ensuring that the reduced-scale bearings exhibited reliable and consistent sliding behavior. Furthermore,

substantial emphasis was placed on proper installation of the isolation system to provide conditions representative of those in practice, considering the different construction/assembly methods and reduced-scale encountered in laboratory testing. These are issues of considerable importance in experimental testing of seismically isolated structures that are either overlooked or at the very least not reported with the necessary level of rigor by other researchers. It is these details that determine the accuracy and validity of the entire experiment.
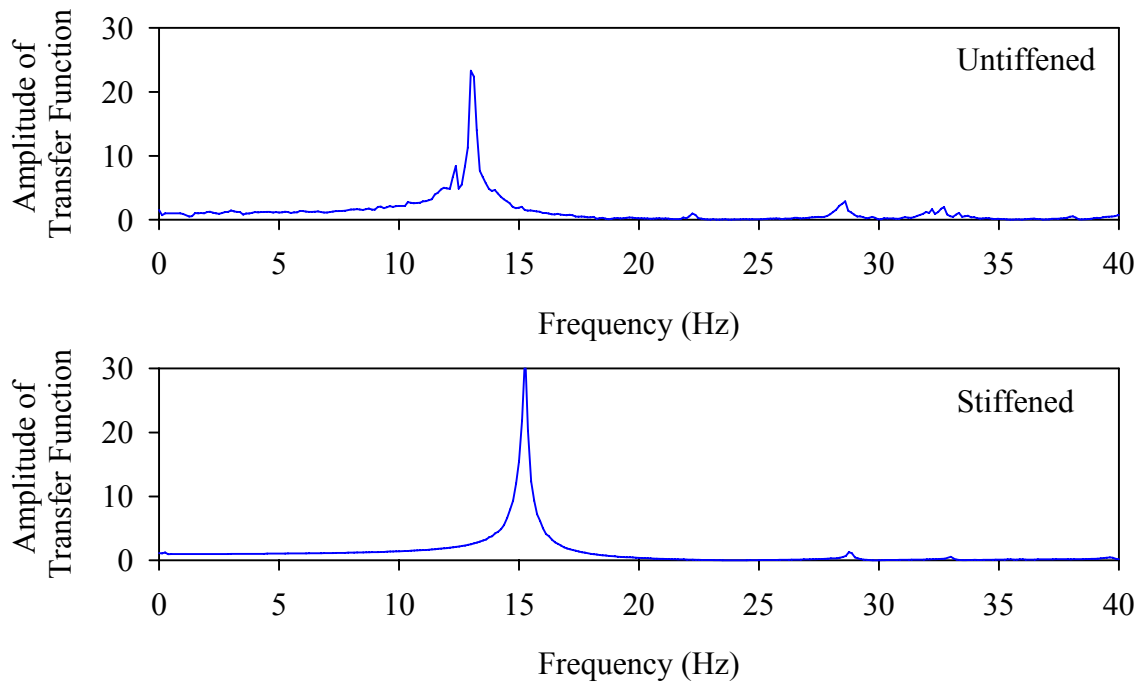
FIGURE 4-9 Transfer Function Amplitudes Obtained from Vertical White Noise Excitation of Model with Before and After Stiffening the HSS Sections

4.3.1 Description of Reduced-Scale Bearing Specimens

The bearing specimens had the same dimensions of the double and triple FP specimens previously used for characterization testing. Drawings of the double and triple FP specimens are provided in figure 4-10. The bearings have a period based on the post-elastic stiffness (pendulum period) of approximately 2 sec when simultaneous sliding is occurring on the outermost concave plates and offer a total displacement capacity of approximately 150 mm. These correspond to 4 sec and 600 mm in the prototype scale, which are in the range of values typical for these devices in practice (see table 4-1 of Constantinou *et al.*, 2007 for a list of standard sizes of FP bearings). Furthermore the sliders are sized appropriately so that (a) pressures can be achieved that result in proper performance of the sliding materials, (b) displacement capacities of individual surfaces of the triple FP bearing are suitable for demonstrating adaptive behavior and (c) the bearings remain stable at large displacements.

(a)

(b)
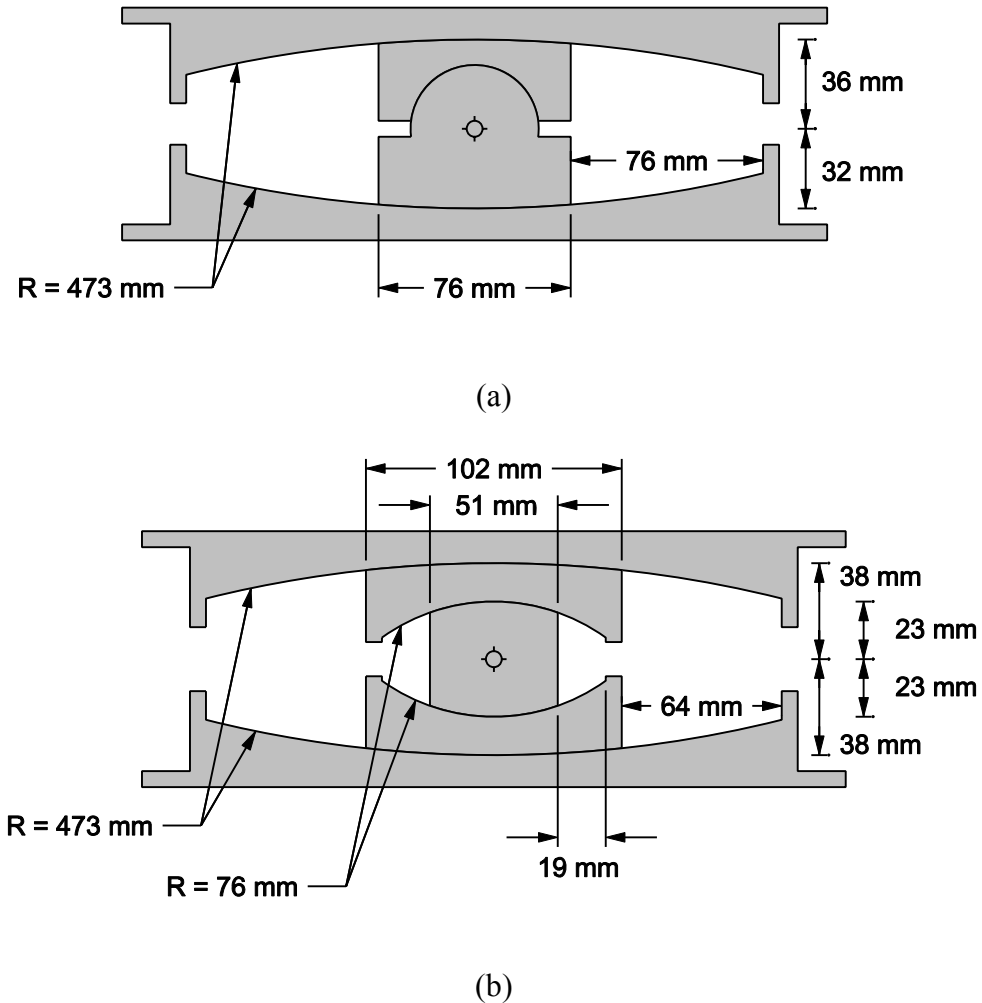
FIGURE 4-10 Dimensions of the (a) Double and (b) Triple FP Specimens Tested

By minimizing the number of different size concave plates and sliders, there was the highest degree of interoperability and versatility in the test arrangement. This way, different configurations of double FP and triple FP bearings could be tested using the same outer concave plates simply by swapping out various parts of the internal sliders. Different types and degrees of adaptive behavior were achieved simply by varying the liner materials that coat the different sliders. A full range of adaptive behaviors were tested ranging from none (double FP bearing with concave surfaces of equal friction) to fully adaptive (triple FP bearing with outermost concave surfaces of different friction). Although the double FP bearing with concave surfaces of equal friction gives hysteretic behavior essentially the same as the traditional single FP bearing, these tests were useful both as a means of comparison to the adaptive systems and for investigation into the effects of uplift. A qualitative description of the different configurations tested is provided in table 4-6. These configurations permitted validation of the dynamic analysis models over the full range of adaptive behaviors.

TABLE 4-6 Qualitative Description of the Various Configurations Tested

Configuration	Description	Behavior
Double 1	Same low friction material on top and bottom interfaces	Single FP bearing with low friction (rigid-linear)
Double 2	Same intermediate friction material on top and bottom interfaces	Single FP bearing with intermediate friction(rigid-linear)
Triple 1	Same low friction material on inner sliding interfaces, same intermediate friction material on the outer sliding interfaces	Double FP bearing with one surface of low friction and one surface of intermediate friction (rigid-bilinear)
Triple 2	Same low friction material on inner sliding interfaces, same high friction material on the outer sliding interfaces	Double FP bearing with one surface of low friction and one surface of high friction (rigid-bilinear)
Triple 3	Same low friction material on inner sliding interfaces, intermediate friction material on the bottom surface, high friction material on the top surface	Triple FP bearing with fully adaptive stiffness and damping

4.3.2 Friction Identification and Selection of Sliding Materials

In table 4-6, the friction at the sliding interfaces were described simply in qualitative terms "low", "intermediate" and "high". In relative terms, "low" friction is on the order of 0.02 to 0.03, "intermediate" friction is on the order of 0.05 to 0.10 and "high" friction is on the order of 0.15 to 0.20. More important than the specific friction values is that the materials provide consistent and reliable values of friction for the duration of the tests – several DBE and MCE level events, much more travel than the bearings would experience in practice. This is not a trivial task, especially for high friction materials. By nature friction dissipates the kinetic energy of the system as heat energy. Logically, high friction materials will generate substantial amounts of heat, which in turn can lead to changes in friction and excessive wear. The high friction interfaces of the triple FP bearing require friction that is much larger than what has been used by manufacturers of sliding bearings in the past. Accordingly, it was necessary to determine a material that exhibits the desired friction coefficient combined with appropriate wear characteristics and thermal properties to give smooth sliding and reliable properties over time.

Additional issues with the consistency of sliding behavior arise due to the relatively small vertical loads on the bearings. The model's weight of approximately 225kN is carried uniformly by four bearings, meaning that each bearing carries only approximately 56kN

of vertical load. For the triple FP specimens, this results in bearing pressure at the interface between the slide plates and the outer concave plates on the order of only 7MPa, which is below the typical minimum value used in practice of 14MPa (Constantinou *et al.*, 2007). High friction materials at low bearing pressures are more likely to experience stick-slip sliding which is undesirable and different from the sliding behavior exhibited by bearings in actual implementation.

Rather than increasing the mass of the model (which is limited by the capabilities of the shake table), this issue was resolved by reducing the contact area. The radius of curvature of the slide plate's interface was manufactured slightly larger than that of the mating concave plate, resulting in bearing only over approximately a 6mm annular area around the perimeter of the slide plate that resulted in increased bearing pressure. Although there is smooth sliding, wear occurs non-uniformly when the interface is manufactured in this way, which compromises the consistency of behavior over time (Zayas, 2007). This method of manufacture was employed to avoid unrealistic stick-slip behavior in the short term, with the understanding that it is not exactly representative of actual construction.

Recognizing these difficulties, component tests under representative conditions were performed on several sliding materials prior to shake table testing. The objective of these tests was to identify three suitable materials that gave "low", "intermediate" and "high" friction respectively. The test apparatus used was the small bearing testing machine in the SEESL shown in figures 4-11 and 4-12. The reader is referred to Kasalanati and Constantinou (1999) for a complete description of the test apparatus and instrumentation. The specimen used for the tests was a prototype triple FP bearing having the dimensions shown in figure 4-10 and both lower and upper slide plates coated with the same liner material. The behavior of each material was characterized using a series of displacement controlled tests with sinusoidal displacement history. The vertical load for all tests is 56kN, corresponding to the vertical load imposed on each bearing by the structure model.
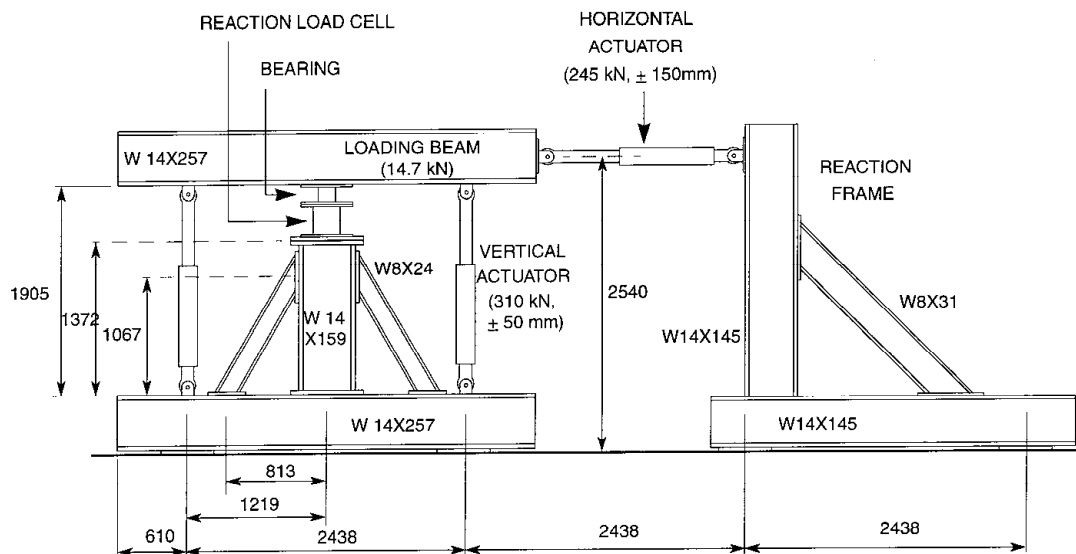
FIGURE 4-11 Dimensioned Drawing of Test Apparatus – Stability Bracing not Shown (Reproduced from Kasalanati and Constantinou, 1999)
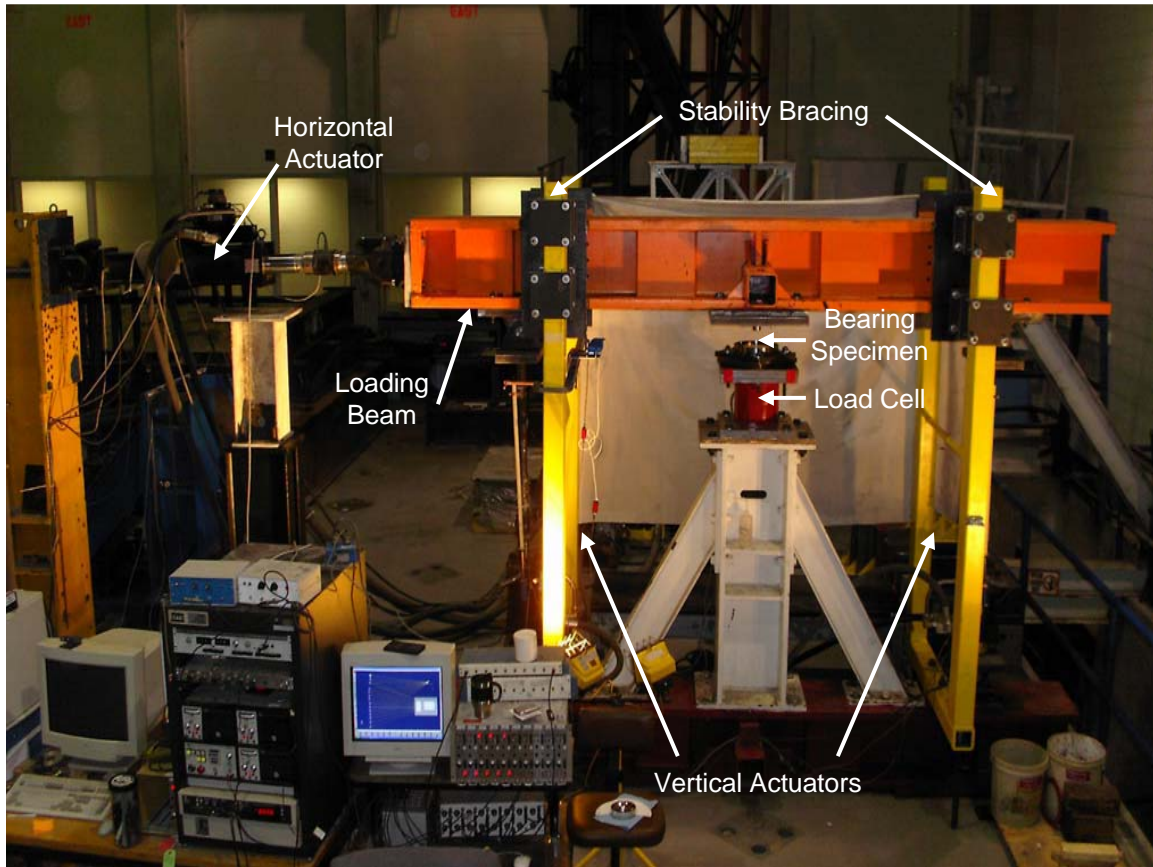
FIGURE 4-12 Apparatus Used for Experimental Testing

Based on this testing, liners denoted Material 1 and Material 8 were chosen for the intermediate and high friction surfaces, respectively. Both of these materials gave uniform and consistent friction under the conditions representative of shake table testing. The hysteresis loops obtained from low speed and high speed tests of the prototype bearing with Material 1 sliders are shown in figures 4-13 and 4-14, those from the prototype having Material 8 sliders are shown in figures 4-15 and 4-16. These represent configurations Triple 1 and Triple 2 respectively. The variation in the coefficient of friction of Material 1 with sliding velocity is shown in figure 4-17. Since it is of high friction, this test was not performed for Material 8 to prevent unnecessary wear prior to the shake table testing. Lastly, the Triple 3 configuration (Material 1 on the bottom slide plate and Material 8 on the top slide plate) was tested at various displacement amplitudes at the approximate dynamic period of the bearing (0.50Hz frequency). The force-displacement loops from these tests are presented in figure 4-18.
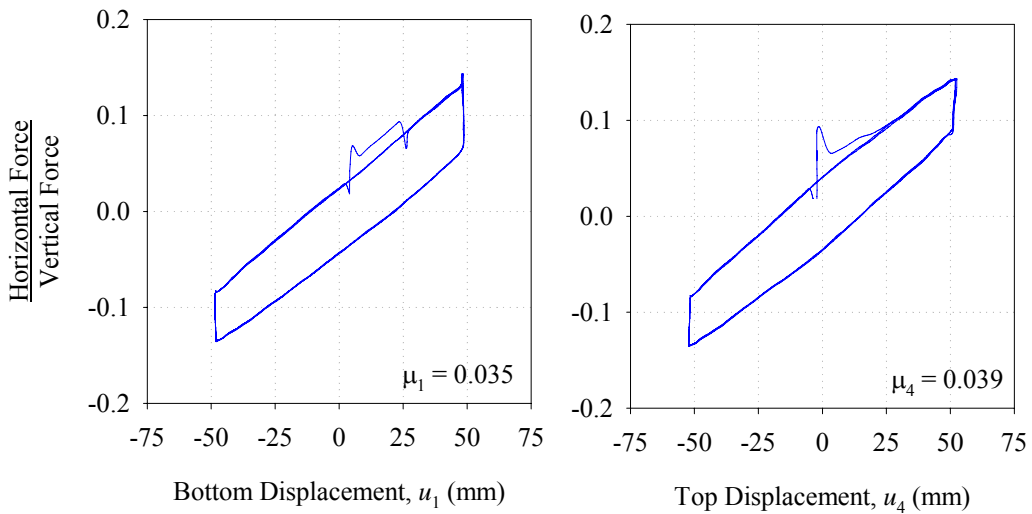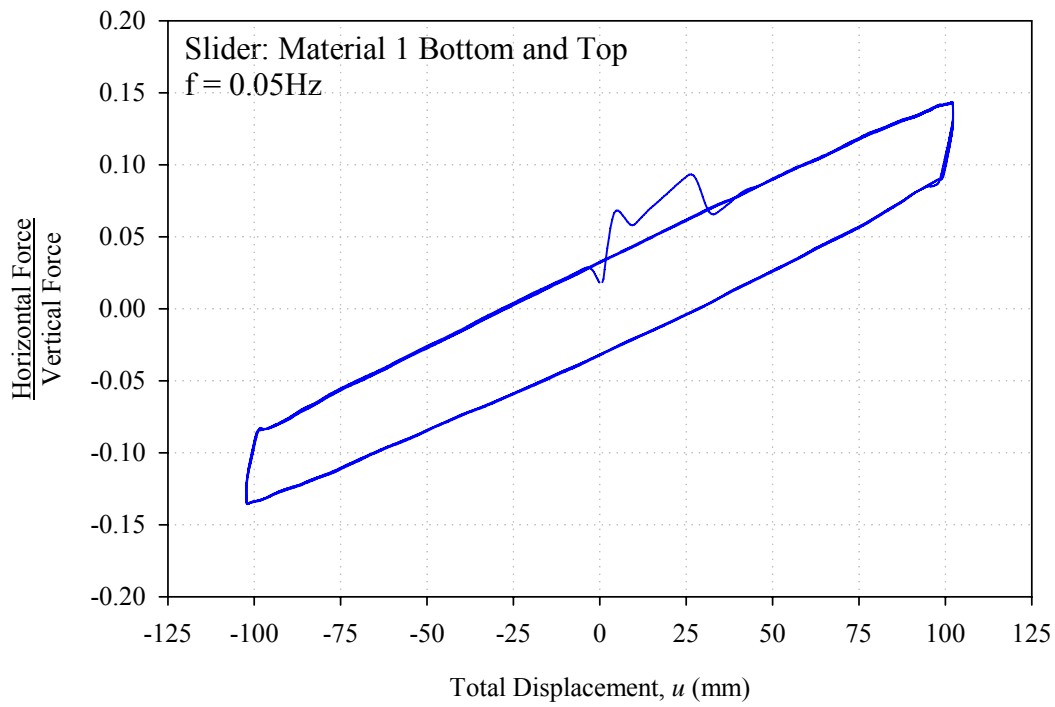
FIGURE 4-13 Total and Decomposed Force-Displacement Loops for f=0.10Hz Test of Prototype Triple 1 Configuration (Lower and Upper Sliders Coated with Material 1)
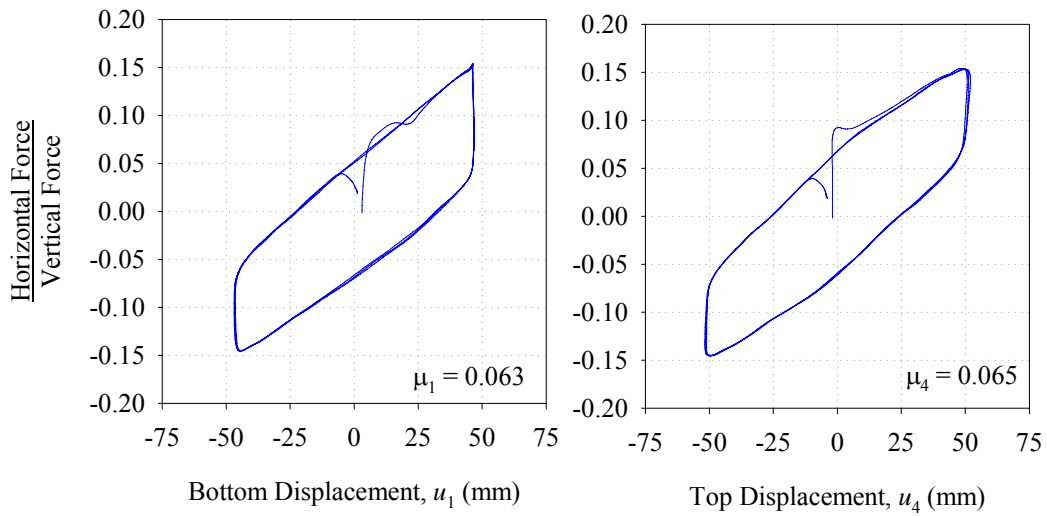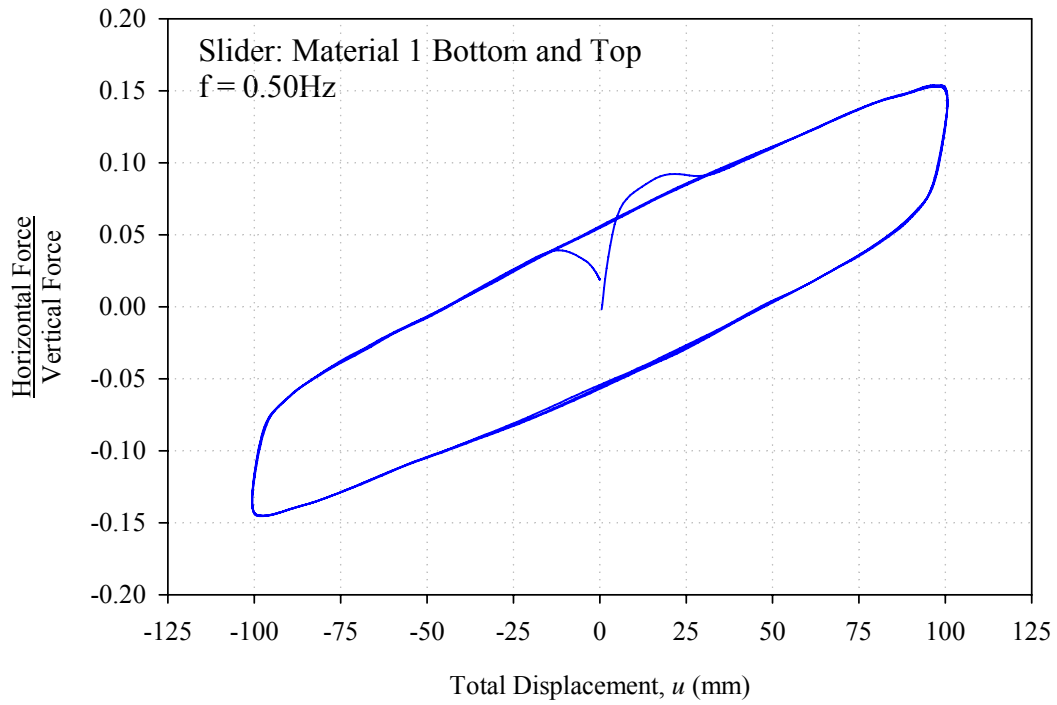
FIGURE 4-14 Total and Decomposed Force-Displacement Loops for f=0.50Hz Test of Prototype Triple 1 Configuration (Lower and Upper Sliders Coated with Material 1)
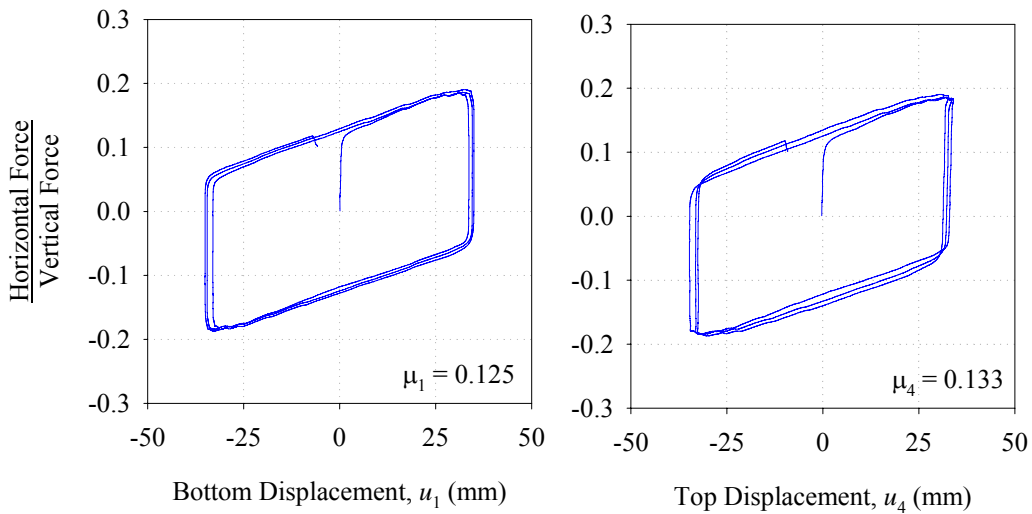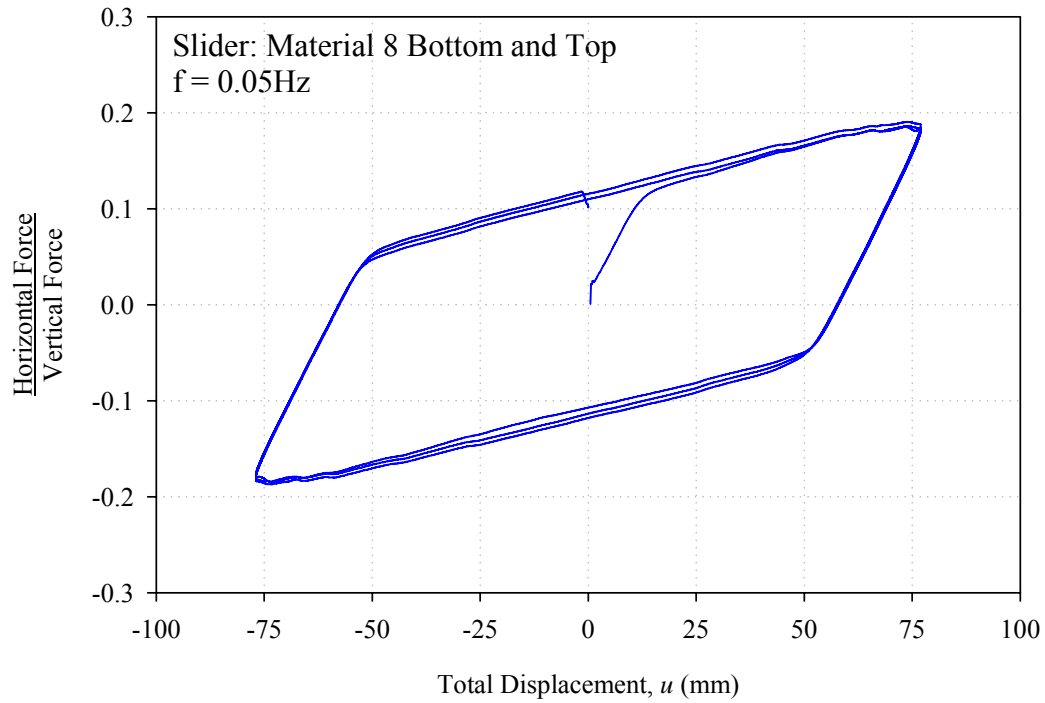
FIGURE 4-15 Total and Decomposed Force-Displacement Loops for f=0.05Hz Test of Prototype Triple 2 Configuration (Lower and Upper Sliders Coated with Material 8)
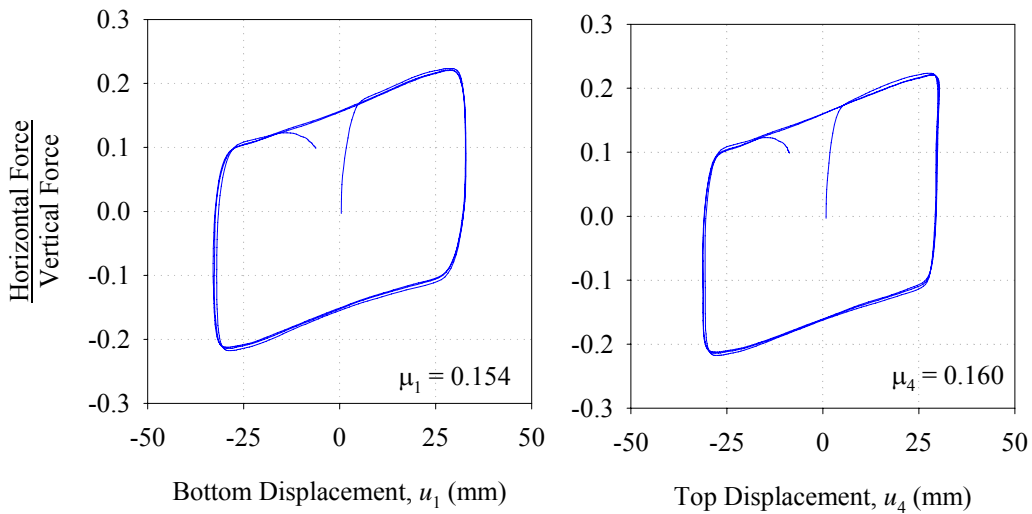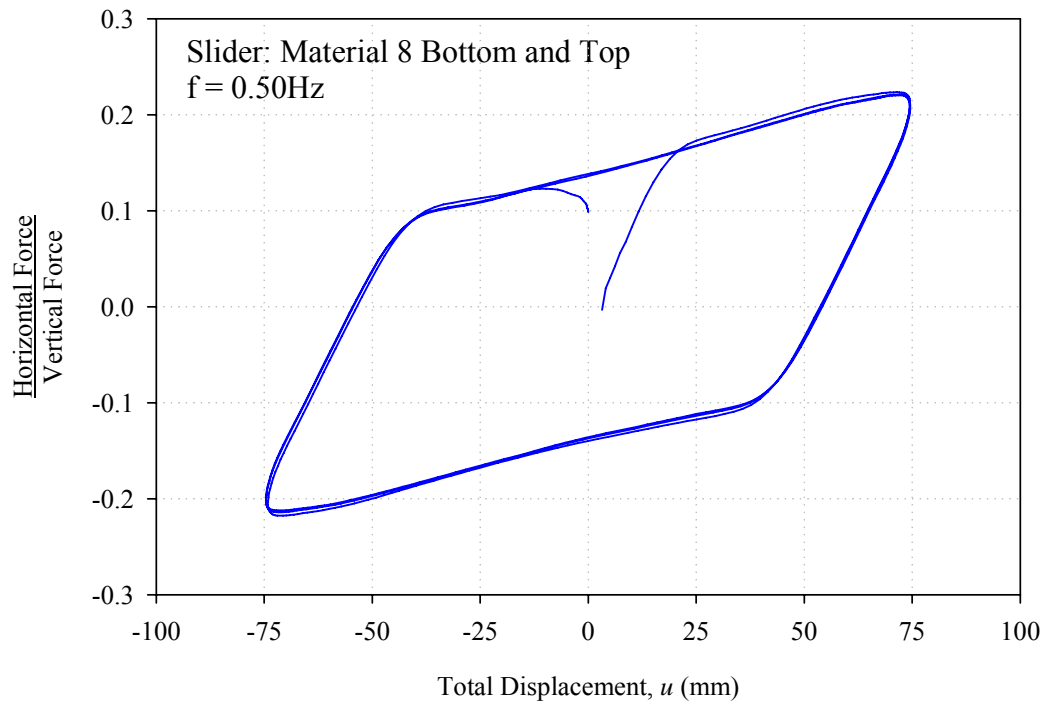
FIGURE 4-16 Total and Decomposed Force-Displacement Loops for f=0.50Hz Test of Prototype Triple 2 Configuration (Lower and Upper Sliders Coated with Material 8)
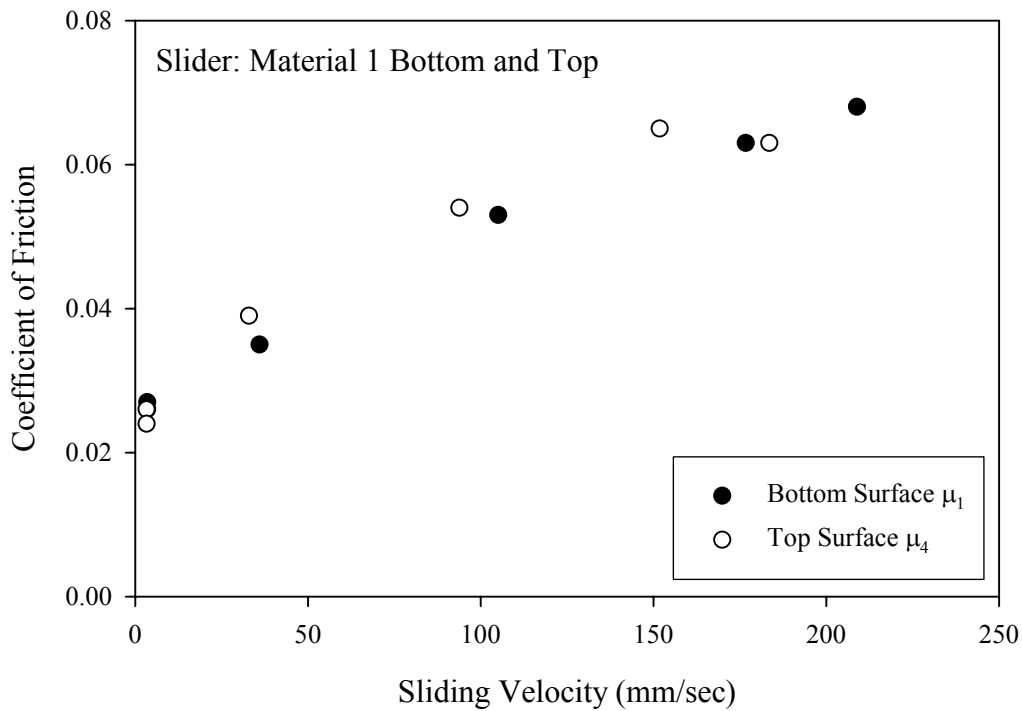
FIGURE 4-17 Variation of Coefficient of Friction of Material 1 as a Function of Sliding Velocity
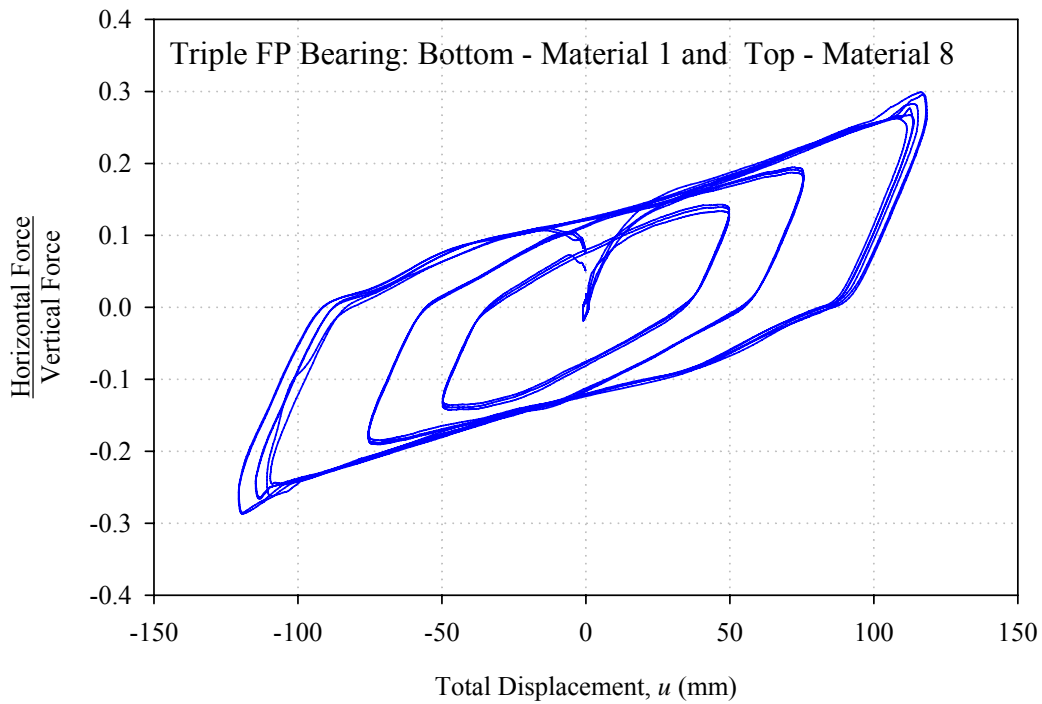
FIGURE 4-18 Force-Displacement Loops for Triple FP Configuration 3 Tested at 0.50 Hz (Slide Plates Coated with Material 1 and Material 8)

For the low friction material used on the inner surfaces of the Triple 1, 2 and 3 configurations, Material 1 lubricated with high temperature silicone grease was used. A lubricated PTFE composite material similar to Material 1, denoted Material 0, was used for the Double 1 (low friction) configuration in the 2004 tests. The velocity dependence of this material is shown in figure 4-19. In the 2007 tests, the Double 2 configuration (intermediate friction) used sliders coated with Material 1.
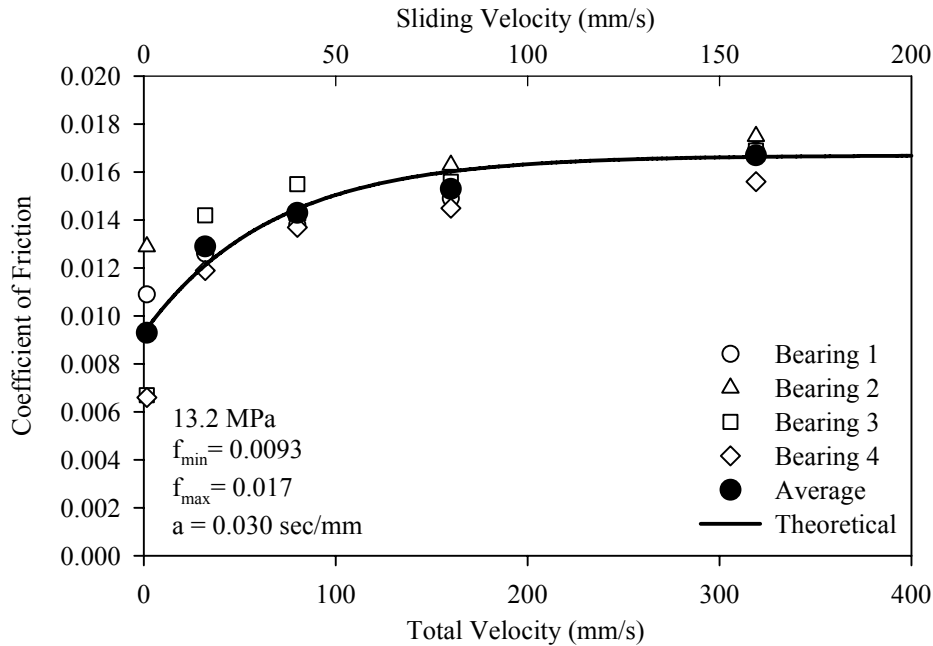
FIGURE 4-19   Friction Exhibited by Material 0 used in the Double FP Configuration 1 (2004 Test Sequence)

4.3.3 Installation of the Isolation System

Special care must be exercised when installing the bearings in order to ensure proper and realistic performance of the isolation system. Sliding bearings are after all, devices adapted from mechanical engineering that have been increased in size for civil engineering applications. Accordingly, higher precision is required in their manufacture and installation. The issues requiring special attention in the installation of multi-spherical sliding bearings are (a) the levelness of each bearing, (b) the distribution of vertical load to each bearing and (c) the alignment of the internal sliding parts.

Typical installation specifications for isolators require that individual bearings be installed level within 0.005 radians or 0.3 degrees. Whenever the concave plates are installed out of level, there is an additional component of force that acts in the horizontal direction due to the fact that there is sliding either up or down the incline. The effect of concave plate rotations can be accounted for analytically as described earlier, however this would introduce an unwanted layer of complexity into the analysis. Second, the bearings must be installed so that there is an even distribution of vertical load on all four bearings. This is an issue of particular importance for shake table testing that is not

encountered in regular construction. In practice, the isolators are installed first and the structure is subsequently built atop the isolators. For this type of construction the load will naturally distribute itself according to tributary area. In the laboratory tests, the structure is completely assembled ahead of time and then set atop the isolators. Analytically the structure is symmetric, however due to imperfections in construction and the vertical rigidity of the isolators the load does not automatically equalize itself among the four isolators.

To solve both of these aforementioned issues, leveling bolts were placed at the four corners of the base plates upon which the bearings and load cells sit. This arrangement is shown in figure 4-20. By properly adjusting the four bolts, each base plate could be individually raised and lowered as well as rotated to evenly distribute the axial load and level each bearing. After the leveling bolts were adjusted properly, the base plates are shimmed beneath and then the 1-⅛ in diameter (28.5mm) rods anchoring the plates to the shake table were tightened.

(a)

(b)
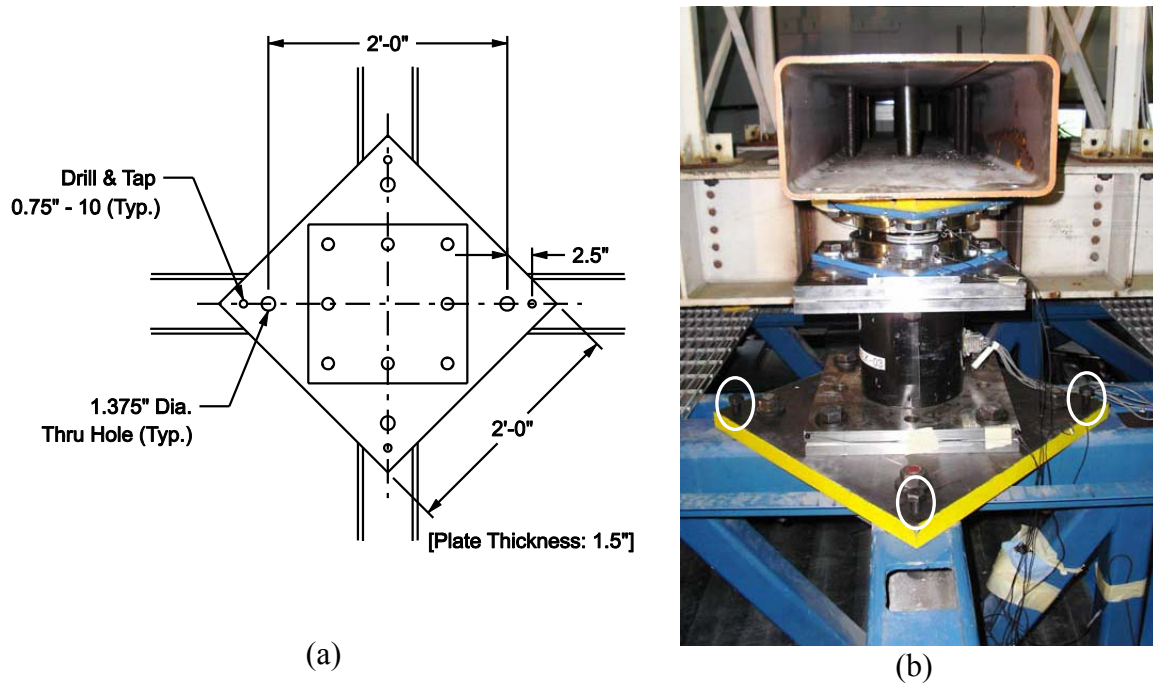
FIGURE 4-20 Base Plate Arrangement with Leveling Bolts Circled

In order to demonstrate this, data was collected as the leveling bolts were adjusted and the vertical load on each isolator was equalized. These datasets are shown in figures 4-21 and 4-22 for the 2004 and 2007 tests respectively. When the assembled model was initially lowered onto the isolation system it sat predominantly on the NE and SW bearings and loads were equalized by jacking up the SE bearing. Perhaps due to the greater vertical flexibility, a more even distribution of loads was achieved during the 2004 tests. However, the distribution of loading during the 2007 tests was still adequate. After the loads were equalized, the base plates were adjusted to level the bearings in each orthogonal direction prior to the final shimming and tightening. Figures 4-23 and 4-24
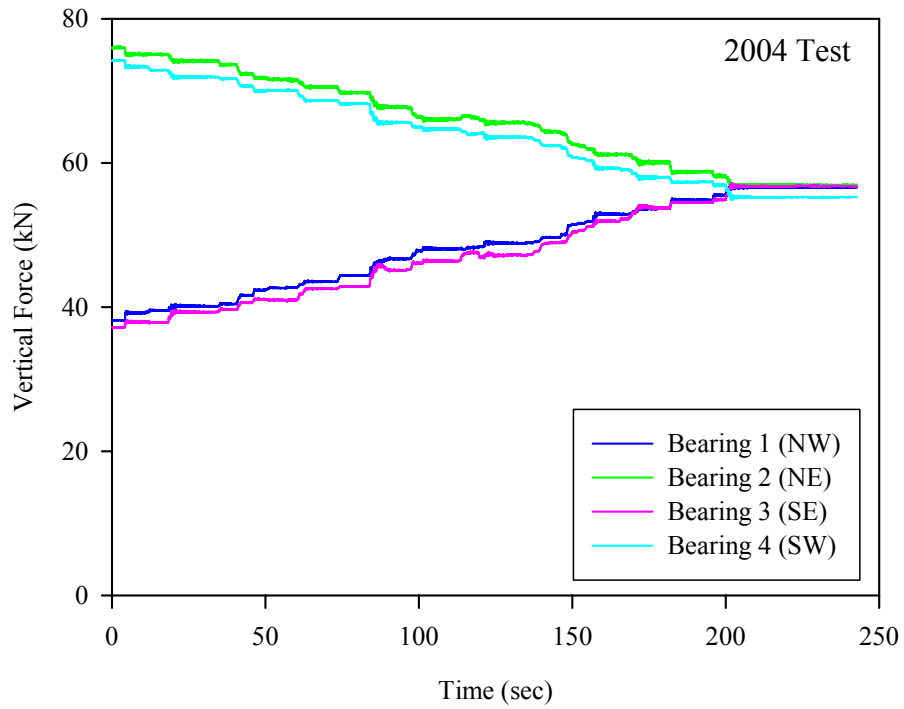
FIGURE 4-21 Equalizing of Vertical Loads on the Bearings (2004 Tests)
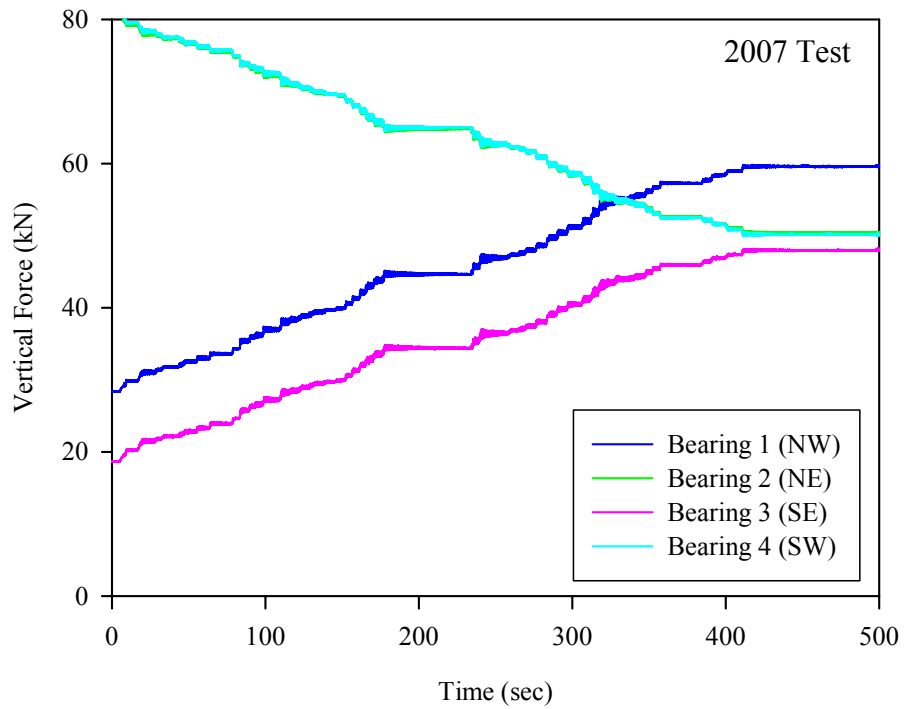
FIGURE 4-22 Equalizing of Vertical Loads on the Bearings (2007 Tests)

document the inclination of the bearings prior to the 2007 tests. In each direction, the maximum rotation of any given bearing is 0.2° or less which introduces negligible error. Similar tolerances were achieved in the 2004 tests but were not photographed.

Alignment of the slider's components is important because the bearing's unique stiffening behavior results from contacting the external displacement restrainer. If there is some initial misalignment or offset and the slider does not start in the middle of the bearing, then the displacement capacity in one direction will be different from the displacement capacity in the other. For example, if the slider is offset by an amount δ_i, then the displacement capacity in one direction is $d_i + \delta_i$ and the displacement capacity in the other is $d_i - \delta_i$. This results in behavior of the isolation system that is slightly different for motion in one direction than for the other. Nevertheless, during testing the bearings had some permanent displacement. A portion of this permanent displacement represented initial displacement in the next test of which the effects were both observed and evaluated in the analysis.
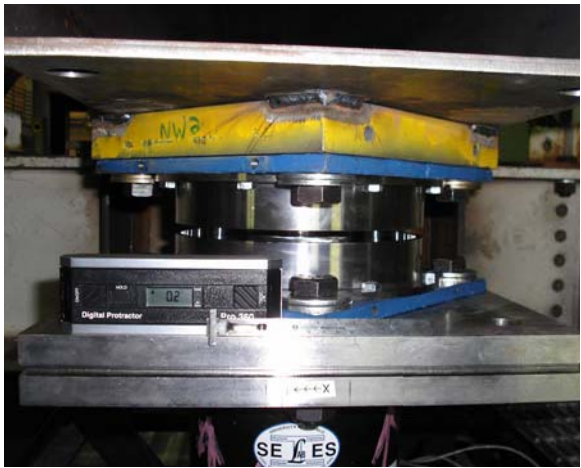
(a) Bearing 1 – NW, 0.2°	(b) Bearing 2 – NE, 0.0°
(c) Bearing 4 – SW, 0.0°	(d) Bearing 3 – SE, 0.0°
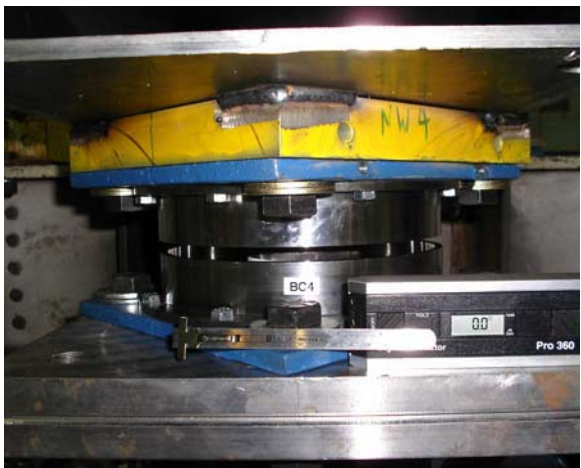
FIGURE 4-23 Inclination of Bearings (Degrees) in the Longitudinal (EW) Direction
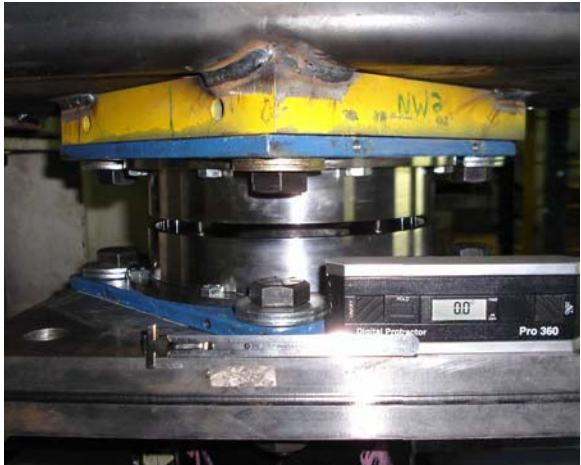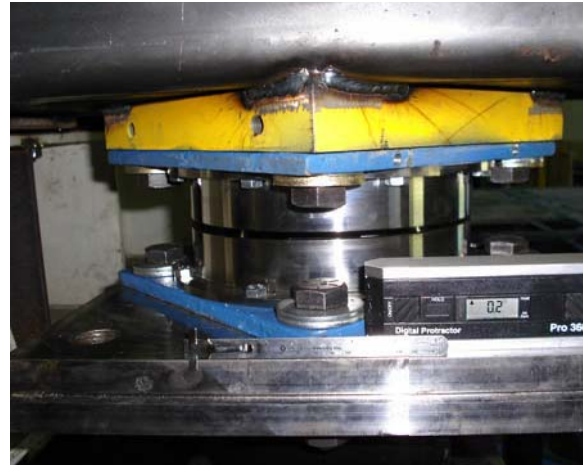
(a) Bearing 1 – NW, 0.0°   (b) Bearing 2 – NE, 0.2°
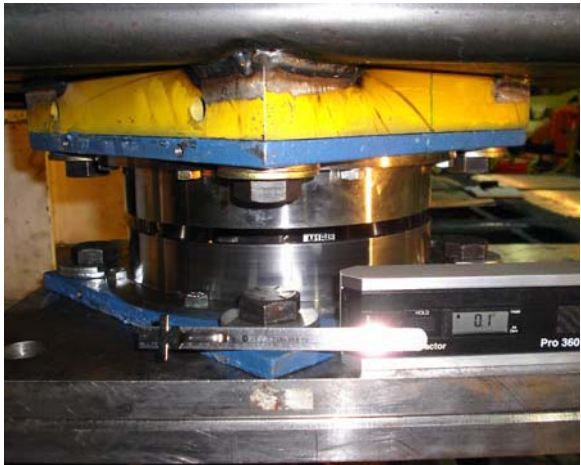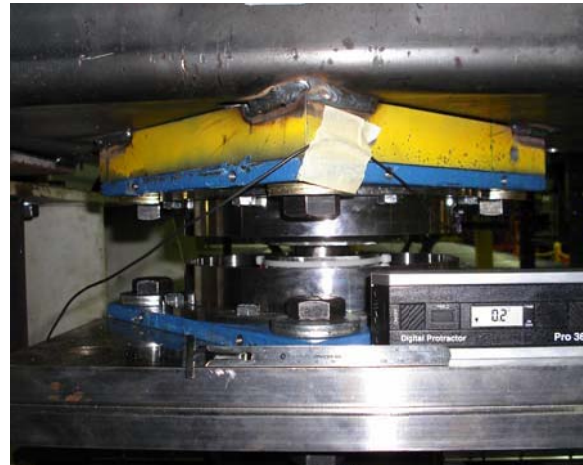
(c) Bearing 4 – SW, 0.1°   (d) Bearing 3 – SE, 0.2°

FIGURE 4-24 Inclination of Bearings (Degrees) in the Transverse (NS) Direction

Because of this issue, care was taken during installation to align the various parts of the bearing and maintain this alignment throughout construction and testing. For the triple FP bearing, prior to assembly the slider components were first aligned and then taped together as a complete unit around the outside. The tape would prevent movement of the various parts with respect to each other during construction but could also be removed easily prior to testing. Following this, the aligned slider unit was centered within the lower concave plate using a removable template and then the upper concave plate was set atop in the correct position. The taped slider unit is shown set in the bearing with the removable template in figure 4-25. With the top plate properly in place, the locking side plates were attached which essentially made the entire bearing an aligned rigid unit. This unit was placed on the load cells, the superstructure was lowered atop the isolators and then everything was bolted in place. With the top concave plates bolted to the basemat tubes and the bottom concave plates bolted to the load cells, the superstructure could be raised and lowered during testing to separate the bearings and still maintain the proper

alignment. This allowed for cleaning and replacement of sliders. Upon resetting the superstructure, the sliders simply had to be centered within the lower concave plate and the top concave plates aligned and set down.

From test to test, effort was made to recenter and realign the sliders using approximately 30 seconds of white noise excitation, which tended to nearly return the sliders back to their equilibrium positions. Nevertheless, the effect of initial displacements on the overall response is minor and can be accounted for in the analysis. In previous tests of sliding isolation systems in which there were initial displacements, it was observed that the isolation system recenters itself upon initial movement. After this, the bearings follow basically the same displacement history regardless of the initial displacement and end up with the same permanent displacement (Tsopelas, 1994).

FIGURE 4-25 Taped Slider and Template Used to Align and Center the Slider

4.4 Instrumentation

Instrumentation was installed to record the actual shake table motion, superstructure response (absolute accelerations and displacements of each story) and the isolation system response (bearing displacements, horizontal and vertical forces). Response quantities in each principal direction were measured, however the longitudinal direction was the most heavily instrumented as it was in this direction that the majority of testing took place.

The basic types of instruments used were:

1. Load Cells – Five component load cells built in house and calibrated in the SEESL. The load cells convert various strains of an instrumented steel cylinder into three force and two moment readings (all forces and moments except torsion).
2. Accelerometers – Sensotec model JTF flat pack accelerometers, acceleration range ±10g.
3. Displacement transducers – Series D62 miniature position transducers (string potentiometers) manufactured by Space Age Control Inc. having ±546mm travel capability.
4. Krypton coordinate tracking system – An advanced camera system that triangulates and records the XYZ positions in space of up to 15 active light emitting diodes (LED).

Additional details and specifications can be found in the SEESL Lab Manual (SEESL, 2004). All instruments had valid calibrations performed in accordance with the methods described in the SEESL Lab Manual (2004). Accelerometers are calibrated using a two-point flip calibration, which provides the output voltages at the known accelerations of +1g and -1g. String potentiometers are calibrated with two point calibrations using a certified test fixture. Load cells are calibrated in each direction by bolting them together in specialized arrangements which provide either pure axial, pure shear or pure moment and then applying a known force as measured by a certified reference load cell.

The instrumentation diagram and instrumentation list for the 2007 test sequence are provided in figure 4-26 and table 4-7 respectively. The text and figures provided herein detail the instrumentation used in the 2007 test sequence, however the 2004 test was essentially the same.

To record the longitudinal input motion, the shake table was instrumented with two displacement transducers and two accelerometers. These were located at the NE and SE corners of the shake table extension. In addition, the north side (NE and NW corners) was instrumented with displacement transducers and accelerometers to record the transverse input motion. Accelerometers were also placed at the four corners to record vertical ground accelerations and rotations of the table. The locations of these instruments are documented by the photographs in figure 4-27. Generally, they were placed along the centerlines of the HSS tubes that form the structure of the shake table extension.

In the longitudinal direction, the structure was instrumented with two accelerometers and two string potentiometers at each of the six floor levels plus the basemat. The accelerometers and displacement transducers are placed at the NE and SE corners to record any torsional response of the isolation system and/or superstructure. In the transverse direction, accelerometers and displacement transducers were placed at the basemat, third and sixth stories. For illustrative purposes, the longitudinal and transverse instrumentation at the third story is shown in figures 4-28(a) and 4-28(b) respectively. In addition, the W14×90 sections were instrumented at each corner to record vertical accelerations of the basemat and monitor the vertical flexibility of the tubes. This is shown in figure 4-29.
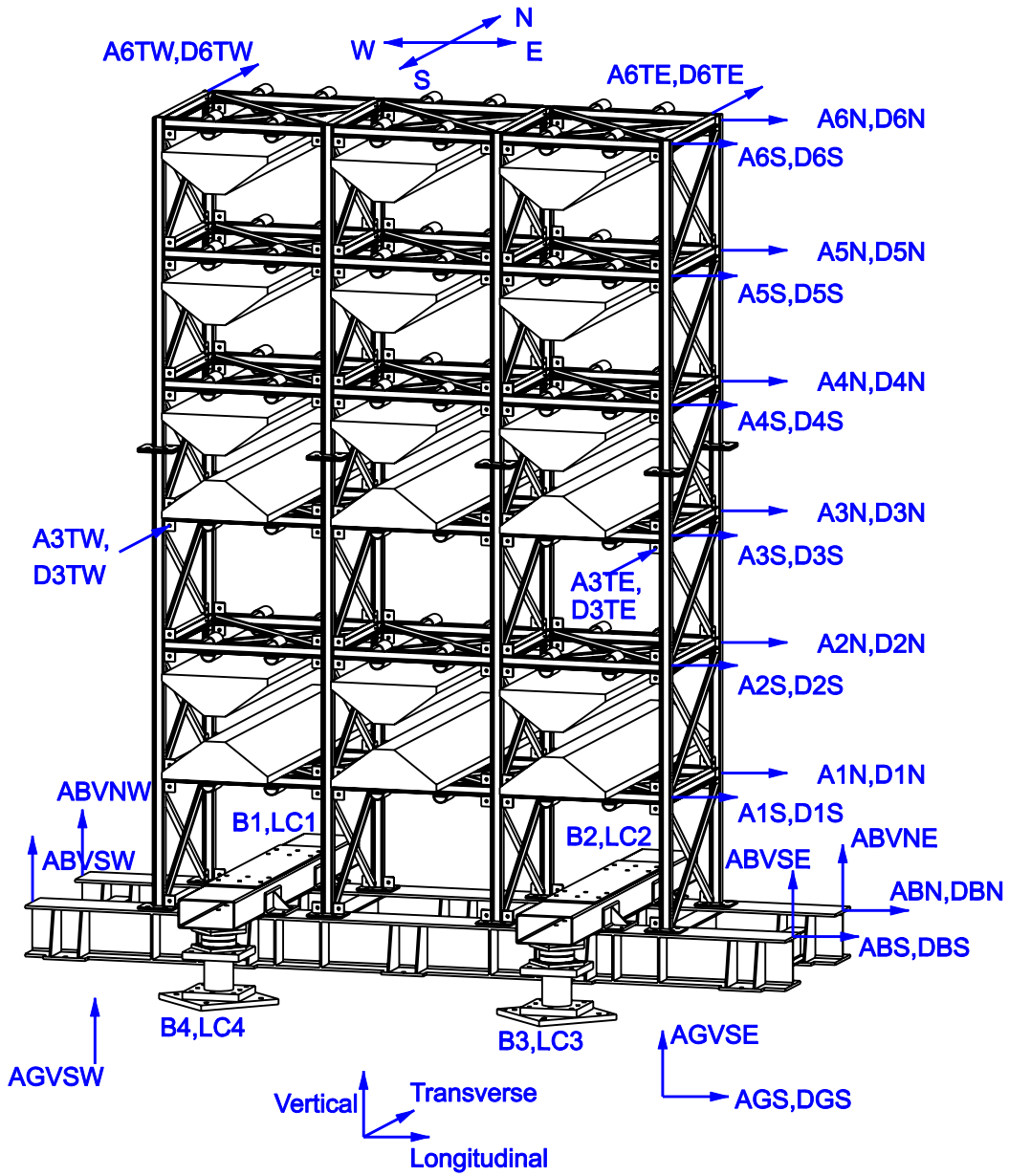
FIGURE 4-26 Instrumentation Diagram

TABLE 4-7 List of Instrumentation Used and Response Quantities Measured

Channel	Notation	Instrument	Measured Quantity	Location	Axis
0	-	clock	time		
1	lc1n	load cell	vertical force	NW table	V
2	lc1sx	load cell	shear force	NW table	L
3	lc1sy	load cell	shear force	NW table	T
4	lc1mx	load cell	moment	NW table	L
5	lc1my	load cell	moment	NW table	T
6	lc2n	load cell	vertical force	NE table	V
7	lc2sx	load cell	shear force	NE table	L
8	lc2sy	load cell	shear force	NE table	T
9	lc2mx	load cell	moment	NE table	L
10	lc2my	load cell	moment	NE table	T
11	lc3n	load cell	vertical force	SE table	V
12	lc3sx	load cell	shear force	SE table	L
13	lc3sy	load cell	shear force	SE table	T
14	lc3mx	load cell	moment	SE table	L
15	lc3my	load cell	moment	SE table	T
16	lc4n	load cell	vertical force	SW table	V
17	lc4sx	load cell	shear force	SW table	L
18	lc4sy	load cell	shear force	SW table	T
19	lc4my	load cell	moment	SW table	T
20	agn	accelerometer	ground acceleration	NE table	L
21	ags	accelerometer	ground acceleration	SE table	L
22	abn	accelerometer	basemat acceleration	NE base	L
23	abs	accelerometer	basemat acceleration	SE base	L
24	a1n	accelerometer	1st story acceleration	NE corner	L
25	a1s	accelerometer	1st story acceleration	SE corner	L
26	a2n	accelerometer	2nd story acceleration	NE corner	L
27	a2s	accelerometer	2nd story acceleration	SE corner	L
28	a3n	accelerometer	3rd story acceleration	NE corner	L
29	a3s	accelerometer	3rd story acceleration	SE corner	L
30	a4n	accelerometer	4th story acceleration	NE corner	L
31	a4s	accelerometer	4th story acceleration	SE corner	L
32	a5n	accelerometer	5th story acceleration	NE corner	L
33	a5s	accelerometer	5th story acceleration	SE corner	L
34	a6n	accelerometer	6th story acceleration	NE corner	L
35	a6s	accelerometer	6th story acceleration	SE corner	L

TABLE 4-7 (ctd) List of Instrumentation Used and Response Quantities Measured

Channel	Notation	Instrument	Measured Quantity	Location	Axis
36	agtw	accelerometer	ground acceleration	NW table	T
37	agte	accelerometer	ground acceleration	NE table	T
38	ab1t	accelerometer	basemat acceleration	NW base	T
39	ab2t	accelerometer	basemat acceleration	NE base	T
40	a3tw	accelerometer	3rd story acceleration	NW corner	T
41	a3te	accelerometer	3rd story acceleration	NE corner	T
42	a6tw	accelerometer	6th story acceleration	NW corner	T
43	a6te	accelerometer	6th story acceleration	NE corner	T
44	agvnw	accelerometer	ground acceleration	NW table	V
45	agvne	accelerometer	ground acceleration	NE table	V
46	agvse	accelerometer	ground acceleration	SE table	V
47	agvsw	accelerometer	ground acceleration	SW table	V
48	abvnw	accelerometer	basemat acceleration	NW base	V
49	abvne	accelerometer	basemat acceleration	NE base	V
50	abvse	accelerometer	basemat acceleration	SE base	V
51	abvsw	accelerometer	basemat acceleration	SW base	V
52	dgn	string pot	ground displacement	NE table	L
53	dgs	string pot	ground displacement	SE table	L
54	dbn	string pot	basemat displacement	NE base	L
55	dbs	string pot	basemat displacement	SE base	L
56	d1n	string pot	1st story displacement	NE corner	L
57	d1s	string pot	1st story displacement	SE corner	L
58	d2n	string pot	2nd story displacement	NE corner	L
59	d2s	string pot	2nd story displacement	SE corner	L
60	d3n	string pot	3rd story displacement	NE corner	L
61	d3s	string pot	3rd story displacement	SE corner	L
62	d4n	string pot	4th story displacement	NE corner	L
63	d4s	string pot	4th story displacement	SE corner	L
64	d5n	string pot	5th story displacement	NE corner	L
65	d5s	string pot	5th story displacement	SE corner	L
66	d6n	string pot	6th story displacement	NE corner	L
67	d6s	string pot	6th story displacement	SE corner	L
68	db1tot	string pot	bearing 1 displacement	B1 (NW)	L
69	db2tot	string pot	bearing 2 displacement	B2 (NE)	L
70	db3tot	string pot	bearing 3 displacement	B3 (SE)	L
71	db3top	string pot	slider 3 displacement	B3 (SE)	L

TABLE 4-7 (ctd) List of Instrumentation Used and Response Quantities Measured

Channel	Notation	Instrument	Measured Quantity	Location	Axis
72	db3bot	string pot	slider 3 displacement	B3 (SE)	L
73	db4tot	string pot	bearing 4 displacement	B4 (SW)	L
74	dgtw	string pot	ground displacement	NW table	T
75	dgte	string pot	ground displacement	NE table	T
76	db1t	string pot	basemat displacement	NW base	T
77	db2t	string pot	basemat displacement	NE base	T
78	d3tw	string pot	3rd story displacement	NW corner	T
79	d3te	string pot	3rd story displacement	NE corner	T
80	d6tw	string pot	6th story displacement	NW corner	T
81	d6te	string pot	6th story displacement	NE corner	T

The isolation system's relative total displacements are monitored for all bearings using string potentiometers. Relative total displacement refers to the displacement of the topmost plate of the bearing with respect to the lowermost plate (which is assumed to be rigidly connected to the shake table). In addition, internal displacements of the SE bearing were also monitored to determine the relative sliding displacements on the individual sliding surfaces. Two string potentiometers were attached to the upper and lower slide plates as was done in the component testing. This bearing had each displacement restrainer ring milled down by 3mm to provide clearance to attach instrumentation so that the slider's motion could be captured by video. To supplement the string potentiometers, the Krypton coordinate tracking camera system was also used to monitor the SE bearing's displacements. The locations of the Krypton LEDs can be seen in the various photographs of the SE bearing. This provided redundancy and was also able to capture additional response quantities, such as vertical displacements of the bearings during uplift. This is an important measurement that is difficult to measure accurately using string potentiometers. Axial and shear forces in the isolation system were measured by a load cell mounted beneath each bearing. Those used were the five component load cells referred to by the SEESL as 5D-LC-12-BLK-01 through 5D-LC-12-BLK-04.

Important response quantities need to be recorded by both direct and indirect means to provide redundancy for checking the accuracy of important measurements. The instrumentation plan described here was designed to provide such redundancy. For example, to check accelerations, the absolute displacement at that location can be double differentiated to obtain the history of acceleration. To check shear force measured by the load cells, the base shear can be calculated by summing the inertial forces at each floor level. Each floor's inertial force is calculated by multiplying the recorded average acceleration by the tributary mass of that floor.

(a) NW Corner

(b) NE Corner

(c) SW Corner

(d) SE Corner

FIGURE 4-27 Instrumentation used to Record Input Ground Accelerations and Displacements

(a)

(b)

FIGURE 4-28 (a) Longitudinal and (b) Transverse Instrumentation at the Third Story of the Superstructure

(a) NW Corner

(b) NE Corner

(c) SW Corner

(d) SE Corner

FIGURE 4-29 Instrumentation of the W14×90 Base

4.5 Description of Ground Motions Used in Study

The ground motions for this study were chosen simply to validate the dynamic analysis models across all sliding regimes. Ground motions used for the 2007 tests are described in table 4-8 and those used in the 2004 test are described in table 4-9. Plots of the acceleration, velocity and displacement histories as well as response spectra for each motion are provided in Appendix A. All motions used are from historical records – the time histories used in the 2007 tests were downloaded directly from the PEER NGA database of ground motions and those used in the 2004 tests are from the library of motions on file with the shake table in the SEESL. Earthquakes were applied primarily in the longitudinal direction; however those motions with multiple components listed in tables 4-8 and 4-9 were used for bidirectional and tridirectional excitation. To satisfy the similitude requirements, in all cases the records were time scaled by a factor of two in accordance with the length scale factor of four.

For the 2007 tests, motions ranging from low to severe intensity were chosen and typically scaled to 100% amplitude to demonstrate the different types of response possible with the adaptive systems (the isolation system used in the 2004 test was not adaptive so each record was run with increasing amplitude scale to cause the largest displacement response safely possible). Low level records such as Wrightwood, Golden Gate Park and Taft were either small magnitude earthquakes or occurred in the far field. These are examples of motions in which isolation systems designed to have sufficient damping to control displacements in larger events would be unlikely to activate. They are chosen to show motion on the innermost surfaces (with high stiffness and low friction) of the triple FP. Intermediate events will show the first transition in stiffness and damping as sliding begins to occur on the outer concave surfaces. Large magnitude events such as the Newhall, Sylmar and Pacoima records were chosen because they will cause substantial sliding on both outer surfaces. These motions all have near fault characteristics. Lastly, to investigate stiffening after contact with the displacement restrainer, the adaptive triple configuration (Triple 3) was tested using the near fault motions scaled beyond 100%. These motions and this range of operation are considered to be MCE level or even beyond MCE level.

TABLE 4-8 Earthquake Ground Motions Used in 2007 Test Sequence

Notation	Earthquake	Station	Component	Moment Magnitude	Distance (km)	Peak Ground Motion[1]		
						Displ. (mm)	Vel. (mm/s)	Accl. (g)
WTW 115	Lytle Creek 9-12-1970	USGS290 Wrightwood	115	5.33	13.0	2.6	51	0.16
GGP 100	San Francisco 3-22-1957	USGS1117 Golden Gate Park	100	5.28	11.1	1.1	23	0.11
TAF 021	Kern County 7-21-1952	USGS1095 Taft Lincoln School	021	7.36	43.5	23	77	0.16
ELC 180	Imperial Valley 5-19-1940	USGS117 El Centro Array #9	180	6.95	13.0	33	149	0.31
ELC 270			270			55	148	0.22
ELC UP			UP			21	53	0.21
CLS 090	Loma Prieta 10-18-1989	CDMG57007 Corralitos	090	6.93	7.2	28	226	0.48
YPT 330	Kocaeli 8-17-1999	KOERI99999 Yarmica	330	7.51	19.3	127	311	0.35
YPT 060			060			143	329	0.27
YPT UP			UP			74	154	0.24
NWH 360	Northridge 1-17-1994	CDMG24279 Newhall Fire Station	360	6.69	20.3	96	486	0.59
NWH 090			090			44	378	0.58
NWH UP			UP			37	157	0.55
SYL 360	Northridge 1-17-1994	CDMG24514 Sylmar-Olive View Med FF	360	6.69	16.7	80	649	0.84
PUL 164	San Fernando 2-9-1971	CDMG279 Pacoima Dam Upper Left Abutment	164	6.61	11.9	89	563	1.23

1. Model Scale

TABLE 4-9 Earthquake Ground Motions Used in 2004 Test Sequence

Notation	Earthquake	Station	Component	Peak Ground Motion[1]		
				Displ. (mm)	Vel. (mm/s)	Accel. (g)
ELC S00E	Imperial Valley 5-19-1940	El Centro	S00E	27	168	0.34
ELC S90W			S90W	55	148	0.22
ELC UP			UP	21	53	0.21
TFT N21E	Kern County 7-21-1952	Taft Lincoln School	N21E	17	79	0.16
KOBE N-S	Kobe 1-17-1995	Kobe Station, Japan	N-S	52	457	0.83
TCU 129 EW	Chi Chi Taiwan 9-20-1999	TCU 129	EW	126	300	0.98
TCU 129 NS			NS	72	180	0.63
TCU 129 UP			UP	59	177	0.34
MXC N90W	Mexico City 9-19-1985	SCT Building	N90W	53	303	0.17
NWH 360	Northridge 1-17-1994	Newhall Fire Station	360	76	474	0.59
NWH 090			90	44	374	0.58
NWHUP			UP	37	157	0.55
SYL 90	Northridge 1-17-1994	Sylmar Parking Lot	90	38	385	0.60
PAC S16E	San Fernando 2-9-1971	Pacoima Dam	S16E	91	566	1.17
PAC S74W			S74W	27	284	1.08
PAC UP			UP	46	283	0.70

1. Model Scale

SECTION 5
SHAKE TABLE TEST RESULTS

5.1 Introduction

The data analysis and results from shake table testing of the model structure are described in this section. When interpreting the experimental results, it should be recognized that the various isolation systems were not designed to fulfill any particular performance requirements - the properties of the bearings were chosen simply to allow for testing of isolation systems with a variety of characteristics for the purpose of providing a database of experimental data upon which the analytical models can be verified. In addition, experimental observation of behavior during uplift or upon contacting the displacement restrainer aids in understanding these localized phenomena and contributes towards demonstrating the overall safety of these devices under extreme conditions.

5.2 Results for Fixed Base Structure

In addition to the various structural identification tests reported in Section 8.2, a limited number of seismic tests were also conducted when the bearings were locked. The earthquakes used were of low intensity and served both to validate the analytical model of the superstructure and to serve as a control group for investigation into the effects of early activation of the adaptive systems. The results of these tests are provided in table 5-1. Reported are the peak table motion and peak structural responses from excitation of the braced frame with the El Centro S00E and Taft N21E motions and the moment frame with the Wrightwood 115 and Golden Gate Park 100 motions. The peak values shown are the maxima after smoothing the dataset with a five point moving average. In each test it was observed that the isolation system moved approximately 0.5mm due to slippage of the locking plates. Although this is relatively small, it does represent a potential source of error between analysis and experiment.

TABLE 5-1 Summary of Peak Responses from Shake Table Testing of Fixed Base Structure

Excitation	Scale	Frame	Direct.	Peak Table Motion			Base Shear/ Weight	Superstructure Response	
				Accel. (g)	Vel. (mm/sec)	Disp. (mm)		Abs. Accel. (g)	Drift/ Height (%)
El Centro S00E	30%	Braced	L	0.117	52	5.9	0.189	0.442 (6)[1]	0.20 (1)[1]
Taft N21E	50%	Braced	L	0.076	58	5.4	0.130	0.244 (6)	0.16 (1)
Wrightwood 115	100%	Moment	L	0.091	37	2.0	0.094	0.354 (6)	0.21 (2)
Golden Gate 100	100%	Moment	L	0.049	8	0.6	0.035	0.230 (6)	0.08 (2)

1. Value in parenthesis indicates the floor corresponding to the peak value.

5.3 Data Analysis and Results for Isolated Structure

Tables 5-2 through 5-7 provide a summary of the peak primary response quantities of the model with the various isolation systems. Again, the peak values are the maxima after smoothing with a five point moving average. The following results are reported in these tables:

(a) The peak table motion for each test. Acceleration and displacement were measured directly as described in section 8.4 and velocity was calculated from numerical differentiation of the displacement data. Longitudinal accelerations and displacements are the average values of the data collected at the north and south sides of the shake table (i.e. the response at the midpoint). Transverse accelerations and displacements were determined similarly using the data collected from the east and west sides. The vertical acceleration reported is the average of the four vertical accelerometers installed at each corner of the shake table.

In general, the data from the two longitudinal transducer pairs was essentially the same (see figure 5-1 for a representative example), indicating that there was negligible torsional motion of the table platform. However, rocking motion was apparent as demonstrated in figure 5-2 by the out of phase histories of vertical acceleration. For purely longitudinal excitation, the vertical accelerations on the east and west sides are equal and opposite, indicating cyclic rocking of the table platform about the transverse axis. To corroborate this, very small vertical displacements of the shake table at the base of the SW load cell were also measured directly by the Krypton system. This is shown in figure 5-3 for a motion of large amplitude (Sylmar 360 from the test of the Double 2 configuration).

The rocking motion of the table platform results from the large overturning moment caused by the structure model. Vertical accelerations are most pronounced at larger bearing displacements, corresponding to when the overturning moment is the largest. Such behavior is unavoidable since it is a result of the model's substantial mass in comparison to the finite dynamic capacity of the shake table's vertical actuators. This is not a major issue however as minor vertical accelerations have only a small impact on primary response quantities. This fact has been demonstrated in numerous studies of traditional single FP bearings over the past twenty years (Zayas *et al.*, 1987; Constantinou *et al.*, 1993; Mosqueda *et al.*, 2004). These findings apply here since single, double and triple FP bearings all have similar vertical rigidity.

TABLE 5-2 Summary of Primary Response Quantities from Shake Table Testing of Braced Frame Specimen with Isolation System Double 1

Excitation	Scale	Direct.	Peak Table Motion			Isolation System Response					Superstructure Response	
			Accel. (g)	Vel. (mm/sec)	Disp. (mm)	Isol. Disp. (mm)	Perm. Disp. (mm)	Base Shear / Weight	Max. Vertic. (kN)	Min. Vertic. (kN)	Abs. Accel. (g)	Drift / Height (%)
El Centro S00E	100%	L	0.38	186	27	32	0.7	0.077	-228	-218	0.239 (6)[1]	0.11 (1)[1]
El Centro S00E	200%	L	0.80	390	54	92	0.2	0.130	-238	-193	0.193 (6)	0.18 (1)
Kobe N-S	100%	L	0.85	525	46	85	1.8	0.120	-241	-206	0.220 (6)	0.18 (1)
Taft N21E	100%	L	0.19	75	15	10	2.3	0.047	-224	-223	0.158 (6)	0.12 (1)
Taft N21E	500%	L	1.04	357	69	76	3.3	0.105	-241	-202	0.249 (6)	0.21 (5)
Taiwan TCU 129 EW	100%	L	1.33	449	75	65	1.0	0.095	-248	-185	0.209 (6)	0.21 (2)
Taiwan TCU 129 EW	125%	L	1.64	547	94	88	0.6	0.128	-262	-162	0.203 (6)	0.31 (2)
Mexico N90W	50%	L	0.12	179	31	58	1.1	0.081	-225	-219	0.137 (6)	0.16 (6)
NR Newhall 360	100%	L	0.99	471	67	98	1.0	0.137	-249	-194	0.205 (6)	0.20 (1)
NR Sylmar 90	100%	L	0.68	396	57	117	1.3	0.160	-234	-205	0.207 (6)	0.24 (1)
Pacoima 164 (1)	100%	L	1.25	535	87	96	0.6	0.131	-247	-198	0.261 (6)	0.27 (2)
Pacoima 164 (2)	100%	L	1.26	537	87	91	2.1	0.138	-247	-197	0.280 (6)	0.28 (2)
El Centro S00E	100%	L	0.39	190	27	28	0.3	0.062	-278	-172	0.193 (6)	0.15 (5)
El Centro UP		V	0.14	-	-	-	-	-	-	-	-	-
El Centro S00E	200%	L	0.79	392	54	92	0.4	0.128	-325	-122	0.264 (6)	0.21 (5)
El Centro UP		V	0.29	-	-	-	-	-	-	-	-	-
Kobe N-S	100%	L	0.85	513	46	86	0.5	0.125	-336	-88	0.297 (6)	0.26 (1)
Kobe UP		V	0.36	-	-	-	-	-	-	-	-	-
Taft N21E	500%	L	1.05	372	71	80	3.7	0.115	-462	-73	0.333 (6)	0.28 (1)
vertical component		V	0.69	-	-	-	-	-	-	-	-	-
Taiwan TCU 129 EW	125%	L	1.62	542	94	88	0.5	0.117	-327	-125	0.355 (6)	0.34 (1)
Taiwan TCU 129 UP		V	0.38	-	-	-	-	-	-	-	-	-
NR Newhall 90	100%	L	0.97	484	67	108	0.7	0.184	-485	-58	0.482 (1)	0.33 (1)
NR Newhall UP		V	0.53	-	-	-	-	-	-	-	-	-
NR Sylmar 90	100%	L	0.68	395	57	120	0.6	0.166	-376	-63	0.256 (6)	0.28 (1)
NR Sylmar UP		V	0.25	-	-	-	-	-	-	-	-	-

1. Value in parenthesis indicates the floor corresponding to the peak value.

TABLE 5-2 (continued) Summary of Primary Response Quantities from Shake Table Testing of Braced Frame Specimen with Isolation System Double 1

Excitation	Scale	Direct.	Peak Table Motion			Isolation System Response					Superstructure Response	
			Accel. (g)	Vel. (mm/sec)	Disp. (mm)	Isol. Disp. (mm)	Perm. Disp. (mm)	Base Shear / Weight	Max. Vertic. (kN)	Min. Vertic. (kN)	Abs. Accel. (g)	Drift / Height (%)
Pacoima S16E	100%	L	1.26	523	86	90	2.8	0.184	-452	-29	0.459 (6)[1]	0.39 (1)[1]
Pacoima UP		V	0.90	-	-	-	-	-	-	-	-	-
El Centro S00E	200%	L	0.79	400	57	112	0.9	0.410	-361	-116	4.198 (6)	0.62 (6)
El Centro S90W		T	0.54	366	92	122	1.0	0.520	-	-	0.949 (6)	-
El Centro UP		V	0.30	-	-	-	-	-	-	-	-	-
Taiwan TCU 129 EW	100%	L	1.31	444	75	74	0.1	0.091	-305	-141	0.286 (6)	0.42 (1)
Taiwan TCU 129 NS		T	0.67	183	38	54	0.7	0.053	-	-	0.135 (6)	-
Taiwan TCU 129 UP		V	0.31	-	-	-	-	-	-	-	-	-
Pacoima S16E	100%	L	1.27	525	85	97	8.7	0.212	-452	-30	0.451 (6)	0.43 (1)
Pacoima S74W		T	1.10	356	33	43	4.0	0.121	-	-	0.275 (6)	-
Pacoima UP		V	0.91	-	-	-	-	-	-	-	-	-

1. Value in parenthesis indicates the floor corresponding to the peak value.

84

TABLE 5-3 Summary of Primary Response Quantities from Shake Table Testing of Moment Frame Specimen with Isolation System Double 2

Excitation	Scale	Direct.	Peak Table Motion			Bearing Displacements				Bearing Vertical Force		Base Shear/ Weight	Superstructure Response	
			Accel. (g)	Vel. (mm/sec)	Disp. (mm)	Init. (mm)	Max. (mm)	Min. (mm)	Perm. (mm)	Max. (kN)	Min. (kN)		Abs. Accel. (g)	Drift/Height(%)
Wrightwood 115	100%	L	0.102	41	2.0	-0.1	0.1	-0.6	-0.3	74.1 (1)[1]	33.2 (2)	0.109	0.287 (6)[2]	0.22 (2)
Golden Gate 100	100%	L	0.073	13	0.7	-0.3	-0.2	-0.4	-0.3	62.0 (1)	42.8 (4)	0.037	0.141 (6)	0.08 (6)
Taft 021	100%	L	0.132	69	11.9	-0.3	2.6	-1.8	-0.1	79.6 (1)	27.9 (2)	0.110	0.318 (6)	0.37 (2)
El Centro 180	100%	L	0.273	167	20.7	-0.3	13.2	-9.6	0.2	91.8 (3)	12.8 (4)	0.125	0.592 (6)	0.55 (2)
Corralitos 090	100%	L	0.503	236	25.2	0.0	7.5	-19.6	-3.5	96.7 (1)	11.9 (2)	0.135	0.681 (6)	0.65 (2)
Kocaeli 330	100%	L	0.326	303	94.4	-3.2	22.4	-24.2	-6.4	86.0 (1)	21.0 (4)	0.142	0.370 (6)	1.50 (2)
Newhall 360	100%	L	0.883	451	63.7	-5.3	30.3	-50.2	-2.3	94.5 (3)	11.5 (4)	0.163	0.741 (6)	1.11 (2)
Sylmar 360 (a)	100%	L	1.122	583	80.9	-2.4	48.1	-81.8	-4.1	93.8 (1)	15.0 (2)	0.179	0.645 (6)	1.15 (2)
Sylmar 360 (b)	100%	L	1.119	583	81.3	0.1	50.3	-82.4	-3.9	93.6 (1)	15.6 (2)	0.180	0.633 (6)	1.14 (2)
Pacoima 164	100%	L	0.831	485	80.6	-3.7	58.4	-62.5	1.3	98.8 (3)	8.6 (4)	0.169	0.954 (6)	1.36 (2)
El Centro 180	100%	L	0.274	168	20.9	-3.2	14.0	-10.3	-0.4	90.0 (3)	11.5 (4)	0.125	0.571 (6)	0.54 (2)
El Centro UP	100%	V	0.105	-	-	-	-	-	-	-	-	-	-	-
El Centro 180	100%	L	0.288	170	20.9	-0.5	12.6	-9.9	1.0	100.9 (1)	6.2 (2)	0.128	0.535 (6)	0.60 (6)
El Centro 270	100%	T	0.187	134	24.5	-2.0	5.8	-7.2	-3.1	-	-	0.128	0.334 (6)	-
El Centro UP	100%	V	0.099	-	-	-	-	-	-	-	-	-	-	-
Kocaeli 330	100%	L	0.325	308	95.4	0.9	23.3	-27.1	-6.0	98.7 (1)	6.9 (2)	0.141	0.383 (6)	1.44 (2)
Kocaeli UP	100%	V	0.218	-	-	-	-	-	-	-	-	-	-	-
Kocaeli 330	100%	L	0.317	307	94.6	-5.3	31.1	-32.9	-12.7	98.9 (3)	9.3 (4)	0.148	0.330(6)	1.53 (2)
Kocaeli 060	100%	T	0.304	327	97.4	-2.2	15.7	-23.2	-0.6	-	-	0.138	0.294 (6)	-
Kocaeli UP	100%	V	0.216	-	-	-	-	-	-	-	-	-	-	-
Newhall 360	100%	L	0.859	441	63.4	-3.2	27.4	-49.4	-1.9	148.4 (3)	0 (1,3,4)	0.165	0.772 (6)	1.20 (2)
Newhall UP	100%	V	0.414	-	-	-	-	-	-	-	-	-	-	-
Newhall 360	100%	L	0.875	445	63.3	-1.9	30.3	-52.5	-3.5	149.9 (2)	0 (1,2,3,4)	0.167	0.699 (6)	1.17 (2)
Newhall 090	100%	T	0.762	306	42.5	-3.9	32.5	-23.2	-7.2	-	-	0.135	0.446 (6)	-
Newhall UP	100%	V	0.419	-	-	-	-	-	-	-	-	-	-	-

1. Value in parenthesis indicates bearing number corresponding to the maximum value.
2. Value in parenthesis indicates the floor corresponding to the peak value.

85

TABLE 5-4 Summary of Primary Response Quantities from Shake Table Testing of Moment Frame Specimen with Isolation System Triple 1

Excitation	Scale	Direct.	Peak Table Motion			Bearing Displacements				Bearing Vertical Force		Base Shear/Weight	Superstructure Response	
			Accel. (g)	Vel. (mm/sec)	Disp. (mm)	Init. (mm)	Max. (mm)	Min. (mm)	Perm. (mm)	Max. (kN)	Min. (kN)		Abs. Accel. (g)	Drift/Height(%)
Wrightwood 115	100%	L	0.117	42	2.1	0.0	0.6	-1.2	-0.6	67.8 (4)[1]	33.7 (3)	0.074	0.287 (6)[2]	0.20 (2)
Golden Gate 100	100%	L	0.086	13	0.8	-0.6	-0.5	-0.8	-0.6	60.2 (2)	42.3 (3)	0.042	0.163 (6)	0.10 (5)
Taft 021	100%	L	0.150	66	12.3	-0.6	5.6	-1.2	0.6	70.2 (1)	30.4 (3)	0.081	0.275 (6)	0.34 (2)
El Centro 180	100%	L	0.291	170	21.4	0.3	11.9	-9.9	3.6	82.7 (2)	26.3 (3)	0.090	0.442 (6)	0.44 (2)
Corralitos 090	100%	L	0.507	244	26.7	2.9	13.9	-28.2	-5.4	81.5 (1)	21.2 (3)	0.110	0.397 (6)	0.62 (2)
Kocaeli 330	100%	L	0.329	313	99.4	-5.4	49.8	-31.0	-1.7	75.1 (2)	32.2 (3)	0.122	0.214 (6)	1.71 (2)
Newhall 360	100%	L	0.859	441	63.2	-2.5	43.0	-61.7	1.1	85.2 (2)	13.4 (3)	0.151	0.408 (6)	1.20 (2)
Sylmar 360	100%	L	1.157	580	80.8	0.6	56.0	-91.5	3.3	86.8 (1)	19.9 (3)	0.176	0.387 (6)	1.32 (2)
Pacoima 164	100%	L	0.880	481	80.0	2.9	72.0	-60.3	6.1	90.1 (2)	17.2 (4)	0.157	0.663 (6)	1.33 (2)
El Centro 180	100%	L	0.300	162	20.9	0.1	15.8	-13.2	1.6	83.1 (1)	21.2 (4)	0.129	0.388 (6)	0.63 (2)
El Centro UP	100%	V	0.097	-	-	-	-	-	-	-	-	-	-	-
El Centro 180	100%	L	0.292	164	21.2	1.0	24.0	-12.2	3.7	89.0 (1)	19.6 (1)	0.132	0.299 (6)	0.76 (6)
El Centro 270	100%	T	0.186	131	24.1	-0.2	11.9	-18.2	-3.0	-	-	0.128	0.201 (6)	-
El Centro UP	100%	V	0.092	-	-	-	-	-	-	-	-	-	-	-
Kocaeli 330	100%	L	0.318	290	95.2	3.2	50.3	-38.3	2.1	89.0 (3)	15.2 (4)	0.156	0.357 (6)	1.66 (2)
Kocaeli UP	100%	V	0.212	-	-	-	-	-	-	-	-	-	-	-
Kocaeli 330	100%	L	0.319	292	94.6	2.2	43.6	-38.6	-1.5	103.5 (3)	7.8 (1)	0.147	0.351 (6)	1.60 (2)
Kocaeli 060	100%	T	0.296	321	97.5	-1.8	33.8	-22.9	-3.0	-	-	0.130	0.186 (6)	-
Kocaeli UP	100%	V	0.211	-	-	-	-	-	-	-	-	-	-	-
Newhall 360	100%	L	0.839	440	62.6	-1.4	37.9	-71.9	1.0	159.7 (3)	0 (1,4)	0.181	0.753 (6)	1.47 (2)
Newhall UP	100%	V	0.427	-	-	-	-	-	-	-	-	-	-	-
Newhall 360	100%	L	0.859	443	62.6	0.7	39.7	-74.4	-0.4	161.5 (2)	0 (1,3,4)	0.179	0.748 (6)	1.50 (2)
Newhall 090	100%	T	0.737	301	41.5	-0.4	48.1	-41.3	-3.6	-	-	0.136	0.270 (6)	-
Newhall UP	100%	V	0.435	-	-	-	-	-	-	-	-	-	-	-

1. Value in parenthesis indicates bearing number corresponding to the maximum value.
2. Value in parenthesis indicates the floor corresponding to the peak value.

TABLE 5-5   Summary of Primary Response Quantities from Shake Table Testing of Moment Frame Specimen with Isolation System Triple 2

Excitation	Scale	Direct.	Peak Table Motion			Bearing Displacements				Bearing Vertical Force		Base Shear/ Weight	Superstructure Response	
			Accel. (g)	Vel. (mm/sec)	Disp. (mm)	Init. (mm)	Max. (mm)	Min. (mm)	Perm. (mm)	Max. (kN)	Min. (kN)		Abs. Accel. (g)	Drift/Height(%)
Wrightwood 115	100%	L	0.110	40	2.1	-2.2	-1.6	-3.0	-2.2	70.9 (4)[1]	31.5 (3)	0.077	0.264 (6)[2]	0.19 (2)
Golden Gate 100	100%	L	0.073	18	0.7	-2.2	-2.1	-2.4	-2.2	62.3 (2)	39.3 (3)	0.038	0.142 (6)	0.08 (2)
Taft 021	100%	L	0.135	67	11.9	-2.2	1.8	-5.5	-1.9	73.0 (4)	27.5 (3)	0.104	0.248 (6)	0.35 (2)
El Centro 180	100%	L	0.293	163	20.7	-2.1	9.0	-13.2	-1.8	88.9 (2)	15.4 (1)	0.157	0.515 (6)	0.60 (2)
Corralitos 090	100%	L	0.510	236	25.2	-2.3	14.9	-21.6	-2.0	93.6 (2)	9.8 (3)	0.208	0.449 (6)	0.73 (2)
Kocaeli 330	100%	L	0.317	291	95.5	-2.4	50.2	-34.4	11.7	90.9 (2)	11.9 (3)	0.219	0.373 (6)	1.95 (2)
Newhall 360	100%	L	0.845	443	63.0	11.1	39.0	-69.3	-8.5	111.3 (2)	0 (3)	0.263	0.644 (6)	1.80 (2)
Sylmar 360	100%	L	1.123	579	81.9	-8.9	63.2	-89.3	-2.2	99.8 (4)	0 (3)	0.301	0.595 (6)	1.96 (2)
Pacoima 164	100%	L	0.870	481	80.2	-2.6	97.2	-50.2	5.5	114.8 (2)	0 (1)	0.253	0.897 (6)	1.88 (2)
El Centro 180	100%	L	0.299	163	20.9	5.2	16.3	-5.5	5.6	86.0 (2)	14.3 (1)	0.155	0.506 (6)	0.57 (2)
El Centro UP	100%	V	0.104	-	-	-	-	-	-	-	-	-	-	-
El Centro 180	100%	L	0.291	162	20.8	5.3	18.1	-5.5	5.9	86.9 (4)	7.1 (3)	0.139	0.365 (6)	0.57 (2)
El Centro 270	100%	T	0.190	138	24.4	0.2	10.6	-14.3	-0.4	-	-	0.161	0.230 (6)	-
El Centro UP	100%	V	0.102	-	-	-	-	-	-	-	-	-	-	-
Kocaeli 330	100%	L	0.314	295	96.6	5.4	58.7	-24.0	17.1	96.3 (2)	0 (1)	0.222	0.436 (6)	1.90 (2)
Kocaeli UP	100%	V	0.215	-	-	-	-	-	-	-	-	-	-	-
Kocaeli 330	100%	L	0.315	289	95.5	16.8	64.5	-24.0	25.2	116.8 (4)	0 (1,3)	0.225	0.561 (6)	1.94 (2)
Kocaeli 060	100%	T	0.296	318	97.7	0.1	19.8	-16.5	-1.4	-	-	0.170	0.241 (6)	-
Kocaeli UP	100%	V	0.215	-	-	-	-	-	-	-	-	-	-	-
Newhall 360	100%	L	0.832	443	62.8	-11.4	23.9	-68.3	-8.0	168.2 (2)	0 (1,3,4)	0.297	0.703 (6)	1.70 (2)
Newhall UP	100%	V	0.446	-	-	-	-	-	-	-	-	-	-	-
Newhall 360	100%	L	0.847	445	62.6	-8.4	20.3	-72.0	-6.0	193.8 (2)	0 (1,3,4)	0.295	0.762 (6)	1.72 (2)
Newhall 090	100%	T	0.751	302	41.6	-1.6	38.0	-44.5	-11.1	-	-	0.218	0.367 (6)	-
Newhall UP	100%	V	0.457	-	-	-	-	-	-	-	-	-	-	-

1. Value in parenthesis indicates bearing number corresponding to the maximum value.
2. Value in parenthesis indicates the floor corresponding to the peak value.

TABLE 5-6 Summary of Primary Response Quantities from Shake Table Testing of Moment Frame Specimen with Isolation System Triple 3

Excitation	Scale	Direct.	Peak Table Motion Accel. (g)	Vel. (mm/sec)	Disp. (mm)	Init. (mm)	Bearing Displacements Max. (mm)	Min. (mm)	Perm. (mm)	Bearing Vertical Force Max. (kN)	Min. (kN)	Base Shear/ Weight	Superstructure Response Abs. Accel. (g)	Drift/ Height(%)
Wrightwood 115	100%	L	0.104	41	2.1	0.0	0.3	-1.1	-0.7	72.8 (2)[1]	32.4 (1)	0.090	0.271 (6)[2]	0.20 (2)
Golden Gate 100	100%	L	0.072	18	0.7	-0.7	-0.5	-0.8	-0.7	64.0 (2)	41.5 (1)	0.038	0.146 (6)	0.07 (2)
Taft 021	100%	L	0.135	68	11.8	-0.6	3.4	-4.1	0.6	70.9 (2)	32.0 (1)	0.095	0.201 (6)	0.33 (2)
El Centro 180	100%	L	0.300	162	20.8	0.2	18.6	-12.1	4.9	85.2 (2)	20.0 (1)	0.134	0.384 (6)	0.58 (2)
Corralitos 090	100%	L	0.506	242	25.3	4.3	14.1	-29.1	-2.9	90.5 (4)	16.4 (3)	0.149	0.418 (6)	0.60 (2)
Kocaeli 330	100%	L	0.315	287	94.4	-3.1	52.7	-32.0	2.1	80.4 (2)	25.6 (1)	0.140	0.236 (6)	1.67 (2)
Newhall 360	100%	L	0.857	445	62.7	1.7	42.7	-66.8	-2.4	98.3 (2)	6.1 (1)	0.199	0.432 (6)	1.34 (2)
Sylmar 360	100%	L	1.148	579	81.3	-2.7	68.2	-91.8	4.9	91.3 (4)	11.5 (3)	0.242	0.424 (6)	1.72 (2)
Pacoima 164	100%	L	0.886	480	79.6	4.8	94.0	-52.2	11.7	100.9 (2)	0 (1)	0.200	0.763 (6)	1.62 (2)
El Centro 180	100%	L	0.299	162	20.8	11.2	24.3	-3.7	8.9	87.7 (2)	15.6 (1)	0.123	0.399 (6)	0.60 (2)
El Centro UP	100%	V	0.093	-	-	-	-	-	-	-	-	-	-	-
El Centro 180	100%	L	0.290	164	21.0	8.4	30.4	-5.8	9.9	96.1 (2)	11.9 (3)	0.138	0.295 (6)	0.76 (2)
El Centro 270	100%	T	0.189	131	23.9	2.5	14.8	-14.9	1.7	-	-	0.144	0.189 (6)	-
El Centro UP	100%	V	0.096	-	-	-	-	-	-	-	-	-	-	-
Kocaeli 330	100%	L	0.315	289	95.7	9.9	59.2	-34.6	7.6	96.1 (2)	5.3 (1)	0.173	0.441 (6)	1.78 (2)
Kocaeli UP	100%	V	0.217	-	-	-	-	-	-	-	-	-	-	-
Kocaeli 330	100%	L	0.316	288	94.8	7.7	54.2	-32.3	4.0	100.6 (4)	0 (1)	0.164	0.433 (6)	1.71 (2)
Kocaeli 060	100%	T	0.296	319	97.5	1.8	29.3	-26.7	0.9	-	-	0.148	0.210 (6)	-
Kocaeli UP	100%	V	0.216	-	-	-	-	-	-	-	-	-	-	-
Newhall 360	100%	L	0.840	444	62.4	-6.7	31.7	-73.9	-2.6	166.7 (2)	0 (1,3,4)	0.220	0.921 (6)	1.63 (2)
Newhall UP	100%	V	0.436	-	-	-	-	-	-	-	-	-	-	-
Newhall 360	100%	L	0.859	444	62.2	-2.8	35.6	-75.3	-4.7	177.3 (2)	0 (1,3,4)	0.221	0.916 (6)	1.65 (2)
Newhall 090	100%	T	0.764	305	41.3	-0.4	42.5	-50.0	-0.3	-	-	0.173	0.327 (6)	-
Newhall UP	100%	V	0.429	-	-	-	-	-	-	-	-	-	-	-

1. Value in parenthesis indicates bearing number corresponding to the maximum value.
2. Value in parenthesis indicates the floor corresponding to the peak value.

TABLE 5-7 Summary of Primary Response Quantities from Shake Table Testing of Moment Frame Specimen with Isolation System Triple 3 at Larger Amplitude Motions

Excitation	Scale	Direct.	Peak Table Motion			Bearing Displacements				Bearing Vertical Force		Base Shear/ Weight	Superstructure Response	
			Accel. (g)	Vel. (mm/sec)	Disp. (mm)	Init. (mm)	Max. (mm)	Min. (mm)	Perm. (mm)	Max. (kN)	Min. (kN)		Abs. Accel. (g)	Drift/ Height(%)
Sylmar 360 (a)	100%	L	1.142	578	81.3	0.0	59.0	-98.9	-1.4	89.9 (4)[1]	10.7 (1)	0.247	0.397 (6)[2]	1.63 (2)
Sylmar 360 (b)	110%	L	1.274	633	90.2	-0.8	66.4	-109.5	2.1	94.8 (4)	5.1 (2)	0.273	0.430 (6)	1.76 (2)
Sylmar 360 (c)	115%	L	1.334	661	94.3	2.7	65.3	-116.5	0.9	96.0 (4)	0 (3)	0.290	0.485 (6)	1.78 (2)
Newhall 360 (a)	100%	L	0.846	440	62.9	1.9	37.5	-75.5	-10.5	100.3 (4)	0 (1,3)	0.227	0.512 (6)	1.56 (2)
Newhall 360 (b)	110%	L	0.948	485	69.3	-10.2	33.3	-85.8	-11.2	104.5 (4)	0 (1,2,3)	0.239	0.573 (6)	1.57 (2)
Pacoima 164 (a)	100%	L	0.899	483	79.8	-10.8	88.5	-65.3	6.8	106.5 (2)	0 (1)	0.221	0.816 (6)	1.73 (2)
Pacoima 164 (b)	110%	L	0.987	532	88.2	5.8	95.0	-60.4	9.0	109.9 (2)	0 (1)	0.225	0.884 (6)	1.64 (2)
Pacoima 164 (c)	110%	L	0.986	533	88.3	6.9	96.4	-58.5	10.5	109.6 (2)	0 (1)	0.229	0.884 (6)	1.69 (2)

1. Value in parenthesis indicates bearing number corresponding to the maximum value.
2. Value in parenthesis indicates the floor corresponding to the peak value.
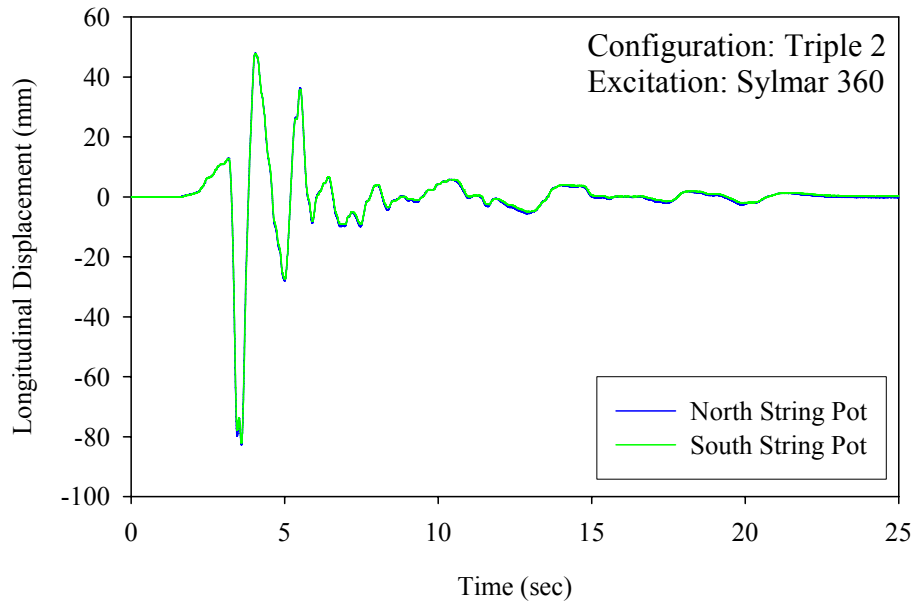
FIGURE 5-1   Histories of Longitudinal Displacement for a Large-Scale Representative Motion Demonstrating Negligible Torsional Motion of the Shake Table
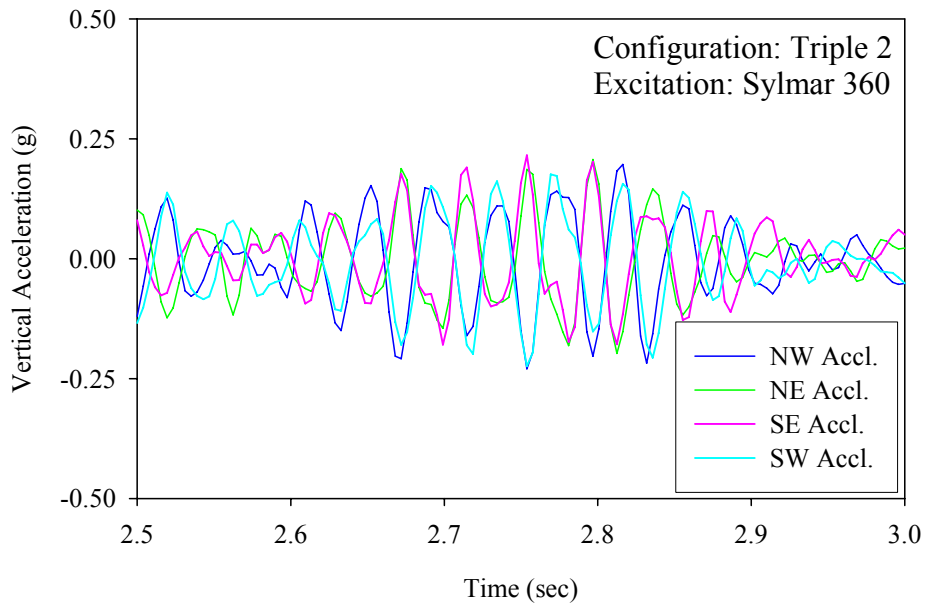
FIGURE 5-2 Histories of Vertical Acceleration for a Large Scale Representative Motion (Longitudinal Excitation Only) Demonstrating Rocking Motion of the Shake Table

90
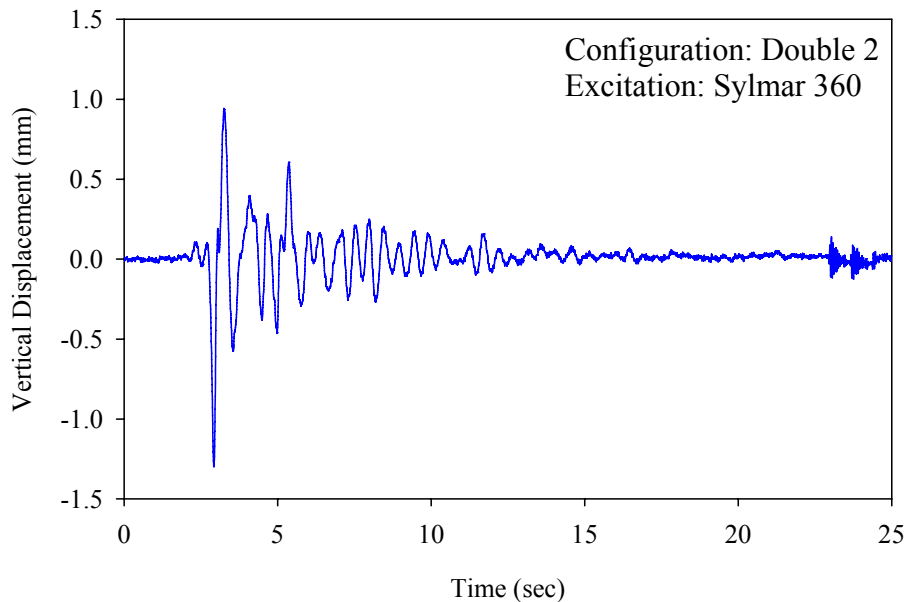
FIGURE 5-3 Histories of Vertical Displacement for a Large Scale Representative Motion (Longitudinal Excitation Only) Measured at the Base of the Southeast Load Cell that Demonstrates Rocking Motion of the Shake Table

(b) The isolation system displacements. The displacement values reported are the relative displacements of the basemat with respect to the table displacement, where the basemat displacements are calculated as the average of the displacement readings on each opposing side. For the 2007 test sequence, the displacement transducers were not zeroed prior to each test. In this way, the initial and permanent displacements from each test could be monitored. As described in figure 5-4, the maximum and minimum displacements reported are the maxima with respect to the absolute zero position from the start of the initial test. In the 2004 tests, the displacement channels were zeroed prior to each test. Therefore, the reported maximum displacement in the table for configuration double 1 is actually the peak travel displacement (the maximum between $max.-init.$ and $min.-init.$). For the 2007 tests it was important to continuously monitor initial and final displacements since materials of higher friction were used which resulted in larger permanent displacements. Low friction materials were used in the 2004 tests resulting in much smaller initial and permanent displacements.

(c) The maximum and minimum bearing vertical forces as measured directly from the load cells beneath each bearing. For the 2004 test sequence the force reported is the sum from all four isolators and for the 2007 test sequence the values reported are the maximum and minimum among the individual bearings.

91
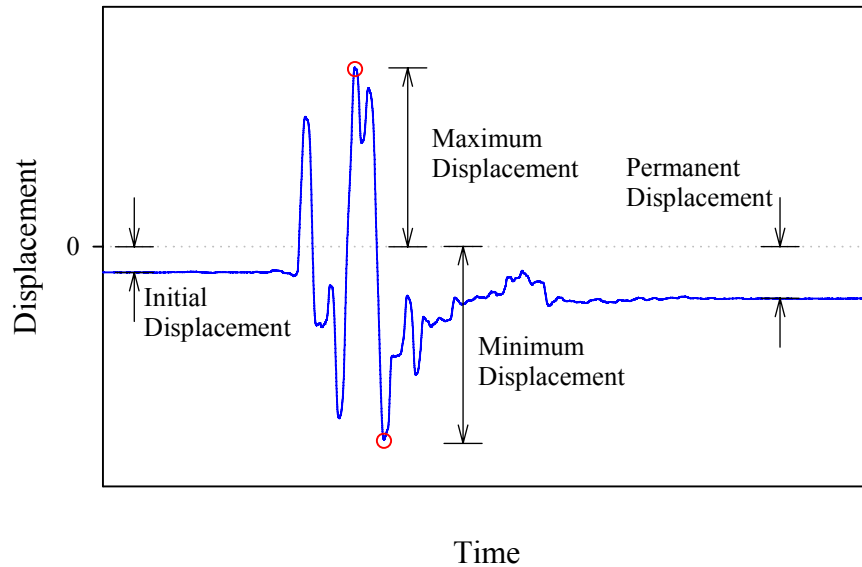
FIGURE 5-4 Description of Data Analysis for Bearing Displacement Histories

(d) The peak value of base shear normalized by structure weight. For the 2007 tests, the reported values in the tables are the sum of the shear forces measured directly from each load cell divided by the sum of vertical forces measured directly from each load cell. To validate the shear force data from the load cells, these values were checked against the shear force calculated as the product of floor mass and the corresponding acceleration. As shown in figure 5-5 for a representative motion, there is very good agreement between the values of base shear obtained using these two sources of data. The peak values are overestimated slightly by the accelerometer data since there is also a component of horizontal acceleration resulting from rocking motion atop the flexible basemat.

For the 2004 tests, the values of shear force reported are the product of the floor mass and the corresponding floor acceleration. The shear force from the accelerometer data was also used to construct the hysteresis loops for the double 1 configuration throughout this report. There was noticeable error in the shear force data from the load cells due to crosstalk. Evidence of this error can be seen in figures 5-6 and 5-7. The shear force from the load cells is substantially less than the shear force calculated using the acceleration data. This is most noticeable in the hysteresis loops, where the post-elastic stiffness using the load cell data is substantially less than the theoretical value based on the effective radius. The post-elastic stiffness in the loops obtained using the accelerometer data matches nearly exactly the theoretical value.

The error in the stiffness calculated using the load cell data means that there is increased error in the shear force measurement as the displacement (and accordingly the overturning moment) increases. This indicates crosstalk in the shear and overturning moment readings. Crosstalk is essentially coupling between

92

the various readings of a multi-axis load cell. This means, for example, that an applied overturning moment will cause spurious (either additive or in this case subtractive) shear force readings. The crosstalk in this case was likely caused by misalignment of the strain gauges. Between the 2004 and 2007 test sequences, the load cells were completely re-gauged and this problem was resolved.
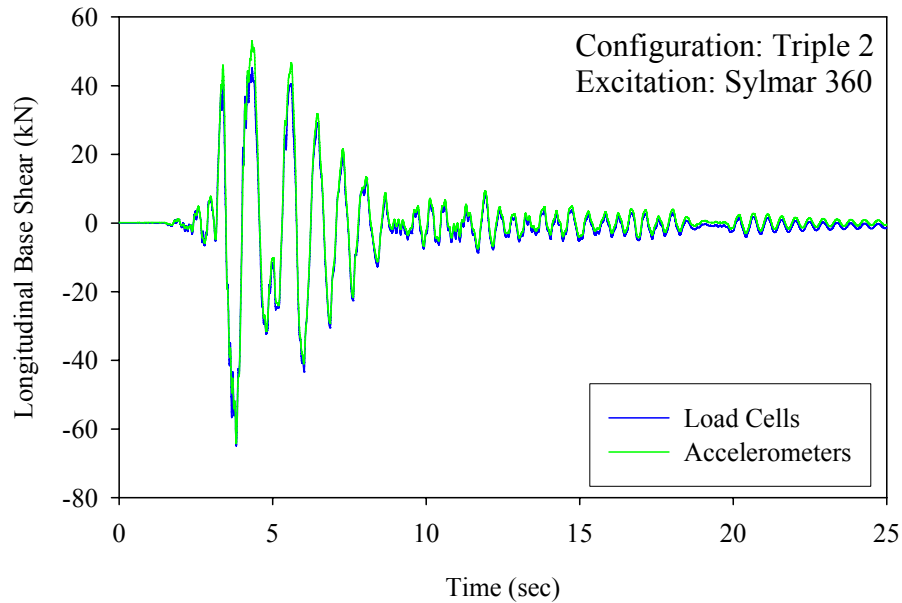
FIGURE 5-5 Comparison Between Base Shear Determined Directly from Load Cell Readings and Calculated Using the Acceleration Data from the 2007 Test Sequence
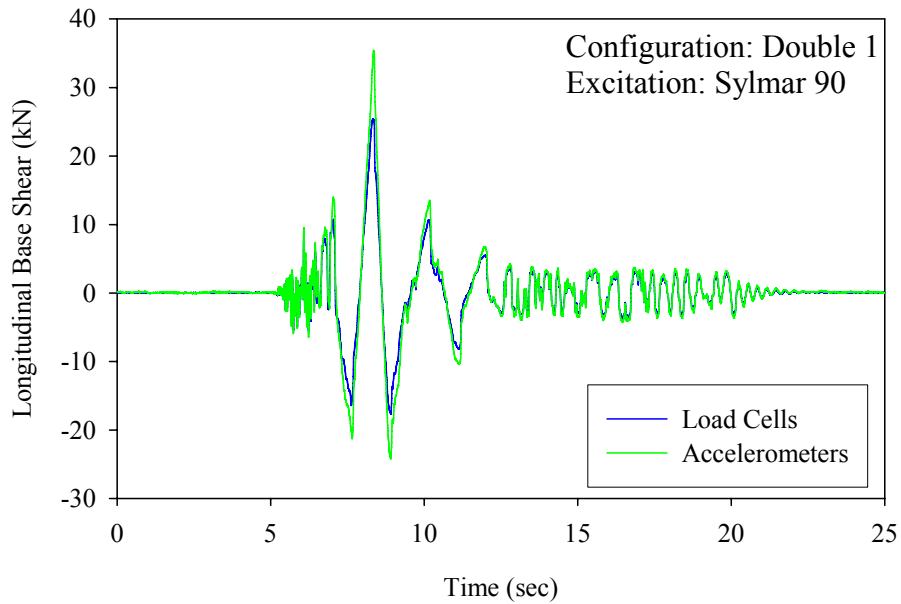
FIGURE 5-6 Comparison Between Base Shear Determined Directly from Load Cell Readings and Calculated Using the Acceleration Data from the 2004 Test Sequence
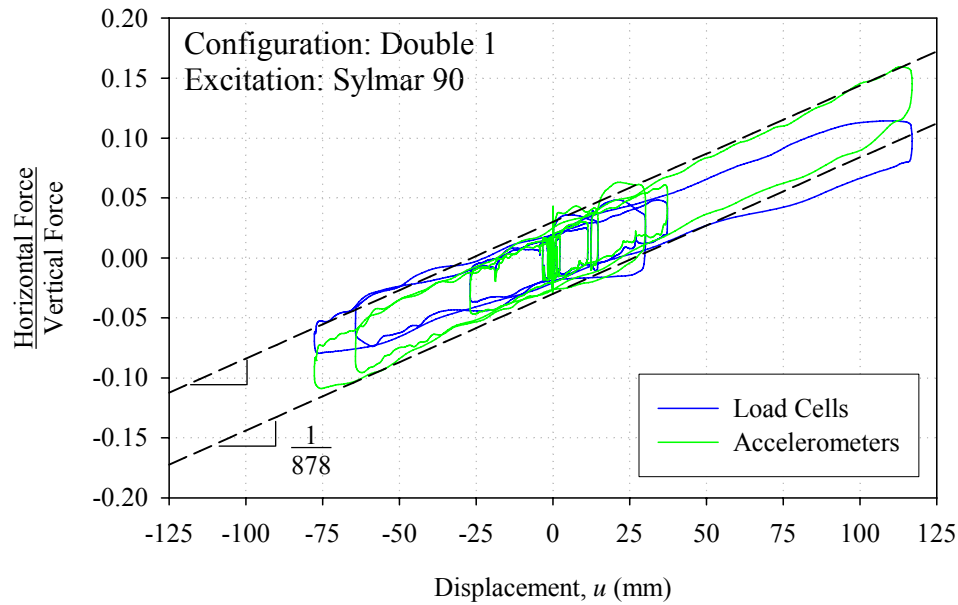
FIGURE 5-7   Comparison of Hysteresis Loops Using Base Shear Determined Directly from Load Cell Readings and from Acceleration Data to the Theoretical Stiffness using R_{eff}, $W/878$ kN/mm (2004 Test Sequence)

(e) The peak absolute floor acceleration and the corresponding floor. The acceleration of each floor measured directly from the accelerometers and determined as the average of the two readings on opposing sides of the structure model.

(f) The peak inter-story drift and the corresponding floor. The displacements of each floor measured directly from the string pots and determined as the average of the two readings on opposing sides of the structure model.

Normalized force-displacement loops of each isolation system from unidirectional testing are presented in figures 5-8 through 5-14. The loops highlight the significant differences in hysteretic behavior between the various systems. Lastly, to evaluate the response of secondary systems and nonstructural components, the 5% damped floor response spectra of the sixth-story, third-story and base of the moment frame are shown in figures 5-15 through 5-22 (the Double 1 configuration is excluded from the plots as it was tested using the braced frame model).

94
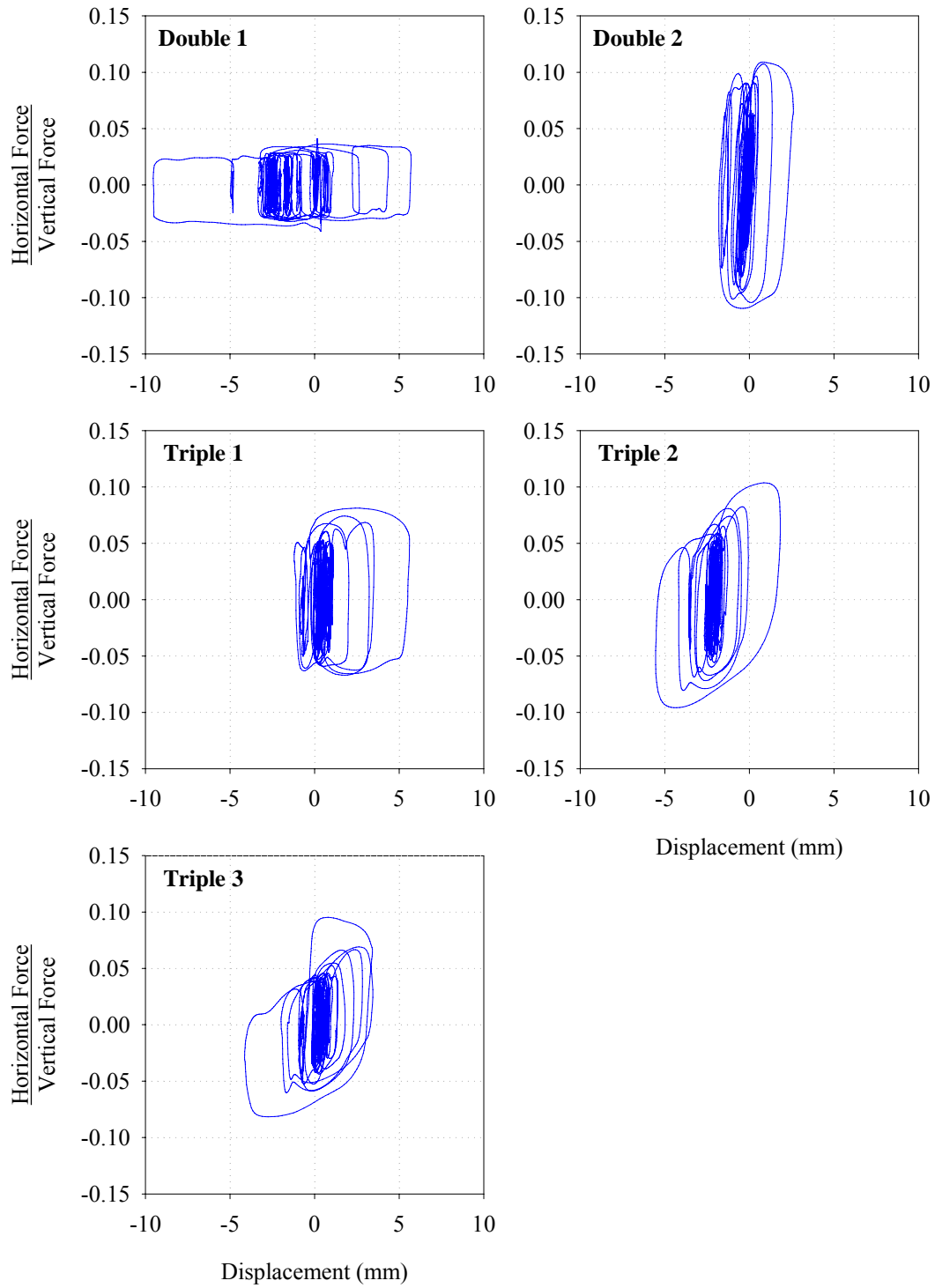
FIGURE 5-8 Hysteresis Loops from Each Isolation System when Tested with Ground Motion Taft 021

95
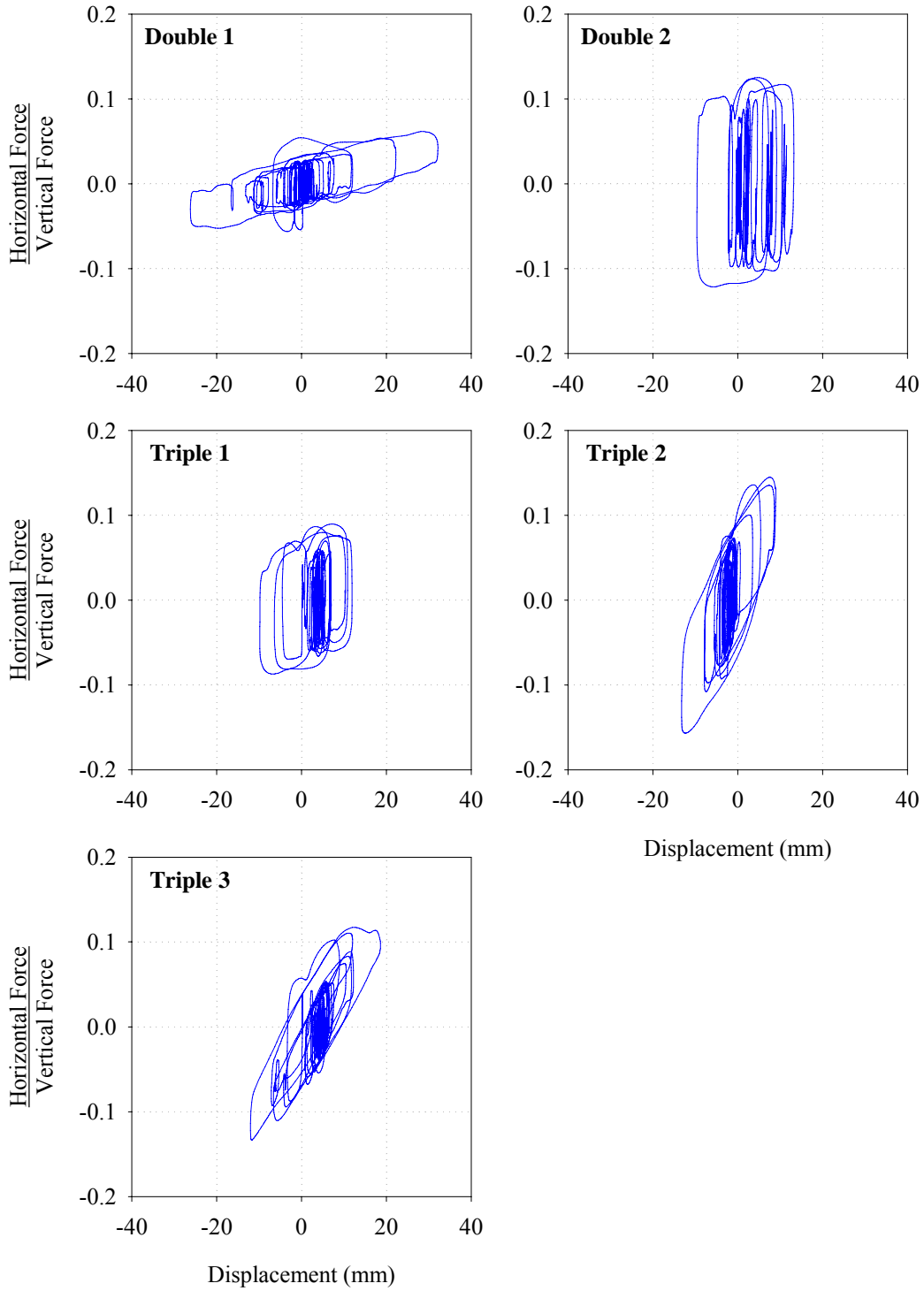
FIGURE 5-9 Hysteresis Loops from Each Isolation System when Tested with Ground Motion El Centro 180
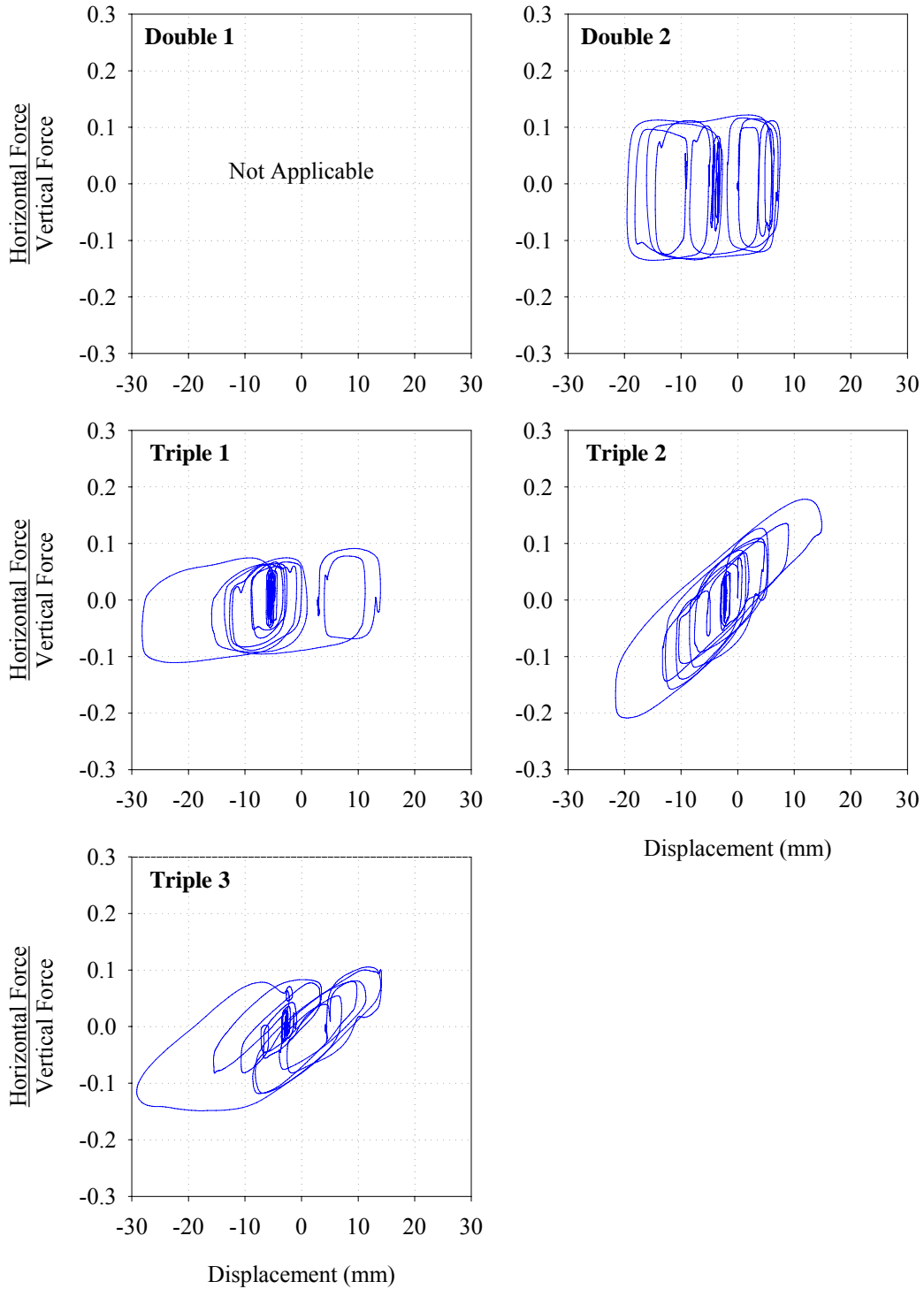
FIGURE 5-10 **Hysteresis Loops from Each Isolation System when Tested with Ground Motion Corralitos 090**

97
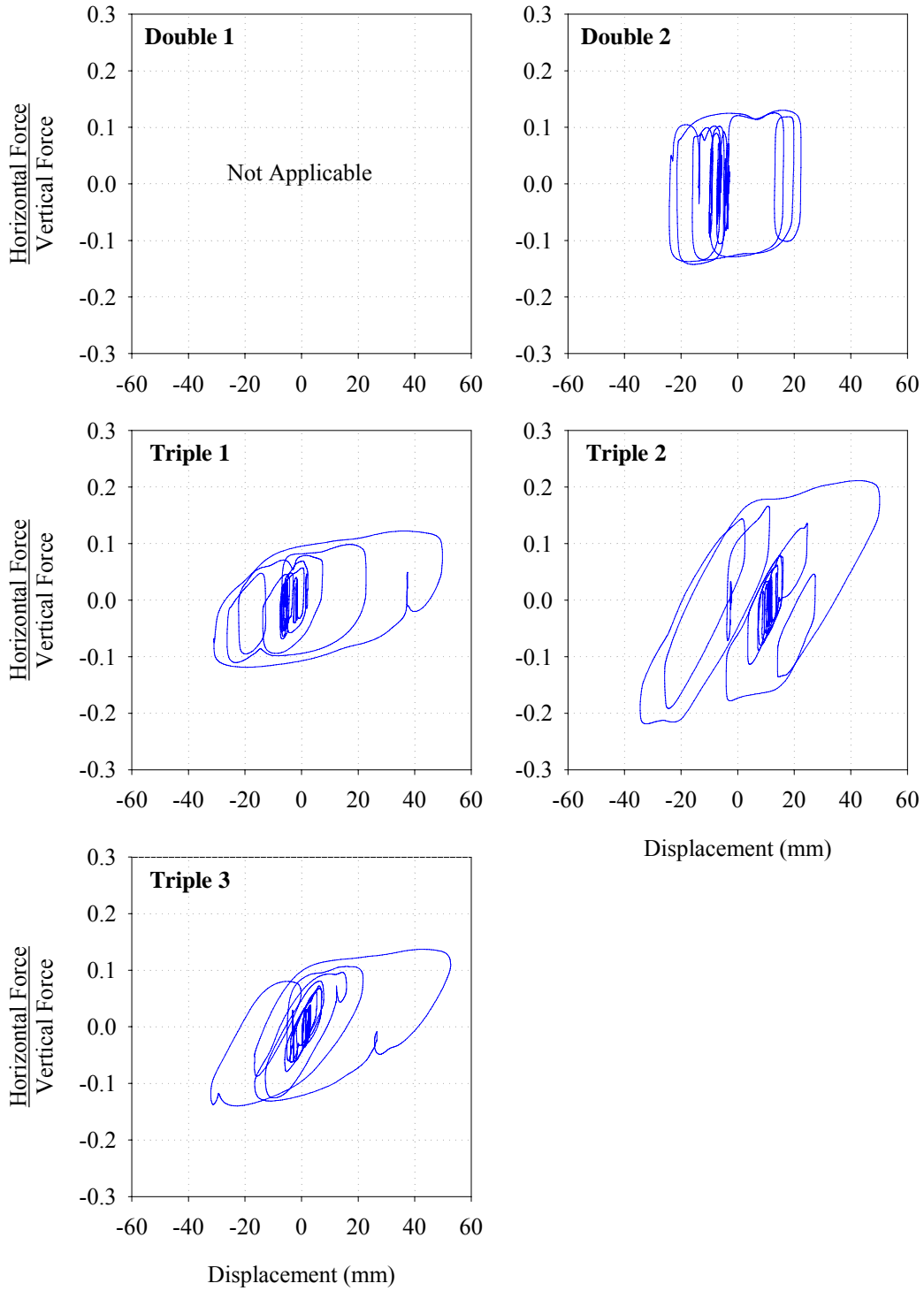
FIGURE 5-11   Hysteresis Loops from Each Isolation System when Tested with Ground Motion Kocaeli 330
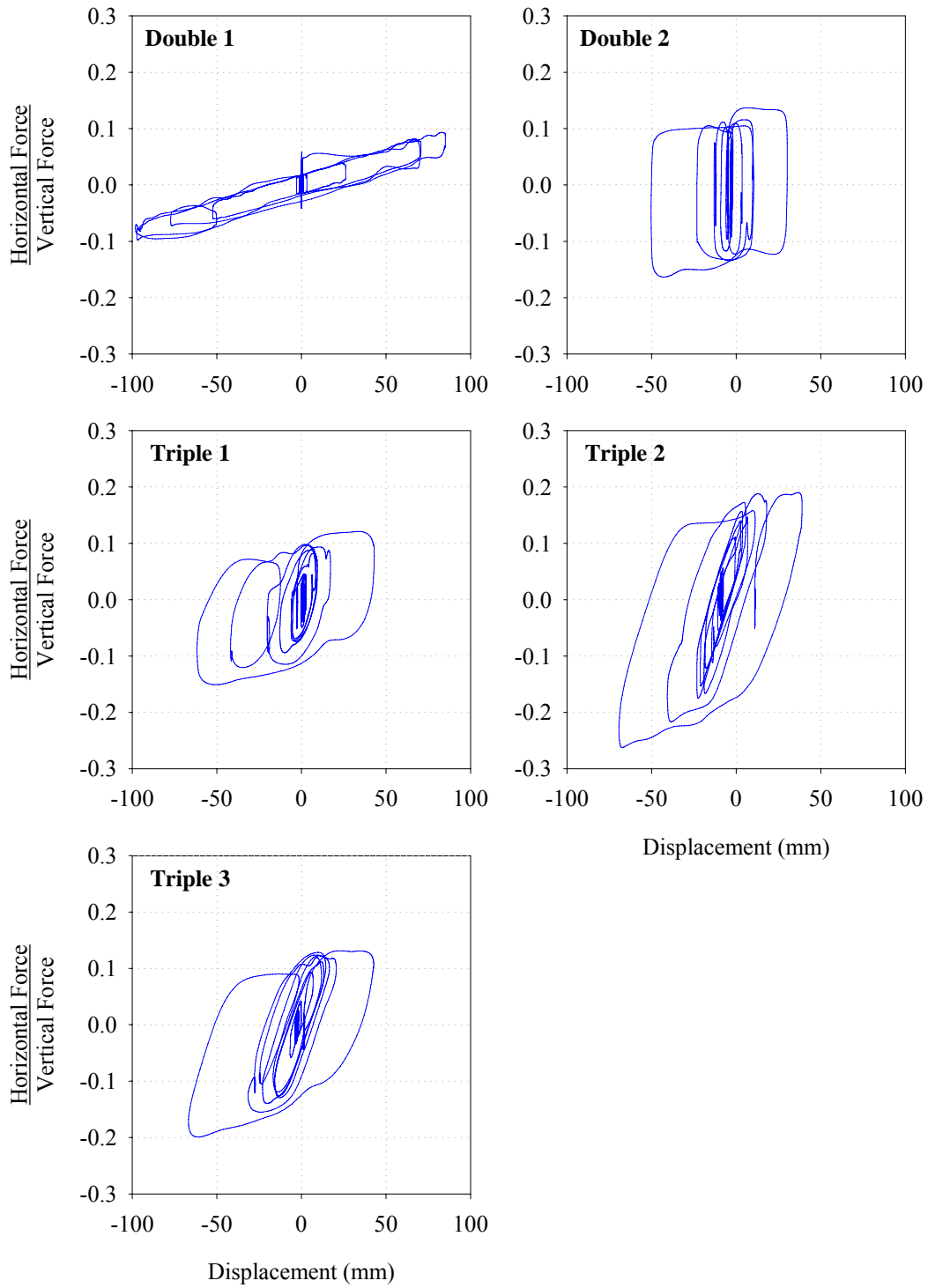
FIGURE 5-12 Hysteresis Loops from Each Isolation System when Tested with Ground Motion Newhall 360
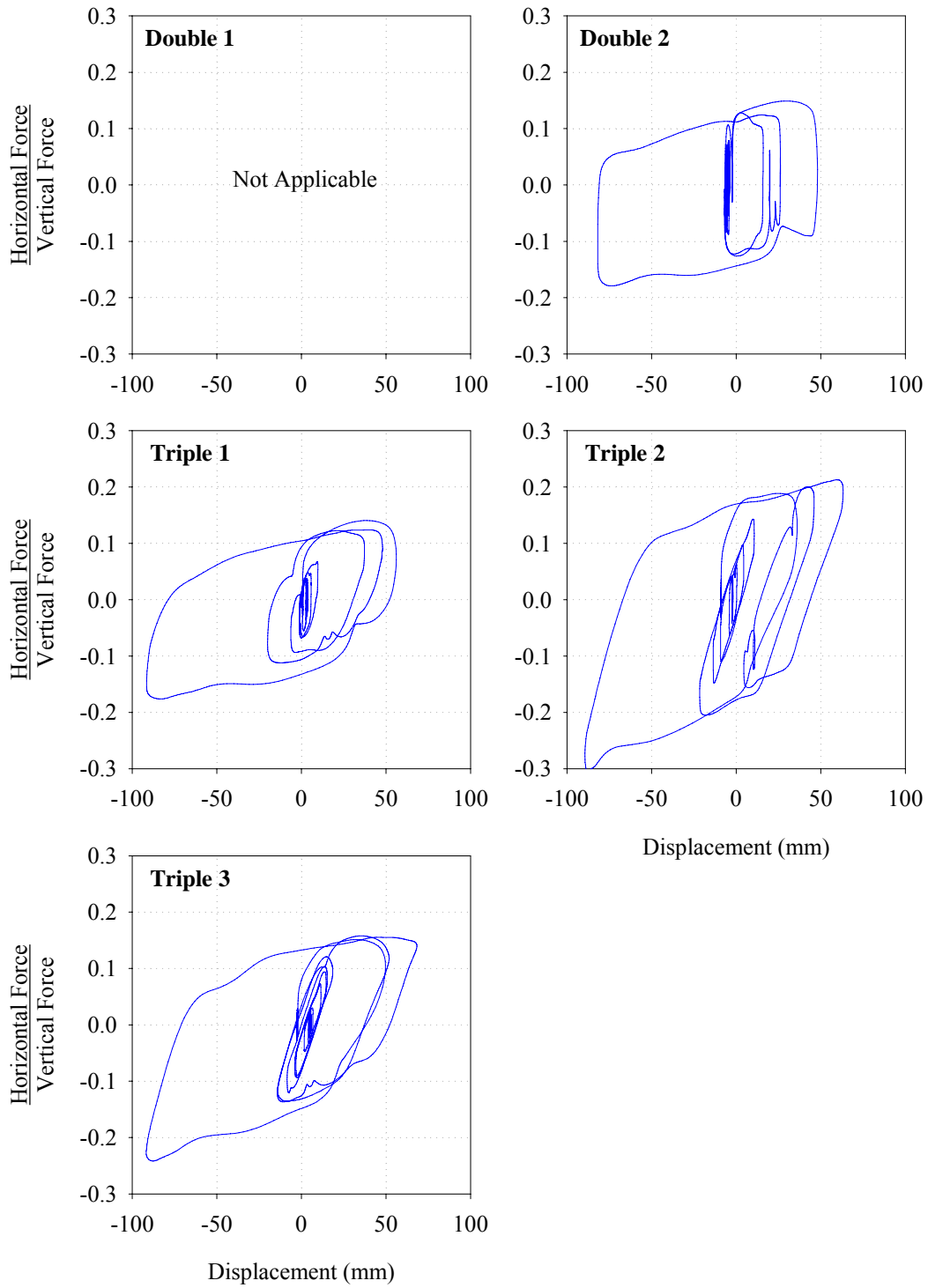
FIGURE 5-13 Hysteresis Loops from Each Isolation System when Tested with Ground Motion Sylmar 360
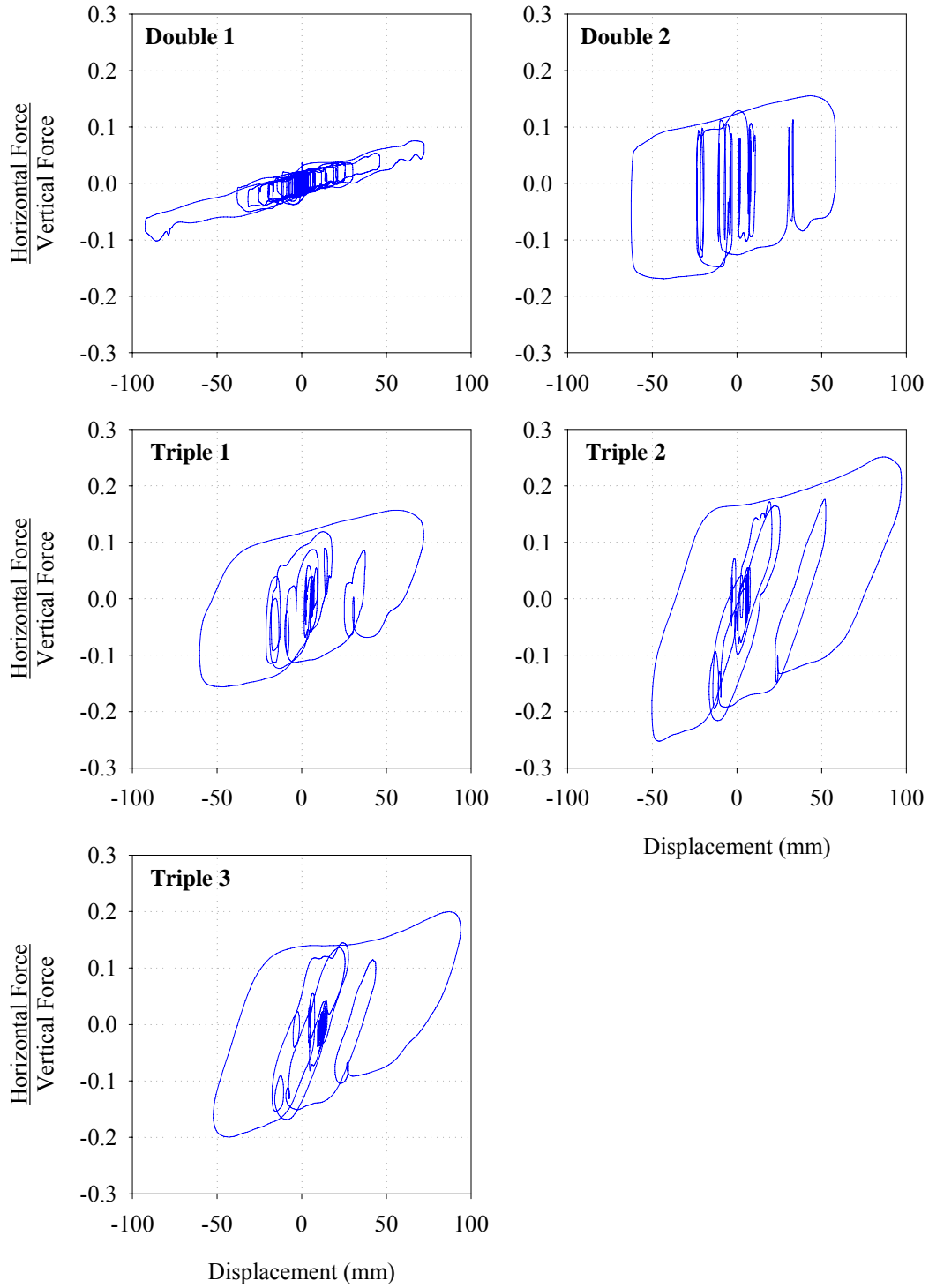
FIGURE 5-14 Hysteresis Loops from Each Isolation System when Tested with Ground Motion Pacoima 164

101
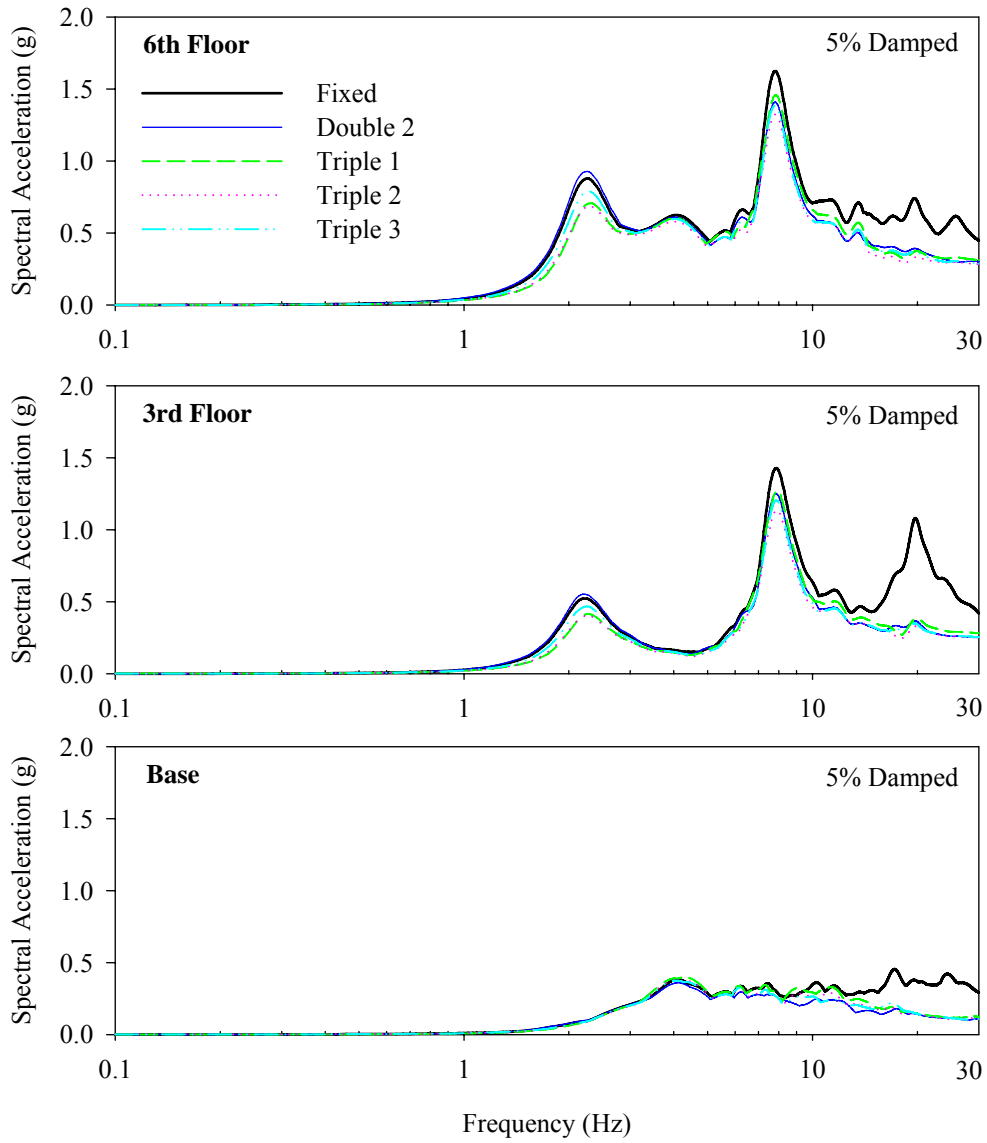
FIGURE 5-15 Floor Response Spectra for Each Isolation System from Testing of Moment Frame Specimen with Ground Motion Wrightwood 115
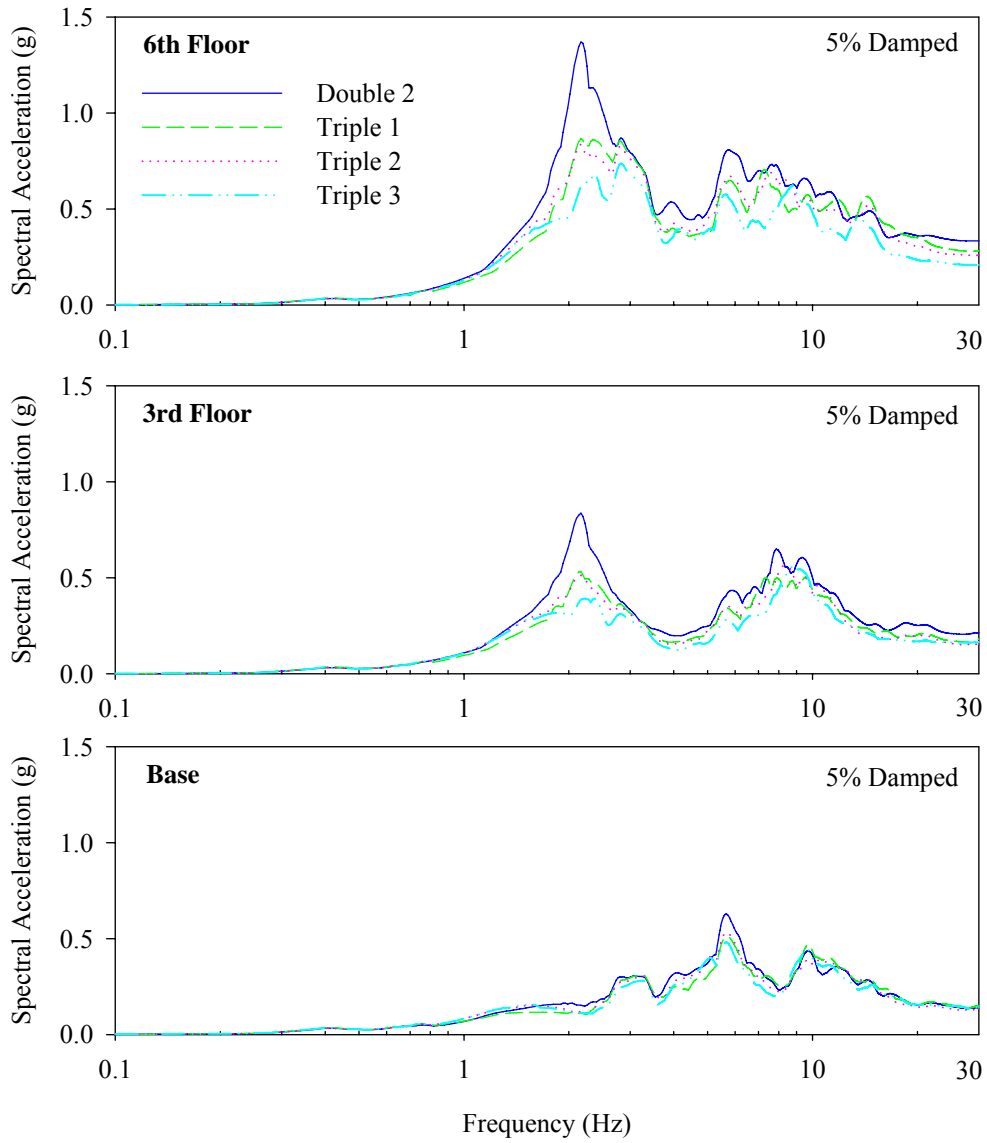
FIGURE 5-16 Floor Response Spectra for Each Isolation System from Testing of Moment Frame Specimen with Ground Motion Taft 021
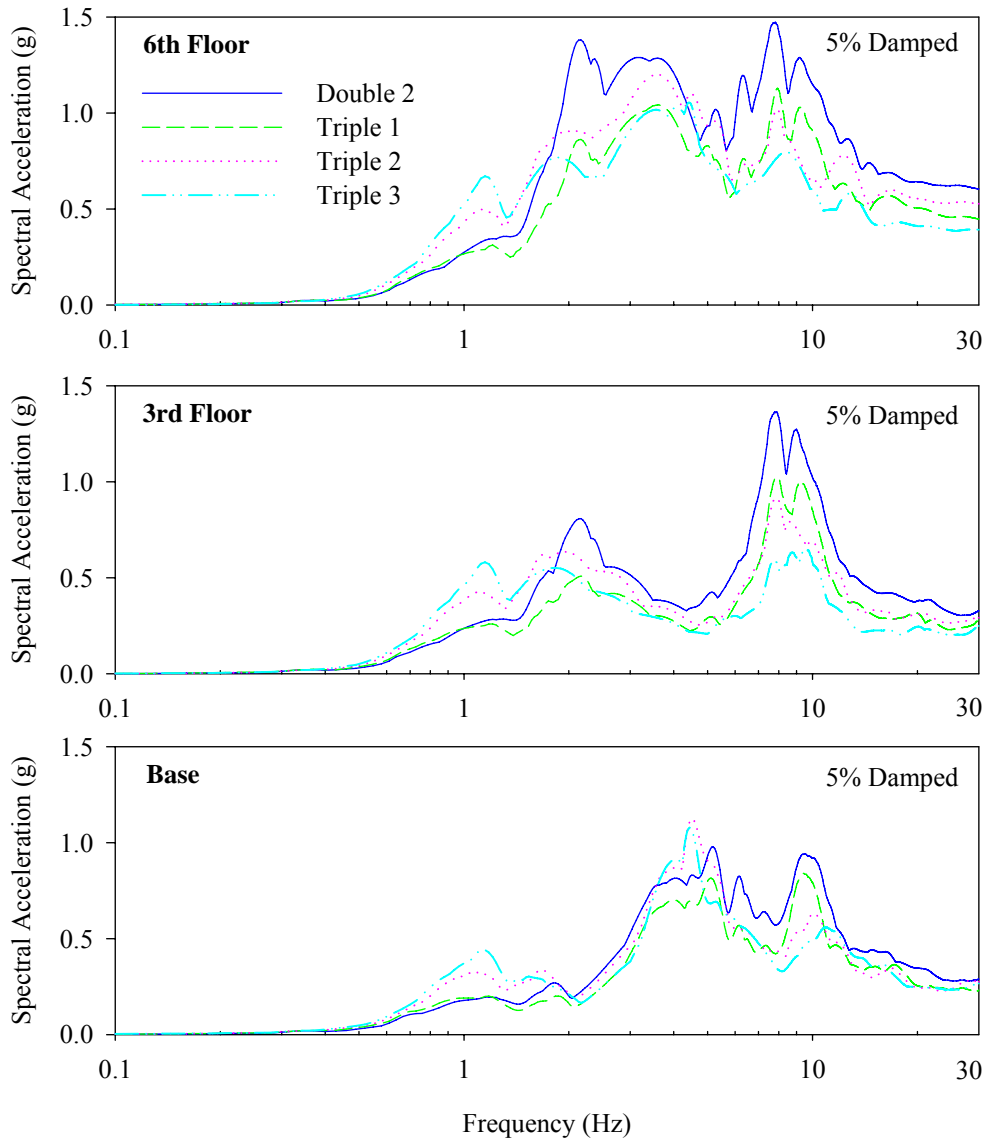
FIGURE 5-17 Floor Response Spectra for Each Isolation System from Testing of Moment Frame Specimen with Ground Motion El Centro 180
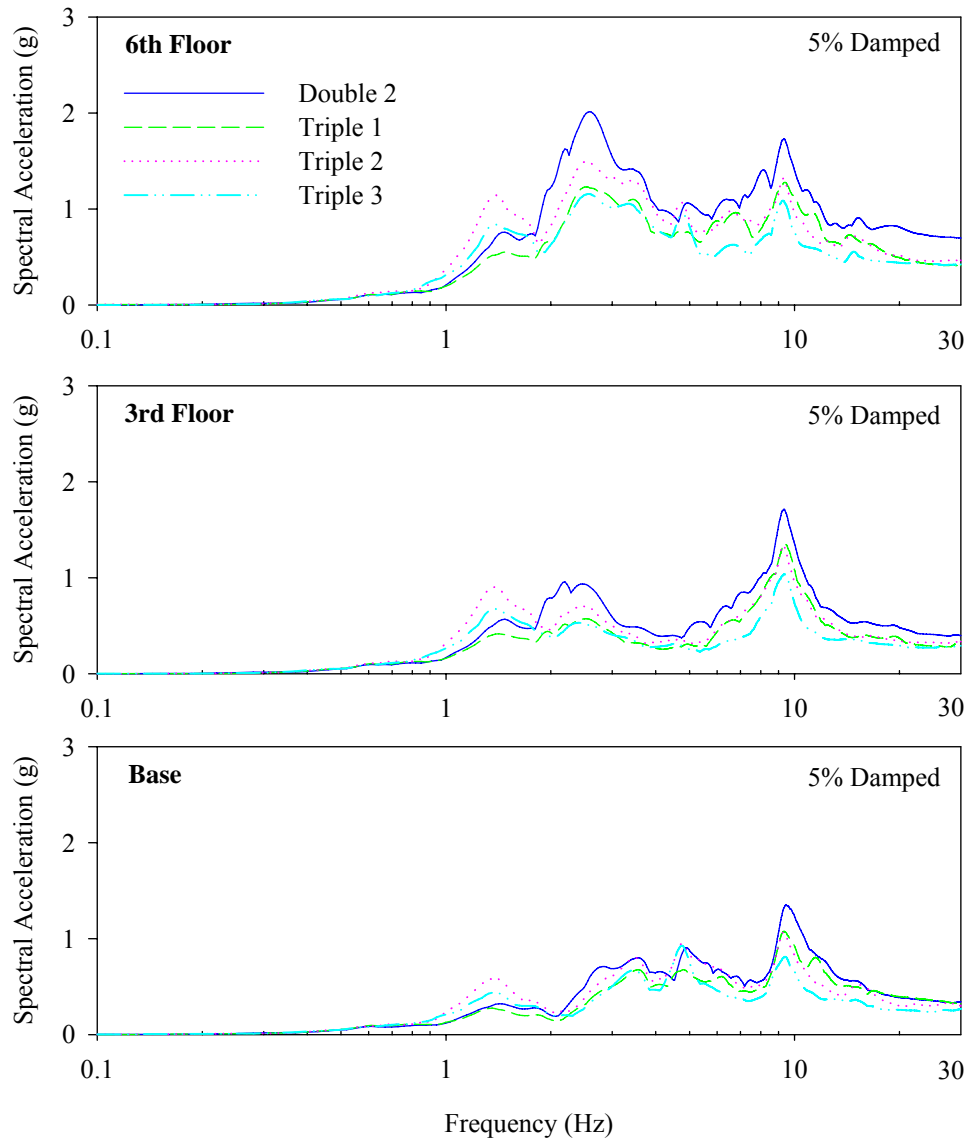
FIGURE 5-18   Floor Response Spectra for Each Isolation System from Testing of Moment Frame Specimen with Ground Motion Corralitos 090
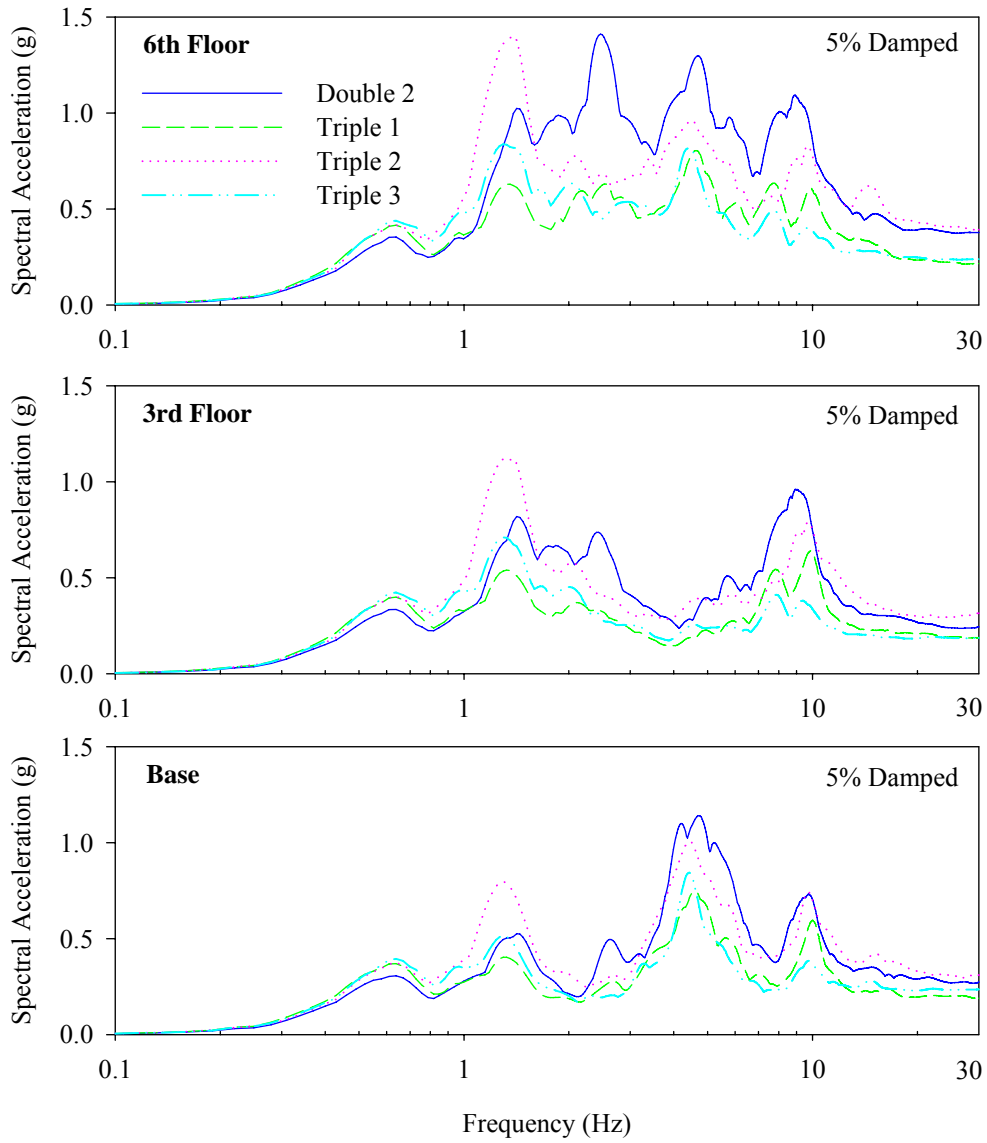
FIGURE 5-19 Floor Response Spectra for Each Isolation System from Testing of Moment Frame Specimen with Ground Motion Kocaeli 330
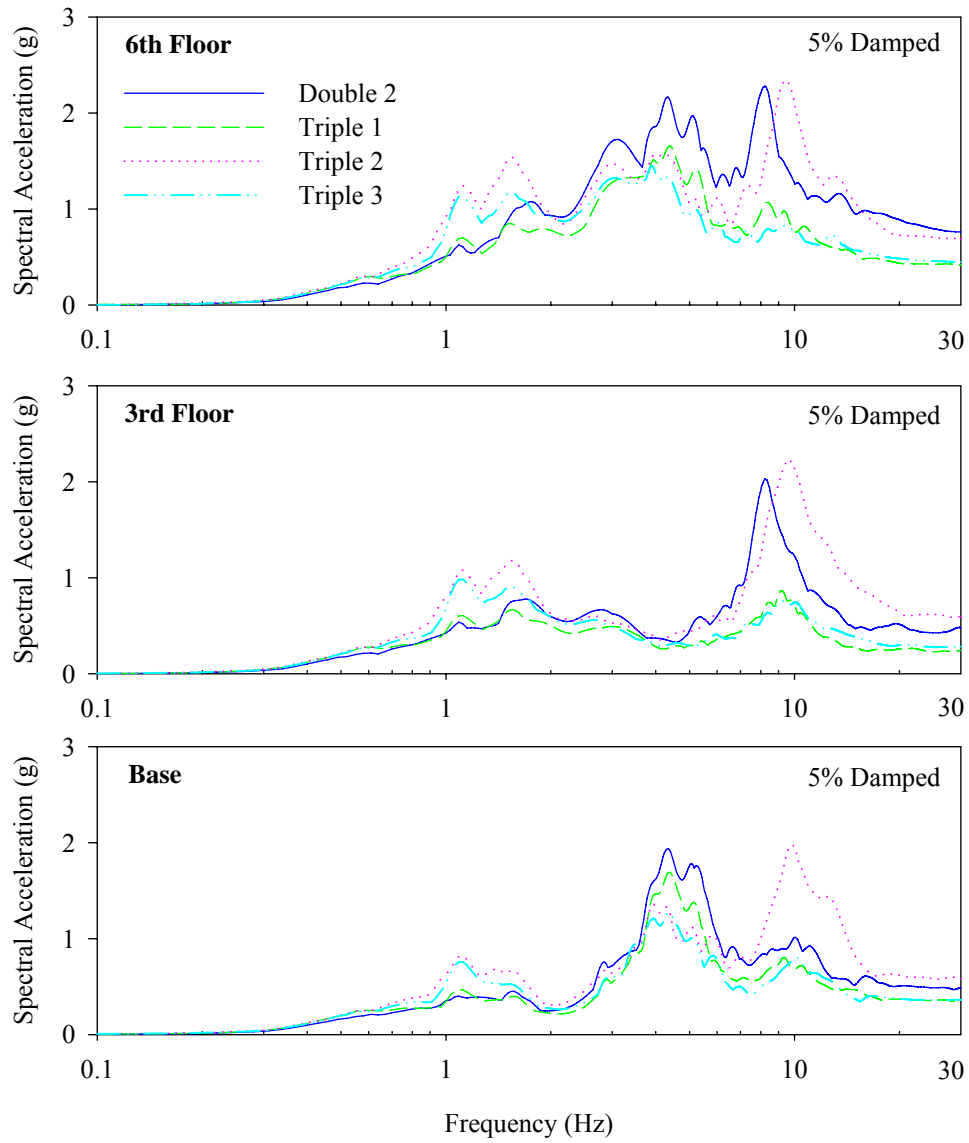
FIGURE 5-20   Floor Response Spectra for Each Isolation System from Testing of Moment Frame Specimen with Ground Motion Newhall 360
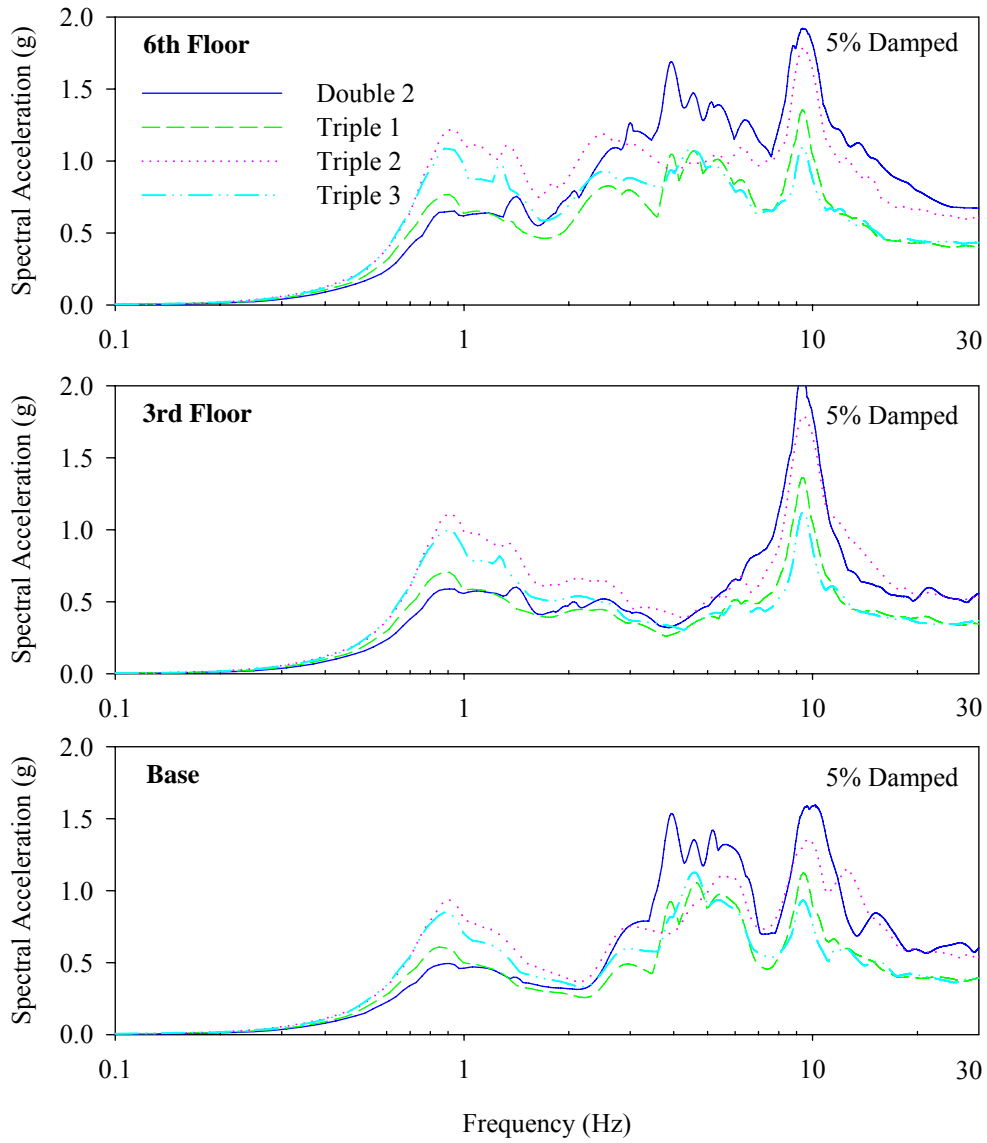
FIGURE 5-21 Floor Response Spectra for Each Isolation System from Testing of Moment Frame Specimen with Ground Motion Sylmar 360
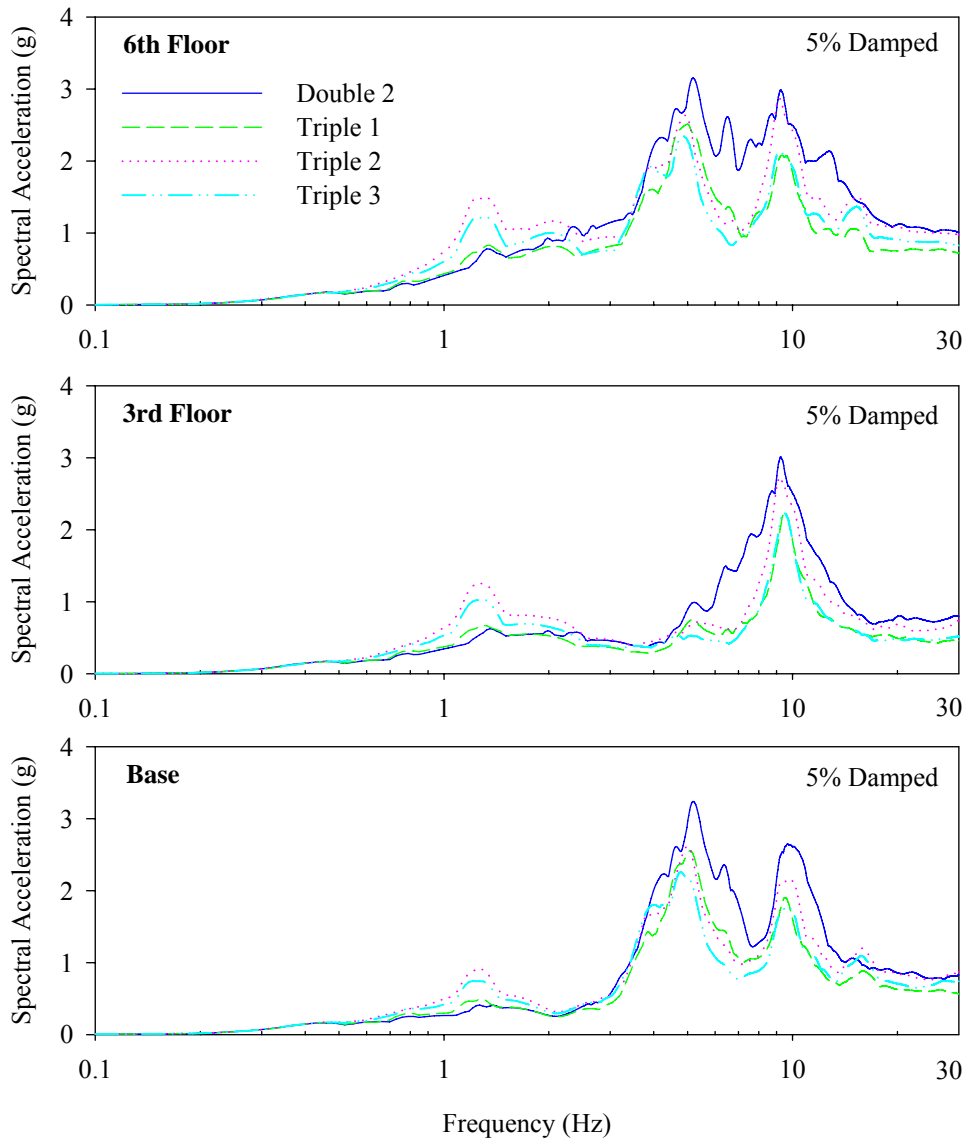
FIGURE 5-22 Floor Response Spectra for Each Isolation System from Testing of Moment Frame Specimen with Ground Motion Pacoima 164

5.4 Comments on Results

5.4.1 Effect of Vertical Motion

Past studies of the traditional single FP system have found that if vertical components of excitation are present there is little or no dynamic amplification of the motion within the structure due to the vertical rigidity of the bearing (Zayas *et al.*, 1987; Constantinou *et al.*, 1993; Mosqueda *et al.*, 2004). Furthermore, it has been observed that the addition of vertical motion has little impact on lateral response due to the fact that the vertical

components of motion are typically of high frequency and short duration. Furthermore, the peaks of the horizontal and vertical components occur at different times.

Similar trends were observed in this study as in the past due to the fact that multi-spherical sliding bearings have similar vertical rigidity as the traditional FP bearing. The differences in peak displacement response, peak base shear and peak superstructure response were very minor when the vertical component of ground motion was added. Although still minor, the differences were slightly more noticeable for the triple FP configurations. This is due to the fact that the addition of the vertical component induces a wider variation in axial load on the isolators; this is evident from tables 5-2 through 5-6. This means that there is a larger variation in the (pressure dependent) coefficient of friction on each surface, which controls when motion initiates on the various concave surfaces. Since the addition of the vertical component changes the instants at which motion starts on the various surfaces, it is not surprising that the differences are slightly larger in comparison to the non-adaptive double FP configuration.

5.4.2 Uplift of Double and Triple FP Bearings

Shake table testing proved a very valuable means of investigating the behavior of multi-spherical sliding bearings under uplift conditions. Since the sliders consist of an assembly of parts that are not mechanically connected, engineers have been understandably concerned about the safety and stability of these devices when uplift occurs. Furthermore, tests under uplift or near uplift conditions are very demanding analytically and are consequently excellent tests of the dynamic analysis methods.

The most compelling evidence for the overall safety of these devices under extreme conditions comes from testing of the Double 1 configuration with 200% of the El Centro ground motion applied tri-directionally. This test was accidentally conducted at increased amplitude of motion without prior evaluation of the displacement demand. The histories of displacement and bearing axial force from this test are presented in figures 5-23 and 5-24 respectively (in figure 5-23, the actual displacement capacity of the isolation system calculated based on equation (2-15) was 141mm; slightly less than the nominal value of 150mm due to the effects of slider height and rotation). In this test the displacement demand exceeded the capacity of the isolation system and there was simultaneously substantial contact of the slider with the displacement restrainer and significant uplift. The uplift displacements were likely magnified due to the impact, which induced rigid body rocking motion of the model. The rocking motion is a result of the 4 bearing isolation system, and differs from the uplift in typical structures with numerous bearings where the uplift is a result of structural deformation. The peak base shear and peak acceleration response are much larger due to the impact, but still significantly less that what would result if the fixed base structure were subjected to the same motion. Moreover, without the displacement restrainer, the isolators would have dislodged, with the slider moving beyond the concave surface, and likely bring about the collapse of the model.
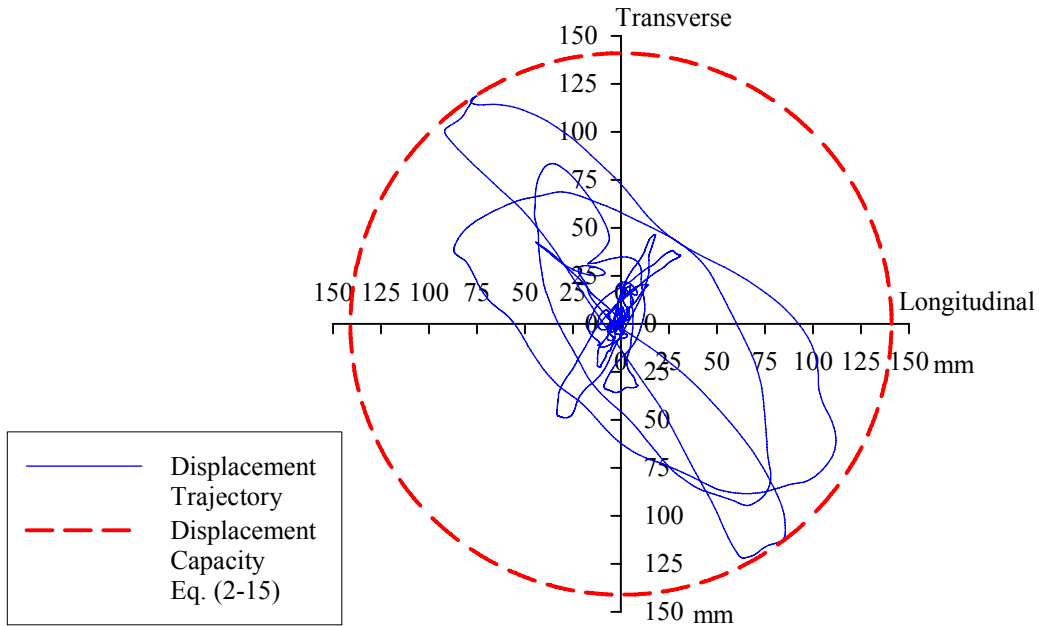
(a)
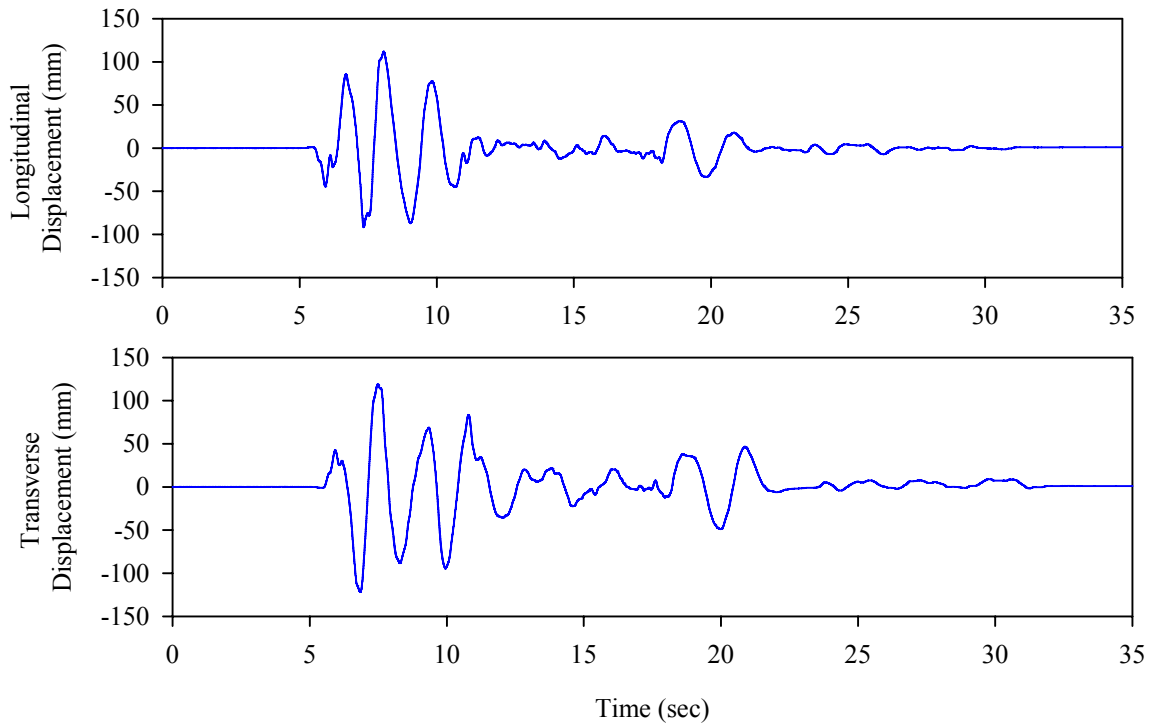
(b)

FIGURE 5-23 (a) Displacement Orbit and (b) Histories of Longitudinal and Transverse Displacements of SE Bearing from 200% El Centro Tridirectional Test of Double 1 Isolation System
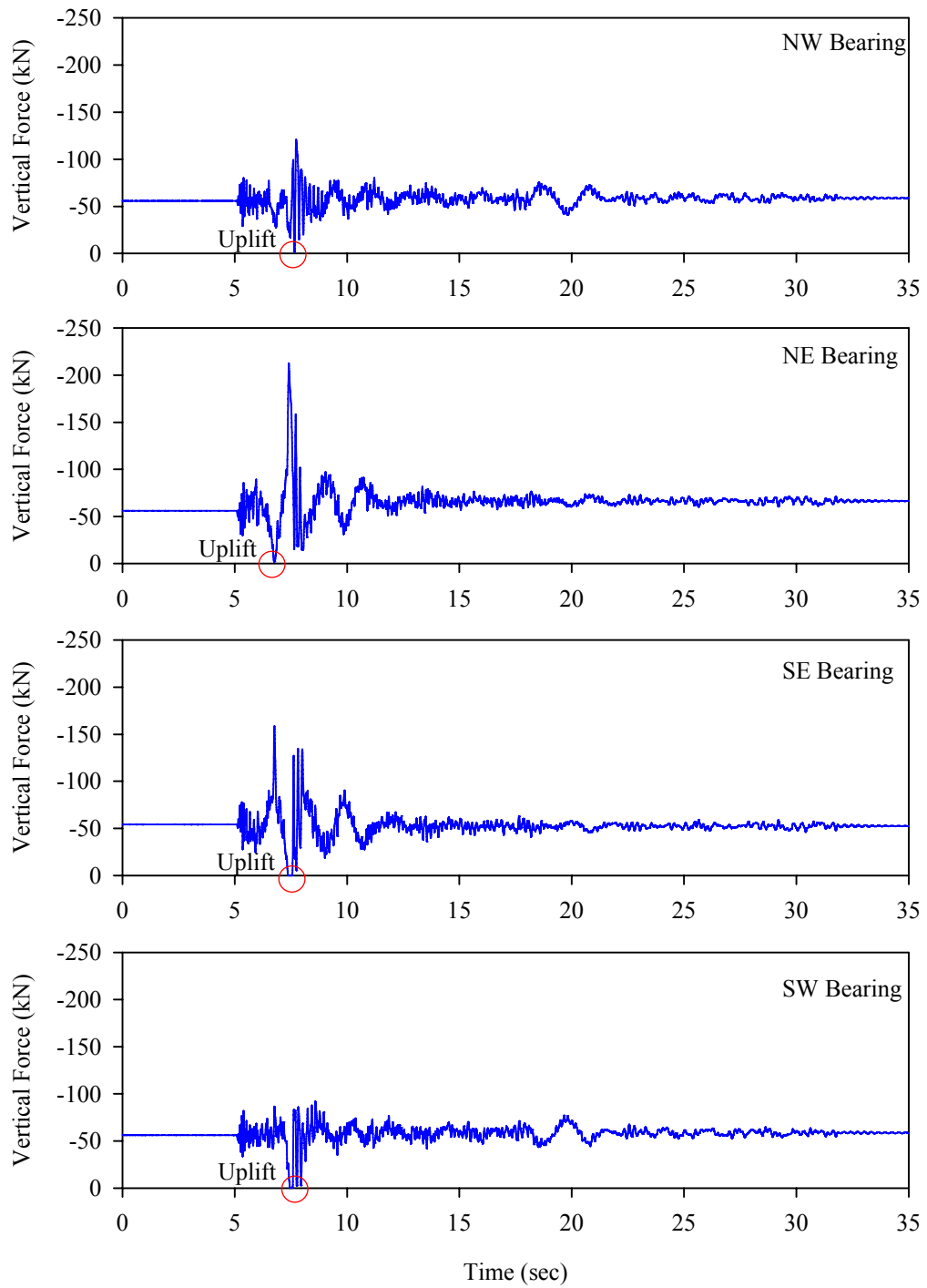
FIGURE 5-24   Histories of Bearing Vertical Force from 200% El Centro Tridirectional Test of Double 1 Isolation System

Data from the Krypton coordinate tracking camera (up to the point at which the stream from the LED was lost due to the impact) is shown in figure 5-25 and indicates that there was over 27mm of vertical movement of the top end plate with respect to the bottom end plate. The vertical displacement due to the curvature of the concave plates is approximately 10mm at a displacement of 140mm, meaning the uplift or separation displacement was 17mm. The uplift behavior can clearly be seen in figure 5-26, which tracks the frame by frame the sequence of uplift and displacement restrainer contact from this test.

FIGURE 5-25 History of Vertical Displacements Relative to the Bottom Concave Plate of Various Parts of the SE Bearing in the 200% Tridirectional El Centro Test

Based on the data in figure 5-25 and the visual evidence in figure 5-26, it appears that the articulated slider remains on the lower concave plate when the large uplift displacements occur. The histories of slider vertical displacement show displacements in the initial part of the test due to sliding up the bottom concave surface, but do not show the slider following the path of the upper plate. This is corroborated in frames 5 through 8 of figure 5-26. The separation between the top concave plate and the slider is clearly visible; however there appears to be no relative motion between the slider and the bottom concave plate. Furthermore, despite the fact that there is no mechanical connection between them, there is no apparent separation between the upper and lower halves of the slider. This is demonstrated by the identical histories of vertical displacement of the upper and lower halves. This also makes sense physically, since there is no force causing the different parts of the slider to separate.

Upon returning from uplift, the bearing is able to resume normal operation. As shown in the final frames of figure 5-26, the top concave plate sets back down on the slider without causing it to topple over or become unstable in anyway. Even after this very serious episode of uplift, the isolation system functioned properly for the remainder of the excitation, including recentering to the initial position. The isolation system preformed normally for the remainder of the test program without need of any repairs, aside from reattaching the LED. The remaining tests included various severe multi-component excitations.

113
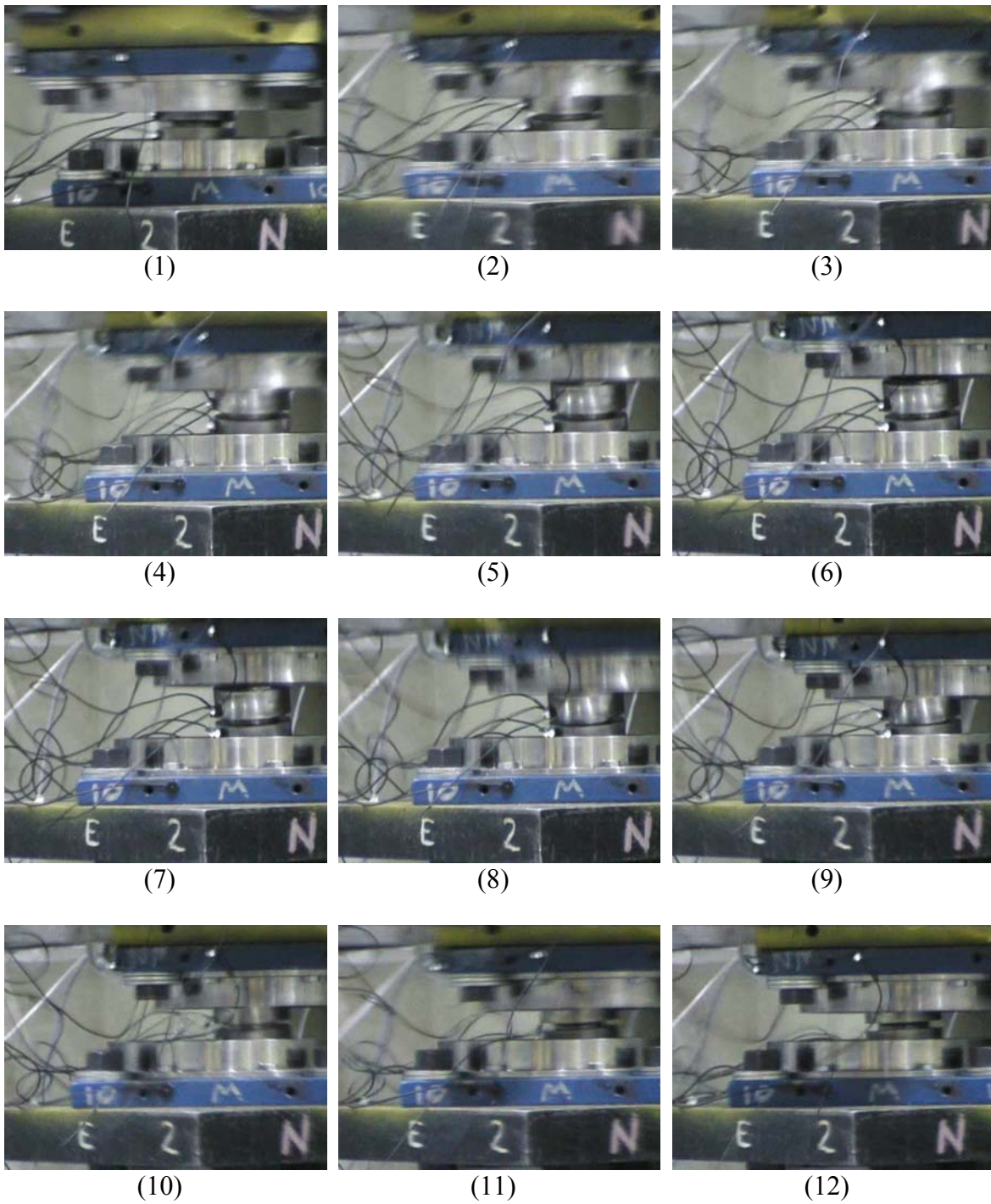
FIGURE 5-26 Frame by Frame Sequence Showing Contact with the Displacement Restrainer and Uplift of SE Bearing in Isolation System Double 1

Uplift of double and triple FP bearings can be particularly serious if the vertical separation displacement exceeds the height of the displacement restrainer ring. If the slide plate is in contact with the displacement restrainer (which is part of the normal course of operation) and a large uplift displacement occurs, it is possible for the concave plate and restrainer to rise over the edge of the slider as shown in figure 5-27 for the triple FP bearing with the higher friction material on the bottom surface. When the upper concave plate returns back down the displacement restrainer can land atop the slide plate damaging the liner material or even causing the slider to become unstable. In the worst case the upper concave plate can land completely outside of the slider causing the bearing to completely lose its lateral functionality-although this is an unlikely event due to the large size of the slider.

Although a similar circumstance occurred in the previously described tridirectional El Centro test of the double FP (simultaneous contact with the displacement restrainer and uplift), the situation was not as serious since the top plate rose up and down nearly vertically. This is due to the fact that the uplift occurred after, or as a result of, the bearing reaching the full displacement capacity. When the isolation system hit both displacement limits, its horizontal motion essentially stopped. Therefore, when the vertical separation occurred, there was little or no horizontal momentum to cause the bearing to land out of alignment. In contrast, for the triple FP, it is possible to still have large sliding velocities when one of the slide plates is in contact with the displacement restrainer since sliding can be occurring on the other surface. If there is uplift under these circumstances there can be considerable lateral movement when the top part of the bearing is airborne causing it to land askew.

For this reason the maximum uplift displacement, with some margin of safety, should be used to size the height of the restrainer ring. Ideally, analysis programs will be able to predict this quantity since gap behavior is assumed in the vertical direction (this will be addressed in the following section). However, appropriate caution should be exercised in assessing its validity due to the localized nature of this type of response. As an added margin of safety, it would be considered good practice when outer concave surfaces of unequal friction are used to use the higher friction material on the top surface. This follows from the previous observation of the slider components remaining together and in contact with the bottom concave surface when the uplift occurs. In this way the slide plate that more commonly contacts the displacement restrainer ring will be on the bottom. If separation and horizontal translation occur the upper slide plate will be more likely to end up within the displacement restrainer when the bearing lands since it is not already at the displacement limit.

Due to a malfunction of the Krypton system's controller during the 2007 testing, coordinate tracking was only possible for the Triple 1 configuration. Although this was not the most demanding configuration in terms of uplift, the behavior was observed during the tridirectional Newhall test. Uplift can actually be heard during testing due to the metallic pinging sound caused by the impact of the various parts. Histories of the isolation system's displacement and each bearing's vertical force are presented in figures 5-28 and 5-29. The displacement demands were small enough so that there was no

contact with the displacement restrainer when the uplift occurred. The vertical displacement history of the SE bearing is presented in figure 5-30. At the time uplift occurred in this bearing, its total lateral displacement was 78mm resulting in approximately 3mm of vertical displacement from sliding up the concave surfaces. Therefore there were approximately 2mm of separation.

Assume Motion to the Right

1.) Slide plate comes into contact with restrainer

2.) Uplift occurs with the concave plate lifting over the displacement restrainer

3.) Horizontal translation of the top plate continues

4.) Upon landing, the restrainer impacts the slider causing damage to the liner material and/or bearing components
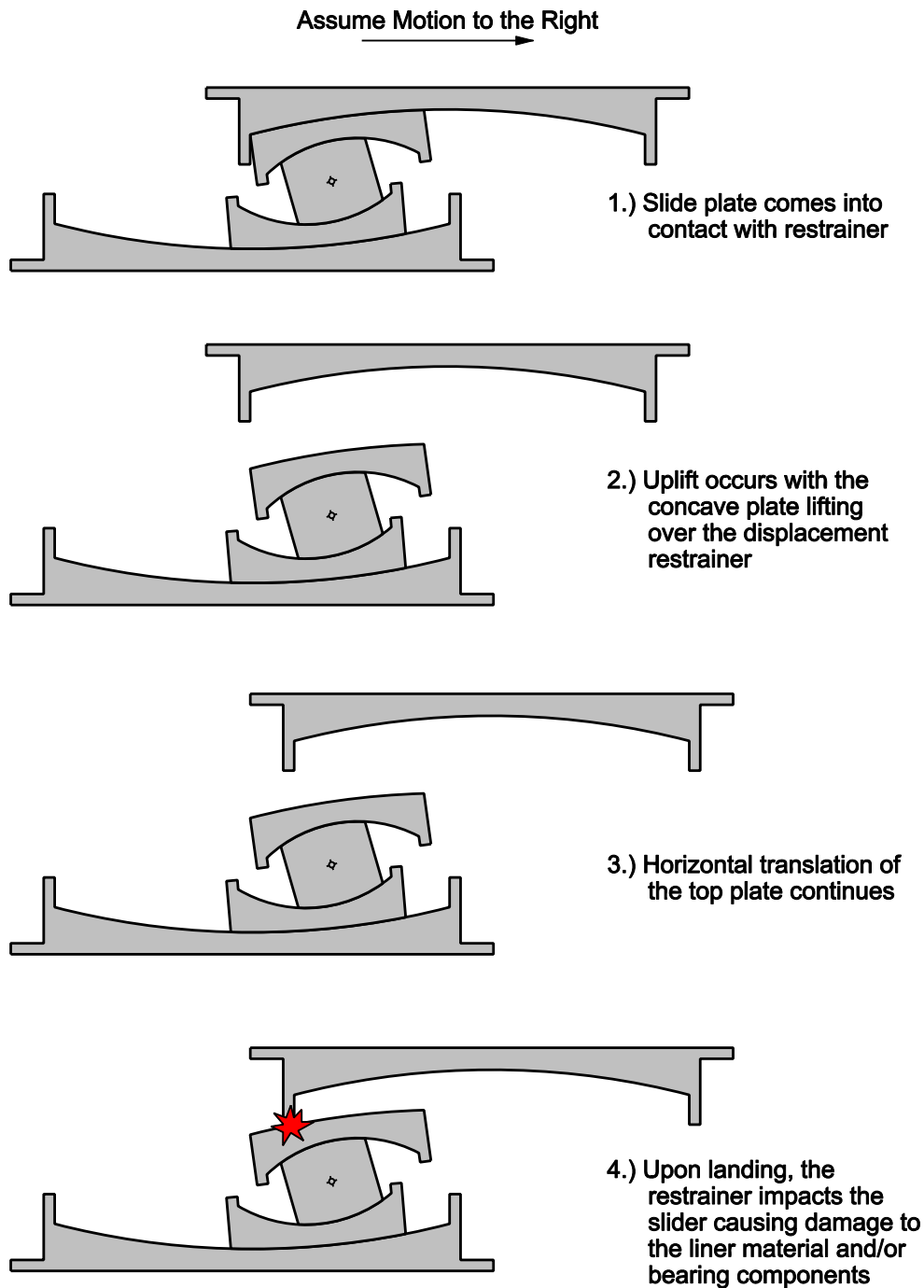
FIGURE 5-27 Sketch of Uplift Occurring After the Slide Plate is in Contact with the Displacement Restrainer (Triple FP Bearing with High Friction on the Bottom Surface)
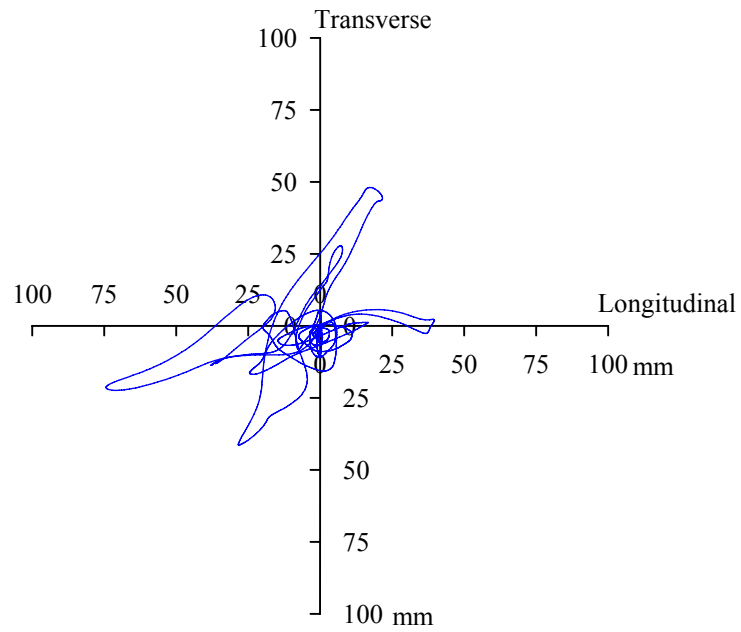
(a)
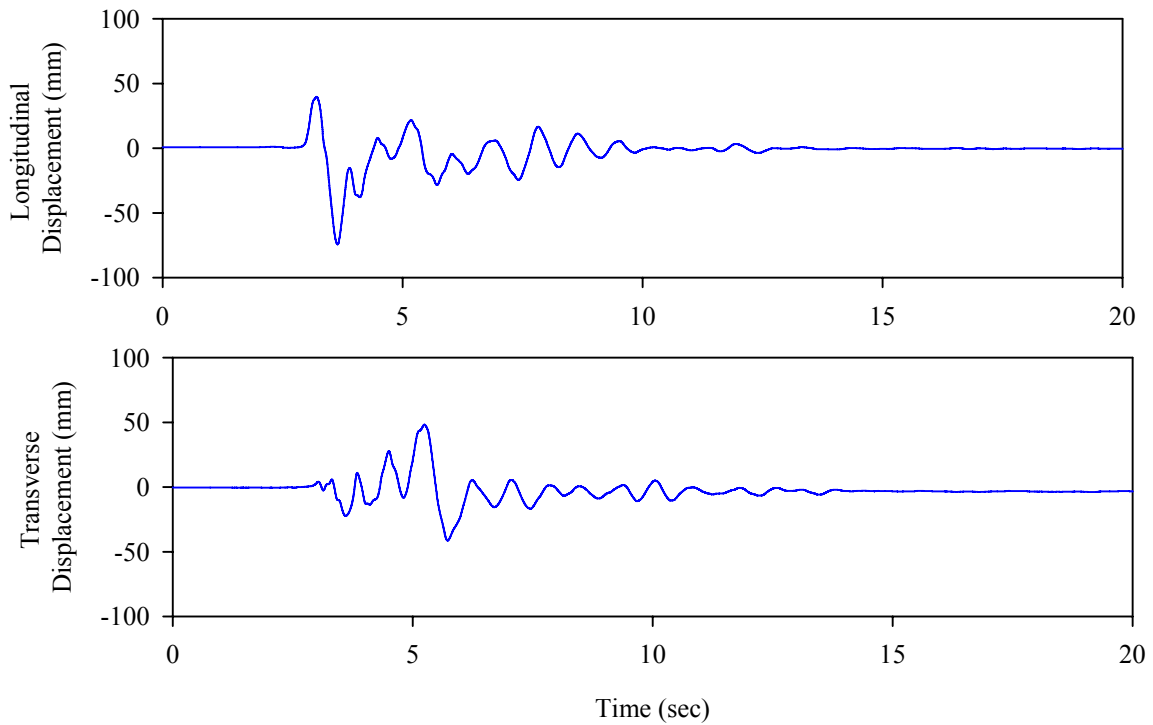
(b)

FIGURE 5-28 (a) Displacement Orbit and (b) Histories of Longitudinal and Transverse Displacements of SE Bearing from 100% Newhall Tridirectional Test of Triple 1 Isolation System
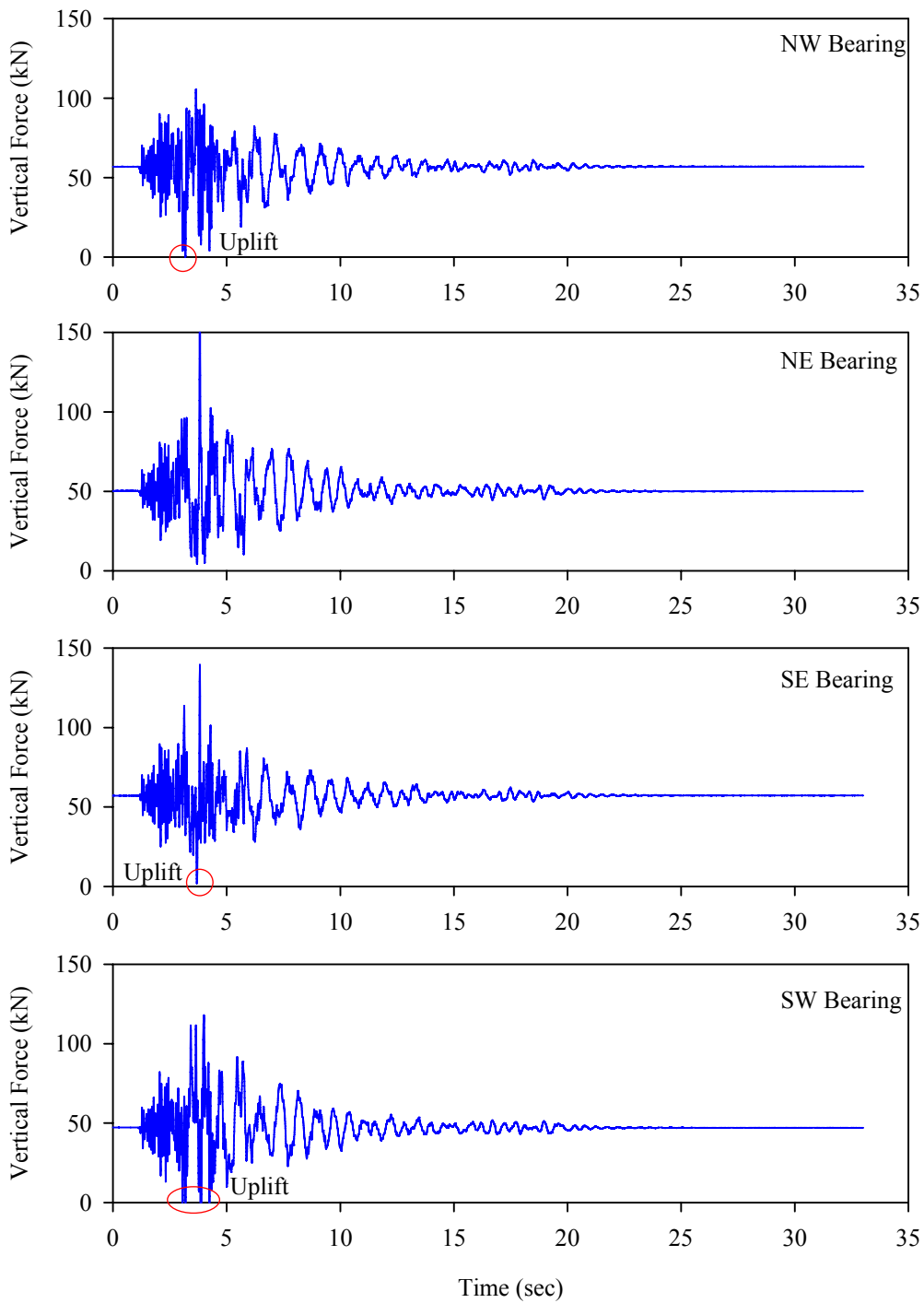
FIGURE 5-29 **Histories of Bearing Vertical Force from 100% Newhall Tridirectional Test of Triple 1 Isolation System**
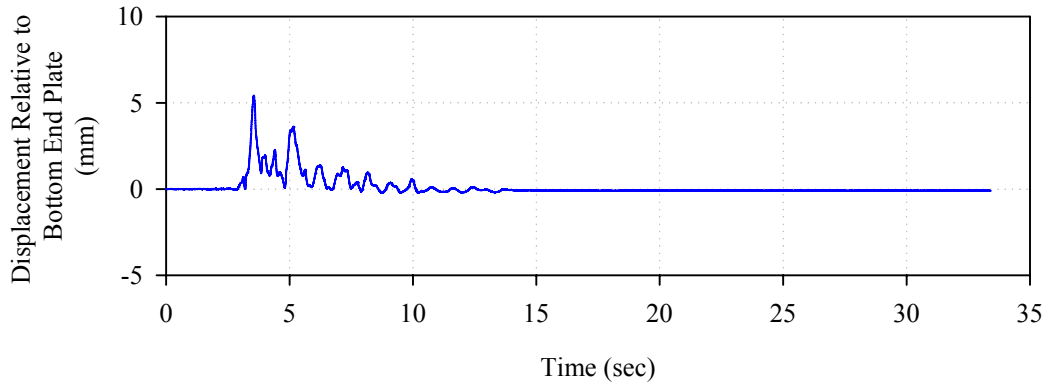
FIGURE 5-30 History of Vertical Displacements Relative to the Bottom Concave Plate of the SE Bearing in the 100% Tridirectional Newhall Test

The uplift behavior observed for triple FP bearings in this experimental program typically lasted for only fractions of a second with very small separation distances. Under these circumstances, there is no adverse effect on the performance of the bearing or danger of the slider falling apart. The uplift occurs over such a short time that the pieces of the slider simply have nowhere to go. In practice, there will be an added margin of safety keeping the slider together in the form of a rubber boot that will be wrapped around the slide plates (see figure 5-31). Its primary function will be to prevent debris from entering the lubricated inner concave surfaces, but it will also help to keep the various pieces of the slider together during extreme response.

FIGURE 5-31 Triple FP Bearing Slider Assembly with Prototype Rubber Boot Attached to the Slide Plates

5.4.3 Behavior of Triple 3 Configuration Upon Contacting the Displacement Restrainer

Various tests were carried out using the Triple 3 configuration with the Sylmar 360, Newhall 360 and Pacoima 164 ground motions scaled at 100% and beyond. For these tests, the slider assembly was wrapped with the rubber boot as shown in figure 5-31 due to the possibility of extreme response. The resulting hysteresis loops are presented in figures 5-32 through 5-34. In these loops, there is apparent stiffening at displacements of

approximately 50mm. This is not due to contact with the displacement restrainer but rather a combination of the effects of (a) velocity dependence when motion initiates on the high friction surface (b) the influence of overturning and (c) inherent variability in the loops due to the random nature of earthquake ground motion. For materials with friction on the order of 0.20, there is larger absolute variation in the coefficient of friction due to velocity dependence, which will have noticeable impact on the bearing's hysteresis loops.
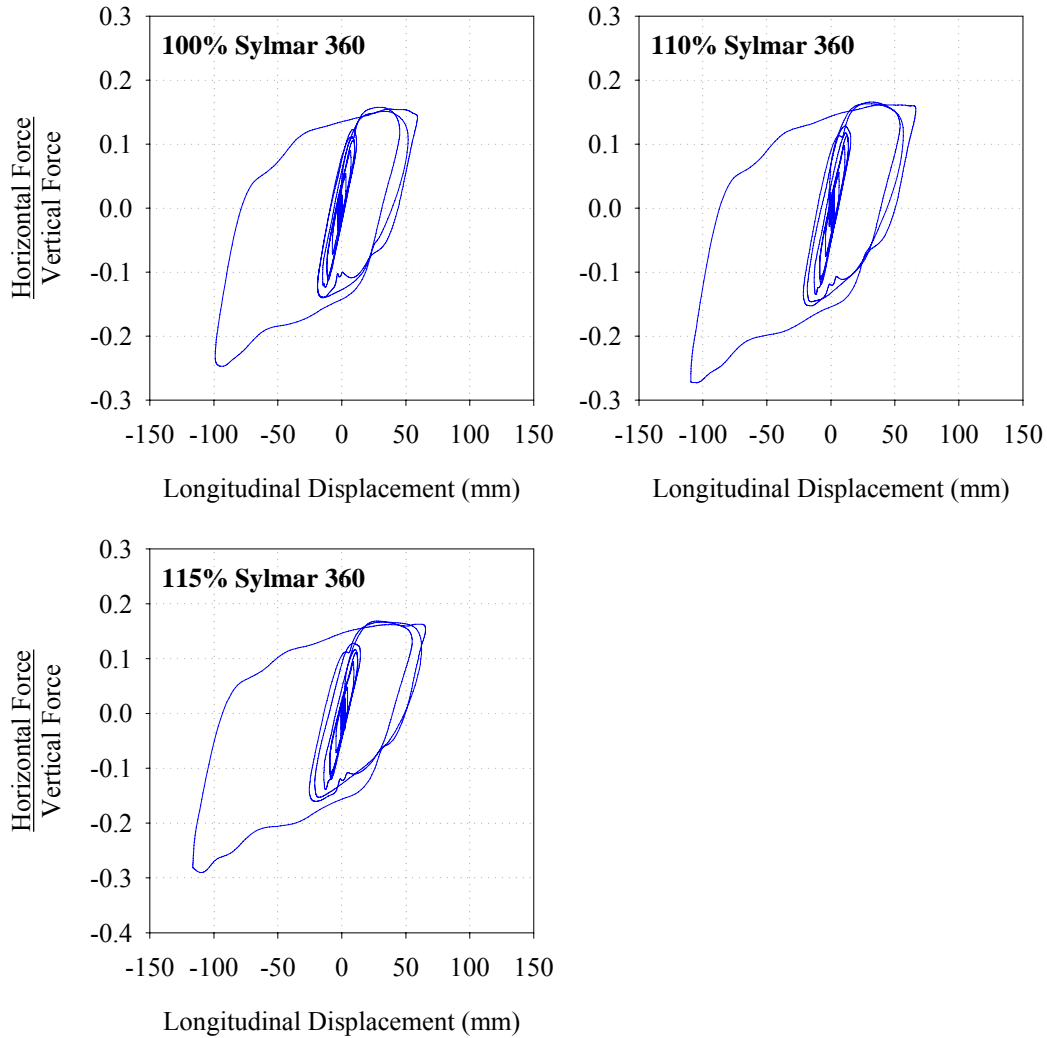
FIGURE 5-32   Hysteresis Loops of Triple 3 Isolation System with Sylmar 360 Ground Motion of Large Amplitude
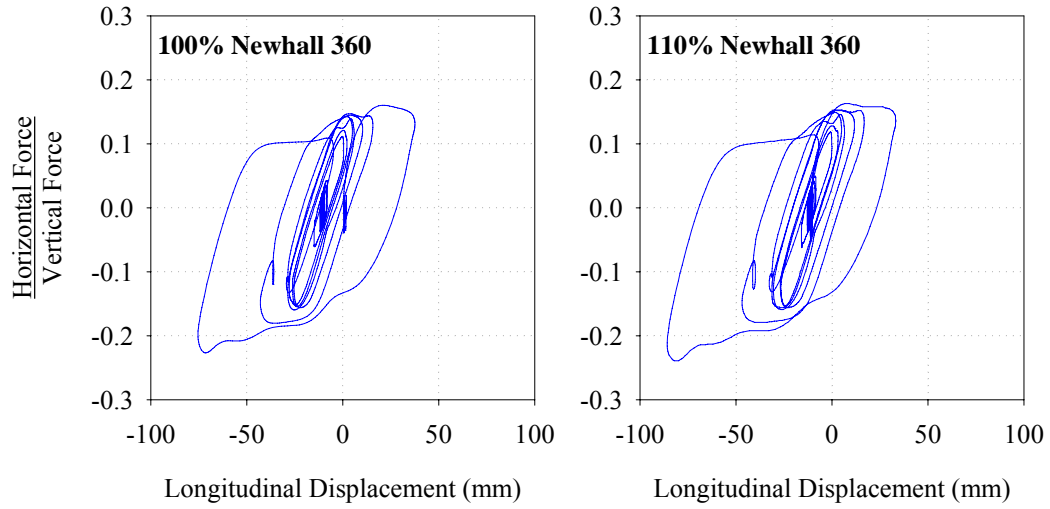
FIGURE 5-33   Hysteresis Loops of Triple 3 Isolation System with Newhall 360 Ground Motion of Large Amplitude
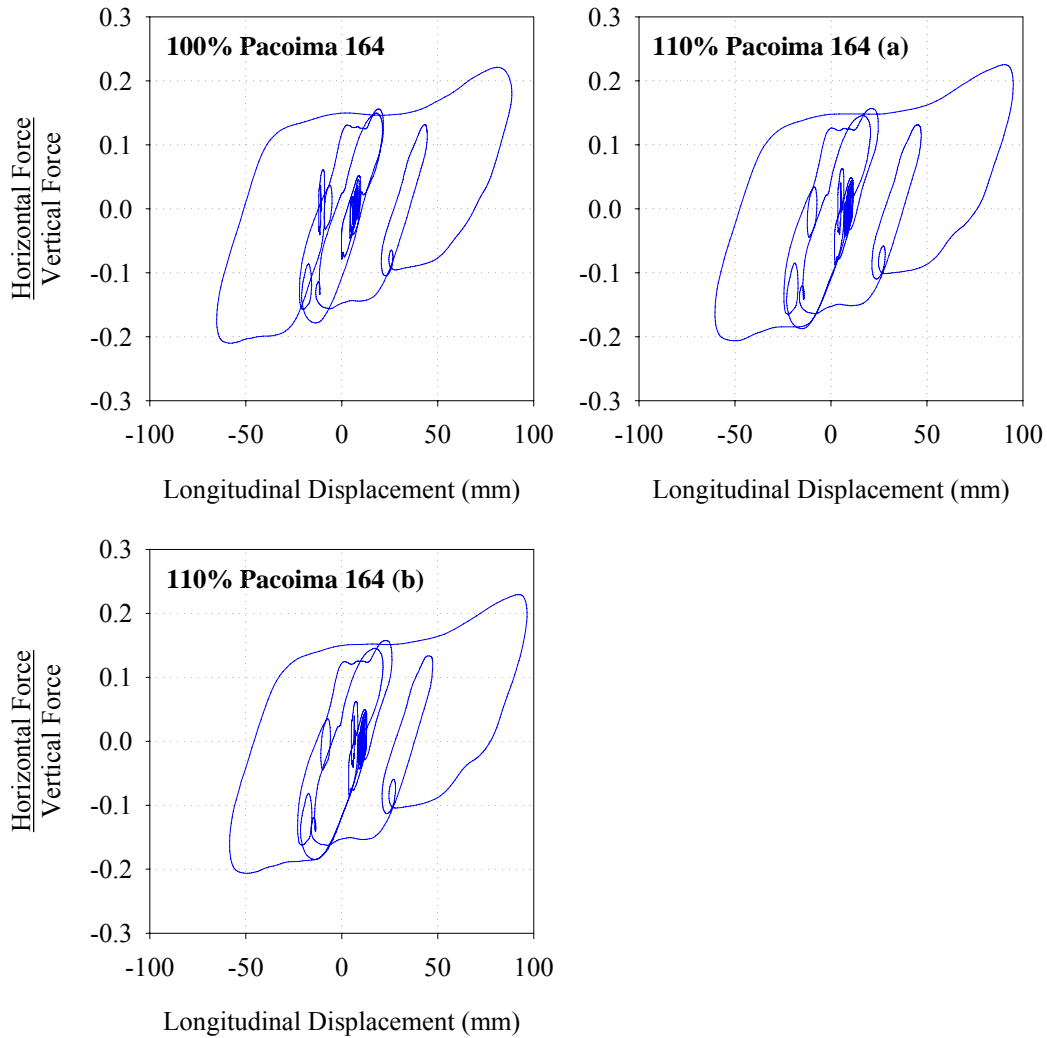
FIGURE 5-34 Hysteresis Loops of Triple 3 Isolation System with Pacoima 164 Ground Motion of Large Amplitude

Out of this test sequence, contact was made with the displacement restrainer only in the 115% Sylmar 360 test. For all motions, substantial uplift was starting to occur across the entire isolation system as the magnitudes of motion were increased and testing was capped at these levels in the interest of safety. The histories of displacements and vertical force from the test with 115% Sylmar 360 excitation are presented in figures 5-35 and 5-36 respectively. This test is noteworthy since there was uplift occurring as the bottom slide plate was in contact with the displacement restrainer. This all occurred over a very short time interval; the slide plate is in contact with the displacement restrainer from $t = 3.52 \sec$ until motion reverses direction at $t = 3.70 \sec$. Uplift of bearing 3 occurs from $t = 3.64 \sec$ to $t = 3.67 \sec$. The frame by frame sequence in which this occurred is shown in figure 5-37. This shows the bottom slide plate coming into contact with the displacement restrainer and remaining there while motion continues on the upper surface and subsequently returning to normal operation even after the uplift occurs.
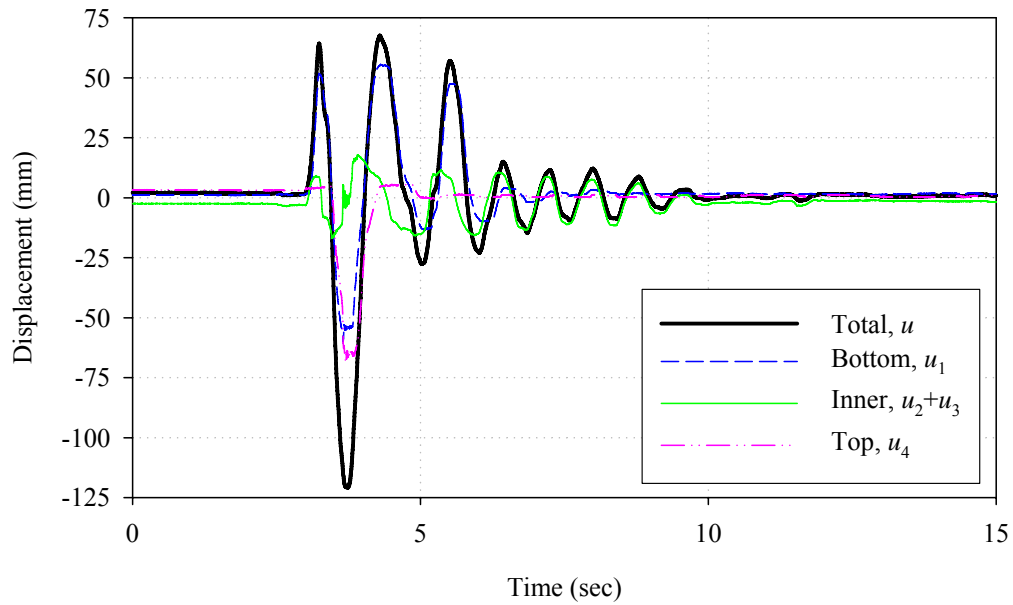
FIGURE 5-35 Decomposed Displacements of SE Bearing in Isolation System Triple 3 During 115% Sylmar 360 Excitation
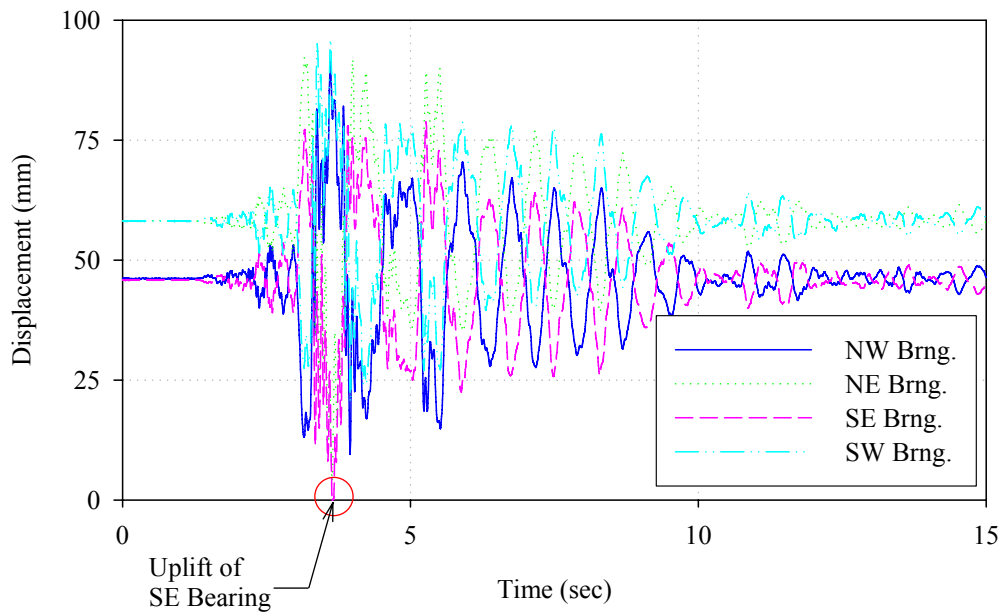
FIGURE 5-36   Histories of Bearing Vertical Force for Triple 3 Isolation System During 115% Sylmar 360 Excitation
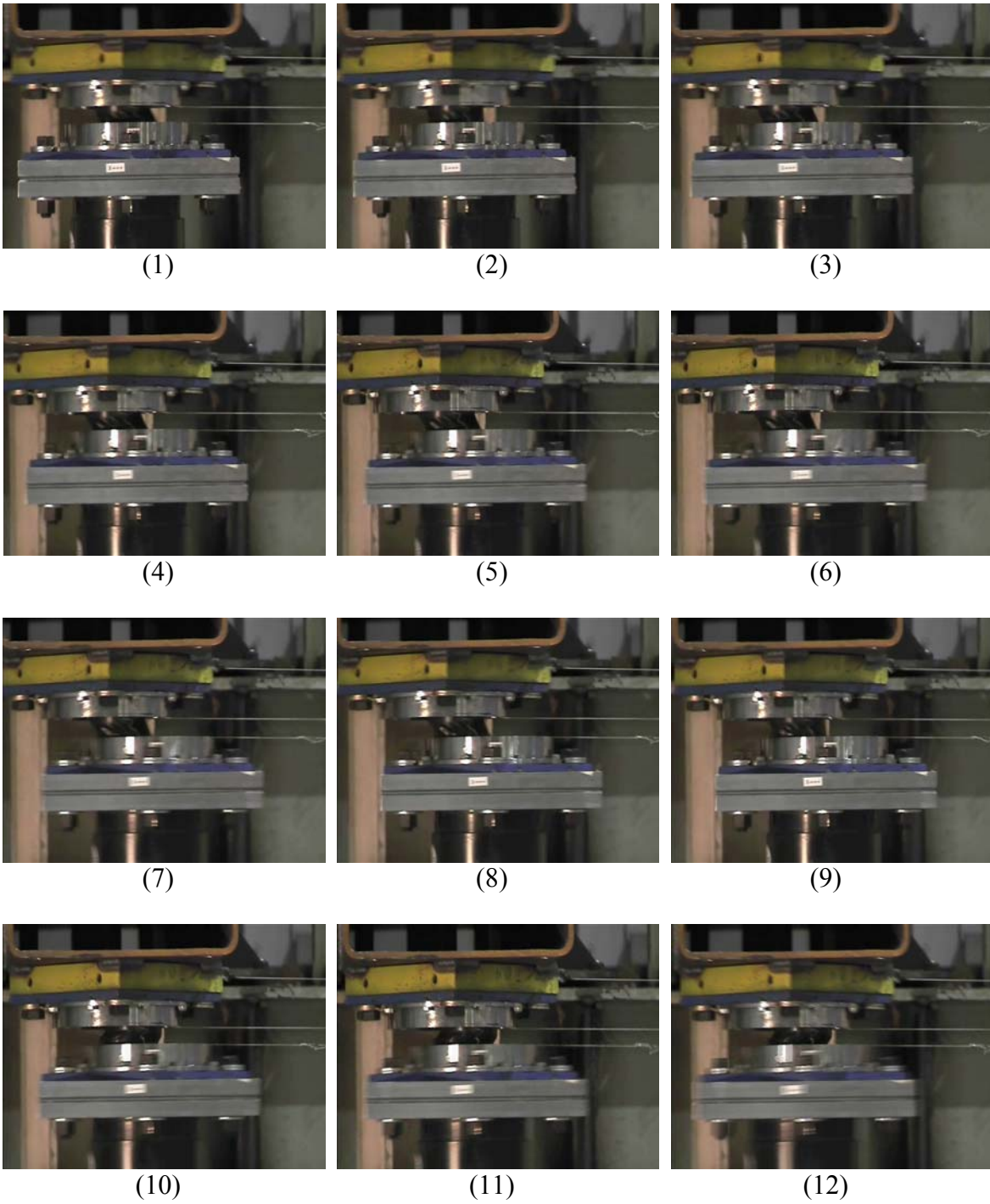
FIGURE 5-37 Frame by Frame Sequence Showing Contact with the Displacement Restrainer and Uplift of SE Bearing in Isolation System Triple 3 During 115% Sylmar 360 Excitation

Despite these seemingly extreme conditions, there was actually very little danger due to the fact that (a) the uplift duration and consequently the uplift displacements were small, (b) the outer surface of least friction (that contacts the displacement restrainer first) was used on the bottom surface so that even if large uplift displacements did occur when the slide plate was bearing on the displacement restrainer it would not be possible to have the restrainer ring lift up and over the slider and (c) the slider was wrapped in a rubber boot as a final protection against coming apart.

5.4.4 Permanent Displacements of Multi-Spherical Sliding Bearings

An important issue related to the design of multi-spherical sliding bearings is the permanent displacement that results after earthquake excitation. On each surface the slider can exist in an equilibrium position of nonzero displacement in which the static friction force balances the restoring force:

$$u_{pi} = R_{effi}\mu_{\min i} \tag{5-1}$$

The coefficient of friction at low velocity is used because as the bearing comes to rest the slider approaches zero velocity from above. The permanent displacements on each surface add to give the total possible permanent displacement of

$$u_p = R_{eff1}\mu_{\min1} + R_{eff2}\mu_{\min2} \tag{5-2}$$

for double FP bearings and

$$u_p = R_{eff1}\mu_{\min1} + \left(R_{eff2} + R_{eff3}\right)\mu_{\min2,3} + R_{eff4}\mu_{\min4} \tag{5-3}$$

for triple FP bearings. The issue of permanent displacements is more significant for double FP and triple FP bearings than for traditional single concave FP bearings since there are multiple surfaces on which the permanent displacements can accumulate. Moreover, for triple FP bearings there is the possibility that high friction materials will be used for at least one of the surfaces.

The value of u_p given by equations (5-1) through (5-3) represents the theoretical upper bound of the permanent displacement. Typically earthquakes end with a period of very low level excitation which tends to recenter the bearings. Past shake table tests of structures isolated with single FP bearings (Tsopelas *et al.*, 1996; Wolff and Constantinou, 2004) have shown that the actual permanent displacements are approximately one order of magnitude less than the theoretical upper bound given by equations (5-1) through (5-3). Figure 5-38 demonstrates that the permanent displacements recorded from the various configurations are consistent with the results of previous studies. The values are reported for both the unidirectional and multidirectional tests. There is no apparent correlation between the number of components in the excitation and the resulting components of permanent displacement. This is an important observation since past studies have pertained to longitudinal and longitudinal plus

vertical excitation. This means that the addition of transverse excitation, for example, does not amplify the permanent displacements in the longitudinal direction. For combined longitudinal and transverse excitation of course, the resultant permanent displacements will be larger than the orthogonal components reported here.

Comparing the performance of the various systems the triple systems with high friction Material 8 exhibited the largest permanent displacements. Naturally, the system with both surfaces of high friction exhibited larger permanent displacements than the system with one surface of high friction. One of the proposed benefits of adaptive behavior is less permanent displacements in small earthquakes. In these tests, the non-adaptive system of intermediate friction and the adaptive triple FP bearings both exhibited equally small permanent displacements in small earthquakes. The adaptive bearings recenter well due to the high stiffness low friction inner surface whereas the non-adaptive systems recenter well due to the velocity dependence of the coefficient of friction. Even though the Double 2 configuration exhibits intermediate friction at high velocity, the coefficient of friction at slow speeds, which determines the permanent displacement, is still reasonably small.
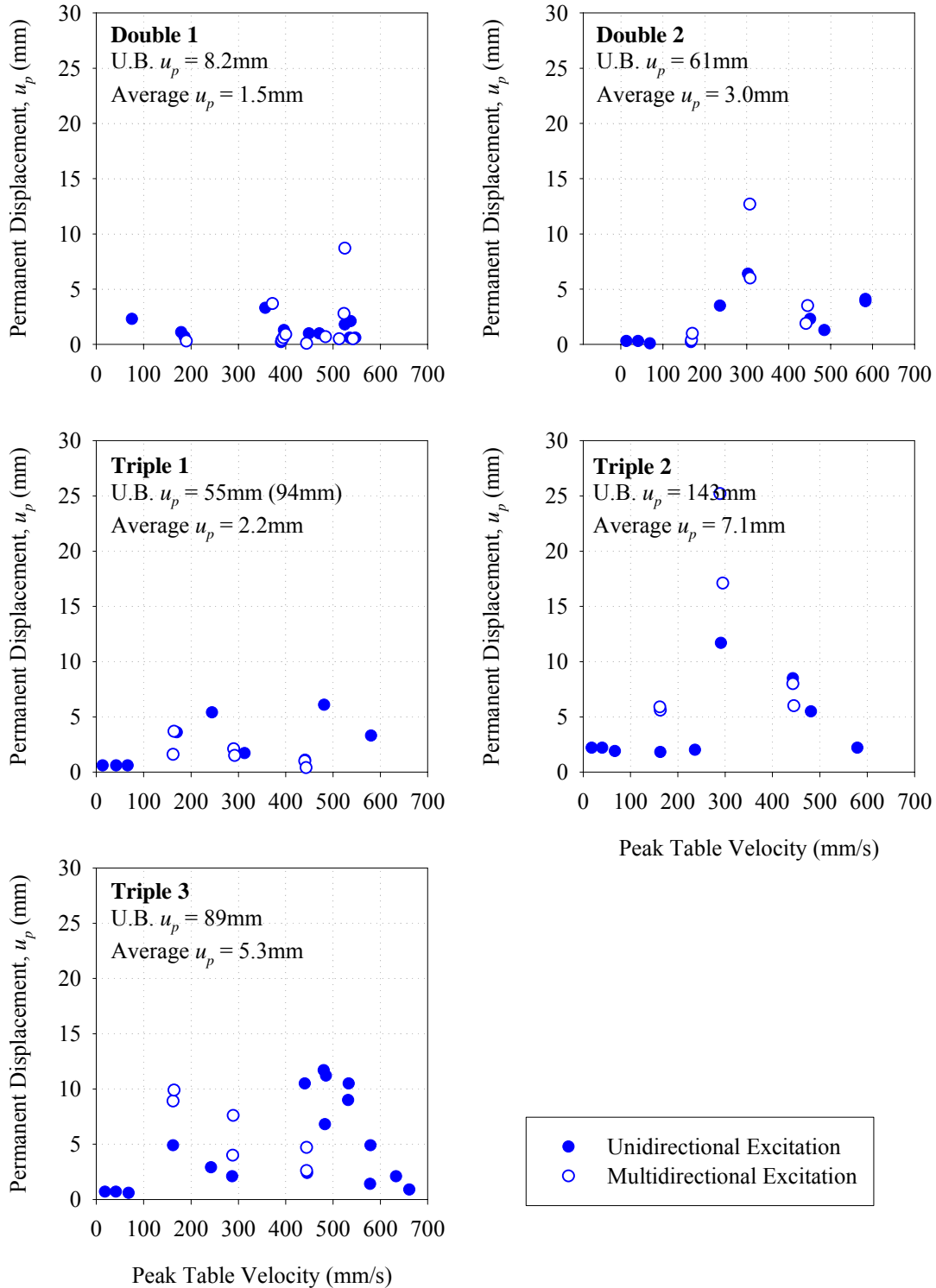
FIGURE 5-38 Comparison of Permanent Displacements from Testing of Each Isolation System (U.B. u_p Refers the Theoretical Upper Bound Value Based on Equations (5-2) and (5-3) and the Average u_p is the Average Permanent Displacement from all Tests of that Particular Configuration)

SECTION 6
ANALYTICAL PREDICTION OF RESPONSE

6.1 Introduction

Implementation of valid dynamic analysis techniques is one of the most critical steps towards practical use of multi-spherical sliding bearings as it demonstrates that the behavior is sufficiently well understood to reliably predict response. This section describes the modeling and response history analysis of the experimental specimen using the commercially available program SAP2000. The intent of this part of the work was to determine the capabilities and limitations of this program in order to assess its overall validity for analysis of these devices. In addition to properly capturing the force-displacement relationship of the individual isolators (which was demonstrated in Sections 6 and 7 of this report), it was necessary to experimentally verify the analytical models of multi-spherical sliding bearings when part of a complex structural system.

Beyond accurately representing the force-displacement relationship of the individual isolators, Section 17.6.2.1 of the ASCE/SEI 7-05 Standard requires that the dynamic analysis procedures used for response history analysis be capable of modeling the isolation system

"…with sufficient detail to
   (a) Account for the spatial distribution of isolator units.
   (b) Calculate the translation, in both horizontal directions, and torsion of the structure above the isolation interface considering the most disadvantageous location of eccentric mass.
   (c) Assess the overturning/uplift forces on individual isolator units.
   (d) Account for the effects of vertical load, bilateral load, and/or the rate of loading if the force-displacement properties of the isolation system are dependent on one or more of these attributes…"

These requirements form the basis upon which the analytical results are compared to the experimental results in this section. In addition, the accuracy of the analysis in predicting secondary system response is also evaluated through comparison of the experimental and analytical floor spectra.

6.2 Description and Verification of Superstructure Analytical Model

The three-dimensional analytical model shown in figure 6-1 was created based on the members, dimensions and connection details of the actual model. A complete list of properties assigned to the frame members is provided in table 6-1. All beam-column connections were fixed and all brace connections were pinned. Rigid end offsets of 38mm, corresponding to half the depth of the S3×5.7 members, were assigned at the ends of each beam and column member. Use of rigid end offsets permits more accurate

calculation of the bending stiffness because the clear span, rather than the centerline to centerline length, is used to determine the flexibility coefficients. End offsets are not used by SAP2000 in the calculation of axial stiffness. In addition, all nodes of each floor were constrained to have the same *xy* displacements by assigning a diaphragm constraint at each *z* level of the superstructure. The rigid diaphragm is a reasonable assumption as each floor bay of the actual model is fully braced.
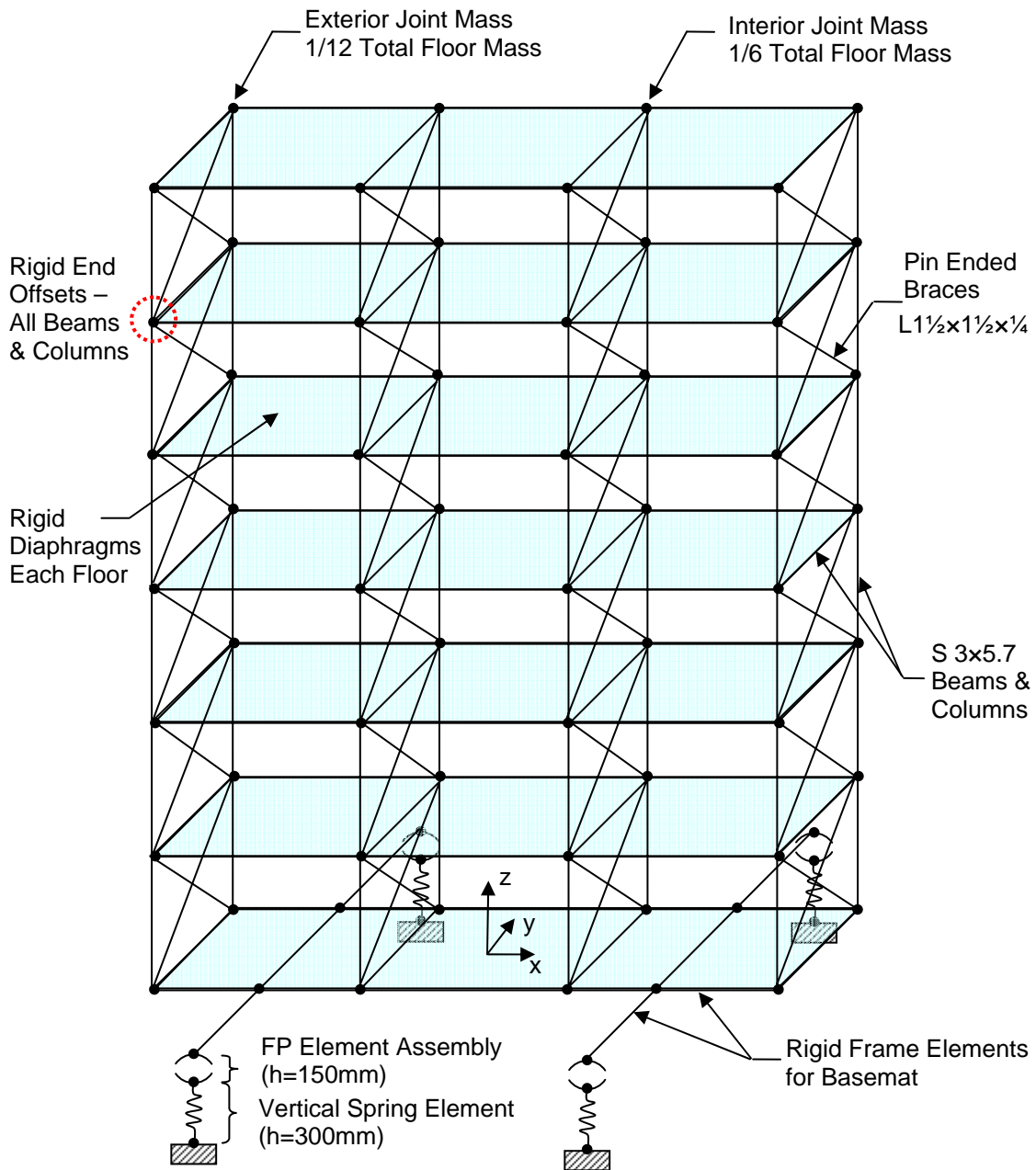
FIGURE 6-1 Analytical Model of Superstructure in SAP2000

TABLE 6-1 Section Properties of Fame Elements

	S3×5.7	L1½×1½×¼	Rigid
Cross Section Area (mm^2)	1071	444	5×10^5
Torsion Constant (mm^4)	18,023	8,325	1×10^8
Moment of Inertia 3-3 (mm^4)	4.162×10^5	5.786×10^4	5×10^9
Moment of Inertia 2-2 (mm^4)	1.861×10^5	5.786×10^4	5×10^9
Shear Area 2 (mm^2)	363	242	5×10^5
Shear Area 3 (mm^2)	782	242	5×10^5
Width (mm)	59.2	38.1	300
Depth (mm)	76.2	38.1	300
Mass and Weight (kg, kN)	0	0	0

Each frame member was assigned to be weightless, with all mass lumped at the beam-column connections. Based on the load cell measurements, the total weight of the braced frame specimen used in the 2004 tests was 222 kN, with 20.9 kN assigned to the basemat and the remaining distributed as 33.6 kN to each floor. For the moment frame used in the 2007 tests the total weight was 209 kN, with 23.6 kN assigned to the basemat and 30.9 kN assigned to each floor (the basemat weight in the 2007 tests was larger due to the addition of the flange stiffener plates). In this study there was no mass eccentricity, though this could easily have been modeled by assigning the joint masses appropriately.

Accurate calculation of the exact section properties of the built up HSS tubes was complicated by the fact that full composite action was not achieved across the entire cross section with the stitch welds that were around the perimeter of the cover plates. Therefore, instead of explicitly assigning section properties to the tubes, the entire basemat was modeled as rigid elements with the vertical flexibility accounted for by using four linear spring elements. Each spring was modeled as a two node linear link element vertically aligned with the FP link elements at the location of each load cell. The length of each spring element corresponded to the height of the load cell. To model the configuration of the 2004 tests, each spring was assigned a stiffness of 45.5 kN/mm. This provided the analytical model a fundamental vertical frequency of 12.98 Hz, which compares well with the actual experimental value of 12.99 Hz. To model the stiffened basemat of the 2007 tests, the vertical springs were each assigned a stiffness of 63.9 kN/mm (analytical first mode = 15.27 Hz, experimental first mode = 15.25 Hz). Each spring element was also fixed in the two remaining translational degrees of freedom and the three rotational degrees of freedom.

In order to verify the accuracy of the superstructure model, the results of modal analysis performed using Ritz vectors are compared to the experimentally measured dynamic properties in tables 6-2 through 6-5. The analytical model describes the dynamic properties very well in the longitudinal direction for both the braced frame and moment frame specimens. However, in the transverse direction the agreement is not as good. The most likely cause of this discrepancy is error in the experimental measurements due to rocking motion. Rocking of the superstructure atop the flexible base is worse in the transverse direction due to the larger aspect ratio. Instead of measuring the accelerations

of pure horizontal translation, the accelerometers used to determine the dynamic properties measured acceleration comprised of both translational and rotational components. This issue is not of great concern however as it is the response of the specimen in the longitudinal direction that is primarily of interest.

TABLE 6-2 Comparison of Experimental and Analytical Values of Frequencies and Mode Shapes of Braced Frame in Longitudinal Direction

		Mode					
		1		**2**		**3**	
		Exp.	**Ana.**	**Exp.**	**Ana.**	**Exp.**	**Ana.**
Frequency (Hz)		**3.50**	**3.73**	**17.38**	**17.85**	**30.63**	**35.42**
Damping Ratio		**0.033**	**-**	**0.017**	**-**	**0.003**	**-**
Story	6th	1.000	1.000	0.834	0.979	0.669	0.750
	5th	0.850	0.832	0.235	0.230	-0.551	-0.491
	4th	0.652	0.653	-0.414	-0.518	-1.000	-0.992
	3rd	0.513	0.472	-0.888	-0.981	-0.236	-0.173
	2nd	0.371	0.295	-1.000	-1.000	0.996	0.950
	1st	0.173	0.133	-0.572	-0.594	0.958	1.000

TABLE 6-3 Comparison of Experimental and Analytical Values of Frequencies and Mode Shapes of Moment Frame in Longitudinal Direction

		Experimental					
		Mode					
		1	**2**	**3**	**4**	**5**	**6**
Frequency (Hz)		**2.25**	**8.00**	**13.63**	**20.13**	**25.63**	**29.88**
Damping Ratio		**0.056**	**0.015**	**0.019**	**0.006**	**0.004**	**0.004**
Story	6th	1.000	0.998	0.819	0.419	0.311	0.145
	5th	0.904	0.383	-0.464	-0.705	-1.000	-0.480
	4th	0.760	-0.418	-1.000	-0.097	0.821	0.748
	3rd	0.585	-0.986	-0.185	0.845	0.051	-1.000
	2nd	0.384	-1.000	0.816	-0.207	-0.593	0.930
	1st	0.177	-0.479	0.817	-1.000	0.834	-0.631

		Analytical					
		Mode					
		1	**2**	**3**	**4**	**5**	**6**
Frequency (Hz)		**2.26**	**7.45**	**13.08**	**19.47**	**25.71**	**30.51**
Story	6th	1.000	0.991	0.797	0.650	0.418	0.194
	5th	0.913	0.389	-0.400	-0.898	-0.972	-0.581
	4th	0.777	-0.399	-1.000	-0.278	0.815	0.881
	3rd	0.597	-0.963	-0.227	0.997	-0.015	-1.000
	2nd	0.386	-1.000	0.862	-0.068	-0.795	0.916
	1st	0.161	-0.511	0.804	-1.000	1.000	-0.656

TABLE 6-4 Comparison of Experimental and Analytical Values of Frequencies and Mode Shapes of Braced Frame in Transverse Direction

		Mode					
		1		2		3	
		Exp.	Ana.	Exp.	Ana.	Exp.	Ana.
Frequency (Hz)		3.75	5.48	15.86	22.37	19.36	45.77
Damping Ratio		0.029	-	0.012	-	0.006	-
Story	6th	1.000	1.000	0.728	0.842	0.084	0.631
	5th	0.867	0.802	0.166	0.070	-0.377	-0.554
	4th	0.686	0.599	-0.481	-0.620	-0.292	-0.919
	3rd	0.457	0.403	-0.881	-1.000	-0.089	-0.082
	2nd	0.318	0.227	-1.000	-0.958	1.000	0.964
	1st	0.144	0.087	-0.597	-0.553	0.190	1.000

TABLE 6-5 Comparison of Experimental and Analytical Values of Frequencies and Mode Shapes of Moment Frame in Transverse Direction

		Mode					
		1		2		3	
		Exp.	Ana.	Exp.	Ana.	Exp.	Ana.
Frequency (Hz)		3.63	5.63	16.00	23.12	18.88	47.39
Damping Ratio		0.110	-	0.010	-	0.005	-
Story	6th	1.000	1.000	0.671	0.838	0.184	0.624
	5th	0.879	0.800	0.387	0.064	-0.222	-0.560
	4th	0.710	0.597	-0.338	-0.625	-0.638	-0.913
	3rd	0.532	0.400	-0.717	-1.000	-0.615	-0.070
	2nd	0.377	0.225	-1.000	-0.953	1.000	0.971
	1st	0.210	0.086	-0.620	-0.548	0.587	1.000

To further verify the analytical model of the superstructure, response history analysis of a linear model of the fixed base structure was performed for the four seismic tests listed in table 9-1 (30% El Centro S00E and 50% Taft N21E for the braced frame and 100% Wrightwood 115 and 100% Golden Gate Park 100 for the moment frame). The input ground motions used in the analysis were the actual histories of table motion recorded during the tests. For these analysis cases, frequency dependent modal damping was specified based on the experimental values of the damping ratios of each modal frequency. The experimental and analytical histories of normalized base shear, interstory drift and sixth floor absolute acceleration are presented in figures 6-2 through 6-5. The agreement for the braced frame tests is reasonable but not great. For both ground motions, the SAP2000 analysis overestimates base shear and acceleration and underestimates the first story drift. This discrepancy results from slippage of the braces during the experiment, which is difficult to model analytically. There is much better agreement between experimental and analytical results for the moment frame specimen

(figures 6-4 and 6-5). With the braces and the associated behavioral discontinuities removed, the specimen acts as a more "analytic" structure for excitation in the longitudinal direction.
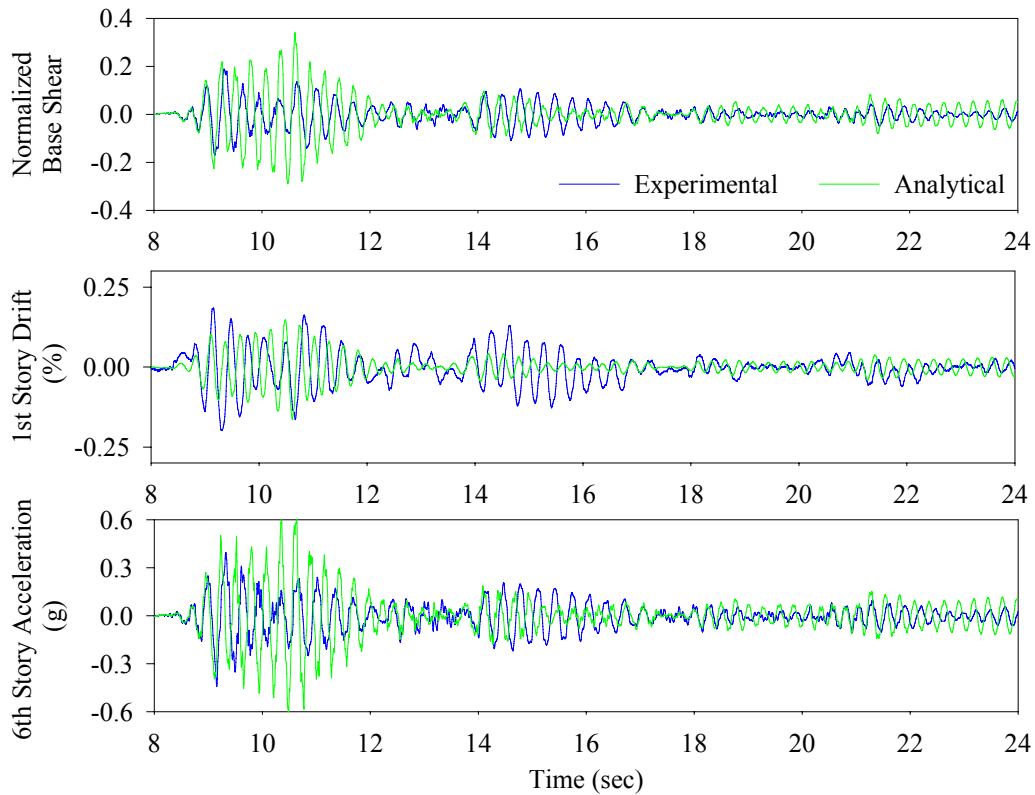
FIGURE 6-2 Comparison of Experimental and Analytical Response for Fixed Base Braced Frame with 30% El Centro S00E Excitation Applied Longitudinally
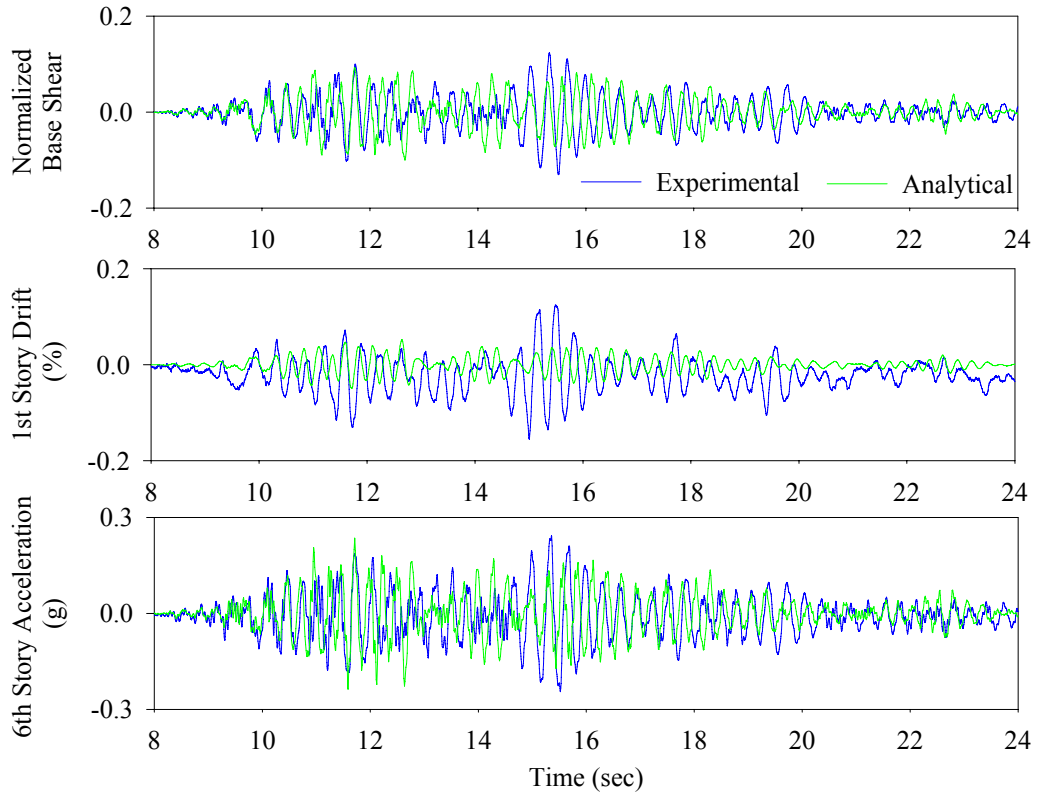
FIGURE 6-3 Comparison of Experimental and Analytical Response for Fixed Base Braced Frame with 50% Taft N21E Excitation Applied Longitudinally
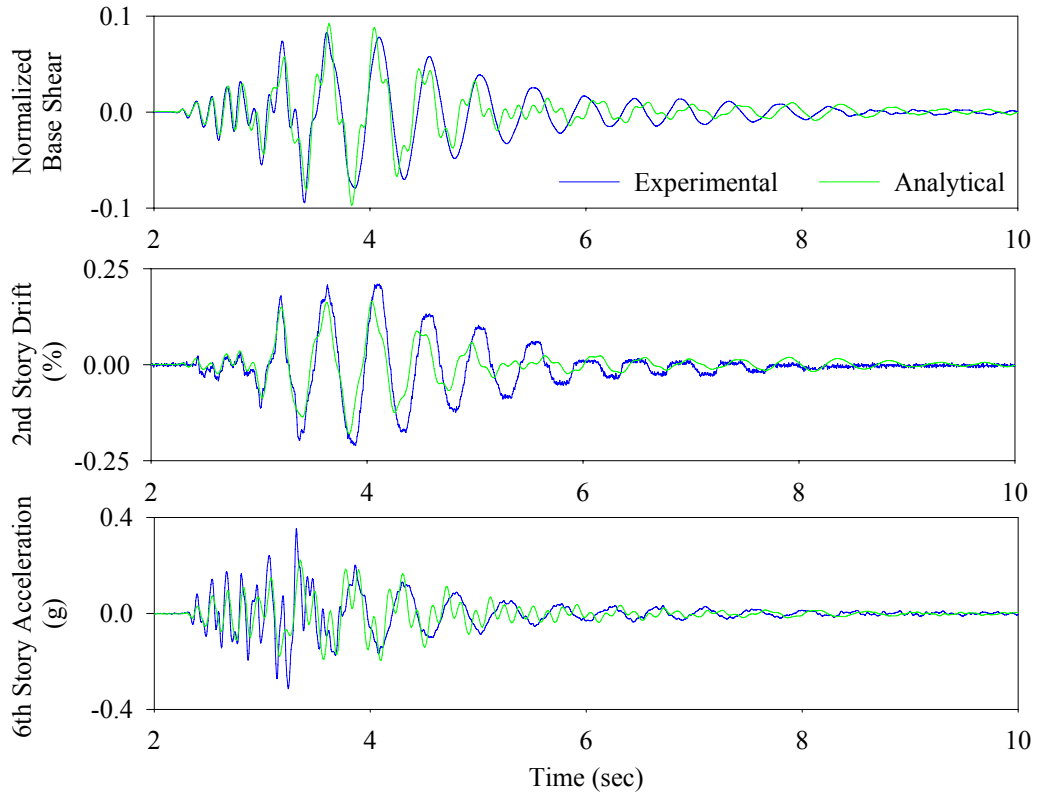
FIGURE 6-4 Comparison of Experimental and Analytical Response for Fixed Base Moment Frame with 100% Wrightwood 115 Excitation Applied Longitudinally
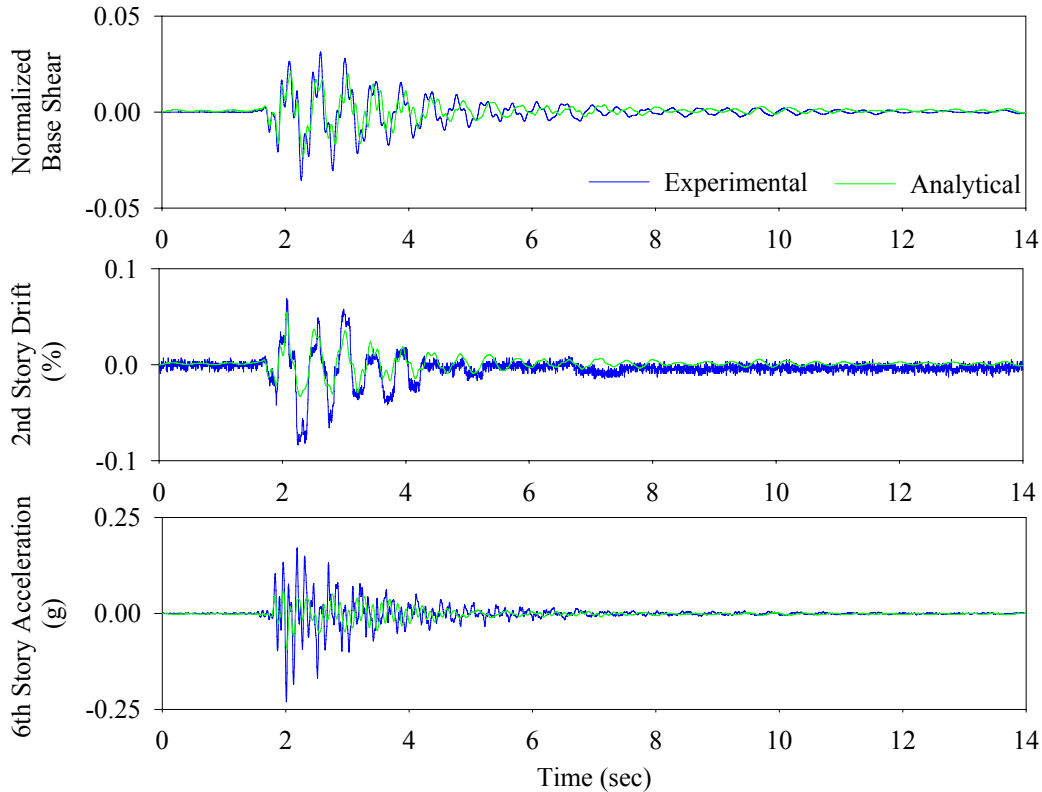
FIGURE 6-5 Comparison of Experimental and Analytical Response for Fixed Base Moment Frame with 100% Golden Gate 100 Excitation Applied Longitudinally

Since one of the proposed benefits of adaptive behavior is earlier activation and consequently better performance of secondary systems in minor earthquakes, it was also useful to evaluate the analytical predictions of floor response spectra. Experimental and analytical floor response spectra for the moment frame subjected to the Wrightwood 115 ground motion are presented in figure 6-6. For lower frequencies (say, below 7 Hz, which approximately corresponds to the second modal frequency), the analytical results are in very good agreement with the experimental results. Beyond this however, the experimental data capture the high frequency content with much greater fidelity than provided by the analysis.

These results contribute toward establishing the accuracy of the superstructure model. This step was necessary in order to be able to more suitably evaluate the analytical models of the various isolation systems and assess the relative contributions of isolation system modeling error and superstructure modeling error to the total error. To summarize, response can be very accurately predicted for the moment frame in the longitudinal direction. Even the floor response spectra at lower frequencies are captured well. There is greater error in the modeling of the braced frame due to slippage of the braces; however the analytical results are still within reasonable agreement. Lastly, it should be qualified that these results are obtained for a highly regular, bare frame structure whose mass is known with a good degree of certainty. Judgments on the

137

accuracy of the analysis for actual structures with asymmetry, exterior cladding and interior partitions whose mass is estimated are left to the reader's discretion.
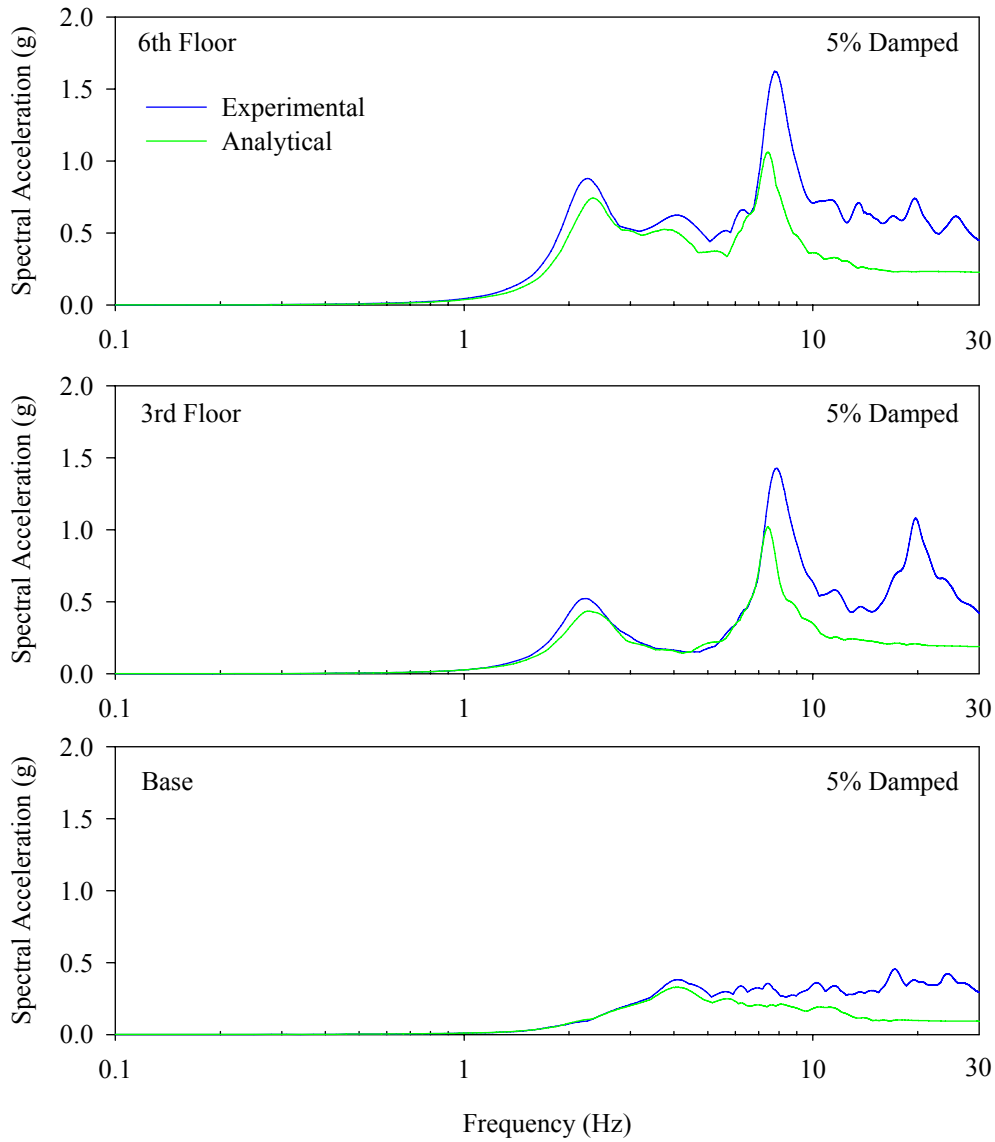
FIGURE 6-6 Comparison of Experimental and Analytical Floor Response Spectra for Moment Frame Structure Subjected to 100% Wrightwood 115 Excitation

6.3 Modeling and Analysis of Isolated Specimens

SAP2000 models each isolator as a discrete nonlinear link element that can be placed anywhere within the model. Frequency dependent modal damping was specified as shown in figure 6-7 based on the experimental values of the damping ratios at each modal frequency. Below the fundamental frequency of the superstructure, near zero equivalent viscous damping is assigned. This way, in the modes associated with the isolators all of

the energy dissipation results from hysteretic energy dissipation based on the friction assigned to the isolator elements. Furthermore, damping is also properly represented in the modes associated with the superstructure above. This prevents error from having viscous damping in addition to hysteretic damping in the modes associated with isolator deformation which would result if the default scheme in SAP2000 of constant damping in all modes were to be used.
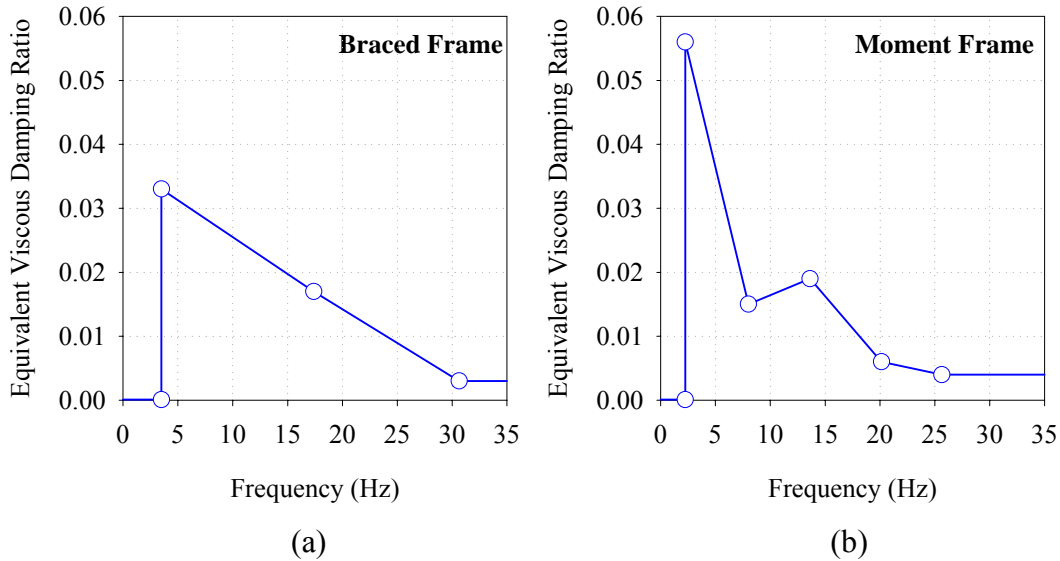
FIGURE 6-7 Frequency Dependent Modal Damping Used in Analysis of (a) Braced Frame Specimen and (b) Moment Frame Specimen

The isolators are modeled following the basic methodology proposed in Sections 6 and 7. For the Double 1 and Double 2 configurations, a single link element is used at each bearing location; the Triple 1 and Triple 2 configurations are modeled with two vertically aligned link elements connected in series at each bearing location and the Triple 3 configuration is modeled with three vertically aligned FP link elements connected in series at each bearing location. The minimum number of link elements needed to properly describe the behavior is dependent on the degree of adaptability of each configuration. More specific details regarding the properties assigned to each element of each configuration are presented in the following sub-sections.

For response history analysis, the input excitation is the actual acceleration of the shake table in each principal translational direction as measured from the experiments. Although there were noticeable rotational accelerations of the shake table, these were not considered in the analysis as there effects were found to be negligible. This was verified by performing analysis for a few motions including the rotational accelerations about the transverse axis as calculated from the vertical accelerations at the west and east sides of the shake table extension. The results from the analysis of the Triple 3 configuration for the Sylmar 360 motion including rotational acceleration of the shake table extension are shown in figure 6-8 and demonstrate that there is very small effect when the rotations are

considered in the analysis. There is negligible effect on all response quantities including horizontal shear, isolator displacements and permanent displacements.
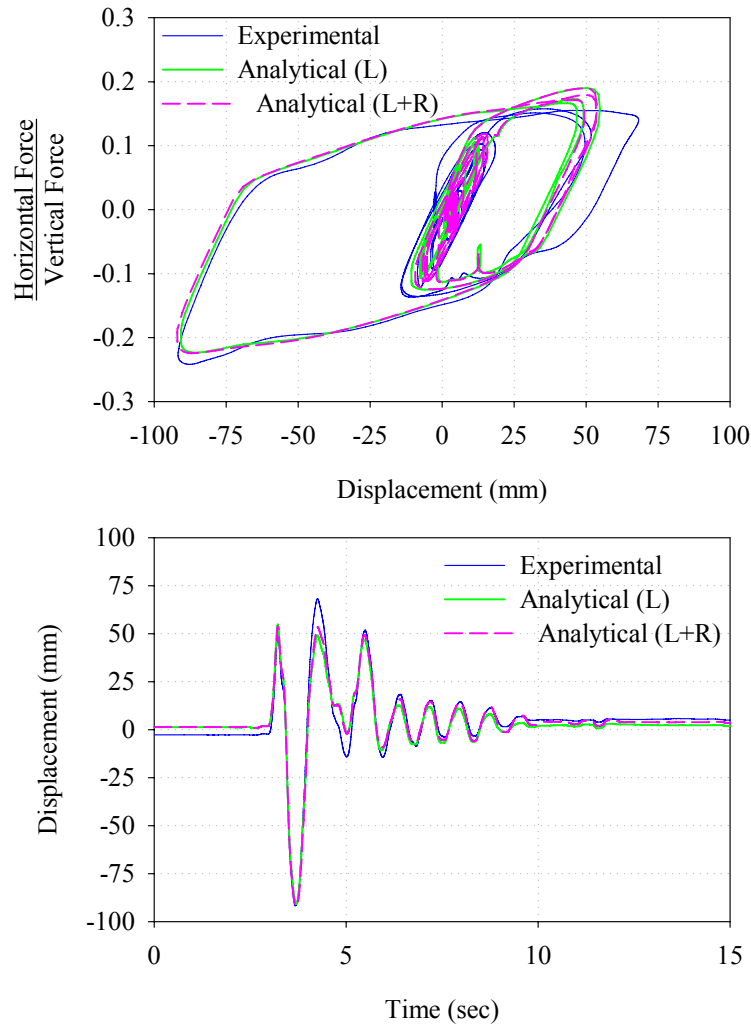
FIGURE 6-8 Comparison of Analysis Results when the Rotational Accelerations of the Shake Table are Included in the Analysis (Triple 3 Configuration Subjected to Sylmar 360 Ground Motion Applied in the Longitudinal Direction)

When experimental data regarding initial displacements are available, as is the case for all configurations tested except Double 1, the initial conditions of each analysis case are those at the end of the previous case. To ensure that the superstructure comes to rest so that the final condition of the model (and accordingly the initial condition for the following analysis case) is only a permanent displacement of the isolation system, there are several seconds of zero acceleration appended to the end of each record.

6.4 Comparison of Isolation System Primary Response Quantities

Though Sections 6 and 7 demonstrate that there are modeling techniques for properly representing the various types of adaptive behavior exhibited by these devices, they establish the validity of the analysis essentially only at the component level. Comparison to the shake table test results is necessary to verify that the behavior predicted by the proposed assemblies of nonlinear elements is accurate in the context of a complex structural system.

6.4.1 Modeling and Analysis Results for the Double 1 and Double 2 Configurations

The Double 1 and Double 2 configurations are each double FP bearings having concave surfaces of equal friction. There is simultaneous sliding on both surfaces throughout the entire course of motion. As a result, no transitions in stiffness occur. The hysteretic behavior of these devices is identical to the single FP bearing, which allows them to be modeled using a single FP link element with radius equal to the sum of the effective radii of the upper and lower surfaces, $R_{eff1} + R_{eff2}$, and rate parameter equal to half of the actual value. Therefore, for the analysis program these configurations are no more demanding analytically than the single FP bearing. The validity of SAP2000 for analyzing single FP bearings has been established for some time now (Scheller and Constantinou, 1999; Computers and Structures, Inc., 2006)

The properties assigned to the link elements used to model each configuration are given in table 6-6. The friction coefficients and rate parameter were assigned based on the experimental results, with the same value specified in every analysis case for each configuration. For the Double 1 configuration, the reason for the slight increase in f_{max} from 0.017 in the characterization tests (see figure 8-19) to 0.03 in the shake table tests is likely due to contamination from flaked off material in repetitive testing and airborne dust collecting in the lubricant in the unsealed model bearings.

The results of analysis of the braced frame with the Double 1 configuration and the moment frame with the Double 2 configuration are compared to the experimental results in figures B-1 through B-21 of Appendix B. Representative results from the Sylmar 360 and Pacoima 164 motions are provided in figures 6-9 and 6-10. There is generally very good agreement in terms of tracking the isolation system displacements and in the prediction of the shear force. This applies also for the bidirectional (longitudinal + vertical) and tridirectional tests. When there is excitation in both the longitudinal and transverse directions, the analytical model is capable of accurately reproducing the actual displacement orbits and the shear forces in each principal direction. Mosqueda *et al.* (2004) were able to get results of similar accuracy from bidirectional tests of a simpler rigid block frame using a coupled plasticity model for the single FP bearings. The results of this present study help to further experimentally validate single FP link elements in SAP2000 for bidirectional (longitudinal + transverse) excitation.

TABLE 6-6 **Properties of FP Elements Used in Response History Analysis of Double 1 and Double 2 Configurations**

Parameter	Double 1	Double 2
Supported Weight (kN)	55.6	52.3
FP Link Element Height (mm)	150	150
Dynamic Mass (kN-sec^2/mm)	1.75×10^{-6}	1.75×10^{-6}
Shear Deformation Location (mm)	75	75
Vertical Stiffness (kN/mm)	3000	3000
Effective Stiffness (kN/mm)	0.255	0.466
Yield Displacement (mm)	0.025	0.025
Elastic Stiffness (kN/mm)	65	290
Coefficient of Friction, Slow	0.0093	0.07
Coefficient of Friction, Fast	0.03	0.14
Radius (mm)	878	878
Rate Parameter (sec/mm)	0.015	0.0079
Torsional Stiffness (kN-mm/rad)	0	0
Rotational Stiffness (kN-mm/rad)	Fixed	Fixed

The analysis also predicts the permanent displacement of the isolators with a good deal of accuracy. The predictions are better for the Double 1 configuration since there is a smaller range of displacements for which the static friction force balances the restoring force. There is slightly larger error in the prediction of permanent displacements for the Double 2 configuration, but this system is of relatively high friction and there is a larger range of displacements for which the two forces balance. The theoretical upper bound permanent displacement for the Double 1 and Double 2 configurations are 8.2mm and 61mm respectively. Considering the large range of displacements for which the Double 2 configuration will be in equilibrium, these analytical estimates of the permanent displacement are actually quite good.

6.4.2 Modeling and Analysis Results for the Triple 1, Triple 2 and Triple 3 Configurations

The Triple 1 and Triple 2 configurations both have coefficients of friction with relative values $\mu_2 = \mu_3 < \mu_1 = \mu_4$. It was described in Section 7 that for this type of configuration the behavior can be modeled with two FP link elements connected in series; the first representing the inner surfaces having radius of $R_{eff\,2} + R_{eff\,3}$ and friction coefficient of $\mu_2 = \mu_3$, the second representing the outer concave surfaces and having radius of $R_{eff\,1} + R_{eff\,4} - R_{eff\,2} - R_{eff\,3}$ and friction coefficient of $\mu_1 = \mu_4$. The rate parameter that is assigned must also be equal to half of the actual value for each material to reflect the fact that one link element is being used to represent sliding on two surfaces. For the Triple 3 configuration, three FP link elements are used to model the behavior since there are different liner materials on the two outer surfaces. To simplify the analysis, gap elements are only used for the analysis cases in which there is the possibility of contact with the displacement restrainer.

FIGURE 6-9   Comparison of Experimental and Analytical Results for Sylmar 090 and Pacoima 164 Ground Motions with Isolation System Double 1

143

FIGURE 6-10 Comparison of Experimental and Analytical Results for Sylmar 090 and Pacoima 164 Ground Motions with Isolation System Double 2

The parameters assigned to the link elements used to represent the Triple 1, Triple 2 and Triple 3 configurations are listed in tables 6-7, 6-8 and 6-9 respectively. Again, the friction coefficients and rate parameter used in the analysis were assigned based on the experimental results, with the same value specified in each analysis case for a particular configuration.

TABLE 6-7 Properties of FP Elements Used in Response History Analysis of Triple 1 Configuration

Parameter	Element FP 1	Element FP 2
Supported Weight (kN)	52.3	52.3
FP Link Element Height (mm)	75	75
Dynamic Mass (kN-sec^2/mm)	1.75×10^{-6}	1.75×10^{-6}
Shear Deformation Location (mm)	0	75
Vertical Stiffness (kN/mm)	2660	2660
Effective Stiffness (kN/mm)	0.492 (0.492[1])	0.440 (0.481)
Yield Displacement (mm)	0.025	0.025
Elastic Stiffness (kN/mm)	125 (125)	270 (310)
Coefficient of Friction, Slow	0.05 (0.02)	0.065 (0.12)
Coefficient of Friction, Fast	0.06 (0.06)	0.13 (0.15)
Radius (mm)	106	764
Rate Parameter (sec/mm)	0.0079	0.0059
Torsional Stiffness (kN-mm/rad)	0	0
Rotational Stiffness (kN-mm/rad)	Fixed	Fixed

1. Value in parenthesis is value used in analysis of multidirectional tests. Sliders were disassembled and reassembled in between test sequences.

TABLE 6-8 Properties of FP Elements Used in Response History Analysis of Triple 2 Configuration

Parameter	Element 1	Element 2
Supported Weight (kN)	52.3	52.3
FP Link Element Height (mm)	75	75
Dynamic Mass (kN-sec^2/mm)	1.75×10^{-6}	1.75×10^{-6}
Shear Deformation Location (mm)	0	75
Vertical Stiffness (kN/mm)	2660	2660
Effective Stiffness (kN/mm)	0.511	0.583
Yield Displacement (mm)	0.025	0.025
Elastic Stiffness (kN/mm)	145	410
Coefficient of Friction, Slow	0.05	0.18
Coefficient of Friction, Fast	0.07	0.20
Radius (mm)	106	764
Rate Parameter (sec/mm)	0.0079	0.0059
Torsional Stiffness (kN-mm/rad)	0	0
Rotational Stiffness (kN-mm/rad)	Fixed	Fixed

TABLE 6-9 Properties of FP Elements Used in Response History Analysis of Triple 3 Configuration

Parameter	Element 1	Element 2	Element 3
Supported Weight (kN)	52.3	52.3	52.3
FP Link Element Height (mm)	50	50	50
Dynamic Mass (kN-sec^2/mm)	1.75×10^{-6}	1.75×10^{-6}	1.75×10^{-6}
Shear Deformation Location (mm)	0	25	50
Vertical Stiffness (kN/mm)	4000	4000	4000
Effective Stiffness (kN/mm)	0.438	0.406	0.559
Yield Displacement (mm)	0.025	0.025	0.025
Elastic Stiffness (kN/mm)	75	255	410
Coefficient of Friction, Slow	0.015	0.11	0.12
Coefficient of Friction, Fast	0.045	0.15	0.20
Radius (mm)	106	382	382
Rate Parameter (sec/mm)	0.0079	0.0158	0.0118
Torsional Stiffness (kN-mm/rad)	0	0	0
Rotational Stiffness (kN-mm/rad)	Fixed	Fixed	Fixed

The results of analysis of the moment frame with the Triple 1, Triple 2 and Triple 3 configurations are compared to the experimental results in figures B-22 through B-45 of Appendix B. Representative results from the Sylmar 360 and Pacoima 164 motions for these three configurations are provided in figures 6-11, 6-12 and 6-13. The SAP2000 analysis results reproduce quite accurately the hysteresis loops and displacement histories measured from the experiment. The analysis captures the transitions in stiffness and the correct forces and displacements at which these occur. This applies regardless of whether two FP link elements (Triple 1 and Triple 2 configurations) or three FP link elements (Triple 3 configuration) are used to represent behavior. There is good accuracy in reproducing the experimental displacement orbits and hysteresis loops for the bidirectional (longitudinal + vertical) and tridirectional analysis cases as well. Since the model also captures the velocity dependence of the coefficient of friction, this experimentally verifies that the analytical model is capable of capturing the behavior accounting for the effects of bilateral loading and rate dependent phenomena. This extends the basic capabilities in Sections 6 and 7 since the model is shown to reproduce the response of a complex, vertically flexible MDOF system with multiple isolators for random earthquake excitation.

Due to the multiple phases in sliding behavior, random motion is much more demanding analytically the sinusoidal input that was used to experimentally verify the behavior in Section 7. After a large displacement excursion, it is possible for the slider to oscillate on the innermost surfaces with the slide plates still in an offset position. Sometimes there is a slight error in the analytical prediction of the outer concave surfaces' displacement when they come to rest during the motion. Since sliding occurs on these surfaces only during the more intense periods of ground shaking, if there is some error in the displacement calculation when motion on one of these surfaces stops then it will manifest itself as an offset in the total bearing displacement throughout the remainder of the excitation. This is

equivalent to error in prediction of the permanent displacement of one of the FP link elements. In general, for all three systems there is good agreement in reproducing the experimental displacement results; however when there is error, it is primarily displacement offsets attributed to this phenomenon.
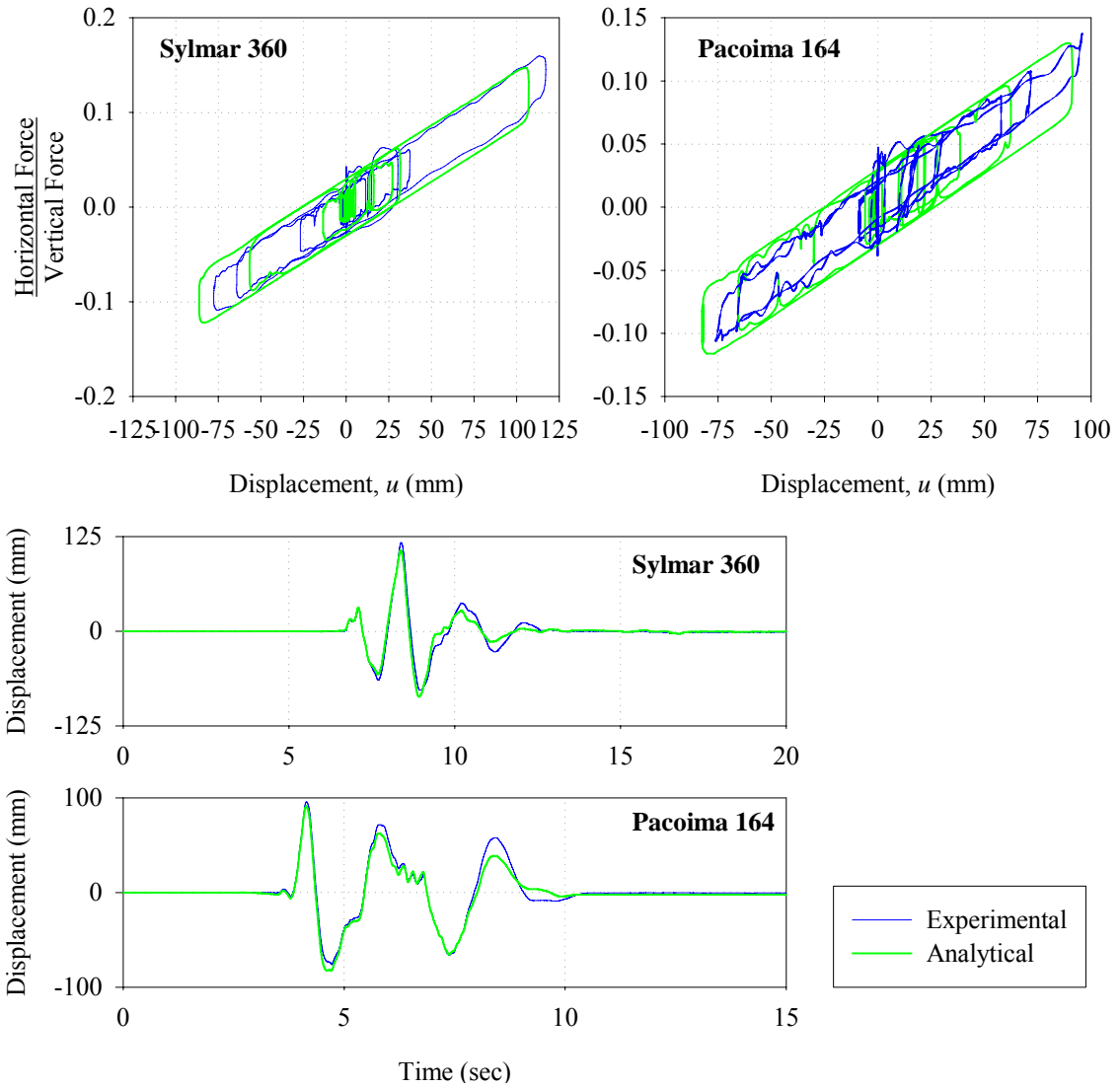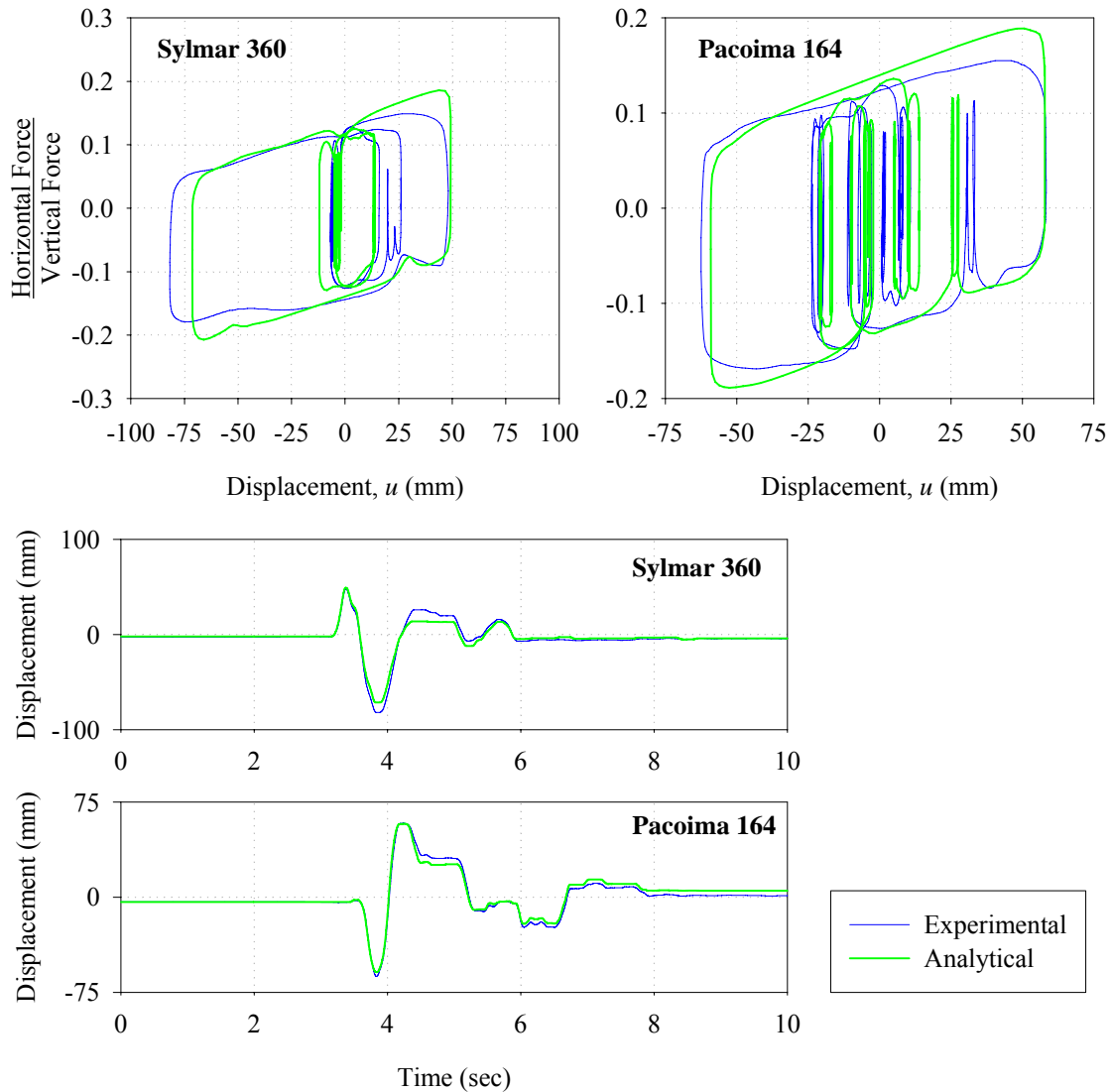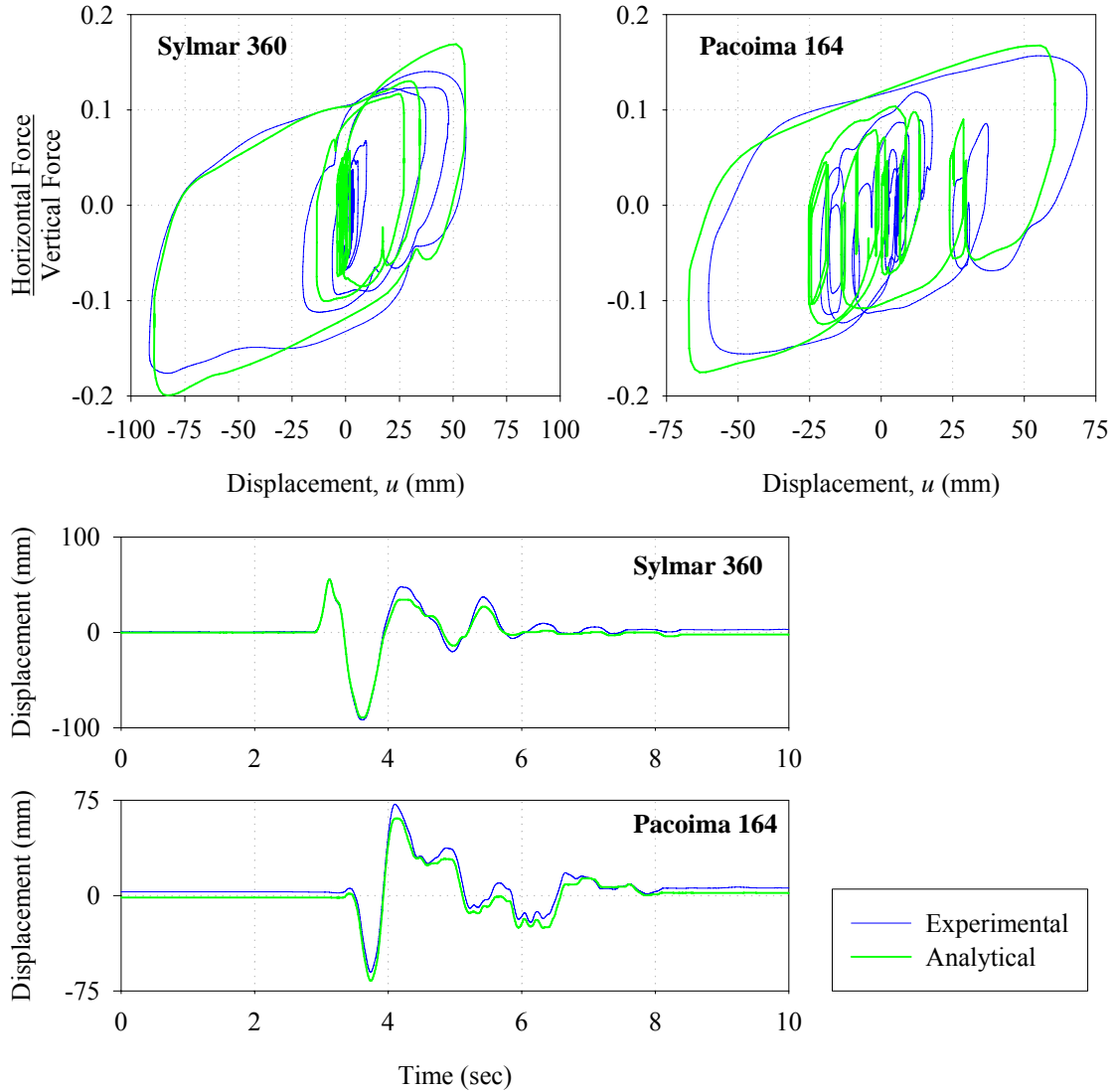

FIGURE 6-11 Comparison of Experimental and Analytical Results for Sylmar 090 and Pacoima 164 Ground Motions with Isolation System Triple 1
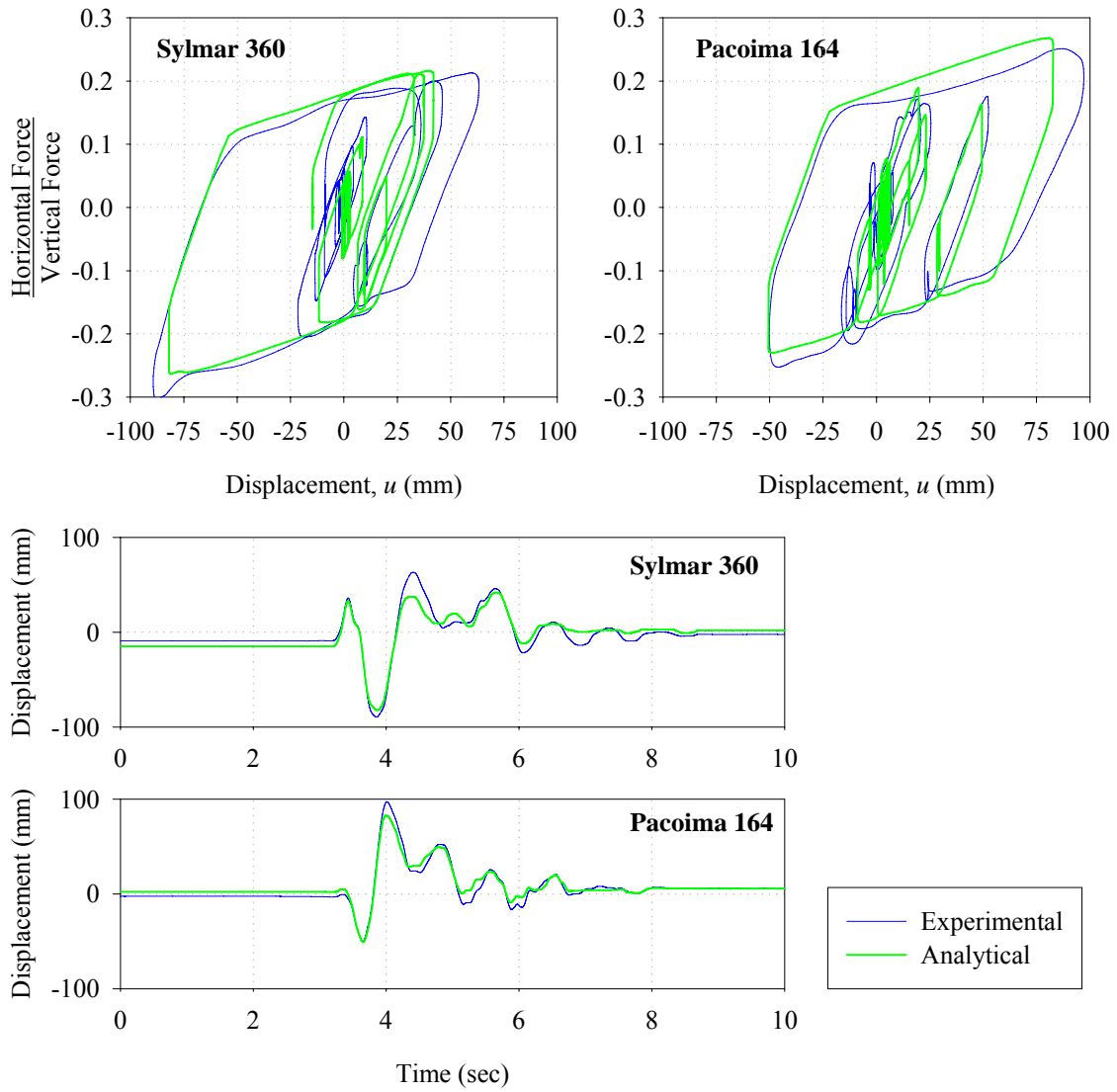
FIGURE 6-12 Comparison of Experimental and Analytical Results for Sylmar 090 and Pacoima 164 Ground Motions with Isolation System Triple 2
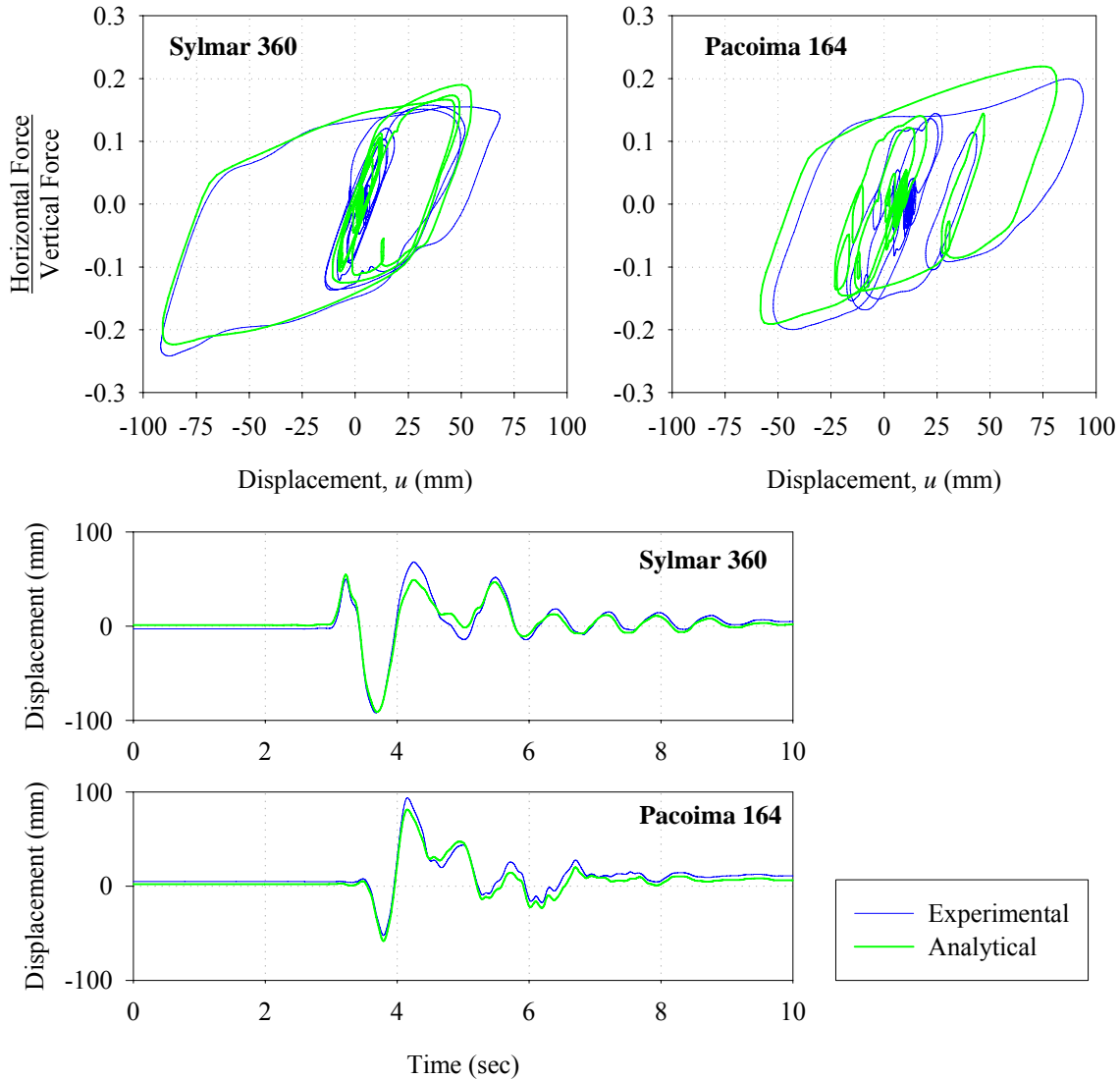
FIGURE 6-13 Comparison of Experimental and Analytical Results for Sylmar 090 and Pacoima 164 Ground Motions with Isolation System Triple 3

6.4.3 Large Amplitude Motions and Contact with the Displacement Restrainer

In larger amplitude tests (those listed in table 9-7), gap elements were included in the analytical model of the isolators to capture the behavior upon contact with the displacement restrainer. Since contact was expected only on the outer surface of lower friction, only one set of gap elements was used per isolator. Each gap element was a pin-ended two-joint link, 150mm in length and aligned along the longitudinal direction of the structure. The specific properties assigned to the elements are given in table 6-10. Note that the gap size of 53.5mm assigned to each element was calculated based on the actual displacement capacity of the outer sliding surface, 61mm. This is less than the nominal displacement capacity of 64mm due to the effects of slider height and slider rotation.

TABLE 6-10 Properties of Gap Elements Used in Response History Analysis of Triple 3 Isolation System

Parameter	Gap Element 2-3
Dynamic Mass (kN-sec^2/mm)	1.75×10^{-7}
Effective Stiffness (kN/mm)	0.5
Gap Size (mm)	53.5
Stiffness After Closing (kN/mm)	250

The results of these large amplitude analysis cases for the Sylmar 360, Newhall 360 and Pacoima 164 motions are provided in figures B-46 through B-49 of Appendix B. There is good agreement in terms of reproducing the hysteresis loops and displacement histories including the residual displacements. Moreover, it is also correctly predicted that there is contact with the displacement restrainer only for the 115% Sylmar excitation. The experimental and analytical hysteresis loops from this test are shown in figure 6-14. The stiffening behavior after contact with the restrainer (after engaging the gap element in the analytical model) is evident in the force-displacement loops. However, due to the velocity dependence of the coefficient of friction which causes the roundedness of the loops near the maximum displacement, it is difficult to absolutely confirm that the stiffness after contact is the same in both the experiment and the analysis. The agreement however, seems reasonable based on the inset of figure 6-14. Furthermore, the validation provided in Section 7 should give added confidence in the accuracy of the analytical model in capturing the stiffening behavior after contact. The history of gap element axial force for the SE bearing, which is the force that would be imparted to the displacement restrainer, is provided in figure 6-15. Consistent with the experimental results, the analysis predicts contact over only a short duration of time – 0.15sec in the analysis compared to 0.18sec observed in the experiment.

As an additional example to evaluate the analytical prediction of behavior upon contact, the 200% tridirectional El Centro test of the Double 1 configuration is investigated. Recall that in this test there was substantial impact with the displacement restrainers as well as uplift. For this configuration, contact with the displacement restrainer is made only as the bearing reaches its full displacement capacity. Therefore there is an abrupt transition to high stiffness as opposed to the gradual stiffening exhibited by the triple FP bearing.

For this analysis, the bearings were modeled the same as before (refer to the properties of the Double 1 configuration listed in table 6-6). Connected to the top node of each FP link element was an assembly of 16 gap elements spaced radially at 22.5° increments. This very closely approximated the circular displacement restrainer. The gap size of each element was 141mm based on the actual displacement capacity of the bearing accounting for the effects of slider height and slider rotation.
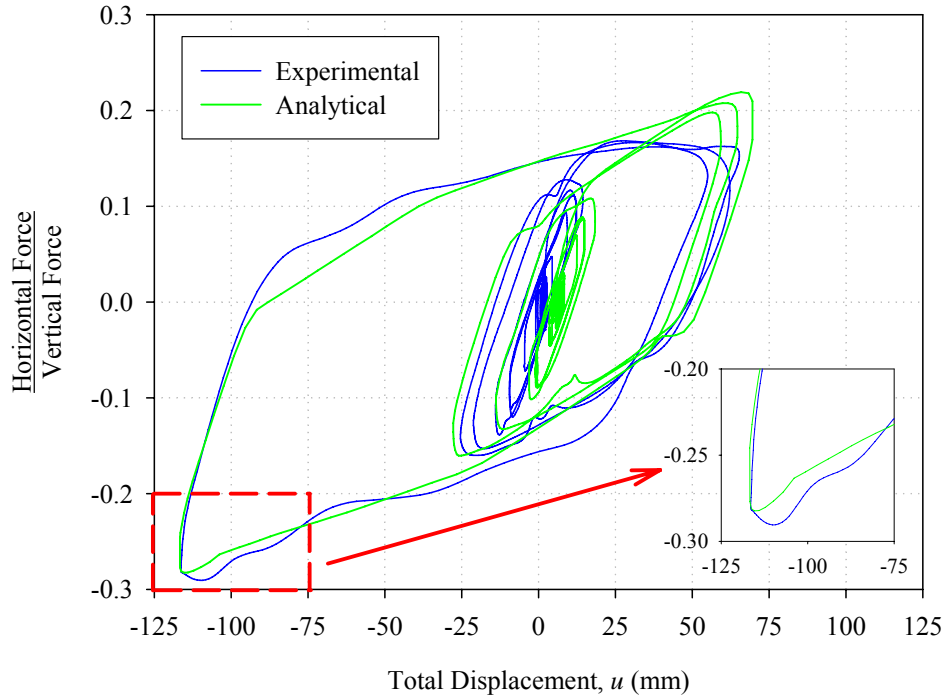
FIGURE 6-14 Comparison of Experimental and Analytical Loops from Testing the Triple 3 Configuration with 115% Sylmar 360 Excitation (Contact Made with Displacement Restrainer)
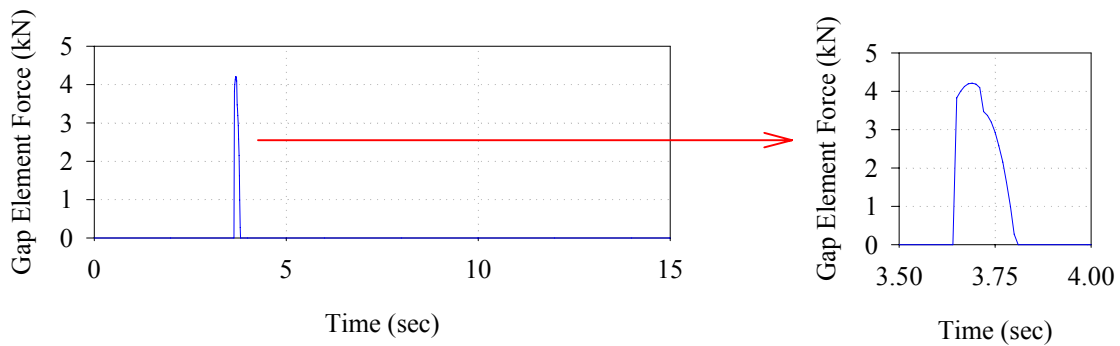
FIGURE 6-15 History of Gap Element Axial Force from the Test of the Triple 3 Configuration with 115% Sylmar 360 Excitation

Initially, the gap elements were assigned very large stiffness following the assumption that they were basically rigid. The stiffness upon closing of each element was 250kN/mm. Figure 6-16 compares the displacement orbits measured from the experiment with those from the analysis and figure 6-17 compares the hysteresis loops in the longitudinal and transverse directions. The analysis reproduces well the displacement orbits and the effect of the displacement restrainer in arresting motion. However, the hysteresis loops clearly do not agree well with the experimental results. The base shear is substantially overpredicted when the displacement restrainer is contacted and there are

151

additional spikes in shear due to the model predicting contact which did not occur in the experiment. The later phenomenon is due to the slider rebounding off the displacement restraint at one end with overestimated velocity and subsequently impacting the displacement restrainer at the other end of travel. These observations are consistent with those of Zayas *et al*. (1989) when they modeled the single FP with a rigid displacement restrainer. The authors of that study also point out that use of a rigid displacement restrainer in the model results in purely elastic response of the bearing upon contact, which is inconsistent with the true behavior. In actuality there is energy dissipation due to (a) impact, (b) friction from steel on steel contact between the displacement restrainer and the slider and (c) plastic deformation of the restrainer ring itself.

FIGURE 6-16 Comparison of Displacement Orbits Measured from Experiment and those Obtained from Analysis Using Gap Elements to Model the Displacement Restrainer (Gap Element Stiffness = 250 kN/mm)

A more accurate approach is to assign a smaller stiffness value to the gap elements upon engagement of the displacement restrainer. A second analysis was carried out using a stiffness of 0.5kN/mm upon engagement of each gap element, which corresponds to approximately ten times the stiffness of the bearing after the initiation of sliding ($10W/R_{eff}$). The displacement orbits and hysteresis loops from this analysis are presented in figures 6-18 and 6-19. Using a finite value for the displacement restrainer stiffness, the model quite accurately estimates the base shear in the longitudinal and transverse directions. The most obvious error is that displacements beyond the restrainer are erroneously predicted. However, for engineering purposes it is much more important to accurately predict the peak base shear upon contacting the displacement restrainer. This value is important as it could be used for design of the superstructure or foundation

152

elements. Common sense dictates that displacements beyond those of the displacement restrainer are only possible when failure of the restrainer occurs.

FIGURE 6-17 Comparison of Longitudinal and Transverse Hysteresis Loops Measured from Experiment and those Obtained from Analysis Using Gap Elements to Model the Displacement Restrainer (Gap Element Stiffness = 250 kN/mm)
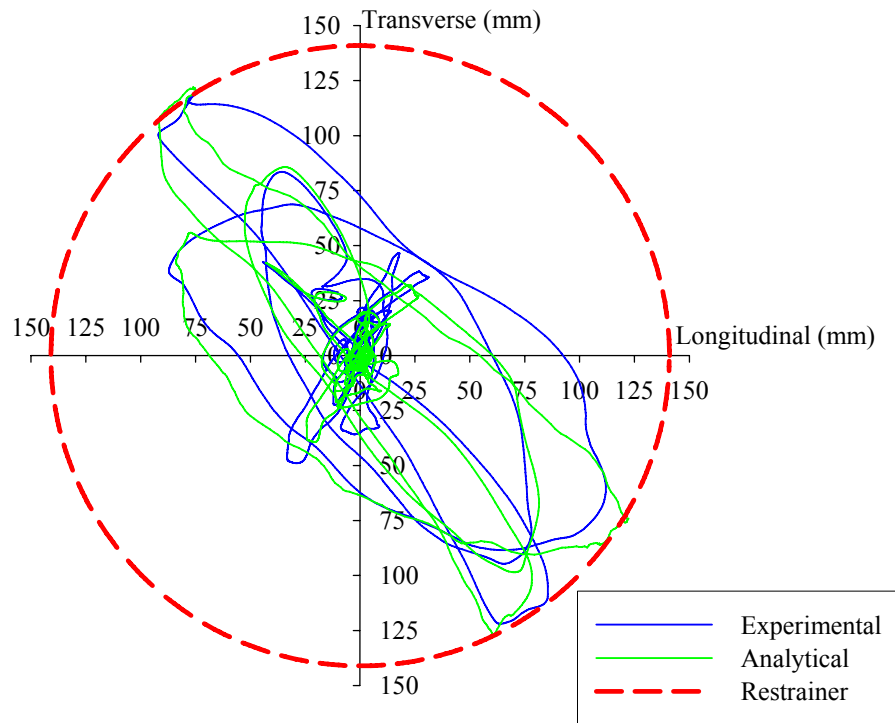

FIGURE 6-18 Comparison of Displacement Orbits Measured from Experiment and those Obtained from Analysis Using Gap Elements to Model the Displacement Restrainer (Gap Element Stiffness = 0.50 kN/mm)
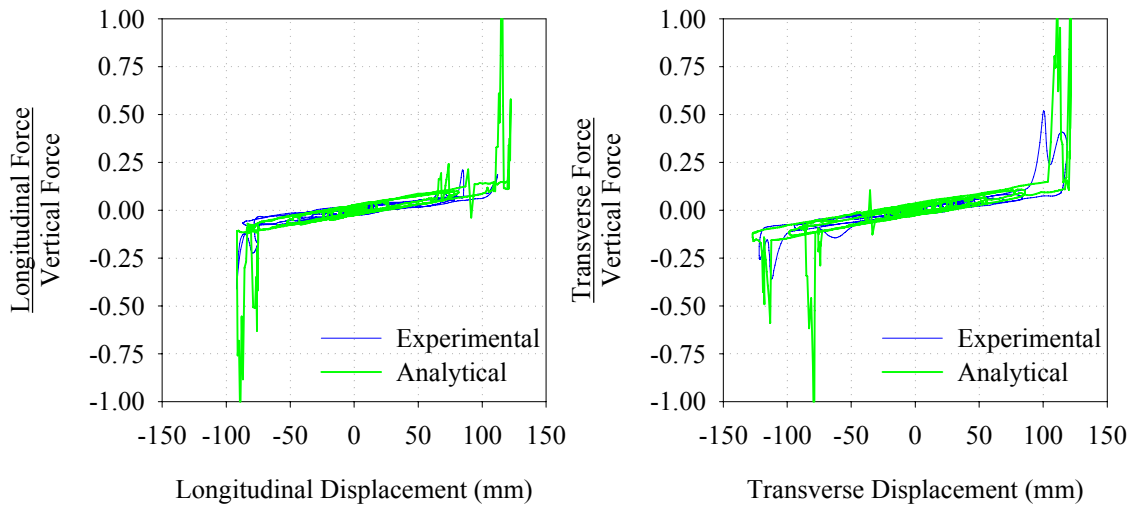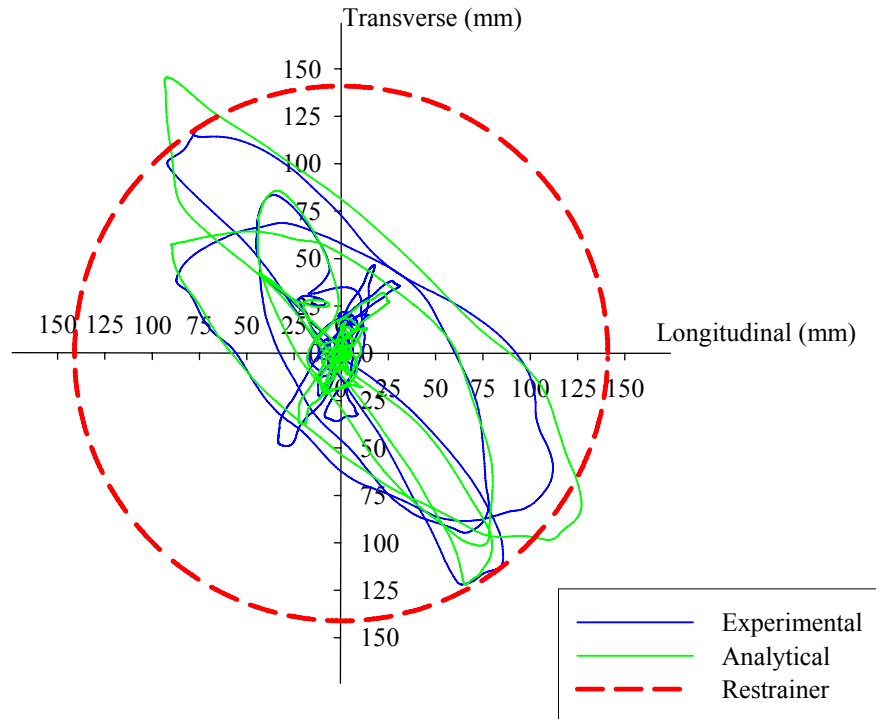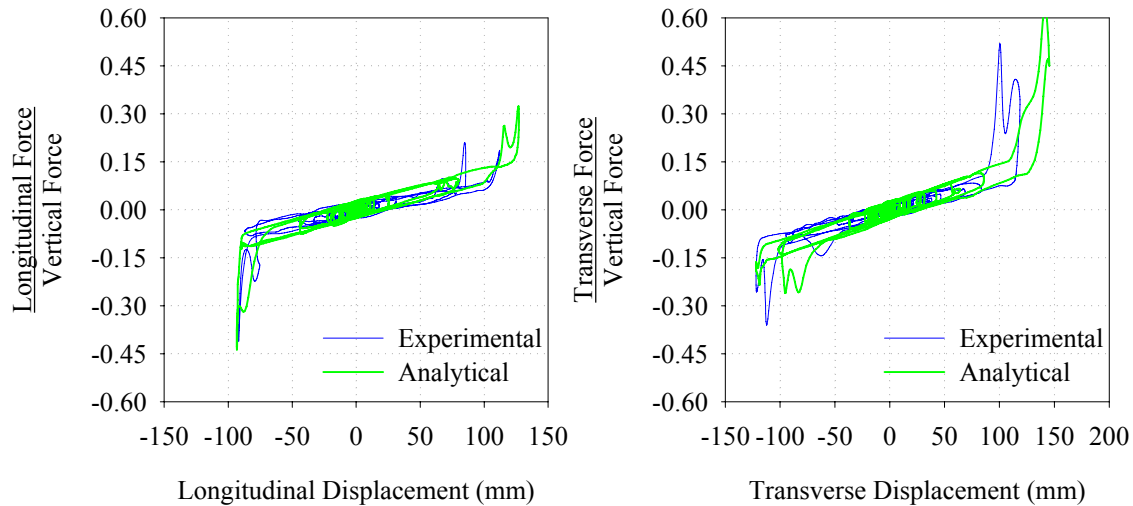
153

FIGURE 6-19   Comparison of Longitudinal and Transverse Hysteresis Loops Measured from Experiment and those Obtained from Analysis Using Gap Elements to Model the Displacement Restrainer (Gap Element Stiffness = 0.50 kN/mm)

It should be noted that the tested model bearings had substantial strength in the restrainer, whereas full size bearings would have a restrainer strength that is only marginally more than the maximum force that the bearings can mobilize just short of their displacement capacity. Therefore, realistic models for analysis should account for the limited strength of the restrainer. In the tested model, there was no need to model this strength as the peak force measured on contact in the tests remained within the elastic limits since no failure or permanent deformation of the restrainer was observed.

6.4.4 Prediction of Variation of Axial Load and Vertical Displacements

Validating the analytical predictions of behavior under extreme dynamic conditions such as bearing uplift is important since it demonstrates the robustness of the analytical models and gives engineers added confidence in the model's capability to predict behavior for more moderate events. In addition to being able to track the histories of vertical load on the bearings, for triple FP bearings it is also useful for design if the uplift displacements can be accurately predicted.

The histories of vertical load on each bearing as well as the histories of vertical displacement for the Triple 1 and Triple 3 configurations tested with tridirectional Newhall excitation are compared in figures 6-20 through 6-23 (the Triple 1 configuration is shown because there is experimental data for vertical displacements and the Triple 3 configuration is shown because it is the most general configuration consisting of three FP link elements). The maximum and minimum bearing axial forces are compared in tables 6-11 and 6-12. This motion is very demanding analytically because (a) excitation along the longitudinal and transverse directions results in each of the four bearings having a different history of vertical load and (b) it has the strongest

154

FIGURE 6-20 Comparison of Experimental and Analytical Vertical Load Histories from Testing the Triple 1 Configuration with Tridirectional Newhall Excitation

FIGURE 6-21 Comparison of Experimental and Analytical Vertical Displacement Histories from Testing the Triple 1 Configuration with Tridirectional Newhall Excitation

156

FIGURE 6-22 Comparison of Experimental and Analytical Vertical Load Histories from Testing the Triple 3 Configuration with Tridirectional Newhall Excitation

157

FIGURE 6-23 Analytical Vertical Displacement Histories from Testing the Triple 3 Configuration with Tridirectional Newhall Excitation

TABLE 6-11 Comparison Experimental and Analytical Values of Bearing Vertical Forces from Test of Triple 1 Configuration with Tridirectional Newhall Excitation

	Minimum Vertical Load (kN)		Maximum Vertical Load (kN)	
	Experimental	Analytical	Experimental	Analytical
NW Bearing	0	0	106	111
NE Bearing	5	0	162	138
SE Bearing	0	0	140	136
SW Bearing	0	0	118	111

TABLE 6-12 Comparison Experimental and Analytical Values of Bearing Vertical Forces from Test of Triple 3 Configuration with Tridirectional Newhall Excitation

	Minimum Vertical Load (kN)		Maximum Vertical Load (kN)	
	Experimental	Analytical	Experimental	Analytical
NW Bearing	0	0	101	118
NE Bearing	4	0	177	142
SE Bearing	0	0	140	139
SW Bearing	0	0	135	119

vertical component of all motions considered resulting in considerable uplift and variation in total axial load. For both configurations, the analysis qualitatively reproduces the experimental histories of vertical load and predicts the peak values within approximately 10%-15% on average. Results of this accuracy for such extreme response are typically suitable for engineering purposes.

The analysis less accurately estimates the vertical displacements during the test. The analytical values of vertical displacement reported are the relative vertical displacements of the top node of the FP link assembly with respect to the bottom node. Experimental data from the Triple 1 configuration indicates that there was a maximum of approximately 5.5mm of vertical motion of the top concave plate relative to the bottom plate. Approximately 3mm of this motion is from sliding up the concave surfaces meaning that there was approximately 2.5mm of separation during the test. Although the FP link elements in SAP2000 do not reproduce the vertical displacements due to sliding up the curved plates, it was originally thought that it would be possible to predict the separation displacements upon uplift since there is gap behavior in the vertical degree of freedom. However, as shown in figure 6-21, the analysis largely underestimates the vertical displacements upon separation. Although no experimental data is available, vertical displacements of similar magnitude and likely similar error are predicted for the Triple 3 configuration.

Analytical predictions of the vertical load on the bearings and the vertical displacements from the 200% tridirectional El Centro test of the Double 1 configuration are shown in figures 6-24 and 6-25 respectively. The maximum and minimum vertical loads for each bearing are shown in table 6-13. These results are shown for the analysis in which the gap elements representing the displacement restrainer were not rigid after contact, but rather assigned the smaller stiffness of 0.5kN/mm. These results demonstrate that even under extreme uplift and impact conditions, the bearing axial forces can be calculated with suitable accuracy. There is some discrepancy during the intervals of extreme uplift and rebounding, due likely to localized phenomena such as impact and radiation damping that are present in reality but not modeled in the analysis. As before, the uplift displacements are largely underestimated in comparison to the experimental results.
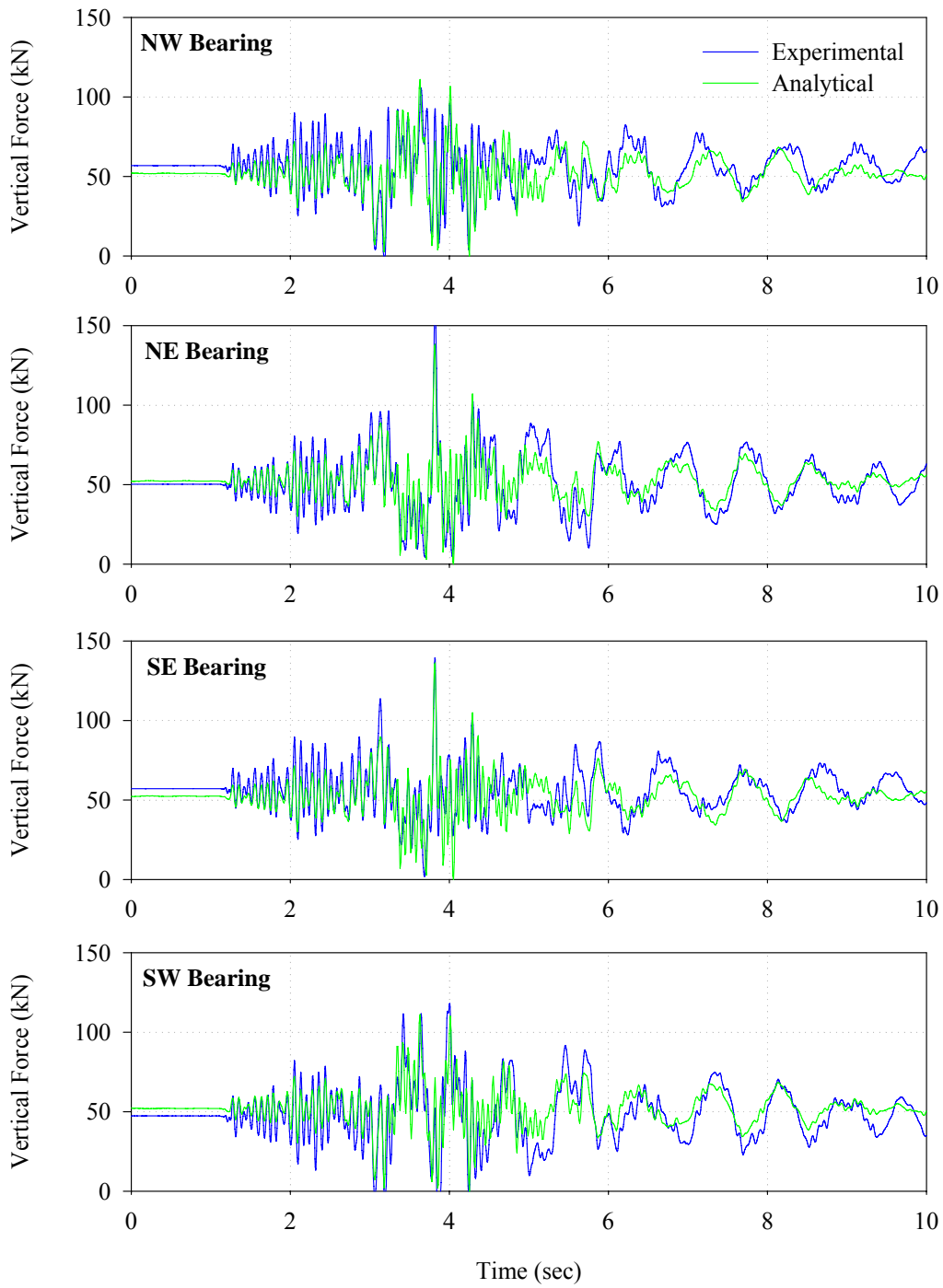
FIGURE 6-24 Comparison of Experimental and Analytical Vertical Load Histories from Testing the Double 1 Configuration with 200% Tridirectional El Centro Excitation
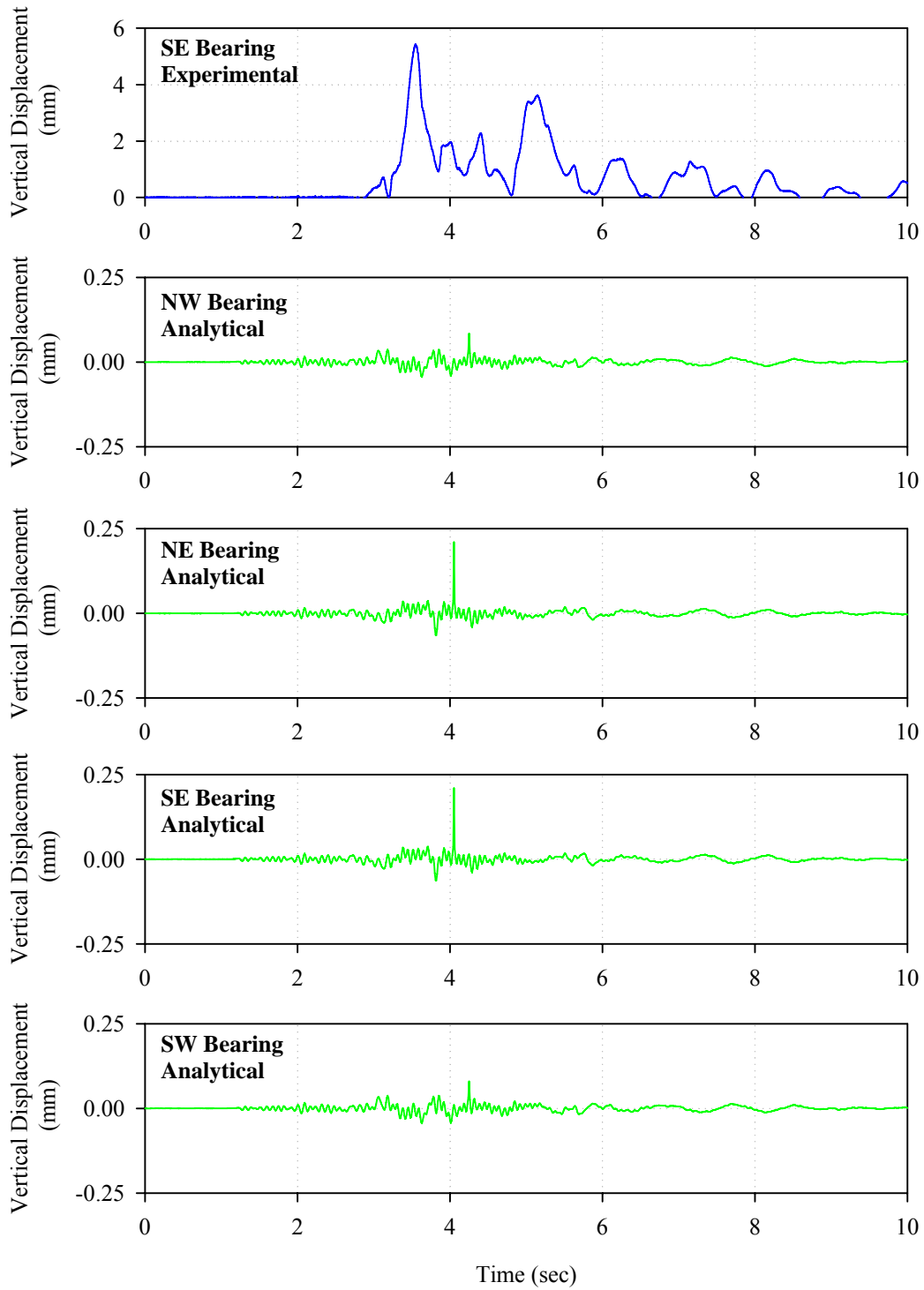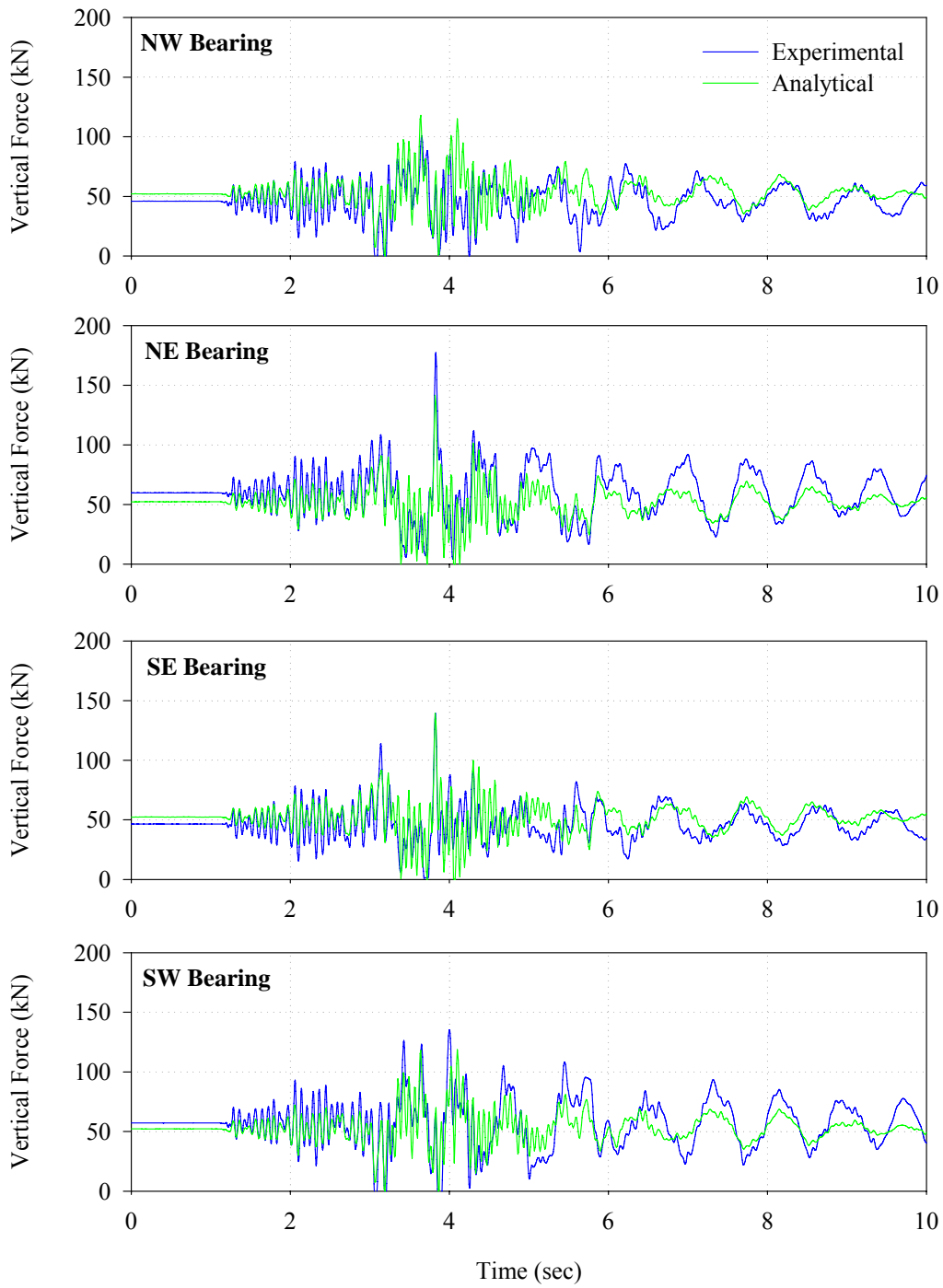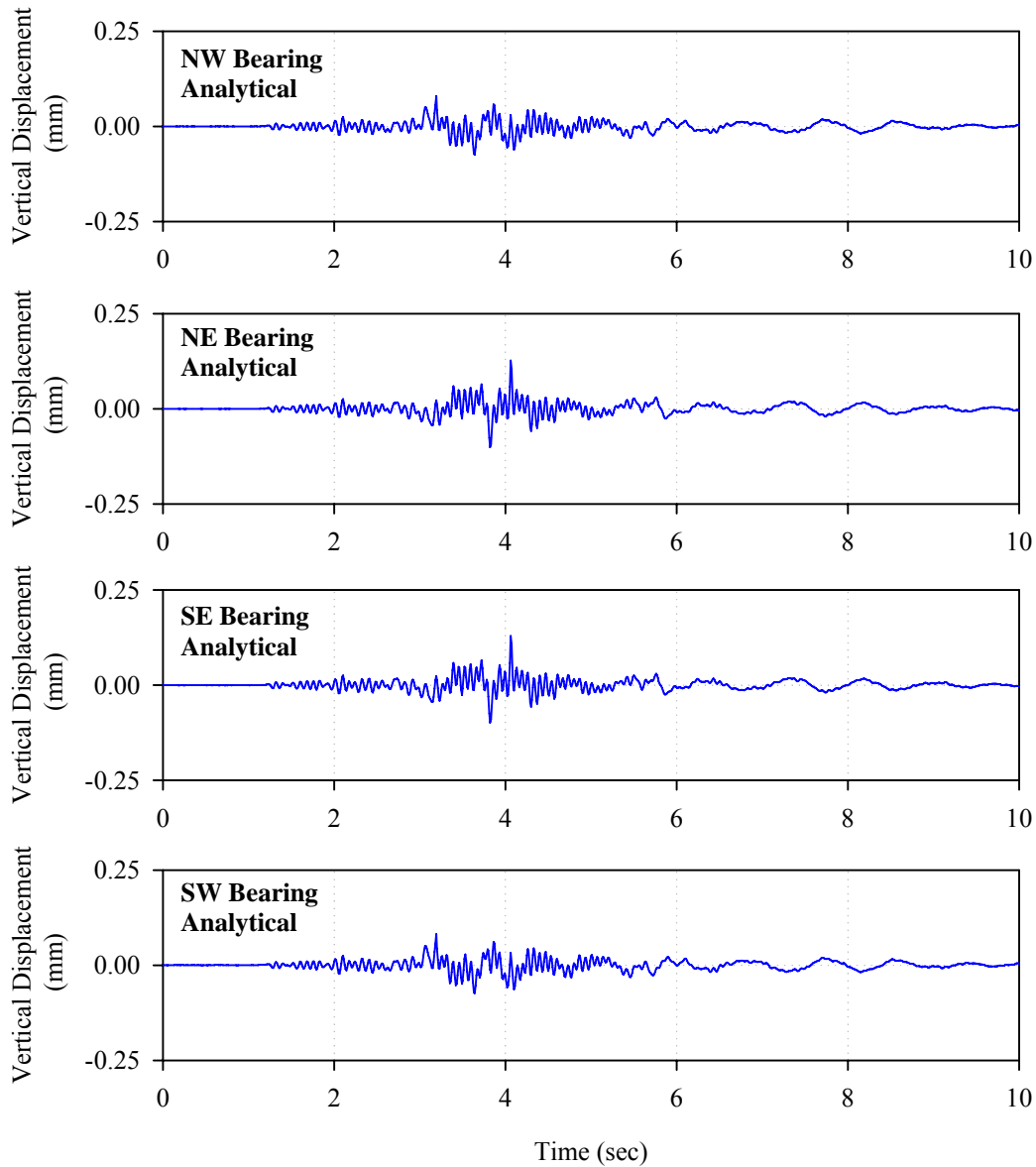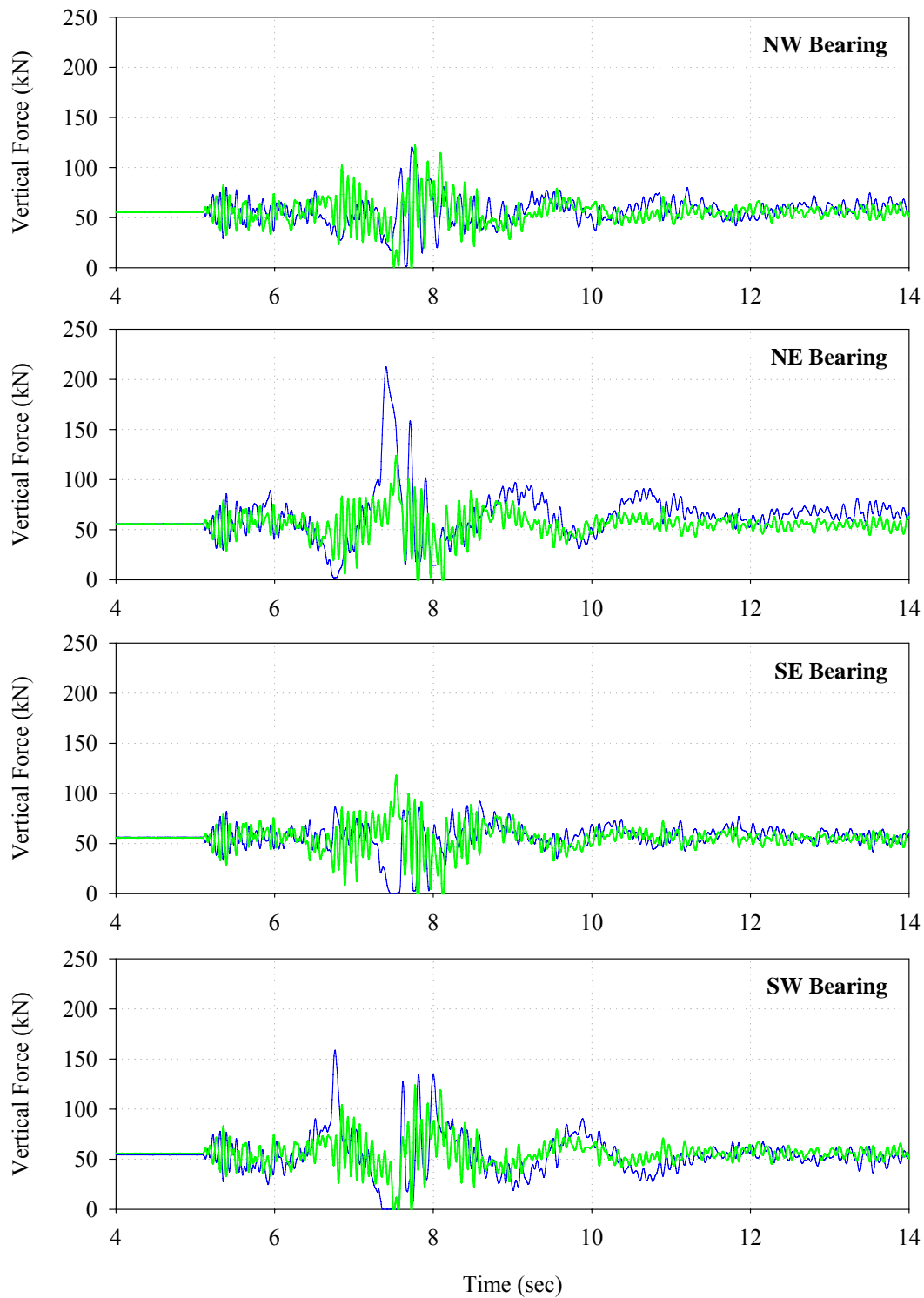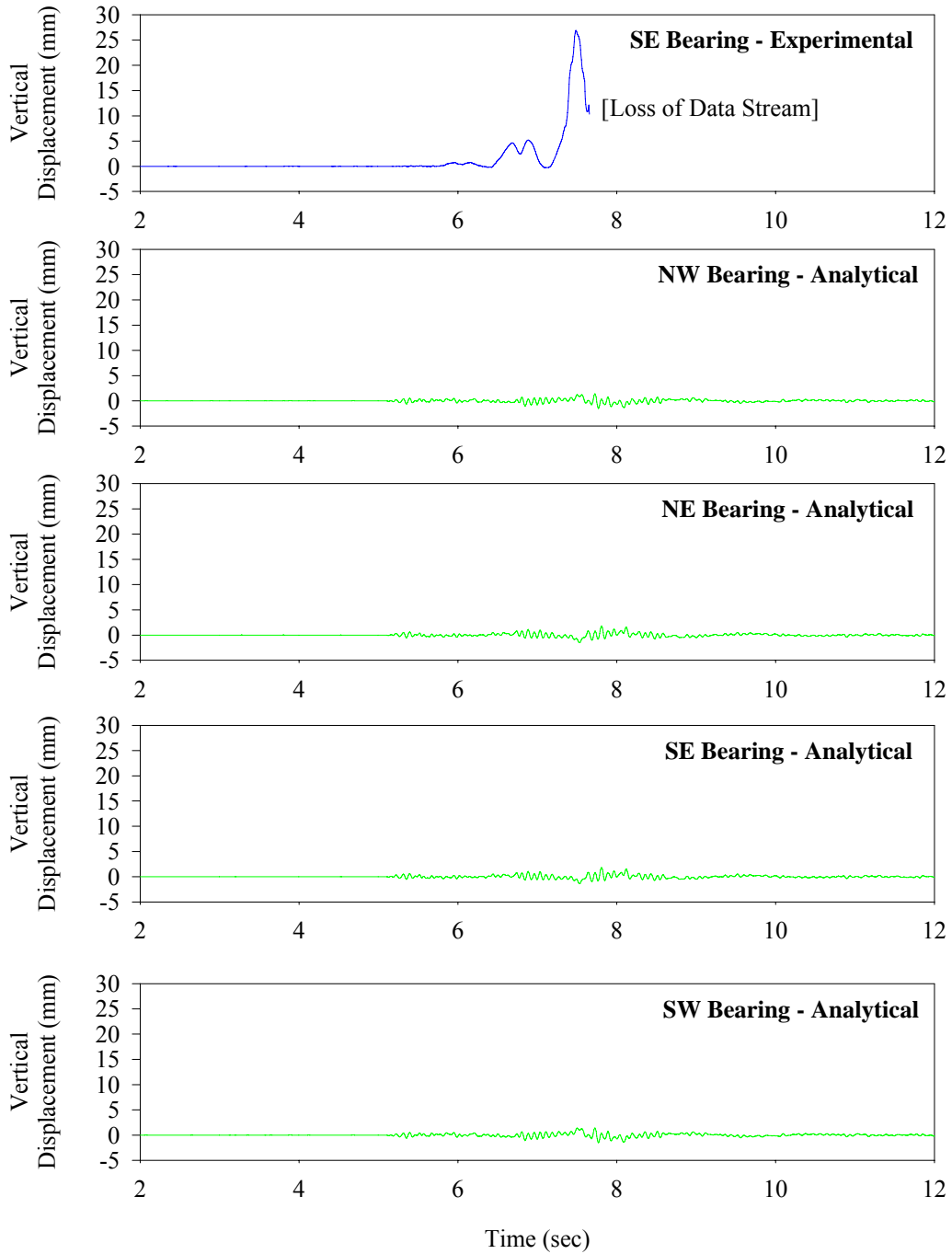
FIGURE 6-25 Comparison of Experimental and Analytical Vertical Displacement Histories from Testing the Double 1 Configuration with 200% Tridirectional El Centro Excitation

TABLE 6-13 Comparison Experimental and Analytical Values of Bearing Vertical Forces from Test of Triple 3 Configuration with 200% Tridirectional El Centro Excitation (Gap Element Stiffness = 0.5kN/mm)

	Minimum Vertical Load (kN)		Maximum Vertical Load (kN)	
	Experimental	Analytical	Experimental	Analytical
NW Bearing	0	0	121	123
NE Bearing	0	0	213	124
SE Bearing	0	0	92	118
SW Bearing	0	0	159	124

The likely reason for the inability of program SAP2000 to accurately predict substantial uplift displacement is due to the fact that such displacement was caused by rigid body rocking of the model that rested on four isolators and effectively rocked with two isolators being airborne during the uplift episode. Such behavior cannot be modeled in SAP2000 as it requires large displacement analysis capability. On the other hand, isolator uplift displacements associated with structural deformation but not rigid body rocking should be accurately predictable by small displacement analysis as that of program SAP2000 (e.g., see Scheller and Constantinou, 1999).

More accurate prediction of the uplift displacements could possibly be obtained using a finite element program such as ABAQUS and explicitly modeling the individual components of the bearing and superstructure and activating large displacement analysis. This type of analysis reproduces the actual physics of the bearing's motion rather than using a mathematical representation of springs, plasticity elements and gap elements like in programs such as SAP2000 and 3D-BASIS. However, such an analysis would likely become exceedingly complex for all but the simplest structures and is likely beyond the capabilities of most design offices. Moreover, such modeling is warranted for isolation system configurations in which uplift with rigid body rocking motion is possible.

6.4.5 Prediction of Floor Response Spectra

Floor spectra are compared in order to evaluate the accuracy of the analysis in predicting the response of nonstructural components and secondary systems in structures isolated with multi-spherical sliding bearings. Floor spectra were chosen as the best means of evaluation since they give information on the response of systems ranging from rigidly mounted components to flexibly mounted components. They also assess the accuracy of analysis over the entire duration of the response rather than just the accuracy in the prediction of the peak response.

The 5% damped floor response spectra of the sixth-story, third-story and base are shown for the Corralitos 090 and Pacoima 164 motions in figures 6-26 through 6-33. Spectra were generated for the Double 2, Triple 1, Triple 2 and Triple 3 configurations. The Pacoima 164 record was selected as it consistently resulted in the largest floor accelerations and the Corralitos 090 record was selected as it is typical of a more moderate earthquake. The figures demonstrate that the floor spectra can accurately and

reliably be calculated regardless of the degree of adaptability of the isolation system or the magnitude of the ground motion. There is good agreement even for the 200% tridirectional El Centro test of the Double 1 configuration in which there was substantial uplift and impact, as shown in Figure 6-34.

For all configurations, the results are in very good agreement up to approximately 12Hz. Beyond this, the analysis overestimated the response. Recall that for analysis of the fixed base structure (figure 6-6), response was also predicted well at lower frequencies but underestimated at higher frequencies. The source of the error and the reason the analytical results begin to deviate above 12Hz is not known. The error could either be the result of some physical phenomenon or could have also resulted from the data processing. However, at lower frequencies, both for the fixed base and isolated models the analysis predicts the floor response spectra very well. This means that the analysis can reliably be used to estimate the demands on flexibly mounted equipment in structures isolated with multi-spherical sliding bearings. Moreover, these results generally provide further evidence of the robustness and validity of the dynamic analysis methods.

FIGURE 6-26 Comparison of Experimental and Analytical Floor Response Spectra for the Double 2 System Subjected to Corralitos 090 Ground Motion

FIGURE 6-27 Comparison of Experimental and Analytical Floor Response Spectra for the Triple 1 System Subjected to Corralitos 090 Ground Motion

FIGURE 6-28 Comparison of Experimental and Analytical Floor Response Spectra for the Triple 2 System Subjected to Corralitos 090 Ground Motion

FIGURE 6-29 Comparison of Experimental and Analytical Floor Response Spectra for the Triple 3 System Subjected to Corralitos 090 Ground Motion

FIGURE 6-30 Comparison of Experimental and Analytical Floor Response Spectra for the Double 2 System Subjected to Pacoima 164 Ground Motion

FIGURE 6-31 Comparison of Experimental and Analytical Floor Response Spectra for the Triple 1 System Subjected to Pacoima 164 Ground Motion

FIGURE 6-32 Comparison of Experimental and Analytical Floor Response Spectra for the Triple 2 System Subjected to Pacoima 164 Ground Motion
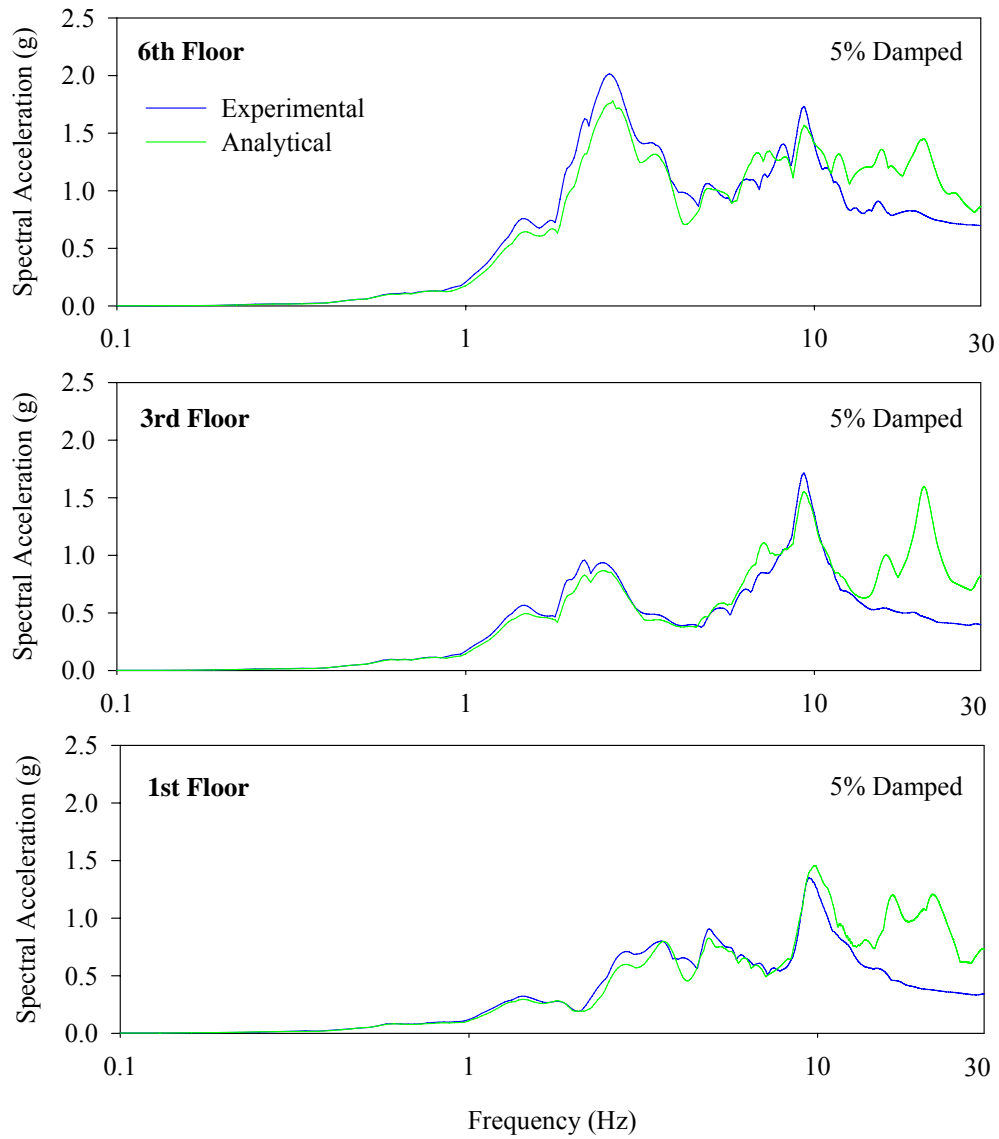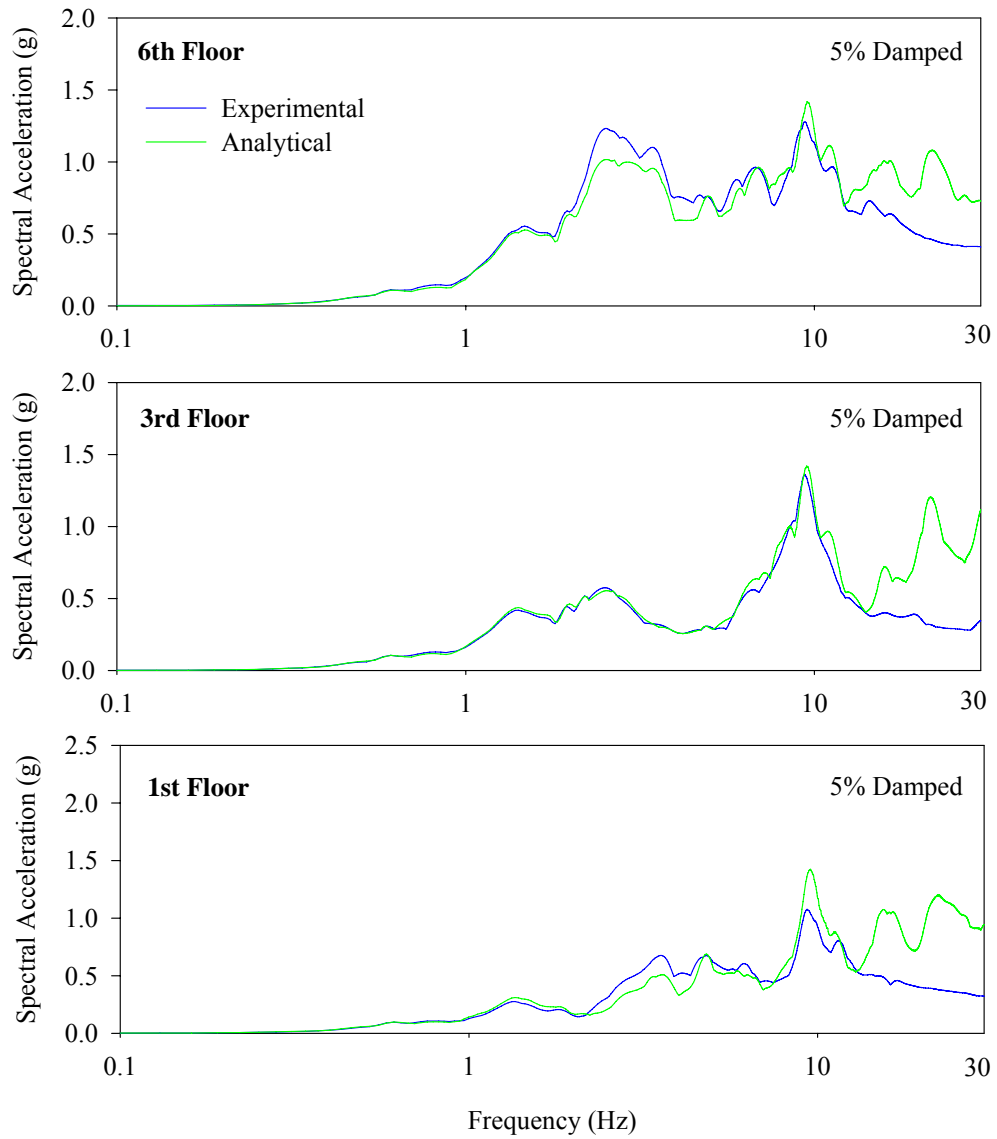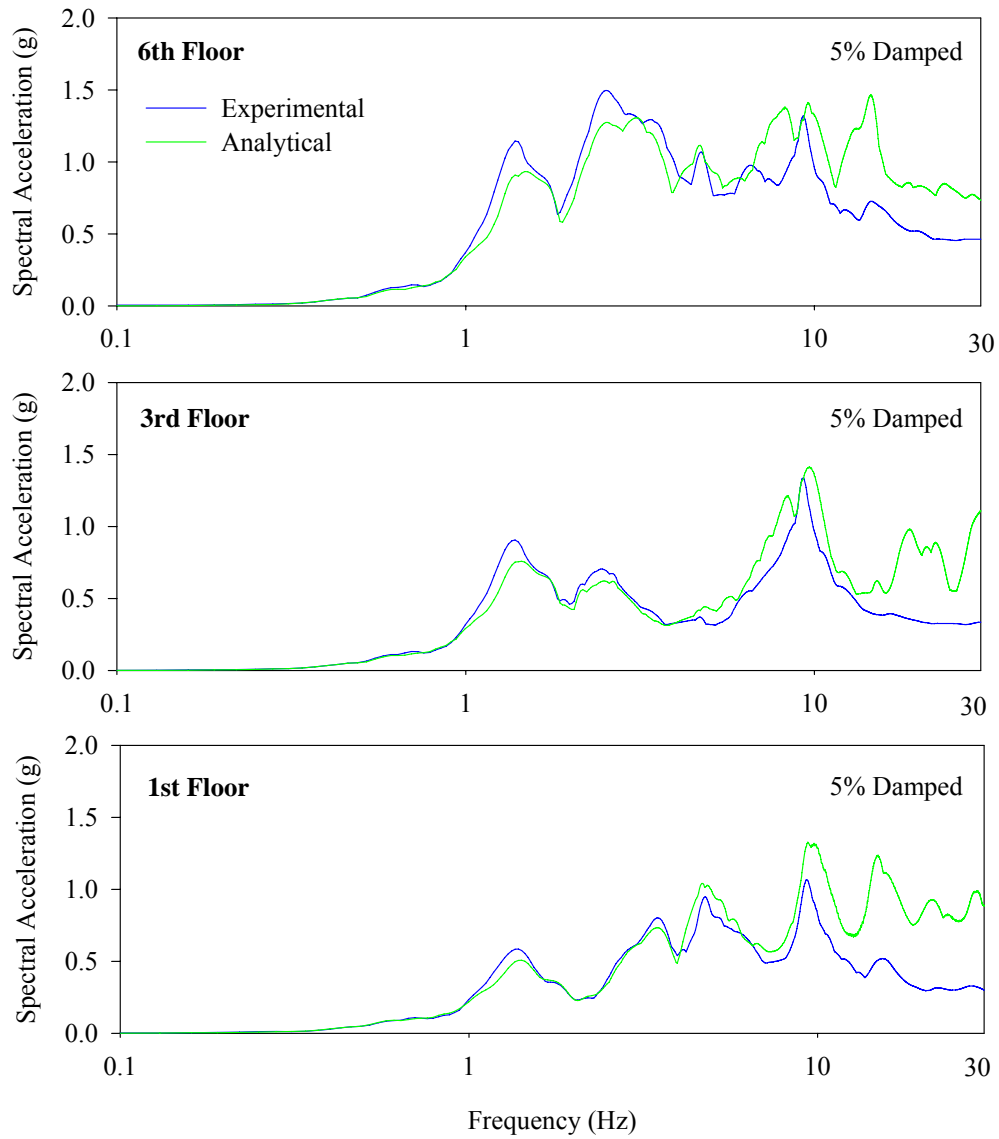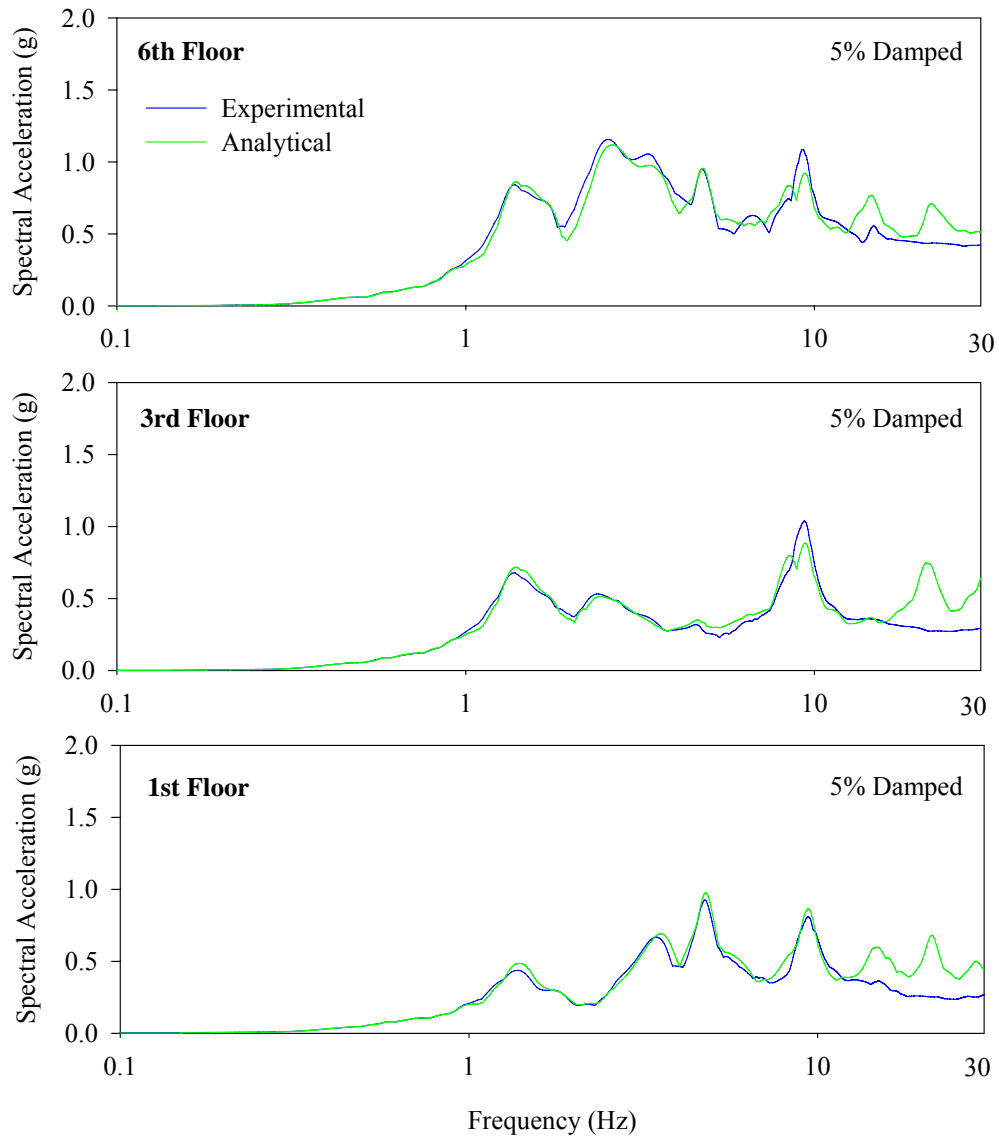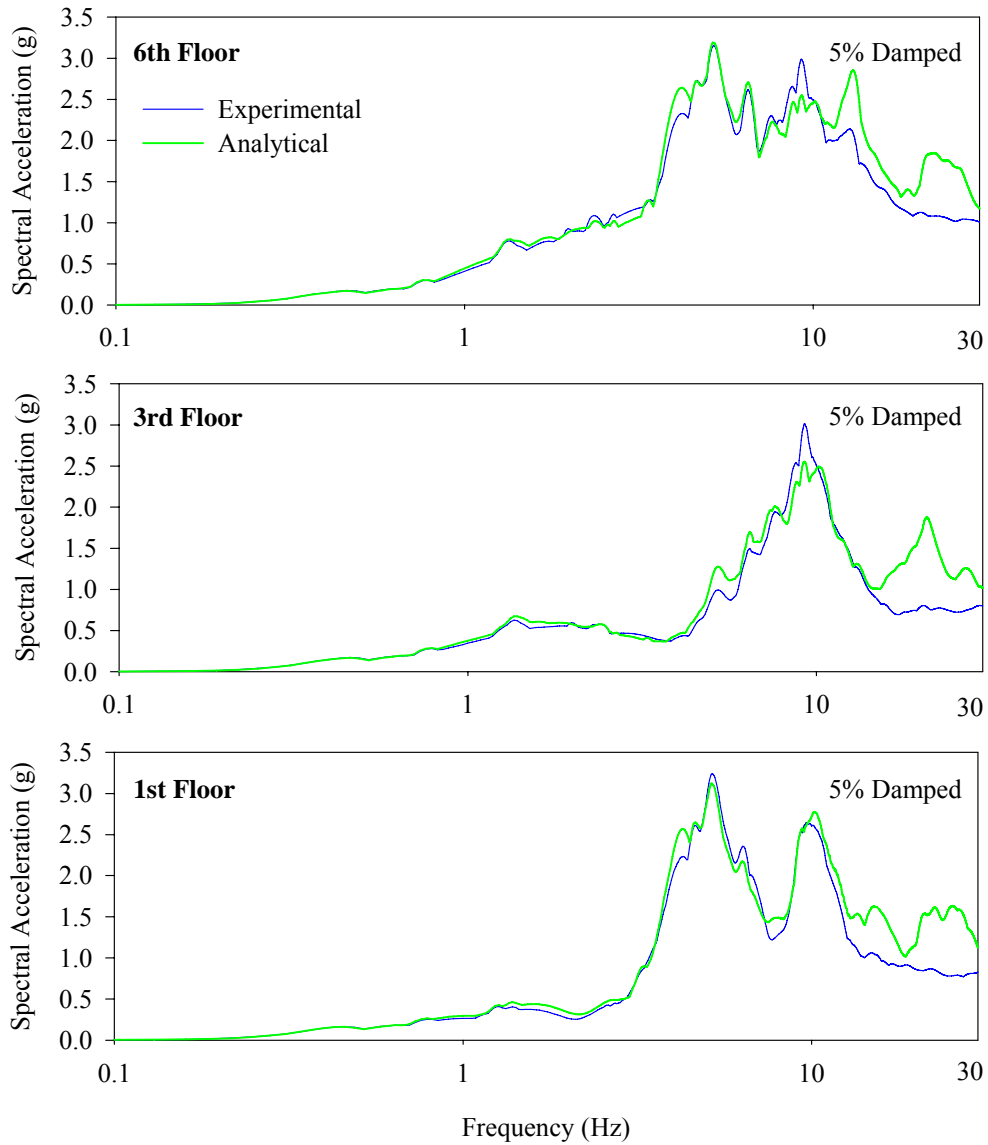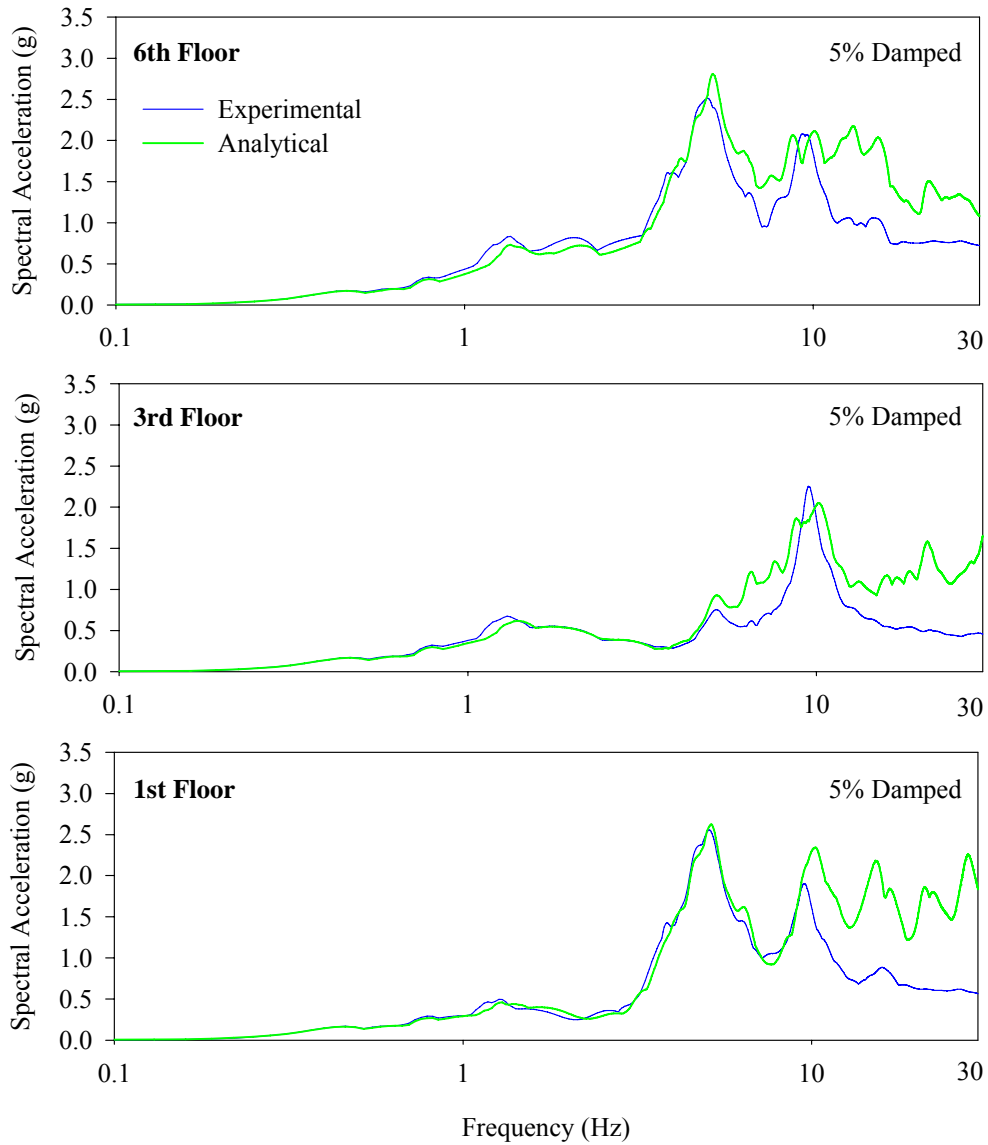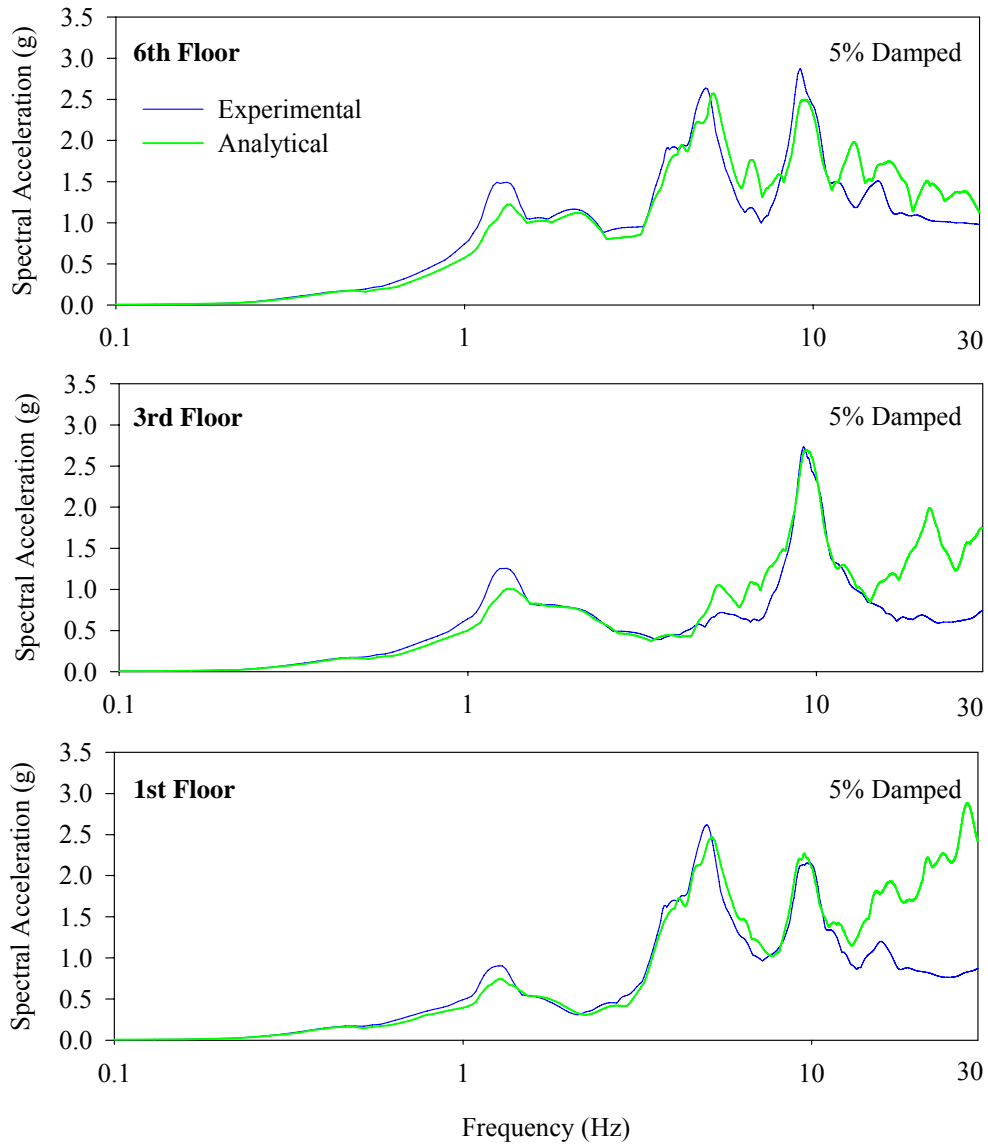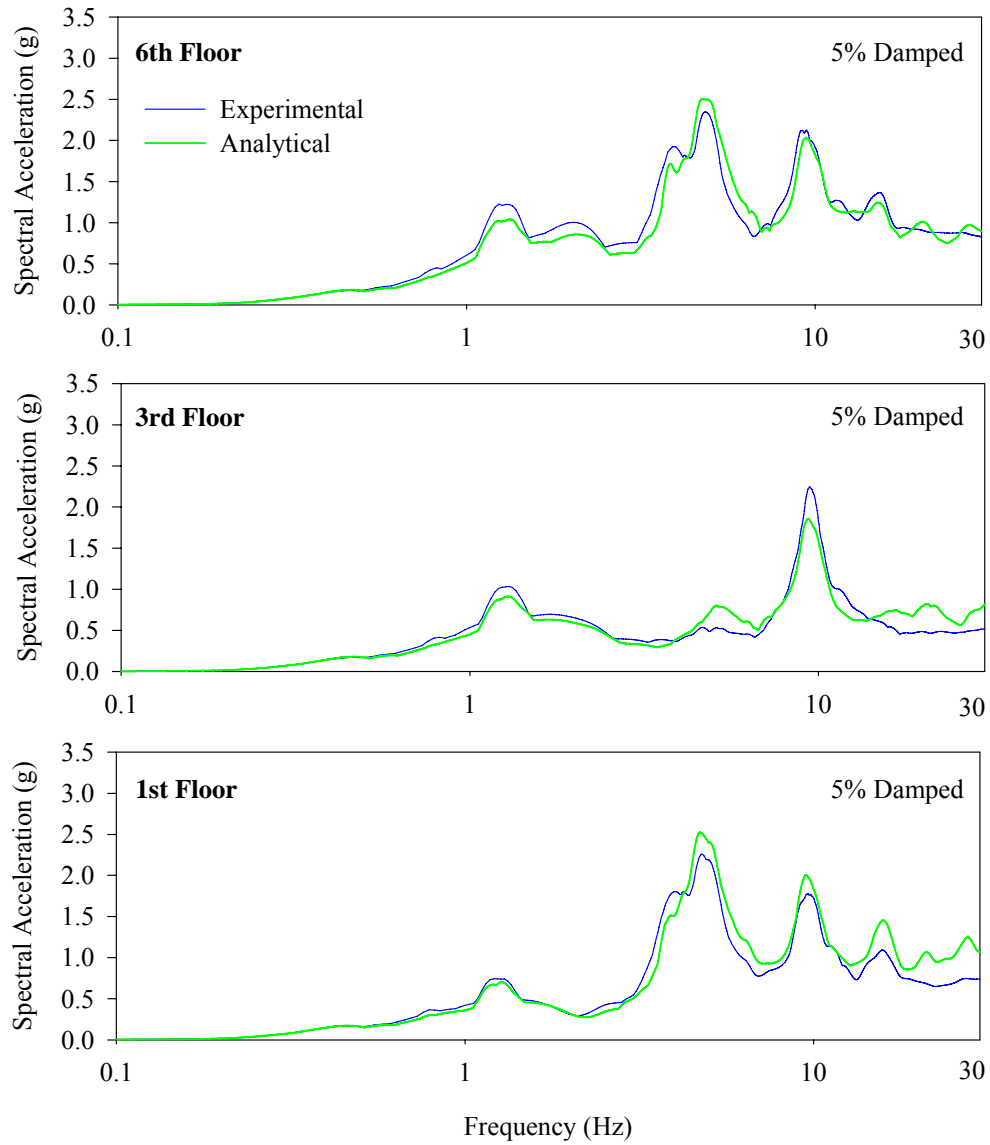
170

FIGURE 6-33 Comparison of Experimental and Analytical Floor Response Spectra for the Triple 3 System Subjected to Pacoima 164 Ground Motion
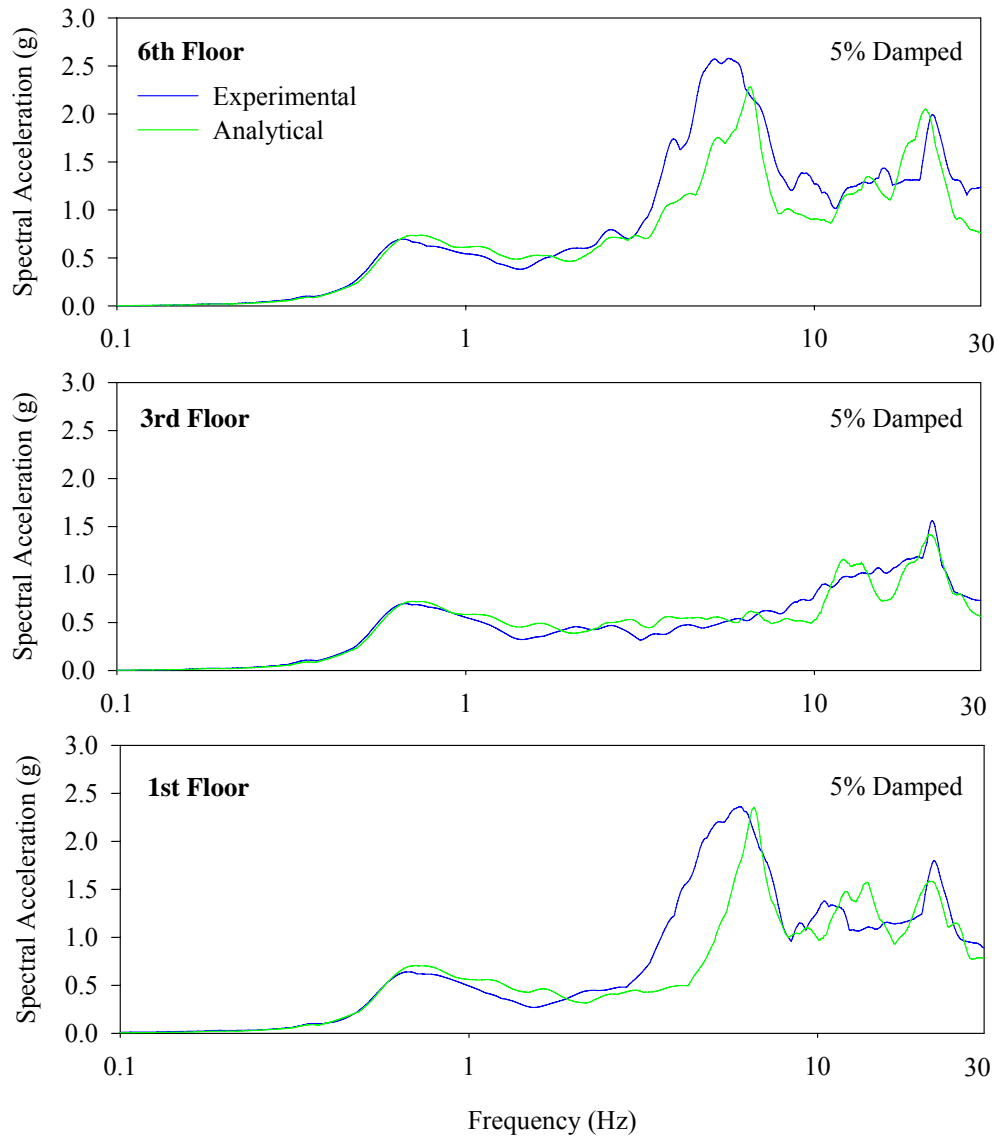
FIGURE 6-34 Comparison of Experimental and Analytical Floor Response Spectra for the Double 1 System Subjected to Tridirectional El Centro Ground Motion

172

SECTION 7
CONCLUSION

The primary objective of this work has been to develop and verify models of a new class of multi-spherical sliding bearings that can be used for dynamic response history analysis. The double and triple FP bearings discussed in this document are extremely promising devices and are likely to see widespread implementation due to the fact that

(a) Sliding displacements are shared among multiple concave surfaces. These bearings can be constructed with plan dimensions approximately half those of the single concave FP bearing and still have the same displacement capacity. This clearly represents important savings in the cost of producing the bearings and has likely been the driving factor behind the practical implementation of these devices to date. In addition to the economic benefits, there are also performance benefits associated with sharing the displacements among multiple surfaces. Frictional heating and the associated phenomenon of wear are directly related to the sliding velocity. By sharing displacements among multiple surfaces, sliding velocities are approximately halved. Therefore in applications in which wear can be an issue, these devices combat the driving factors on two fronts: both through a reduction in the travel displacements on each surface and through a reduction in velocity and the associated frictional heating.

(b) Varying degrees of adaptive behavior can be achieved. The stiffness and effective friction exhibited by these devices changes depending upon which surfaces sliding is occurring. Since there are more sliding surfaces associated with the triple FP bearing, more highly adaptive behavior is possible than with the double FP bearing. Displacement dependent stiffness and damping mean that the design can be optimized for different performance objectives in different levels of earthquakes. For example, the triple FP isolation system can be optimized to reduce floor acceleration in minor earthquakes with high stiffness and low friction, minimize the base shear transmitted to the structure in the DBE with reduced stiffness and intermediate friction and control displacements in the MCE and beyond with stiffening of the bearings at a predefined displacement. An adaptive isolation system is nothing new, there have been numerous active and semi-active systems proposed over the past 20 years. However, there is skepticism in the engineering community regarding the reliability and consistency of these devices over time. The double and triple FP bearings here are completely passive systems that are simple derivatives of the widely used single concave FP bearing, a device with over 20 years of field proven reliability and longevity.

(c) In configurations where sliding surfaces are of equal friction, the adaptive behavior collapses to simpler types of hysteretic behavior. For example, when the double FP bearing is used with both surfaces of equal friction, the hysteretic behavior is identical to that of the single FP bearing. Engineers can use the same analysis methods developed for single FP bearings but gain the economic and

173

performance benefits associated with the double FP bearing. When the triple FP bearing is used with inner surfaces with very low friction and outer surfaces of equal friction, the behavior is nearly the same as that of a lead rubber bearing (approximately bilinear with velocity dependent strength, no sharp transitions in stiffness and stiffening at large displacements).

In order for engineers to be able to capitalize on these attractive features and effectively use these devices, their behavior must be sufficiently well understood and demonstrated to be predictable. Furthermore, methods of dynamic analysis that are within the capabilities of most design offices must be developed and experimentally verified. These efforts have been the principal contributions of this work. Specifically, this meant for the double and triple FP bearings

(a) Based on the mechanical behavior of these devices presented in Fenz and Constantinou (2006,2008a,2008b,2008c), developing models capturing this complex force-displacement relationship for response history analysis in SAP2000. This was straightforward for the double FP bearing as the mechanical behavior is that of two single concave FP elements in series. However, the behavior of the triple FP bearing is not that of a series arrangement of single FP bearings. Consequently, procedures were developed for modifying the model's parameters in order to reproduce the true behavior of the triple FP bearing using a series arrangement.

(b) Performing shake table testing to generate data for validation of the analytical models. In general, it was shown that the dynamic analysis models are capable of accurately reproducing primary response quantities such as the shear force, displacements and vertical force in the isolation system as well as secondary response quantities such as floor spectra. The accuracy was also demonstrated for more analytically demanding scenarios such as isolator uplift, contact with the displacement restrainer and excitation consisting of multiple components. Just as important as establishing the capabilities of the dynamic analysis models, various limitations such as the inaccuracy of the calculation of uplift displacements were identified, although likely restricted to configurations in which uplift is associated with rigid body rocking behavior.

(c) Using the shake table tests to examine localized phenomena with double and triple FP bearings. Localized phenomena, such as uplift, and their effects on the structure are difficult to realistically simulate in conditions other than shake table testing.

Looking forward, it was important to validate the dynamic analysis models under extreme conditions such as uplift and contact with the displacement restrainer not only to demonstrate their robustness, but to demonstrate that they can be used to accurately evaluate the response of seismically isolated structures approaching collapse. As codes for base isolated structures evolve from deterministic to probabilistic, engineers will have to do more than just demonstrate that the designs are safe for a certain level of ground

shaking. Instead, it will have to be shown that the design satisfies a certain minimum probability of collapse. This will involve analysis of the isolated structure at or near conditions of collapse, where the isolation system will very likely experience uplift and/or contact with the displacement restraints (or possibly the moat). Furthermore, it was important to demonstrate the validity of the dynamic analysis models so that they can be used as the basis of future parametric studies into how best to take advantage of the adaptive behavior exhibited by these devices.

SECTION 8
REFERENCES

American Society of Civil Engineers (2006). "Minimum Design Loads for Buildings and Other Structures", *Standard ASCE/SEI 7-05*, ASCE, Reston, VA, USA.

Bracci JM, Reinhorn AM, Mander JB (1992). "Seismic Resistance of Reinforced Concrete Frame Structures Designed Only for Gravity Loads: Part I – Design and Properties of a One-Third Scale Model Structure", *Technical Report NCEER-92-0027*, National Center for Earthquake Engineering Research, State University of New York at Buffalo, Buffalo, NY, USA.

Clarke CSJ, Buchanan R, Efthymiou M, Shaw C (2005). "Structural Platform Solution for Seismic Arctic Environments – Sakhalin II Offshore Facilities", *Proceedings, 2005 Offshore Technology Conference*, Houston, TX, USA, paper OTC-17378.

Computers and Structures Inc. (2006). "SAP2000 Software Verification Examples: Version 11", Computers and Structures, Inc., Berkeley, CA, USA.

Computers and Structures Inc. (2007). "SAP2000: Static and Dynamic Finite Element Analysis of Structures (Version 11.0.2) Analysis Reference Manual", Computers and Structures, Inc., Berkeley, CA, USA.

Constantinou MC, Mokha A, Reinhorn AM (1990). "Teflon Bearings in Base Isolation. II: Modeling", *ASCE Journal of Structural Engineering*, **116**(2), 455-474.

Constantinou MC, Mokha AS, Reinhorn AM (1991). "Study of Sliding Bearing and Helical-Steel-Spring Isolation System", *ASCE Journal of Structural Engineering*, **117**(4), 1257-1275.

Constantinou MC, Tsopelas P, Kim YS, Okamoto S (1993). "NCEER-Taisei Corporation Research Program on Sliding Seismic Isolation Systems for Bridges: Experimental and Analytical Study of a Friction Pendulum System (FPS)", *Technical Report NCEER-93-0020,* National Center for Earthquake Engineering Research, State University of New York at Buffalo, Buffalo, NY, USA.

Constantinou MC, Whittaker AS, Fenz DM, Apostolakis G (2007). "Seismic Isolation of Bridges: Version 2", *Report to Sponsor: California Department of Transportation*.

Fenz DM, Constantinou MC (2006). "Behavior of the Double Concave Friction Pendulum Bearing", *Earthquake Engineering and Structural Dynamics*, **35**(11) 1403-1424, DOI: 10.1002/eqe.589.

Fenz DM, Constantinou MC (2008a). "Spherical Sliding Isolation Bearings with Adaptive Behavior: Theory", *Earthquake Engineering and Structural Dynamics,* **37**(2) 163-183, DOI: 10.1002/eqe.751.

Fenz DM, Constantinou MC (2008b). "Spherical Sliding Isolation Bearings with Adaptive Behavior: Experimental Verification", *Earthquake Engineering and Structural Dynamics,* **37**(2) 185-205, DOI: 10.1002/eqe.750.

Fenz DM, Constantinou MC (2008c). "Mechanical Behavior of Multi-Spherical Sliding Bearings", *Technical Report MCEER-08-0007*, Multidisciplinary Center for Earthquake Engineering Research, State University of New York at Buffalo, Buffalo, NY, USA.

Hibbitt, Karlsson and Sorensen, Inc. (2004). "ABAQUS (Version 6.4)", Hibbitt, Karlsson and Sorensen, Inc., Pawtucket, RI, USA.

Kasalanati A, Constantinou MC (1999). "Experimental Study of Bridge Elastomeric and Other Isolation and Energy Dissipation Systems with Emphasis on Uplift Prevention and High Velocity Near Source Seismic Excitation", *Technical Report MCEER-99-0004*, Multidisciplinary Center for Earthquake Engineering Research, State University of New York at Buffalo, Buffalo, NY, USA.

Mokha A, Constantinou MC, Reinhorn AM (1990). "Experimental Study and Analytical Prediction of Earthquake Response of a Sliding Isolation System with Spherical Surface", *Technical Report NCEER-90-0020*, National Center for Earthquake Engineering Research, State University of New York at Buffalo, Buffalo, NY, USA.

Mosqueda G, Whittaker AS, Fenves GL (2004). "Characterization and Modeling of Friction Pendulum Bearings Subjected to Multiple Components of Excitation", *ASCE Journal of Structural Engineering*, **130**(3), 433-442.

Nagarajaiah S, Reinhorn AM, Constantinou MC (1989). "Nonlinear Dynamic Analysis of Three-Dimensional Base Isolated Structures (3D-BASIS)", *Technical Report NCEER-89-0019*, National Center for Earthquake Engineering Research, Buffalo, NY, USA.

Reinhorn AM, Soong TT, Lin RC, Yang YP, Fukao Y, Abe H, Nakai M (1989). "1:4 Scale Model Studies of Active Tendon Systems and Active Mass Dampers for Aseismic Protection", *Technical Report NCEER-89-0026*, National Center for Earthquake Engineering Research, State University of New York at Buffalo, Buffalo, NY, USA.

Scheller J, Constantinou MC (1999). "Response History Analysis of Structures with Seismic Isolation and Energy Dissipation Systems: Verification Examples for Program SAP2000", *Technical Report MCEER-99-0002*, Multidisciplinary Center

for Earthquake Engineering Research, State University of New York at Buffalo, Buffalo, NY, USA.

Shampine LF, Reichelt MW (1997). "The MATLAB ODE Suite", *SIAM Journal on Scientific Computing*, **18**(1) 1-22.

Sivaselvan MV, Reinhorn AM (2000). "Hysteretic Models for Deteriorating Inelastic Structures", *ASCE Journal of Structural Engineering*, **126**(6) 633-640.

Structural Engineering and Earthquake Simulation Laboratory (2004). "Laboratory Manual", SEESL, Buffalo, NY USA. Available online: http://nees.buffalo.edu/docs/labmanual/html/

Tsopelas P (1994). "Testing and Modeling of a Class of Bridge Seismic Isolation Systems", Ph.D. Dissertation, State University of New York at Buffalo, Buffalo, NY, USA.

Tsopelas P, Constantinou MC, Kim YS, Okamoto S (1996). "Experimental Study of FPS System in Bridge Seismic Isolation", *Earthquake Engineering and Structural Dynamics,* **25**(1) 65-78, DOI: 10.1002/eqe.536.

Tsopelas PC, Roussis PC, Constantinou MC, Buchanan R, Reinhorn AM (2005). "3D-BASIS-ME-MB: Computer Program for Nonlinear Dynamic Analysis of Seismically Isolated Structures", *Technical Report MCEER-05-0009*, Multidisciplinary Center for Earthquake Engineering Research, State University of New York at Buffalo, Buffalo, NY, USA.

Wilson EL (2001). "Three-Dimensional Static and Dynamic Analysis of Structures", Computers and Structures, Inc., Berkeley, CA, USA.

Wolff ED, Constantinou MC (2004). "Experimental Study of Seismic Isolation Systems with Emphasis on Secondary System Response and Verification of Accuracy of Dynamic Response History Analysis Methods", *Technical Report MCEER-04-0001*, Multidisciplinary Center for Earthquake Engineering Research, State University of New York at Buffalo, Buffalo, NY, USA.

Zayas VA, Low SS, Mahin SA (1987). "The FPS Earthquake Resisting System: Experimental Report", *Report No. UCB/EERC-87/01*, Earthquake Engineering Research Center, University of California Berkeley, Berkeley, CA, USA.

Zayas VA, Low SS, Bozzo L, Mahin SA (1989). "Feasibility and Performance Studies on Improving the Earthquake Resistance of New and Existing Buildings Using the Friction Pendulum System", *Report No. UCB/EERC-89/09*, Earthquake Engineering Research Center, UC Berkeley, Berkeley, CA, USA.

Zayas VA (2007). Personal communication on September 19, 2007.

APPENDIX A
HISTORIES OF DISPLACEMENT, VELOCITY, ACCELERATION AND THE ACCELERATION RESPONSE SPECTRUM FOR GROUND MOTIONS USED IN SHAKE TABLE TESTING

Lytle Creek Earthquake, Component WTW115

FIGURE A-1   Histories of Acceleration, Velocity and Displacement and Acceleration Response Spectrum for the WTW 115 Record

San Francisco Earthquake, Component GGP100

FIGURE A-2   Histories of Acceleration, Velocity and Displacement and Acceleration Response Spectrum for the GGP 100 Record

Kern County Earthquake, Component TFT021

FIGURE A-3   Histories of Acceleration, Velocity and Displacement and Acceleration Response Spectrum for the TAF 021 Record

FIGURE A-4 Histories of Acceleration, Velocity and Displacement and Acceleration Response Spectrum for the ELC 180 Record

FIGURE A-5   Histories of Acceleration, Velocity and Displacement and Acceleration Response Spectrum for the ELC 270 Record

FIGURE A-6 **Histories of Acceleration, Velocity and Displacement and Acceleration Response Spectrum for the CLS 090 Record**

FIGURE A-7   Histories of Acceleration, Velocity and Displacement and Acceleration Response Spectrum for the YPT 330 Record

FIGURE A-8   Histories of Acceleration, Velocity and Displacement and Acceleration Response Spectrum for the YPT 060 Record

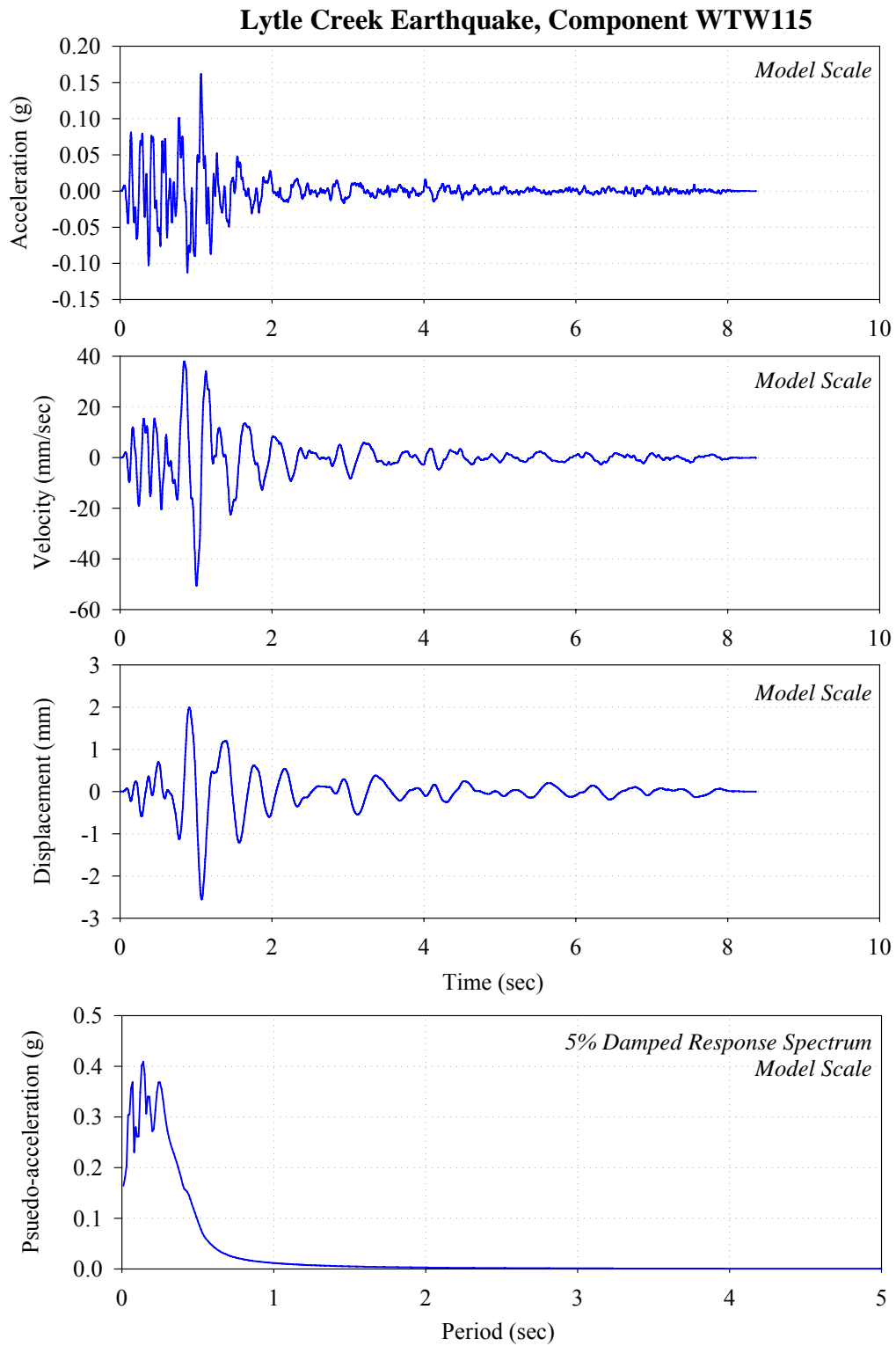**Northridge Earthquake, Component NWH360**

FIGURE A-9   Histories of Acceleration, Velocity and Displacement and Acceleration Response Spectrum for the NWH 360 Record

190
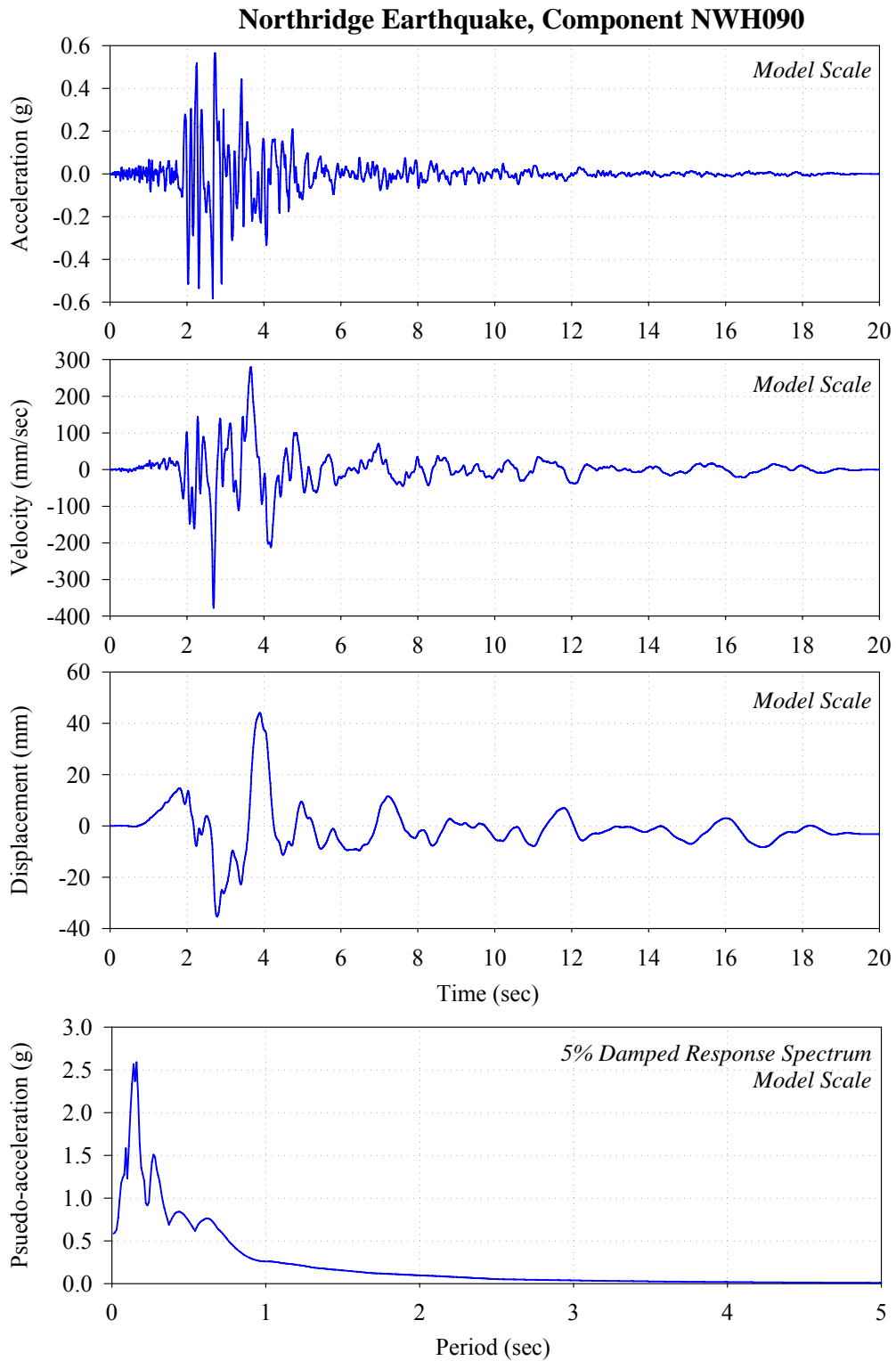
FIGURE A-10   Histories of Acceleration, Velocity and Displacement and Acceleration Response Spectrum for the NWH 090 Record
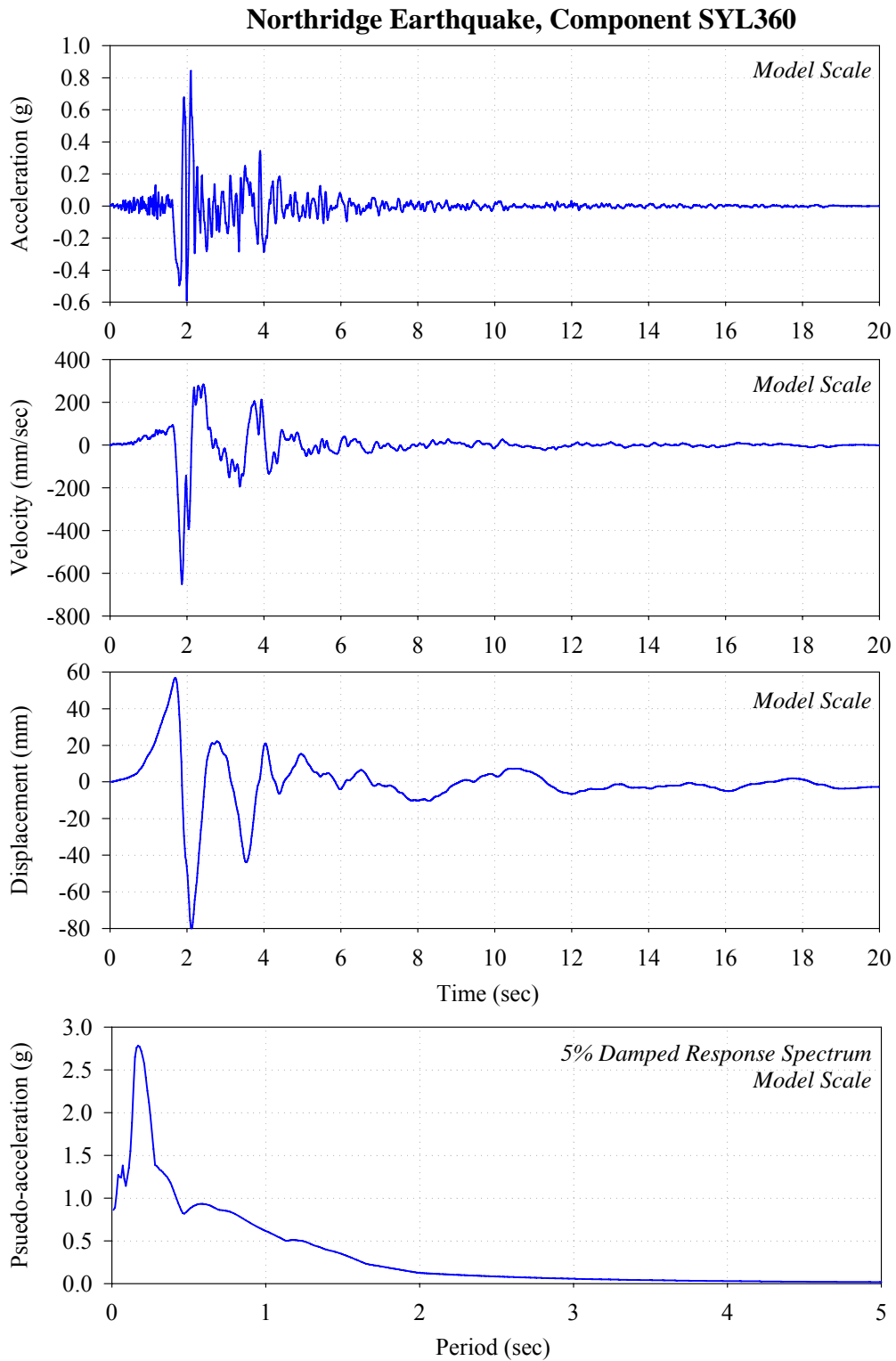
FIGURE A-11 **Histories of Acceleration, Velocity and Displacement and Acceleration Response Spectrum for the SYL 360 Record**
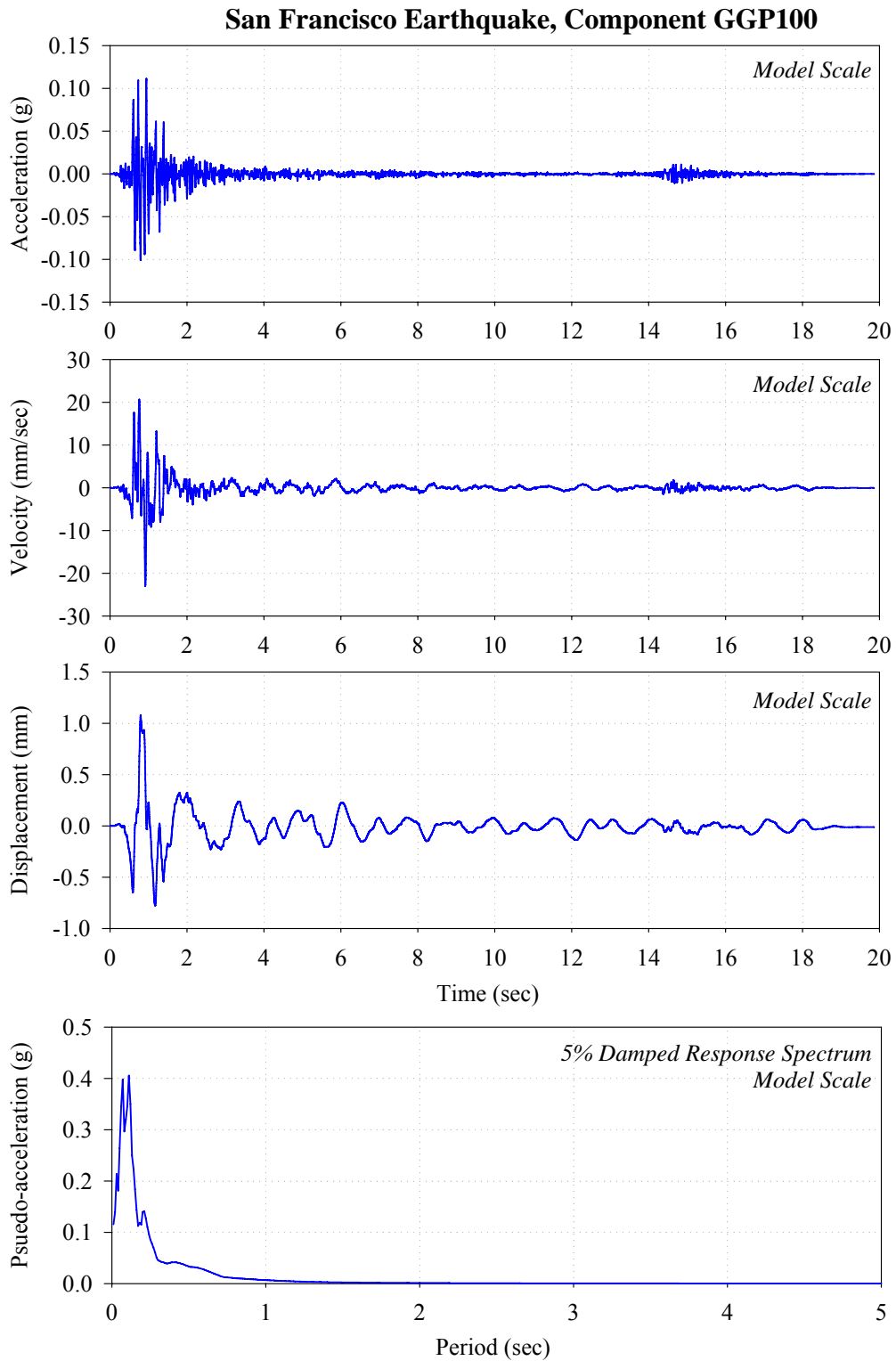
San Fernando Earthquake, Component PUL164
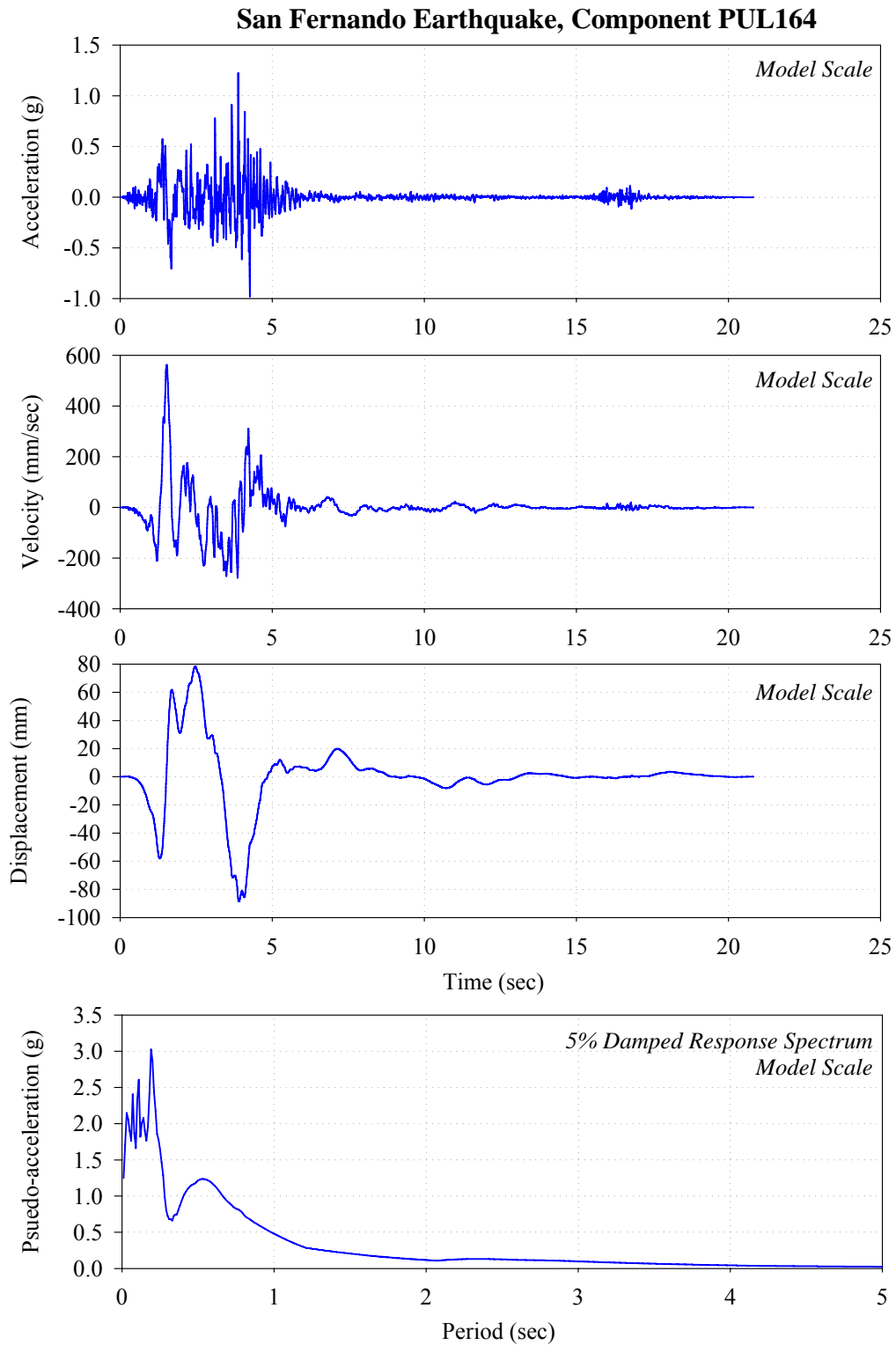
FIGURE A-12   Histories of Acceleration, Velocity and Displacement and Acceleration Response Spectrum for the PUL 164 Record

El Centro S00E 200%
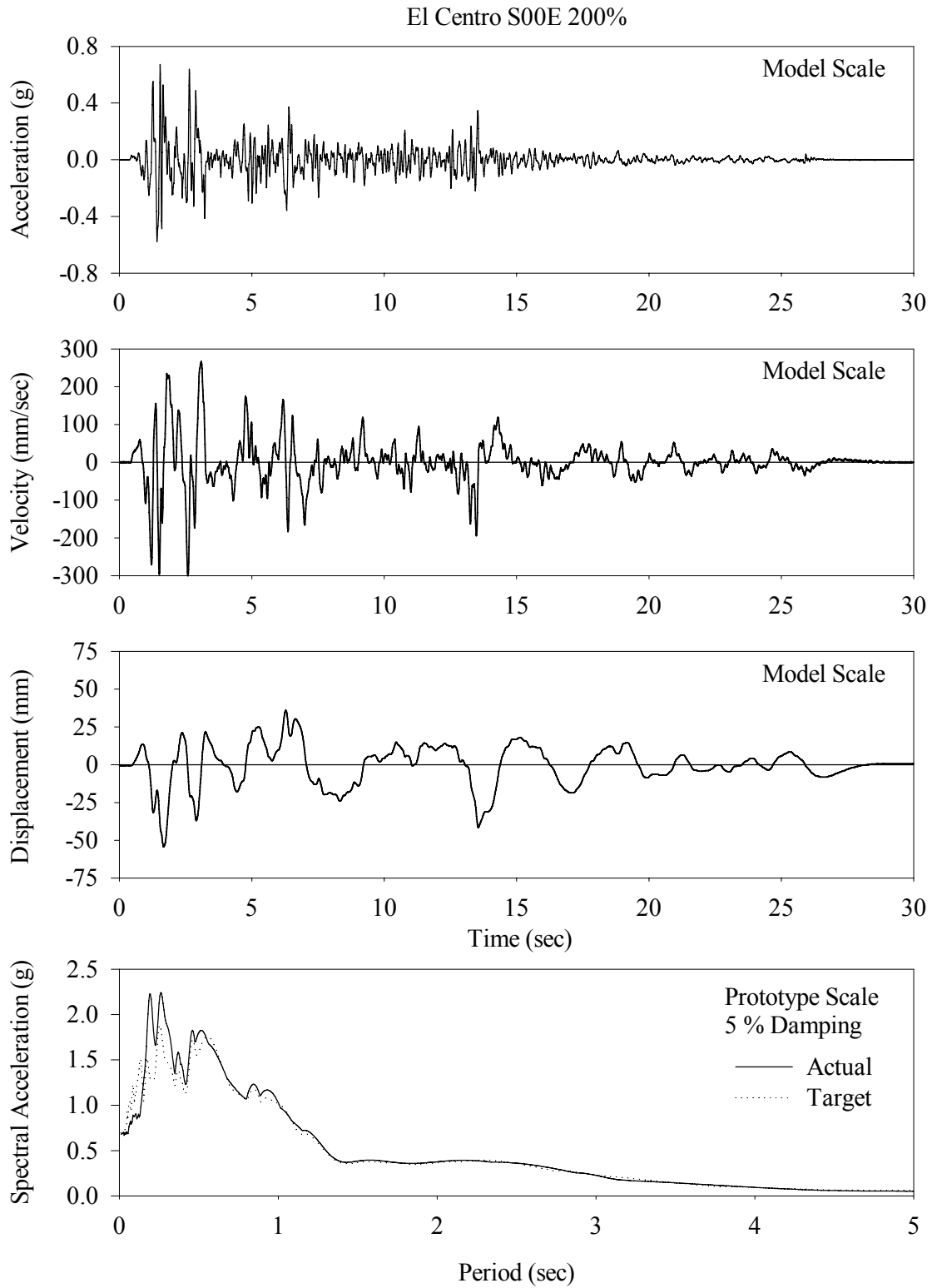
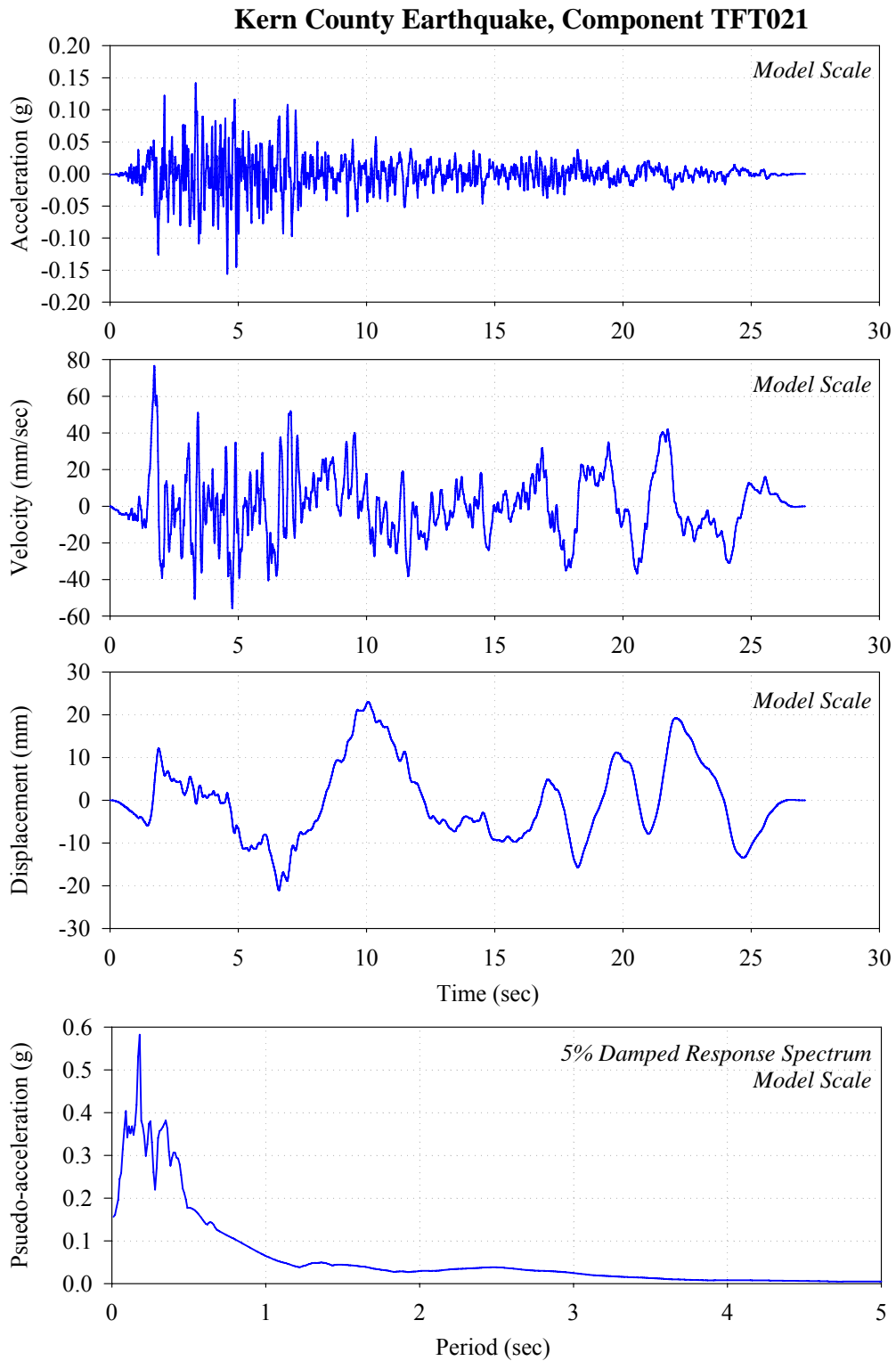**FIGURE A-13   Histories of Acceleration, Velocity and Displacement and Acceleration Response Spectrum for the ELC S00E Record (From Wolff, 2004)**
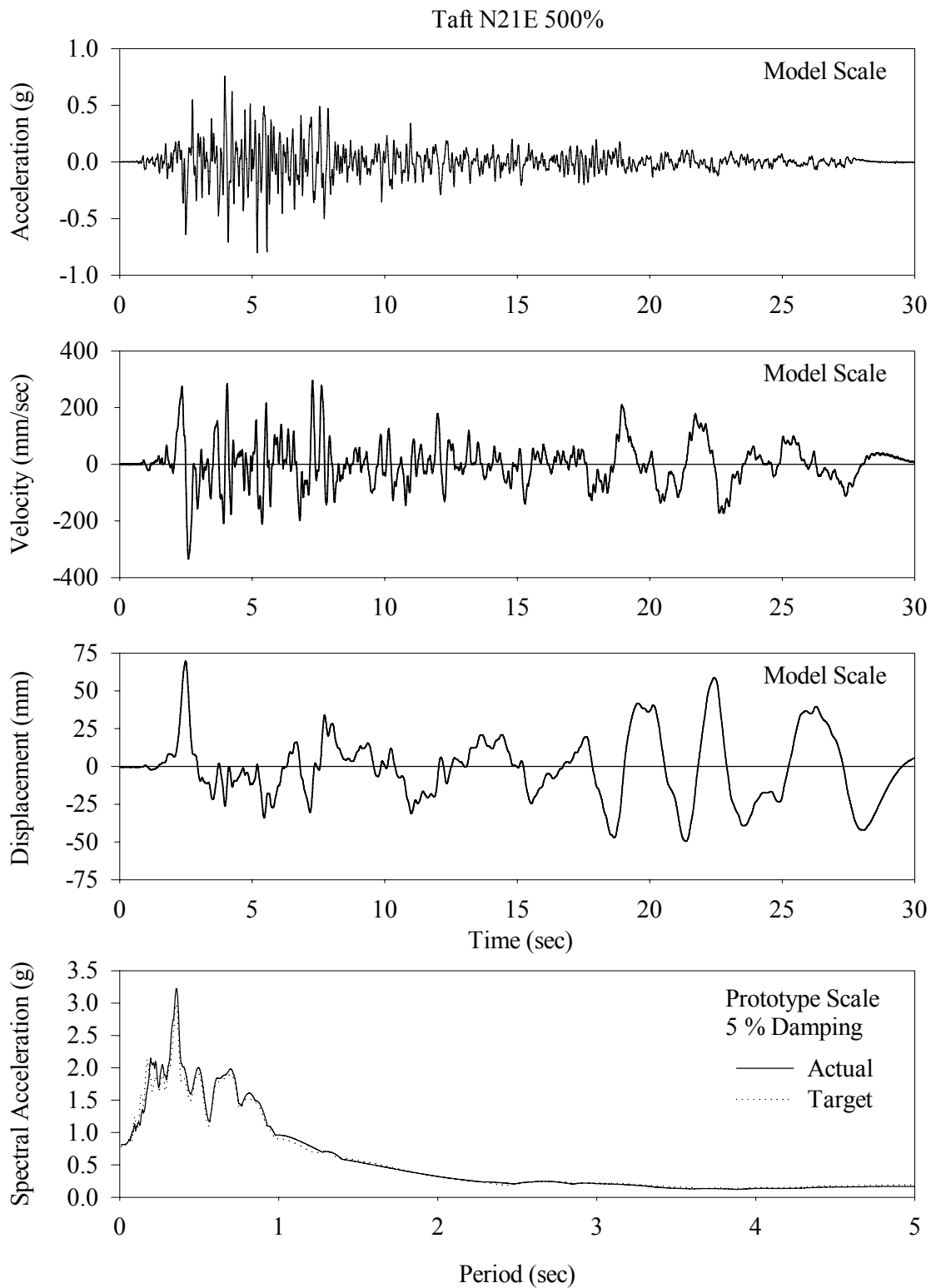
FIGURE A-14 Histories of Acceleration, Velocity and Displacement and Acceleration Response Spectrum for the TFT N21E Record (From Wolff, 2004)
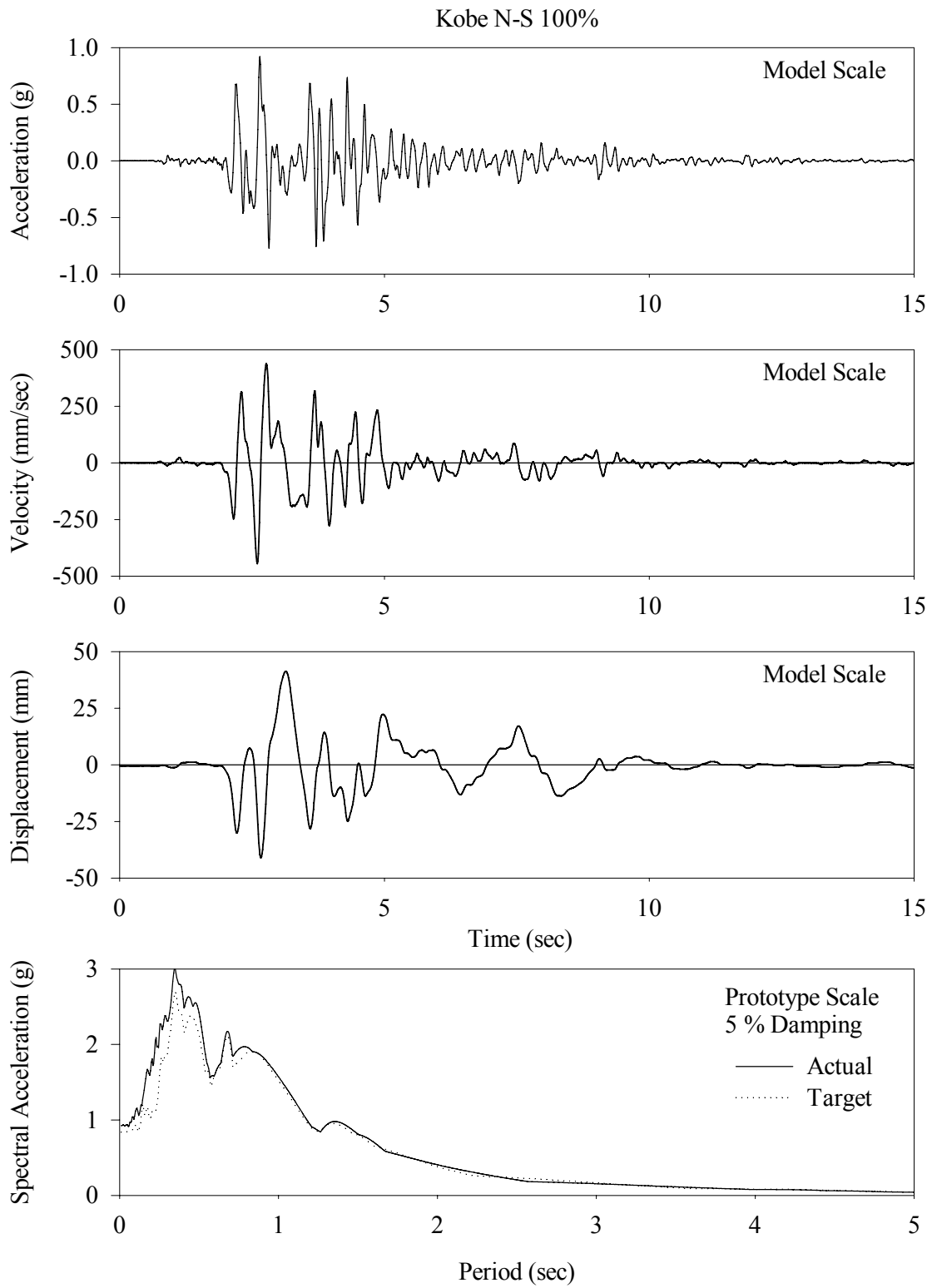
FIGURE A-15 Histories of Acceleration, Velocity and Displacement and Acceleration Response Spectrum for the KOBE N-S Record (From Wolff, 2004)
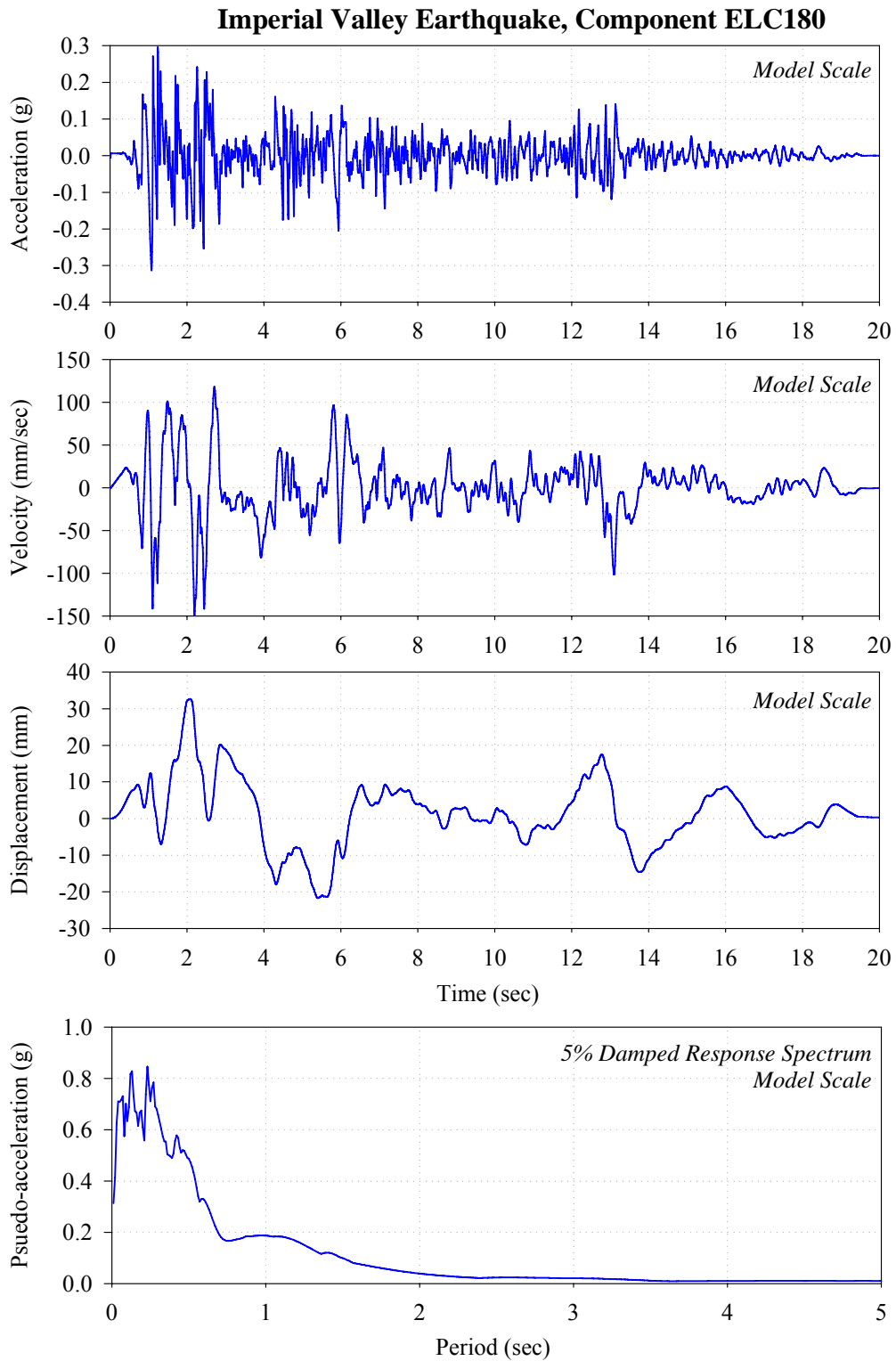
Chi-Chi (Taiwan TCU 129) E-W 100%
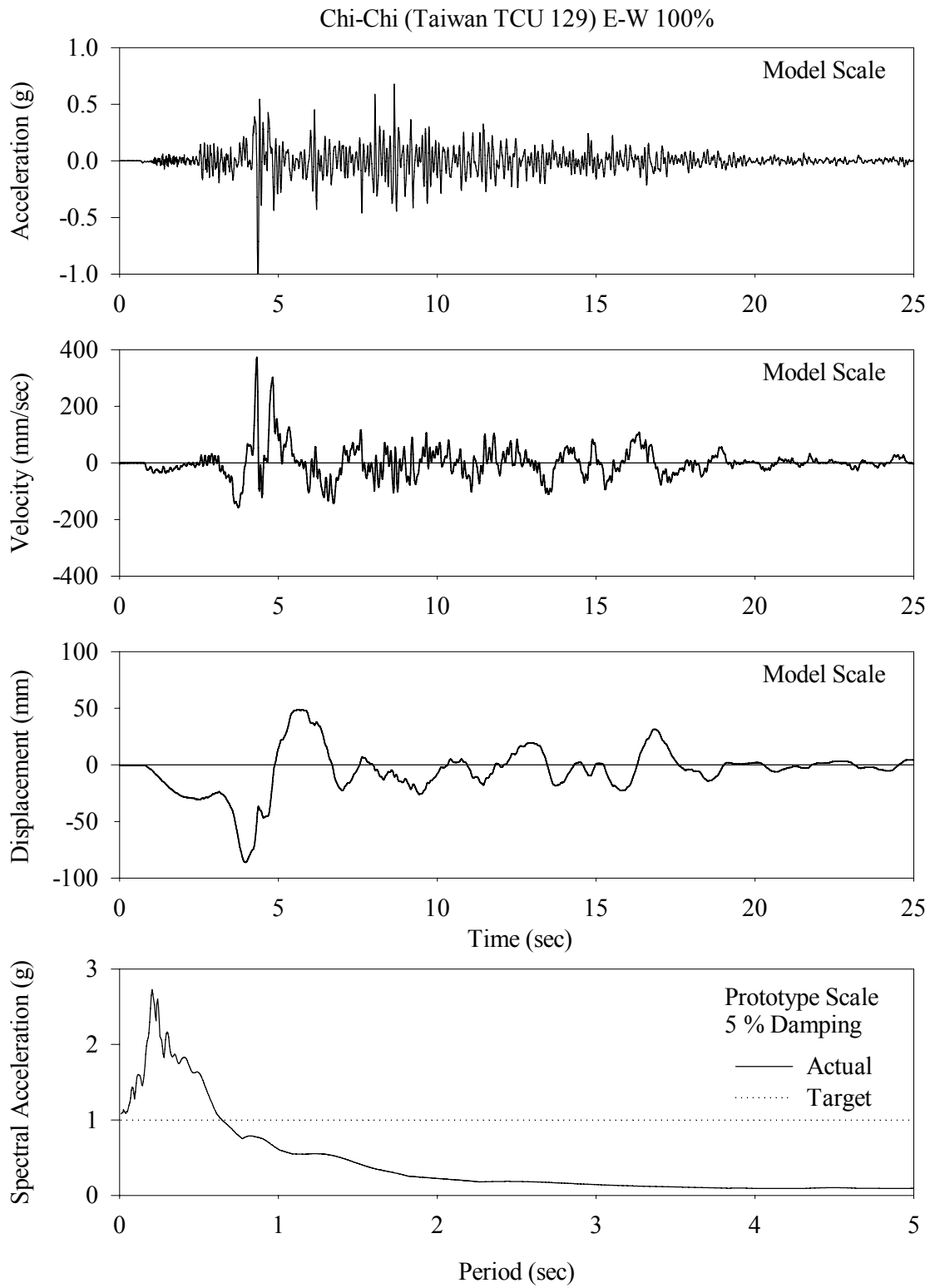
FIGURE A-16 Histories of Acceleration, Velocity and Displacement and Acceleration Response Spectrum for the TCU 129EW Record (From Wolff, 2004)
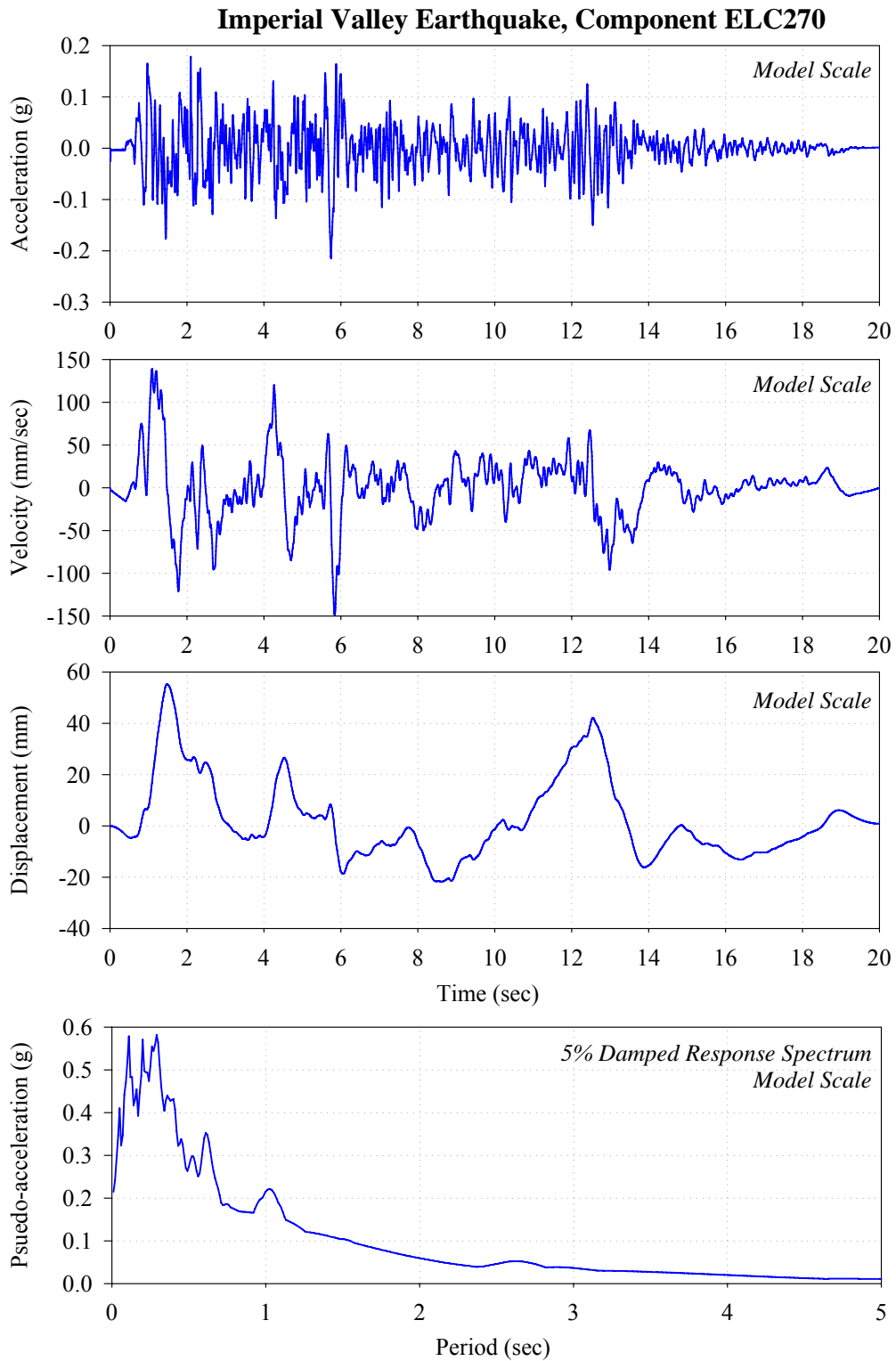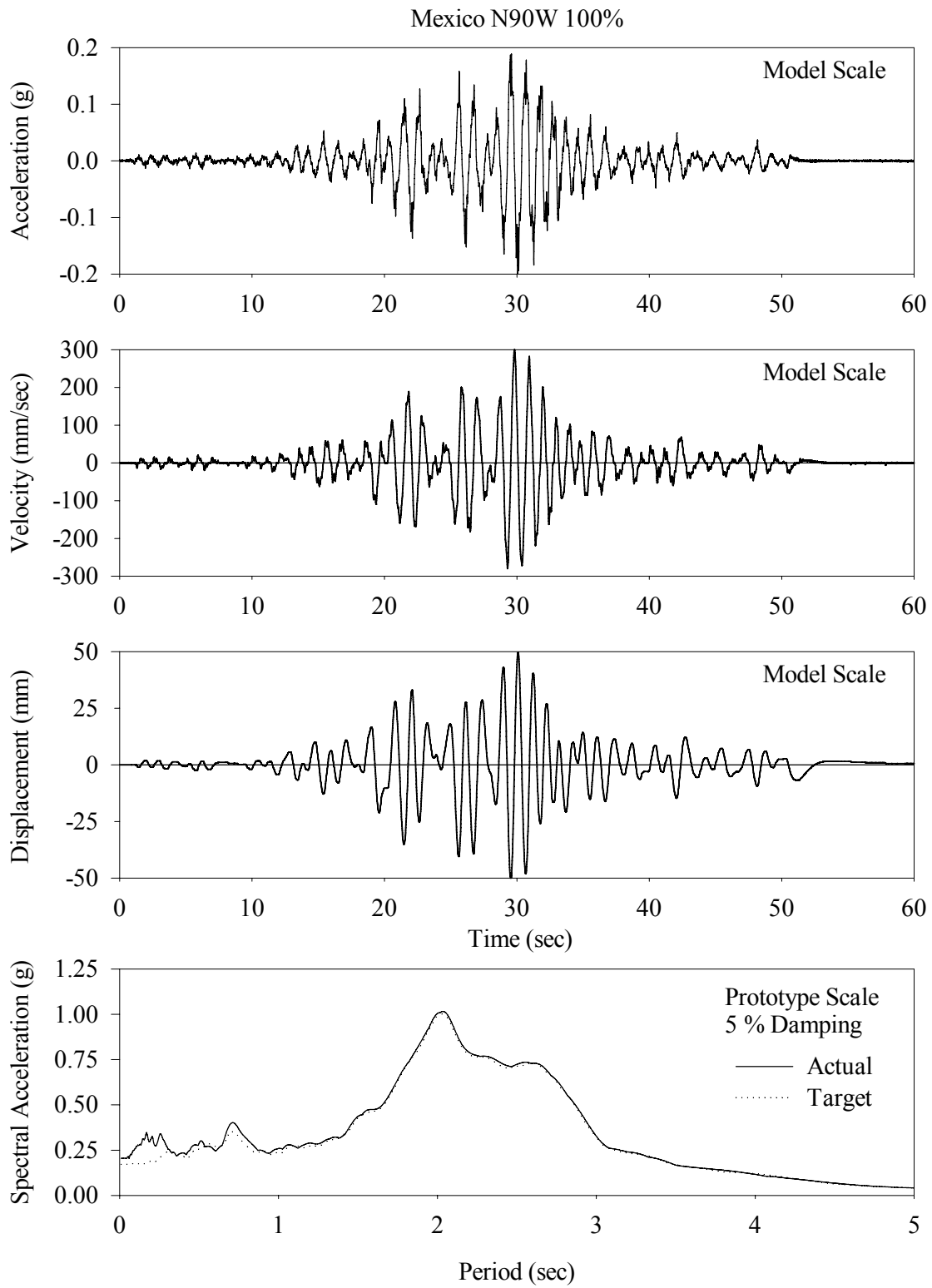
FIGURE A-17   Histories of Acceleration, Velocity and Displacement and Acceleration Response Spectrum for the PAC S16E Record (From Wolff, 2004)
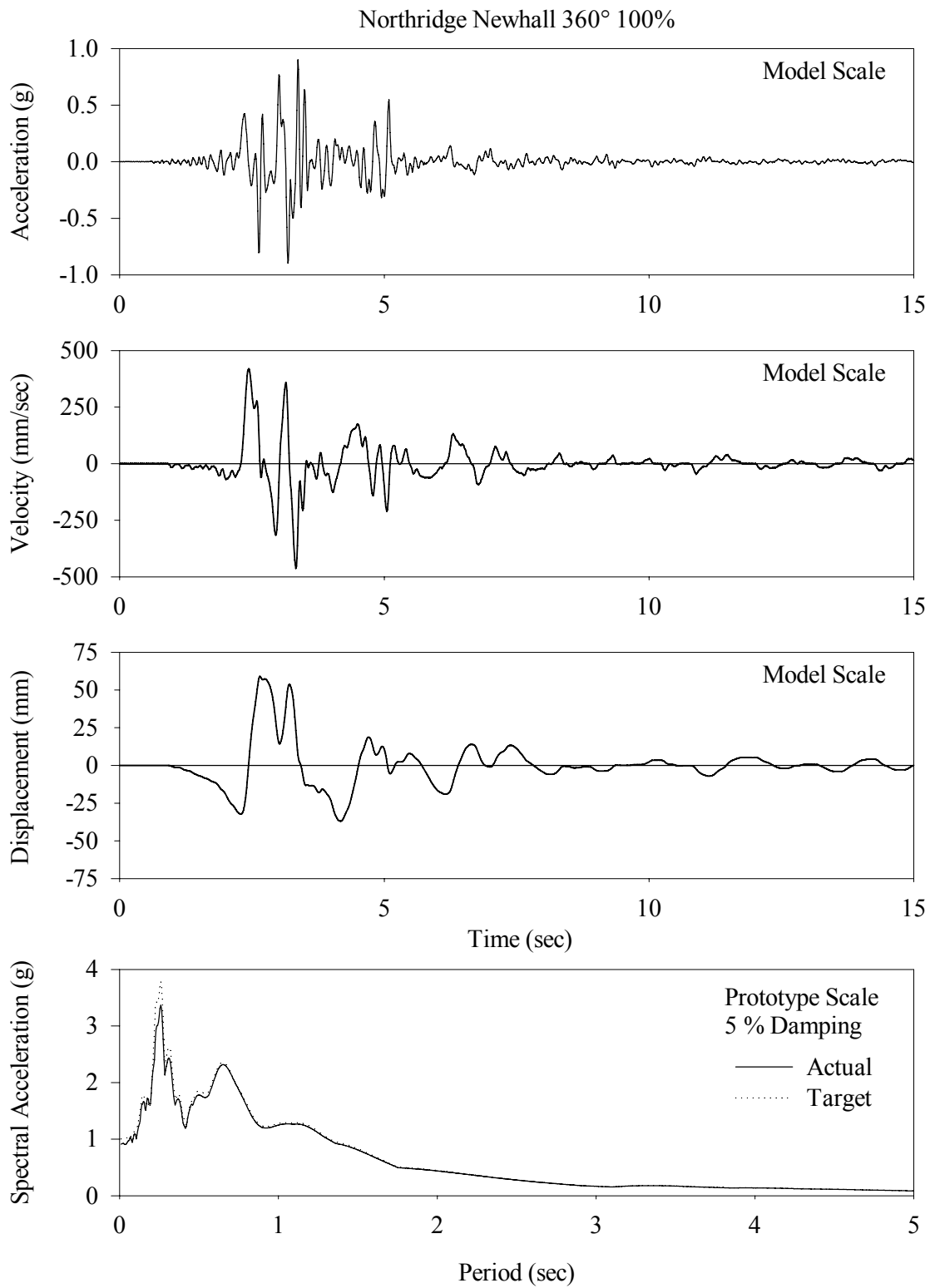
FIGURE A-18 Histories of Acceleration, Velocity and Displacement and Acceleration Response Spectrum for the NWH 360 Record (From Wolff, 2004)
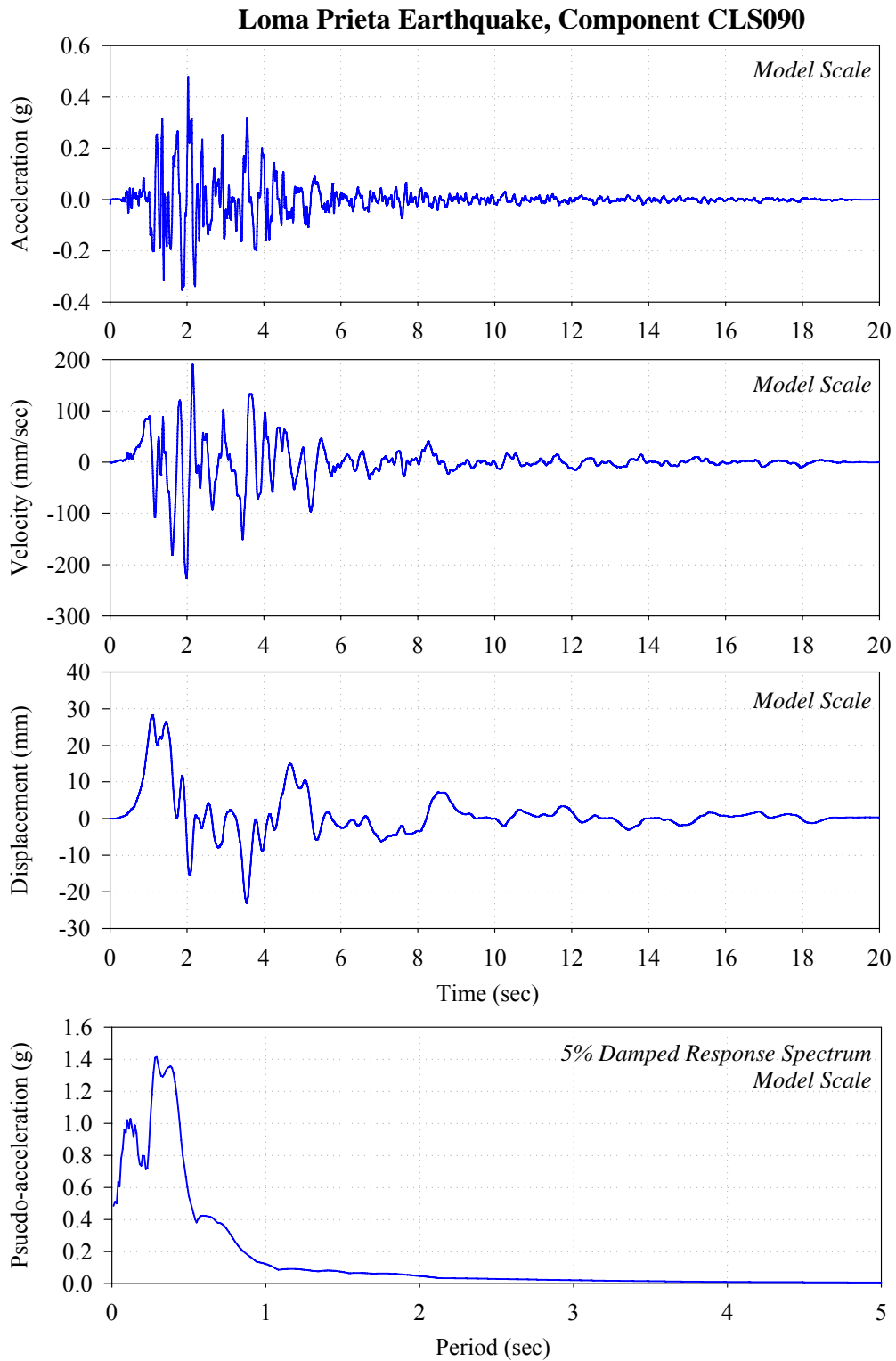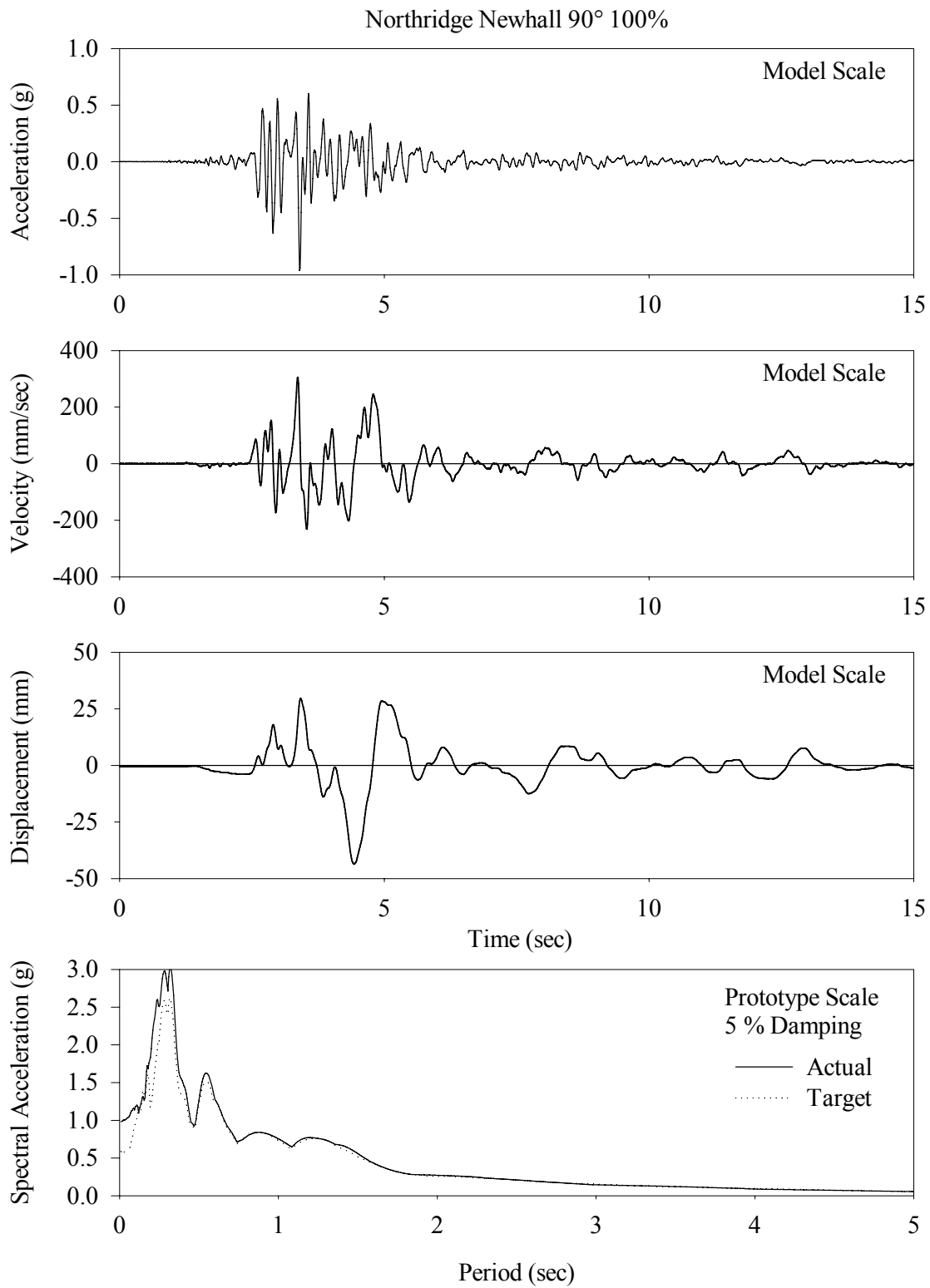
FIGURE A-19   Histories of Acceleration, Velocity and Displacement and Acceleration Response Spectrum for the NWH 90 Record (From Wolff, 2004)
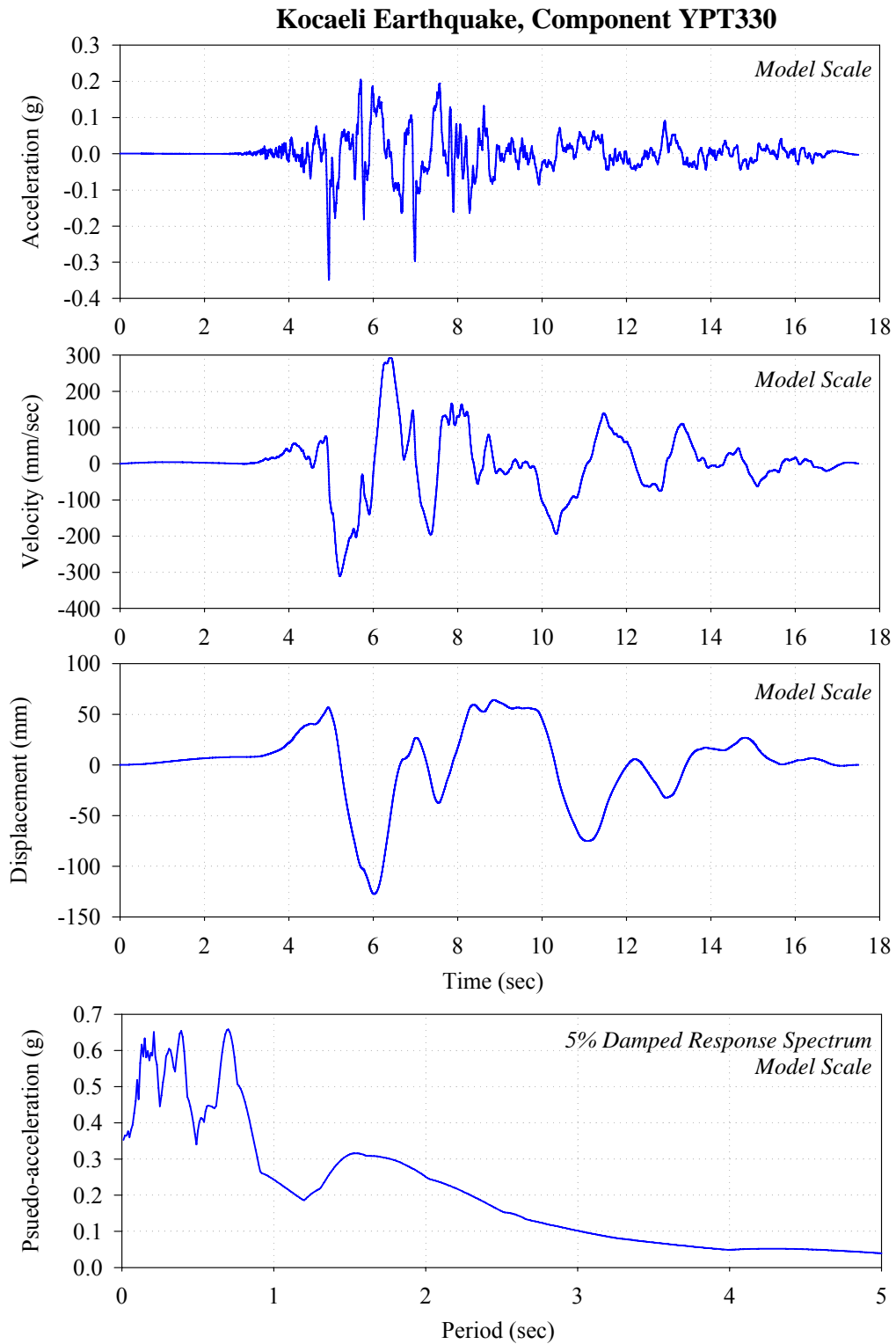
Northridge Sylmar 90° 100%
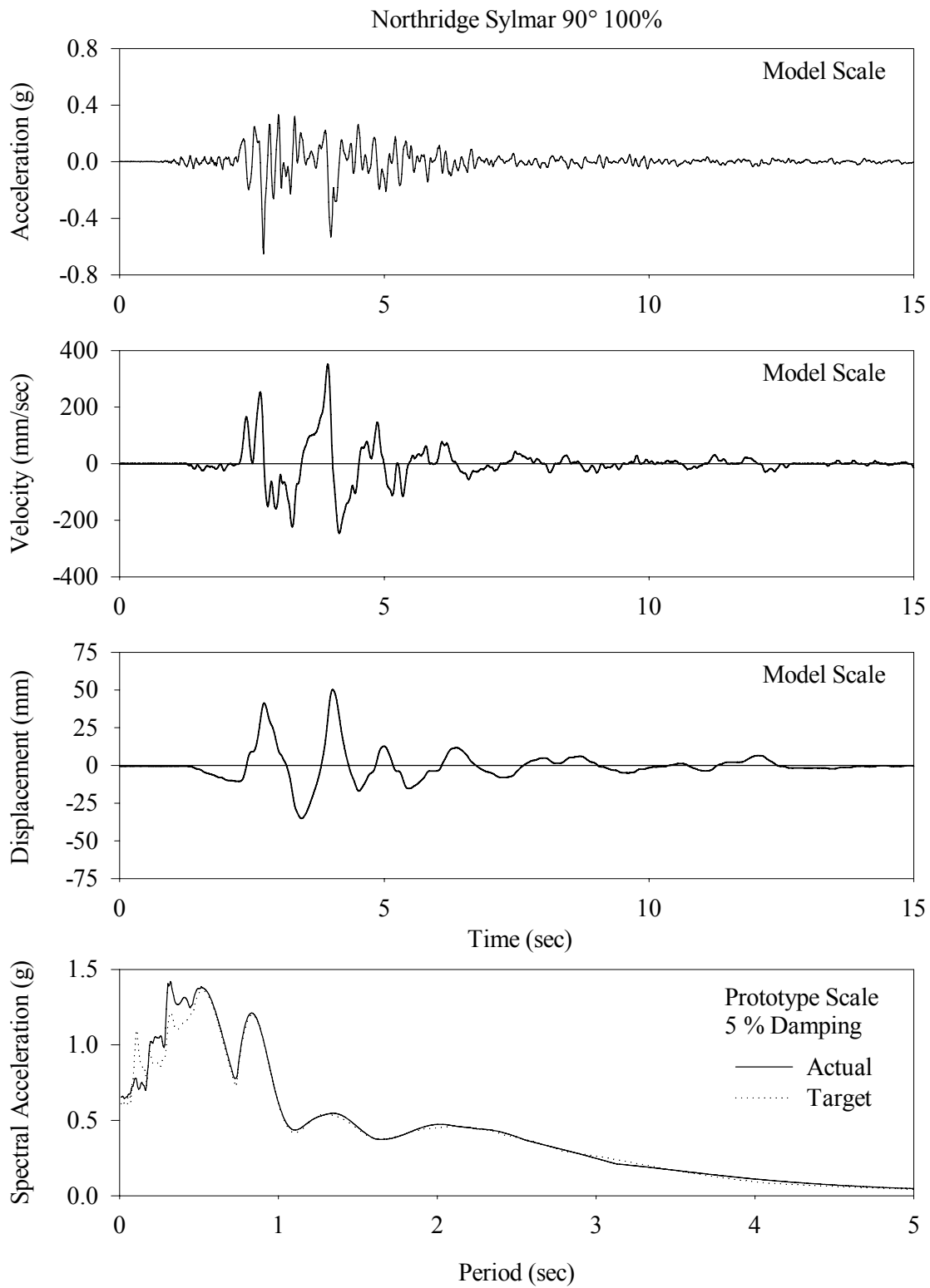
FIGURE A-20 **Histories of Acceleration, Velocity and Displacement and Acceleration Response Spectrum for the SYL 90 Record (From Wolff, 2004)**

201

Pacoima S16E 100%
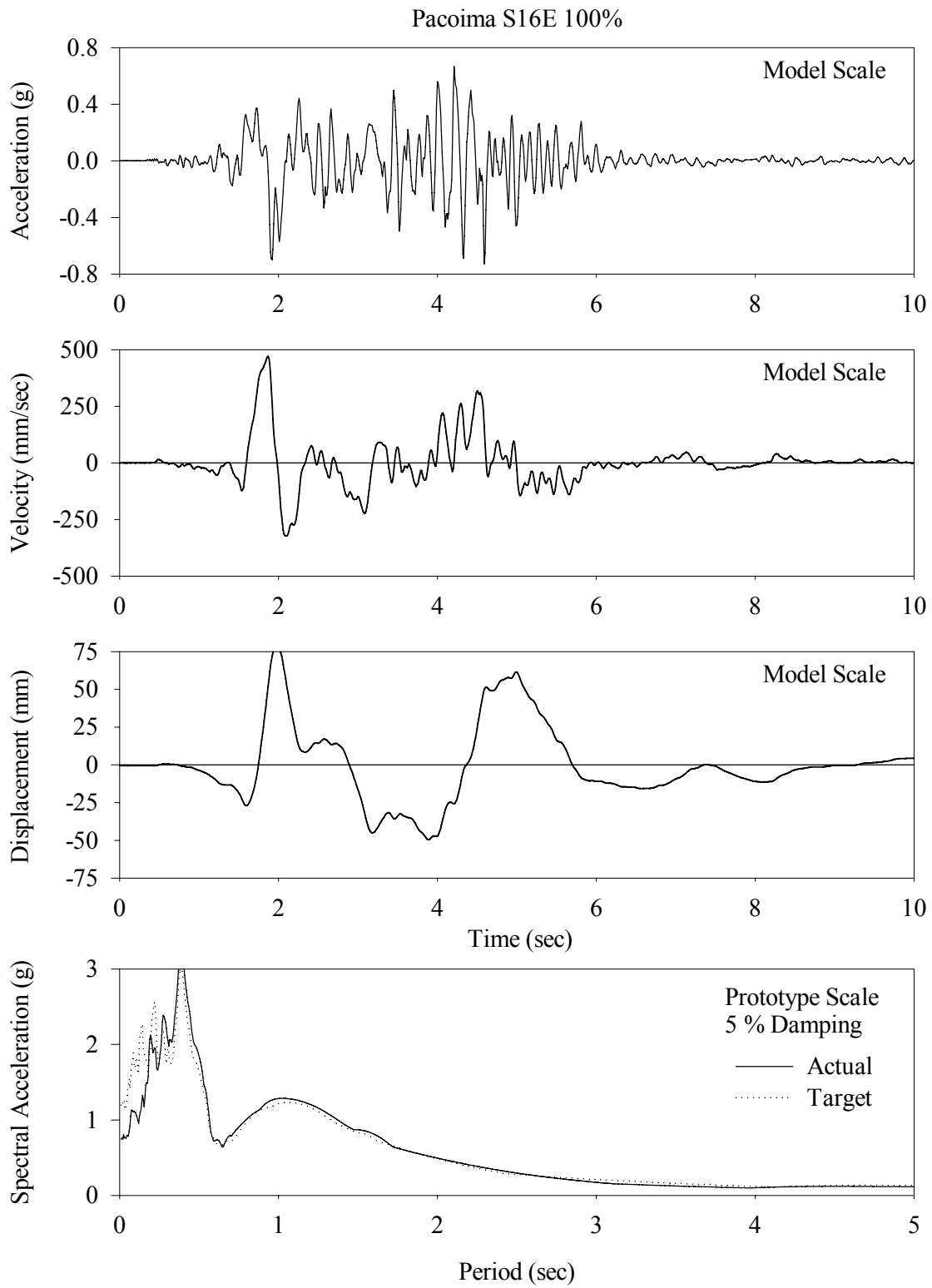
FIGURE A-21 **Histories of Acceleration, Velocity and Displacement and Acceleration Response Spectrum for the PAC S16E Record (From Wolff, 2004)**
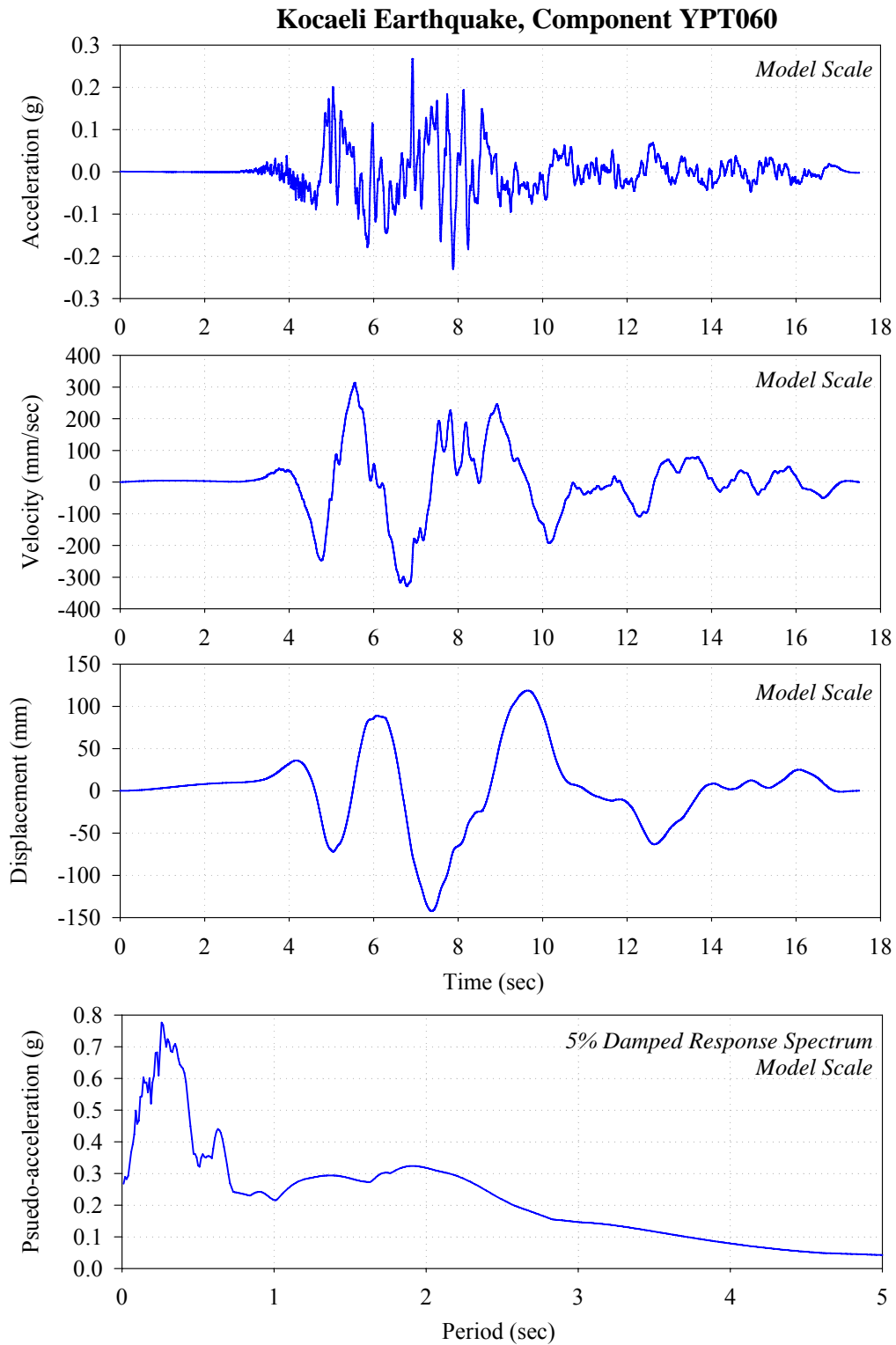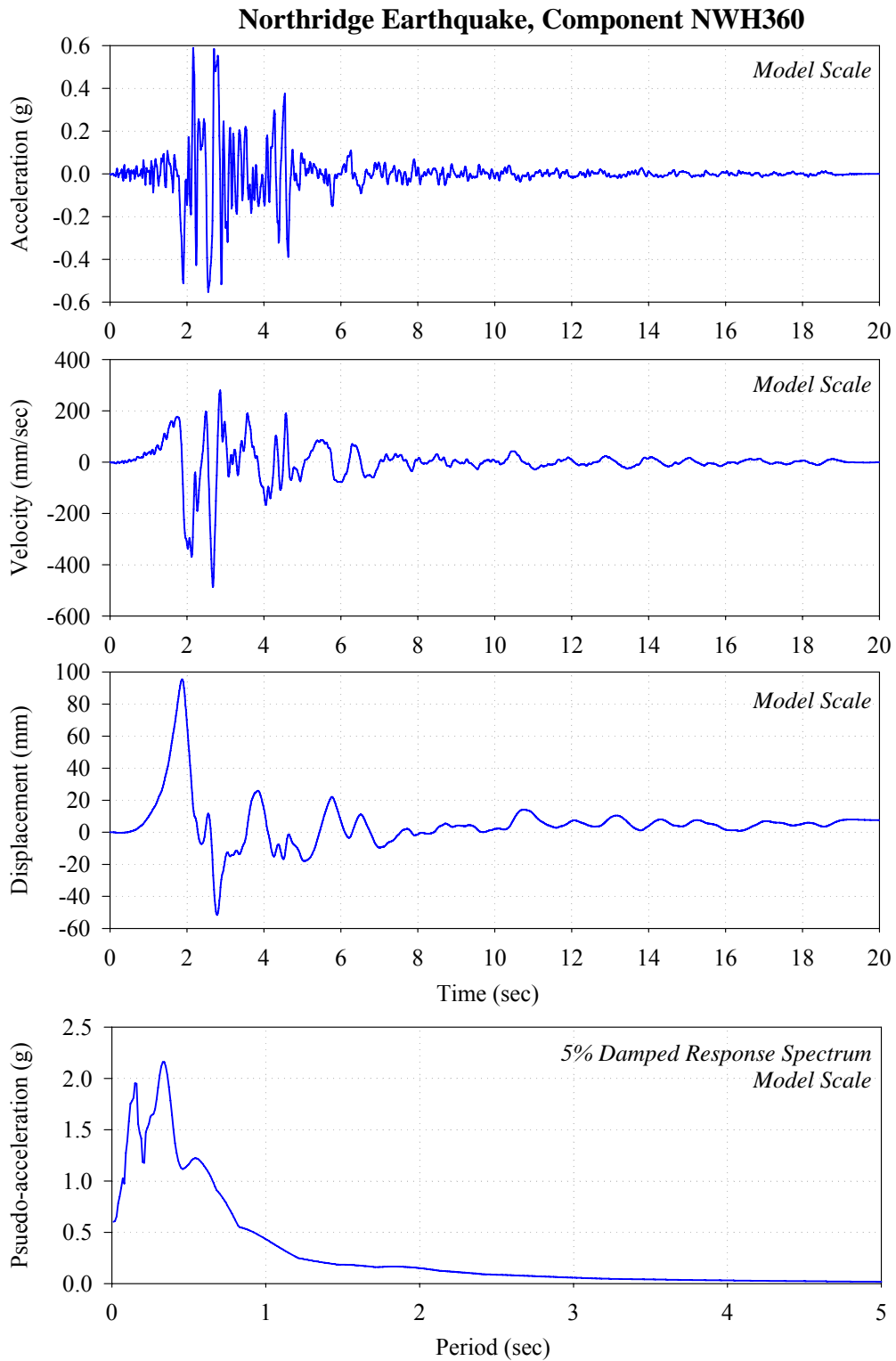
202
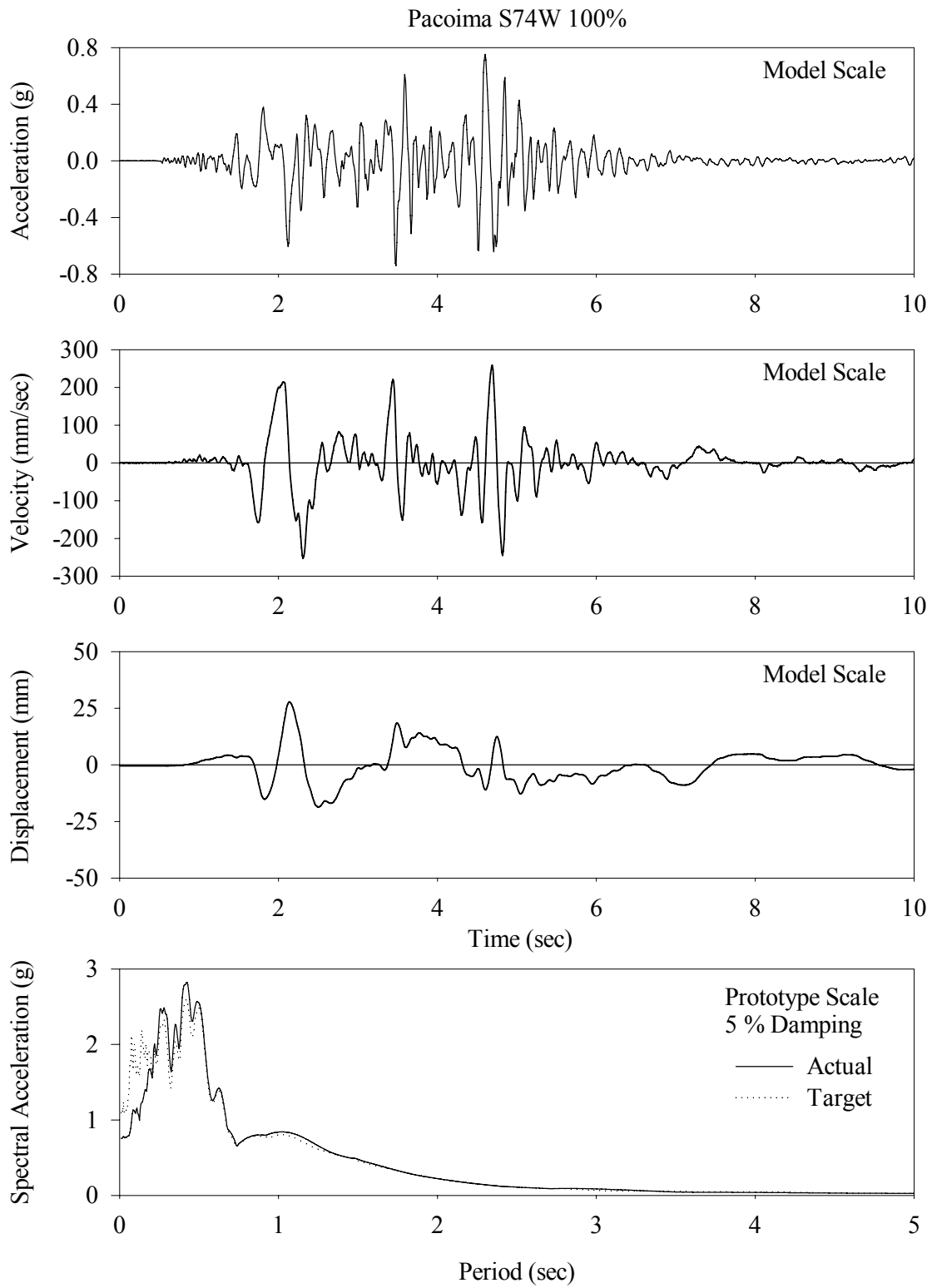
FIGURE A-22   Histories of Acceleration, Velocity and Displacement and Acceleration Response Spectrum for the PAC S74W Record (From Wolff, 2004)

APPENDIX B
COMPARISON OF EXPERIMENTAL AND ANALYTICAL FORCE-DISPLACEMENT LOOPS

FIGURE B-1 Comparison of Experimental Results and Analytical Prediction of Response for Isolation System Double 1 Subjected to the 100% El Centro S00E and 200% El Centro S00E Ground Motions

206

FIGURE B-2 Comparison of Experimental Results and Analytical Prediction of Response for Isolation System Double 1 Subjected to the 100% Kobe N-S and 100% Taft N21E Ground Motions

FIGURE B-3 Comparison of Experimental Results and Analytical Prediction of Response for Isolation System Double 1 Subjected to the 500% Taft N21E and 100% Taiwan TCU 129 EW Ground Motions

FIGURE B-4 Comparison of Experimental Results and Analytical Prediction of Response for Isolation System Double 1 Subjected to the 125% Taiwan TCU 129 EW and 50% Mexico N90W Ground Motions

FIGURE B-5 Comparison of Experimental Results and Analytical Prediction of Response for Isolation System Double 1 Subjected to the 100% Newhall 360 and 100% Sylmar 90 Ground Motions

FIGURE B-6 Comparison of Experimental Results and Analytical Prediction of Response for Isolation System Double 1 Subjected to the 100% Pacoima S16E and 100% Pacoima S74W Ground Motions

FIGURE B-7 Comparison of Experimental Results and Analytical Prediction of Response for Isolation System Double 1 Subjected to the 100% El Centro S00E + Vertical and 200% El Centro S00E + Vertical Ground Motions

FIGURE B-8 Comparison of Experimental Results and Analytical Prediction of Response for Isolation System Double 1 Subjected to the 100% Kobe N-S + Vertical and 500% Taft N21E + Vertical Ground Motions

FIGURE B-9   Comparison of Experimental Results and Analytical Prediction of Response for Isolation System Double 1 Subjected to the 125% Taiwan TCU 129 EW + Vertical and 100% Newhall 90 + Vertical Ground Motions

FIGURE B-10 Comparison of Experimental Results and Analytical Prediction of Response for Isolation System Double 1 Subjected to the 100% Sylmar 90 + Vertical and 100% Pacoima S16E + Vertical Ground Motions

215

FIGURE B-11 Comparison of Experimental Results and Analytical Prediction of Response for Isolation System Double 1 Subjected to 200% Tridirectional El Centro Ground Motion

FIGURE B-12 Comparison of Experimental Results and Analytical Prediction of Response for Isolation System Double 1 Subjected to 100% Tridirectional Taiwan TCU 129 Ground Motion

FIGURE B-13 Comparison of Experimental Results and Analytical Prediction of Response for Isolation System Double 1 Subjected to 100% Tridirectional Pacoima Ground Motion

FIGURE B-14   Comparison of Experimental Results and Analytical Prediction of Response for Isolation System Double 2 Subjected to the Taft 021 and El Centro 180 Ground Motions

FIGURE B-15 Comparison of Experimental Results and Analytical Prediction of Response for Isolation System Double 2 Subjected to the Corralitos 090 and Kocaeli 330 Ground Motions

FIGURE B-16 Comparison of Experimental Results and Analytical Prediction of Response for Isolation System Double 2 Subjected to the Newhall 360 and Sylmar 360 Ground Motions

221

FIGURE B-17   Comparison of Experimental Results and Analytical Prediction of Response for Isolation System Double 2 Subjected to the Pacoima 164 and El Centro 180 + Vertical Ground Motions

FIGURE B-18 Comparison of Experimental Results and Analytical Prediction of Response for Isolation System Double 2 Subjected to the Kocaeli 330 + Vertical and Newhall 360 + Vertical Ground Motions

FIGURE B-19   Comparison of Experimental Results and Analytical Prediction of Response for Isolation System Double 2 Subjected to Tridirectional El Centro Excitation

Kocaeli 330 Longitudinal + Kocaeli 060 Transverse + Vertical

Displacement Orbits

FIGURE B-20 Comparison of Experimental Results and Analytical Prediction of Response for Isolation System Double 2 Subjected to Tridirectional Kocaeli Excitation
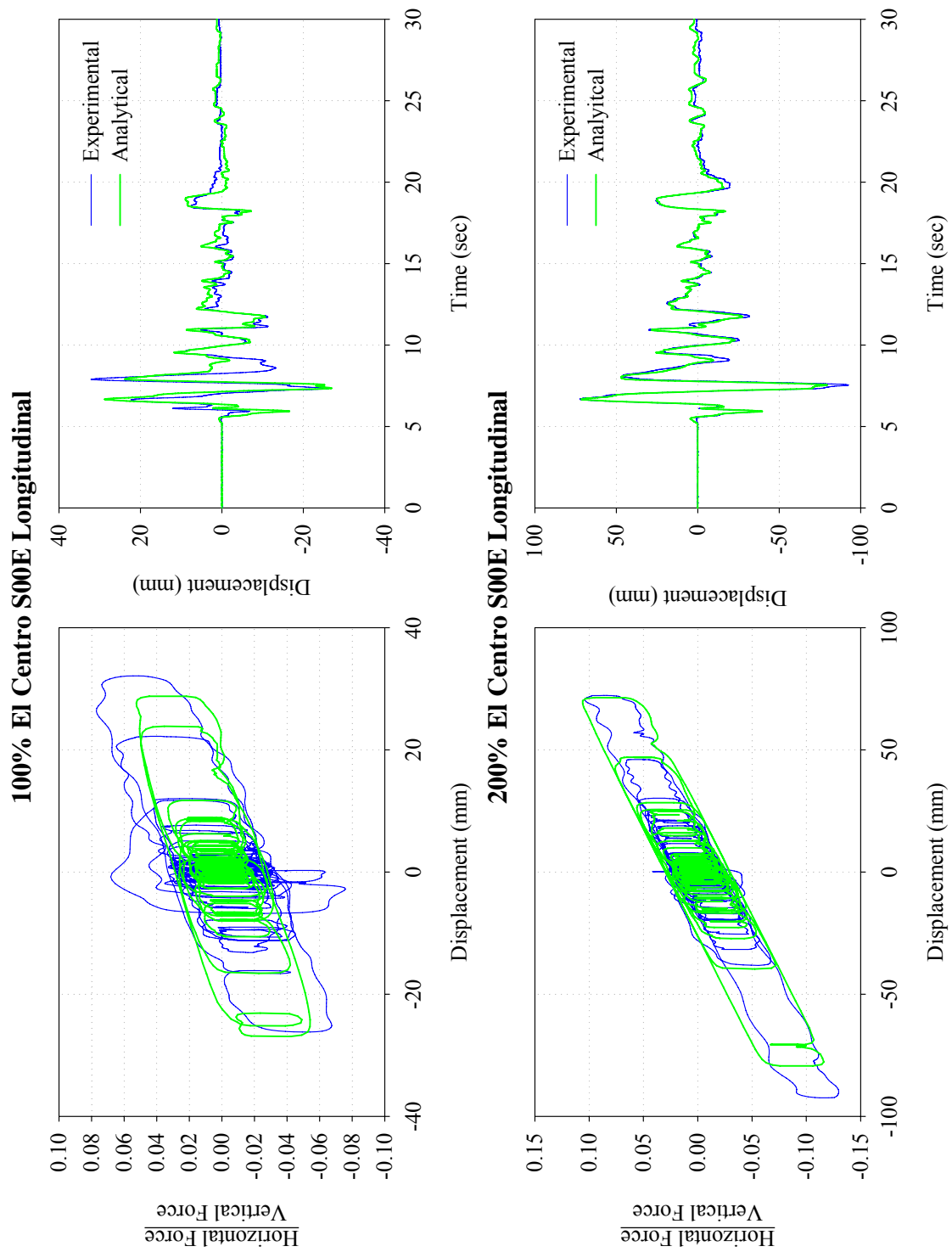
225

FIGURE B-21 Comparison of Experimental Results and Analytical Prediction of Response for Isolation System Double 2 Subjected to Tridirectional Newhall Excitation

FIGURE B-22   Comparison of Experimental Results and Analytical Prediction of Response for Isolation System Triple 1 Subjected to the Taft 021 and El Centro 180 Ground Motions
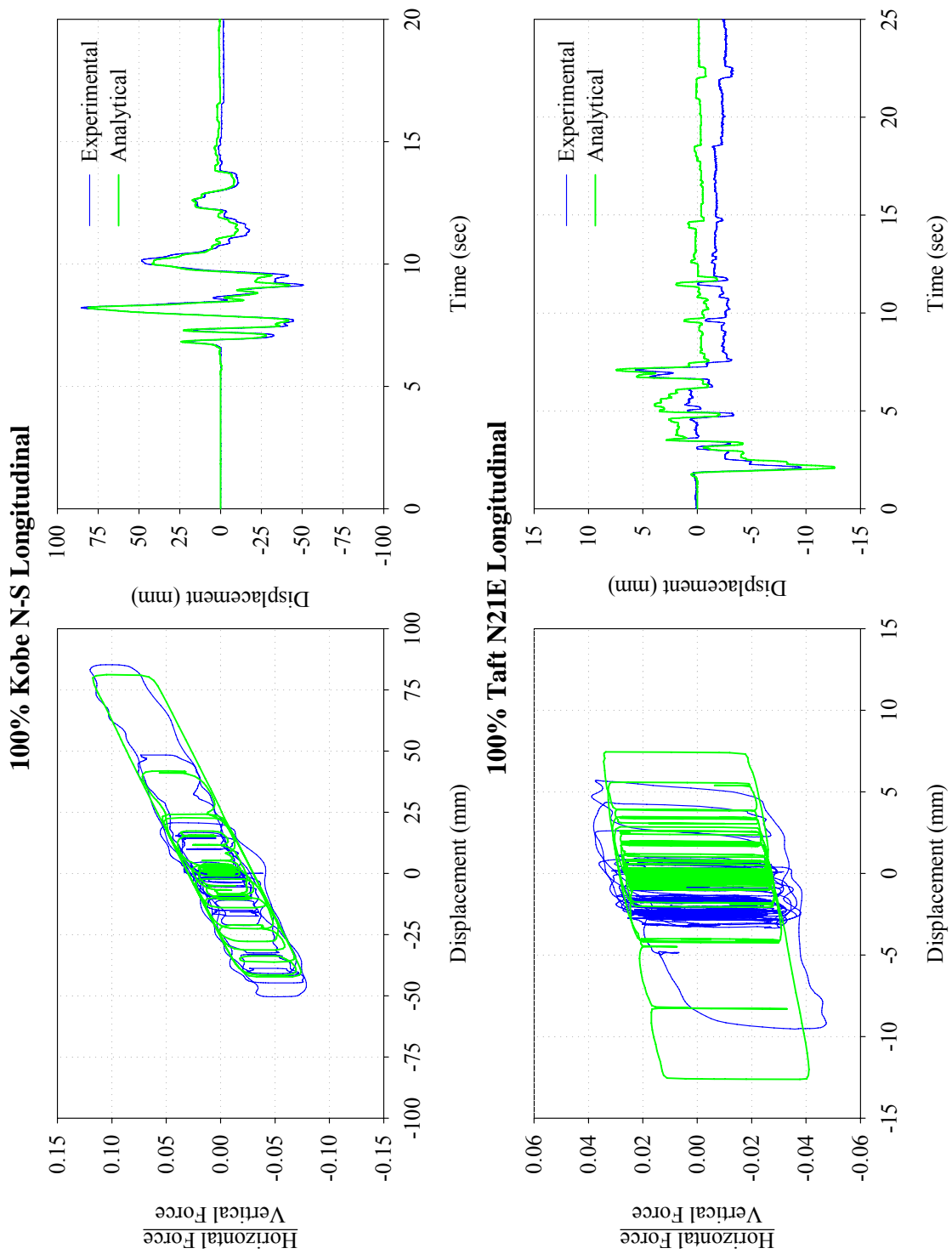
FIGURE B-23 Comparison of Experimental Results and Analytical Prediction of Response for Isolation System Triple 1 Subjected to the Corralitos 090 and Kocaeli 330 Ground Motions

228

FIGURE B-24 Comparison of Experimental Results and Analytical Prediction of Response for Isolation System Triple 1 Subjected to the Newhall 360 and Sylmar 360 Ground Motions
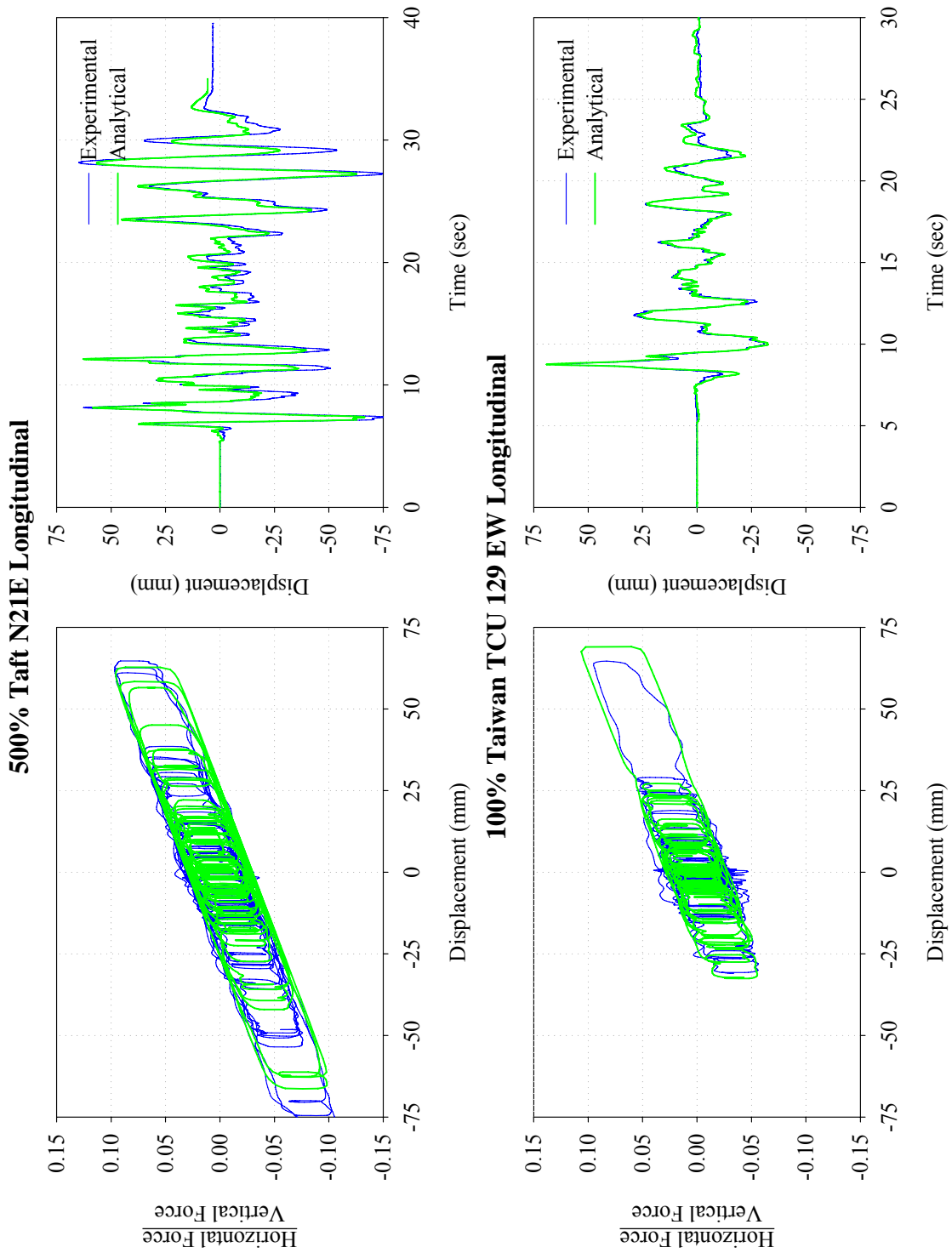
FIGURE B-25   Comparison of Experimental Results and Analytical Prediction of Response for Isolation System Triple 1 Subjected to the Pacoima 164 and El Centro 180 + Vertical Ground Motions

FIGURE B-26 Comparison of Experimental Results and Analytical Prediction of Response for Isolation System Triple 1 Subjected to the Kocaeli 330 + Vertical and Newhall 360 + Vertical Ground Motions
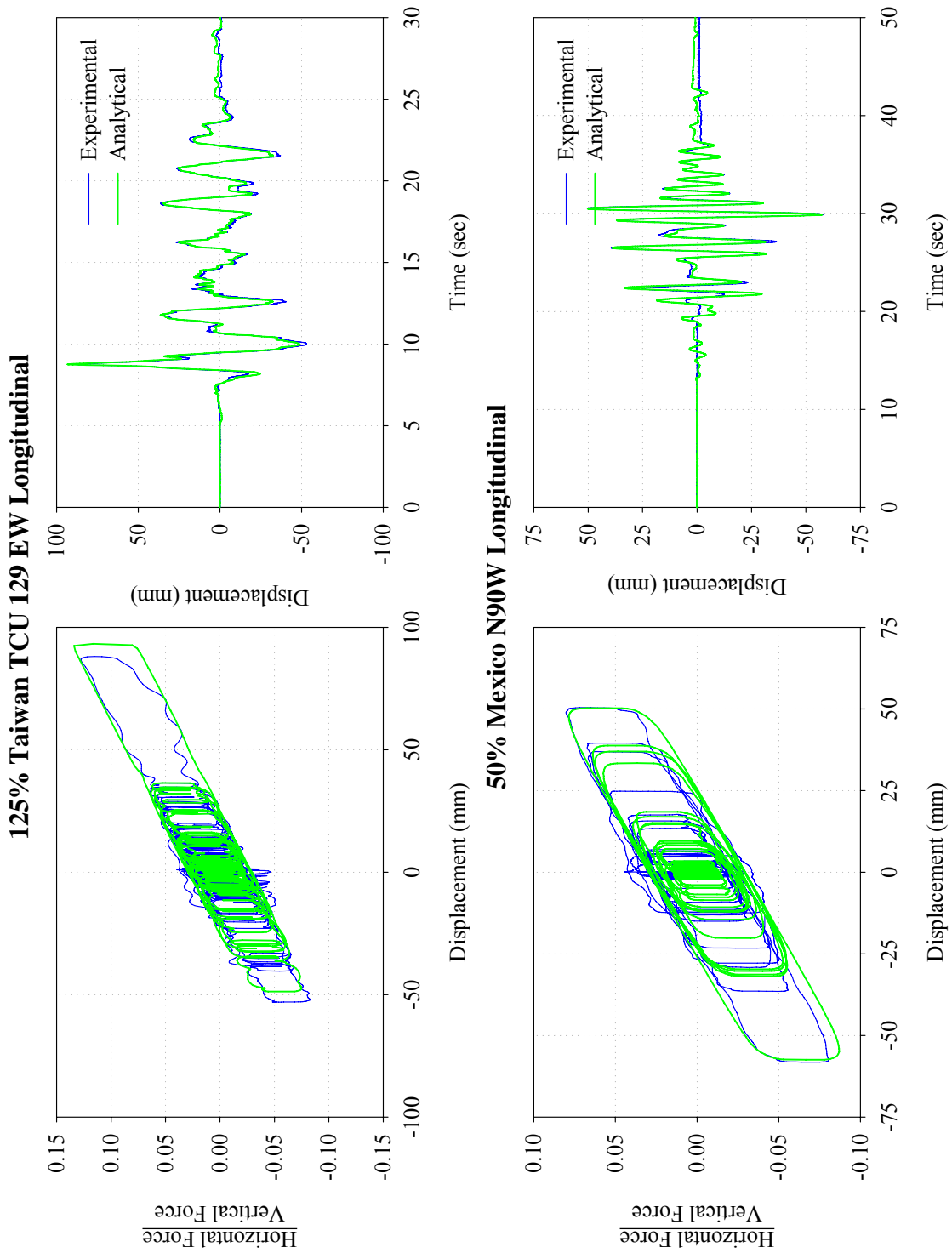
231

FIGURE B-27 Comparison of Experimental Results and Analytical Prediction of Response for Isolation System Triple 1 Subjected to Tridirectional El Centro Excitation
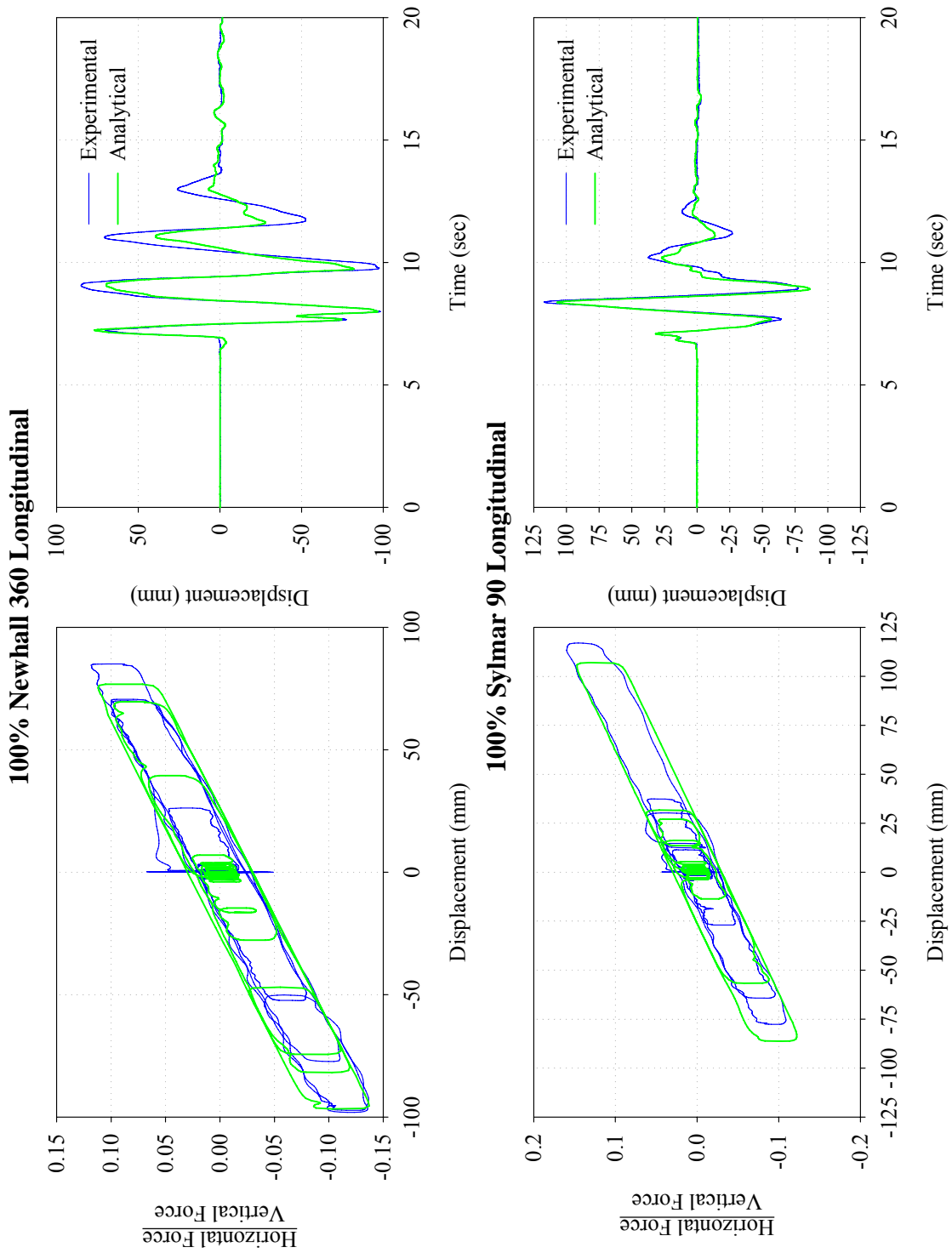
FIGURE B-28   Comparison of Experimental Results and Analytical Prediction of Response for Isolation System Triple 1 Subjected to Tridirectional Kocaeli Excitation

Newhall 360 Longitudinal + Newhall 090 Transverse + Vertical

FIGURE B-29 Comparison of Experimental Results and Analytical Prediction of Response for Isolation System Triple 1 Subjected to Tridirectional Newhall Excitation

234

FIGURE B-30   Comparison of Experimental Results and Analytical Prediction of Response for Isolation System Triple 2 Subjected to the Taft 021 and El Centro 180 Ground Motions
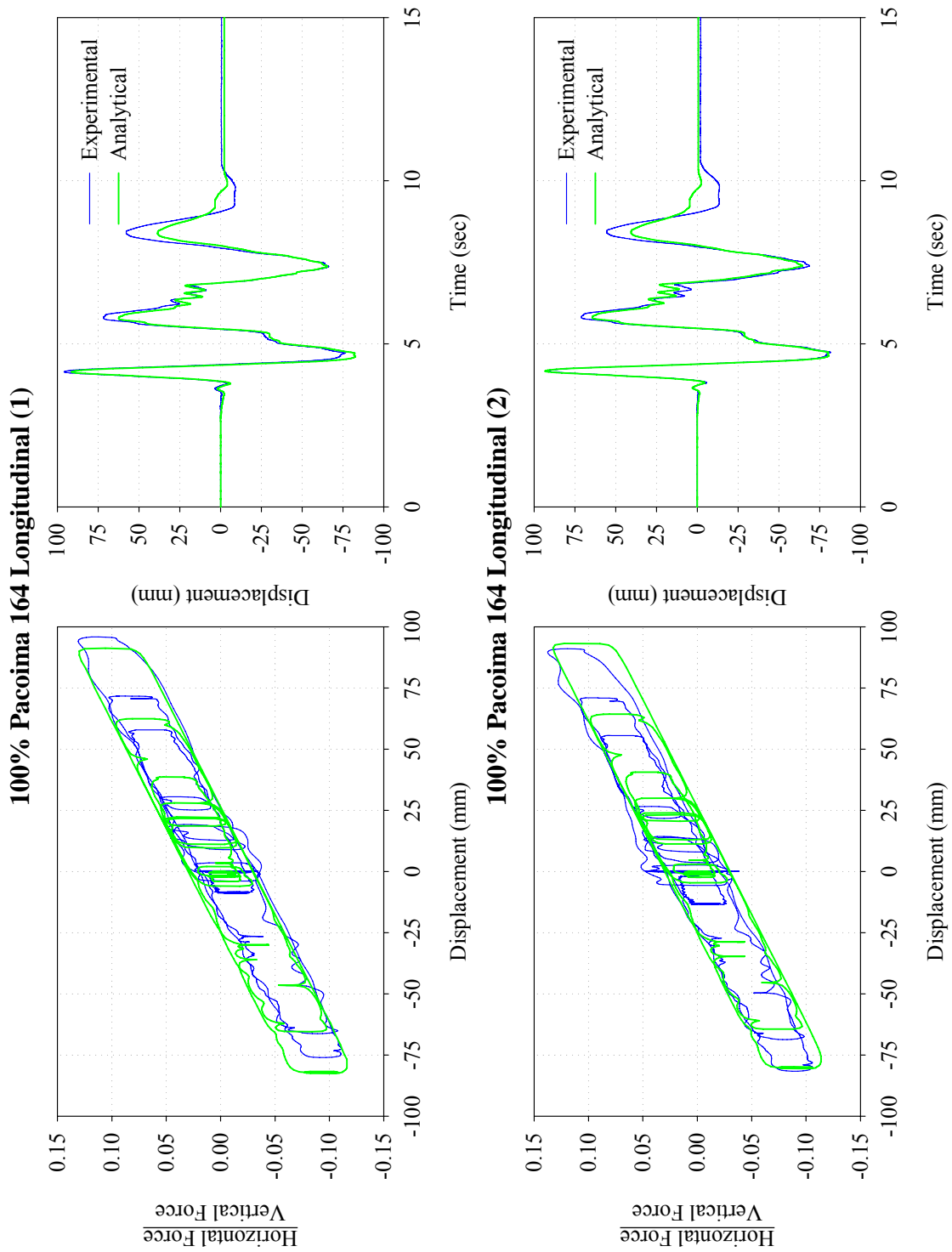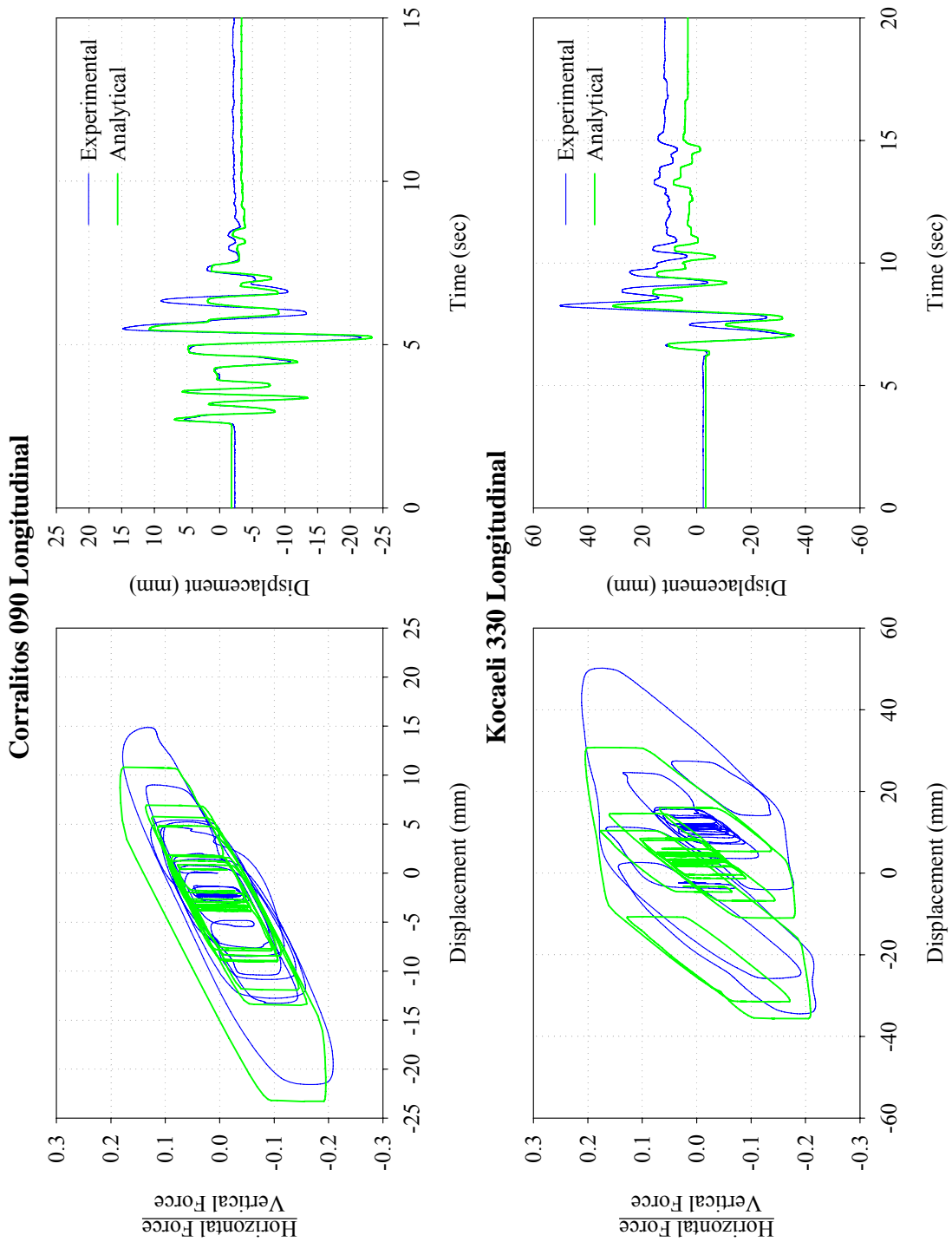
FIGURE B-31 Comparison of Experimental Results and Analytical Prediction of Response for Isolation System Triple 2 Subjected to the Corralitos 090 and Kocaeli 330 Ground Motions
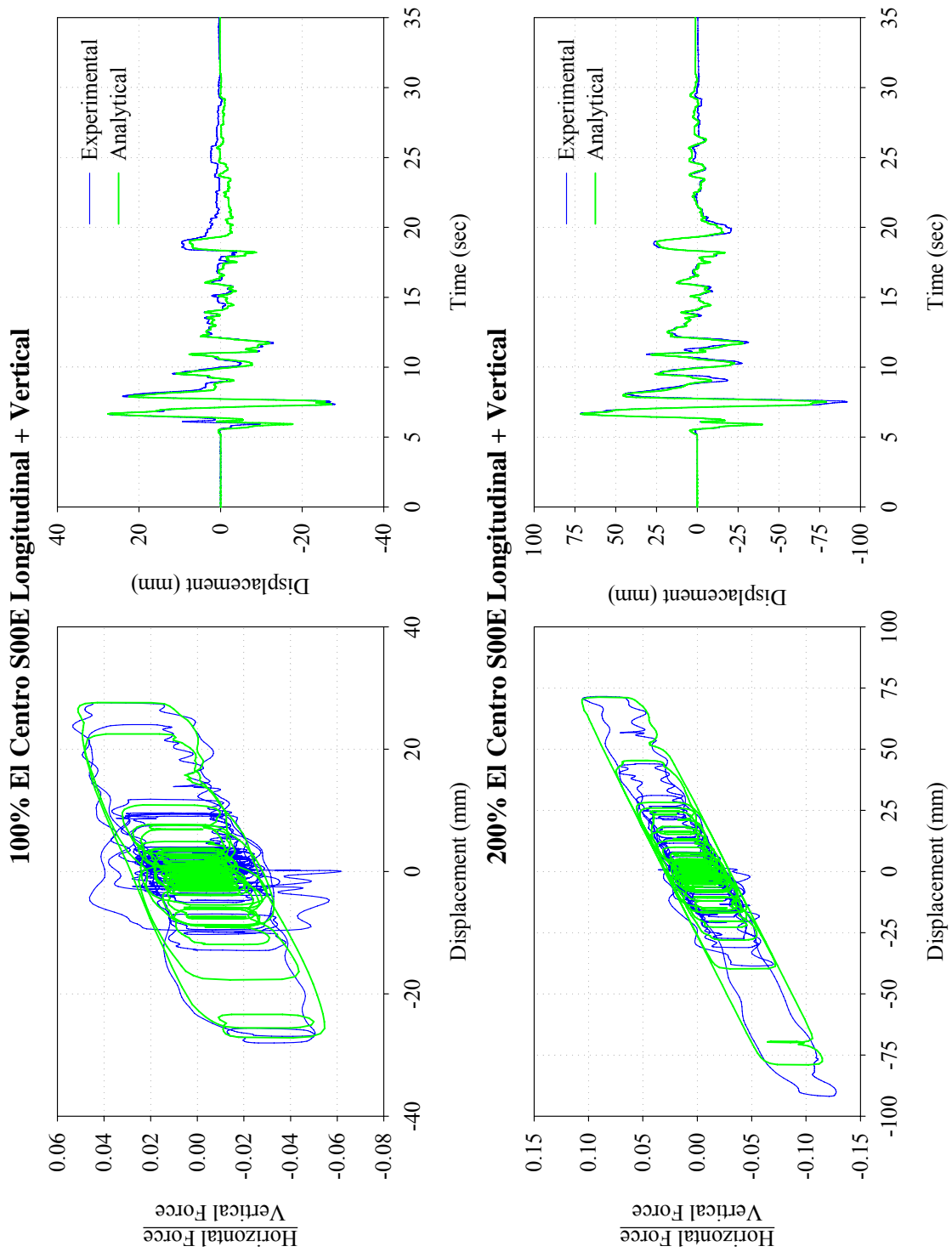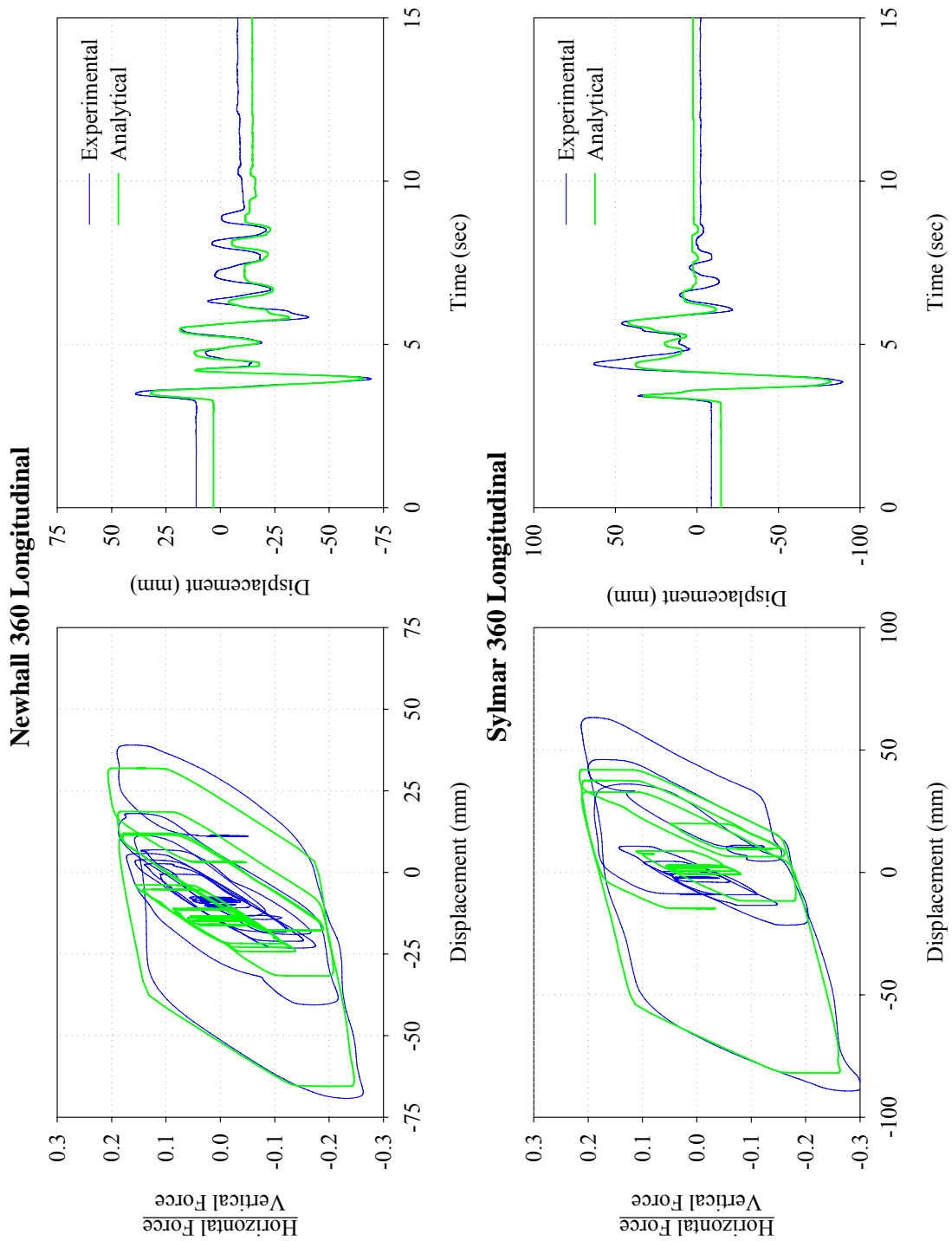
FIGURE B-32 Comparison of Experimental Results and Analytical Prediction of Response for Isolation System Triple 2 Subjected to the Newhall 360 and Sylmar 360 Ground Motions

237
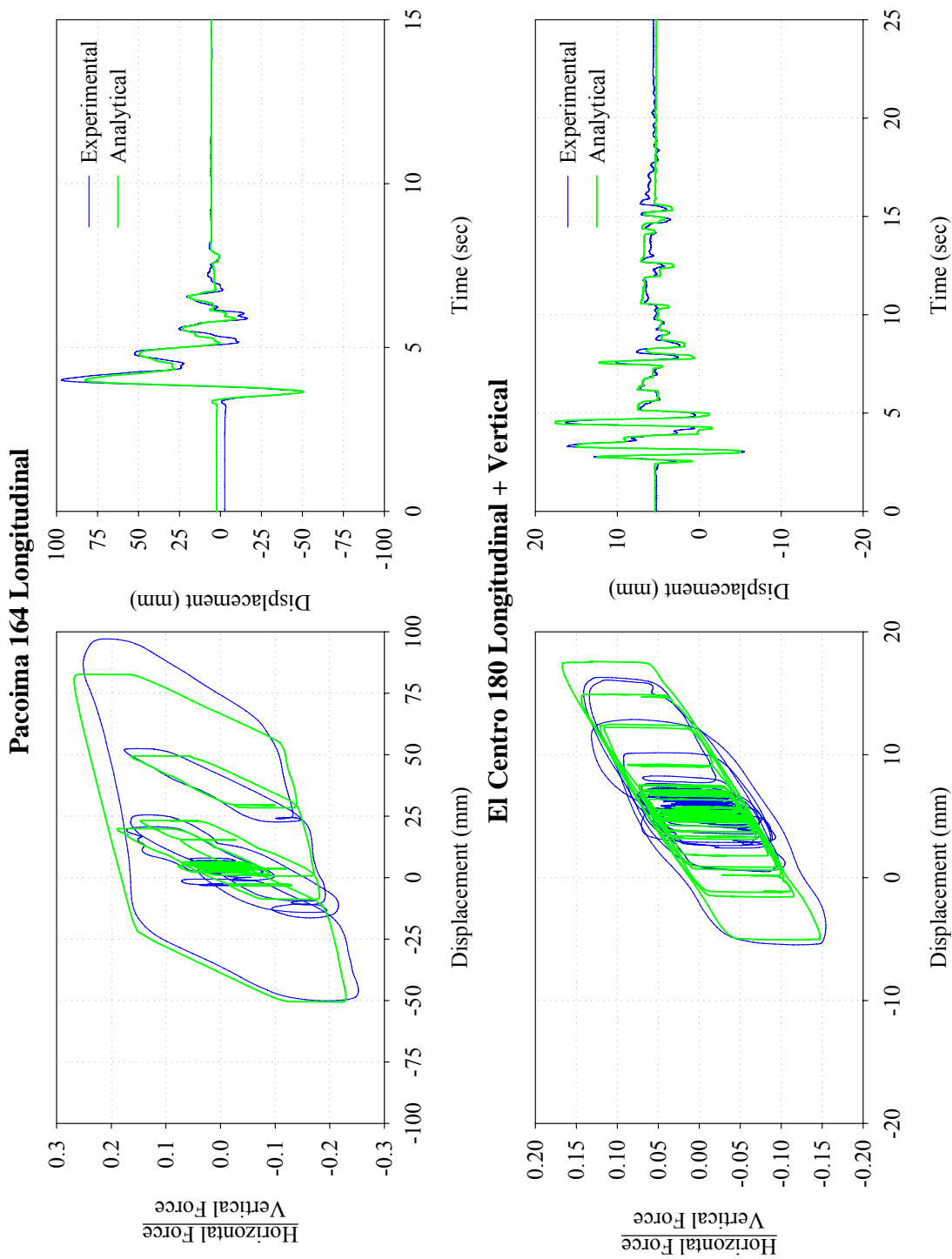
FIGURE B-33 Comparison of Experimental Results and Analytical Prediction of Response for Isolation System Triple 2 Subjected to the Pacoima 164 and El Centro 180 + Vertical Ground Motions
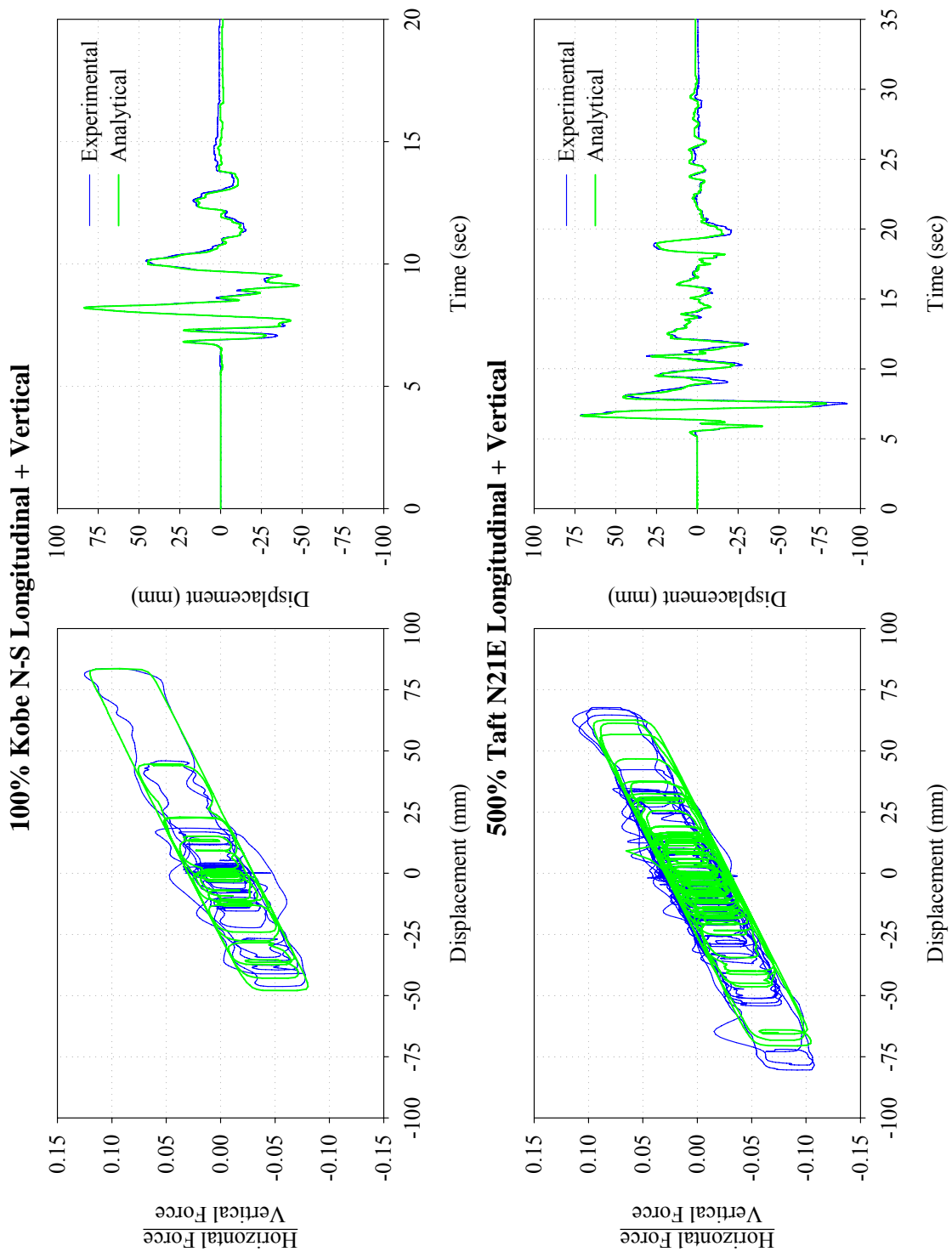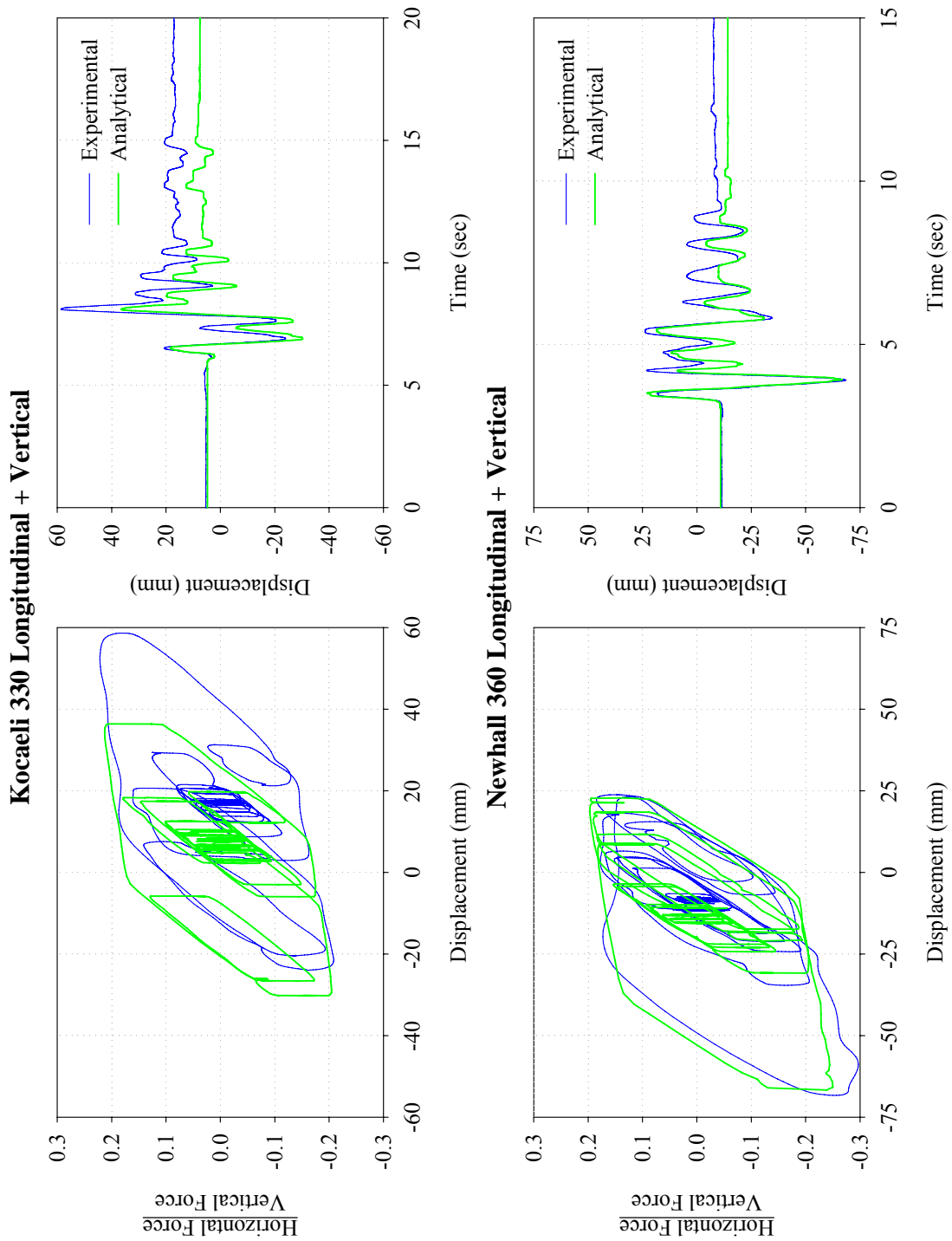
FIGURE B-34 Comparison of Experimental Results and Analytical Prediction of Response for Isolation System Triple 2 Subjected to the Kocaeli 330 + Vertical and Newhall 360 + Vertical Ground Motions

239

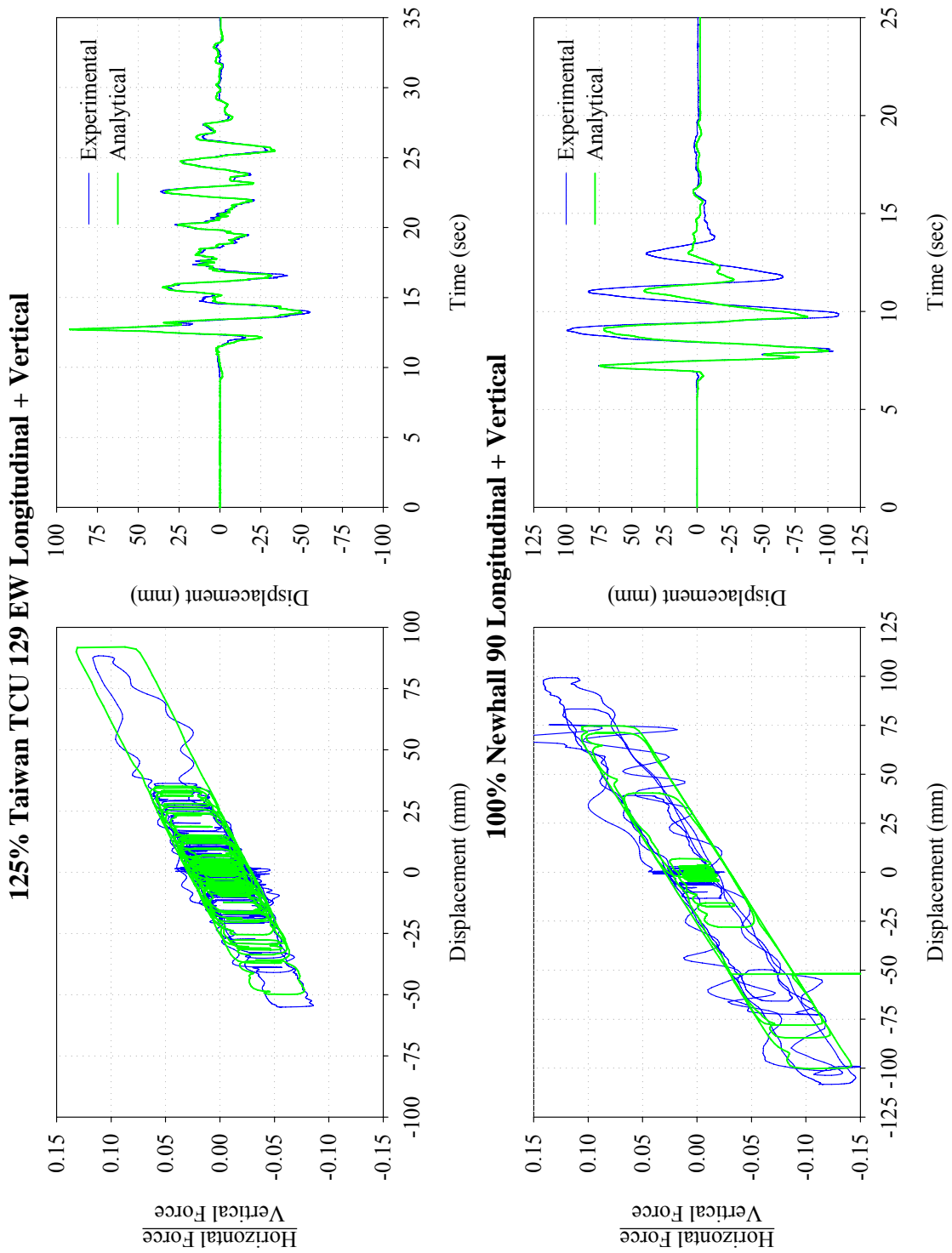**El Centro 180 Longitudinal + El Centro 270 Transverse + Vertical**

Displacement Orbits
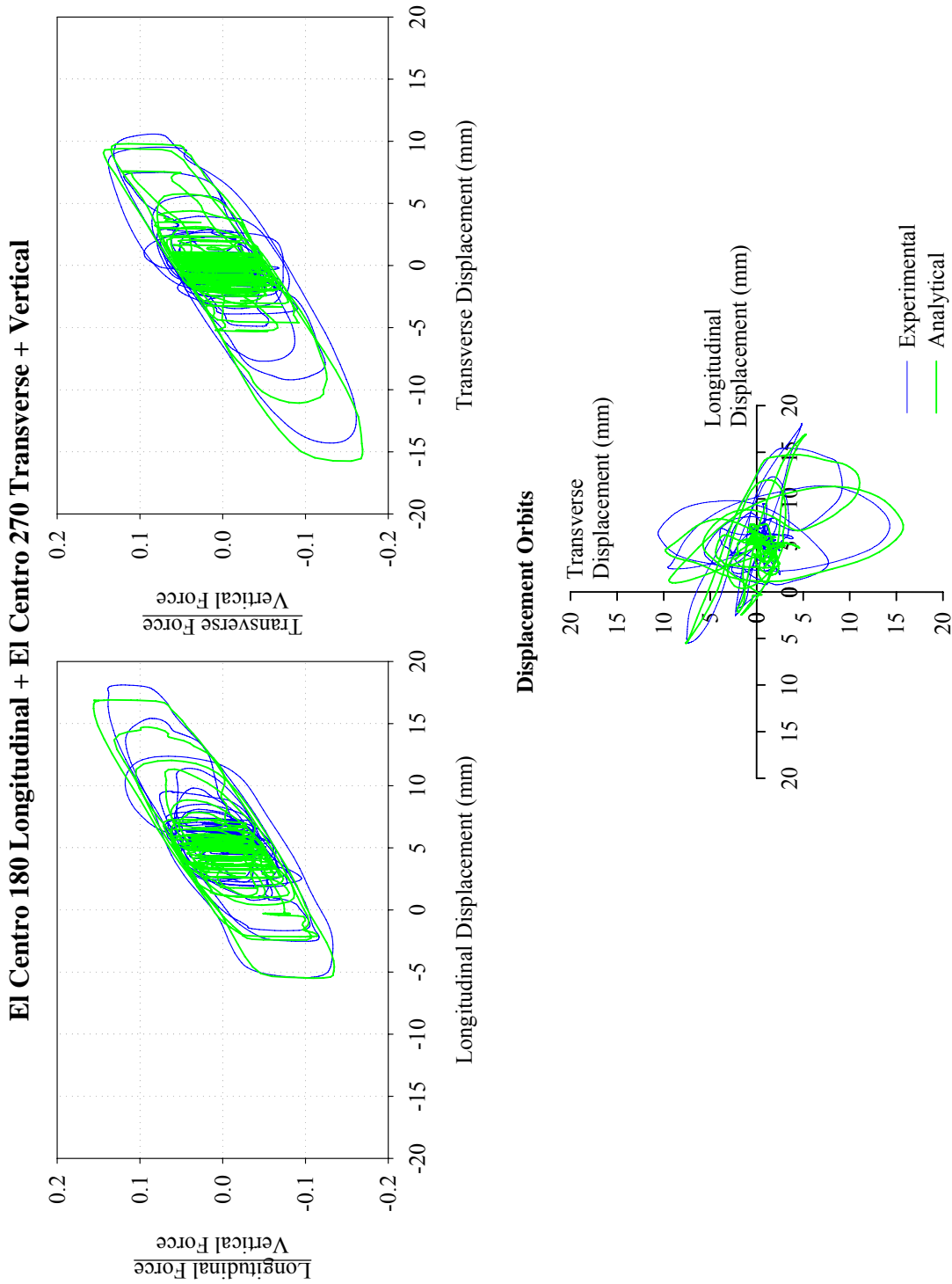
FIGURE B-35   Comparison of Experimental Results and Analytical Prediction of Response for Isolation System Triple 2 Subjected to Tridirectional El Centro Excitation
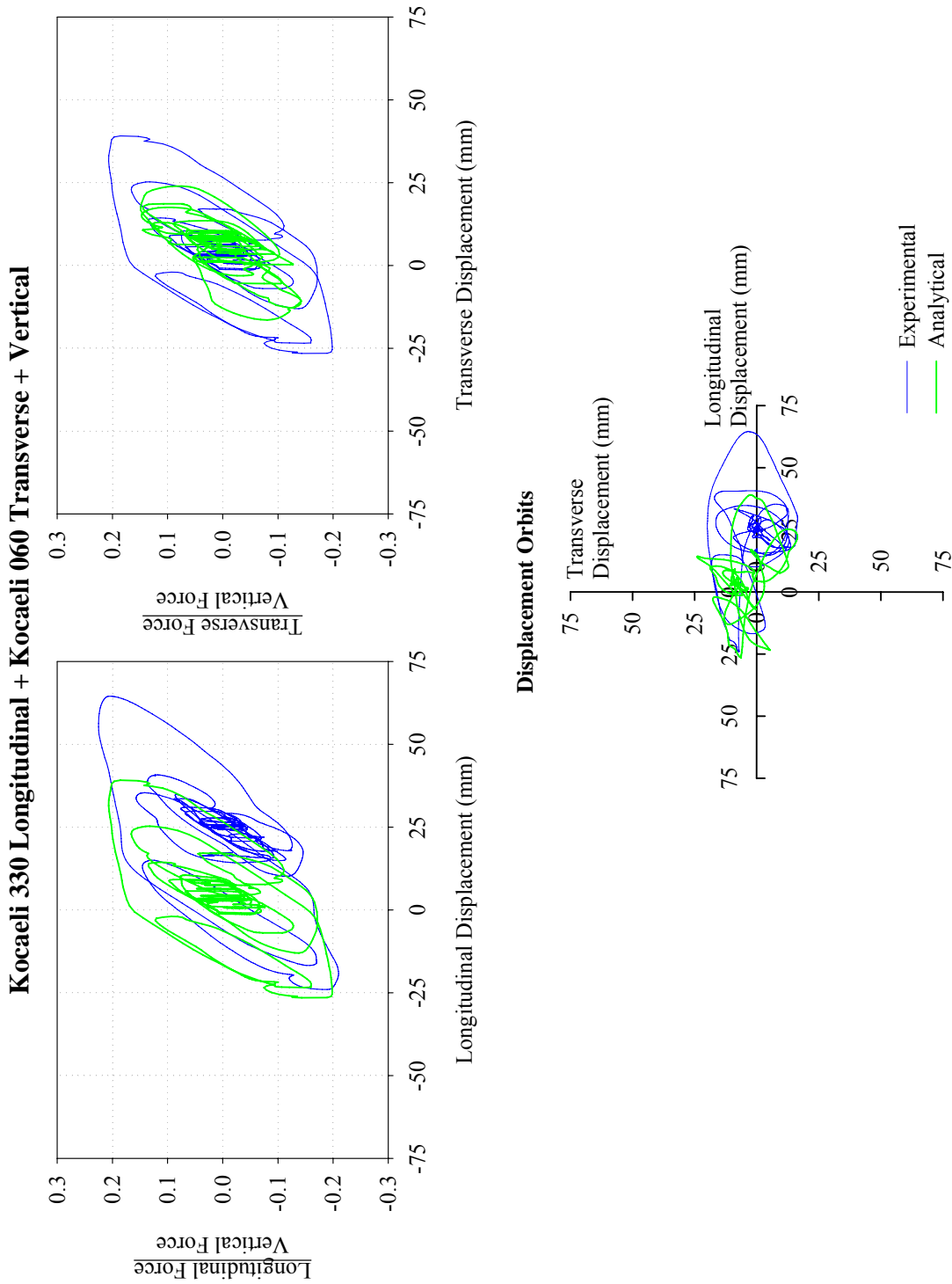
FIGURE B-36 Comparison of Experimental Results and Analytical Prediction of Response for Isolation System Triple 2 Subjected to Tridirectional Kocaeli Excitation
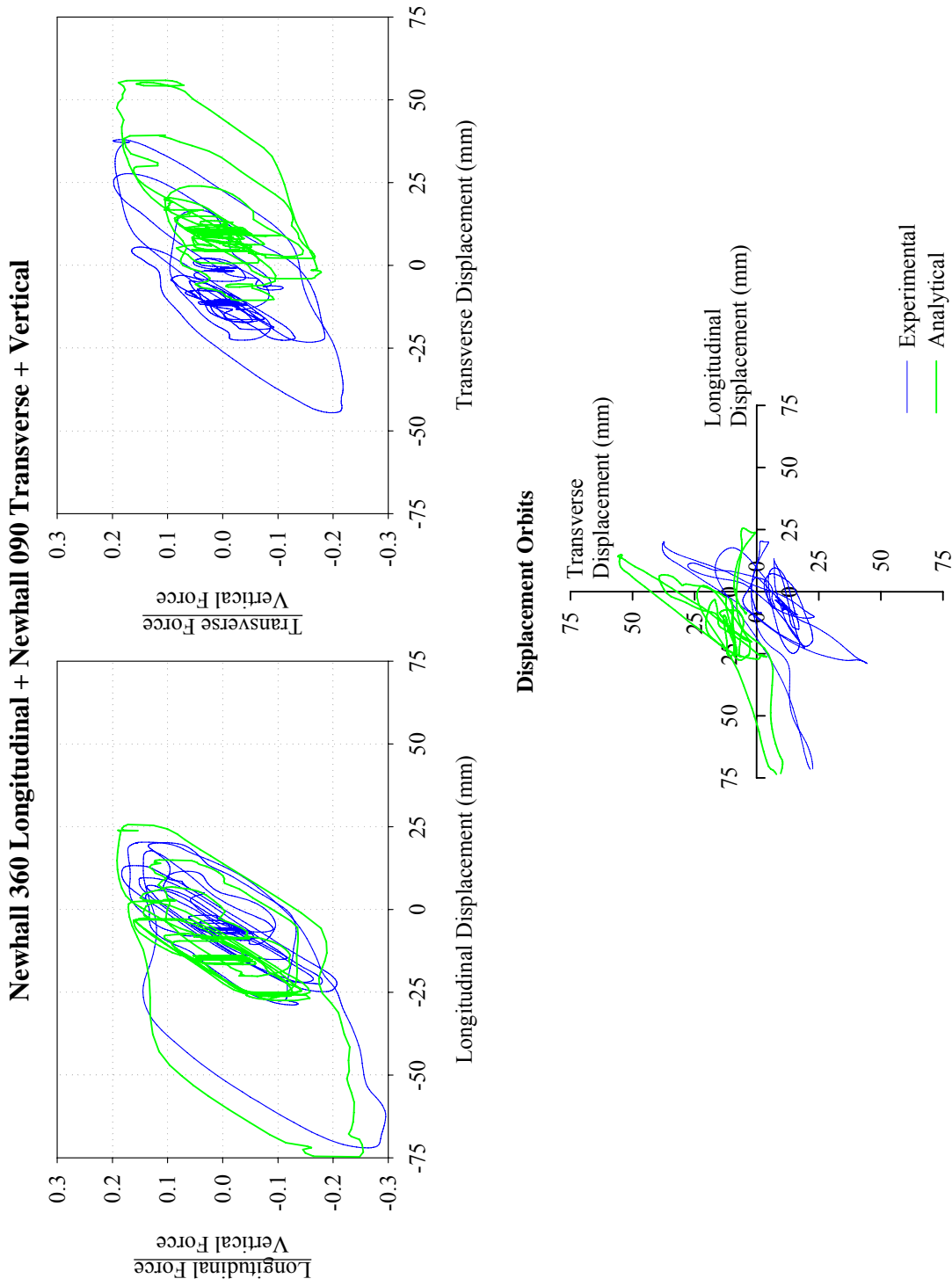
FIGURE B-37 Comparison of Experimental Results and Analytical Prediction of Response for Isolation System Triple 2 Subjected to Tridirectional Newhall Excitation
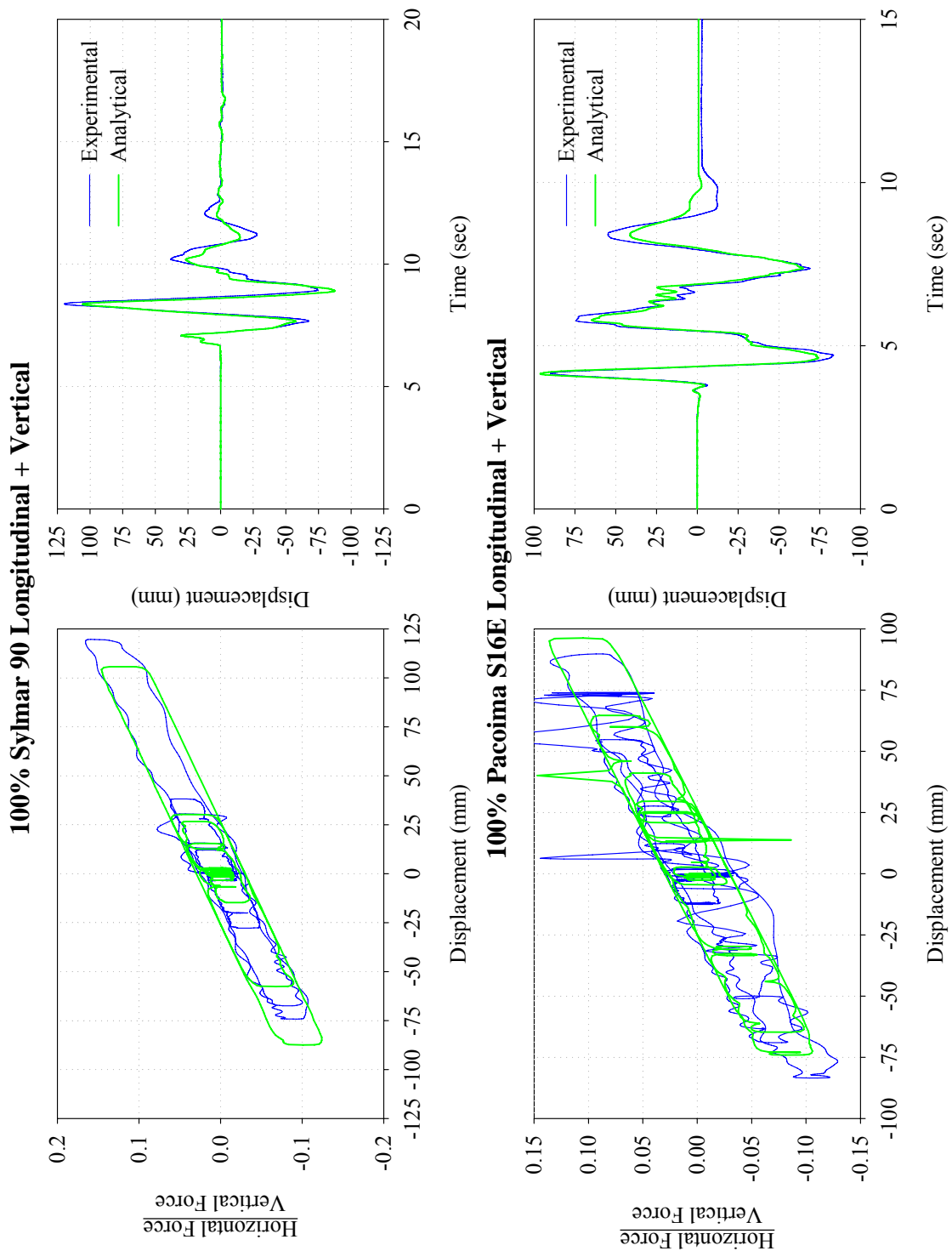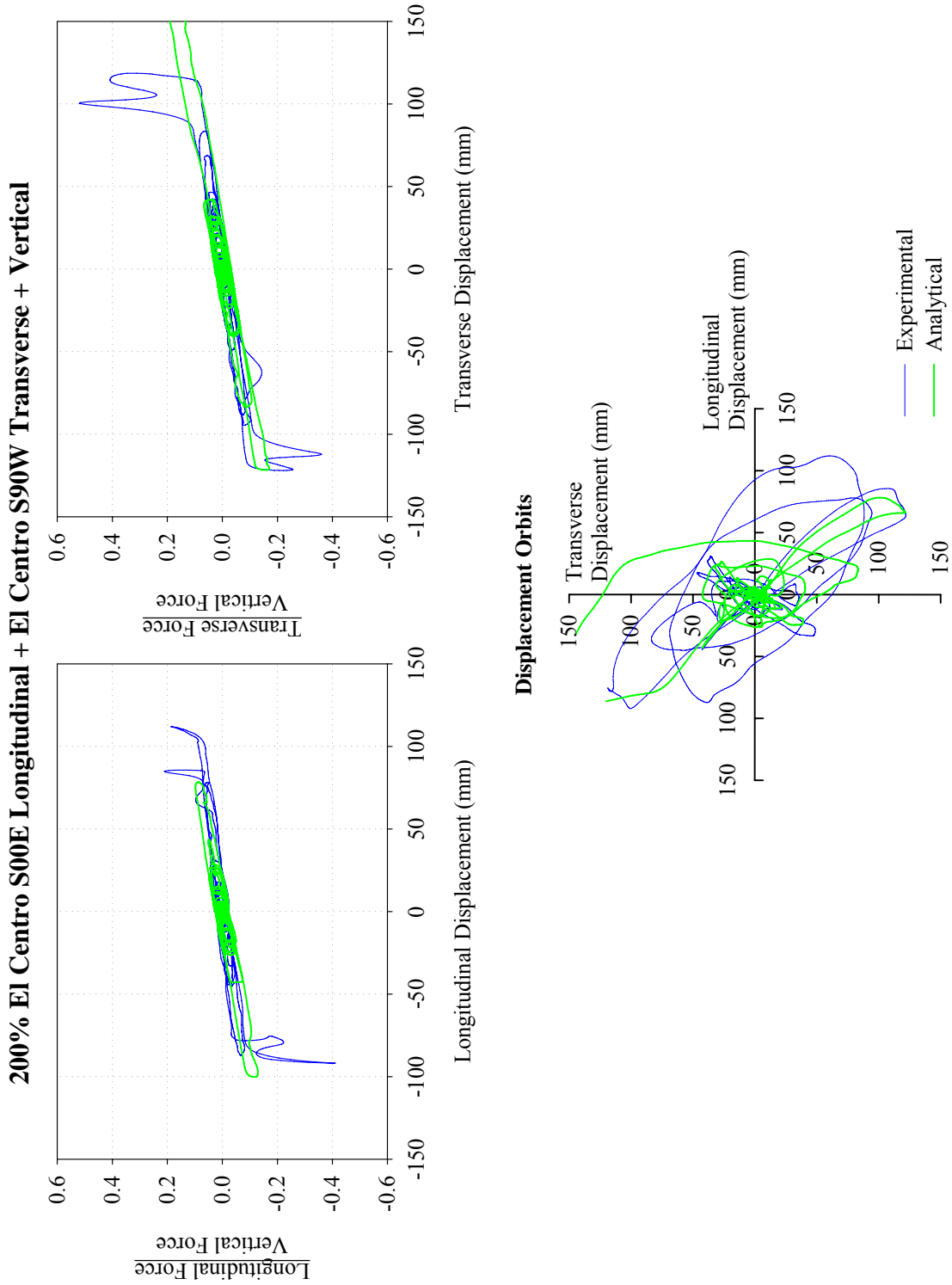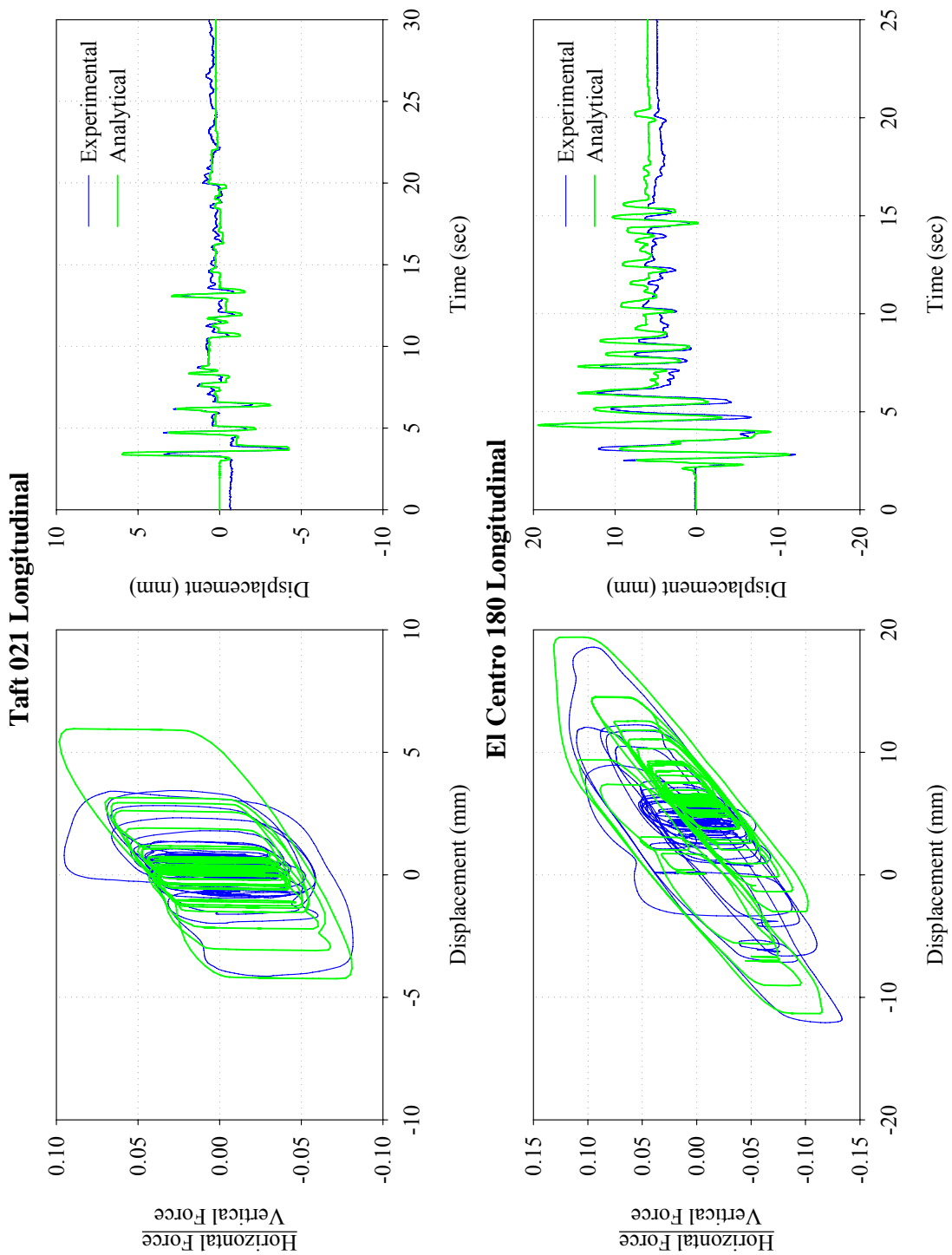
FIGURE B-38 Comparison of Experimental Results and Analytical Prediction of Response for Isolation System Triple 3 Subjected to the Taft 021 and El Centro 180 Ground Motions

243
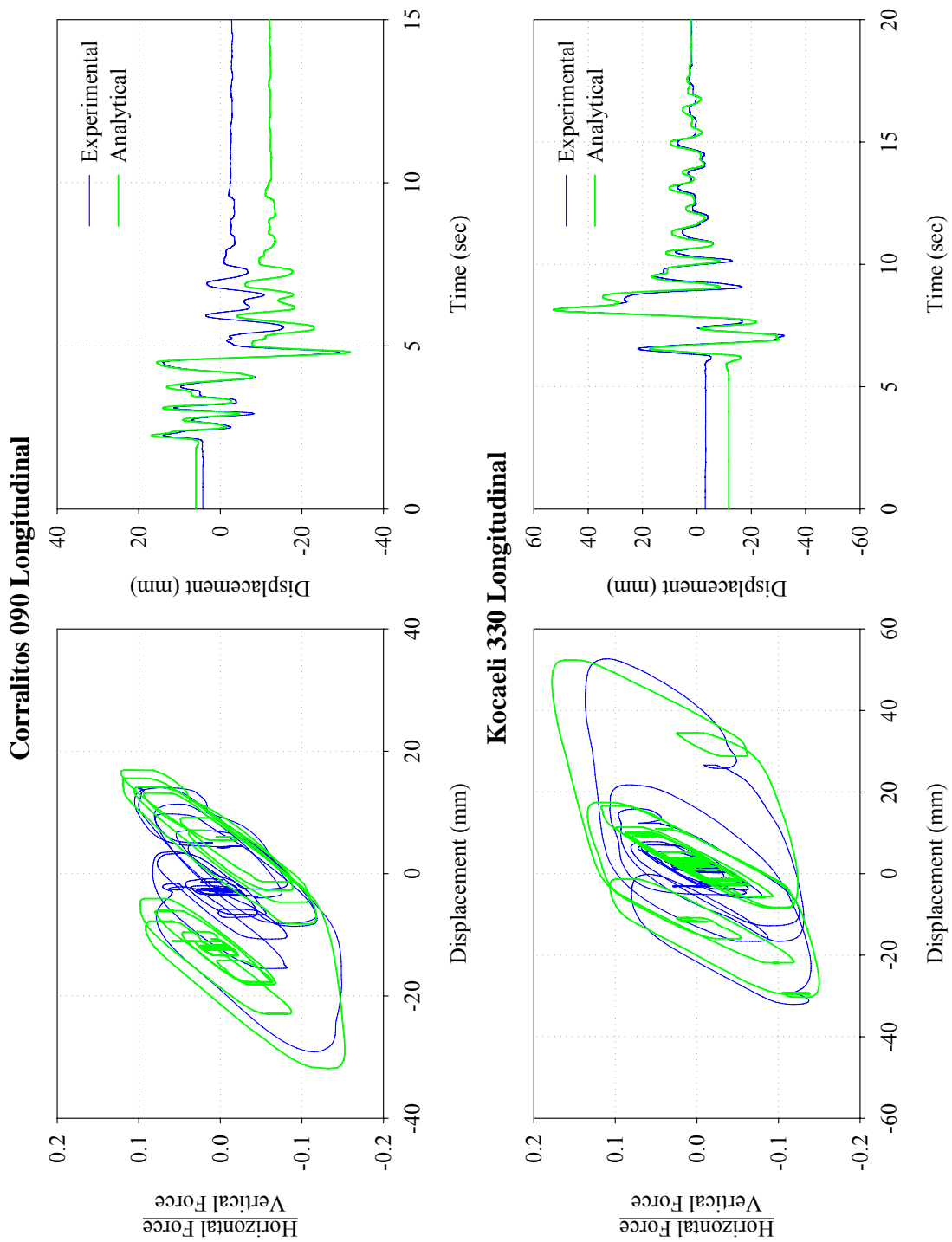
FIGURE B-39   Comparison of Experimental Results and Analytical Prediction of Response for Isolation System Triple 3 Subjected to the Corralitos 090 and Kocaeli 330 Ground Motions

244
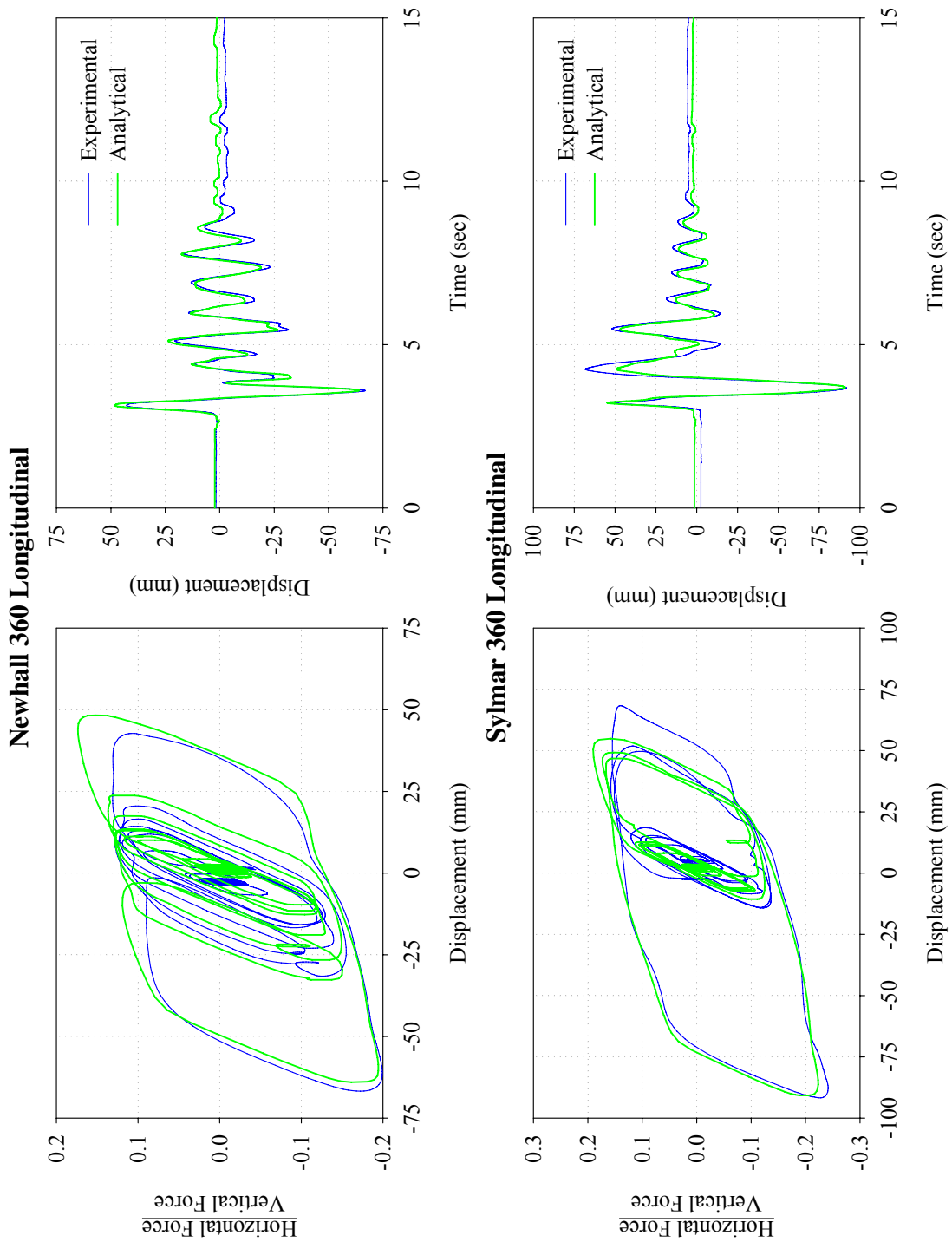
FIGURE B-40 Comparison of Experimental Results and Analytical Prediction of Response for Isolation System Triple 3 Subjected to the Newhall 360 and Sylmar 360 Ground Motions
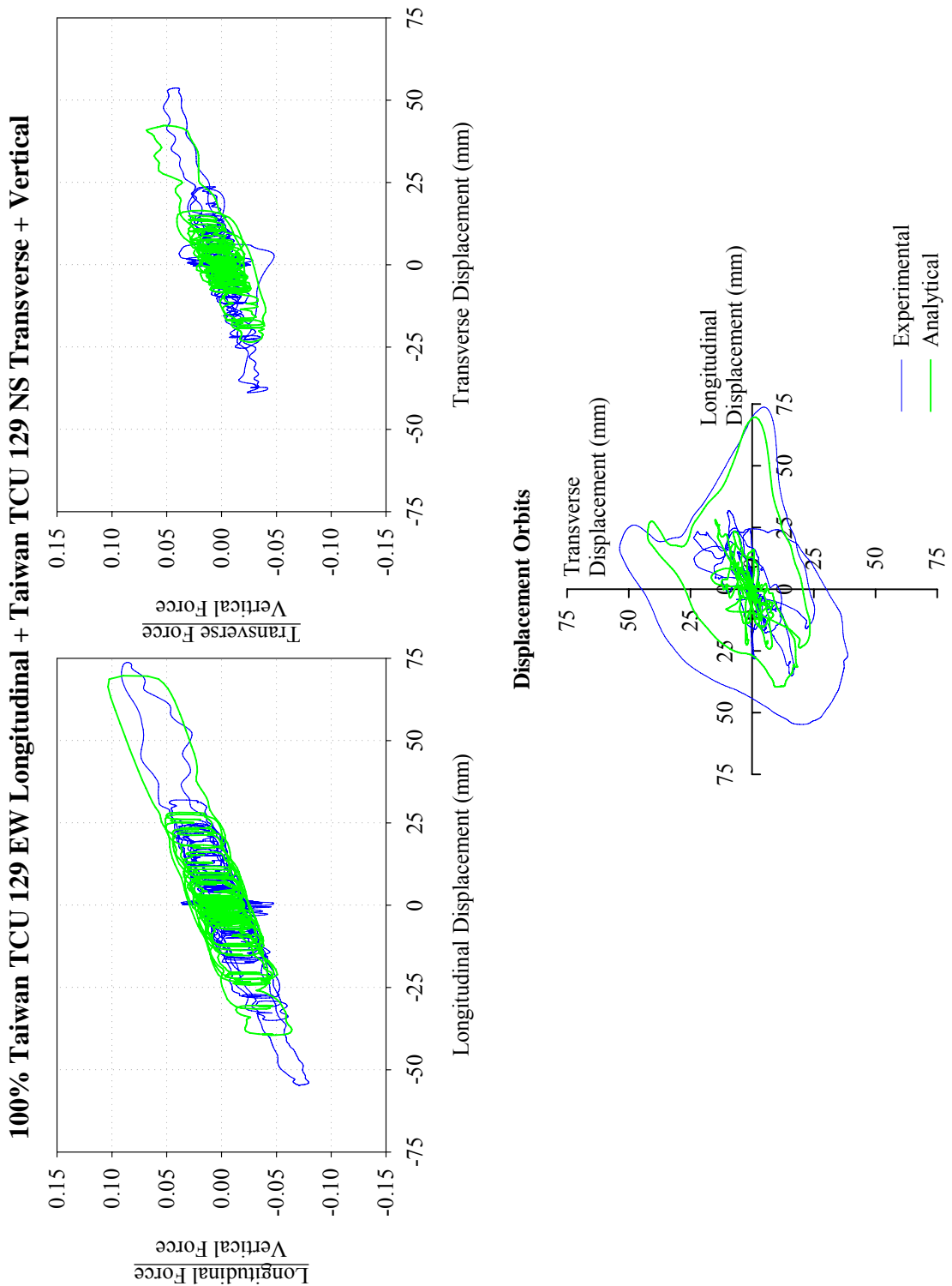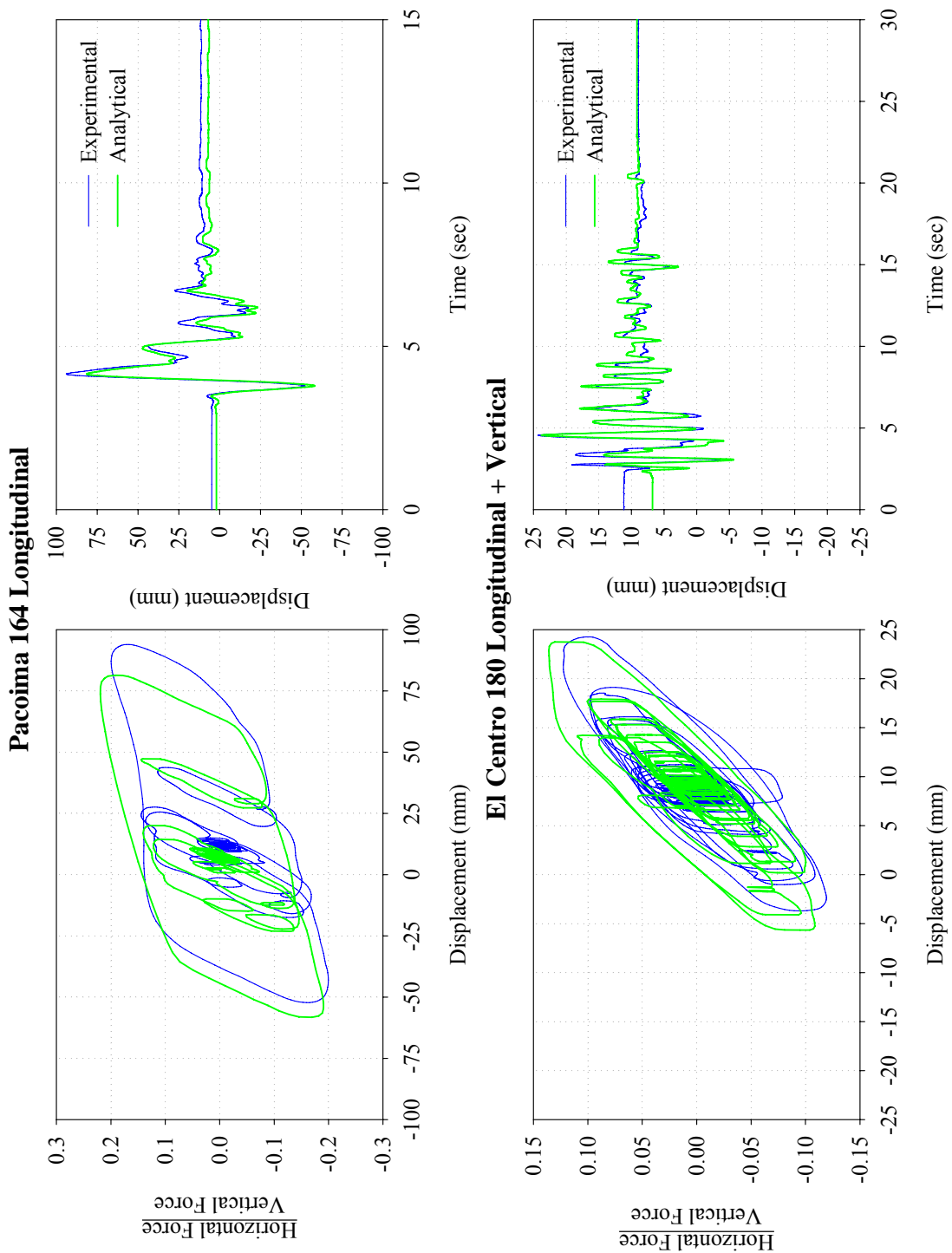
FIGURE B-41 Comparison of Experimental Results and Analytical Prediction of Response for Isolation System Triple 3 Subjected to the Pacoima 164 and El Centro 180 + Vertical Ground Motions
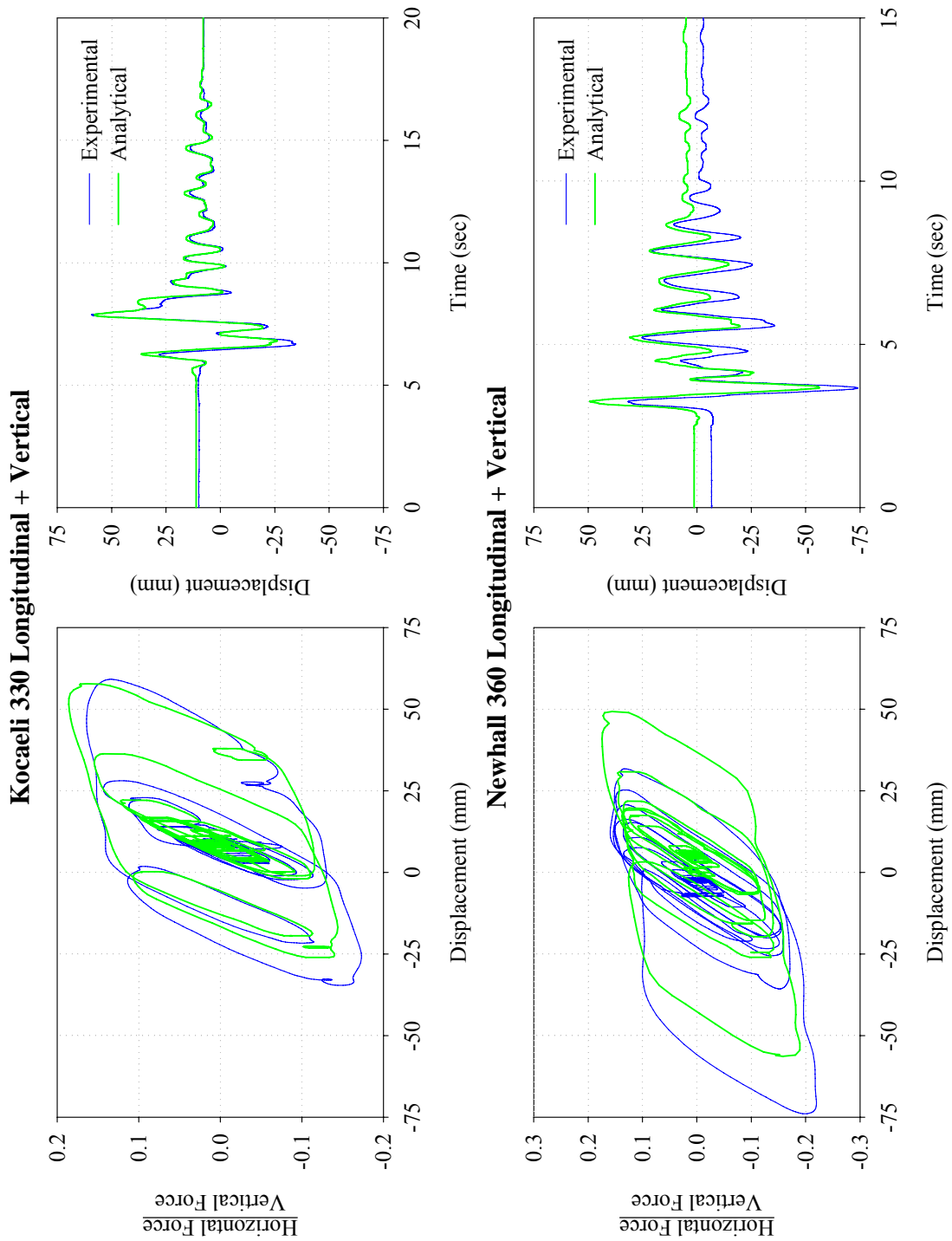
FIGURE B-42 Comparison of Experimental Results and Analytical Prediction of Response for Isolation System Triple 3 Subjected to the Kocaeli 330 + Vertical and Newhall 360 + Vertical Ground Motions
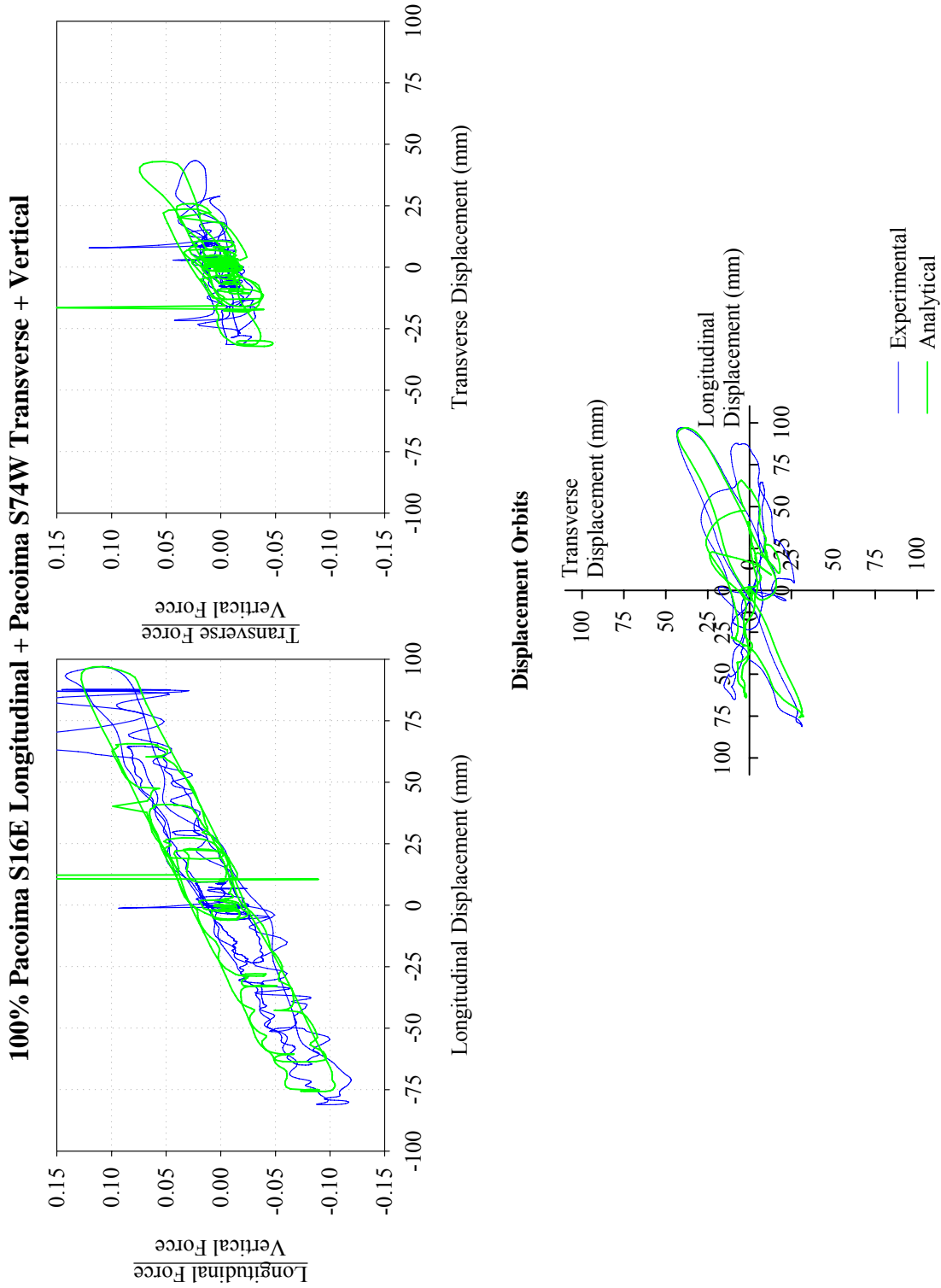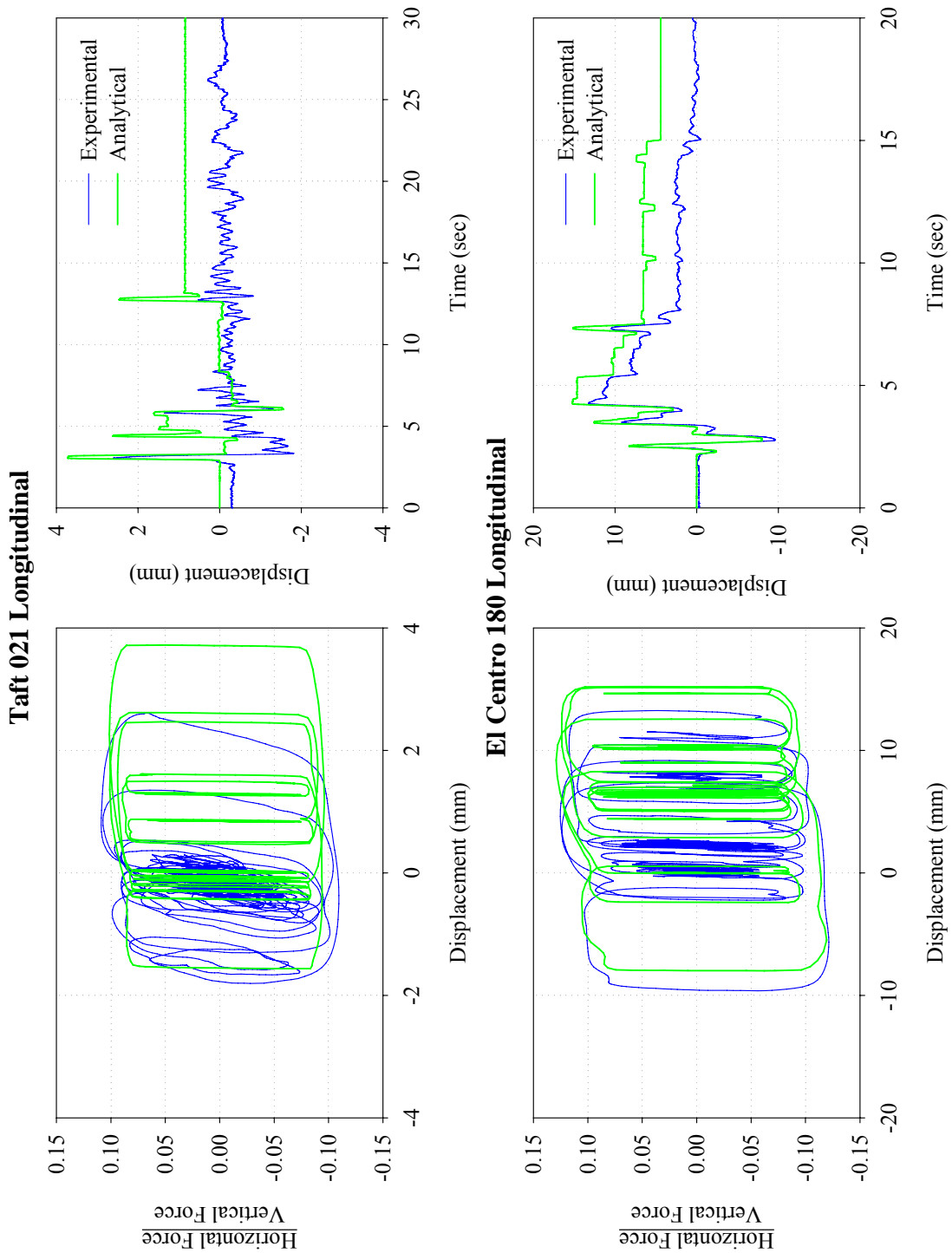
247
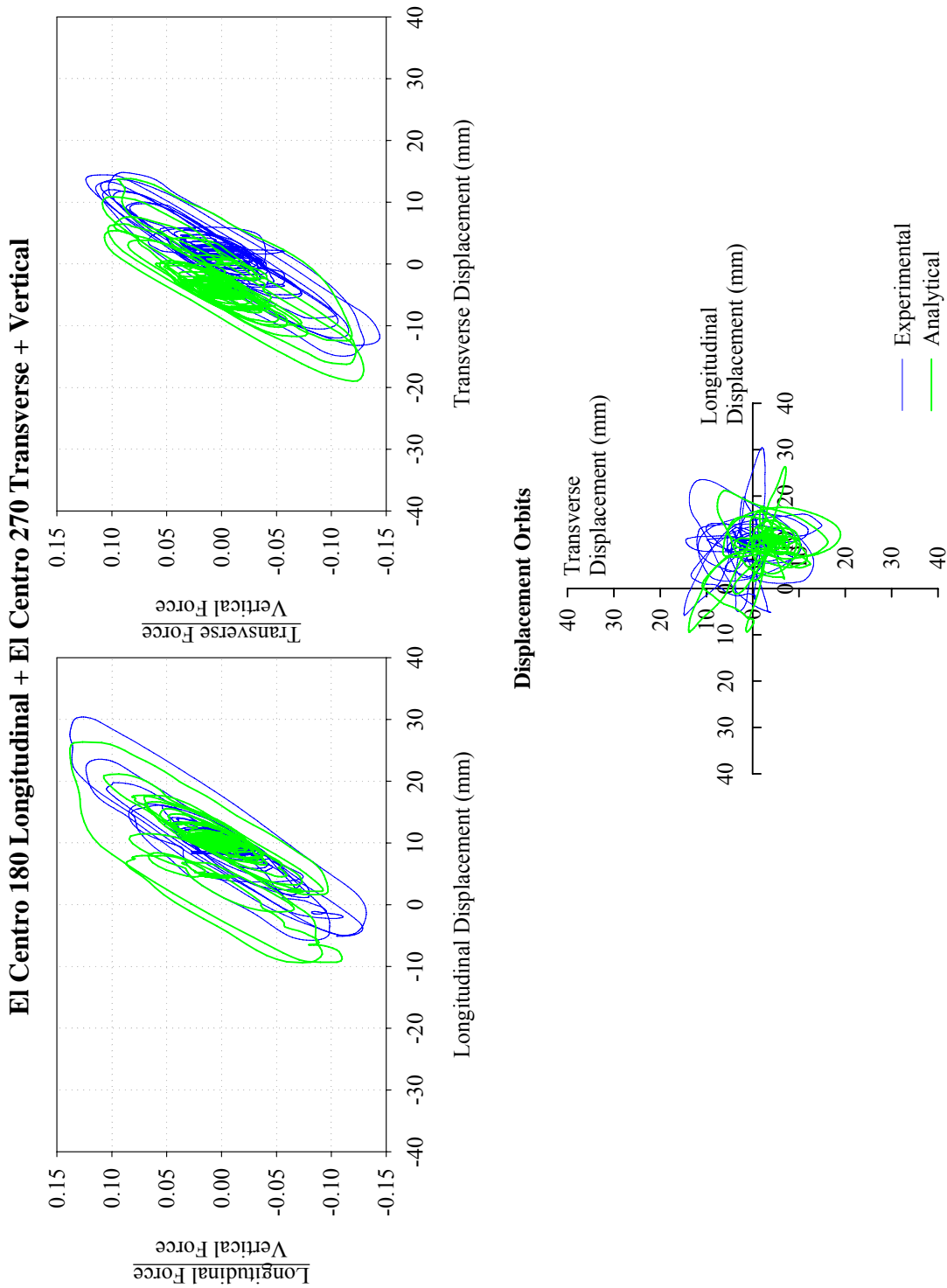
FIGURE B-43   Comparison of Experimental Results and Analytical Prediction of Response for Isolation System Triple 3 Subjected to Tridirectional El Centro Excitation
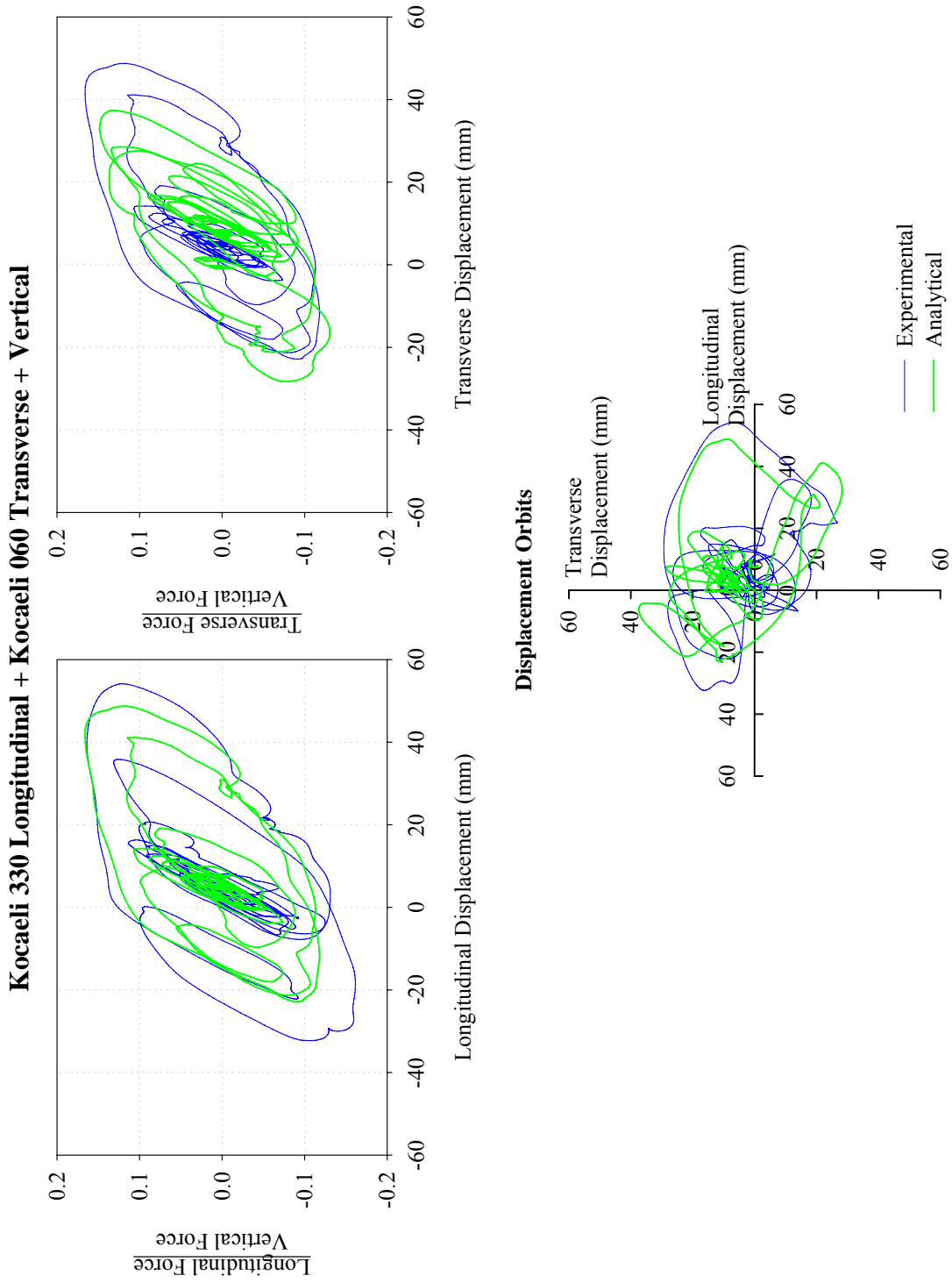
FIGURE B-44 Comparison of Experimental Results and Analytical Prediction of Response for Isolation System Triple 3 Subjected to Tridirectional Kocaeli Excitation
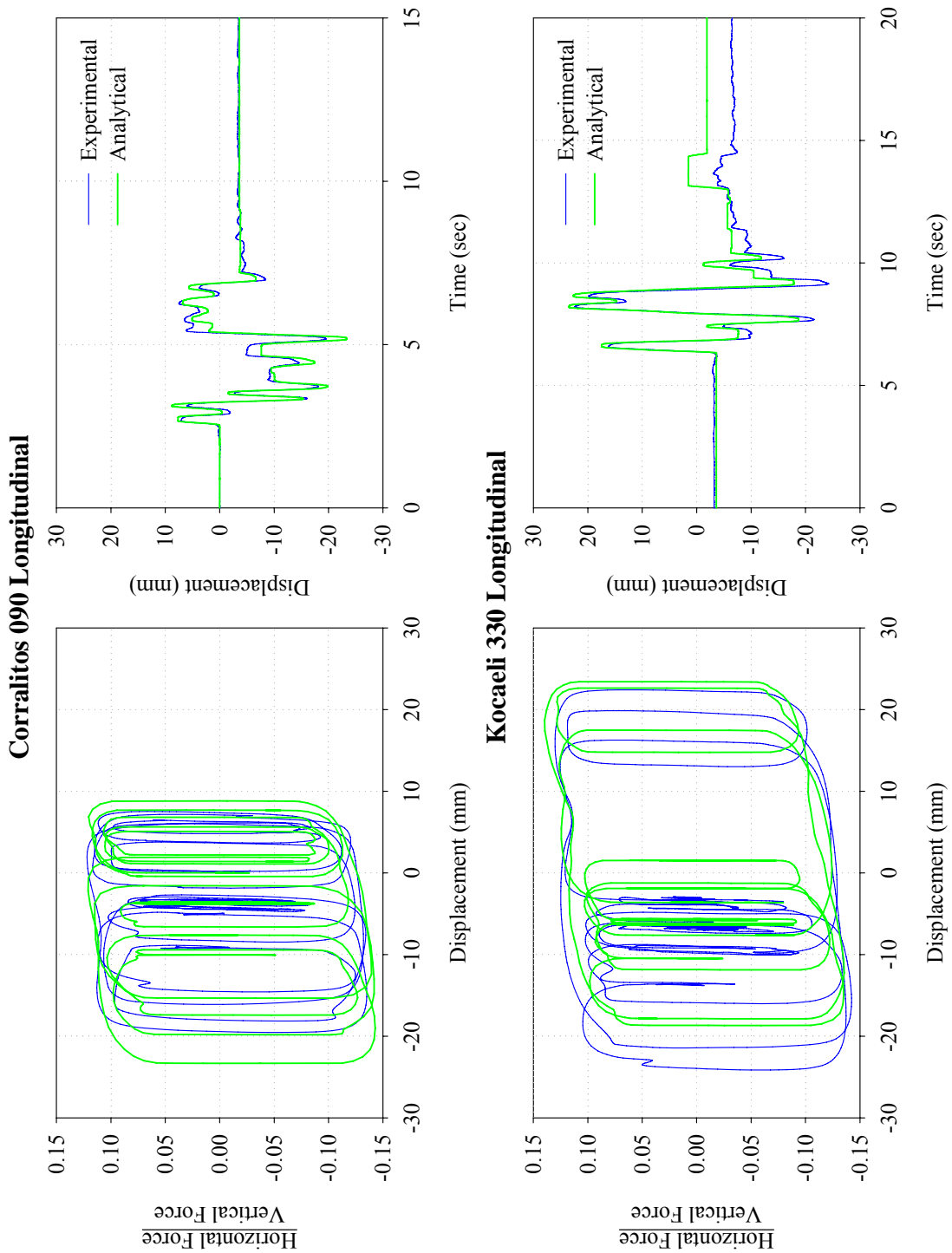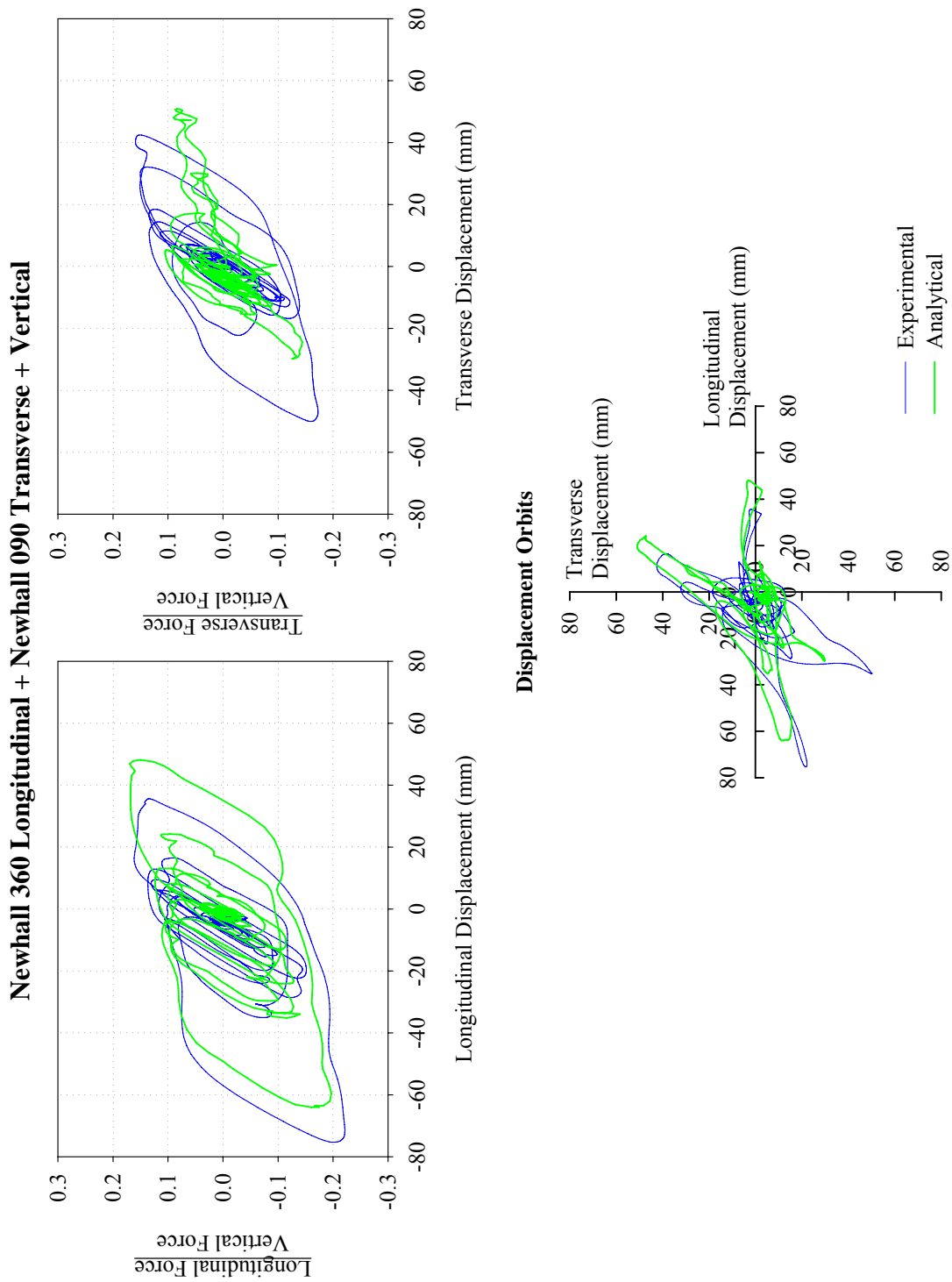
FIGURE B-45 Comparison of Experimental Results and Analytical Prediction of Response for Isolation System Triple 3 Subjected to Tridirectional Newhall Excitation
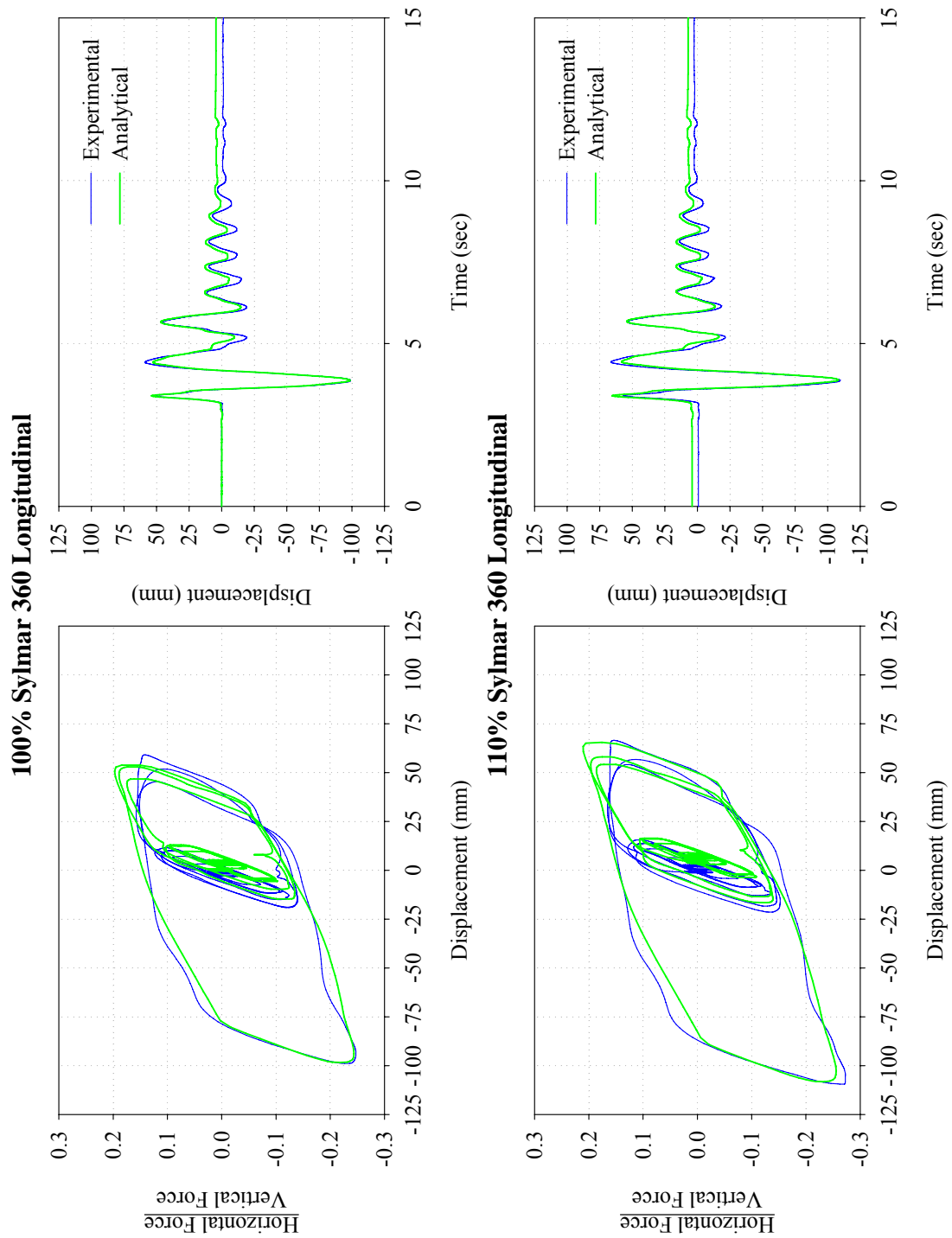
FIGURE B-46 Comparison of Experimental Results and Analytical Prediction of Response for Isolation System Triple 3 Subjected to Large Amplitude Sylmar 360 Excitation
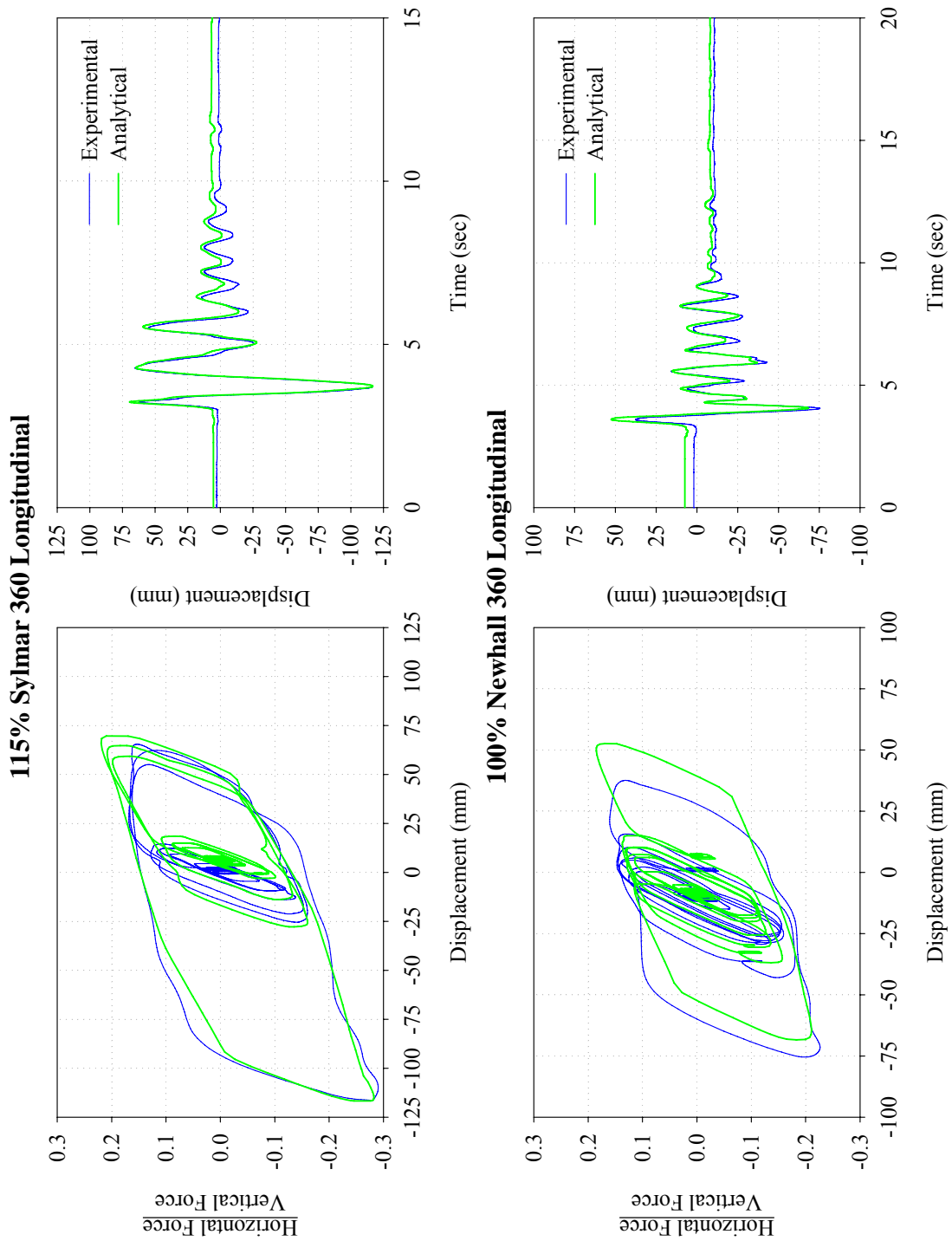
FIGURE B-47   Comparison of Experimental Results and Analytical Prediction of Response for Isolation System Triple 3 Subjected to Large Amplitude Sylmar 360 and Newhall 360 Excitation
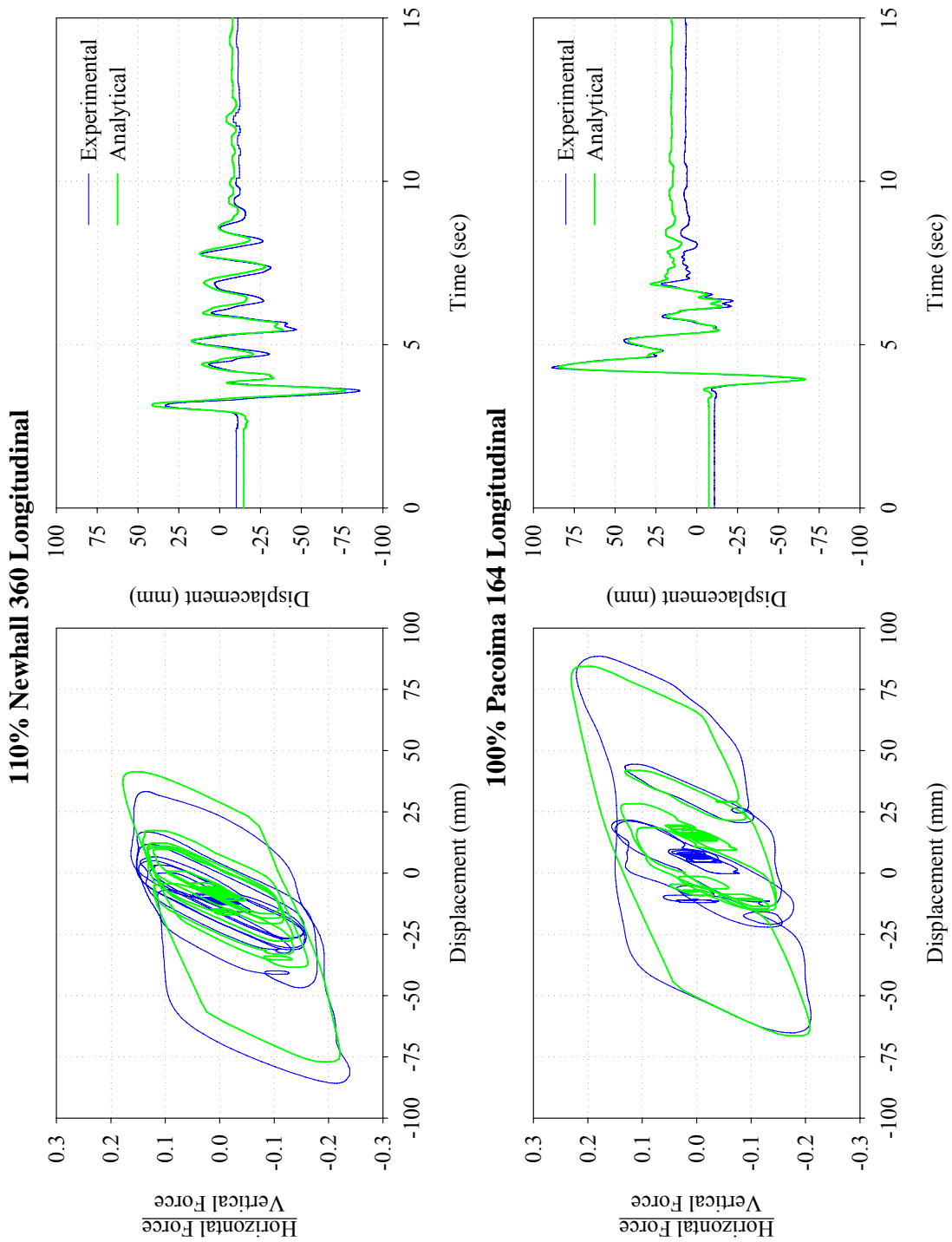
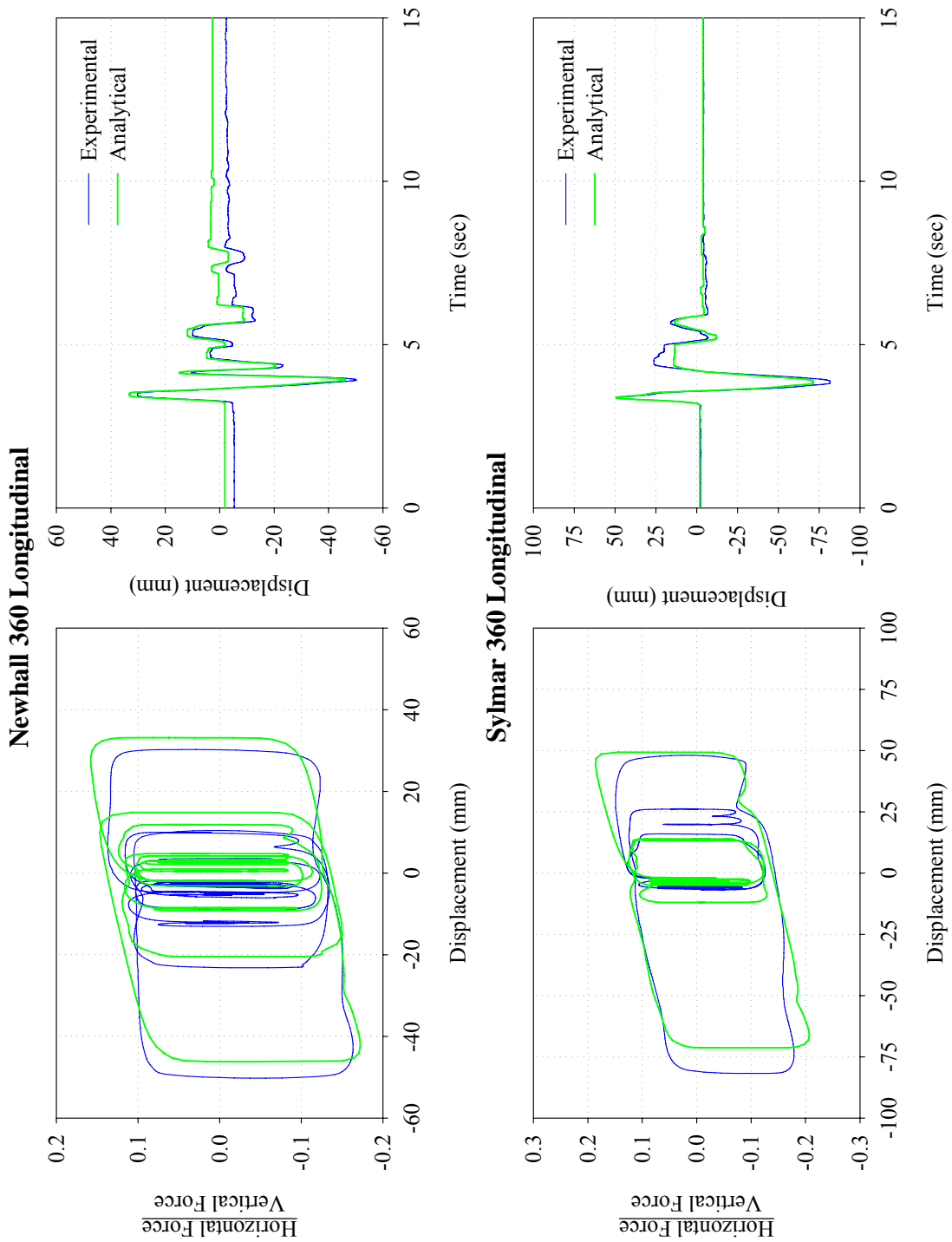**FIGURE B-48   Comparison of Experimental Results and Analytical Prediction of Response for Isolation System Triple 3 Subjected to Large Amplitude Newhall 360 and Pacoima 164 Excitation**
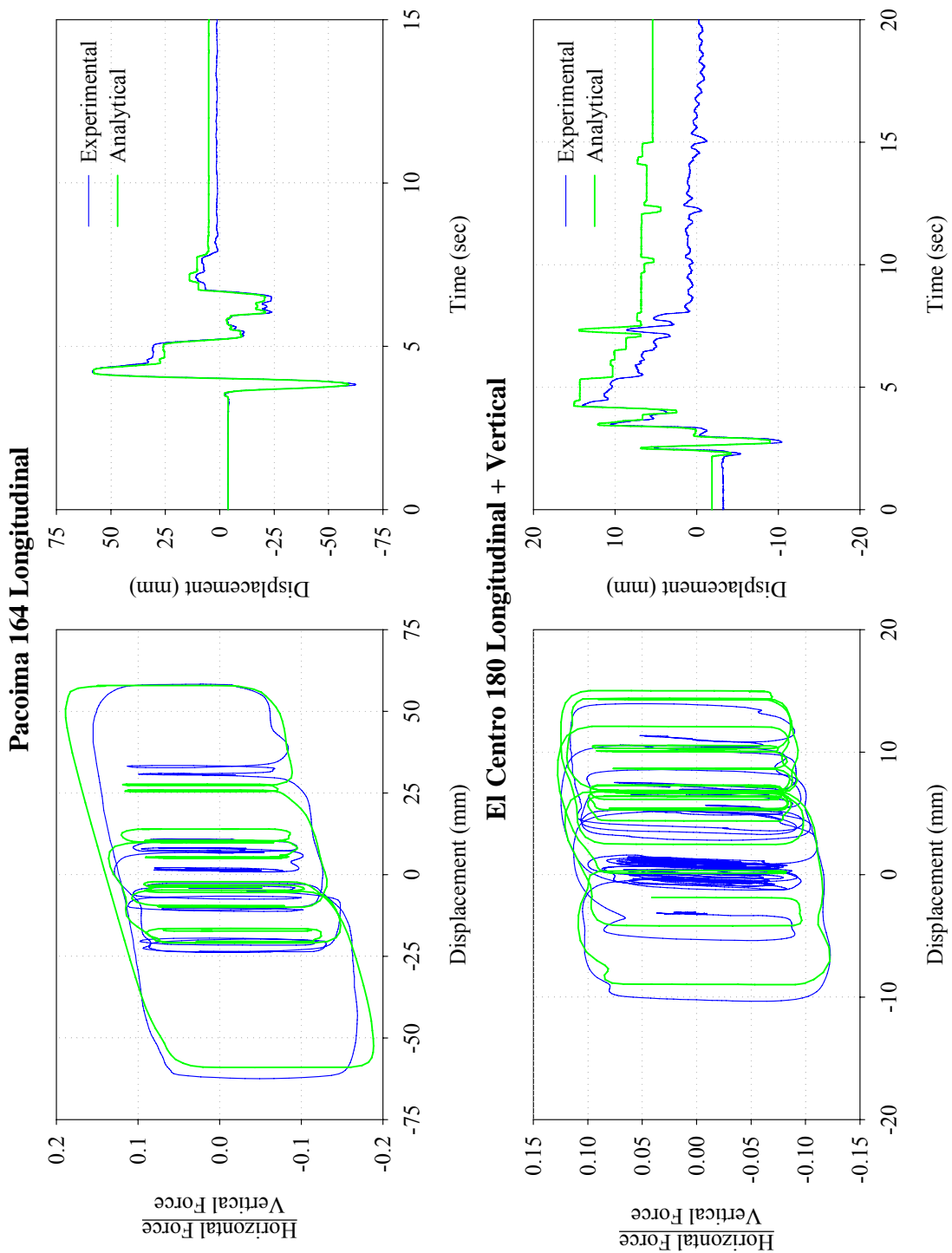
253

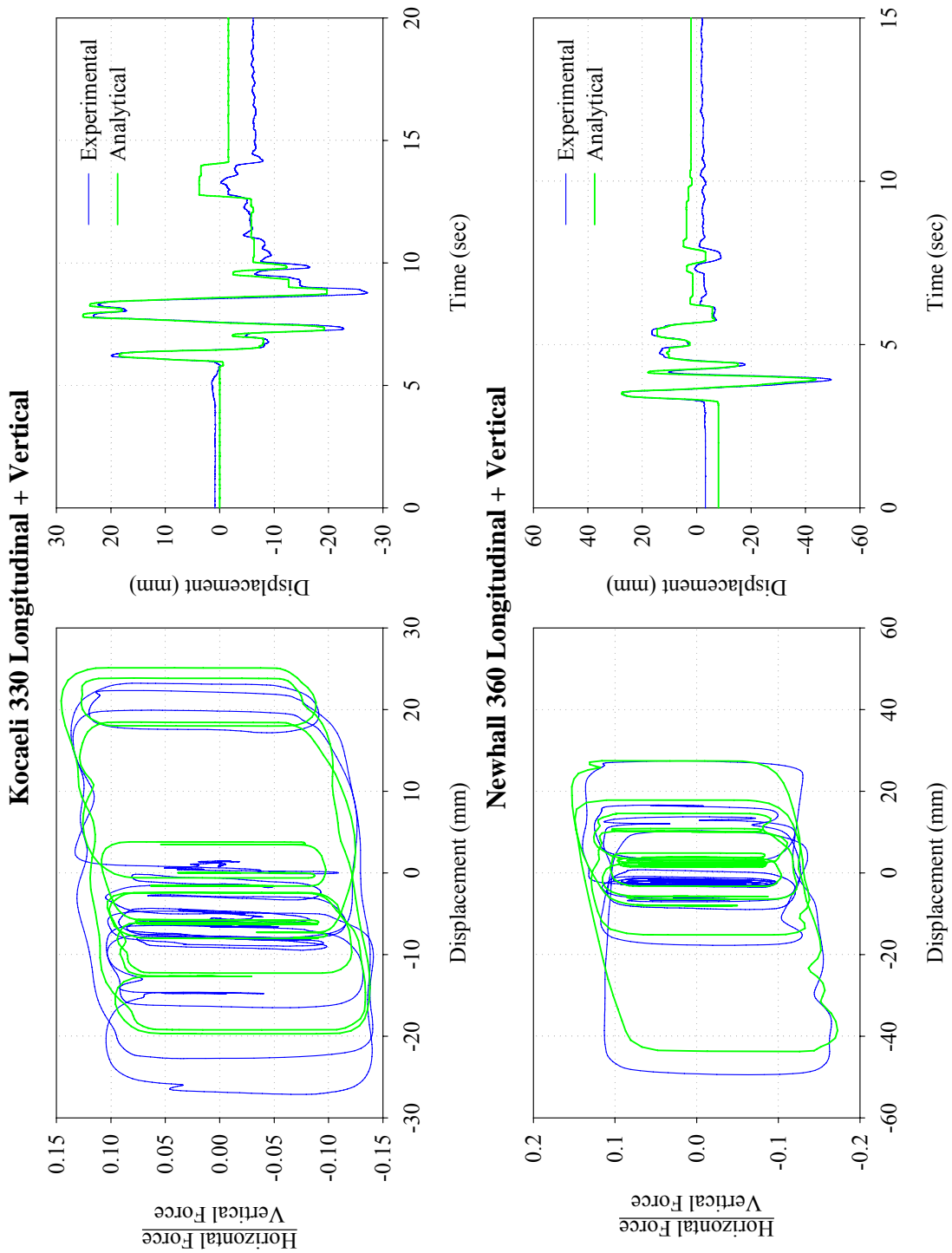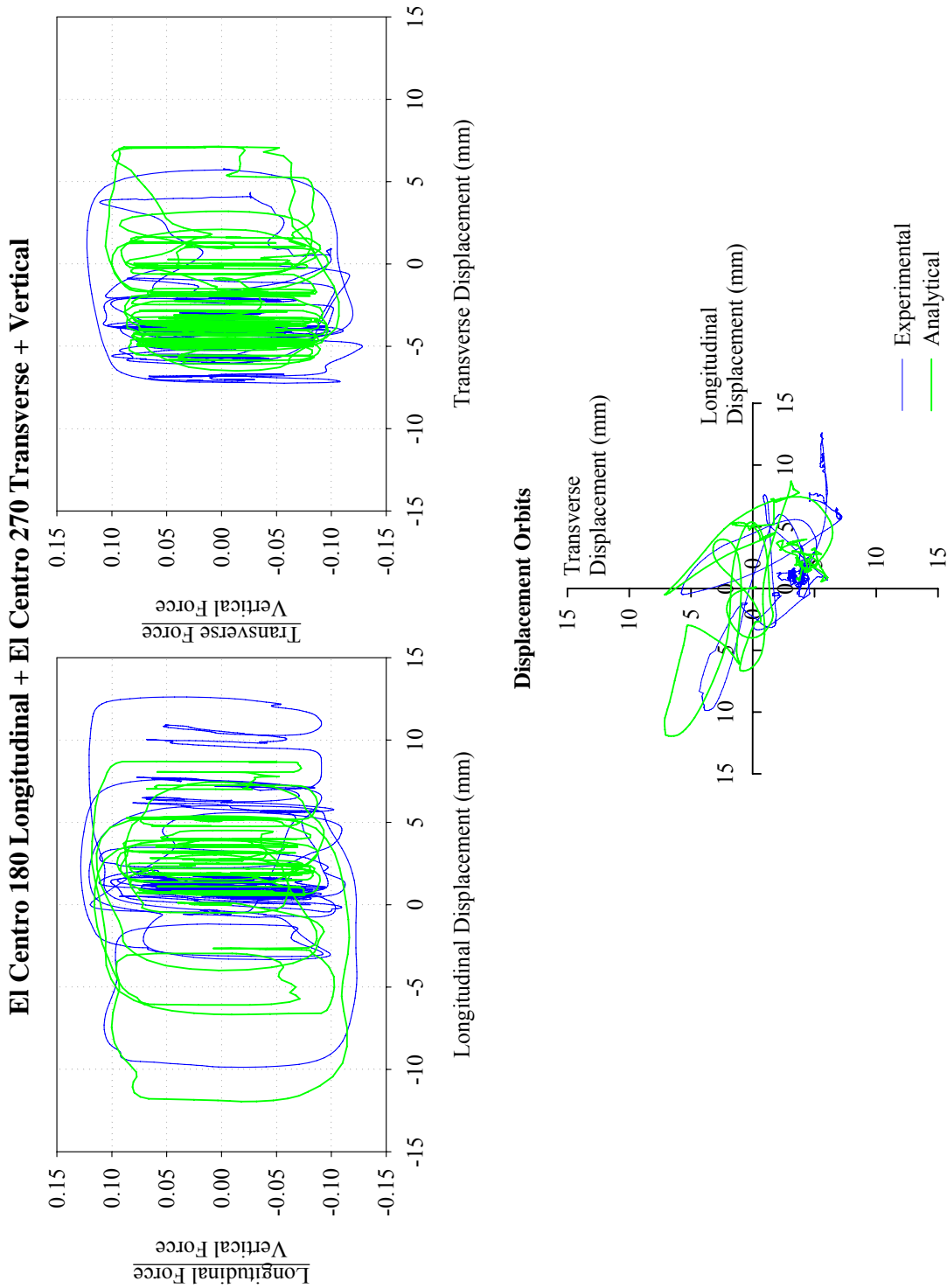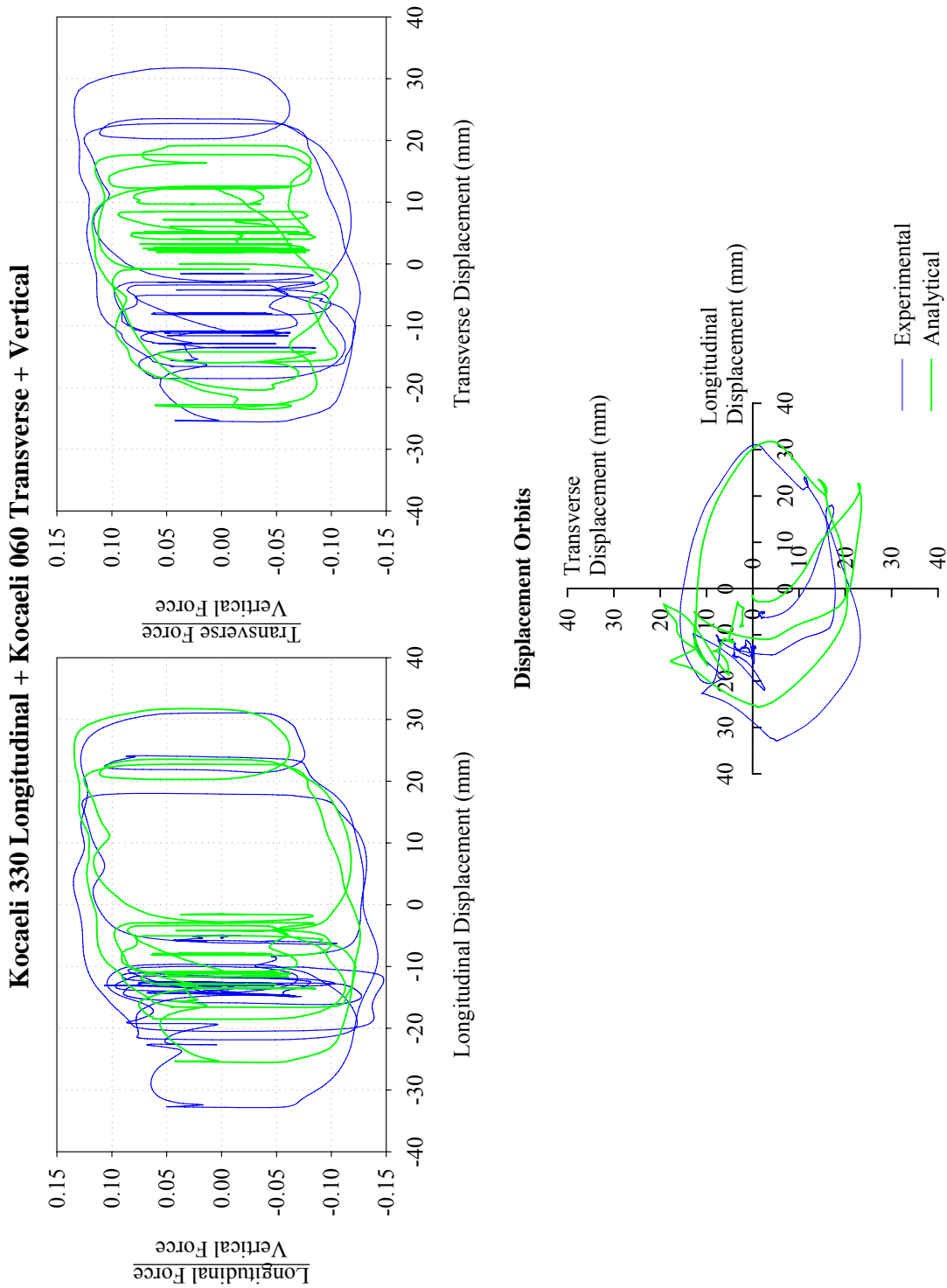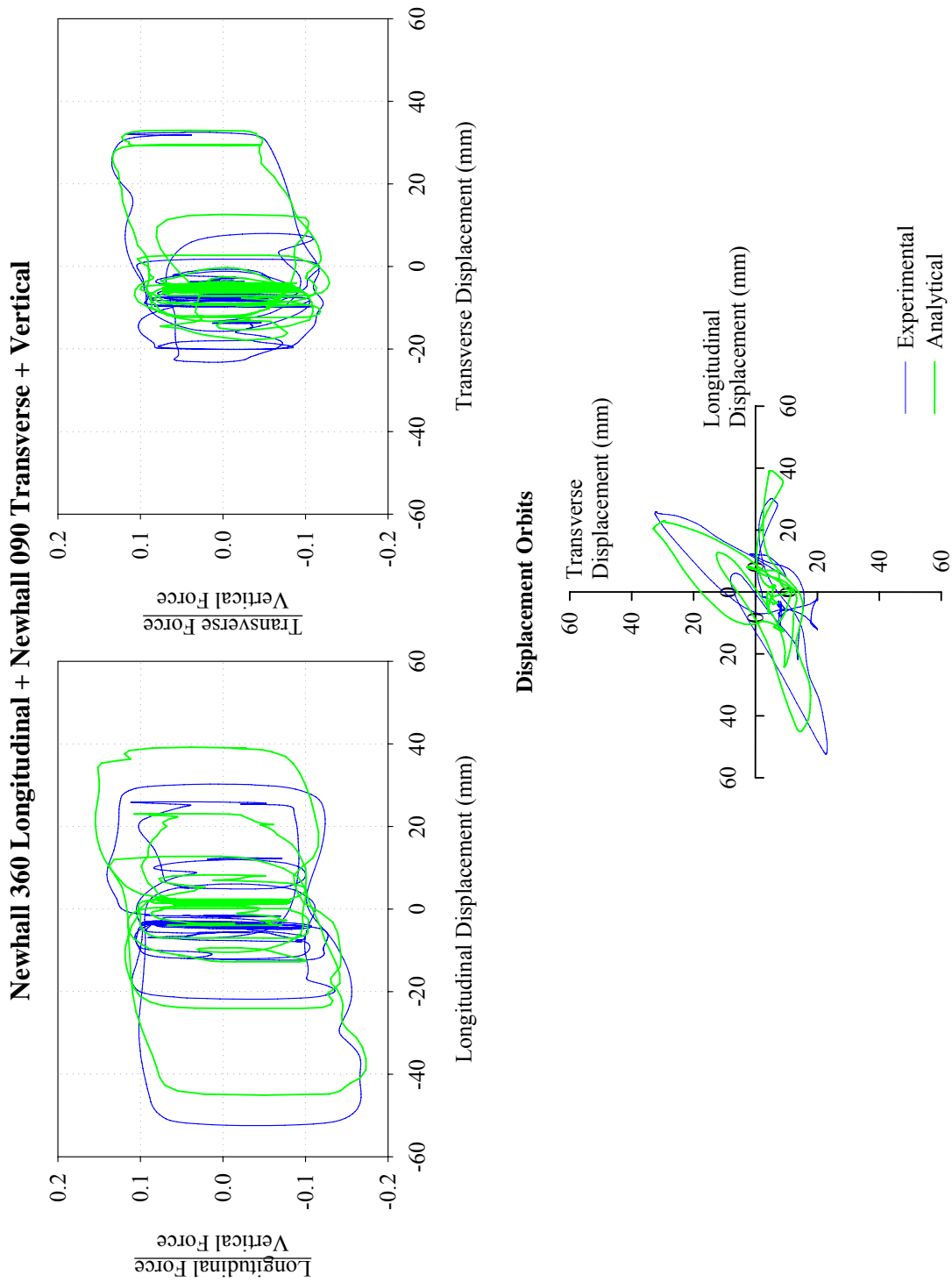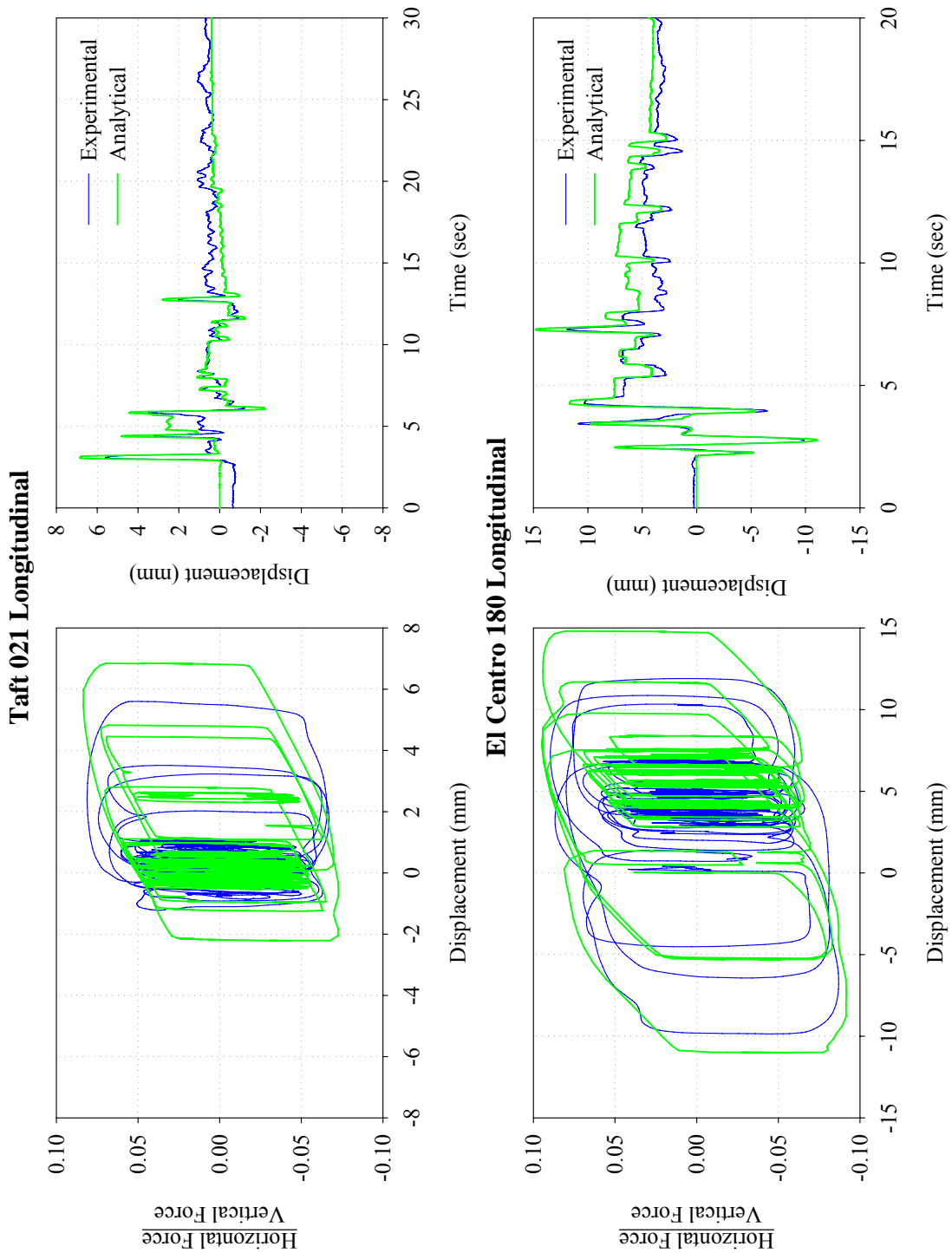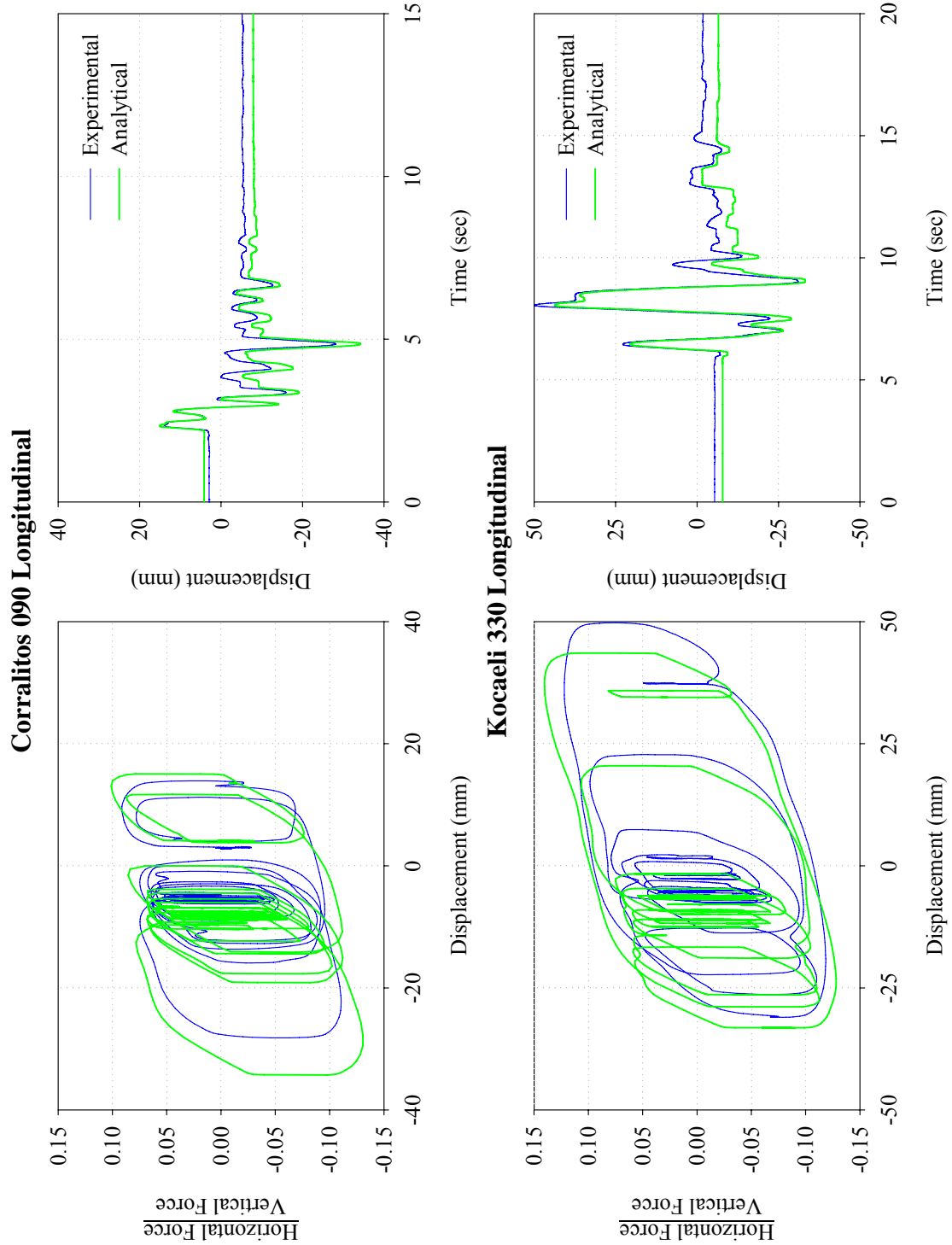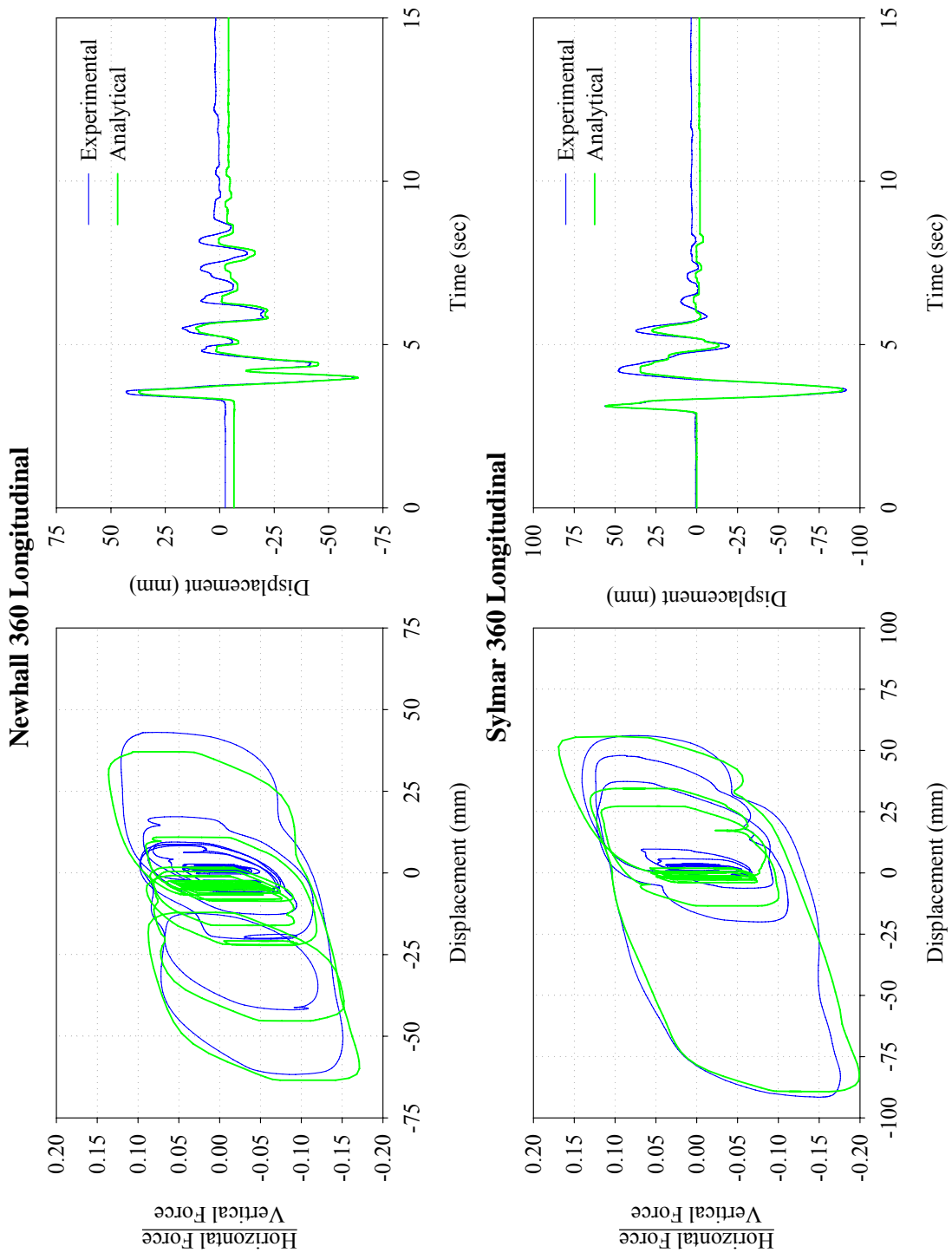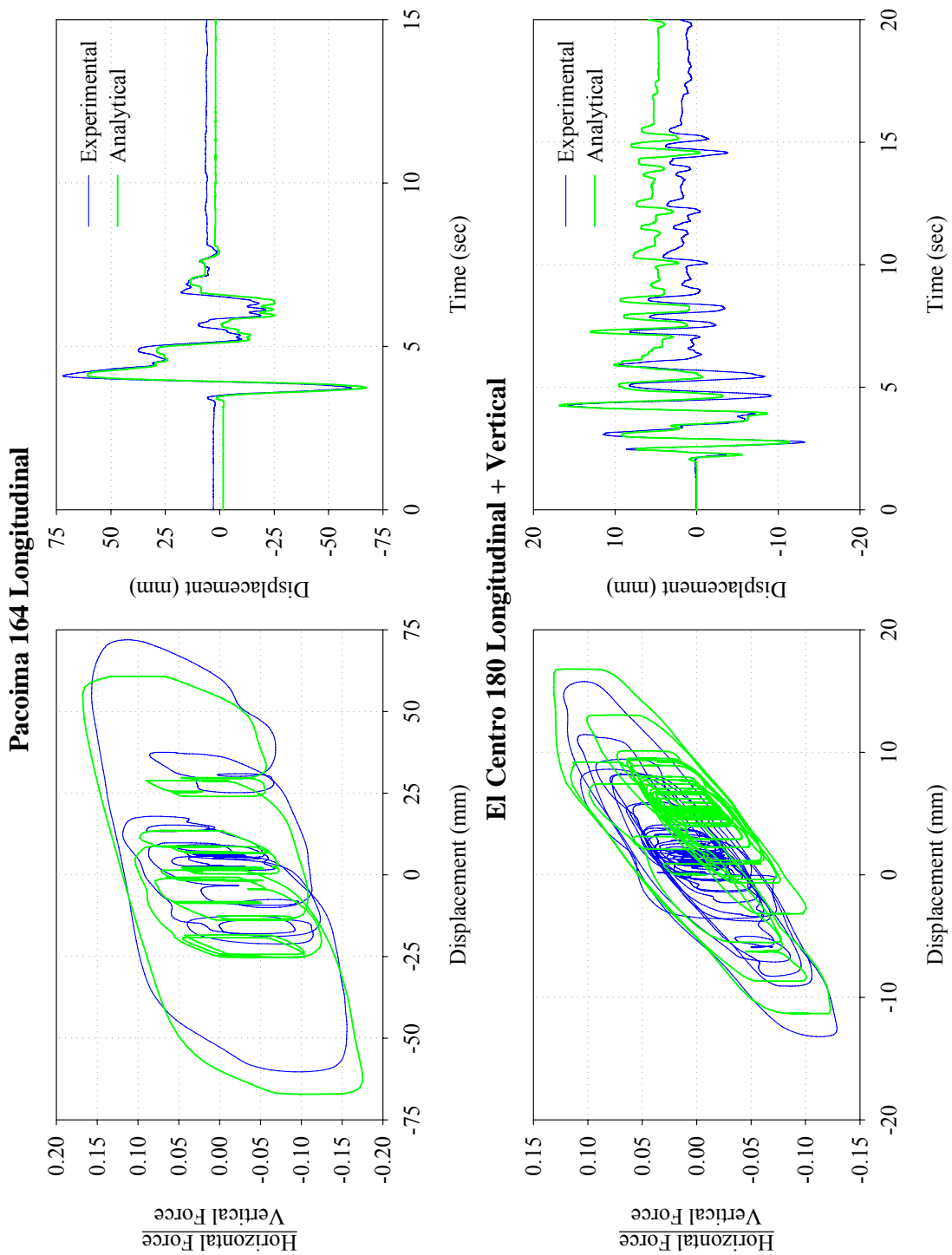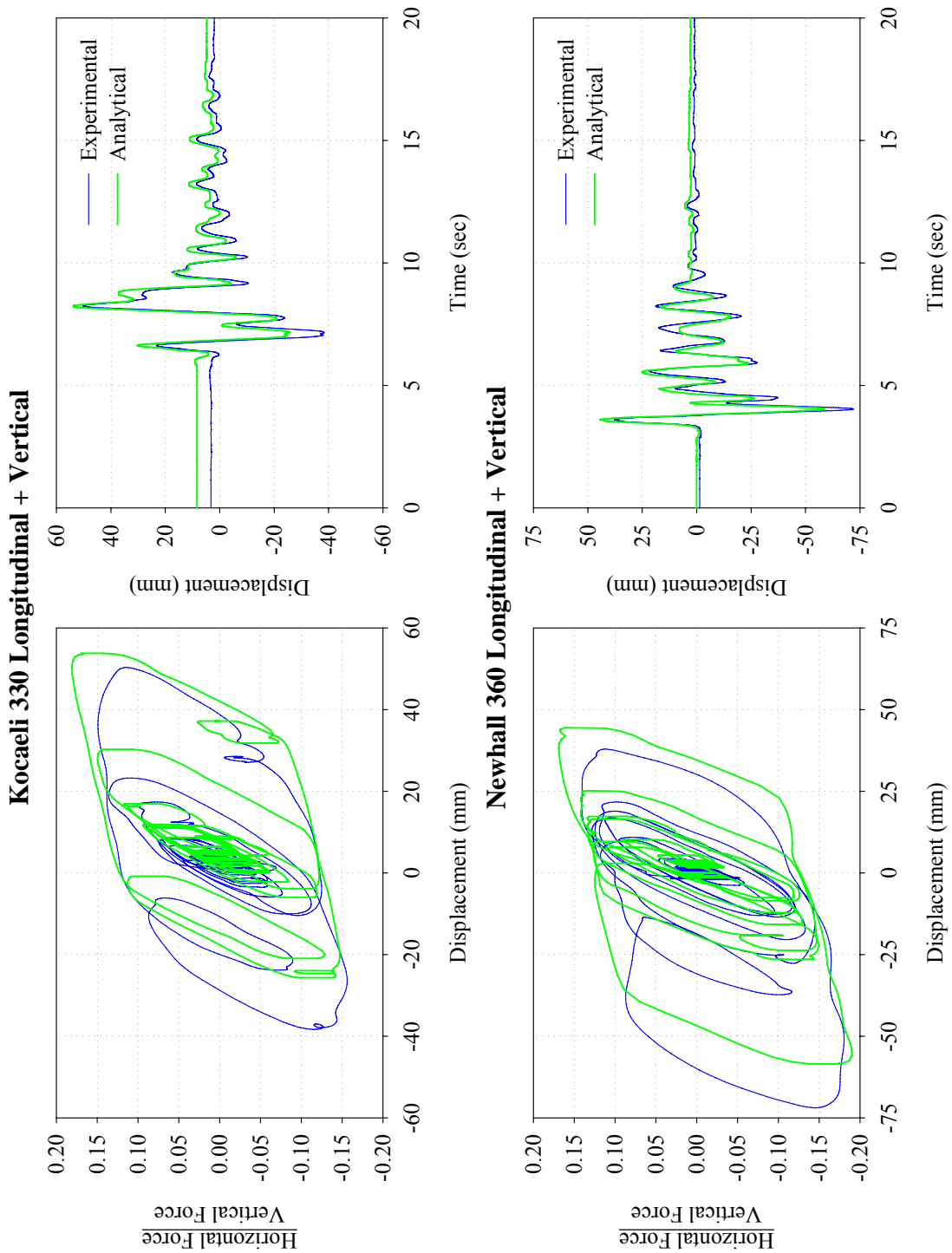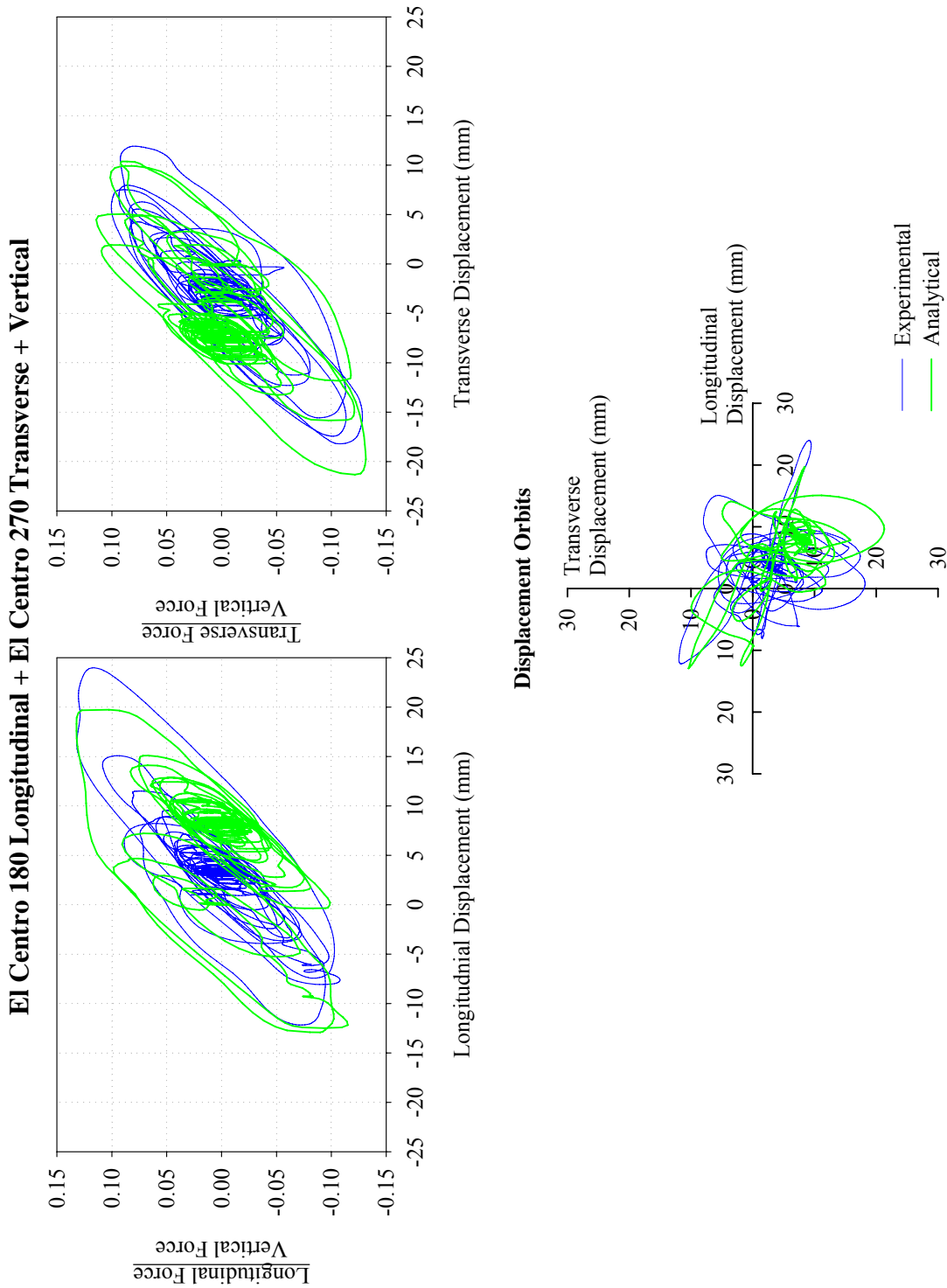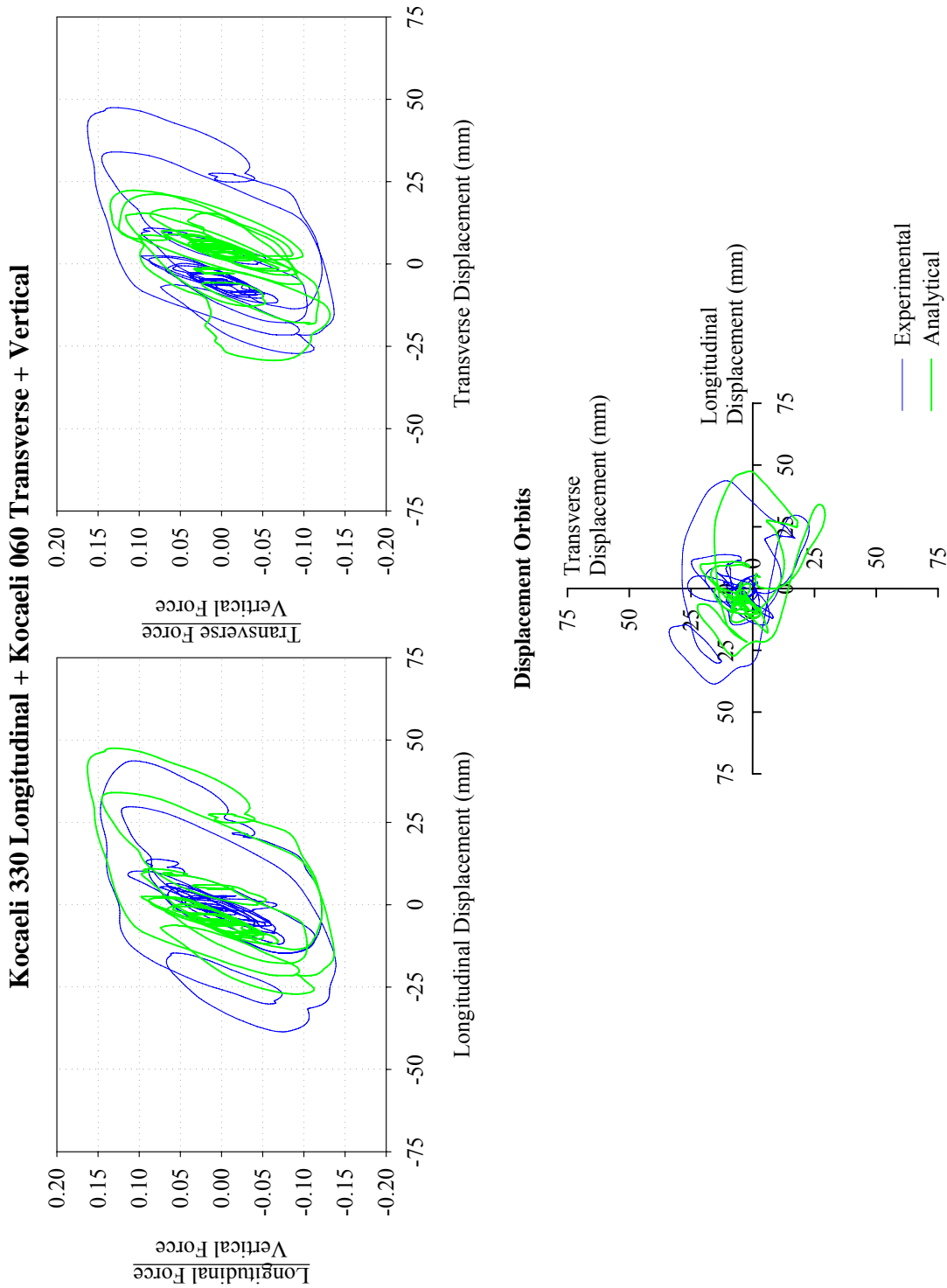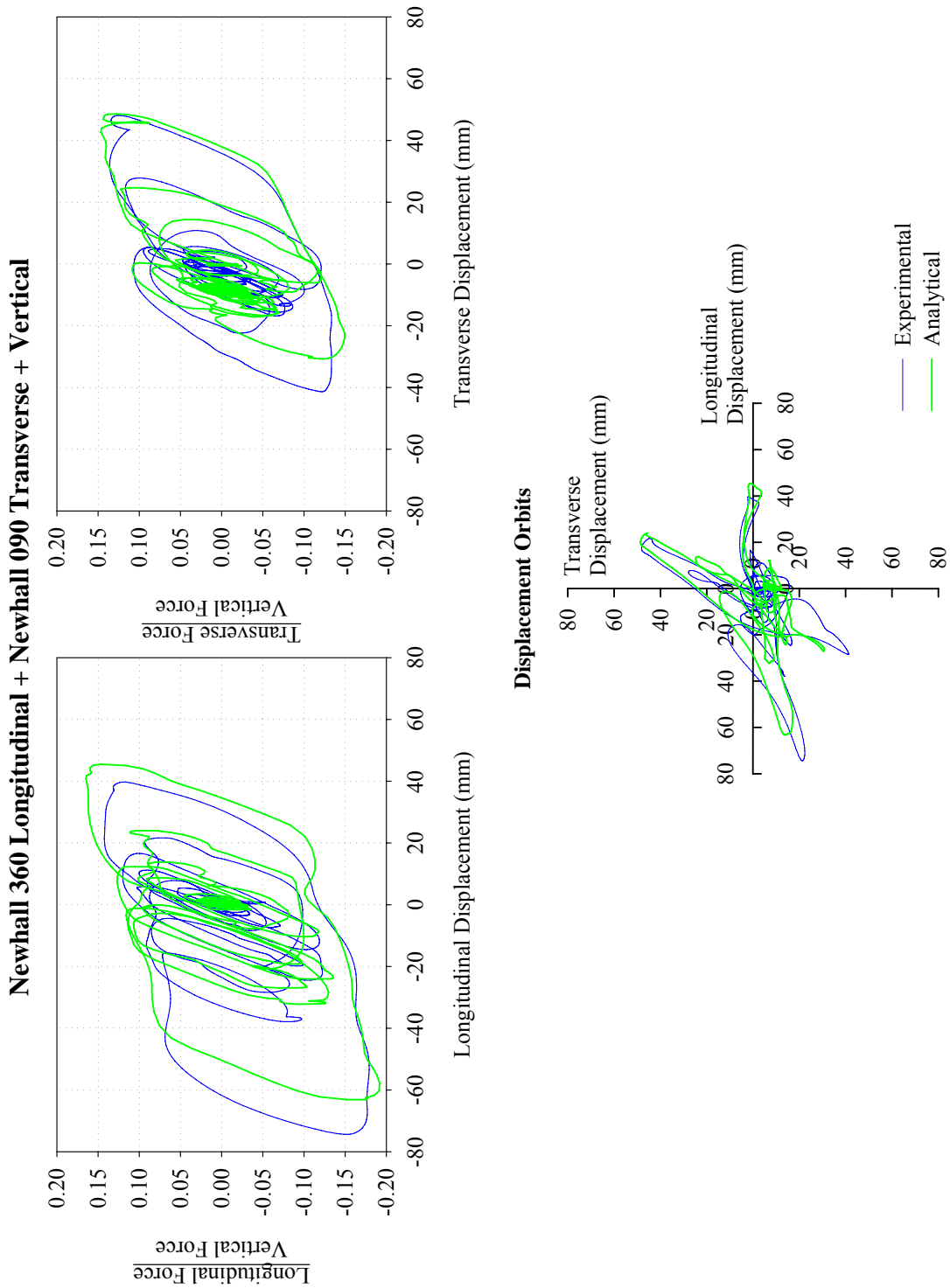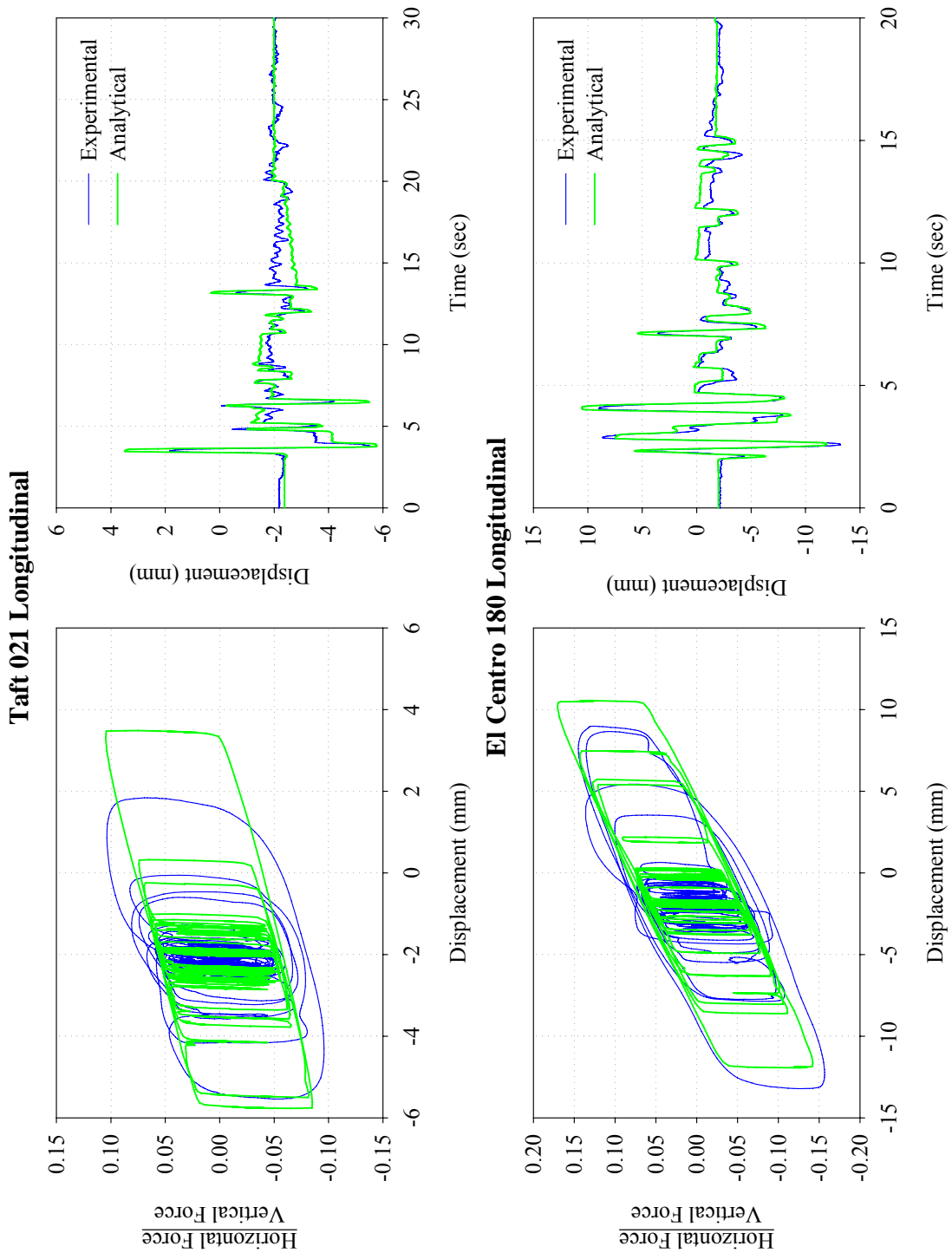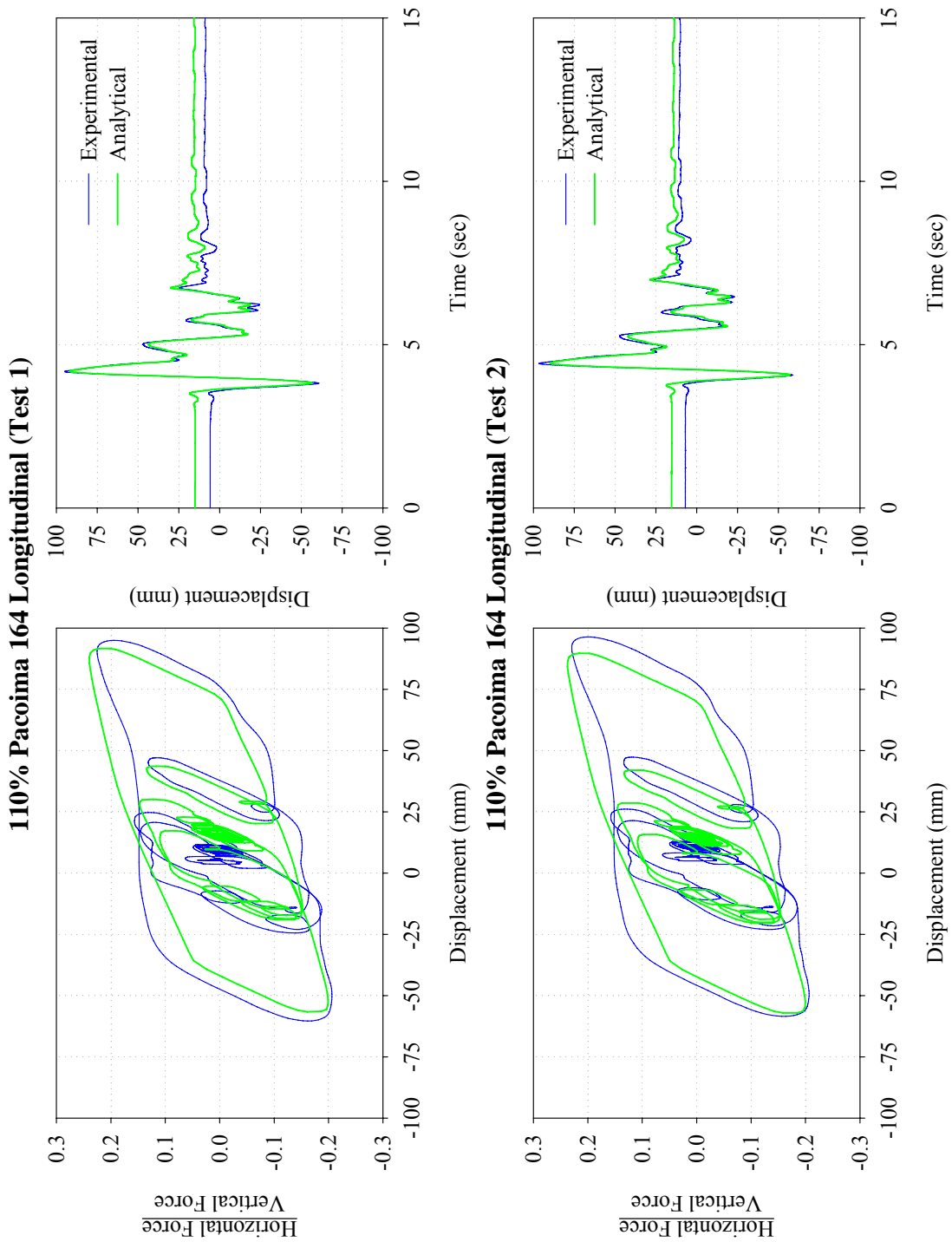**FIGURE B-49 Comparison of Experimental Results and Analytical Prediction of Response for Isolation System Triple 3 Subjected to Large Amplitude Pacoima 164 Excitation**

MCEER Technical Reports

MCEER publishes technical reports on a variety of subjects written by authors funded through MCEER. These reports are available from both MCEER Publications and the National Technical Information Service (NTIS). Requests for reports should be directed to MCEER Publications, MCEER, University at Buffalo, State University of New York, Red Jacket Quadrangle, Buffalo, New York 14261. Reports can also be requested through NTIS, 5285 Port Royal Road, Springfield, Virginia 22161. NTIS accession numbers are shown in parenthesis, if available.

NCEER-87-0001   "First-Year Program in Research, Education and Technology Transfer," 3/5/87, (PB88-134275, A04, MF-A01).

NCEER-87-0002   "Experimental Evaluation of Instantaneous Optimal Algorithms for Structural Control," by R.C. Lin, T.T. Soong and A.M. Reinhorn, 4/20/87, (PB88-134341, A04, MF-A01).

NCEER-87-0003   "Experimentation Using the Earthquake Simulation Facilities at University at Buffalo," by A.M. Reinhorn and R.L. Ketter, to be published.

NCEER-87-0004   "The System Characteristics and Performance of a Shaking Table," by J.S. Hwang, K.C. Chang and G.C. Lee, 6/1/87, (PB88-134259, A03, MF-A01). This report is available only through NTIS (see address given above).

NCEER-87-0005   "A Finite Element Formulation for Nonlinear Viscoplastic Material Using a Q Model," by O. Gyebi and G. Dasgupta, 11/2/87, (PB88-213764, A08, MF-A01).

NCEER-87-0006   "Symbolic Manipulation Program (SMP) - Algebraic Codes for Two and Three Dimensional Finite Element Formulations," by X. Lee and G. Dasgupta, 11/9/87, (PB88-218522, A05, MF-A01).

NCEER-87-0007   "Instantaneous Optimal Control Laws for Tall Buildings Under Seismic Excitations," by J.N. Yang, A. Akbarpour and P. Ghaemmaghami, 6/10/87, (PB88-134333, A06, MF-A01). This report is only available through NTIS (see address given above).

NCEER-87-0008   "IDARC: Inelastic Damage Analysis of Reinforced Concrete Frame - Shear-Wall Structures," by Y.J. Park, A.M. Reinhorn and S.K. Kunnath, 7/20/87, (PB88-134325, A09, MF-A01). This report is only available through NTIS (see address given above).

NCEER-87-0009   "Liquefaction Potential for New York State: A Preliminary Report on Sites in Manhattan and Buffalo," by M. Budhu, V. Vijayakumar, R.F. Giese and L. Baumgras, 8/31/87, (PB88-163704, A03, MF-A01). This report is available only through NTIS (see address given above).

NCEER-87-0010   "Vertical and Torsional Vibration of Foundations in Inhomogeneous Media," by A.S. Veletsos and K.W. Dotson, 6/1/87, (PB88-134291, A03, MF-A01). This report is only available through NTIS (see address given above).

NCEER-87-0011   "Seismic Probabilistic Risk Assessment and Seismic Margins Studies for Nuclear Power Plants," by Howard H.M. Hwang, 6/15/87, (PB88-134267, A03, MF-A01). This report is only available through NTIS (see address given above).

NCEER-87-0012   "Parametric Studies of Frequency Response of Secondary Systems Under Ground-Acceleration Excitations," by Y. Yong and Y.K. Lin, 6/10/87, (PB88-134309, A03, MF-A01). This report is only available through NTIS (see address given above).

NCEER-87-0013   "Frequency Response of Secondary Systems Under Seismic Excitation," by J.A. HoLung, J. Cai and Y.K. Lin, 7/31/87, (PB88-134317, A05, MF-A01). This report is only available through NTIS (see address given above).

NCEER-87-0014   "Modelling Earthquake Ground Motions in Seismically Active Regions Using Parametric Time Series Methods," by G.W. Ellis and A.S. Cakmak, 8/25/87, (PB88-134283, A08, MF-A01). This report is only available through NTIS (see address given above).

NCEER-87-0015   "Detection and Assessment of Seismic Structural Damage," by E. DiPasquale and A.S. Cakmak, 8/25/87, (PB88-163712, A05, MF-A01). This report is only available through NTIS (see address given above).

NCEER-87-0016   "Pipeline Experiment at Parkfield, California," by J. Isenberg and E. Richardson, 9/15/87, (PB88-163720, A03, MF-A01). This report is available only through NTIS (see address given above).

NCEER-87-0017   "Digital Simulation of Seismic Ground Motion," by M. Shinozuka, G. Deodatis and T. Harada, 8/31/87, (PB88-155197, A04, MF-A01). This report is available only through NTIS (see address given above).

NCEER-87-0018   "Practical Considerations for Structural Control: System Uncertainty, System Time Delay and Truncation of Small Control Forces," J.N. Yang and A. Akbarpour, 8/10/87, (PB88-163738, A08, MF-A01). This report is only available through NTIS (see address given above).

NCEER-87-0019   "Modal Analysis of Nonclassically Damped Structural Systems Using Canonical Transformation," by J.N. Yang, S. Sarkani and F.X. Long, 9/27/87, (PB88-187851, A04, MF-A01).

NCEER-87-0020   "A Nonstationary Solution in Random Vibration Theory," by J.R. Red-Horse and P.D. Spanos, 11/3/87, (PB88-163746, A03, MF-A01).

NCEER-87-0021   "Horizontal Impedances for Radially Inhomogeneous Viscoelastic Soil Layers," by A.S. Veletsos and K.W. Dotson, 10/15/87, (PB88-150859, A04, MF-A01).

NCEER-87-0022   "Seismic Damage Assessment of Reinforced Concrete Members," by Y.S. Chung, C. Meyer and M. Shinozuka, 10/9/87, (PB88-150867, A05, MF-A01). This report is available only through NTIS (see address given above).

NCEER-87-0023   "Active Structural Control in Civil Engineering," by T.T. Soong, 11/11/87, (PB88-187778, A03, MF-A01).

NCEER-87-0024   "Vertical and Torsional Impedances for Radially Inhomogeneous Viscoelastic Soil Layers," by K.W. Dotson and A.S. Veletsos, 12/87, (PB88-187786, A03, MF-A01).

NCEER-87-0025   "Proceedings from the Symposium on Seismic Hazards, Ground Motions, Soil-Liquefaction and Engineering Practice in Eastern North America," October 20-22, 1987, edited by K.H. Jacob, 12/87, (PB88-188115, A23, MF-A01). This report is available only through NTIS (see address given above).

NCEER-87-0026   "Report on the Whittier-Narrows, California, Earthquake of October 1, 1987," by J. Pantelic and A. Reinhorn, 11/87, (PB88-187752, A03, MF-A01). This report is available only through NTIS (see address given above).

NCEER-87-0027   "Design of a Modular Program for Transient Nonlinear Analysis of Large 3-D Building Structures," by S. Srivastav and J.F. Abel, 12/30/87, (PB88-187950, A05, MF-A01). This report is only available through NTIS (see address given above).

NCEER-87-0028   "Second-Year Program in Research, Education and Technology Transfer," 3/8/88, (PB88-219480, A04, MF-A01).

NCEER-88-0001   "Workshop on Seismic Computer Analysis and Design of Buildings With Interactive Graphics," by W. McGuire, J.F. Abel and C.H. Conley, 1/18/88, (PB88-187760, A03, MF-A01). This report is only available through NTIS (see address given above).

NCEER-88-0002   "Optimal Control of Nonlinear Flexible Structures," by J.N. Yang, F.X. Long and D. Wong, 1/22/88, (PB88-213772, A06, MF-A01).

NCEER-88-0003   "Substructuring Techniques in the Time Domain for Primary-Secondary Structural Systems," by G.D. Manolis and G. Juhn, 2/10/88, (PB88-213780, A04, MF-A01).

NCEER-88-0004   "Iterative Seismic Analysis of Primary-Secondary Systems," by A. Singhal, L.D. Lutes and P.D. Spanos, 2/23/88, (PB88-213798, A04, MF-A01).

NCEER-88-0005   "Stochastic Finite Element Expansion for Random Media," by P.D. Spanos and R. Ghanem, 3/14/88, (PB88-213806, A03, MF-A01).

NCEER-88-0006   "Combining Structural Optimization and Structural Control," by F.Y. Cheng and C.P. Pantelides, 1/10/88, (PB88-213814, A05, MF-A01).

NCEER-88-0007   "Seismic Performance Assessment of Code-Designed Structures," by H.H-M. Hwang, J-W. Jaw and H-J. Shau, 3/20/88, (PB88-219423, A04, MF-A01). This report is only available through NTIS (see address given above).

NCEER-88-0008   "Reliability Analysis of Code-Designed Structures Under Natural Hazards," by H.H-M. Hwang, H. Ushiba and M. Shinozuka, 2/29/88, (PB88-229471, A07, MF-A01). This report is only available through NTIS (see address given above).

NCEER-88-0009   "Seismic Fragility Analysis of Shear Wall Structures," by J-W Jaw and H.H-M. Hwang, 4/30/88, (PB89-102867, A04, MF-A01).

NCEER-88-0010   "Base Isolation of a Multi-Story Building Under a Harmonic Ground Motion - A Comparison of Performances of Various Systems," by F-G Fan, G. Ahmadi and I.G. Tadjbakhsh, 5/18/88, (PB89-122238, A06, MF-A01). This report is only available through NTIS (see address given above).

NCEER-88-0011   "Seismic Floor Response Spectra for a Combined System by Green's Functions," by F.M. Lavelle, L.A. Bergman and P.D. Spanos, 5/1/88, (PB89-102875, A03, MF-A01).

NCEER-88-0012   "A New Solution Technique for Randomly Excited Hysteretic Structures," by G.Q. Cai and Y.K. Lin, 5/16/88, (PB89-102883, A03, MF-A01).

NCEER-88-0013   "A Study of Radiation Damping and Soil-Structure Interaction Effects in the Centrifuge," by K. Weissman, supervised by J.H. Prevost, 5/24/88, (PB89-144703, A06, MF-A01).

NCEER-88-0014   "Parameter Identification and Implementation of a Kinematic Plasticity Model for Frictional Soils," by J.H. Prevost and D.V. Griffiths, to be published.

NCEER-88-0015   "Two- and Three- Dimensional Dynamic Finite Element Analyses of the Long Valley Dam," by D.V. Griffiths and J.H. Prevost, 6/17/88, (PB89-144711, A04, MF-A01).

NCEER-88-0016   "Damage Assessment of Reinforced Concrete Structures in Eastern United States," by A.M. Reinhorn, M.J. Seidel, S.K. Kunnath and Y.J. Park, 6/15/88, (PB89-122220, A04, MF-A01). This report is only available through NTIS (see address given above).

NCEER-88-0017   "Dynamic Compliance of Vertically Loaded Strip Foundations in Multilayered Viscoelastic Soils," by S. Ahmad and A.S.M. Israil, 6/17/88, (PB89-102891, A04, MF-A01).

NCEER-88-0018   "An Experimental Study of Seismic Structural Response With Added Viscoelastic Dampers," by R.C. Lin, Z. Liang, T.T. Soong and R.H. Zhang, 6/30/88, (PB89-122212, A05, MF-A01). This report is available only through NTIS (see address given above).

NCEER-88-0019   "Experimental Investigation of Primary - Secondary System Interaction," by G.D. Manolis, G. Juhn and A.M. Reinhorn, 5/27/88, (PB89-122204, A04, MF-A01).

NCEER-88-0020   "A Response Spectrum Approach For Analysis of Nonclassically Damped Structures," by J.N. Yang, S. Sarkani and F.X. Long, 4/22/88, (PB89-102909, A04, MF-A01).

NCEER-88-0021   "Seismic Interaction of Structures and Soils: Stochastic Approach," by A.S. Veletsos and A.M. Prasad, 7/21/88, (PB89-122196, A04, MF-A01). This report is only available through NTIS (see address given above).

NCEER-88-0022   "Identification of the Serviceability Limit State and Detection of Seismic Structural Damage," by E. DiPasquale and A.S. Cakmak, 6/15/88, (PB89-122188, A05, MF-A01). This report is available only through NTIS (see address given above).

NCEER-88-0023   "Multi-Hazard Risk Analysis: Case of a Simple Offshore Structure," by B.K. Bhartia and E.H. Vanmarcke, 7/21/88, (PB89-145213, A05, MF-A01).

NCEER-88-0024   "Automated Seismic Design of Reinforced Concrete Buildings," by Y.S. Chung, C. Meyer and M. Shinozuka, 7/5/88, (PB89-122170, A06, MF-A01). This report is available only through NTIS (see address given above).

NCEER-88-0025   "Experimental Study of Active Control of MDOF Structures Under Seismic Excitations," by L.L. Chung, R.C. Lin, T.T. Soong and A.M. Reinhorn, 7/10/88, (PB89-122600, A04, MF-A01).

NCEER-88-0026   "Earthquake Simulation Tests of a Low-Rise Metal Structure," by J.S. Hwang, K.C. Chang, G.C. Lee and R.L. Ketter, 8/1/88, (PB89-102917, A04, MF-A01).

NCEER-88-0027   "Systems Study of Urban Response and Reconstruction Due to Catastrophic Earthquakes," by F. Kozin and H.K. Zhou, 9/22/88, (PB90-162348, A04, MF-A01).

NCEER-88-0028   "Seismic Fragility Analysis of Plane Frame Structures," by H.H-M. Hwang and Y.K. Low, 7/31/88, (PB89-131445, A06, MF-A01).

NCEER-88-0029   "Response Analysis of Stochastic Structures," by A. Kardara, C. Bucher and M. Shinozuka, 9/22/88, (PB89-174429, A04, MF-A01).

NCEER-88-0030   "Nonnormal Accelerations Due to Yielding in a Primary Structure," by D.C.K. Chen and L.D. Lutes, 9/19/88, (PB89-131437, A04, MF-A01).

NCEER-88-0031   "Design Approaches for Soil-Structure Interaction," by A.S. Veletsos, A.M. Prasad and Y. Tang, 12/30/88, (PB89-174437, A03, MF-A01). This report is available only through NTIS (see address given above).

NCEER-88-0032   "A Re-evaluation of Design Spectra for Seismic Damage Control," by C.J. Turkstra and A.G. Tallin, 11/7/88, (PB89-145221, A05, MF-A01).

NCEER-88-0033   "The Behavior and Design of Noncontact Lap Splices Subjected to Repeated Inelastic Tensile Loading," by V.E. Sagan, P. Gergely and R.N. White, 12/8/88, (PB89-163737, A08, MF-A01).

NCEER-88-0034   "Seismic Response of Pile Foundations," by S.M. Mamoon, P.K. Banerjee and S. Ahmad, 11/1/88, (PB89-145239, A04, MF-A01).

NCEER-88-0035   "Modeling of R/C Building Structures With Flexible Floor Diaphragms (IDARC2)," by A.M. Reinhorn, S.K. Kunnath and N. Panahshahi, 9/7/88, (PB89-207153, A07, MF-A01).

NCEER-88-0036   "Solution of the Dam-Reservoir Interaction Problem Using a Combination of FEM, BEM with Particular Integrals, Modal Analysis, and Substructuring," by C-S. Tsai, G.C. Lee and R.L. Ketter, 12/31/88, (PB89-207146, A04, MF-A01).

NCEER-88-0037   "Optimal Placement of Actuators for Structural Control," by F.Y. Cheng and C.P. Pantelides, 8/15/88, (PB89-162846, A05, MF-A01).

NCEER-88-0038   "Teflon Bearings in Aseismic Base Isolation: Experimental Studies and Mathematical Modeling," by A. Mokha, M.C. Constantinou and A.M. Reinhorn, 12/5/88, (PB89-218457, A10, MF-A01). This report is available only through NTIS (see address given above).

NCEER-88-0039   "Seismic Behavior of Flat Slab High-Rise Buildings in the New York City Area," by P. Weidlinger and M. Ettouney, 10/15/88, (PB90-145681, A04, MF-A01).

NCEER-88-0040   "Evaluation of the Earthquake Resistance of Existing Buildings in New York City," by P. Weidlinger and M. Ettouney, 10/15/88, to be published.

NCEER-88-0041   "Small-Scale Modeling Techniques for Reinforced Concrete Structures Subjected to Seismic Loads," by W. Kim, A. El-Attar and R.N. White, 11/22/88, (PB89-189625, A05, MF-A01).

NCEER-88-0042   "Modeling Strong Ground Motion from Multiple Event Earthquakes," by G.W. Ellis and A.S. Cakmak, 10/15/88, (PB89-174445, A03, MF-A01).

NCEER-88-0043   "Nonstationary Models of Seismic Ground Acceleration," by M. Grigoriu, S.E. Ruiz and E. Rosenblueth, 7/15/88, (PB89-189617, A04, MF-A01).

NCEER-88-0044   "SARCF User's Guide: Seismic Analysis of Reinforced Concrete Frames," by Y.S. Chung, C. Meyer and M. Shinozuka, 11/9/88, (PB89-174452, A08, MF-A01).

NCEER-88-0045   "First Expert Panel Meeting on Disaster Research and Planning," edited by J. Pantelic and J. Stoyle, 9/15/88, (PB89-174460, A05, MF-A01).

NCEER-88-0046   "Preliminary Studies of the Effect of Degrading Infill Walls on the Nonlinear Seismic Response of Steel Frames," by C.Z. Chrysostomou, P. Gergely and J.F. Abel, 12/19/88, (PB89-208383, A05, MF-A01).

NCEER-88-0047   "Reinforced Concrete Frame Component Testing Facility - Design, Construction, Instrumentation and Operation," by S.P. Pessiki, C. Conley, T. Bond, P. Gergely and R.N. White, 12/16/88, (PB89-174478, A04, MF-A01).

NCEER-89-0001   "Effects of Protective Cushion and Soil Compliancy on the Response of Equipment Within a Seismically Excited Building," by J.A. HoLung, 2/16/89, (PB89-207179, A04, MF-A01).

NCEER-89-0002   "Statistical Evaluation of Response Modification Factors for Reinforced Concrete Structures," by H.H-M. Hwang and J-W. Jaw, 2/17/89, (PB89-207187, A05, MF-A01).

NCEER-89-0003   "Hysteretic Columns Under Random Excitation," by G-Q. Cai and Y.K. Lin, 1/9/89, (PB89-196513, A03, MF-A01).

NCEER-89-0004   "Experimental Study of `Elephant Foot Bulge' Instability of Thin-Walled Metal Tanks," by Z-H. Jia and R.L. Ketter, 2/22/89, (PB89-207195, A03, MF-A01).

NCEER-89-0005   "Experiment on Performance of Buried Pipelines Across San Andreas Fault," by J. Isenberg, E. Richardson and T.D. O'Rourke, 3/10/89, (PB89-218440, A04, MF-A01). This report is available only through NTIS (see address given above).

NCEER-89-0006   "A Knowledge-Based Approach to Structural Design of Earthquake-Resistant Buildings," by M. Subramani, P. Gergely, C.H. Conley, J.F. Abel and A.H. Zaghw, 1/15/89, (PB89-218465, A06, MF-A01).

NCEER-89-0007   "Liquefaction Hazards and Their Effects on Buried Pipelines," by T.D. O'Rourke and P.A. Lane, 2/1/89, (PB89-218481, A09, MF-A01).

NCEER-89-0008   "Fundamentals of System Identification in Structural Dynamics," by H. Imai, C-B. Yun, O. Maruyama and M. Shinozuka, 1/26/89, (PB89-207211, A04, MF-A01).

NCEER-89-0009   "Effects of the 1985 Michoacan Earthquake on Water Systems and Other Buried Lifelines in Mexico," by A.G. Ayala and M.J. O'Rourke, 3/8/89, (PB89-207229, A06, MF-A01).

NCEER-89-R010   "NCEER Bibliography of Earthquake Education Materials," by K.E.K. Ross, Second Revision, 9/1/89, (PB90-125352, A05, MF-A01). This report is replaced by NCEER-92-0018.

NCEER-89-0011   "Inelastic Three-Dimensional Response Analysis of Reinforced Concrete Building Structures (IDARC-3D), Part I - Modeling," by S.K. Kunnath and A.M. Reinhorn, 4/17/89, (PB90-114612, A07, MF-A01). This report is available only through NTIS (see address given above).

NCEER-89-0012   "Recommended Modifications to ATC-14," by C.D. Poland and J.O. Malley, 4/12/89, (PB90-108648, A15, MF-A01).

NCEER-89-0013   "Repair and Strengthening of Beam-to-Column Connections Subjected to Earthquake Loading," by M. Corazao and A.J. Durrani, 2/28/89, (PB90-109885, A06, MF-A01).

NCEER-89-0014   "Program EXKAL2 for Identification of Structural Dynamic Systems," by O. Maruyama, C-B. Yun, M. Hoshiya and M. Shinozuka, 5/19/89, (PB90-109877, A09, MF-A01).

NCEER-89-0015   "Response of Frames With Bolted Semi-Rigid Connections, Part I - Experimental Study and Analytical Predictions," by P.J. DiCorso, A.M. Reinhorn, J.R. Dickerson, J.B. Radziminski and W.L. Harper, 6/1/89, to be published.

NCEER-89-0016   "ARMA Monte Carlo Simulation in Probabilistic Structural Analysis," by P.D. Spanos and M.P. Mignolet, 7/10/89, (PB90-109893, A03, MF-A01).

NCEER-89-P017   "Preliminary Proceedings from the Conference on Disaster Preparedness - The Place of Earthquake Education in Our Schools," Edited by K.E.K. Ross, 6/23/89, (PB90-108606, A03, MF-A01).

NCEER-89-0017   "Proceedings from the Conference on Disaster Preparedness - The Place of Earthquake Education in Our Schools," Edited by K.E.K. Ross, 12/31/89, (PB90-207895, A012, MF-A02). This report is available only through NTIS (see address given above).

NCEER-89-0018   "Multidimensional Models of Hysteretic Material Behavior for Vibration Analysis of Shape Memory Energy Absorbing Devices, by E.J. Graesser and F.A. Cozzarelli, 6/7/89, (PB90-164146, A04, MF-A01).

NCEER-89-0019   "Nonlinear Dynamic Analysis of Three-Dimensional Base Isolated Structures (3D-BASIS)," by S. Nagarajaiah, A.M. Reinhorn and M.C. Constantinou, 8/3/89, (PB90-161936, A06, MF-A01). This report has been replaced by NCEER-93-0011.

NCEER-89-0020   "Structural Control Considering Time-Rate of Control Forces and Control Rate Constraints," by F.Y. Cheng and C.P. Pantelides, 8/3/89, (PB90-120445, A04, MF-A01).

NCEER-89-0021   "Subsurface Conditions of Memphis and Shelby County," by K.W. Ng, T-S. Chang and H-H.M. Hwang, 7/26/89, (PB90-120437, A03, MF-A01).

NCEER-89-0022   "Seismic Wave Propagation Effects on Straight Jointed Buried Pipelines," by K. Elhmadi and M.J. O'Rourke, 8/24/89, (PB90-162322, A10, MF-A02).

NCEER-89-0023   "Workshop on Serviceability Analysis of Water Delivery Systems," edited by M. Grigoriu, 3/6/89, (PB90-127424, A03, MF-A01).

NCEER-89-0024   "Shaking Table Study of a 1/5 Scale Steel Frame Composed of Tapered Members," by K.C. Chang, J.S. Hwang and G.C. Lee, 9/18/89, (PB90-160169, A04, MF-A01).

NCEER-89-0025   "DYNA1D: A Computer Program for Nonlinear Seismic Site Response Analysis - Technical Documentation," by Jean H. Prevost, 9/14/89, (PB90-161944, A07, MF-A01). This report is available only through NTIS (see address given above).

NCEER-89-0026   "1:4 Scale Model Studies of Active Tendon Systems and Active Mass Dampers for Aseismic Protection," by A.M. Reinhorn, T.T. Soong, R.C. Lin, Y.P. Yang, Y. Fukao, H. Abe and M. Nakai, 9/15/89, (PB90-173246, A10, MF-A02). This report is available only through NTIS (see address given above).

NCEER-89-0027   "Scattering of Waves by Inclusions in a Nonhomogeneous Elastic Half Space Solved by Boundary Element Methods," by P.K. Hadley, A. Askar and A.S. Cakmak, 6/15/89, (PB90-145699, A07, MF-A01).

NCEER-89-0028   "Statistical Evaluation of Deflection Amplification Factors for Reinforced Concrete Structures," by H.H.M. Hwang, J-W. Jaw and A.L. Ch'ng, 8/31/89, (PB90-164633, A05, MF-A01).

NCEER-89-0029   "Bedrock Accelerations in Memphis Area Due to Large New Madrid Earthquakes," by H.H.M. Hwang, C.H.S. Chen and G. Yu, 11/7/89, (PB90-162330, A04, MF-A01).

NCEER-89-0030   "Seismic Behavior and Response Sensitivity of Secondary Structural Systems," by Y.Q. Chen and T.T. Soong, 10/23/89, (PB90-164658, A08, MF-A01).

NCEER-89-0031   "Random Vibration and Reliability Analysis of Primary-Secondary Structural Systems," by Y. Ibrahim, M. Grigoriu and T.T. Soong, 11/10/89, (PB90-161951, A04, MF-A01).

NCEER-89-0032 "Proceedings from the Second U.S. - Japan Workshop on Liquefaction, Large Ground Deformation and Their Effects on Lifelines, September 26-29, 1989," Edited by T.D. O'Rourke and M. Hamada, 12/1/89, (PB90-209388, A22, MF-A03).

NCEER-89-0033 "Deterministic Model for Seismic Damage Evaluation of Reinforced Concrete Structures," by J.M. Bracci, A.M. Reinhorn, J.B. Mander and S.K. Kunnath, 9/27/89, (PB91-108803, A06, MF-A01).

NCEER-89-0034 "On the Relation Between Local and Global Damage Indices," by E. DiPasquale and A.S. Cakmak, 8/15/89, (PB90-173865, A05, MF-A01).

NCEER-89-0035 "Cyclic Undrained Behavior of Nonplastic and Low Plasticity Silts," by A.J. Walker and H.E. Stewart, 7/26/89, (PB90-183518, A10, MF-A01).

NCEER-89-0036 "Liquefaction Potential of Surficial Deposits in the City of Buffalo, New York," by M. Budhu, R. Giese and L. Baumgrass, 1/17/89, (PB90-208455, A04, MF-A01).

NCEER-89-0037 "A Deterministic Assessment of Effects of Ground Motion Incoherence," by A.S. Veletsos and Y. Tang, 7/15/89, (PB90-164294, A03, MF-A01).

NCEER-89-0038 "Workshop on Ground Motion Parameters for Seismic Hazard Mapping," July 17-18, 1989, edited by R.V. Whitman, 12/1/89, (PB90-173923, A04, MF-A01).

NCEER-89-0039 "Seismic Effects on Elevated Transit Lines of the New York City Transit Authority," by C.J. Costantino, C.A. Miller and E. Heymsfield, 12/26/89, (PB90-207887, A06, MF-A01).

NCEER-89-0040 "Centrifugal Modeling of Dynamic Soil-Structure Interaction," by K. Weissman, Supervised by J.H. Prevost, 5/10/89, (PB90-207879, A07, MF-A01).

NCEER-89-0041 "Linearized Identification of Buildings With Cores for Seismic Vulnerability Assessment," by I-K. Ho and A.E. Aktan, 11/1/89, (PB90-251943, A07, MF-A01).

NCEER-90-0001 "Geotechnical and Lifeline Aspects of the October 17, 1989 Loma Prieta Earthquake in San Francisco," by T.D. O'Rourke, H.E. Stewart, F.T. Blackburn and T.S. Dickerman, 1/90, (PB90-208596, A05, MF-A01).

NCEER-90-0002 "Nonnormal Secondary Response Due to Yielding in a Primary Structure," by D.C.K. Chen and L.D. Lutes, 2/28/90, (PB90-251976, A07, MF-A01).

NCEER-90-0003 "Earthquake Education Materials for Grades K-12," by K.E.K. Ross, 4/16/90, (PB91-251984, A05, MF-A05). This report has been replaced by NCEER-92-0018.

NCEER-90-0004 "Catalog of Strong Motion Stations in Eastern North America," by R.W. Busby, 4/3/90, (PB90-251984, A05, MF-A01).

NCEER-90-0005 "NCEER Strong-Motion Data Base: A User Manual for the GeoBase Release (Version 1.0 for the Sun3)," by P. Friberg and K. Jacob, 3/31/90 (PB90-258062, A04, MF-A01).

NCEER-90-0006 "Seismic Hazard Along a Crude Oil Pipeline in the Event of an 1811-1812 Type New Madrid Earthquake," by H.H.M. Hwang and C-H.S. Chen, 4/16/90, (PB90-258054, A04, MF-A01).

NCEER-90-0007 "Site-Specific Response Spectra for Memphis Sheahan Pumping Station," by H.H.M. Hwang and C.S. Lee, 5/15/90, (PB91-108811, A05, MF-A01).

NCEER-90-0008 "Pilot Study on Seismic Vulnerability of Crude Oil Transmission Systems," by T. Ariman, R. Dobry, M. Grigoriu, F. Kozin, M. O'Rourke, T. O'Rourke and M. Shinozuka, 5/25/90, (PB91-108837, A06, MF-A01).

NCEER-90-0009 "A Program to Generate Site Dependent Time Histories: EQGEN," by G.W. Ellis, M. Srinivasan and A.S. Cakmak, 1/30/90, (PB91-108829, A04, MF-A01).

NCEER-90-0010 "Active Isolation for Seismic Protection of Operating Rooms," by M.E. Talbott, Supervised by M. Shinozuka, 6/8/9, (PB91-110205, A05, MF-A01).

NCEER-90-0011   "Program LINEARID for Identification of Linear Structural Dynamic Systems," by C-B. Yun and M. Shinozuka, 6/25/90, (PB91-110312, A08, MF-A01).

NCEER-90-0012   "Two-Dimensional Two-Phase Elasto-Plastic Seismic Response of Earth Dams," by A.N. Yiagos, Supervised by J.H. Prevost, 6/20/90, (PB91-110197, A13, MF-A02).

NCEER-90-0013   "Secondary Systems in Base-Isolated Structures: Experimental Investigation, Stochastic Response and Stochastic Sensitivity," by G.D. Manolis, G. Juhn, M.C. Constantinou and A.M. Reinhorn, 7/1/90, (PB91-110320, A08, MF-A01).

NCEER-90-0014   "Seismic Behavior of Lightly-Reinforced Concrete Column and Beam-Column Joint Details," by S.P. Pessiki, C.H. Conley, P. Gergely and R.N. White, 8/22/90, (PB91-108795, A11, MF-A02).

NCEER-90-0015   "Two Hybrid Control Systems for Building Structures Under Strong Earthquakes," by J.N. Yang and A. Danielians, 6/29/90, (PB91-125393, A04, MF-A01).

NCEER-90-0016   "Instantaneous Optimal Control with Acceleration and Velocity Feedback," by J.N. Yang and Z. Li, 6/29/90, (PB91-125401, A03, MF-A01).

NCEER-90-0017   "Reconnaissance Report on the Northern Iran Earthquake of June 21, 1990," by M. Mehrain, 10/4/90, (PB91-125377, A03, MF-A01).

NCEER-90-0018   "Evaluation of Liquefaction Potential in Memphis and Shelby County," by T.S. Chang, P.S. Tang, C.S. Lee and H. Hwang, 8/10/90, (PB91-125427, A09, MF-A01).

NCEER-90-0019   "Experimental and Analytical Study of a Combined Sliding Disc Bearing and Helical Steel Spring Isolation System," by M.C. Constantinou, A.S. Mokha and A.M. Reinhorn, 10/4/90, (PB91-125385, A06, MF-A01). This report is available only through NTIS (see address given above).

NCEER-90-0020   "Experimental Study and Analytical Prediction of Earthquake Response of a Sliding Isolation System with a Spherical Surface," by A.S. Mokha, M.C. Constantinou and A.M. Reinhorn, 10/11/90, (PB91-125419, A05, MF-A01).

NCEER-90-0021   "Dynamic Interaction Factors for Floating Pile Groups," by G. Gazetas, K. Fan, A. Kaynia and E. Kausel, 9/10/90, (PB91-170381, A05, MF-A01).

NCEER-90-0022   "Evaluation of Seismic Damage Indices for Reinforced Concrete Structures," by S. Rodriguez-Gomez and A.S. Cakmak, 9/30/90, PB91-171322, A06, MF-A01).

NCEER-90-0023   "Study of Site Response at a Selected Memphis Site," by H. Desai, S. Ahmad, E.S. Gazetas and M.R. Oh, 10/11/90, (PB91-196857, A03, MF-A01).

NCEER-90-0024   "A User's Guide to Strongmo: Version 1.0 of NCEER's Strong-Motion Data Access Tool for PCs and Terminals," by P.A. Friberg and C.A.T. Susch, 11/15/90, (PB91-171272, A03, MF-A01).

NCEER-90-0025   "A Three-Dimensional Analytical Study of Spatial Variability of Seismic Ground Motions," by L-L. Hong and A.H.-S. Ang, 10/30/90, (PB91-170399, A09, MF-A01).

NCEER-90-0026   "MUMOID User's Guide - A Program for the Identification of Modal Parameters," by S. Rodriguez-Gomez and E. DiPasquale, 9/30/90, (PB91-171298, A04, MF-A01).

NCEER-90-0027   "SARCF-II User's Guide - Seismic Analysis of Reinforced Concrete Frames," by S. Rodriguez-Gomez, Y.S. Chung and C. Meyer, 9/30/90, (PB91-171280, A05, MF-A01).

NCEER-90-0028   "Viscous Dampers: Testing, Modeling and Application in Vibration and Seismic Isolation," by N. Makris and M.C. Constantinou, 12/20/90 (PB91-190561, A06, MF-A01).

NCEER-90-0029   "Soil Effects on Earthquake Ground Motions in the Memphis Area," by H. Hwang, C.S. Lee, K.W. Ng and T.S. Chang, 8/2/90, (PB91-190751, A05, MF-A01).

NCEER-91-0001   "Proceedings from the Third Japan-U.S. Workshop on Earthquake Resistant Design of Lifeline Facilities and Countermeasures for Soil Liquefaction, December 17-19, 1990," edited by T.D. O'Rourke and M. Hamada, 2/1/91, (PB91-179259, A99, MF-A04).

NCEER-91-0002   "Physical Space Solutions of Non-Proportionally Damped Systems," by M. Tong, Z. Liang and G.C. Lee, 1/15/91, (PB91-179242, A04, MF-A01).

NCEER-91-0003   "Seismic Response of Single Piles and Pile Groups," by K. Fan and G. Gazetas, 1/10/91, (PB92-174994, A04, MF-A01).

NCEER-91-0004   "Damping of Structures: Part 1 - Theory of Complex Damping," by Z. Liang and G. Lee, 10/10/91, (PB92-197235, A12, MF-A03).

NCEER-91-0005   "3D-BASIS - Nonlinear Dynamic Analysis of Three Dimensional Base Isolated Structures: Part II," by S. Nagarajaiah, A.M. Reinhorn and M.C. Constantinou, 2/28/91, (PB91-190553, A07, MF-A01). This report has been replaced by NCEER-93-0011.

NCEER-91-0006   "A Multidimensional Hysteretic Model for Plasticity Deforming Metals in Energy Absorbing Devices," by E.J. Graesser and F.A. Cozzarelli, 4/9/91, (PB92-108364, A04, MF-A01).

NCEER-91-0007   "A Framework for Customizable Knowledge-Based Expert Systems with an Application to a KBES for Evaluating the Seismic Resistance of Existing Buildings," by E.G. Ibarra-Anaya and S.J. Fenves, 4/9/91, (PB91-210930, A08, MF-A01).

NCEER-91-0008   "Nonlinear Analysis of Steel Frames with Semi-Rigid Connections Using the Capacity Spectrum Method," by G.G. Deierlein, S-H. Hsieh, Y-J. Shen and J.F. Abel, 7/2/91, (PB92-113828, A05, MF-A01).

NCEER-91-0009   "Earthquake Education Materials for Grades K-12," by K.E.K. Ross, 4/30/91, (PB91-212142, A06, MF-A01). This report has been replaced by NCEER-92-0018.

NCEER-91-0010   "Phase Wave Velocities and Displacement Phase Differences in a Harmonically Oscillating Pile," by N. Makris and G. Gazetas, 7/8/91, (PB92-108356, A04, MF-A01).

NCEER-91-0011   "Dynamic Characteristics of a Full-Size Five-Story Steel Structure and a 2/5 Scale Model," by K.C. Chang, G.C. Yao, G.C. Lee, D.S. Hao and Y.C. Yeh," 7/2/91, (PB93-116648, A06, MF-A02).

NCEER-91-0012   "Seismic Response of a 2/5 Scale Steel Structure with Added Viscoelastic Dampers," by K.C. Chang, T.T. Soong, S-T. Oh and M.L. Lai, 5/17/91, (PB92-110816, A05, MF-A01).

NCEER-91-0013   "Earthquake Response of Retaining Walls; Full-Scale Testing and Computational Modeling," by S. Alampalli and A-W.M. Elgamal, 6/20/91, to be published.

NCEER-91-0014   "3D-BASIS-M: Nonlinear Dynamic Analysis of Multiple Building Base Isolated Structures," by P.C. Tsopelas, S. Nagarajaiah, M.C. Constantinou and A.M. Reinhorn, 5/28/91, (PB92-113885, A09, MF-A02).

NCEER-91-0015   "Evaluation of SEAOC Design Requirements for Sliding Isolated Structures," by D. Theodossiou and M.C. Constantinou, 6/10/91, (PB92-114602, A11, MF-A03).

NCEER-91-0016   "Closed-Loop Modal Testing of a 27-Story Reinforced Concrete Flat Plate-Core Building," by H.R. Somaprasad, T. Toksoy, H. Yoshiyuki and A.E. Aktan, 7/15/91, (PB92-129980, A07, MF-A02).

NCEER-91-0017   "Shake Table Test of a 1/6 Scale Two-Story Lightly Reinforced Concrete Building," by A.G. El-Attar, R.N. White and P. Gergely, 2/28/91, (PB92-222447, A06, MF-A02).

NCEER-91-0018   "Shake Table Test of a 1/8 Scale Three-Story Lightly Reinforced Concrete Building," by A.G. El-Attar, R.N. White and P. Gergely, 2/28/91, (PB93-116630, A08, MF-A02).

NCEER-91-0019   "Transfer Functions for Rigid Rectangular Foundations," by A.S. Veletsos, A.M. Prasad and W.H. Wu, 7/31/91, to be published.

NCEER-91-0020   "Hybrid Control of Seismic-Excited Nonlinear and Inelastic Structural Systems," by J.N. Yang, Z. Li and A. Danielians, 8/1/91, (PB92-143171, A06, MF-A02).

NCEER-91-0021   "The NCEER-91 Earthquake Catalog: Improved Intensity-Based Magnitudes and Recurrence Relations for U.S. Earthquakes East of New Madrid," by L. Seeber and J.G. Armbruster, 8/28/91, (PB92-176742, A06, MF-A02).

NCEER-91-0022   "Proceedings from the Implementation of Earthquake Planning and Education in Schools: The Need for Change - The Roles of the Changemakers," by K.E.K. Ross and F. Winslow, 7/23/91, (PB92-129998, A12, MF-A03).

NCEER-91-0023   "A Study of Reliability-Based Criteria for Seismic Design of Reinforced Concrete Frame Buildings," by H.H.M. Hwang and H-M. Hsu, 8/10/91, (PB92-140235, A09, MF-A02).

NCEER-91-0024   "Experimental Verification of a Number of Structural System Identification Algorithms," by R.G. Ghanem, H. Gavin and M. Shinozuka, 9/18/91, (PB92-176577, A18, MF-A04).

NCEER-91-0025   "Probabilistic Evaluation of Liquefaction Potential," by H.H.M. Hwang and C.S. Lee," 11/25/91, (PB92-143429, A05, MF-A01).

NCEER-91-0026   "Instantaneous Optimal Control for Linear, Nonlinear and Hysteretic Structures - Stable Controllers," by J.N. Yang and Z. Li, 11/15/91, (PB92-163807, A04, MF-A01).

NCEER-91-0027   "Experimental and Theoretical Study of a Sliding Isolation System for Bridges," by M.C. Constantinou, A. Kartoum, A.M. Reinhorn and P. Bradford, 11/15/91, (PB92-176973, A10, MF-A03).

NCEER-92-0001   "Case Studies of Liquefaction and Lifeline Performance During Past Earthquakes, Volume 1: Japanese Case Studies," Edited by M. Hamada and T. O'Rourke, 2/17/92, (PB92-197243, A18, MF-A04).

NCEER-92-0002   "Case Studies of Liquefaction and Lifeline Performance During Past Earthquakes, Volume 2: United States Case Studies," Edited by T. O'Rourke and M. Hamada, 2/17/92, (PB92-197250, A20, MF-A04).

NCEER-92-0003   "Issues in Earthquake Education," Edited by K. Ross, 2/3/92, (PB92-222389, A07, MF-A02).

NCEER-92-0004   "Proceedings from the First U.S. - Japan Workshop on Earthquake Protective Systems for Bridges," Edited by I.G. Buckle, 2/4/92, (PB94-142239, A99, MF-A06).

NCEER-92-0005   "Seismic Ground Motion from a Haskell-Type Source in a Multiple-Layered Half-Space," A.P. Theoharis, G. Deodatis and M. Shinozuka, 1/2/92, to be published.

NCEER-92-0006   "Proceedings from the Site Effects Workshop," Edited by R. Whitman, 2/29/92, (PB92-197201, A04, MF-A01).

NCEER-92-0007   "Engineering Evaluation of Permanent Ground Deformations Due to Seismically-Induced Liquefaction," by M.H. Baziar, R. Dobry and A-W.M. Elgamal, 3/24/92, (PB92-222421, A13, MF-A03).

NCEER-92-0008   "A Procedure for the Seismic Evaluation of Buildings in the Central and Eastern United States," by C.D. Poland and J.O. Malley, 4/2/92, (PB92-222439, A20, MF-A04).

NCEER-92-0009   "Experimental and Analytical Study of a Hybrid Isolation System Using Friction Controllable Sliding Bearings," by M.Q. Feng, S. Fujii and M. Shinozuka, 5/15/92, (PB93-150282, A06, MF-A02).

NCEER-92-0010   "Seismic Resistance of Slab-Column Connections in Existing Non-Ductile Flat-Plate Buildings," by A.J. Durrani and Y. Du, 5/18/92, (PB93-116812, A06, MF-A02).

NCEER-92-0011   "The Hysteretic and Dynamic Behavior of Brick Masonry Walls Upgraded by Ferrocement Coatings Under Cyclic Loading and Strong Simulated Ground Motion," by H. Lee and S.P. Prawel, 5/11/92, to be published.

NCEER-92-0012   "Study of Wire Rope Systems for Seismic Protection of Equipment in Buildings," by G.F. Demetriades, M.C. Constantinou and A.M. Reinhorn, 5/20/92, (PB93-116655, A08, MF-A02).

NCEER-92-0013   "Shape Memory Structural Dampers: Material Properties, Design and Seismic Testing," by P.R. Witting and F.A. Cozzarelli, 5/26/92, (PB93-116663, A05, MF-A01).

NCEER-92-0014   "Longitudinal Permanent Ground Deformation Effects on Buried Continuous Pipelines," by M.J. O'Rourke, and C. Nordberg, 6/15/92, (PB93-116671, A08, MF-A02).

NCEER-92-0015   "A Simulation Method for Stationary Gaussian Random Functions Based on the Sampling Theorem," by M. Grigoriu and S. Balopoulou, 6/11/92, (PB93-127496, A05, MF-A01).

NCEER-92-0016   "Gravity-Load-Designed Reinforced Concrete Buildings: Seismic Evaluation of Existing Construction and Detailing Strategies for Improved Seismic Resistance," by G.W. Hoffmann, S.K. Kunnath, A.M. Reinhorn and J.B. Mander, 7/15/92, (PB94-142007, A08, MF-A02).

NCEER-92-0017   "Observations on Water System and Pipeline Performance in the Limón Area of Costa Rica Due to the April 22, 1991 Earthquake," by M. O'Rourke and D. Ballantyne, 6/30/92, (PB93-126811, A06, MF-A02).

NCEER-92-0018   "Fourth Edition of Earthquake Education Materials for Grades K-12," Edited by K.E.K. Ross, 8/10/92, (PB93-114023, A07, MF-A02).

NCEER-92-0019   "Proceedings from the Fourth Japan-U.S. Workshop on Earthquake Resistant Design of Lifeline Facilities and Countermeasures for Soil Liquefaction," Edited by M. Hamada and T.D. O'Rourke, 8/12/92, (PB93-163939, A99, MF-E11).

NCEER-92-0020   "Active Bracing System: A Full Scale Implementation of Active Control," by A.M. Reinhorn, T.T. Soong, R.C. Lin, M.A. Riley, Y.P. Wang, S. Aizawa and M. Higashino, 8/14/92, (PB93-127512, A06, MF-A02).

NCEER-92-0021   "Empirical Analysis of Horizontal Ground Displacement Generated by Liquefaction-Induced Lateral Spreads," by S.F. Bartlett and T.L. Youd, 8/17/92, (PB93-188241, A06, MF-A02).

NCEER-92-0022   "IDARC Version 3.0: Inelastic Damage Analysis of Reinforced Concrete Structures," by S.K. Kunnath, A.M. Reinhorn and R.F. Lobo, 8/31/92, (PB93-227502, A07, MF-A02).

NCEER-92-0023   "A Semi-Empirical Analysis of Strong-Motion Peaks in Terms of Seismic Source, Propagation Path and Local Site Conditions, by M. Kamiyama, M.J. O'Rourke and R. Flores-Berrones, 9/9/92, (PB93-150266, A08, MF-A02).

NCEER-92-0024   "Seismic Behavior of Reinforced Concrete Frame Structures with Nonductile Details, Part I: Summary of Experimental Findings of Full Scale Beam-Column Joint Tests," by A. Beres, R.N. White and P. Gergely, 9/30/92, (PB93-227783, A05, MF-A01).

NCEER-92-0025   "Experimental Results of Repaired and Retrofitted Beam-Column Joint Tests in Lightly Reinforced Concrete Frame Buildings," by A. Beres, S. El-Borgi, R.N. White and P. Gergely, 10/29/92, (PB93-227791, A05, MF-A01).

NCEER-92-0026   "A Generalization of Optimal Control Theory: Linear and Nonlinear Structures," by J.N. Yang, Z. Li and S. Vongchavalitkul, 11/2/92, (PB93-188621, A05, MF-A01).

NCEER-92-0027   "Seismic Resistance of Reinforced Concrete Frame Structures Designed Only for Gravity Loads: Part I - Design and Properties of a One-Third Scale Model Structure," by J.M. Bracci, A.M. Reinhorn and J.B. Mander, 12/1/92, (PB94-104502, A08, MF-A02).

NCEER-92-0028   "Seismic Resistance of Reinforced Concrete Frame Structures Designed Only for Gravity Loads: Part II - Experimental Performance of Subassemblages," by L.E. Aycardi, J.B. Mander and A.M. Reinhorn, 12/1/92, (PB94-104510, A08, MF-A02).

NCEER-92-0029   "Seismic Resistance of Reinforced Concrete Frame Structures Designed Only for Gravity Loads: Part III - Experimental Performance and Analytical Study of a Structural Model," by J.M. Bracci, A.M. Reinhorn and J.B. Mander, 12/1/92, (PB93-227528, A09, MF-A01).

NCEER-92-0030   "Evaluation of Seismic Retrofit of Reinforced Concrete Frame Structures: Part I - Experimental Performance of Retrofitted Subassemblages," by D. Choudhuri, J.B. Mander and A.M. Reinhorn, 12/8/92, (PB93-198307, A07, MF-A02).

NCEER-92-0031   "Evaluation of Seismic Retrofit of Reinforced Concrete Frame Structures: Part II - Experimental Performance and Analytical Study of a Retrofitted Structural Model," by J.M. Bracci, A.M. Reinhorn and J.B. Mander, 12/8/92, (PB93-198315, A09, MF-A03).

NCEER-92-0032   "Experimental and Analytical Investigation of Seismic Response of Structures with Supplemental Fluid Viscous Dampers," by M.C. Constantinou and M.D. Symans, 12/21/92, (PB93-191435, A10, MF-A03). This report is available only through NTIS (see address given above).

NCEER-92-0033   "Reconnaissance Report on the Cairo, Egypt Earthquake of October 12, 1992," by M. Khater, 12/23/92, (PB93-188621, A03, MF-A01).

NCEER-92-0034   "Low-Level Dynamic Characteristics of Four Tall Flat-Plate Buildings in New York City," by H. Gavin, S. Yuan, J. Grossman, E. Pekelis and K. Jacob, 12/28/92, (PB93-188217, A07, MF-A02).

NCEER-93-0001   "An Experimental Study on the Seismic Performance of Brick-Infilled Steel Frames With and Without Retrofit," by J.B. Mander, B. Nair, K. Wojtkowski and J. Ma, 1/29/93, (PB93-227510, A07, MF-A02).

NCEER-93-0002   "Social Accounting for Disaster Preparedness and Recovery Planning," by S. Cole, E. Pantoja and V. Razak, 2/22/93, (PB94-142114, A12, MF-A03).

NCEER-93-0003   "Assessment of 1991 NEHRP Provisions for Nonstructural Components and Recommended Revisions," by T.T. Soong, G. Chen, Z. Wu, R-H. Zhang and M. Grigoriu, 3/1/93, (PB93-188639, A06, MF-A02).

NCEER-93-0004   "Evaluation of Static and Response Spectrum Analysis Procedures of SEAOC/UBC for Seismic Isolated Structures," by C.W. Winters and M.C. Constantinou, 3/23/93, (PB93-198299, A10, MF-A03).

NCEER-93-0005   "Earthquakes in the Northeast - Are We Ignoring the Hazard? A Workshop on Earthquake Science and Safety for Educators," edited by K.E.K. Ross, 4/2/93, (PB94-103066, A09, MF-A02).

NCEER-93-0006   "Inelastic Response of Reinforced Concrete Structures with Viscoelastic Braces," by R.F. Lobo, J.M. Bracci, K.L. Shen, A.M. Reinhorn and T.T. Soong, 4/5/93, (PB93-227486, A05, MF-A02).

NCEER-93-0007   "Seismic Testing of Installation Methods for Computers and Data Processing Equipment," by K. Kosar, T.T. Soong, K.L. Shen, J.A. HoLung and Y.K. Lin, 4/12/93, (PB93-198299, A07, MF-A02).

NCEER-93-0008   "Retrofit of Reinforced Concrete Frames Using Added Dampers," by A. Reinhorn, M. Constantinou and C. Li, to be published.

NCEER-93-0009   "Seismic Behavior and Design Guidelines for Steel Frame Structures with Added Viscoelastic Dampers," by K.C. Chang, M.L. Lai, T.T. Soong, D.S. Hao and Y.C. Yeh, 5/1/93, (PB94-141959, A07, MF-A02).

NCEER-93-0010   "Seismic Performance of Shear-Critical Reinforced Concrete Bridge Piers," by J.B. Mander, S.M. Waheed, M.T.A. Chaudhary and S.S. Chen, 5/12/93, (PB93-227494, A08, MF-A02).

NCEER-93-0011   "3D-BASIS-TABS: Computer Program for Nonlinear Dynamic Analysis of Three Dimensional Base Isolated Structures," by S. Nagarajaiah, C. Li, A.M. Reinhorn and M.C. Constantinou, 8/2/93, (PB94-141819, A09, MF-A02).

NCEER-93-0012   "Effects of Hydrocarbon Spills from an Oil Pipeline Break on Ground Water," by O.J. Helweg and H.H.M. Hwang, 8/3/93, (PB94-141942, A06, MF-A02).

NCEER-93-0013   "Simplified Procedures for Seismic Design of Nonstructural Components and Assessment of Current Code Provisions," by M.P. Singh, L.E. Suarez, E.E. Matheu and G.O. Maldonado, 8/4/93, (PB94-141827, A09, MF-A02).

NCEER-93-0014   "An Energy Approach to Seismic Analysis and Design of Secondary Systems," by G. Chen and T.T. Soong, 8/6/93, (PB94-142767, A11, MF-A03).

NCEER-93-0015   "Proceedings from School Sites: Becoming Prepared for Earthquakes - Commemorating the Third Anniversary of the Loma Prieta Earthquake," Edited by F.E. Winslow and K.E.K. Ross, 8/16/93, (PB94-154275, A16, MF-A02).

NCEER-93-0016   "Reconnaissance Report of Damage to Historic Monuments in Cairo, Egypt Following the October 12, 1992 Dahshur Earthquake," by D. Sykora, D. Look, G. Croci, E. Karaesmen and E. Karaesmen, 8/19/93, (PB94-142221, A08, MF-A02).

NCEER-93-0017   "The Island of Guam Earthquake of August 8, 1993," by S.W. Swan and S.K. Harris, 9/30/93, (PB94-141843, A04, MF-A01).

NCEER-93-0018   "Engineering Aspects of the October 12, 1992 Egyptian Earthquake," by A.W. Elgamal, M. Amer, K. Adalier and A. Abul-Fadl, 10/7/93, (PB94-141983, A05, MF-A01).

NCEER-93-0019   "Development of an Earthquake Motion Simulator and its Application in Dynamic Centrifuge Testing," by I. Krstelj, Supervised by J.H. Prevost, 10/23/93, (PB94-181773, A-10, MF-A03).

NCEER-93-0020   "NCEER-Taisei Corporation Research Program on Sliding Seismic Isolation Systems for Bridges: Experimental and Analytical Study of a Friction Pendulum System (FPS)," by M.C. Constantinou, P. Tsopelas, Y-S. Kim and S. Okamoto, 11/1/93, (PB94-142775, A08, MF-A02).

NCEER-93-0021   "Finite Element Modeling of Elastomeric Seismic Isolation Bearings," by L.J. Billings, Supervised by R. Shepherd, 11/8/93, to be published.

NCEER-93-0022   "Seismic Vulnerability of Equipment in Critical Facilities: Life-Safety and Operational Consequences," by K. Porter, G.S. Johnson, M.M. Zadeh, C. Scawthorn and S. Eder, 11/24/93, (PB94-181765, A16, MF-A03).

NCEER-93-0023   "Hokkaido Nansei-oki, Japan Earthquake of July 12, 1993, by P.I. Yanev and C.R. Scawthorn, 12/23/93, (PB94-181500, A07, MF-A01).

NCEER-94-0001   "An Evaluation of Seismic Serviceability of Water Supply Networks with Application to the San Francisco Auxiliary Water Supply System," by I. Markov, Supervised by M. Grigoriu and T. O'Rourke, 1/21/94, (PB94-204013, A07, MF-A02).

NCEER-94-0002   "NCEER-Taisei Corporation Research Program on Sliding Seismic Isolation Systems for Bridges: Experimental and Analytical Study of Systems Consisting of Sliding Bearings, Rubber Restoring Force Devices and Fluid Dampers," Volumes I and II, by P. Tsopelas, S. Okamoto, M.C. Constantinou, D. Ozaki and S. Fujii, 2/4/94, (PB94-181740, A09, MF-A02 and PB94-181757, A12, MF-A03).

NCEER-94-0003   "A Markov Model for Local and Global Damage Indices in Seismic Analysis," by S. Rahman and M. Grigoriu, 2/18/94, (PB94-206000, A12, MF-A03).

NCEER-94-0004   "Proceedings from the NCEER Workshop on Seismic Response of Masonry Infills," edited by D.P. Abrams, 3/1/94, (PB94-180783, A07, MF-A02).

NCEER-94-0005   "The Northridge, California Earthquake of January 17, 1994: General Reconnaissance Report," edited by J.D. Goltz, 3/11/94, (PB94-193943, A10, MF-A03).

NCEER-94-0006   "Seismic Energy Based Fatigue Damage Analysis of Bridge Columns: Part I - Evaluation of Seismic Capacity," by G.A. Chang and J.B. Mander, 3/14/94, (PB94-219185, A11, MF-A03).

NCEER-94-0007   "Seismic Isolation of Multi-Story Frame Structures Using Spherical Sliding Isolation Systems," by T.M. Al-Hussaini, V.A. Zayas and M.C. Constantinou, 3/17/94, (PB94-193745, A09, MF-A02).

NCEER-94-0008   "The Northridge, California Earthquake of January 17, 1994: Performance of Highway Bridges," edited by I.G. Buckle, 3/24/94, (PB94-193851, A06, MF-A02).

NCEER-94-0009   "Proceedings of the Third U.S.-Japan Workshop on Earthquake Protective Systems for Bridges," edited by I.G. Buckle and I. Friedland, 3/31/94, (PB94-195815, A99, MF-A06).

NCEER-94-0010   "3D-BASIS-ME: Computer Program for Nonlinear Dynamic Analysis of Seismically Isolated Single and Multiple Structures and Liquid Storage Tanks," by P.C. Tsopelas, M.C. Constantinou and A.M. Reinhorn, 4/12/94, (PB94-204922, A09, MF-A02).

NCEER-94-0011   "The Northridge, California Earthquake of January 17, 1994: Performance of Gas Transmission Pipelines," by T.D. O'Rourke and M.C. Palmer, 5/16/94, (PB94-204989, A05, MF-A01).

NCEER-94-0012   "Feasibility Study of Replacement Procedures and Earthquake Performance Related to Gas Transmission Pipelines," by T.D. O'Rourke and M.C. Palmer, 5/25/94, (PB94-206638, A09, MF-A02).

NCEER-94-0013   "Seismic Energy Based Fatigue Damage Analysis of Bridge Columns: Part II - Evaluation of Seismic Demand," by G.A. Chang and J.B. Mander, 6/1/94, (PB95-18106, A08, MF-A02).

NCEER-94-0014   "NCEER-Taisei Corporation Research Program on Sliding Seismic Isolation Systems for Bridges: Experimental and Analytical Study of a System Consisting of Sliding Bearings and Fluid Restoring Force/Damping Devices," by P. Tsopelas and M.C. Constantinou, 6/13/94, (PB94-219144, A10, MF-A03).

NCEER-94-0015   "Generation of Hazard-Consistent Fragility Curves for Seismic Loss Estimation Studies," by H. Hwang and J-R. Huo, 6/14/94, (PB95-181996, A09, MF-A02).

NCEER-94-0016   "Seismic Study of Building Frames with Added Energy-Absorbing Devices," by W.S. Pong, C.S. Tsai and G.C. Lee, 6/20/94, (PB94-219136, A10, A03).

NCEER-94-0017   "Sliding Mode Control for Seismic-Excited Linear and Nonlinear Civil Engineering Structures," by J. Yang, J. Wu, A. Agrawal and Z. Li, 6/21/94, (PB95-138483, A06, MF-A02).

NCEER-94-0018   "3D-BASIS-TABS Version 2.0: Computer Program for Nonlinear Dynamic Analysis of Three Dimensional Base Isolated Structures," by A.M. Reinhorn, S. Nagarajaiah, M.C. Constantinou, P. Tsopelas and R. Li, 6/22/94, (PB95-182176, A08, MF-A02).

NCEER-94-0019   "Proceedings of the International Workshop on Civil Infrastructure Systems: Application of Intelligent Systems and Advanced Materials on Bridge Systems," Edited by G.C. Lee and K.C. Chang, 7/18/94, (PB95-252474, A20, MF-A04).

NCEER-94-0020   "Study of Seismic Isolation Systems for Computer Floors," by V. Lambrou and M.C. Constantinou, 7/19/94, (PB95-138533, A10, MF-A03).

NCEER-94-0021   "Proceedings of the U.S.-Italian Workshop on Guidelines for Seismic Evaluation and Rehabilitation of Unreinforced Masonry Buildings," Edited by D.P. Abrams and G.M. Calvi, 7/20/94, (PB95-138749, A13, MF-A03).

NCEER-94-0022   "NCEER-Taisei Corporation Research Program on Sliding Seismic Isolation Systems for Bridges: Experimental and Analytical Study of a System Consisting of Lubricated PTFE Sliding Bearings and Mild Steel Dampers," by P. Tsopelas and M.C. Constantinou, 7/22/94, (PB95-182184, A08, MF-A02).

NCEER-94-0023   "Development of Reliability-Based Design Criteria for Buildings Under Seismic Load," by Y.K. Wen, H. Hwang and M. Shinozuka, 8/1/94, (PB95-211934, A08, MF-A02).

NCEER-94-0024   "Experimental Verification of Acceleration Feedback Control Strategies for an Active Tendon System," by S.J. Dyke, B.F. Spencer, Jr., P. Quast, M.K. Sain, D.C. Kaspari, Jr. and T.T. Soong, 8/29/94, (PB95-212320, A05, MF-A01).

NCEER-94-0025   "Seismic Retrofitting Manual for Highway Bridges," Edited by I.G. Buckle and I.F. Friedland, published by the Federal Highway Administration (PB95-212676, A15, MF-A03).

NCEER-94-0026   "Proceedings from the Fifth U.S.-Japan Workshop on Earthquake Resistant Design of Lifeline Facilities and Countermeasures Against Soil Liquefaction," Edited by T.D. O'Rourke and M. Hamada, 11/7/94, (PB95-220802, A99, MF-E08).

NCEER-95-0001   "Experimental and Analytical Investigation of Seismic Retrofit of Structures with Supplemental Damping: Part 1 - Fluid Viscous Damping Devices," by A.M. Reinhorn, C. Li and M.C. Constantinou, 1/3/95, (PB95-266599, A09, MF-A02).

NCEER-95-0002   "Experimental and Analytical Study of Low-Cycle Fatigue Behavior of Semi-Rigid Top-And-Seat Angle Connections," by G. Pekcan, J.B. Mander and S.S. Chen, 1/5/95, (PB95-220042, A07, MF-A02).

NCEER-95-0003   "NCEER-ATC Joint Study on Fragility of Buildings," by T. Anagnos, C. Rojahn and A.S. Kiremidjian, 1/20/95, (PB95-220026, A06, MF-A02).

NCEER-95-0004   "Nonlinear Control Algorithms for Peak Response Reduction," by Z. Wu, T.T. Soong, V. Gattulli and R.C. Lin, 2/16/95, (PB95-220349, A05, MF-A01).

NCEER-95-0005   "Pipeline Replacement Feasibility Study: A Methodology for Minimizing Seismic and Corrosion Risks to Underground Natural Gas Pipelines," by R.T. Eguchi, H.A. Seligson and D.G. Honegger, 3/2/95, (PB95-252326, A06, MF-A02).

NCEER-95-0006   "Evaluation of Seismic Performance of an 11-Story Frame Building During the 1994 Northridge Earthquake," by F. Naeim, R. DiSulio, K. Benuska, A. Reinhorn and C. Li, to be published.

NCEER-95-0007   "Prioritization of Bridges for Seismic Retrofitting," by N. Basöz and A.S. Kiremidjian, 4/24/95, (PB95-252300, A08, MF-A02).

NCEER-95-0008   "Method for Developing Motion Damage Relationships for Reinforced Concrete Frames," by A. Singhal and A.S. Kiremidjian, 5/11/95, (PB95-266607, A06, MF-A02).

NCEER-95-0009   "Experimental and Analytical Investigation of Seismic Retrofit of Structures with Supplemental Damping: Part II - Friction Devices," by C. Li and A.M. Reinhorn, 7/6/95, (PB96-128087, A11, MF-A03).

NCEER-95-0010   "Experimental Performance and Analytical Study of a Non-Ductile Reinforced Concrete Frame Structure Retrofitted with Elastomeric Spring Dampers," by G. Pekcan, J.B. Mander and S.S. Chen, 7/14/95, (PB96-137161, A08, MF-A02).

NCEER-95-0011   "Development and Experimental Study of Semi-Active Fluid Damping Devices for Seismic Protection of Structures," by M.D. Symans and M.C. Constantinou, 8/3/95, (PB96-136940, A23, MF-A04).

NCEER-95-0012   "Real-Time Structural Parameter Modification (RSPM): Development of Innervated Structures," by Z. Liang, M. Tong and G.C. Lee, 4/11/95, (PB96-137153, A06, MF-A01).

NCEER-95-0013   "Experimental and Analytical Investigation of Seismic Retrofit of Structures with Supplemental Damping: Part III - Viscous Damping Walls," by A.M. Reinhorn and C. Li, 10/1/95, (PB96-176409, A11, MF-A03).

NCEER-95-0014   "Seismic Fragility Analysis of Equipment and Structures in a Memphis Electric Substation," by J-R. Huo and H.H.M. Hwang, 8/10/95, (PB96-128087, A09, MF-A02).

NCEER-95-0015   "The Hanshin-Awaji Earthquake of January 17, 1995: Performance of Lifelines," Edited by M. Shinozuka, 11/3/95, (PB96-176383, A15, MF-A03).

NCEER-95-0016   "Highway Culvert Performance During Earthquakes," by T.L. Youd and C.J. Beckman, available as NCEER-96-0015.

NCEER-95-0017   "The Hanshin-Awaji Earthquake of January 17, 1995: Performance of Highway Bridges," Edited by I.G. Buckle, 12/1/95, to be published.

NCEER-95-0018   "Modeling of Masonry Infill Panels for Structural Analysis," by A.M. Reinhorn, A. Madan, R.E. Valles, Y. Reichmann and J.B. Mander, 12/8/95, (PB97-110886, MF-A01, A06).

NCEER-95-0019   "Optimal Polynomial Control for Linear and Nonlinear Structures," by A.K. Agrawal and J.N. Yang, 12/11/95, (PB96-168737, A07, MF-A02).

NCEER-95-0020   "Retrofit of Non-Ductile Reinforced Concrete Frames Using Friction Dampers," by R.S. Rao, P. Gergely and R.N. White, 12/22/95, (PB97-133508, A10, MF-A02).

NCEER-95-0021   "Parametric Results for Seismic Response of Pile-Supported Bridge Bents," by G. Mylonakis, A. Nikolaou and G. Gazetas, 12/22/95, (PB97-100242, A12, MF-A03).

NCEER-95-0022   "Kinematic Bending Moments in Seismically Stressed Piles," by A. Nikolaou, G. Mylonakis and G. Gazetas, 12/23/95, (PB97-113914, MF-A03, A13).

NCEER-96-0001   "Dynamic Response of Unreinforced Masonry Buildings with Flexible Diaphragms," by A.C. Costley and D.P. Abrams," 10/10/96, (PB97-133573, MF-A03, A15).

NCEER-96-0002   "State of the Art Review: Foundations and Retaining Structures," by I. Po Lam, to be published.

NCEER-96-0003   "Ductility of Rectangular Reinforced Concrete Bridge Columns with Moderate Confinement," by N. Wehbe, M. Saiidi, D. Sanders and B. Douglas, 11/7/96, (PB97-133557, A06, MF-A02).

NCEER-96-0004   "Proceedings of the Long-Span Bridge Seismic Research Workshop," edited by I.G. Buckle and I.M. Friedland, to be published.

NCEER-96-0005   "Establish Representative Pier Types for Comprehensive Study: Eastern United States," by J. Kulicki and Z. Prucz, 5/28/96, (PB98-119217, A07, MF-A02).

NCEER-96-0006   "Establish Representative Pier Types for Comprehensive Study: Western United States," by R. Imbsen, R.A. Schamber and T.A. Osterkamp, 5/28/96, (PB98-118607, A07, MF-A02).

NCEER-96-0007   "Nonlinear Control Techniques for Dynamical Systems with Uncertain Parameters," by R.G. Ghanem and M.I. Bujakov, 5/27/96, (PB97-100259, A17, MF-A03).

NCEER-96-0008   "Seismic Evaluation of a 30-Year Old Non-Ductile Highway Bridge Pier and Its Retrofit," by J.B. Mander, B. Mahmoodzadegan, S. Bhadra and S.S. Chen, 5/31/96, (PB97-110902, MF-A03, A10).

NCEER-96-0009   "Seismic Performance of a Model Reinforced Concrete Bridge Pier Before and After Retrofit," by J.B. Mander, J.H. Kim and C.A. Ligozio, 5/31/96, (PB97-110910, MF-A02, A10).

NCEER-96-0010   "IDARC2D Version 4.0: A Computer Program for the Inelastic Damage Analysis of Buildings," by R.E. Valles, A.M. Reinhorn, S.K. Kunnath, C. Li and A. Madan, 6/3/96, (PB97-100234, A17, MF-A03).

NCEER-96-0011   "Estimation of the Economic Impact of Multiple Lifeline Disruption: Memphis Light, Gas and Water Division Case Study," by S.E. Chang, H.A. Seligson and R.T. Eguchi, 8/16/96, (PB97-133490, A11, MF-A03).

NCEER-96-0012   "Proceedings from the Sixth Japan-U.S. Workshop on Earthquake Resistant Design of Lifeline Facilities and Countermeasures Against Soil Liquefaction, Edited by M. Hamada and T. O'Rourke, 9/11/96, (PB97-133581, A99, MF-A06).

NCEER-96-0013   "Chemical Hazards, Mitigation and Preparedness in Areas of High Seismic Risk: A Methodology for Estimating the Risk of Post-Earthquake Hazardous Materials Release," by H.A. Seligson, R.T. Eguchi, K.J. Tierney and K. Richmond, 11/7/96, (PB97-133565, MF-A02, A08).

NCEER-96-0014   "Response of Steel Bridge Bearings to Reversed Cyclic Loading," by J.B. Mander, D-K. Kim, S.S. Chen and G.J. Premus, 11/13/96, (PB97-140735, A12, MF-A03).

NCEER-96-0015   "Highway Culvert Performance During Past Earthquakes," by T.L. Youd and C.J. Beckman, 11/25/96, (PB97-133532, A06, MF-A01).

NCEER-97-0001   "Evaluation, Prevention and Mitigation of Pounding Effects in Building Structures," by R.E. Valles and A.M. Reinhorn, 2/20/97, (PB97-159552, A14, MF-A03).

NCEER-97-0002   "Seismic Design Criteria for Bridges and Other Highway Structures," by C. Rojahn, R. Mayes, D.G. Anderson, J. Clark, J.H. Hom, R.V. Nutt and M.J. O'Rourke, 4/30/97, (PB97-194658, A06, MF-A03).

NCEER-97-0003   "Proceedings of the U.S.-Italian Workshop on Seismic Evaluation and Retrofit," Edited by D.P. Abrams and G.M. Calvi, 3/19/97, (PB97-194666, A13, MF-A03).

NCEER-97-0004   "Investigation of Seismic Response of Buildings with Linear and Nonlinear Fluid Viscous Dampers," by A.A. Seleemah and M.C. Constantinou, 5/21/97, (PB98-109002, A15, MF-A03).

NCEER-97-0005   "Proceedings of the Workshop on Earthquake Engineering Frontiers in Transportation Facilities," edited by G.C. Lee and I.M. Friedland, 8/29/97, (PB98-128911, A25, MR-A04).

NCEER-97-0006   "Cumulative Seismic Damage of Reinforced Concrete Bridge Piers," by S.K. Kunnath, A. El-Bahy, A. Taylor and W. Stone, 9/2/97, (PB98-108814, A11, MF-A03).

NCEER-97-0007   "Structural Details to Accommodate Seismic Movements of Highway Bridges and Retaining Walls," by R.A. Imbsen, R.A. Schamber, E. Thorkildsen, A. Kartoum, B.T. Martin, T.N. Rosser and J.M. Kulicki, 9/3/97, (PB98-108996, A09, MF-A02).

NCEER-97-0008   "A Method for Earthquake Motion-Damage Relationships with Application to Reinforced Concrete Frames," by A. Singhal and A.S. Kiremidjian, 9/10/97, (PB98-108988, A13, MF-A03).

NCEER-97-0009   "Seismic Analysis and Design of Bridge Abutments Considering Sliding and Rotation," by K. Fishman and R. Richards, Jr., 9/15/97, (PB98-108897, A06, MF-A02).

NCEER-97-0010   "Proceedings of the FHWA/NCEER Workshop on the National Representation of Seismic Ground Motion for New and Existing Highway Facilities," edited by I.M. Friedland, M.S. Power and R.L. Mayes, 9/22/97, (PB98-128903, A21, MF-A04).

NCEER-97-0011   "Seismic Analysis for Design or Retrofit of Gravity Bridge Abutments," by K.L. Fishman, R. Richards, Jr. and R.C. Divito, 10/2/97, (PB98-128937, A08, MF-A02).

NCEER-97-0012   "Evaluation of Simplified Methods of Analysis for Yielding Structures," by P. Tsopelas, M.C. Constantinou, C.A. Kircher and A.S. Whittaker, 10/31/97, (PB98-128929, A10, MF-A03).

NCEER-97-0013   "Seismic Design of Bridge Columns Based on Control and Repairability of Damage," by C-T. Cheng and J.B. Mander, 12/8/97, (PB98-144249, A11, MF-A03).

NCEER-97-0014   "Seismic Resistance of Bridge Piers Based on Damage Avoidance Design," by J.B. Mander and C-T. Cheng, 12/10/97, (PB98-144223, A09, MF-A02).

NCEER-97-0015   "Seismic Response of Nominally Symmetric Systems with Strength Uncertainty," by S. Balopoulou and M. Grigoriu, 12/23/97, (PB98-153422, A11, MF-A03).

NCEER-97-0016   "Evaluation of Seismic Retrofit Methods for Reinforced Concrete Bridge Columns," by T.J. Wipf, F.W. Klaiber and F.M. Russo, 12/28/97, (PB98-144215, A12, MF-A03).

NCEER-97-0017   "Seismic Fragility of Existing Conventional Reinforced Concrete Highway Bridges," by C.L. Mullen and A.S. Cakmak, 12/30/97, (PB98-153406, A08, MF-A02).

NCEER-97-0018   "Loss Asssessment of Memphis Buildings," edited by D.P. Abrams and M. Shinozuka, 12/31/97, (PB98-144231, A13, MF-A03).

NCEER-97-0019   "Seismic Evaluation of Frames with Infill Walls Using Quasi-static Experiments," by K.M. Mosalam, R.N. White and P. Gergely, 12/31/97, (PB98-153455, A07, MF-A02).

NCEER-97-0020   "Seismic Evaluation of Frames with Infill Walls Using Pseudo-dynamic Experiments," by K.M. Mosalam, R.N. White and P. Gergely, 12/31/97, (PB98-153430, A07, MF-A02).

NCEER-97-0021   "Computational Strategies for Frames with Infill Walls: Discrete and Smeared Crack Analyses and Seismic Fragility," by K.M. Mosalam, R.N. White and P. Gergely, 12/31/97, (PB98-153414, A10, MF-A02).

NCEER-97-0022   "Proceedings of the NCEER Workshop on Evaluation of Liquefaction Resistance of Soils," edited by T.L. Youd and I.M. Idriss, 12/31/97, (PB98-155617, A15, MF-A03).

MCEER-98-0001   "Extraction of Nonlinear Hysteretic Properties of Seismically Isolated Bridges from Quick-Release Field Tests," by Q. Chen, B.M. Douglas, E.M. Maragakis and I.G. Buckle, 5/26/98, (PB99-118838, A06, MF-A01).

MCEER-98-0002   "Methodologies for Evaluating the Importance of Highway Bridges," by A. Thomas, S. Eshenaur and J. Kulicki, 5/29/98, (PB99-118846, A10, MF-A02).

MCEER-98-0003   "Capacity Design of Bridge Piers and the Analysis of Overstrength," by J.B. Mander, A. Dutta and P. Goel, 6/1/98, (PB99-118853, A09, MF-A02).

MCEER-98-0004   "Evaluation of Bridge Damage Data from the Loma Prieta and Northridge, California Earthquakes," by N. Basoz and A. Kiremidjian, 6/2/98, (PB99-118861, A15, MF-A03).

MCEER-98-0005   "Screening Guide for Rapid Assessment of Liquefaction Hazard at Highway Bridge Sites," by T. L. Youd, 6/16/98, (PB99-118879, A06, not available on microfiche).

MCEER-98-0006   "Structural Steel and Steel/Concrete Interface Details for Bridges," by P. Ritchie, N. Kauhl and J. Kulicki, 7/13/98, (PB99-118945, A06, MF-A01).

MCEER-98-0007   "Capacity Design and Fatigue Analysis of Confined Concrete Columns," by A. Dutta and J.B. Mander, 7/14/98, (PB99-118960, A14, MF-A03).

MCEER-98-0008   "Proceedings of the Workshop on Performance Criteria for Telecommunication Services Under Earthquake Conditions," edited by A.J. Schiff, 7/15/98, (PB99-118952, A08, MF-A02).

MCEER-98-0009   "Fatigue Analysis of Unconfined Concrete Columns," by J.B. Mander, A. Dutta and J.H. Kim, 9/12/98, (PB99-123655, A10, MF-A02).

MCEER-98-0010   "Centrifuge Modeling of Cyclic Lateral Response of Pile-Cap Systems and Seat-Type Abutments in Dry Sands," by A.D. Gadre and R. Dobry, 10/2/98, (PB99-123606, A13, MF-A03).

MCEER-98-0011   "IDARC-BRIDGE: A Computational Platform for Seismic Damage Assessment of Bridge Structures," by A.M. Reinhorn, V. Simeonov, G. Mylonakis and Y. Reichman, 10/2/98, (PB99-162919, A15, MF-A03).

MCEER-98-0012   "Experimental Investigation of the Dynamic Response of Two Bridges Before and After Retrofitting with Elastomeric Bearings," by D.A. Wendichansky, S.S. Chen and J.B. Mander, 10/2/98, (PB99-162927, A15, MF-A03).

MCEER-98-0013   "Design Procedures for Hinge Restrainers and Hinge Sear Width for Multiple-Frame Bridges," by R. Des Roches and G.L. Fenves, 11/3/98, (PB99-140477, A13, MF-A03).

MCEER-98-0014   "Response Modification Factors for Seismically Isolated Bridges," by M.C. Constantinou and J.K. Quarshie, 11/3/98, (PB99-140485, A14, MF-A03).

MCEER-98-0015   "Proceedings of the U.S.-Italy Workshop on Seismic Protective Systems for Bridges," edited by I.M. Friedland and M.C. Constantinou, 11/3/98, (PB2000-101711, A22, MF-A04).

MCEER-98-0016   "Appropriate Seismic Reliability for Critical Equipment Systems: Recommendations Based on Regional Analysis of Financial and Life Loss," by K. Porter, C. Scawthorn, C. Taylor and N. Blais, 11/10/98, (PB99-157265, A08, MF-A02).

MCEER-98-0017   "Proceedings of the U.S. Japan Joint Seminar on Civil Infrastructure Systems Research," edited by M. Shinozuka and A. Rose, 11/12/98, (PB99-156713, A16, MF-A03).

MCEER-98-0018   "Modeling of Pile Footings and Drilled Shafts for Seismic Design," by I. PoLam, M. Kapuskar and D. Chaudhuri, 12/21/98, (PB99-157257, A09, MF-A02).

MCEER-99-0001   "Seismic Evaluation of a Masonry Infilled Reinforced Concrete Frame by Pseudodynamic Testing," by S.G. Buonopane and R.N. White, 2/16/99, (PB99-162851, A09, MF-A02).

MCEER-99-0002   "Response History Analysis of Structures with Seismic Isolation and Energy Dissipation Systems: Verification Examples for Program SAP2000," by J. Scheller and M.C. Constantinou, 2/22/99, (PB99-162869, A08, MF-A02).

MCEER-99-0003   "Experimental Study on the Seismic Design and Retrofit of Bridge Columns Including Axial Load Effects," by A. Dutta, T. Kokorina and J.B. Mander, 2/22/99, (PB99-162877, A09, MF-A02).

MCEER-99-0004   "Experimental Study of Bridge Elastomeric and Other Isolation and Energy Dissipation Systems with Emphasis on Uplift Prevention and High Velocity Near-source Seismic Excitation," by A. Kasalanati and M. C. Constantinou, 2/26/99, (PB99-162885, A12, MF-A03).

MCEER-99-0005   "Truss Modeling of Reinforced Concrete Shear-flexure Behavior," by J.H. Kim and J.B. Mander, 3/8/99, (PB99-163693, A12, MF-A03).

MCEER-99-0006   "Experimental Investigation and Computational Modeling of Seismic Response of a 1:4 Scale Model Steel Structure with a Load Balancing Supplemental Damping System," by G. Pekcan, J.B. Mander and S.S. Chen, 4/2/99, (PB99-162893, A11, MF-A03).

MCEER-99-0007   "Effect of Vertical Ground Motions on the Structural Response of Highway Bridges," by M.R. Button, C.J. Cronin and R.L. Mayes, 4/10/99, (PB2000-101411, A10, MF-A03).

MCEER-99-0008   "Seismic Reliability Assessment of Critical Facilities: A Handbook, Supporting Documentation, and Model Code Provisions," by G.S. Johnson, R.E. Sheppard, M.D. Quilici, S.J. Eder and C.R. Scawthorn, 4/12/99, (PB2000-101701, A18, MF-A04).

MCEER-99-0009   "Impact Assessment of Selected MCEER Highway Project Research on the Seismic Design of Highway Structures," by C. Rojahn, R. Mayes, D.G. Anderson, J.H. Clark, D'Appolonia Engineering, S. Gloyd and R.V. Nutt, 4/14/99, (PB99-162901, A10, MF-A02).

MCEER-99-0010   "Site Factors and Site Categories in Seismic Codes," by R. Dobry, R. Ramos and M.S. Power, 7/19/99, (PB2000-101705, A08, MF-A02).

MCEER-99-0011   "Restrainer Design Procedures for Multi-Span Simply-Supported Bridges," by M.J. Randall, M. Saiidi, E. Maragakis and T. Isakovic, 7/20/99, (PB2000-101702, A10, MF-A02).

MCEER-99-0012   "Property Modification Factors for Seismic Isolation Bearings," by M.C. Constantinou, P. Tsopelas, A. Kasalanati and E. Wolff, 7/20/99, (PB2000-103387, A11, MF-A03).

MCEER-99-0013   "Critical Seismic Issues for Existing Steel Bridges," by P. Ritchie, N. Kauhl and J. Kulicki, 7/20/99, (PB2000-101697, A09, MF-A02).

MCEER-99-0014   "Nonstructural Damage Database," by A. Kao, T.T. Soong and A. Vender, 7/24/99, (PB2000-101407, A06, MF-A01).

MCEER-99-0015   "Guide to Remedial Measures for Liquefaction Mitigation at Existing Highway Bridge Sites," by H.G. Cooke and J. K. Mitchell, 7/26/99, (PB2000-101703, A11, MF-A03).

MCEER-99-0016   "Proceedings of the MCEER Workshop on Ground Motion Methodologies for the Eastern United States," edited by N. Abrahamson and A. Becker, 8/11/99, (PB2000-103385, A07, MF-A02).

MCEER-99-0017   "Quindío, Colombia Earthquake of January 25, 1999: Reconnaissance Report," by A.P. Asfura and P.J. Flores, 10/4/99, (PB2000-106893, A06, MF-A01).

MCEER-99-0018   "Hysteretic Models for Cyclic Behavior of Deteriorating Inelastic Structures," by M.V. Sivaselvan and A.M. Reinhorn, 11/5/99, (PB2000-103386, A08, MF-A02).

MCEER-99-0019   "Proceedings of the 7th U.S.- Japan Workshop on Earthquake Resistant Design of Lifeline Facilities and Countermeasures Against Soil Liquefaction," edited by T.D. O'Rourke, J.P. Bardet and M. Hamada, 11/19/99, (PB2000-103354, A99, MF-A06).

MCEER-99-0020   "Development of Measurement Capability for Micro-Vibration Evaluations with Application to Chip Fabrication Facilities," by G.C. Lee, Z. Liang, J.W. Song, J.D. Shen and W.C. Liu, 12/1/99, (PB2000-105993, A08, MF-A02).

MCEER-99-0021   "Design and Retrofit Methodology for Building Structures with Supplemental Energy Dissipating Systems," by G. Pekcan, J.B. Mander and S.S. Chen, 12/31/99, (PB2000-105994, A11, MF-A03).

MCEER-00-0001   "The Marmara, Turkey Earthquake of August 17, 1999: Reconnaissance Report," edited by C. Scawthorn; with major contributions by M. Bruneau, R. Eguchi, T. Holzer, G. Johnson, J. Mander, J. Mitchell, W. Mitchell, A. Papageorgiou, C. Scaethorn, and G. Webb, 3/23/00, (PB2000-106200, A11, MF-A03).

MCEER-00-0002   "Proceedings of the MCEER Workshop for Seismic Hazard Mitigation of Health Care Facilities," edited by G.C. Lee, M. Ettouney, M. Grigoriu, J. Hauer and J. Nigg, 3/29/00, (PB2000-106892, A08, MF-A02).

MCEER-00-0003   "The Chi-Chi, Taiwan Earthquake of September 21, 1999: Reconnaissance Report," edited by G.C. Lee and C.H. Loh, with major contributions by G.C. Lee, M. Bruneau, I.G. Buckle, S.E. Chang, P.J. Flores, T.D. O'Rourke, M. Shinozuka, T.T. Soong, C-H. Loh, K-C. Chang, Z-J. Chen, J-S. Hwang, M-L. Lin, G-Y. Liu, K-C. Tsai, G.C. Yao and C-L. Yen, 4/30/00, (PB2001-100980, A10, MF-A02).

MCEER-00-0004   "Seismic Retrofit of End-Sway Frames of Steel Deck-Truss Bridges with a Supplemental Tendon System: Experimental and Analytical Investigation," by G. Pekcan, J.B. Mander and S.S. Chen, 7/1/00, (PB2001-100982, A10, MF-A02).

MCEER-00-0005   "Sliding Fragility of Unrestrained Equipment in Critical Facilities," by W.H. Chong and T.T. Soong, 7/5/00, (PB2001-100983, A08, MF-A02).

MCEER-00-0006   "Seismic Response of Reinforced Concrete Bridge Pier Walls in the Weak Direction," by N. Abo-Shadi, M. Saiidi and D. Sanders, 7/17/00, (PB2001-100981, A17, MF-A03).

MCEER-00-0007   "Low-Cycle Fatigue Behavior of Longitudinal Reinforcement in Reinforced Concrete Bridge Columns," by J. Brown and S.K. Kunnath, 7/23/00, (PB2001-104392, A08, MF-A02).

MCEER-00-0008   "Soil Structure Interaction of Bridges for Seismic Analysis," I. PoLam and H. Law, 9/25/00, (PB2001-105397, A08, MF-A02).

MCEER-00-0009   "Proceedings of the First MCEER Workshop on Mitigation of Earthquake Disaster by Advanced Technologies (MEDAT-1), edited by M. Shinozuka, D.J. Inman and T.D. O'Rourke, 11/10/00, (PB2001-105399, A14, MF-A03).

MCEER-00-0010   "Development and Evaluation of Simplified Procedures for Analysis and Design of Buildings with Passive Energy Dissipation Systems, Revision 01," by O.M. Ramirez, M.C. Constantinou, C.A. Kircher, A.S. Whittaker, M.W. Johnson, J.D. Gomez and C. Chrysostomou, 11/16/01, (PB2001-105523, A23, MF-A04).

MCEER-00-0011   "Dynamic Soil-Foundation-Structure Interaction Analyses of Large Caissons," by C-Y. Chang, C-M. Mok, Z-L. Wang, R. Settgast, F. Waggoner, M.A. Ketchum, H.M. Gonnermann and C-C. Chin, 12/30/00, (PB2001-104373, A07, MF-A02).

MCEER-00-0012   "Experimental Evaluation of Seismic Performance of Bridge Restrainers," by A.G. Vlassis, E.M. Maragakis and M. Saiid Saiidi, 12/30/00, (PB2001-104354, A09, MF-A02).

MCEER-00-0013   "Effect of Spatial Variation of Ground Motion on Highway Structures," by M. Shinozuka, V. Saxena and G. Deodatis, 12/31/00, (PB2001-108755, A13, MF-A03).

MCEER-00-0014   "A Risk-Based Methodology for Assessing the Seismic Performance of Highway Systems," by S.D. Werner, C.E. Taylor, J.E. Moore, II, J.S. Walton and S. Cho, 12/31/00, (PB2001-108756, A14, MF-A03).

MCEER-01-0001 "Experimental Investigation of P-Delta Effects to Collapse During Earthquakes," by D. Vian and M. Bruneau, 6/25/01, (PB2002-100534, A17, MF-A03).

MCEER-01-0002 "Proceedings of the Second MCEER Workshop on Mitigation of Earthquake Disaster by Advanced Technologies (MEDAT-2)," edited by M. Bruneau and D.J. Inman, 7/23/01, (PB2002-100434, A16, MF-A03).

MCEER-01-0003 "Sensitivity Analysis of Dynamic Systems Subjected to Seismic Loads," by C. Roth and M. Grigoriu, 9/18/01, (PB2003-100884, A12, MF-A03).

MCEER-01-0004 "Overcoming Obstacles to Implementing Earthquake Hazard Mitigation Policies: Stage 1 Report," by D.J. Alesch and W.J. Petak, 12/17/01, (PB2002-107949, A07, MF-A02).

MCEER-01-0005 "Updating Real-Time Earthquake Loss Estimates: Methods, Problems and Insights," by C.E. Taylor, S.E. Chang and R.T. Eguchi, 12/17/01, (PB2002-107948, A05, MF-A01).

MCEER-01-0006 "Experimental Investigation and Retrofit of Steel Pile Foundations and Pile Bents Under Cyclic Lateral Loadings," by A. Shama, J. Mander, B. Blabac and S. Chen, 12/31/01, (PB2002-107950, A13, MF-A03).

MCEER-02-0001 "Assessment of Performance of Bolu Viaduct in the 1999 Duzce Earthquake in Turkey" by P.C. Roussis, M.C. Constantinou, M. Erdik, E. Durukal and M. Dicleli, 5/8/02, (PB2003-100883, A08, MF-A02).

MCEER-02-0002 "Seismic Behavior of Rail Counterweight Systems of Elevators in Buildings," by M.P. Singh, Rildova and L.E. Suarez, 5/27/02. (PB2003-100882, A11, MF-A03).

MCEER-02-0003 "Development of Analysis and Design Procedures for Spread Footings," by G. Mylonakis, G. Gazetas, S. Nikolaou and A. Chauncey, 10/02/02, (PB2004-101636, A13, MF-A03, CD-A13).

MCEER-02-0004 "Bare-Earth Algorithms for Use with SAR and LIDAR Digital Elevation Models," by C.K. Huyck, R.T. Eguchi and B. Houshmand, 10/16/02, (PB2004-101637, A07, CD-A07).

MCEER-02-0005 "Review of Energy Dissipation of Compression Members in Concentrically Braced Frames," by K.Lee and M. Bruneau, 10/18/02, (PB2004-101638, A10, CD-A10).

MCEER-03-0001 "Experimental Investigation of Light-Gauge Steel Plate Shear Walls for the Seismic Retrofit of Buildings" by J. Berman and M. Bruneau, 5/2/03, (PB2004-101622, A10, MF-A03, CD-A10).

MCEER-03-0002 "Statistical Analysis of Fragility Curves," by M. Shinozuka, M.Q. Feng, H. Kim, T. Uzawa and T. Ueda, 6/16/03, (PB2004-101849, A09, CD-A09).

MCEER-03-0003 "Proceedings of the Eighth U.S.-Japan Workshop on Earthquake Resistant Design f Lifeline Facilities and Countermeasures Against Liquefaction," edited by M. Hamada, J.P. Bardet and T.D. O'Rourke, 6/30/03, (PB2004-104386, A99, CD-A99).

MCEER-03-0004 "Proceedings of the PRC-US Workshop on Seismic Analysis and Design of Special Bridges," edited by L.C. Fan and G.C. Lee, 7/15/03, (PB2004-104387, A14, CD-A14).

MCEER-03-0005 "Urban Disaster Recovery: A Framework and Simulation Model," by S.B. Miles and S.E. Chang, 7/25/03, (PB2004-104388, A07, CD-A07).

MCEER-03-0006 "Behavior of Underground Piping Joints Due to Static and Dynamic Loading," by R.D. Meis, M. Maragakis and R. Siddharthan, 11/17/03, (PB2005-102194, A13, MF-A03, CD-A00).

MCEER-04-0001 "Experimental Study of Seismic Isolation Systems with Emphasis on Secondary System Response and Verification of Accuracy of Dynamic Response History Analysis Methods," by E. Wolff and M. Constantinou, 1/16/04 (PB2005-102195, A99, MF-E08, CD-A00).

MCEER-04-0002 "Tension, Compression and Cyclic Testing of Engineered Cementitious Composite Materials," by K. Kesner and S.L. Billington, 3/1/04, (PB2005-102196, A08, CD-A08).

MCEER-04-0003   "Cyclic Testing of Braces Laterally Restrained by Steel Studs to Enhance Performance During Earthquakes," by O.C. Celik, J.W. Berman and M. Bruneau, 3/16/04, (PB2005-102197, A13, MF-A03, CD-A00).

MCEER-04-0004   "Methodologies for Post Earthquake Building Damage Detection Using SAR and Optical Remote Sensing: Application to the August 17, 1999 Marmara, Turkey Earthquake," by C.K. Huyck, B.J. Adams, S. Cho, R.T. Eguchi, B. Mansouri and B. Houshmand, 6/15/04, (PB2005-104888, A10, CD-A00).

MCEER-04-0005   "Nonlinear Structural Analysis Towards Collapse Simulation: A Dynamical Systems Approach," by M.V. Sivaselvan and A.M. Reinhorn, 6/16/04, (PB2005-104889, A11, MF-A03, CD-A00).

MCEER-04-0006   "Proceedings of the Second PRC-US Workshop on Seismic Analysis and Design of Special Bridges," edited by G.C. Lee and L.C. Fan, 6/25/04, (PB2005-104890, A16, CD-A00).

MCEER-04-0007   "Seismic Vulnerability Evaluation of Axially Loaded Steel Built-up Laced Members," by K. Lee and M. Bruneau, 6/30/04, (PB2005-104891, A16, CD-A00).

MCEER-04-0008   "Evaluation of Accuracy of Simplified Methods of Analysis and Design of Buildings with Damping Systems for Near-Fault and for Soft-Soil Seismic Motions," by E.A. Pavlou and M.C. Constantinou, 8/16/04, (PB2005-104892, A08, MF-A02, CD-A00).

MCEER-04-0009   "Assessment of Geotechnical Issues in Acute Care Facilities in California," by M. Lew, T.D. O'Rourke, R. Dobry and M. Koch, 9/15/04, (PB2005-104893, A08, CD-A00).

MCEER-04-0010   "Scissor-Jack-Damper Energy Dissipation System," by A.N. Sigaher-Boyle and M.C. Constantinou, 12/1/04 (PB2005-108221).

MCEER-04-0011   "Seismic Retrofit of Bridge Steel Truss Piers Using a Controlled Rocking Approach," by M. Pollino and M. Bruneau, 12/20/04 (PB2006-105795).

MCEER-05-0001   "Experimental and Analytical Studies of Structures Seismically Isolated with an Uplift-Restraint Isolation System," by P.C. Roussis and M.C. Constantinou, 1/10/05 (PB2005-108222).

MCEER-05-0002   "A Versatile Experimentation Model for Study of Structures Near Collapse Applied to Seismic Evaluation of Irregular Structures," by D. Kusumastuti, A.M. Reinhorn and A. Rutenberg, 3/31/05 (PB2006-101523).

MCEER-05-0003   "Proceedings of the Third PRC-US Workshop on Seismic Analysis and Design of Special Bridges," edited by L.C. Fan and G.C. Lee, 4/20/05, (PB2006-105796).

MCEER-05-0004   "Approaches for the Seismic Retrofit of Braced Steel Bridge Piers and Proof-of-Concept Testing of an Eccentrically Braced Frame with Tubular Link," by J.W. Berman and M. Bruneau, 4/21/05 (PB2006-101524).

MCEER-05-0005   "Simulation of Strong Ground Motions for Seismic Fragility Evaluation of Nonstructural Components in Hospitals," by A. Wanitkorkul and A. Filiatrault, 5/26/05 (PB2006-500027).

MCEER-05-0006   "Seismic Safety in California Hospitals: Assessing an Attempt to Accelerate the Replacement or Seismic Retrofit of Older Hospital Facilities," by D.J. Alesch, L.A. Arendt and W.J. Petak, 6/6/05 (PB2006-105794).

MCEER-05-0007   "Development of Seismic Strengthening and Retrofit Strategies for Critical Facilities Using Engineered Cementitious Composite Materials," by K. Kesner and S.L. Billington, 8/29/05 (PB2006-111701).

MCEER-05-0008   "Experimental and Analytical Studies of Base Isolation Systems for Seismic Protection of Power Transformers," by N. Murota, M.Q. Feng and G-Y. Liu, 9/30/05 (PB2006-111702).

MCEER-05-0009   "3D-BASIS-ME-MB: Computer Program for Nonlinear Dynamic Analysis of Seismically Isolated Structures," by P.C. Tsopelas, P.C. Roussis, M.C. Constantinou, R. Buchanan and A.M. Reinhorn, 10/3/05 (PB2006-111703).

MCEER-05-0010   "Steel Plate Shear Walls for Seismic Design and Retrofit of Building Structures," by D. Vian and M. Bruneau, 12/15/05 (PB2006-111704).

MCEER-05-0011   "The Performance-Based Design Paradigm," by M.J. Astrella and A. Whittaker, 12/15/05 (PB2006-111705).

MCEER-06-0001   "Seismic Fragility of Suspended Ceiling Systems," H. Badillo-Almaraz, A.S. Whittaker, A.M. Reinhorn and G.P. Cimellaro, 2/4/06 (PB2006-111706).

MCEER-06-0002   "Multi-Dimensional Fragility of Structures," by G.P. Cimellaro, A.M. Reinhorn and M. Bruneau, 3/1/06 (PB2007-106974, A09, MF-A02, CD A00).

MCEER-06-0003   "Built-Up Shear Links as Energy Dissipators for Seismic Protection of Bridges," by P. Dusicka, A.M. Itani and I.G. Buckle, 3/15/06 (PB2006-111708).

MCEER-06-0004   "Analytical Investigation of the Structural Fuse Concept," by R.E. Vargas and M. Bruneau, 3/16/06 (PB2006-111709).

MCEER-06-0005   "Experimental Investigation of the Structural Fuse Concept," by R.E. Vargas and M. Bruneau, 3/17/06 (PB2006-111710).

MCEER-06-0006   "Further Development of Tubular Eccentrically Braced Frame Links for the Seismic Retrofit of Braced Steel Truss Bridge Piers," by J.W. Berman and M. Bruneau, 3/27/06 (PB2007-105147).

MCEER-06-0007   "REDARS Validation Report," by S. Cho, C.K. Huyck, S. Ghosh and R.T. Eguchi, 8/8/06 (PB2007-106983).

MCEER-06-0008   "Review of Current NDE Technologies for Post-Earthquake Assessment of Retrofitted Bridge Columns," by J.W. Song, Z. Liang and G.C. Lee, 8/21/06 (PB2007-106984).

MCEER-06-0009   "Liquefaction Remediation in Silty Soils Using Dynamic Compaction and Stone Columns," by S. Thevanayagam, G.R. Martin, R. Nashed, T. Shenthan, T. Kanagalingam and N. Ecemis, 8/28/06 (PB2007-106985).

MCEER-06-0010   "Conceptual Design and Experimental Investigation of Polymer Matrix Composite Infill Panels for Seismic Retrofitting," by W. Jung, M. Chiewanichakorn and A.J. Aref, 9/21/06 (PB2007-106986).

MCEER-06-0011   "A Study of the Coupled Horizontal-Vertical Behavior of Elastomeric and Lead-Rubber Seismic Isolation Bearings," by G.P. Warn and A.S. Whittaker, 9/22/06 (PB2007-108679).

MCEER-06-0012   "Proceedings of the Fourth PRC-US Workshop on Seismic Analysis and Design of Special Bridges: Advancing Bridge Technologies in Research, Design, Construction and Preservation," Edited by L.C. Fan, G.C. Lee and L. Ziang, 10/12/06 (PB2007-109042).

MCEER-06-0013   "Cyclic Response and Low Cycle Fatigue Characteristics of Plate Steels," by P. Dusicka, A.M. Itani and I.G. Buckle, 11/1/06 06 (PB2007-106987).

MCEER-06-0014   "Proceedings of the Second US-Taiwan Bridge Engineering Workshop," edited by W.P. Yen, J. Shen, J-Y. Chen and M. Wang, 11/15/06 (PB2008-500041).

MCEER-06-0015   "User Manual and Technical Documentation for the REDARS^{TM} Import Wizard," by S. Cho, S. Ghosh, C.K. Huyck and S.D. Werner, 11/30/06 (PB2007-114766).

MCEER-06-0016   "Hazard Mitigation Strategy and Monitoring Technologies for Urban and Infrastructure Public Buildings: Proceedings of the China-US Workshops," edited by X.Y. Zhou, A.L. Zhang, G.C. Lee and M. Tong, 12/12/06 (PB2008-500018).

MCEER-07-0001   "Static and Kinetic Coefficients of Friction for Rigid Blocks," by C. Kafali, S. Fathali, M. Grigoriu and A.S. Whittaker, 3/20/07 (PB2007-114767).

MCEER-07-0002   "Hazard Mitigation Investment Decision Making: Organizational Response to Legislative Mandate," by L.A. Arendt, D.J. Alesch and W.J. Petak, 4/9/07 (PB2007-114768).

MCEER-07-0003   "Seismic Behavior of Bidirectional-Resistant Ductile End Diaphragms with Unbonded Braces in Straight or Skewed Steel Bridges," by O. Celik and M. Bruneau, 4/11/07 (PB2008-105141).

MCEER-07-0004   "Modeling Pile Behavior in Large Pile Groups Under Lateral Loading," by A.M. Dodds and G.R. Martin, 4/16/07(PB2008-105142).

MCEER-07-0005   "Experimental Investigation of Blast Performance of Seismically Resistant Concrete-Filled Steel Tube Bridge Piers," by S. Fujikura, M. Bruneau and D. Lopez-Garcia, 4/20/07 (PB2008-105143).

MCEER-07-0006   "Seismic Analysis of Conventional and Isolated Liquefied Natural Gas Tanks Using Mechanical Analogs," by I.P. Christovasilis and A.S. Whittaker, 5/1/07.

MCEER-07-0007   "Experimental Seismic Performance Evaluation of Isolation/Restraint Systems for Mechanical Equipment – Part 1: Heavy Equipment Study," by S. Fathali and A. Filiatrault, 6/6/07 (PB2008-105144).

MCEER-07-0008   "Seismic Vulnerability of Timber Bridges and Timber Substructures," by A.A. Sharma, J.B. Mander, I.M. Friedland and D.R. Allicock, 6/7/07 (PB2008-105145).

MCEER-07-0009   "Experimental and Analytical Study of the XY-Friction Pendulum (XY-FP) Bearing for Bridge Applications," by C.C. Marin-Artieda, A.S. Whittaker and M.C. Constantinou, 6/7/07 (PB2008-105191).

MCEER-07-0010   "Proceedings of the PRC-US Earthquake Engineering Forum for Young Researchers," Edited by G.C. Lee and X.Z. Qi, 6/8/07.

MCEER-07-0011   "Design Recommendations for Perforated Steel Plate Shear Walls," by R. Purba and M. Bruneau, 6/18/07, (PB2008-105192).

MCEER-07-0012   "Performance of Seismic Isolation Hardware Under Service and Seismic Loading," by M.C. Constantinou, A.S. Whittaker, Y. Kalpakidis, D.M. Fenz and G.P. Warn, 8/27/07, (PB2008-105193).

MCEER-07-0013   "Experimental Evaluation of the Seismic Performance of Hospital Piping Subassemblies," by E.R. Goodwin, E. Maragakis and A.M. Itani, 9/4/07, (PB2008-105194).

MCEER-07-0014   "A Simulation Model of Urban Disaster Recovery and Resilience: Implementation for the 1994 Northridge Earthquake," by S. Miles and S.E. Chang, 9/7/07, (PB2008-106426).

MCEER-07-0015   "Statistical and Mechanistic Fragility Analysis of Concrete Bridges," by M. Shinozuka, S. Banerjee and S-H. Kim, 9/10/07, (PB2008-106427).

MCEER-07-0016   "Three-Dimensional Modeling of Inelastic Buckling in Frame Structures," by M. Schachter and AM. Reinhorn, 9/13/07, (PB2008-108125).

MCEER-07-0017   "Modeling of Seismic Wave Scattering on Pile Groups and Caissons," by I. Po Lam, H. Law and C.T. Yang, 9/17/07 (PB2008-108150).

MCEER-07-0018   "Bridge Foundations: Modeling Large Pile Groups and Caissons for Seismic Design," by I. Po Lam, H. Law and G.R. Martin (Coordinating Author), 12/1/07 (PB2008-111190).

MCEER-07-0019   "Principles and Performance of Roller Seismic Isolation Bearings for Highway Bridges," by G.C. Lee, Y.C. Ou, Z. Liang, T.C. Niu and J. Song, 12/10/07.

MCEER-07-0020   "Centrifuge Modeling of Permeability and Pinning Reinforcement Effects on Pile Response to Lateral Spreading," by L.L Gonzalez-Lagos, T. Abdoun and R. Dobry, 12/10/07 (PB2008-111191).

MCEER-07-0021   "Damage to the Highway System from the Pisco, Perú Earthquake of August 15, 2007," by J.S. O'Connor, L. Mesa and M. Nykamp, 12/10/07, (PB2008-108126).

MCEER-07-0022   "Experimental Seismic Performance Evaluation of Isolation/Restraint Systems for Mechanical Equipment – Part 2: Light Equipment Study," by S. Fathali and A. Filiatrault, 12/13/07 (PB2008-111192).

MCEER-07-0023   "Fragility Considerations in Highway Bridge Design," by M. Shinozuka, S. Banerjee and S.H. Kim, 12/14/07 (PB2008-111193).

MCEER-07-0024   "Performance Estimates for Seismically Isolated Bridges," by G.P. Warn and A.S. Whittaker, 12/30/07 (PB2008-112230).

MCEER-08-0001   "Seismic Performance of Steel Girder Bridge Superstructures with Conventional Cross Frames," by L.P. Carden, A.M. Itani and I.G. Buckle, 1/7/08, (PB2008-112231).

MCEER-08-0002   "Seismic Performance of Steel Girder Bridge Superstructures with Ductile End Cross Frames with Seismic Isolators," by L.P. Carden, A.M. Itani and I.G. Buckle, 1/7/08 (PB2008-112232).

MCEER-08-0003   "Analytical and Experimental Investigation of a Controlled Rocking Approach for Seismic Protection of Bridge Steel Truss Piers," by M. Pollino and M. Bruneau, 1/21/08 (PB2008-112233).

MCEER-08-0004   "Linking Lifeline Infrastructure Performance and Community Disaster Resilience: Models and Multi-Stakeholder Processes," by S.E. Chang, C. Pasion, K. Tatebe and R. Ahmad, 3/3/08 (PB2008-112234).

MCEER-08-0005   "Modal Analysis of Generally Damped Linear Structures Subjected to Seismic Excitations," by J. Song, Y-L. Chu, Z. Liang and G.C. Lee, 3/4/08 (PB2009-102311).

MCEER-08-0006   "System Performance Under Multi-Hazard Environments," by C. Kafali and M. Grigoriu, 3/4/08 (PB2008-112235).

MCEER-08-0007   "Mechanical Behavior of Multi-Spherical Sliding Bearings," by D.M. Fenz and M.C. Constantinou, 3/6/08 (PB2008-112236).

MCEER-08-0008   "Post-Earthquake Restoration of the Los Angeles Water Supply System," by T.H.P. Tabucchi and R.A. Davidson, 3/7/08 (PB2008-112237).

MCEER-08-0009   "Fragility Analysis of Water Supply Systems," by A. Jacobson and M. Grigoriu, 3/10/08.

MCEER-08-0010   "Experimental Investigation of Full-Scale Two-Story Steel Plate Shear Walls with Reduced Beam Section Connections," by B. Qu, M. Bruneau, C-H. Lin and K-C. Tsai, 3/17/08.

MCEER-08-0011   "Seismic Evaluation and Rehabilitation of Critical Components of Electrical Power Systems," S. Ersoy, B. Feizi, A. Ashrafi and M. Ala Saadeghvaziri, 3/17/08.

MCEER-08-0012   "Seismic Behavior and Design of Boundary Frame Members of Steel Plate Shear Walls," by B. Qu and M. Bruneau, 4/26/08.

MCEER-08-0013   "Development and Appraisal of a Numerical Cyclic Loading Protocol for Quantifying Building System Performance," by A. Filiatrault, A. Wanitkorkul and M. Constantinou, 4/27/08.

MCEER-08-0014   "Structural and Nonstructural Earthquake Design: The Challenge of Integrating Specialty Areas in Designing Complex, Critical Facilities," by W.J. Petak and D.J. Alesch, 4/30/08.

MCEER-08-0015   "Seismic Performance Evaluation of Water Systems," by Y. Wang and T.D. O'Rourke, 5/5/08.

MCEER-08-0016   "Seismic Response Modeling of Water Supply Systems," by P. Shi and T.D. O'Rourke, 5/5/08.

MCEER-08-0017   "Numerical and Experimental Studies of Self-Centering Post-Tensioned Steel Frames," by D. Wang and A. Filiatrault, 5/12/08.

MCEER-08-0018   "Development, Implementation and Verification of Dynamic Analysis Models for Multi-Spherical Sliding Bearings," by D.M. Fenz and M.C. Constantinou, 8/15/08.